

NASA Contractor Report 3099

NASA
CR
3099
c.1

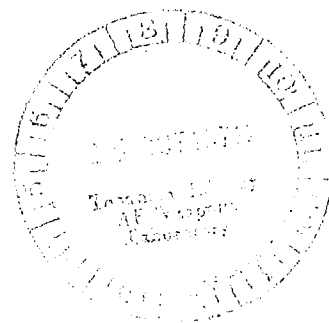
LOAN COPY. RETURN TO
AFWL TECHNICAL LIBRARY
KIRTLAND AFB, N.M.
LOAN COPY. RETURN TO
AFWL TECHNICAL LIBRARY
KIRTLAND AFB, N.M.



Rotary Balance Data for a Single-
Engine Trainer Design for an
Angle-of-Attack Range of 8° to 90°

Paul Pantason and Waldo Dickens

CONTRACT NAS1-14849
AUGUST 1979



NASA



NASA Contractor Report 3099

Rotary Balance Data for a Single-Engine Trainer Design for an Angle-of-Attack Range of 8° to 90°

Paul Pantason and Waldo Dickens
Bihrl Applied Research, Inc.
Jericho, New York

Prepared for
Langley Research Center
under Contract NAS1-14849



National Aeronautics
and Space Administration

Scientific and Technical
Information Branch

1979

SUMMARY

Aerodynamic characteristics obtained in a rotational flow environment utilizing a rotary balance located in the Langley spin tunnel are presented in plotted form for a 1/6-scale, single-engine trainer airplane model. The configurations tested included the basic airplane, various wing leading-edge devices, elevator, aileron and rudder control settings as well as airplane components. Data are presented without analysis for an angle-of-attack range of 8° to 90° and clockwise and counter-clockwise rotations covering an $\frac{\Omega b}{2V}$ range from 0 to 0.85.

INTRODUCTION

The NASA Langley Research Center has initiated a broad general aviation stall/spin research program which includes spin-tunnel and free-flight radio control model tests, as well as full-scale flight tests for a number of configurations typical of light, general aviation airplanes. To support this effort, rotary balance wind tunnel force tests covering these same configurations will be conducted to establish a data base for analysis of model and full-scale flight results, and to develop design charts for desirable stall/spin characteristics.

A 1/6-scale, single-engine trainer airplane model, having a low-wing location was tested in a rotational flow environment utilizing a rotary balance located in the Langley spin tunnel. This report presents the data obtained for the basic configuration, various wing leading-edge devices, elevator, aileron and rudder control settings as well as airplane components.

SYMBOLS

The units for physical quantities used herein are presented in the International System of Units (SI) and U.S. Customary Units. The measurements were made in the U.S. Customary Units; equivalent dimensions were determined by using the conversion factors given in reference 1.

b	wing span, m (ft)
\bar{c}	mean aerodynamic chord, cm (in.)
C_L	lift-force coefficient, $\frac{\text{Lift force}}{qS}$
C_N	normal-force coefficient, $\frac{\text{Normal force}}{qS}$
C_A	axial-force coefficient, $\frac{\text{Axial force}}{qS}$
C_Y	side-force coefficient, $\frac{\text{Side force}}{qS}$
C_ℓ	rolling moment coefficient, $\frac{\text{Rolling moment}}{qSb}$
C_m	pitching-moment coefficient, $\frac{\text{Pitching moment}}{qS\bar{c}}$
C_n	yawing-moment coefficient, $\frac{\text{Yawing moment}}{qSb}$
q	free-stream dynamic pressure, N/m ² (lb/ft ²)
S	wing area, m ² (ft ²)
V	free-stream velocity, m/sec (ft/sec)
α	angle of attack, deg
β	angle of sideslip, deg
Ω	angular velocity about spin axis, rad/sec
$\frac{\Omega b}{2V}$	spin coefficient, positive for clockwise spin
δ_a	aileron deflection, positive when right aileron is down $(\delta_{a_{\text{right}}} - \delta_{a_{\text{left}}})/2$, deg
δ_e	elevator deflection, positive when trailing edge is down, deg

δ_r rudder deflection, positive when trailing edge is to left, deg

Abbreviations:

cg center of gravity

LE leading edge

SR spin radius

TEST EQUIPMENT

A rotary balance measures the forces and moments acting on an airplane while subjected to rotational flow conditions; the background for this apparatus is discussed in reference 2. A photograph and sketch of the rotary balance apparatus installed in the Langley spin tunnel are shown in figures 1 and 2, respectively. The rotating portion of the balance system, mounted on a horizontal supporting boom which is hinged at the wall, is moved from the wall to the center of the tunnel by cables. The rotary arm of the balance system, which rotates about a vertical axis, is attached to the outer end of the horizontal supporting boom and is driven by a drive shaft through couplings and gears.

A test model is mounted on a strain gauge balance which is affixed to the bottom of the rotary balance apparatus. Controls located outside the tunnel are used to activate motors on the rig which position the model to the desired attitude. The angle-of-attack range of the rig is 8 to 90 degrees and the sideslip angle range is ± 15 degrees. The spin radius and the lateral displacement motors allow the operator to position the moment center of

the balance on the spin axis or at a specific distance from the spin axis. This is done for each combination of angle of attack and sideslip angle. The general practice is to mount the moment center of the balance at the cg location about which the aerodynamic moments are desired. Electrical current from the balance, and to the motors on the rig, is conducted through slip-rings located at the rig head. Examples of how the rig is positioned for different angle of attack and sideslip angles are shown in figures 2a and 2b, respectively.

The model can be rotated up to 90 rpm in either direction. By using different rotational speeds and a specific airflow in the tunnel, the motions of a steady spinning airplane can be simulated. The aerodynamic forces and moments can then be measured for values of $\frac{\Omega b}{2V}$, including the case of $\frac{\Omega b}{2V} = 0$, where static aerodynamic forces and moments can be obtained.

A NASA six-component strain gauge balance is mounted inside the model and measures the normal, lateral and longitudinal forces and the yawing, rolling and pitching moments acting about the model body axis. The interactions that exist between the six components are available from balance calibration tests and are accounted for after the balance voltages are converted to forces and moments.

The data acquisition, reduction and presentation system for the rotary balance set-up is composed of a 12-channel scanner/voltmeter, a mini-computer and a plotter. With this equipment,

on-line digital print-out and/or graphical plots of data are possible.

TEST PROCEDURES

Rotary aerodynamic data are obtained in two steps. The first step is to record the inertial forces and moments (tares) acting on the model at different attitudes and rotational speeds. To accomplish this, a covered bird-cage like structure is mounted to the upper rig which encloses the model without touching it. In this manner, the air immediately surrounding the model is rotated with it. As the rig is rotated at the desired attitude and rate, the inertial forces and moments generated by the model are measured and stored on magnetic tape for later use.

The second step in the data-gathering process is to measure aerodynamic and inertial forces at different attitudes and rotational speeds for a selected tunnel velocity with, of course, the cage structure removed. The tares are subtracted from these values, and the remaining aerodynamic forces and moments are then converted to coefficient form and stored on magnetic tape.

MODEL

A 1/6-scale fiberglass/aluminum model of a configuration considered to be a typical low-wing, single-engine trainer airplane was tested in the present study. A three-view drawing of this model is shown in figure 3, dimensional characteristics of the model are presented in Table I, and a photograph of the model installed on the rotary balance located in the Langley spin tunnel is presented in figure 1.

The model control surfaces could be set at any position prior to the test. The maximum deflections for the control surfaces were:

Elevator, deg	20 up, 15 down
Rudder, deg	28 right, 28 left
Aileron, deg	20 up, 20 down

TEST CONDITIONS

The tests were conducted in the spin tunnel at a tunnel velocity of 7.62m/sec (25 ft/sec) which corresponds to a Reynolds number of 145,000 based on the model mean aerodynamic chord. Unless noted otherwise in Table II, all the configurations were tested through an angle-of-attack range of 8 to 90° at a zero sideslip angle with the spin axis passing through the full-scale airplane cg location of .25 \bar{c} for angles of attack above 30°. For angles of attack below 35°, the spin axis was set 91.4 cm (36 in.) forward of the cg. Consequently, data was obtained for both a 0 and 91.4 cm (36 in.) spin radius at angles of attack of 30 and 35°. At each spin attitude, measurements were obtained for nominal $\frac{\Omega b}{2V}$ values of .1, .2, .3, .4, .45, .55, .65, .75 and .85 in both clockwise and counter-clockwise directions, as well as for $\frac{\Omega b}{2V} = 0$ (static value).

DATA PRESENTATION

Table II identifies the configurations tested and the corresponding appendix figure numbers which present the aerodynamic data. The aerodynamic coefficients vs. $\frac{\Omega b}{2V}$ are presented for each configuration in six sequentially numbered

figures in the following order: C_n , C_l , C_m , C_N , C_Y and C_A . Each figure, in turn, consists of four pages which present the subject aerodynamic coefficient vs. $\frac{\Omega b}{2V}$ for the following angles of attack and spin radii, unless noted otherwise in Table II.

- a) $\alpha = 8, 10, 12, 14, 16$ deg $SR = 91.4$ cm (36 in.)
- b) $\alpha = 18, 20, 25, 30, 35$ deg $SR = 91.4$ cm (36 in.)
- c) $\alpha = 30, 35, 40, 45, 50$ deg $SR = 0$
- d) $\alpha = 55, 60, 70, 80, 90$ deg $SR = 0$

All the moment data are presented for a cg position of $0.25\bar{c}$.

Lift coefficient as a function of angle of attack for zero rotation rate is presented at the end of the Appendix for several configurations cited in Table II.

REFERENCES

1. Mechtly, E.C.: The International System of Units - Physical Constants and Conversion Factors. NASA SP-7012, 1973.
2. Bihrlé, William, Jr.; Hultberg, Randy S.; and Mulcay, William: Rotary Balance Data for a Typical Single-Engine Low-Wing General Aviation Design for an Angle-of-Attack Range of 30° to 90° . NASA CR 2972, 1978.

TABLE I.- DIMENSIONAL CHARACTERISTICS OF THE BASIC MODEL

Overall length, m (ft)	1.46 (4.79)
Wing:	
Span, m (ft)	1.70 (5.57)
Area, m ² (ft ²)47 (5.03)
Root chord, cm (in.)	35.56 (14.0)
Tip chord, cm (in.)	17.78 (7.0)
Mean aerodynamic chord, cm (in.)	27.66 (10.89)
Leading edge of \bar{c} , distance rearward of leading	
edge of root chord, cm (in.)	1.98 (.78)
Aspect ratio	6.21
Taper ratio	0.50
Dihedral, deg	7.0
Incidence:	
Root, deg	4.0
Tip, deg	1.0
Airfoil section:	
Root	NASA 23016.5
Tip	NASA 23012
Horizontal tail:	
Span, m (ft)62 (2.03)
Area, m ² (ft ²)10 (1.03)
Incidence, deg	0
Airfoil sectionNASA 0008.2 (modified)
Vertical tail:	
Area, m ² (ft ²)05 (.55)
Sweepback at leading edge, deg.	15
Aspect ratio	1.44
Leading edge canted left, deg	1.0
Airfoil sectionNASA 0006.7 (modified)

TABLE II.- CONFIGURATIONS TESTED AND FIGURE INDEX
(Unless noted otherwise, all configurations tested through $\alpha = 8$ to 90° at $\beta = 0^\circ$.)

FIGURE NO.	CONFIGURATION	δ_e deg	δ_a deg	δ_r deg	REMARKS
^a A1-A6	Basic	0	0	0	$\alpha = 8-35^\circ$ & $55-90^\circ$ only
A7-A12	↓	-20	20	-28	
^a A13-A18	Outboard LE wing droop	0	0	0	
A19-A24	Engine stacks off	↓	↓	↓	
A25-A30	Ventrals and strakes off	↓	↓	↓	
A31-A36	↓	-20	20	-28	
A37-A42	Sharp-edged fuselage bottom	0	0	0	
A43-A48	↓	-20	20	-28	
A49-A54	↓	↓	0	↓	
A55-A60	↓	↓	20	0	
A61-A66	↓	15	0	28	$\alpha = 50-90^\circ$ only
A67-A72	with ventrals and strakes off	0	↓	0	
A73-A78	with ventrals, strakes and engine stacks off	↓	↓	↓	
^a A79-A84	↓ with 4.06cm (1.6in) span outboard LE wing droop tab	↓	↓	↓	$\alpha = 50-90^\circ$ only

^a C_L vs. α presented in figure A85.

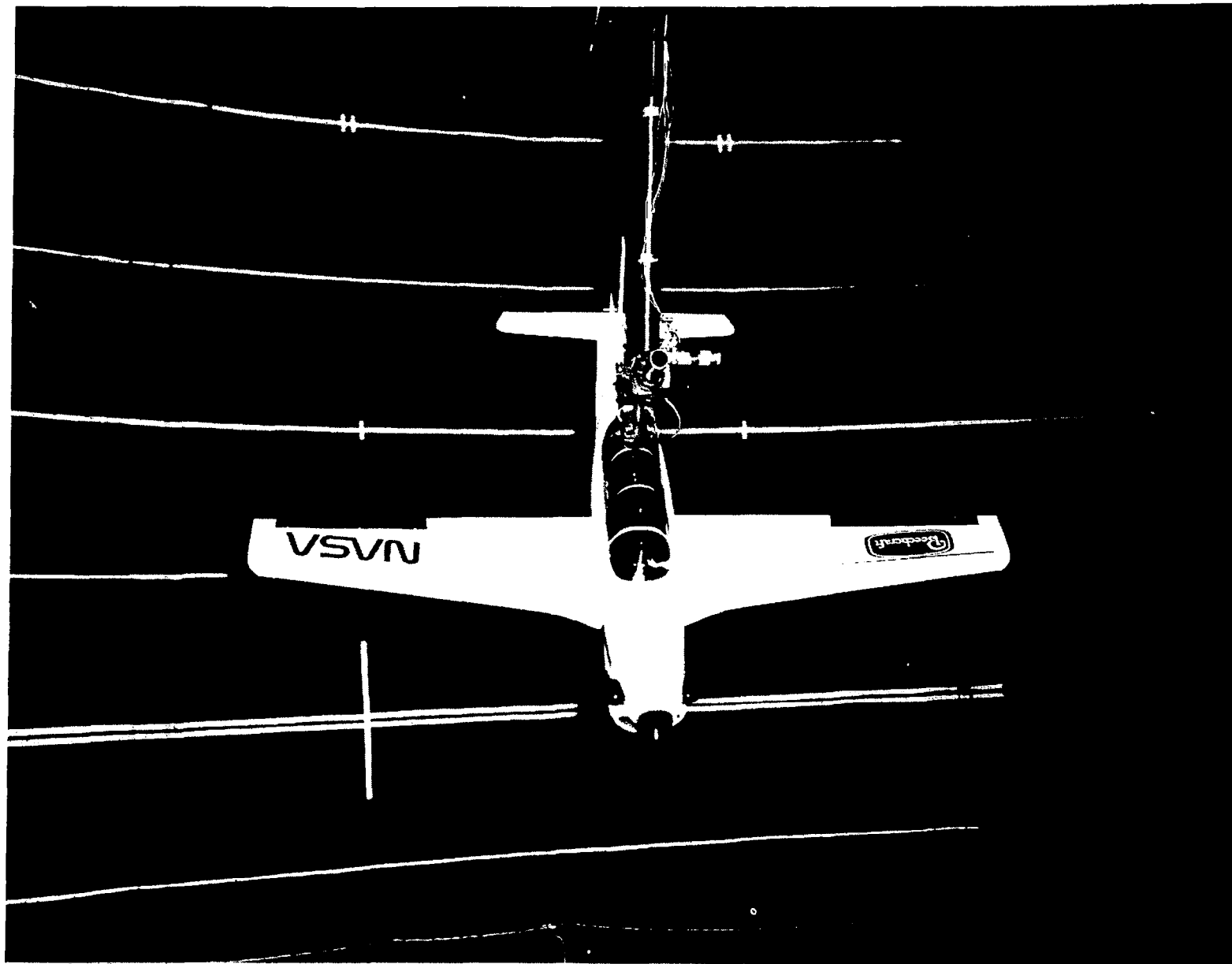
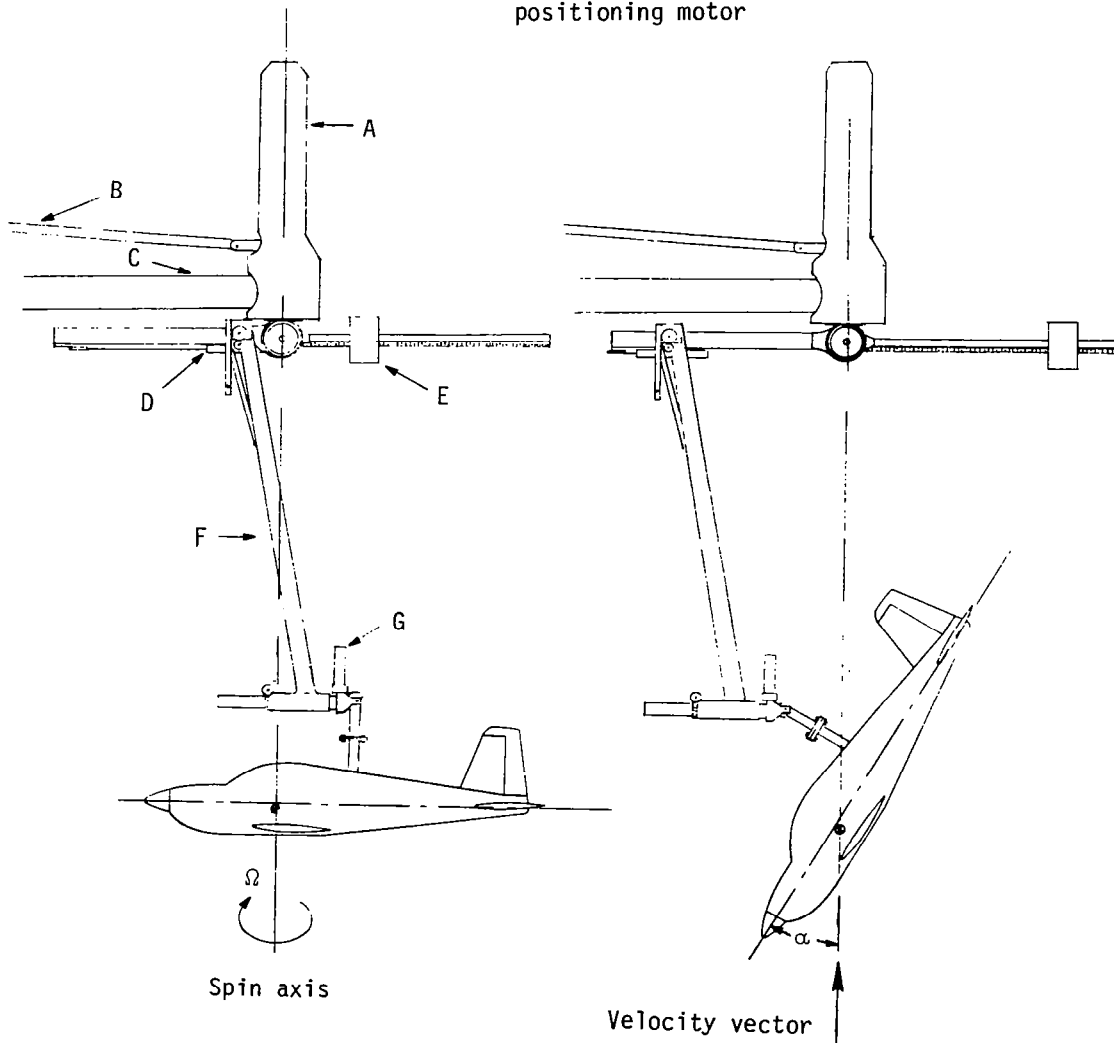


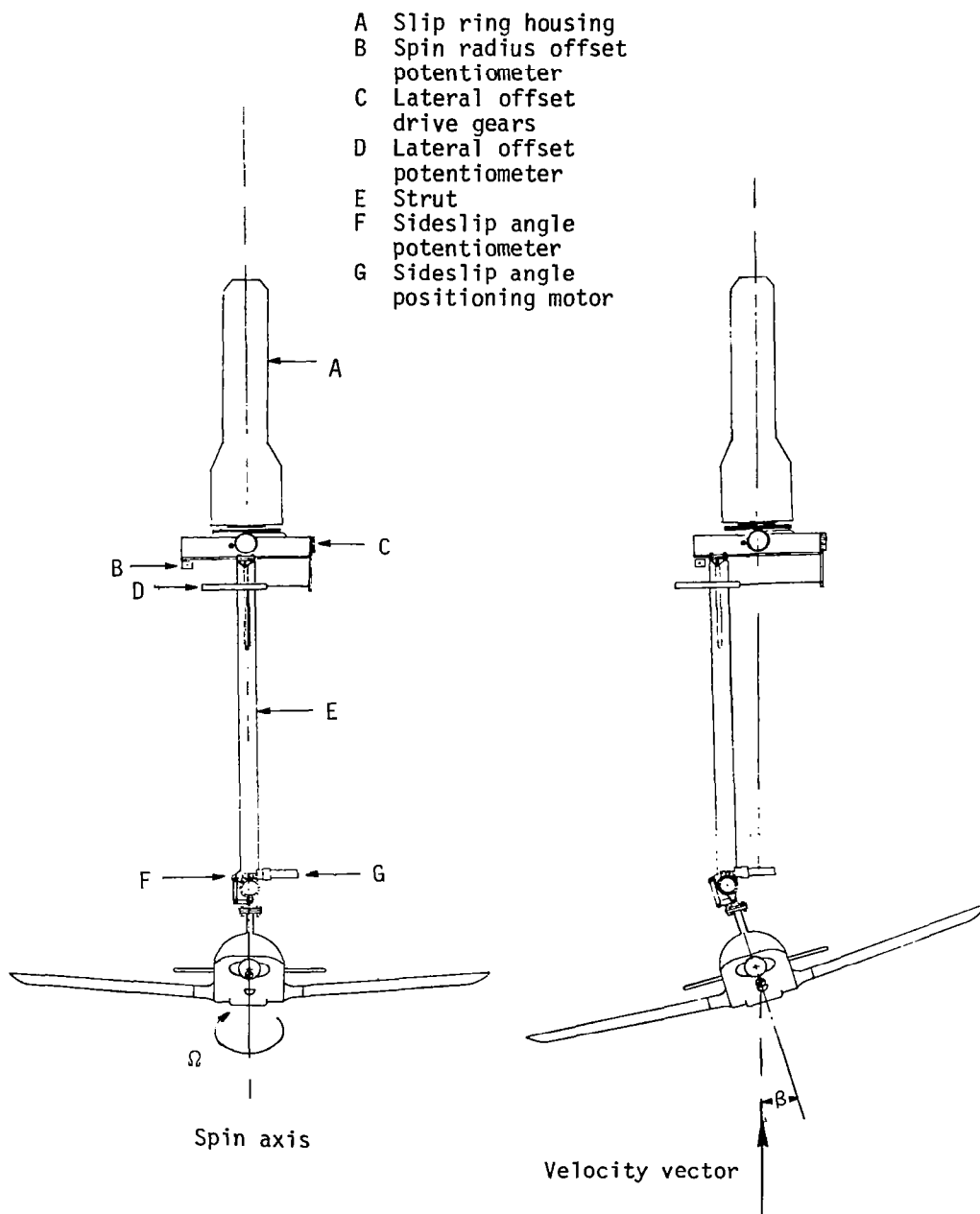
Figure 1.- Photograph of 1/6-scale model installed on rotary balance apparatus.

- A Slip ring housing
- B Drive shaft
- C Support boom
- D Spin radius offset potentiometer
- E Counterweight
- F Strut
- G Angle of attack positioning motor



(a) Side view of model.

Figure 2.- Sketch of rotary balance apparatus.



(b) Front view of model.

Figure 2.- Concluded.

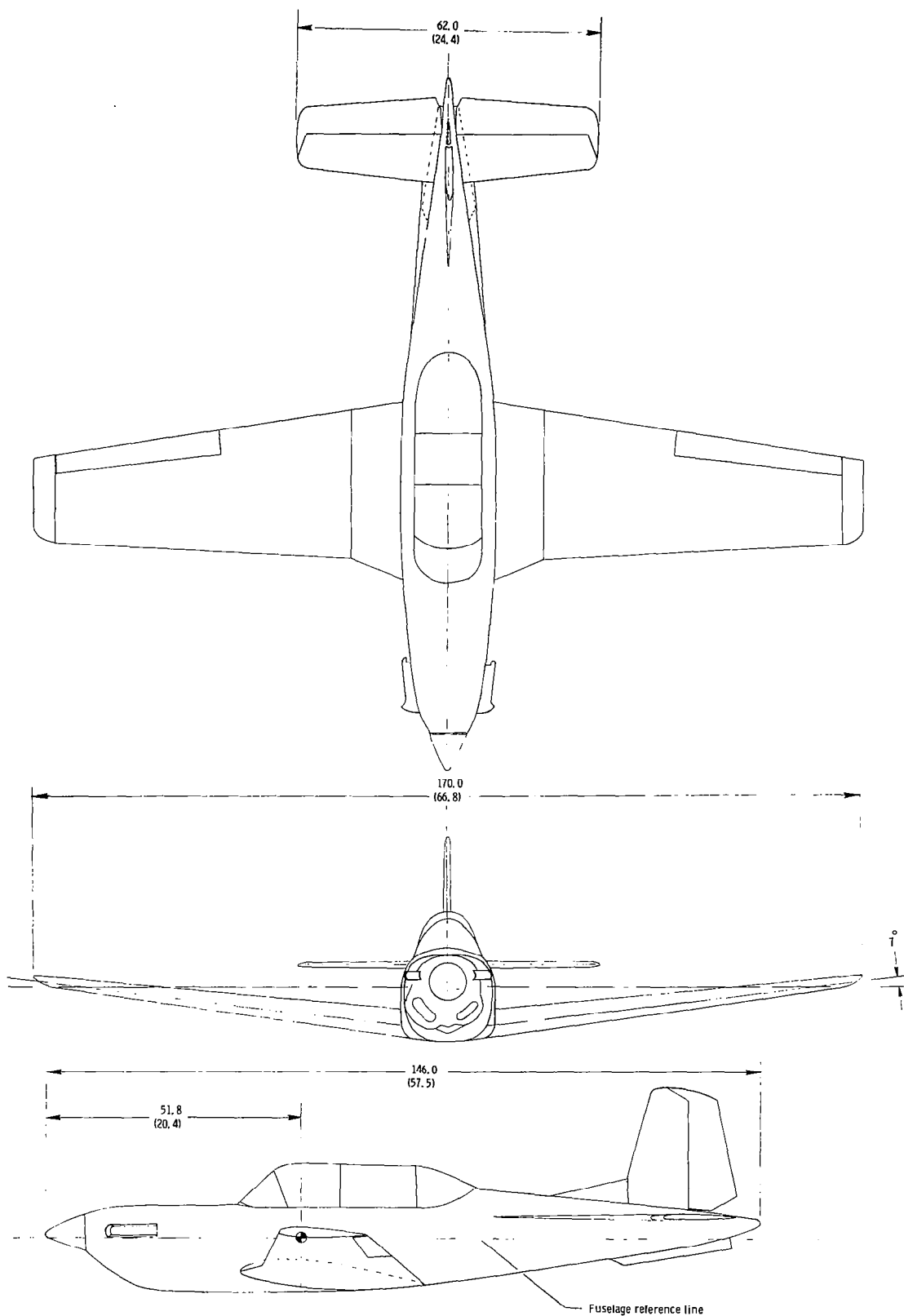


Figure 3. - Three-view drawing of basic 1/6-scale low-wing trainer. Center-of-gravity positioned at 0.25C. Dimensions are given in centimeters (inches), model scale.

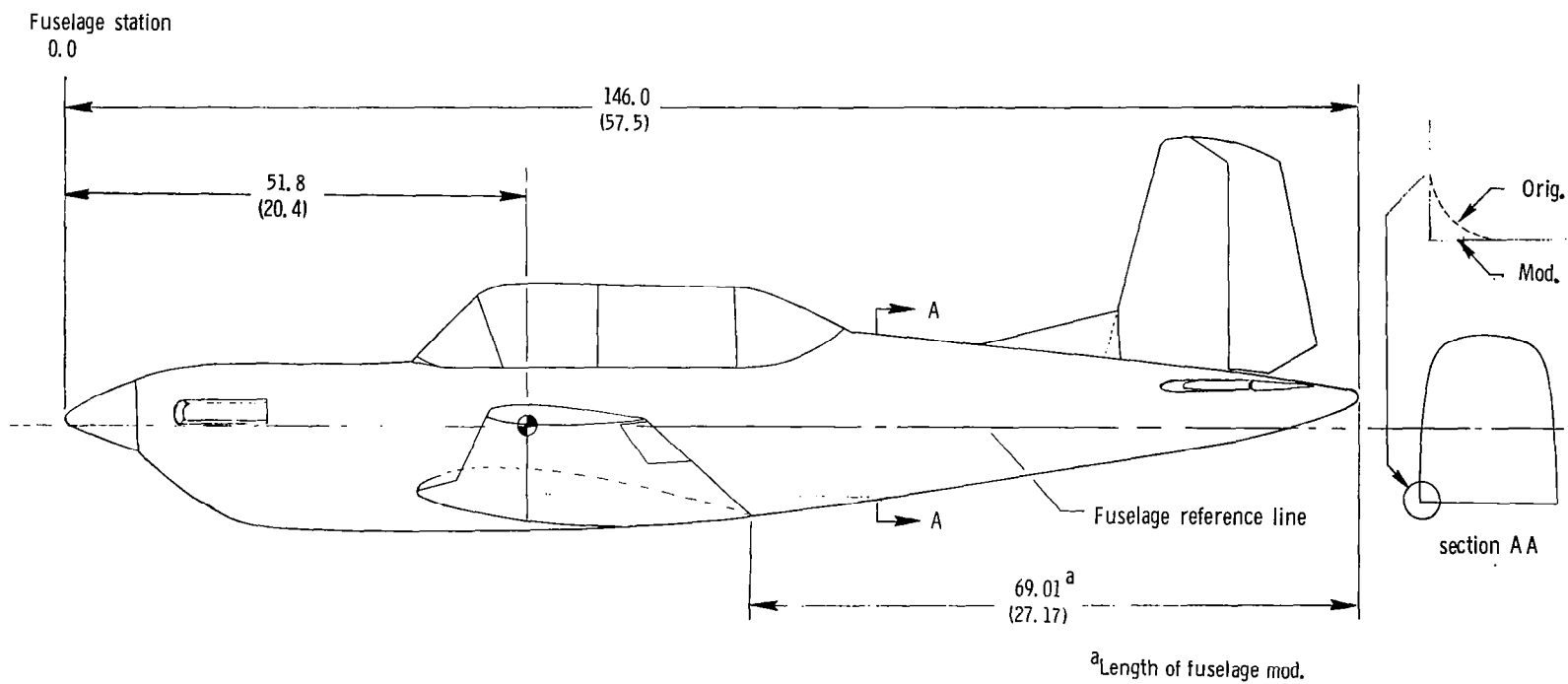
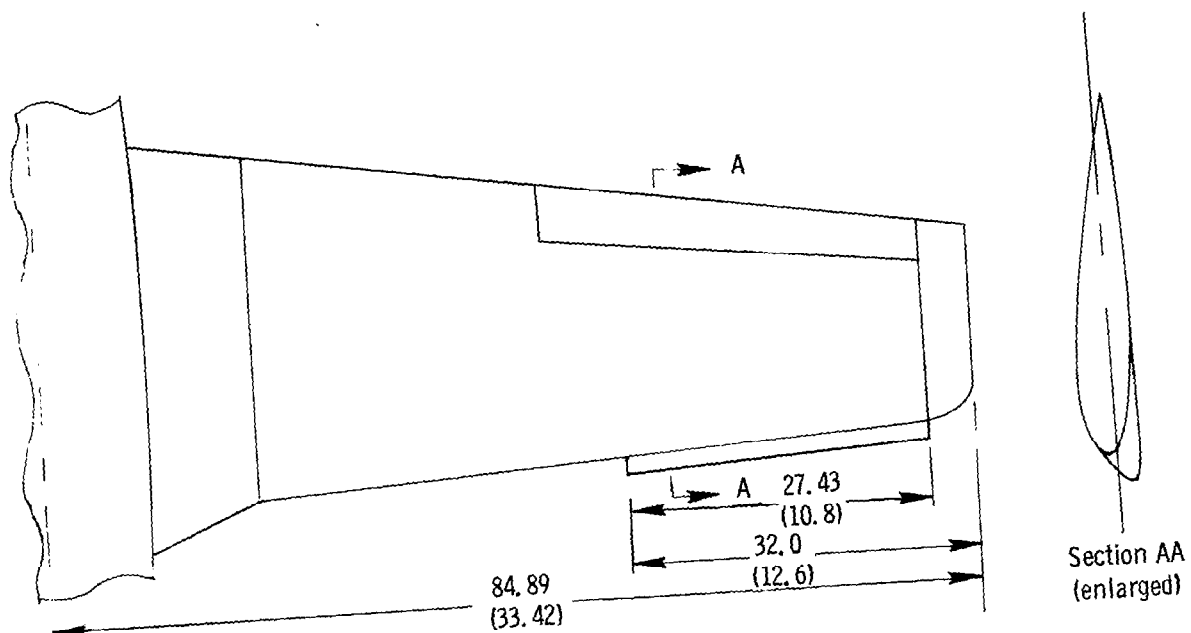
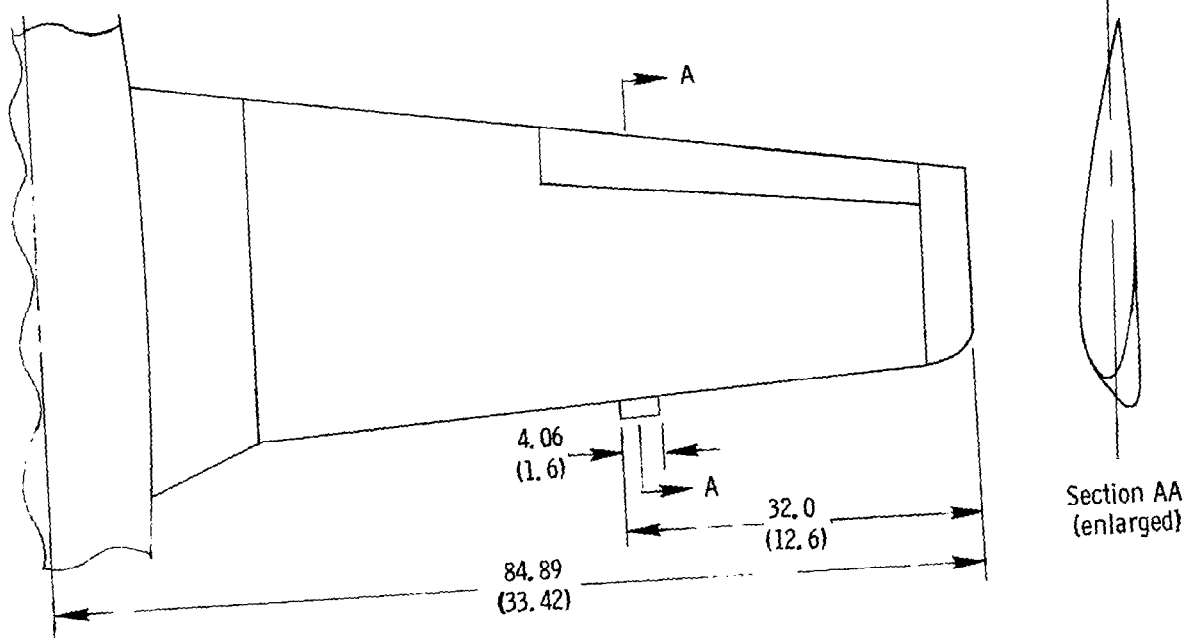


Figure 4. - Fuselage shape modification tested on model. Dimensions are given in centimeters (inches), model scale.



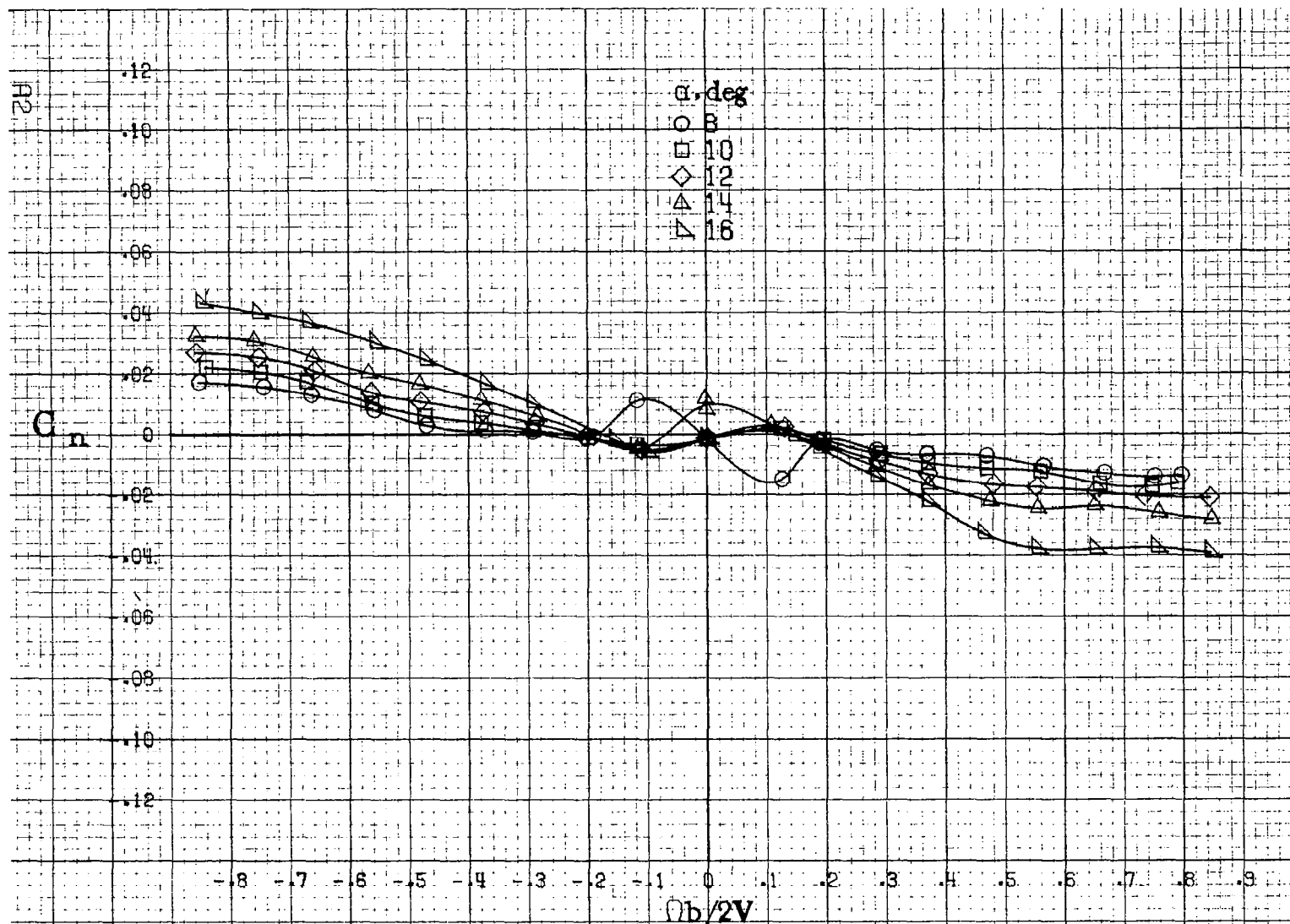
(a) Outboard LE wing droop.



(b) Outboard LE wing droop tab.

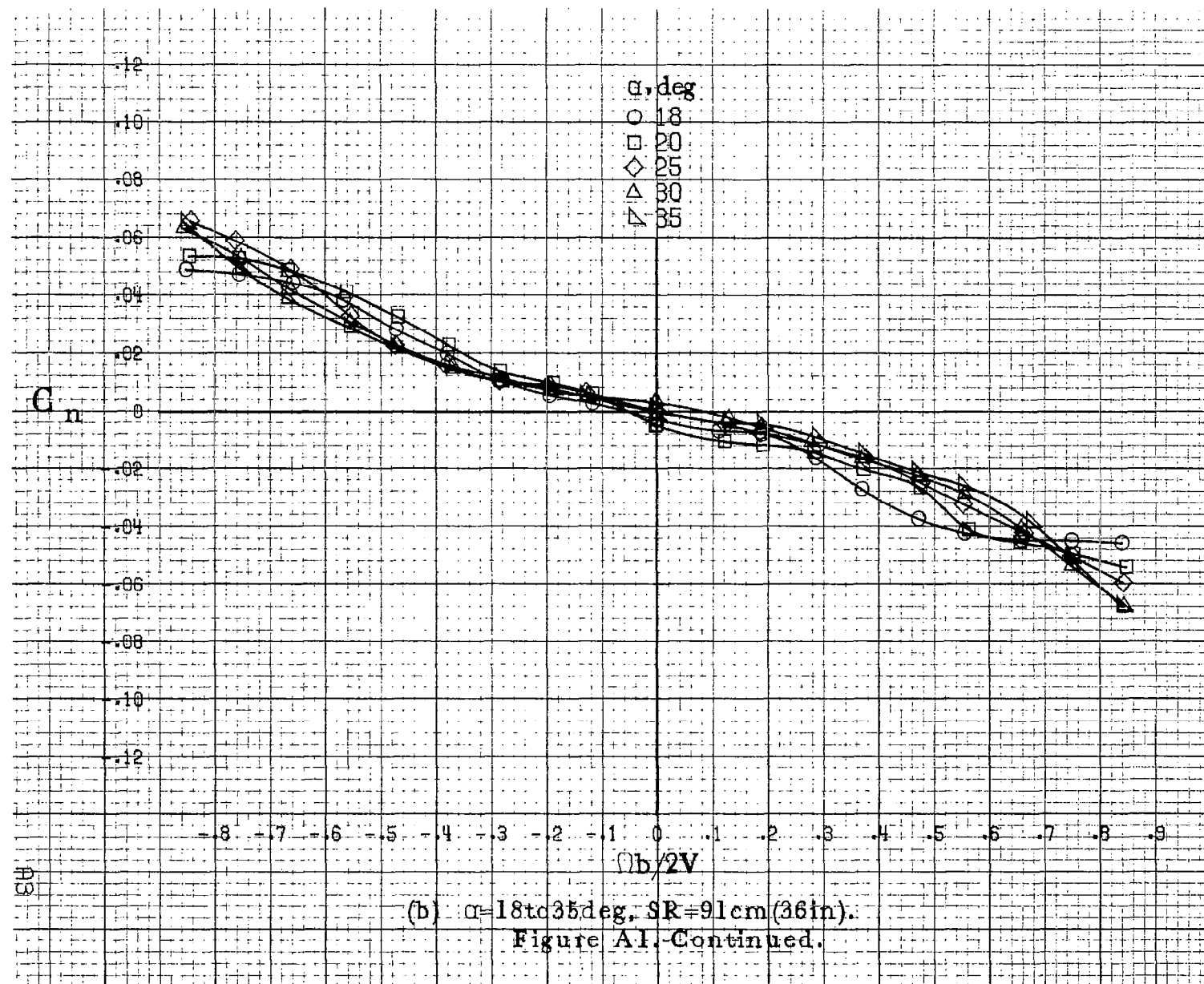
Figure 5. - Wing leading-edge modifications tested on model. Dimensions are given in centimeters (inches), model scale.

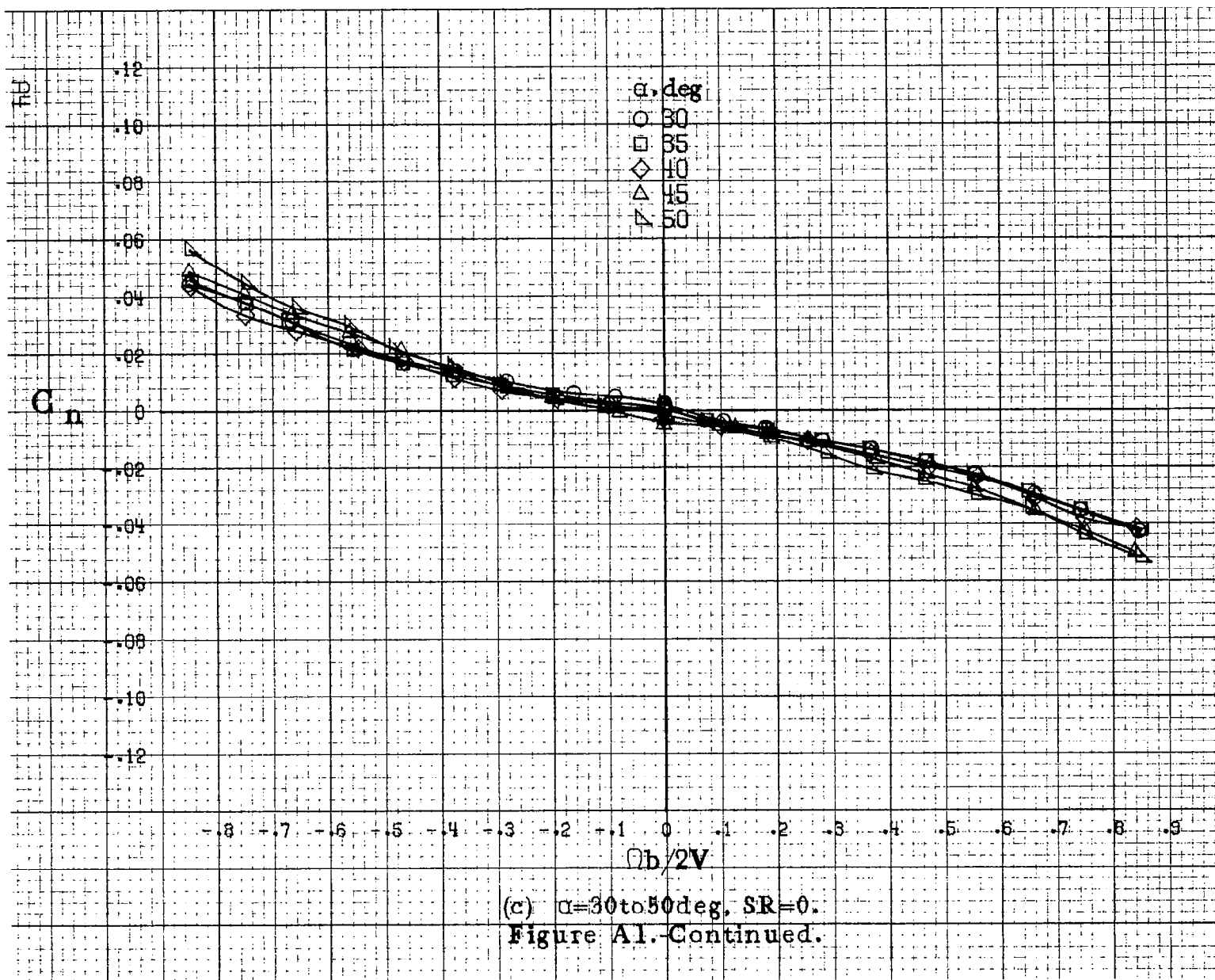
APPENDIX

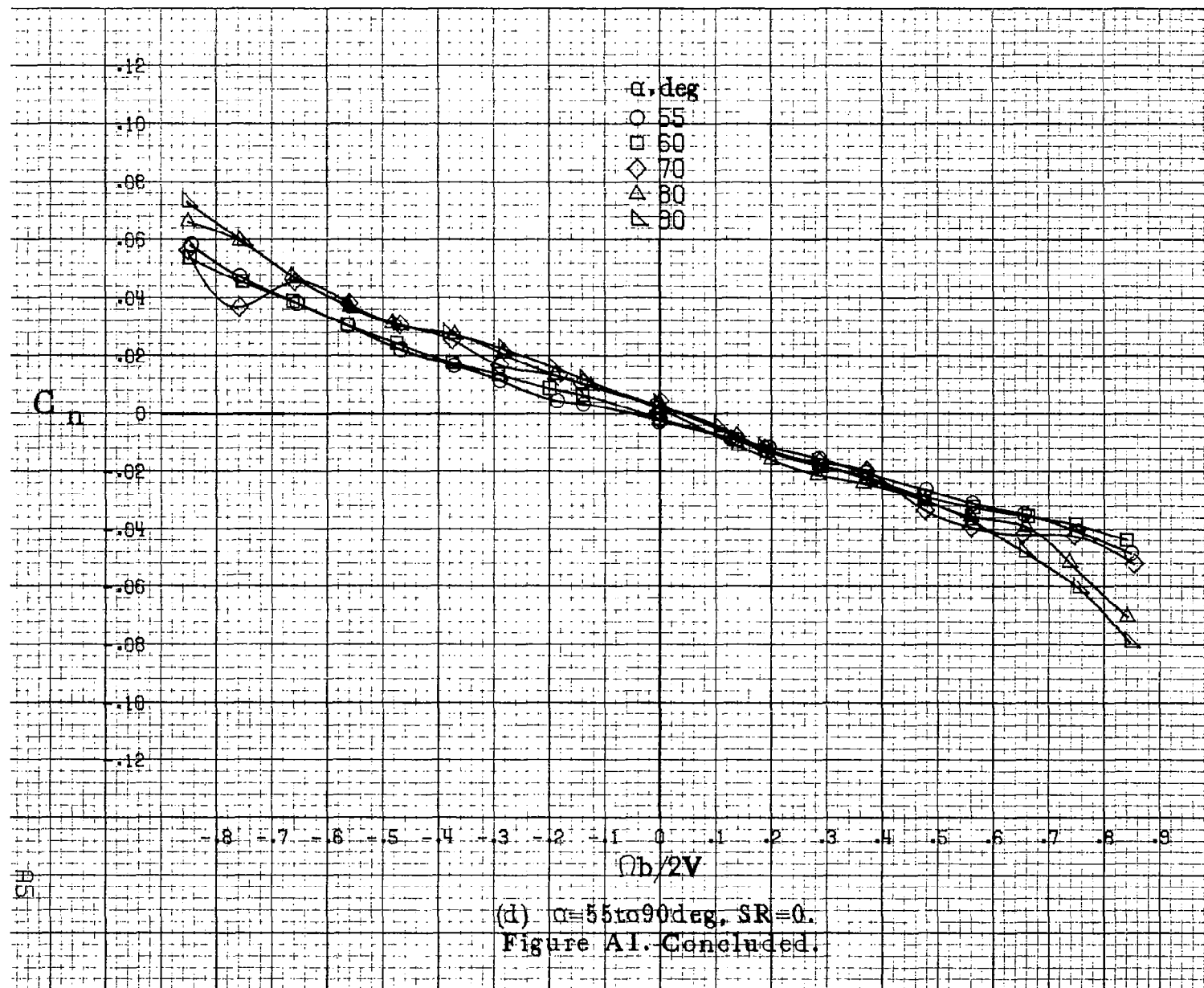


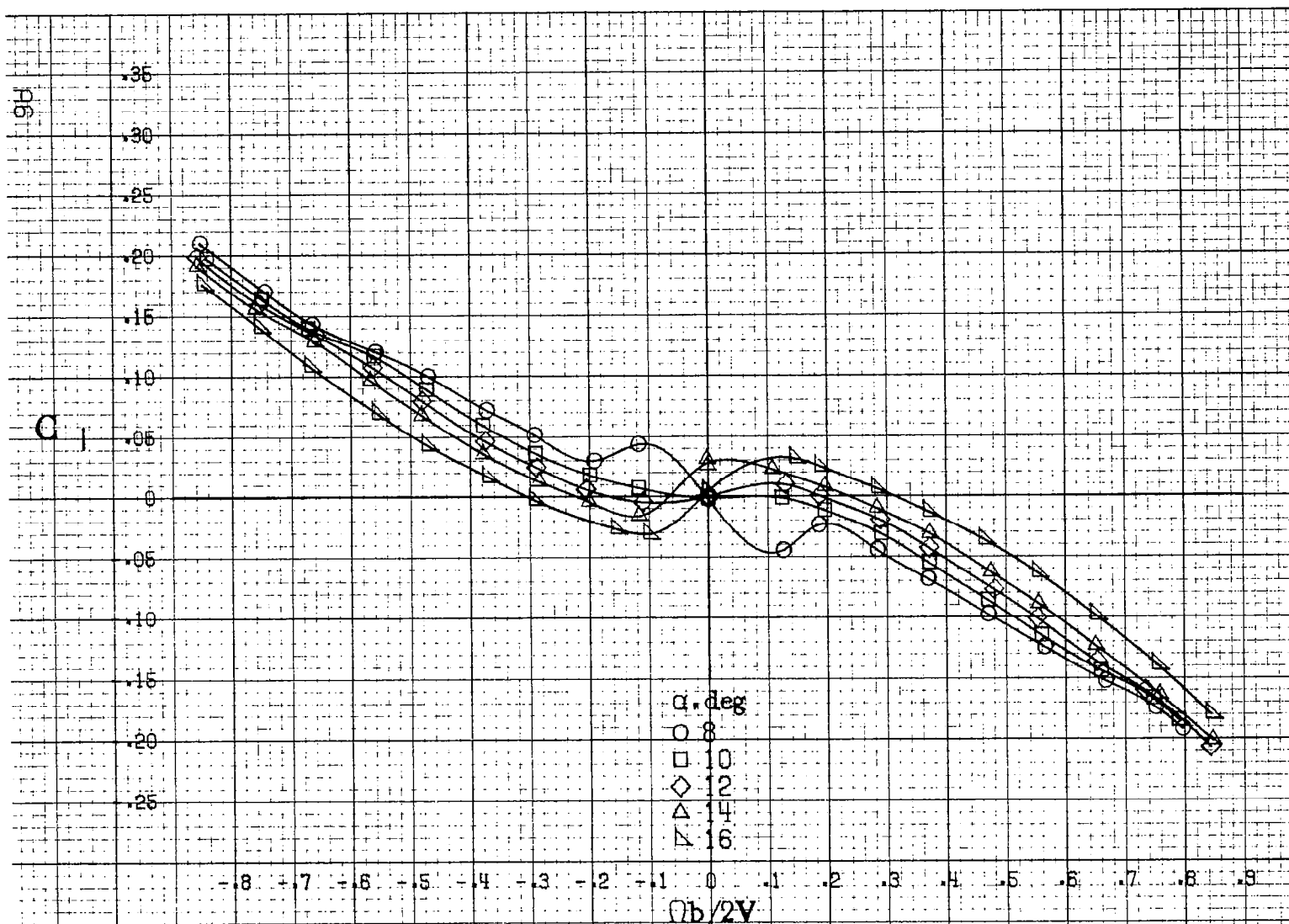
(a) $\alpha = 8$ to 16 deg, $SR = 91$ cm (36 in).

Figure A1. Effect of rotation rate and angle of attack on yawing moment coefficient for basic configuration. $\delta_e = 0^\circ$, $\delta_a = 0^\circ$, $\delta_r = 0^\circ$, $\beta = 0^\circ$.



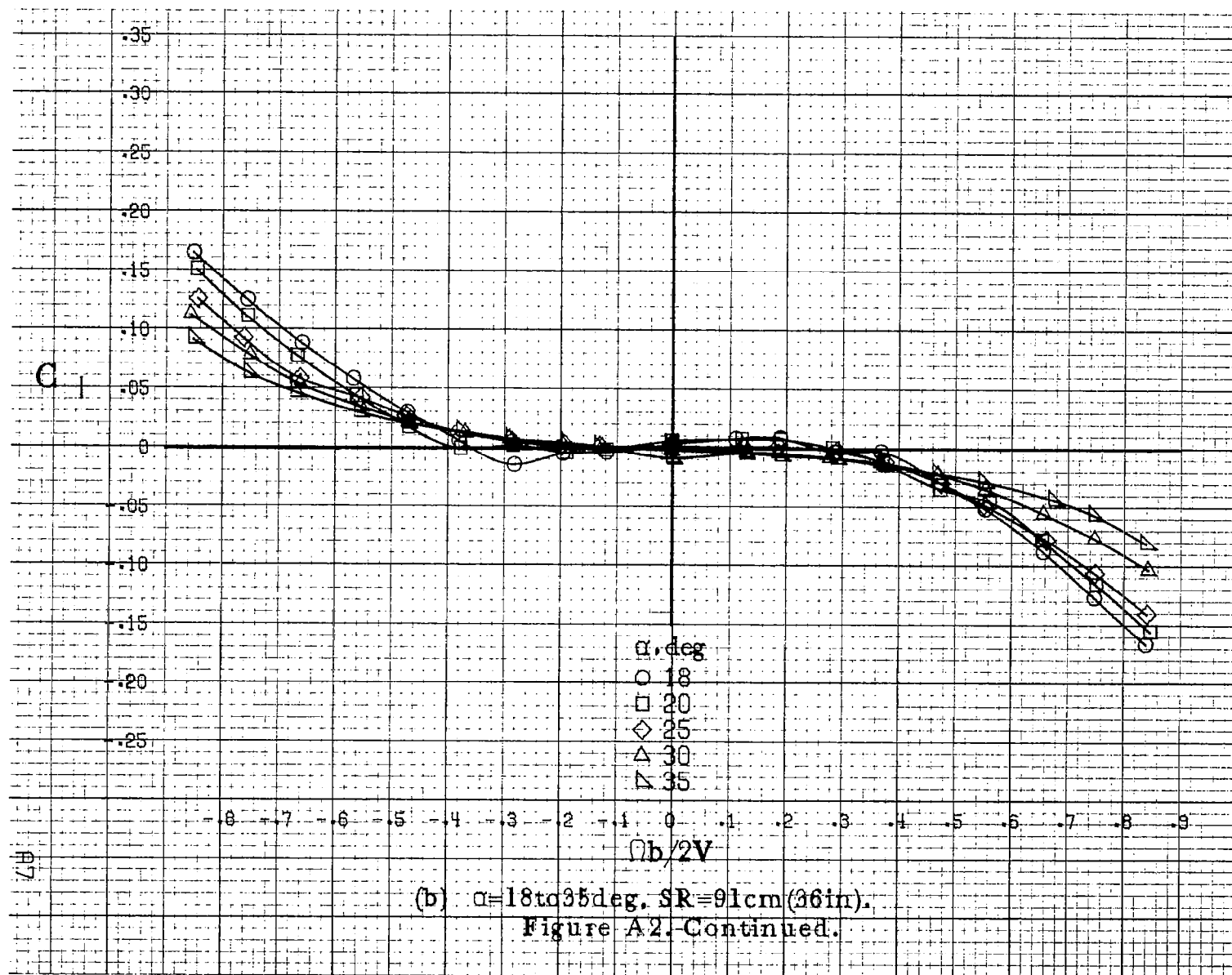


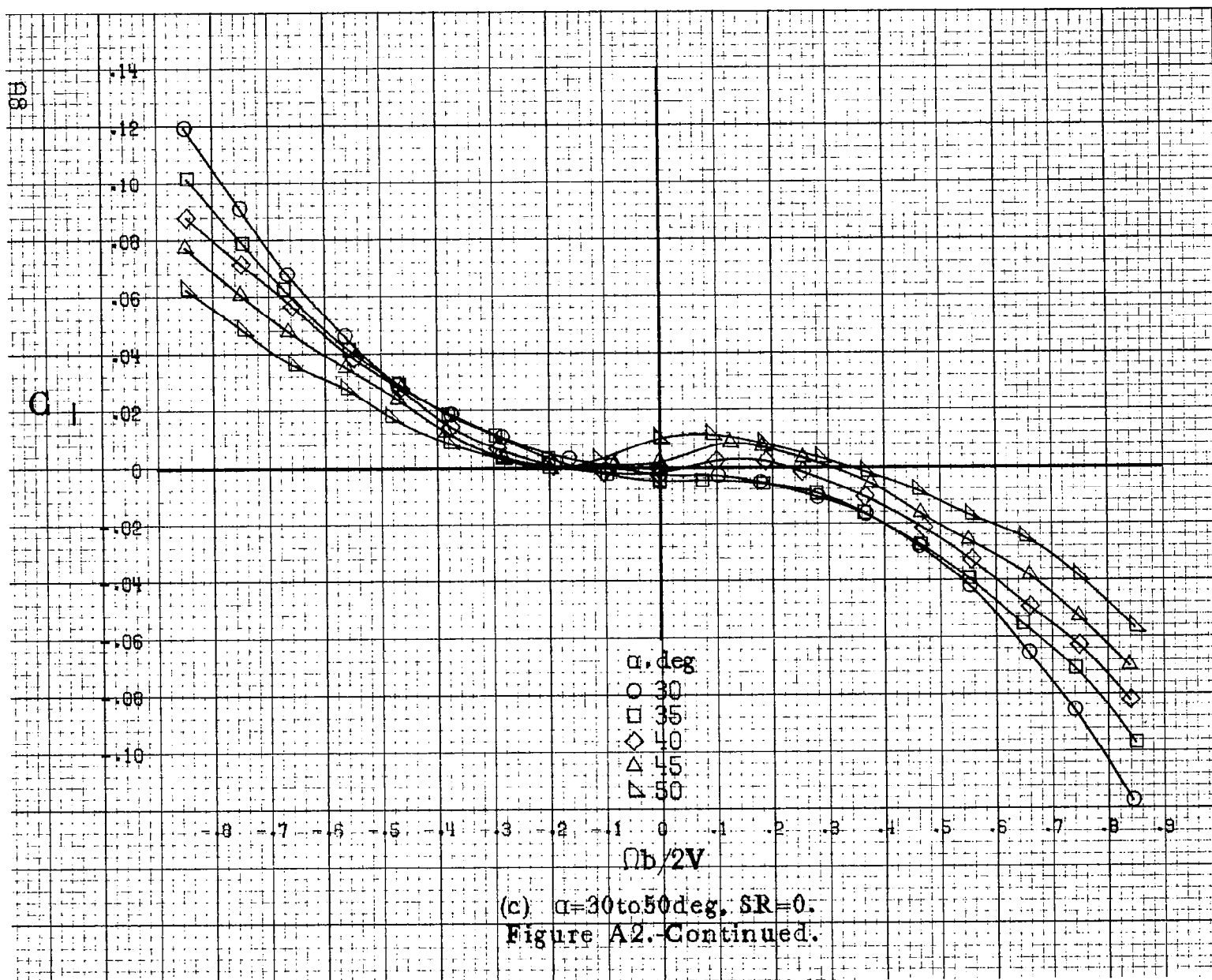


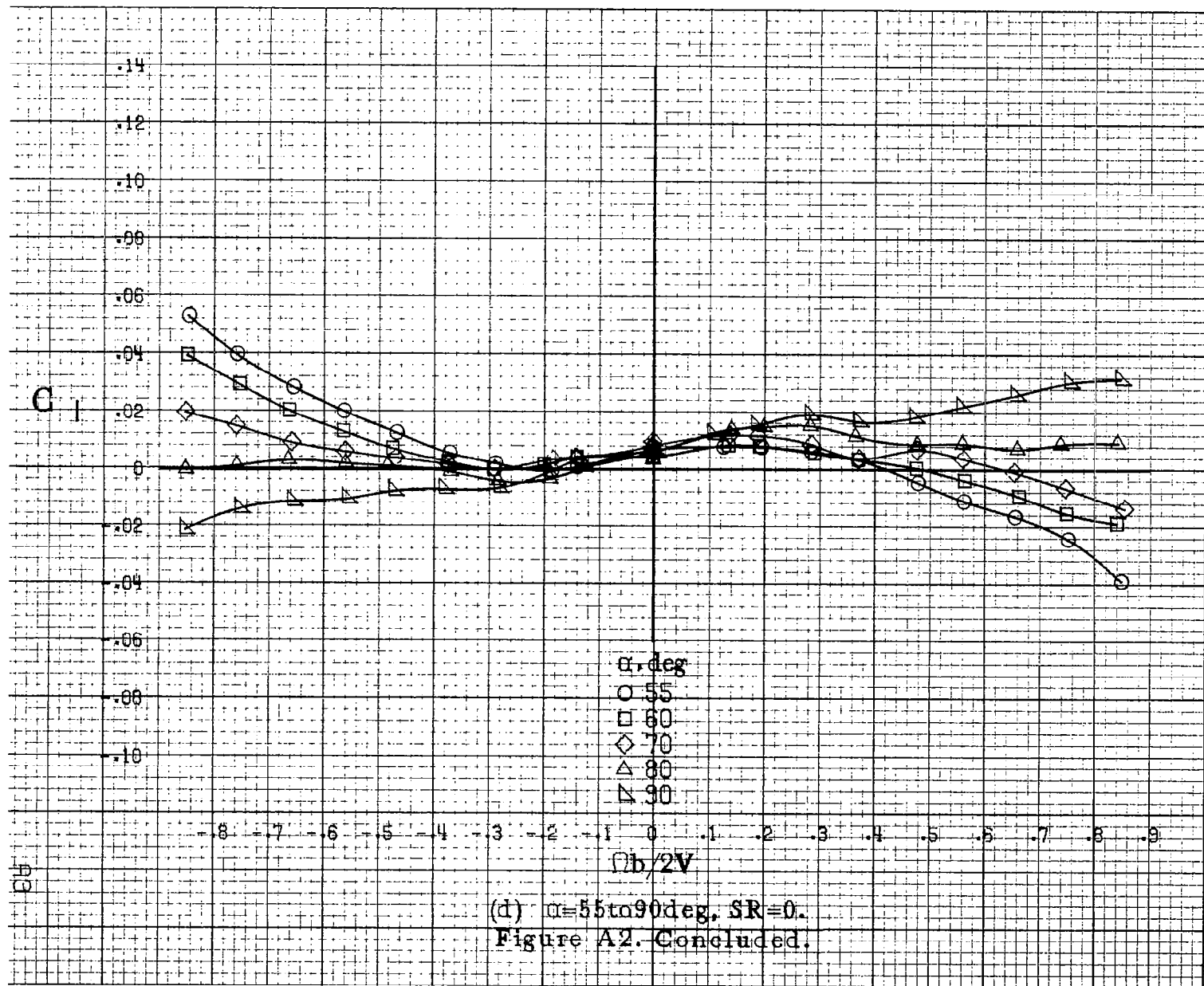


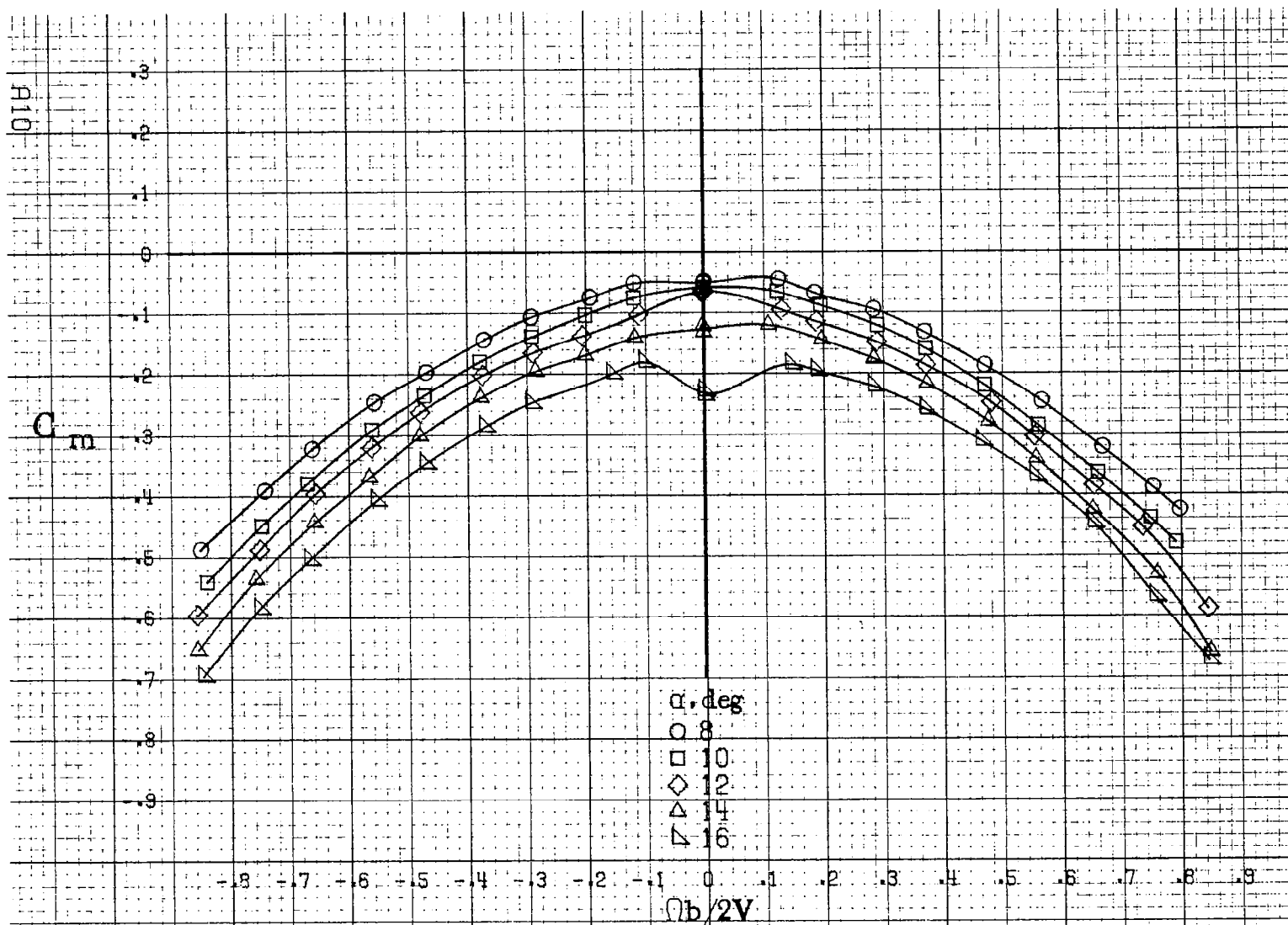
(a) $\alpha = 8$ to 16° , $SR = 91\text{cm} (36\text{in})$.

Figure A2. Effect of rotation rate and angle of attack on rolling moment coefficient for basic configuration. $\delta_e = 0^\circ$, $\delta_a = 0^\circ$, $\delta_r = 0^\circ$, $\theta = 0^\circ$.



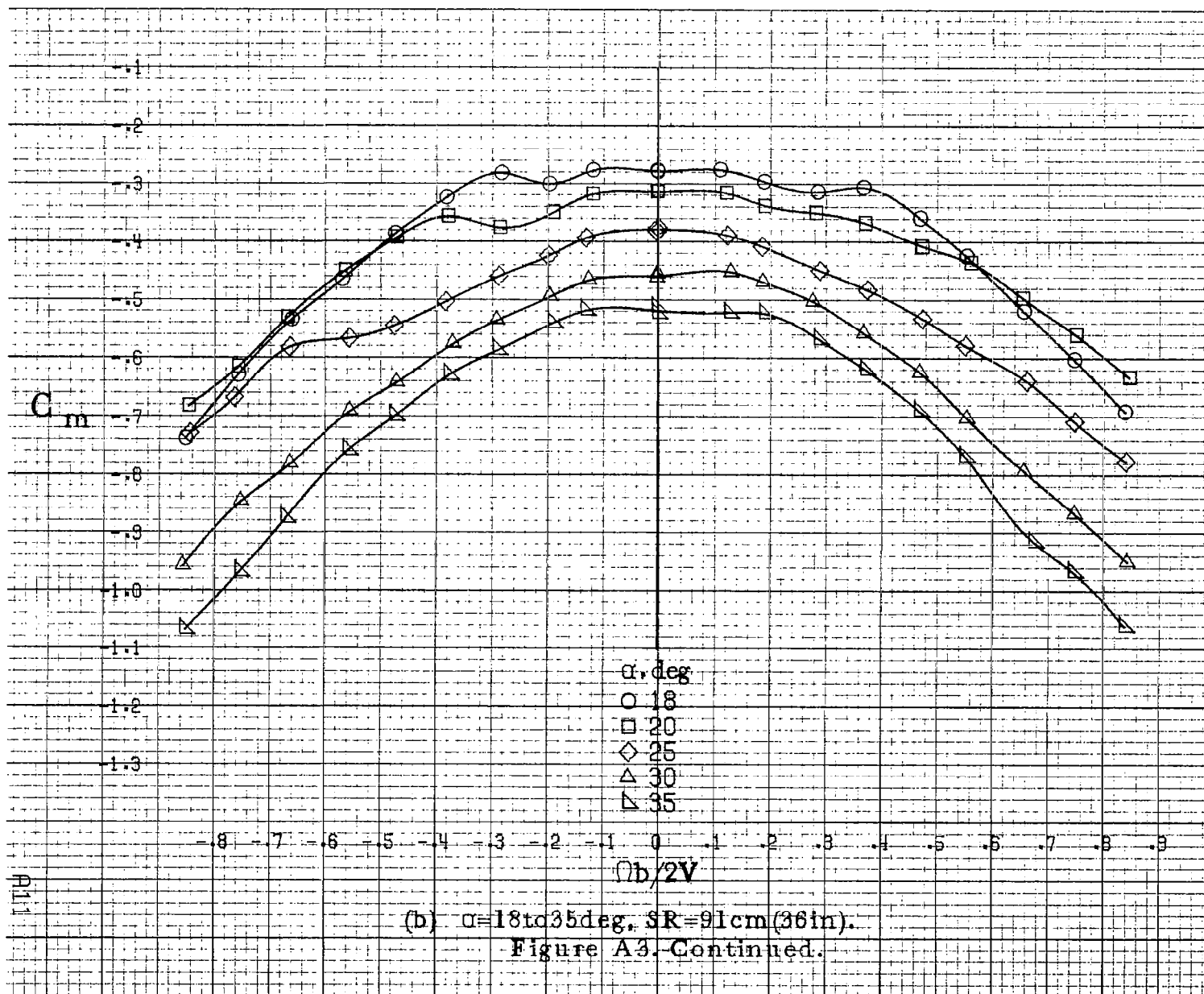


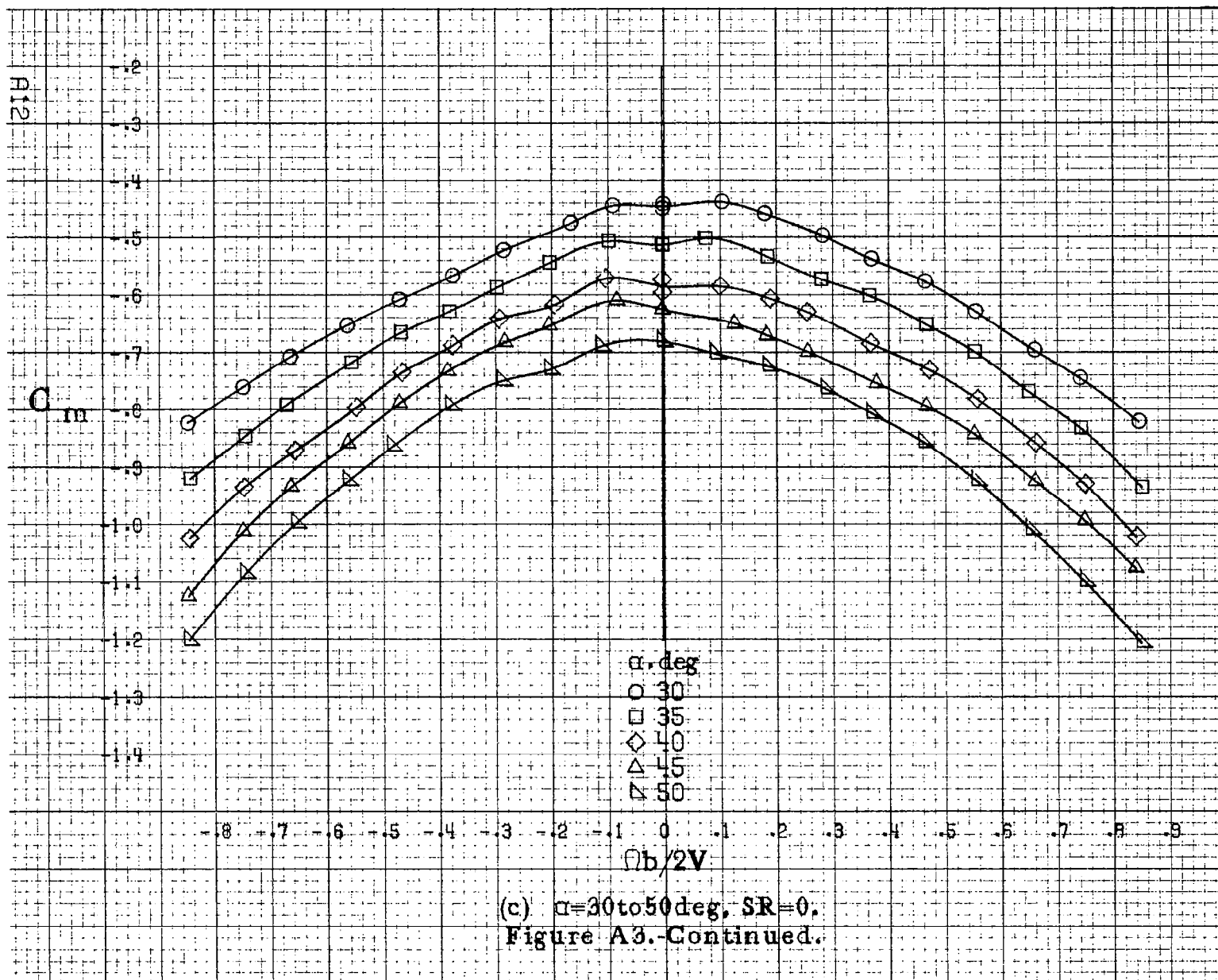


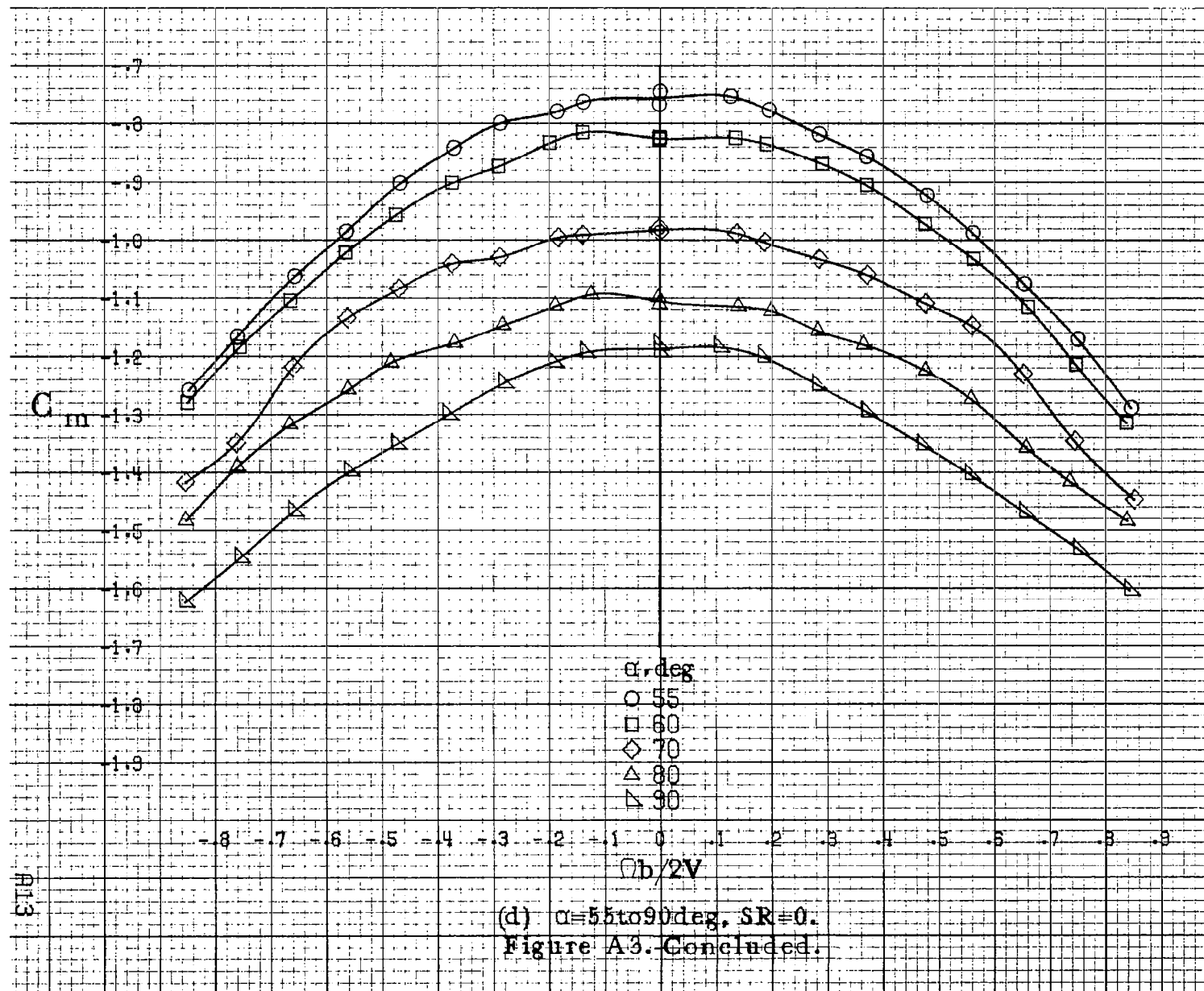


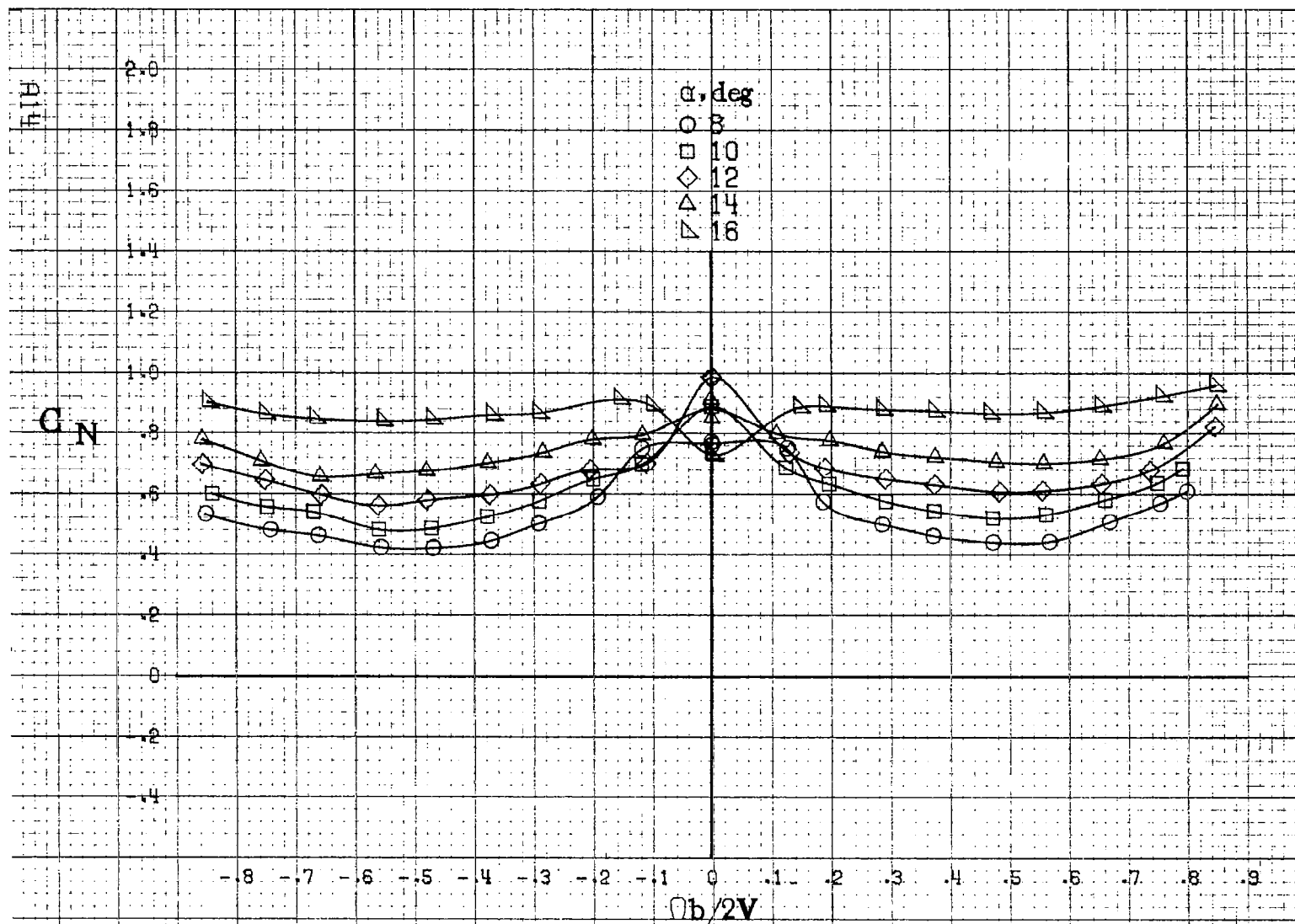
(a) $\alpha = 8$ to 16° , $SR = 91\text{cm} (36\text{in})$.

Figure A3. Effect of rotation rate and angle of attack on pitching moment coefficient for basic configuration. $\delta_e = 0^\circ$, $\delta_a = 0^\circ$, $\delta_r = 0^\circ$, $\beta = 0^\circ$.



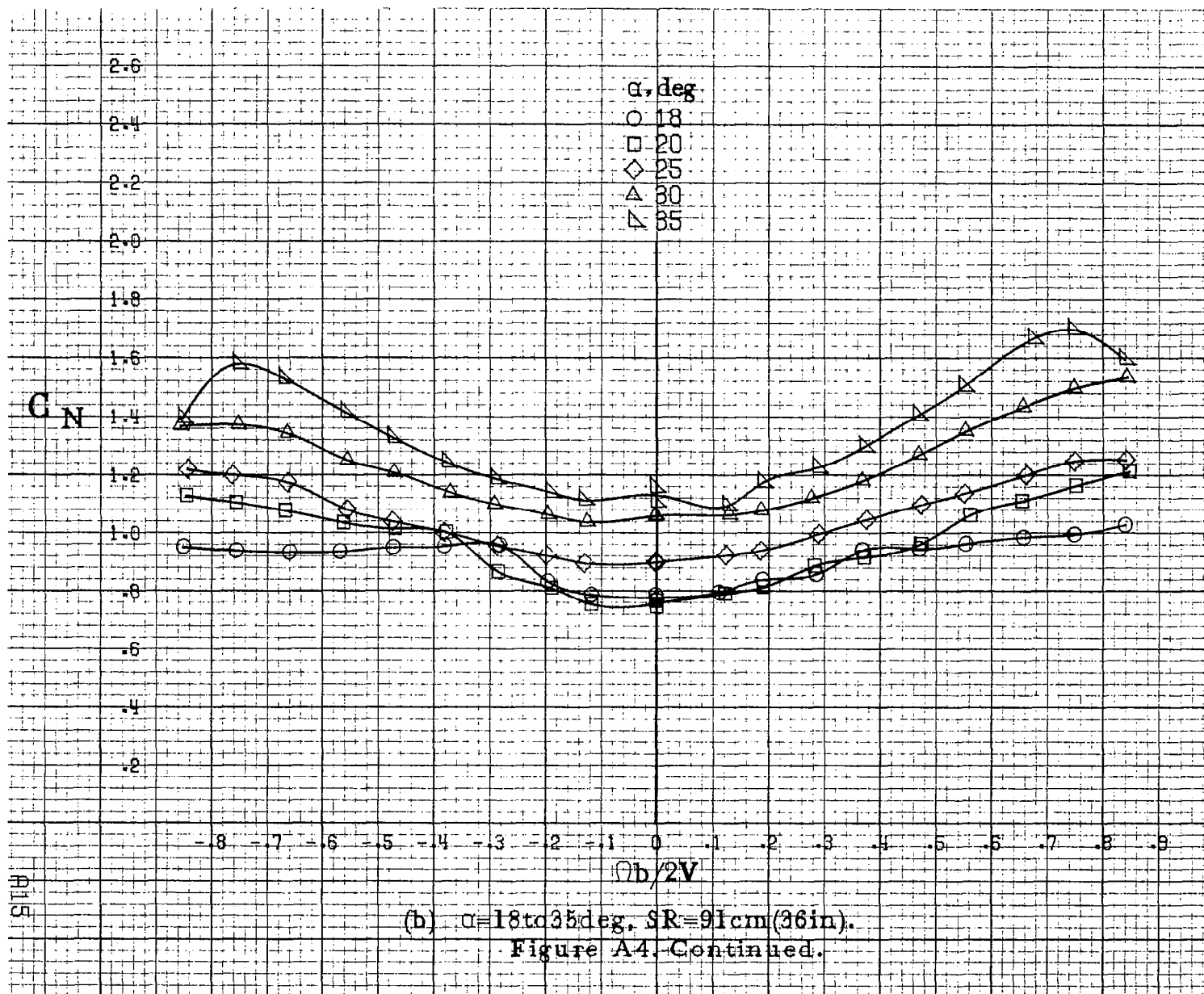


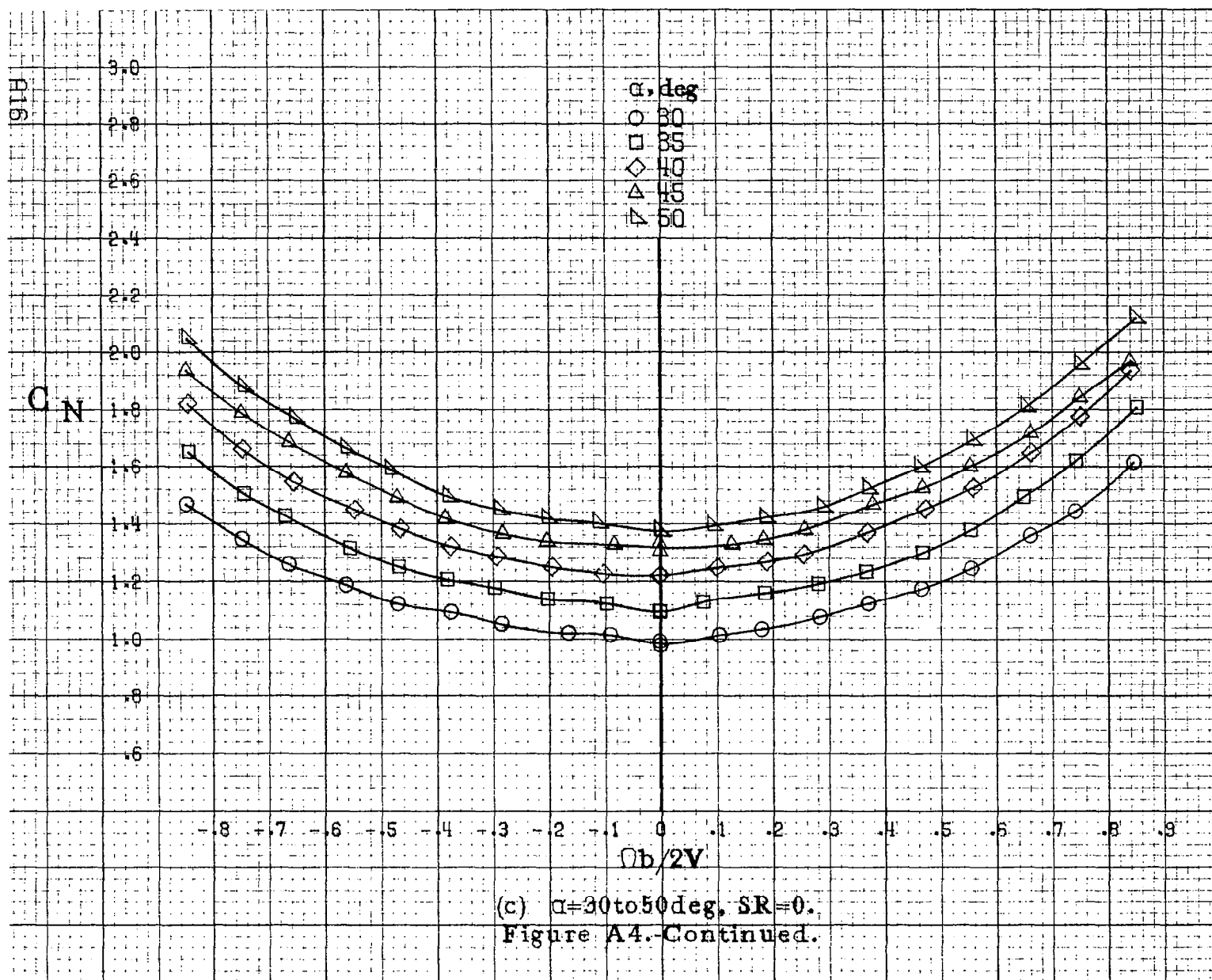


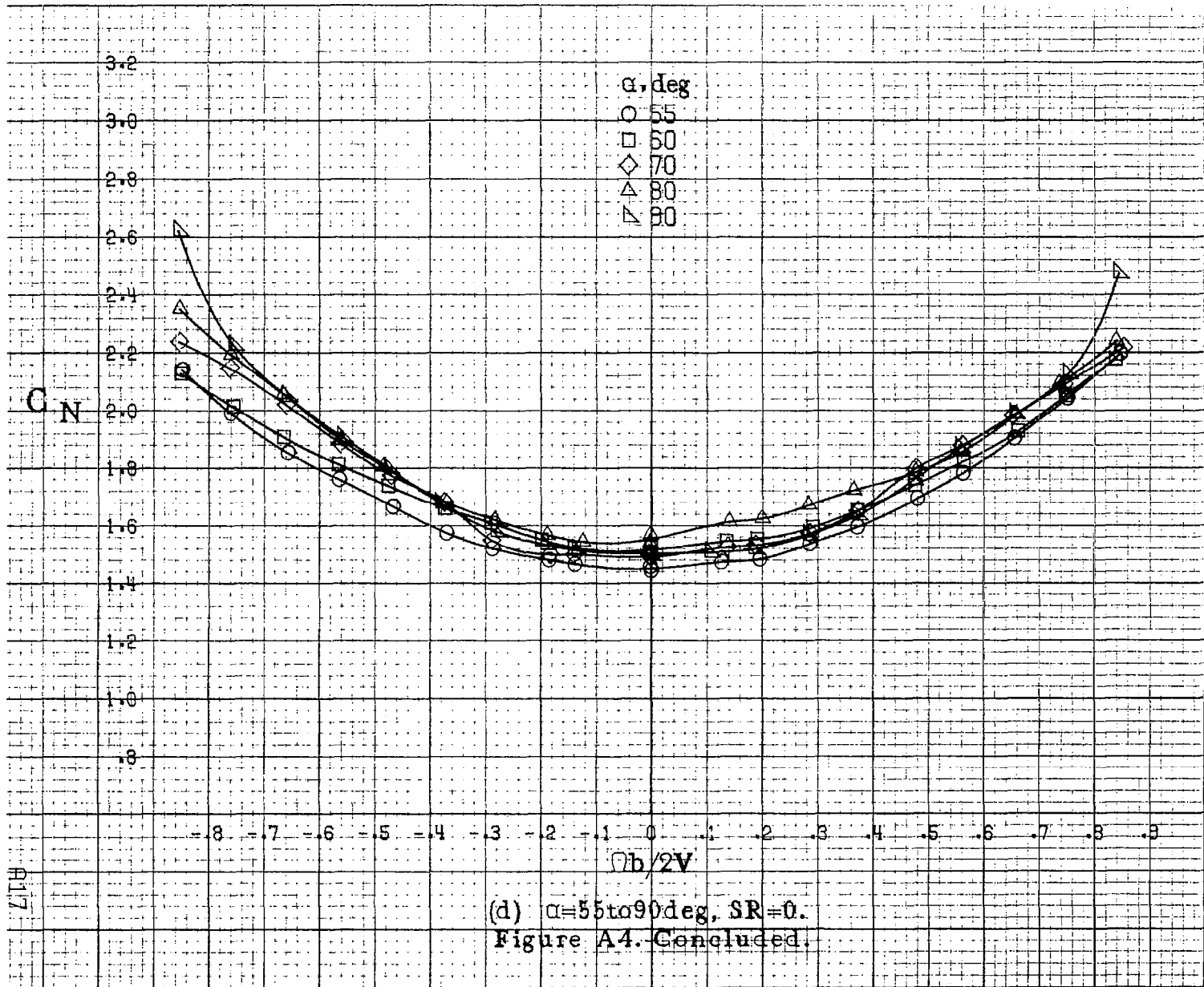


(a) $\alpha = 8$ to 16° , $SR = 91\text{cm}$ (36in).

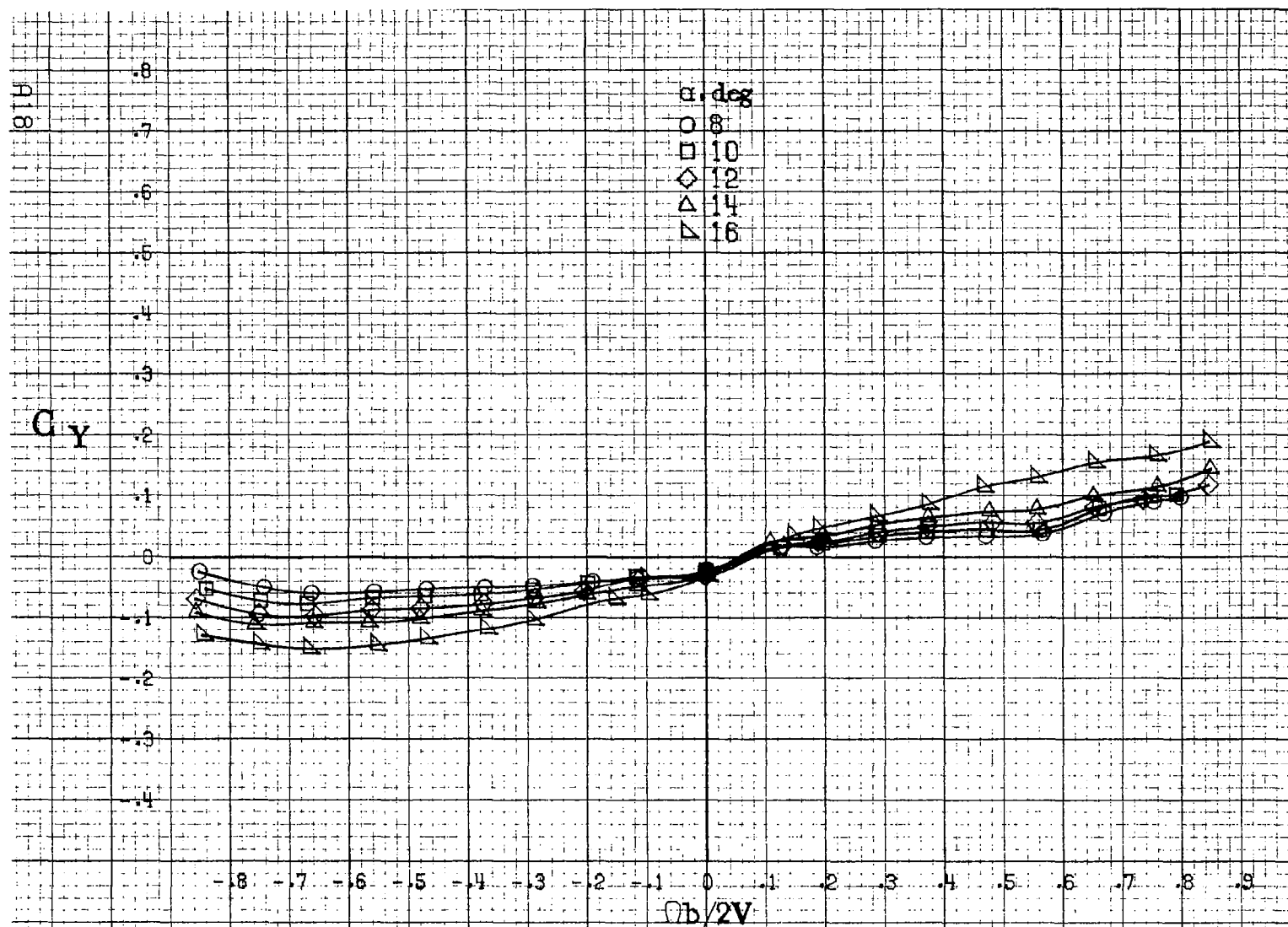
Figure A4. Effect of rotation rate and angle of attack on normal-force coefficient for basic configuration. $\delta_a = 0^\circ$, $\delta_s = 0^\circ$, $\delta_r = 0^\circ$, $\beta = 0^\circ$.





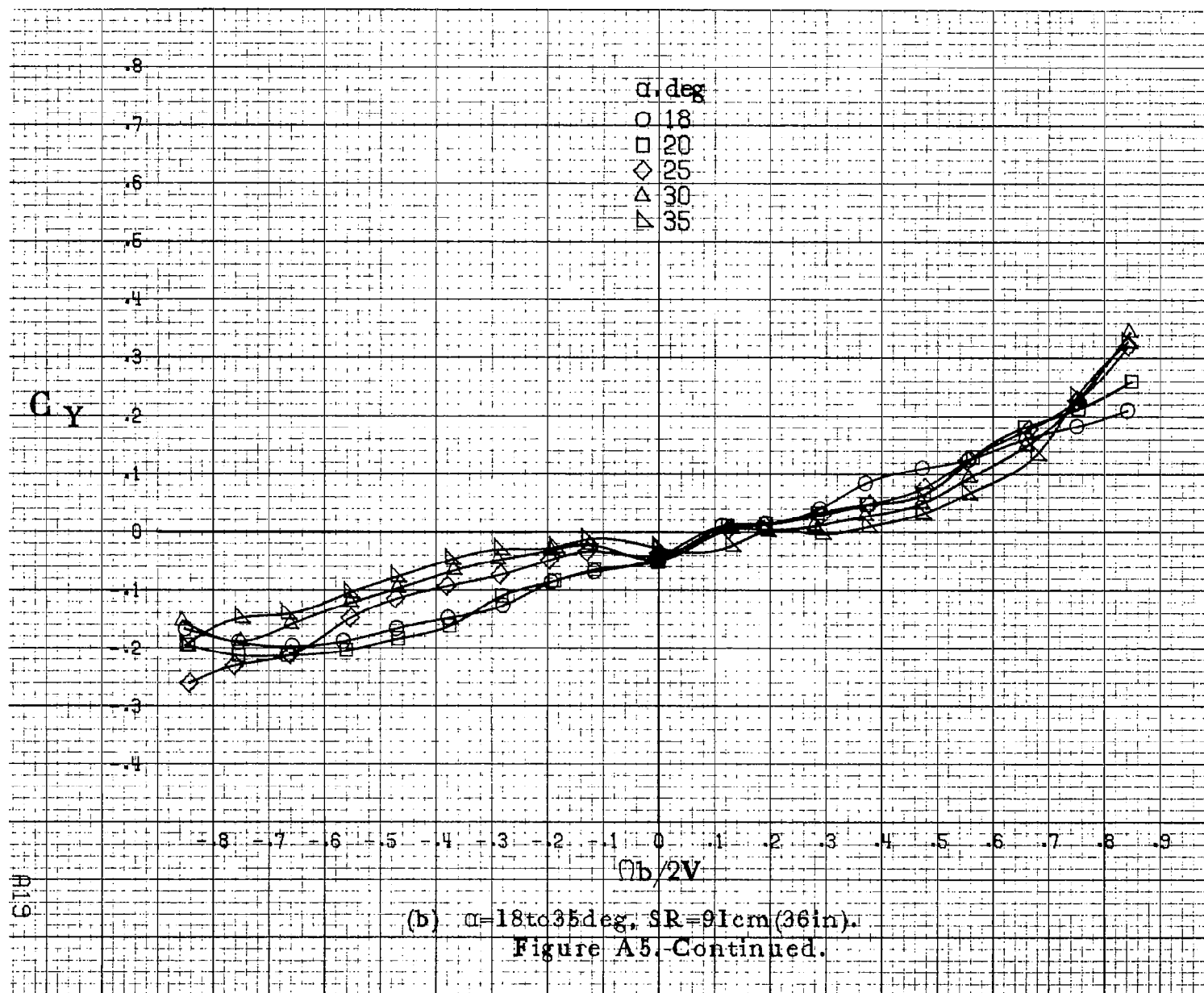


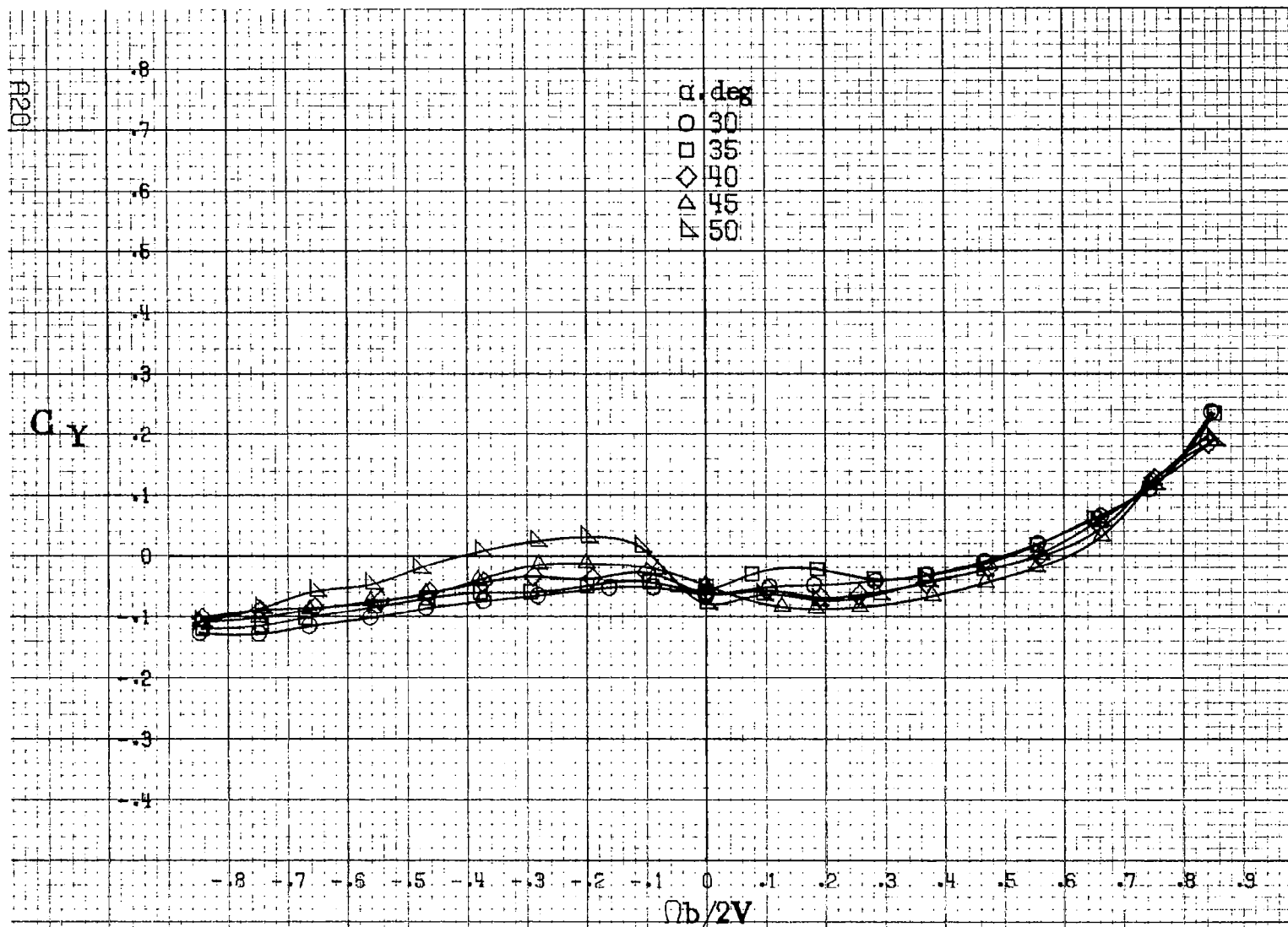
(d) $\alpha=55$ to 90° , $SR=0$.
Figure A4. Concluded.



(a) $\alpha = 8$ to 16° , $SR = 91\text{cm (36in)}$.

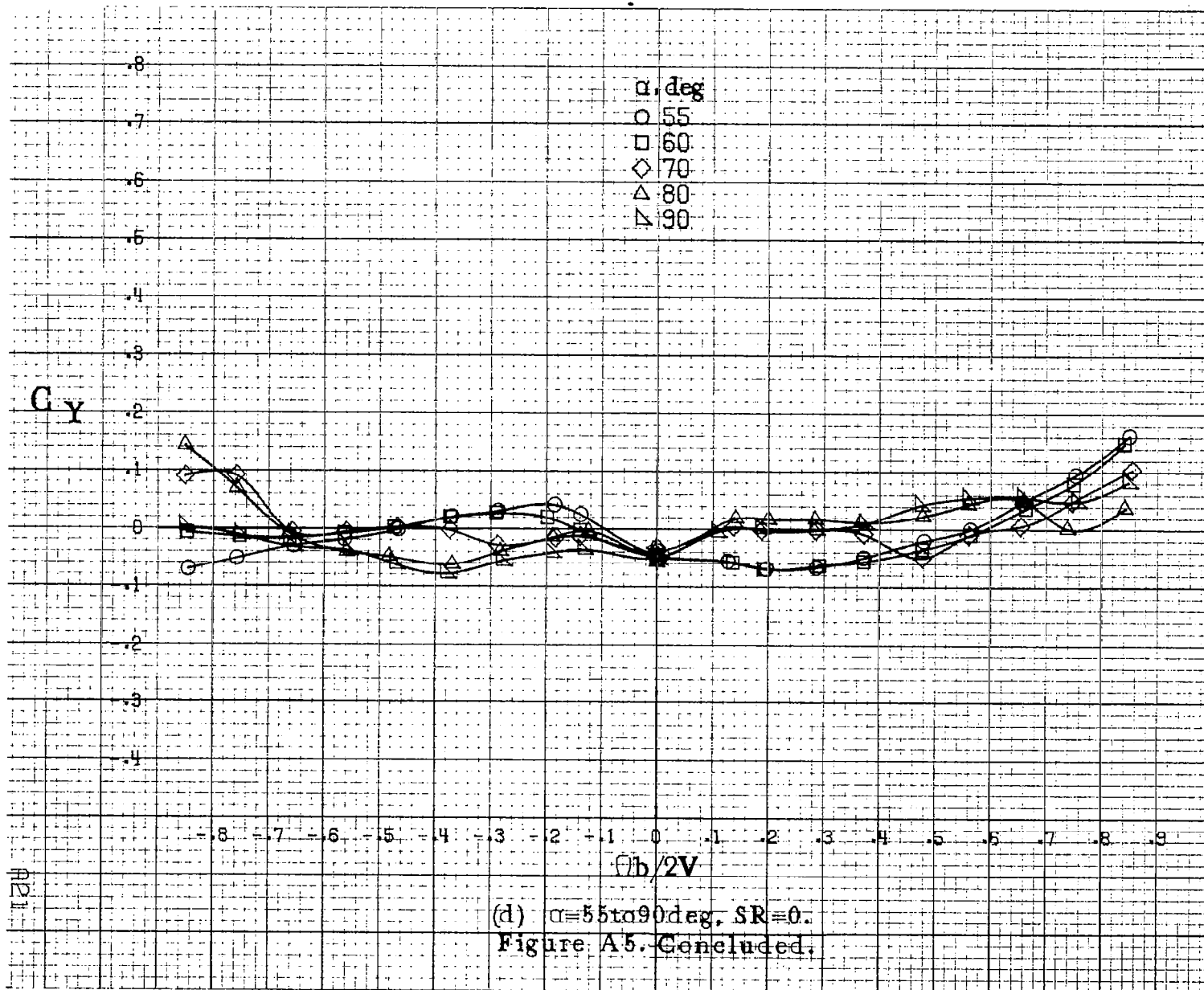
Figure A5. Effect of rotation rate and angle of attack on side-force coefficient for basic configuration. $\delta_e = 0^\circ$, $\delta_a = 0^\circ$, $\delta_r = 0^\circ$, $\beta = 0^\circ$.

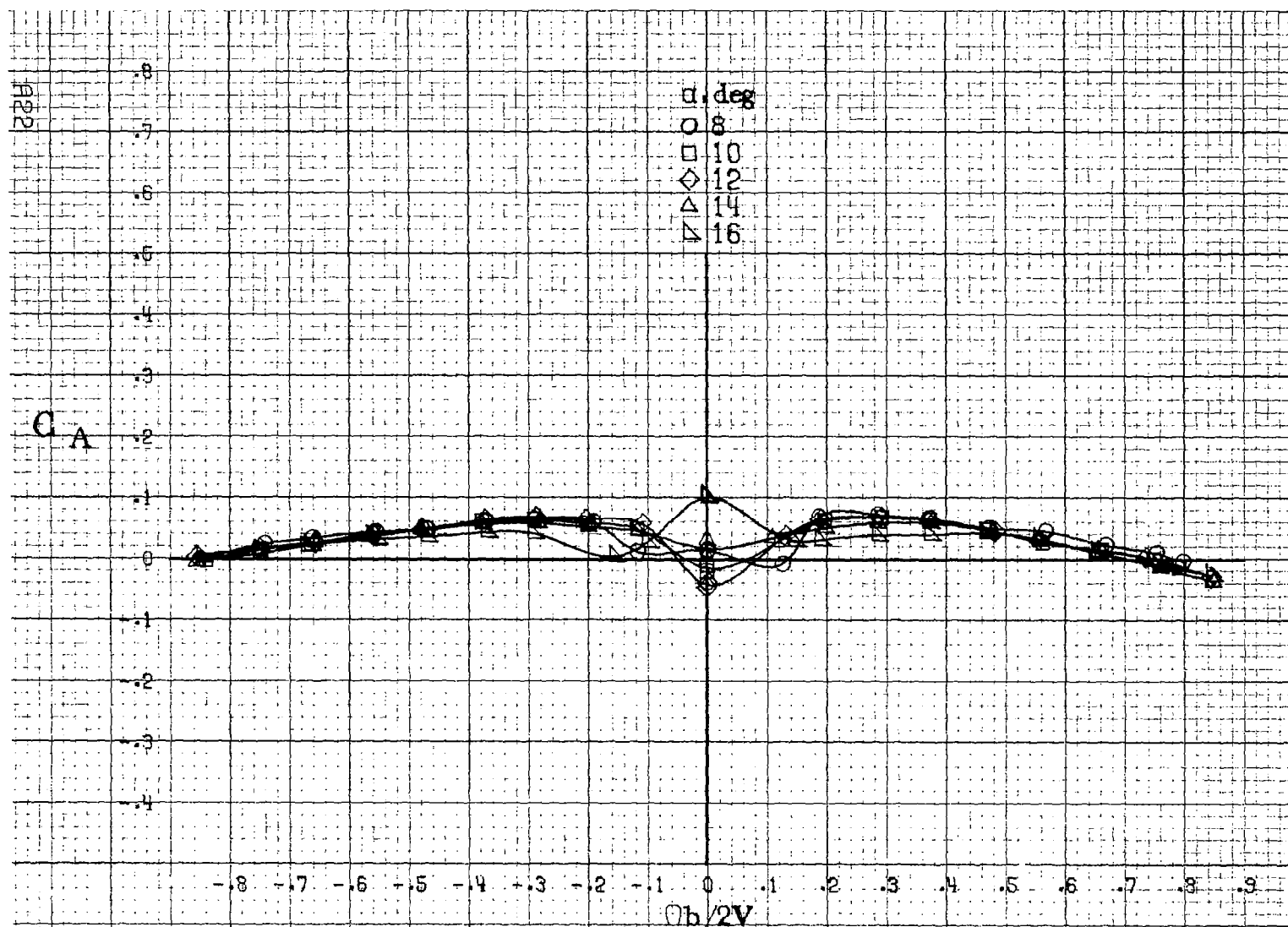




(c) $\alpha = 30$ to 50 deg, $SR = 0$.

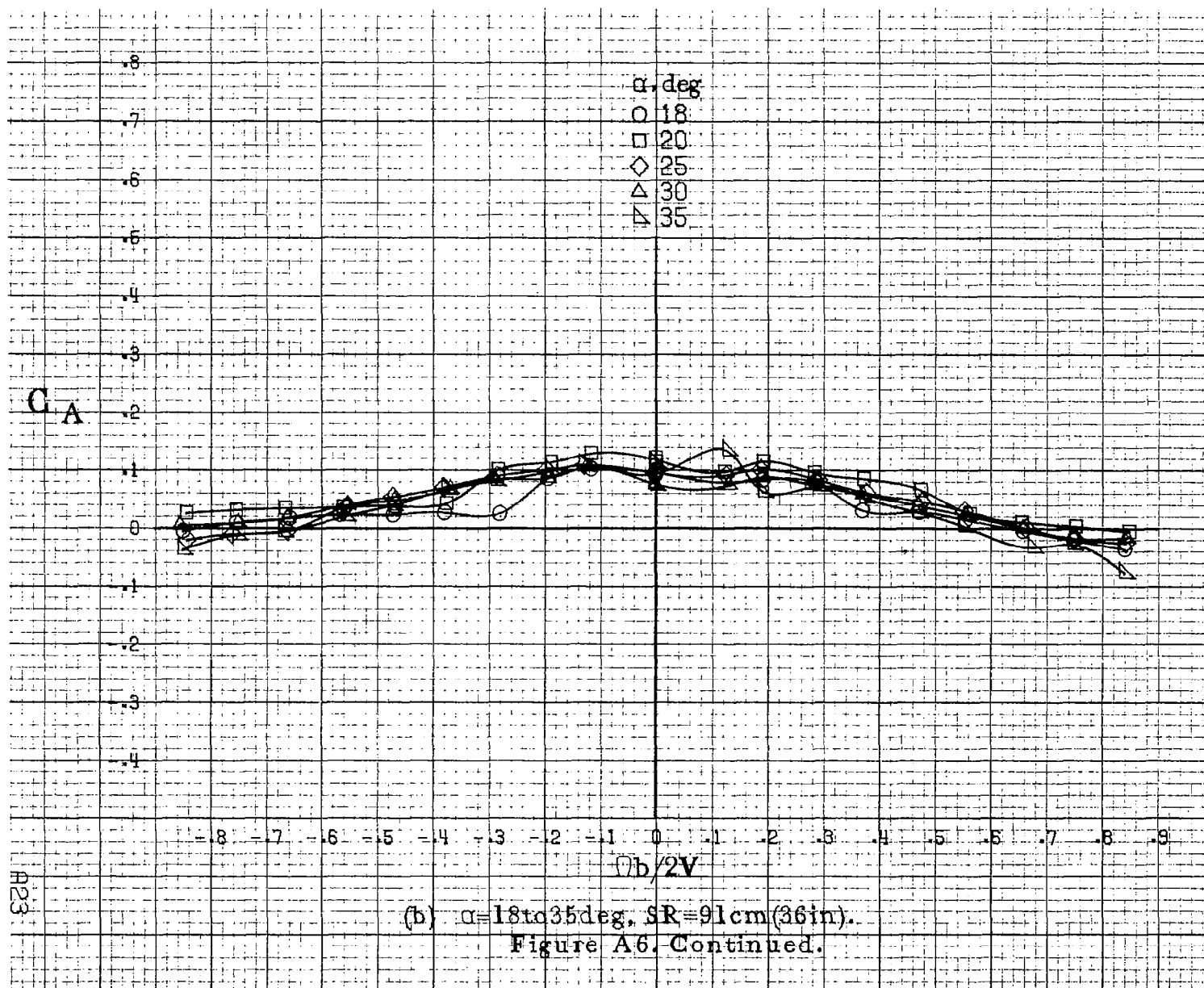
Figure A5. Continued.

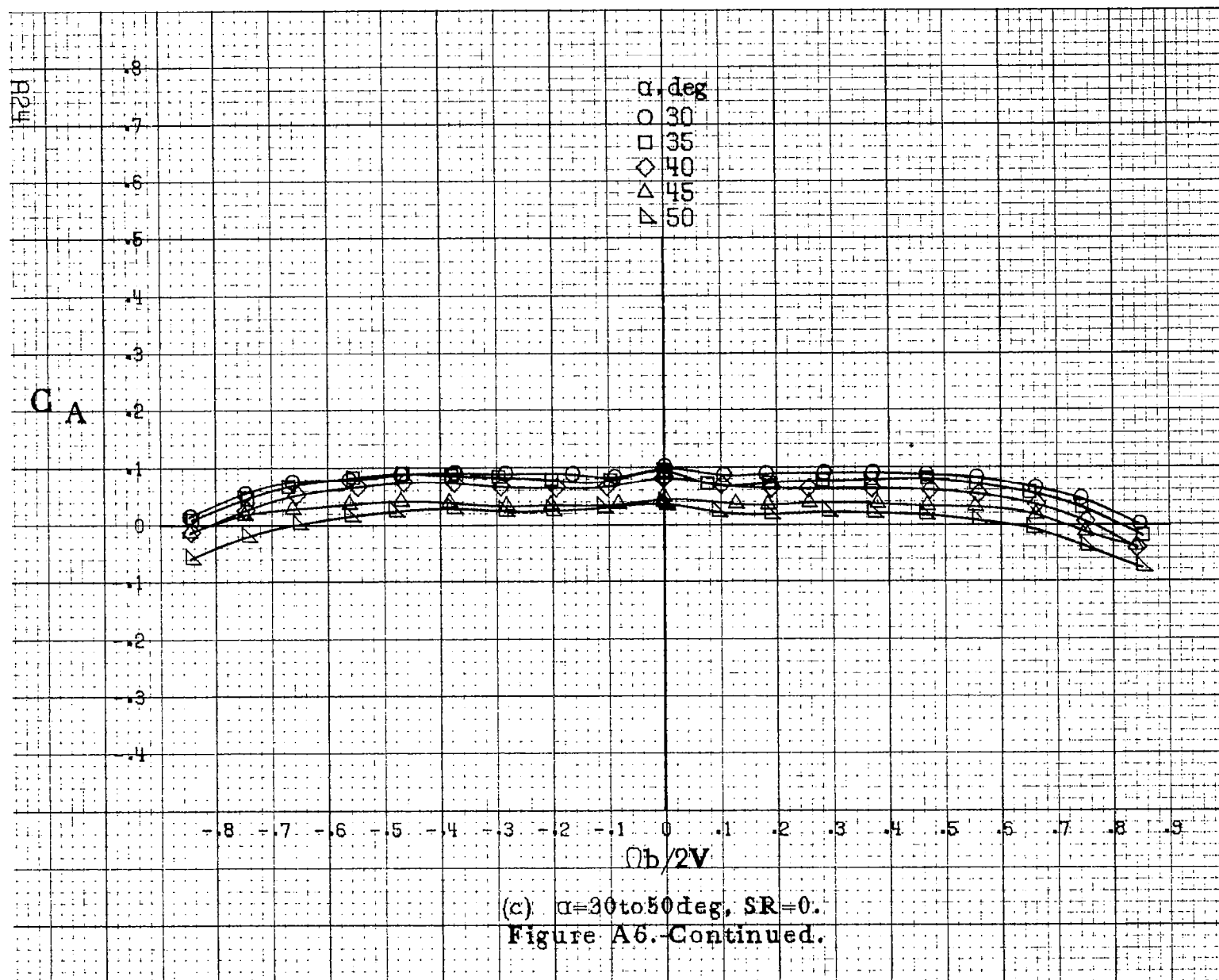


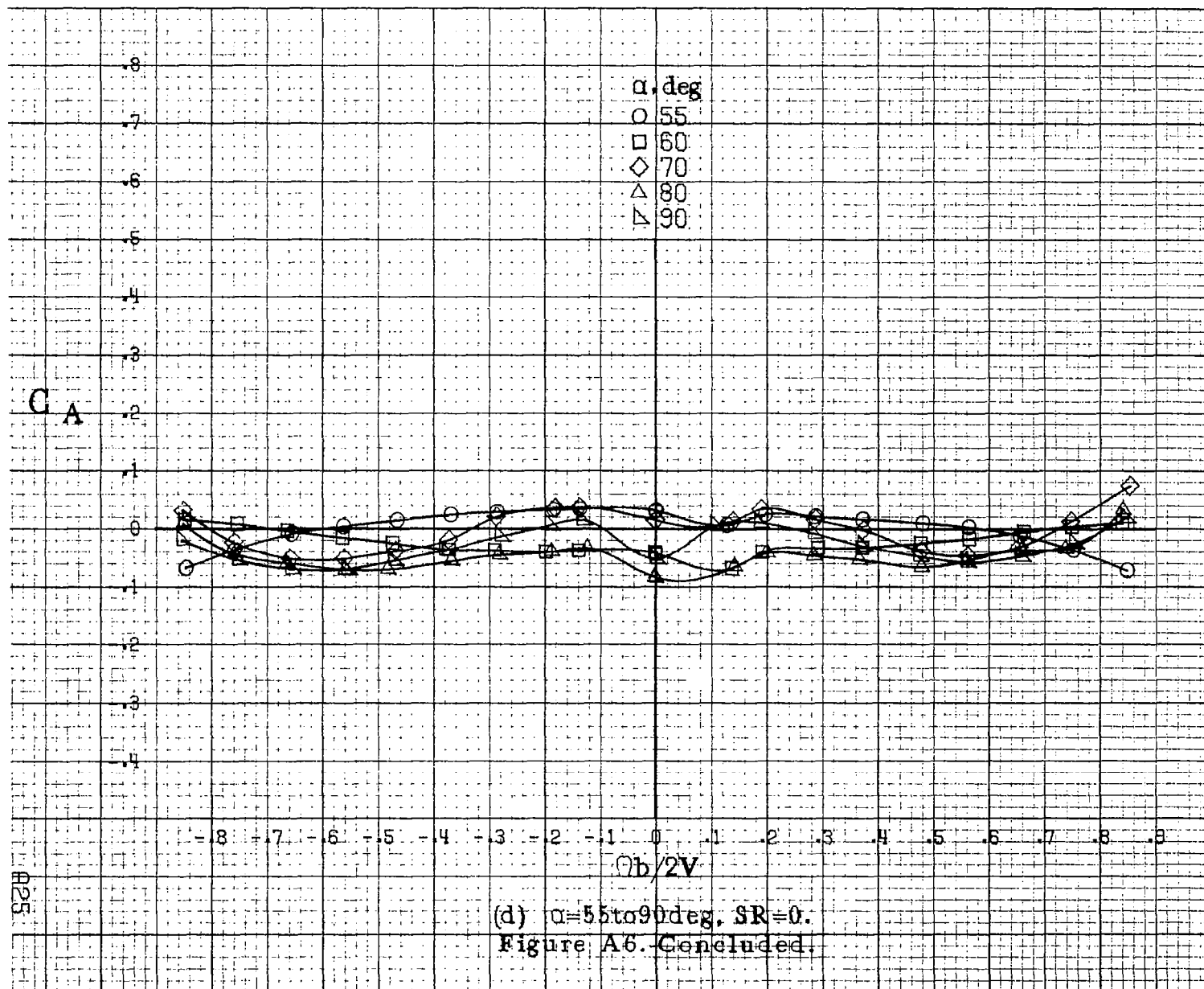


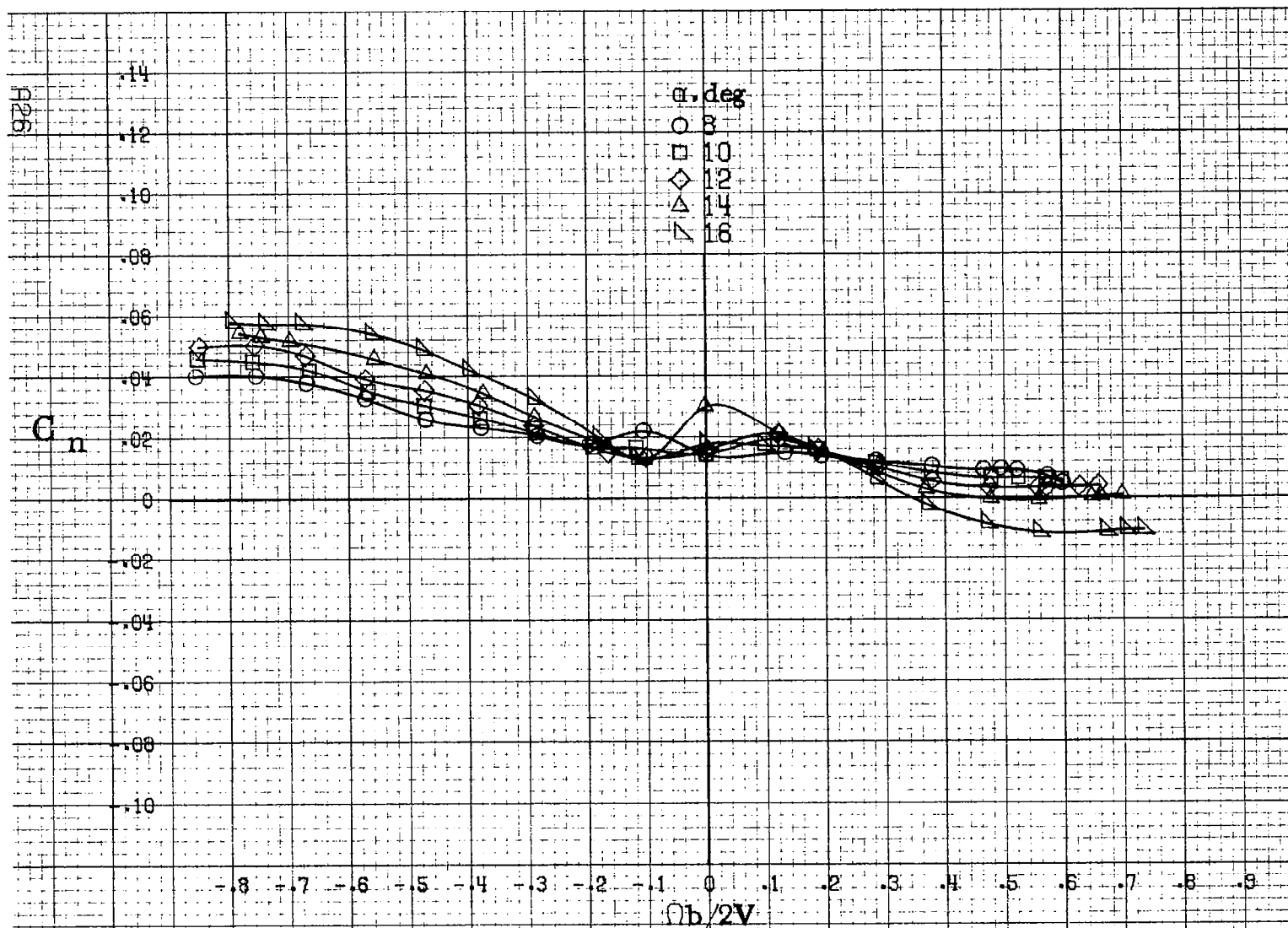
(a) $\alpha = 8$ to 16° , $SR = 91 \text{ cm (36 in.)}$.

Figure A.6. Effect of rotation rate and angle of attack on axial force coefficient for basic configuration. $\delta_e = 0^\circ$, $\delta_a = 0^\circ$, $\delta_r = 0^\circ$, $\beta = 0^\circ$.



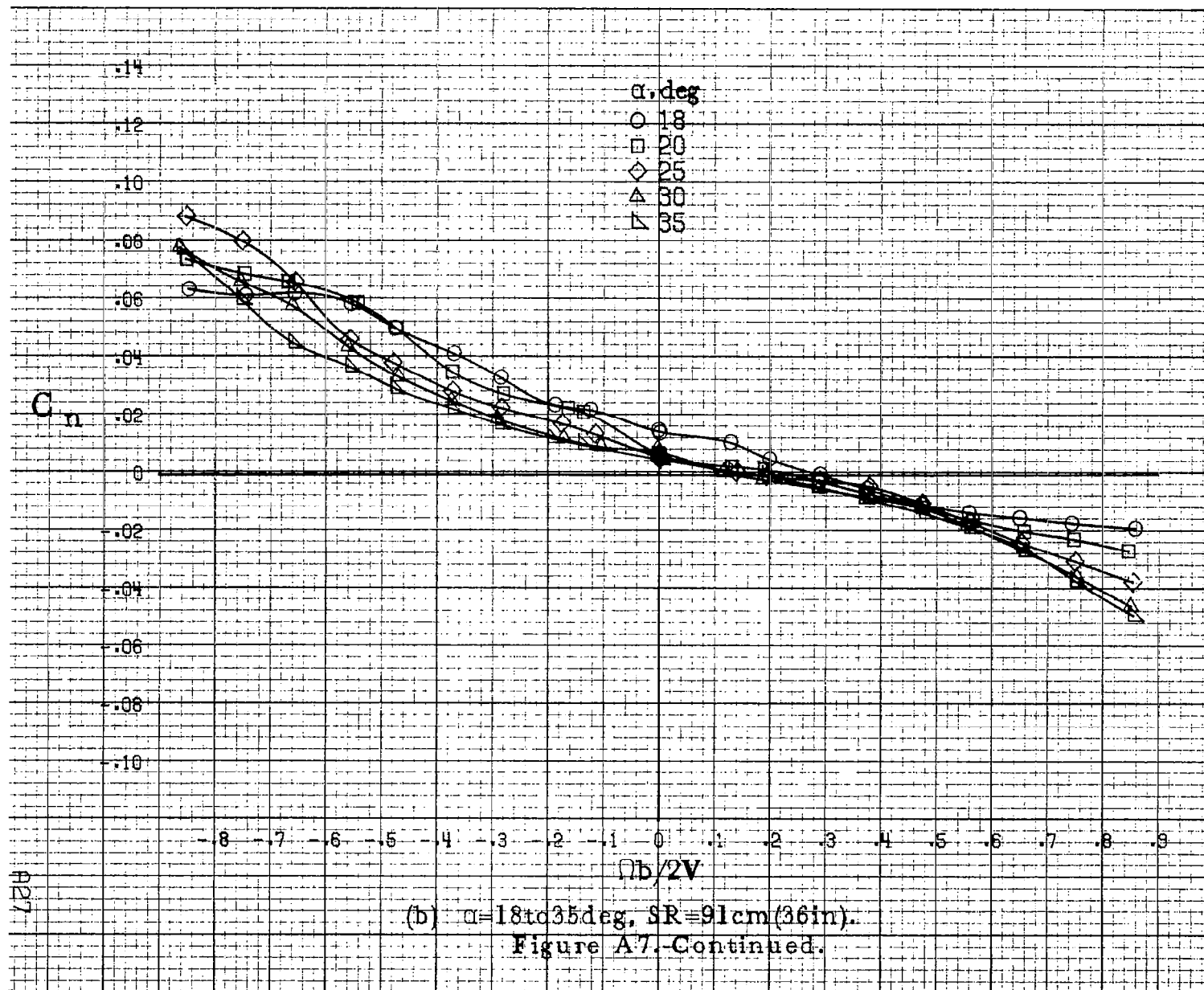


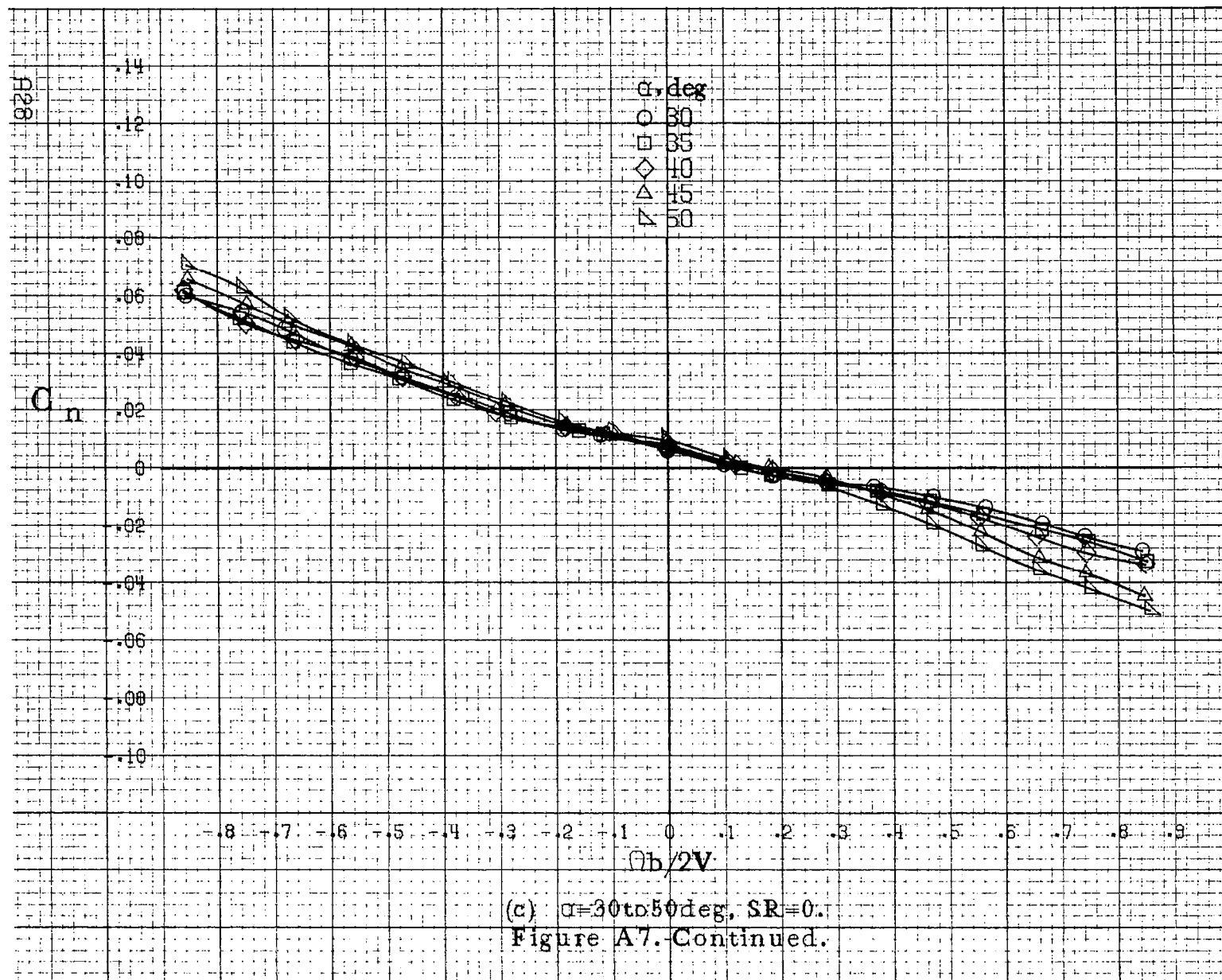


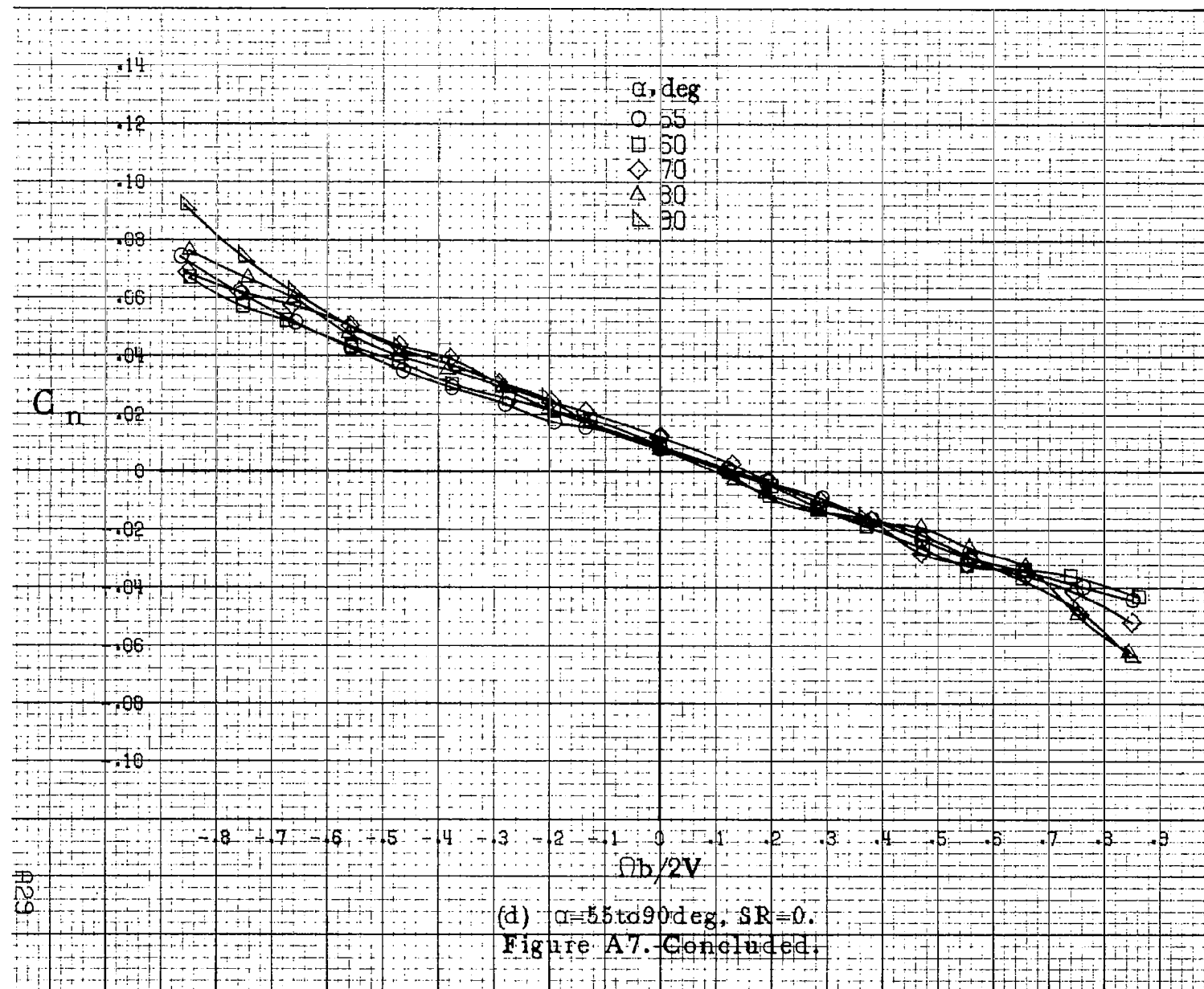


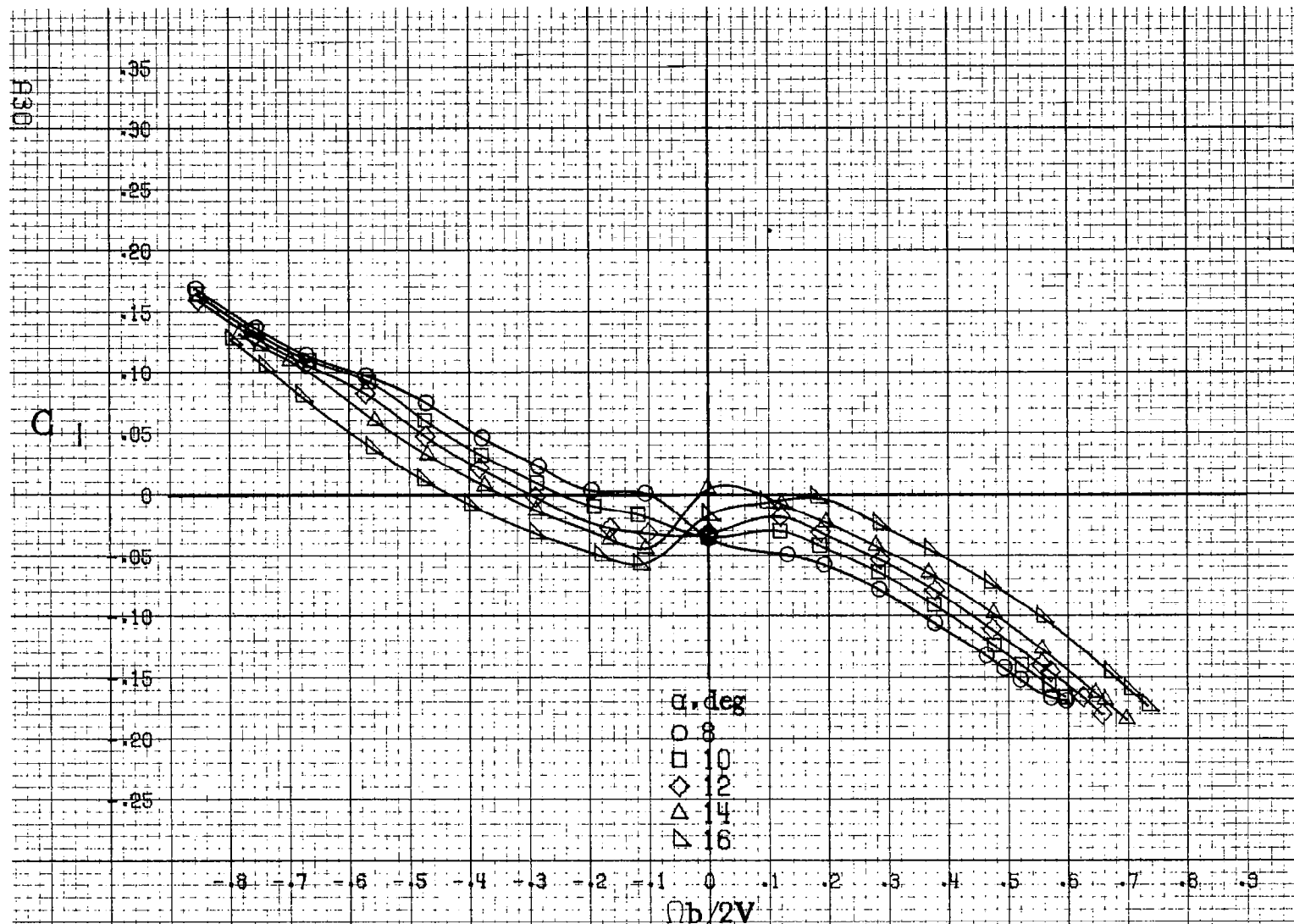
(a) $\alpha = 8$ to 16° , $SR = 91 \text{ cm (36 in.)}$.

Figure A7. Effect of rotation rate and angle of attack on yawing moment coefficient for basic configuration. $\delta_e = -20^\circ$, $\delta_a = 20^\circ$, $\delta_r = -28^\circ$, $\beta = 0^\circ$.



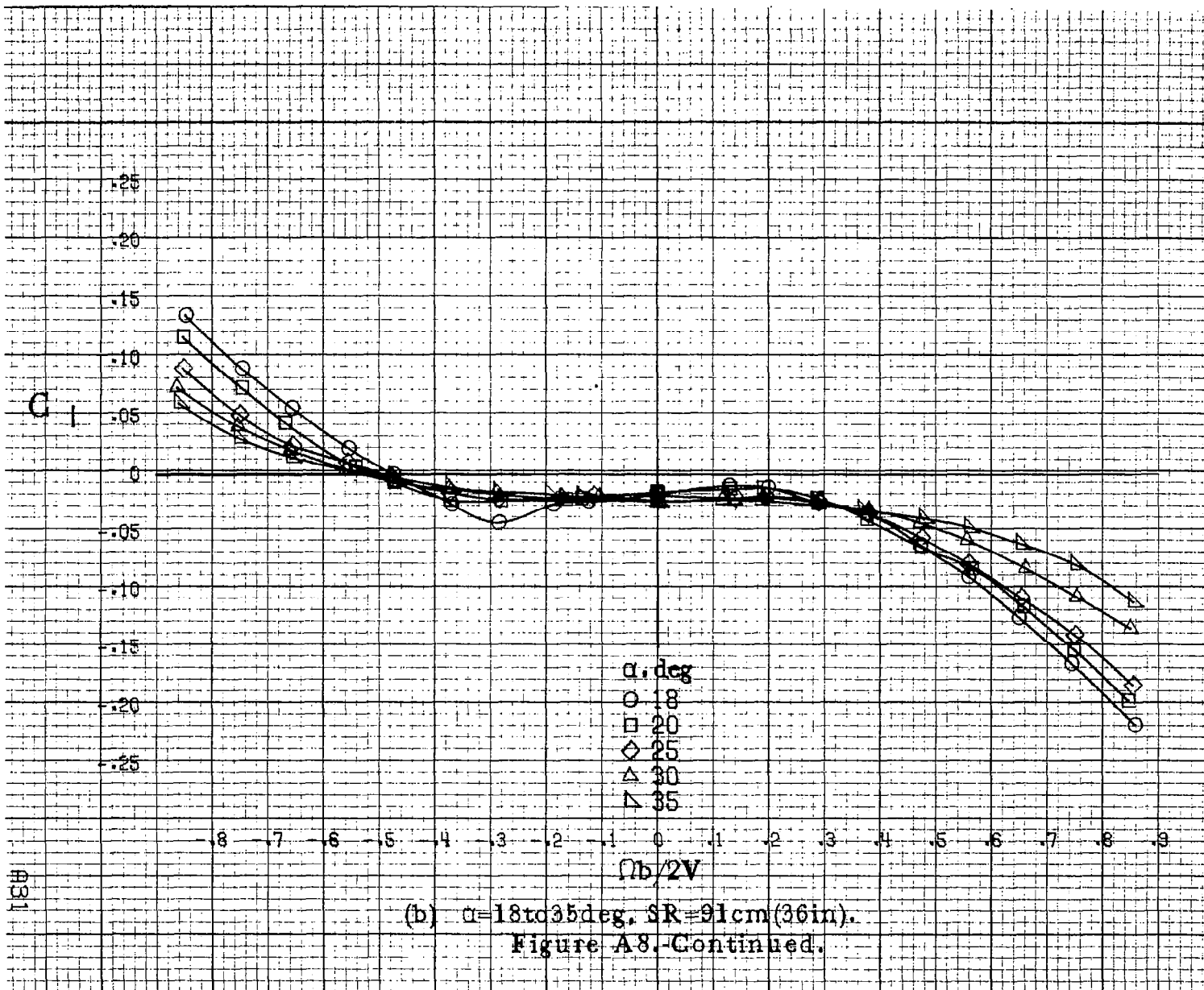


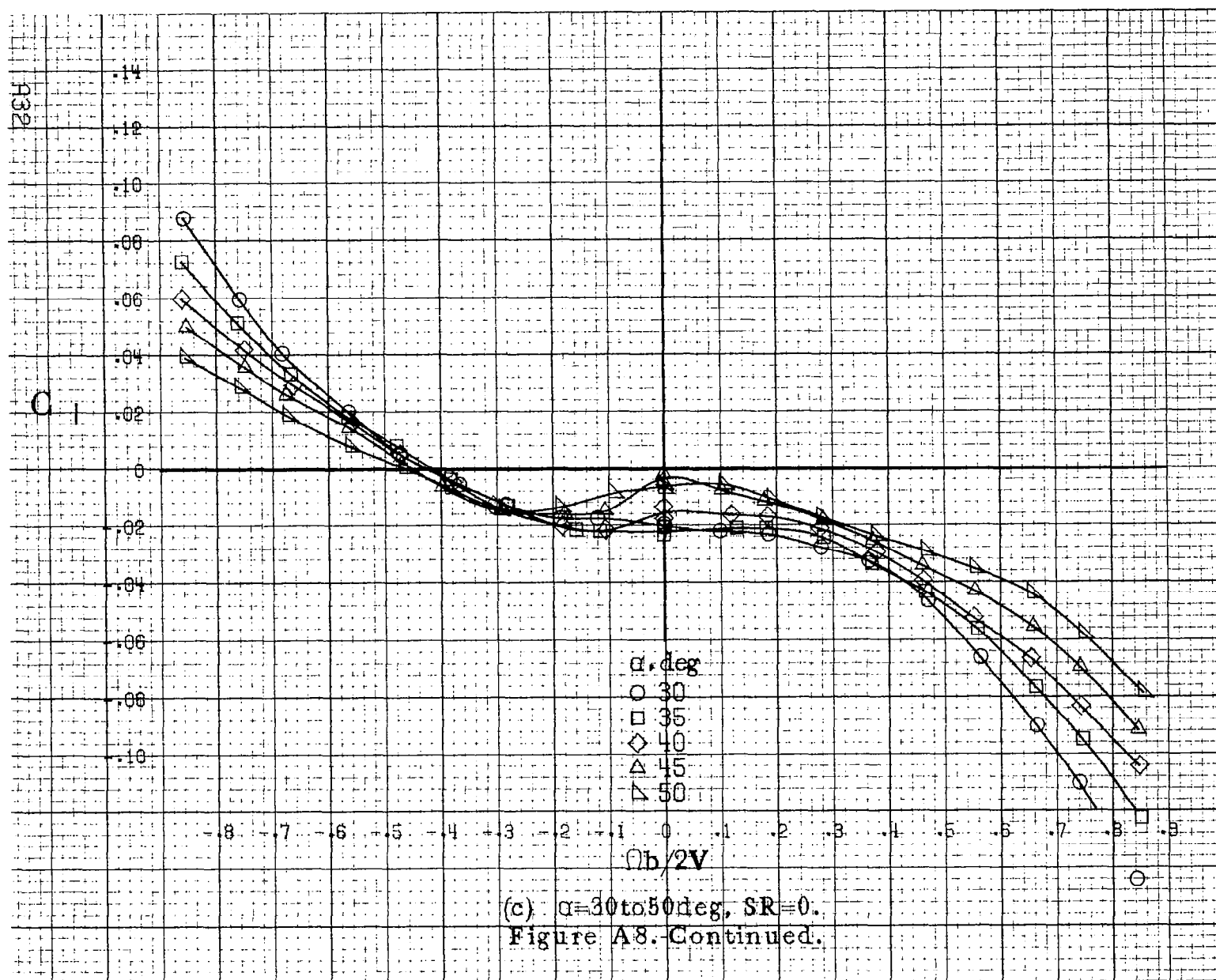


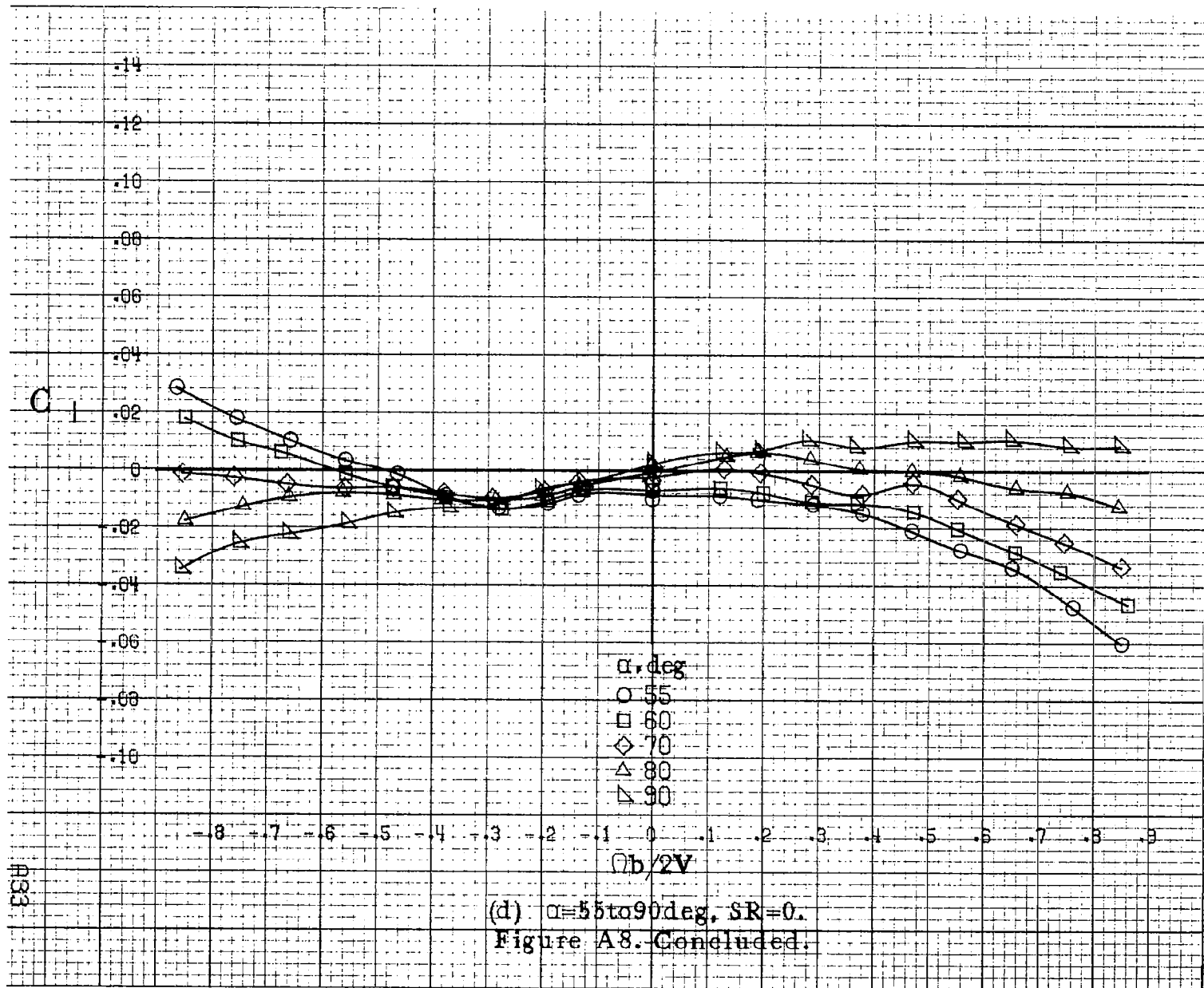


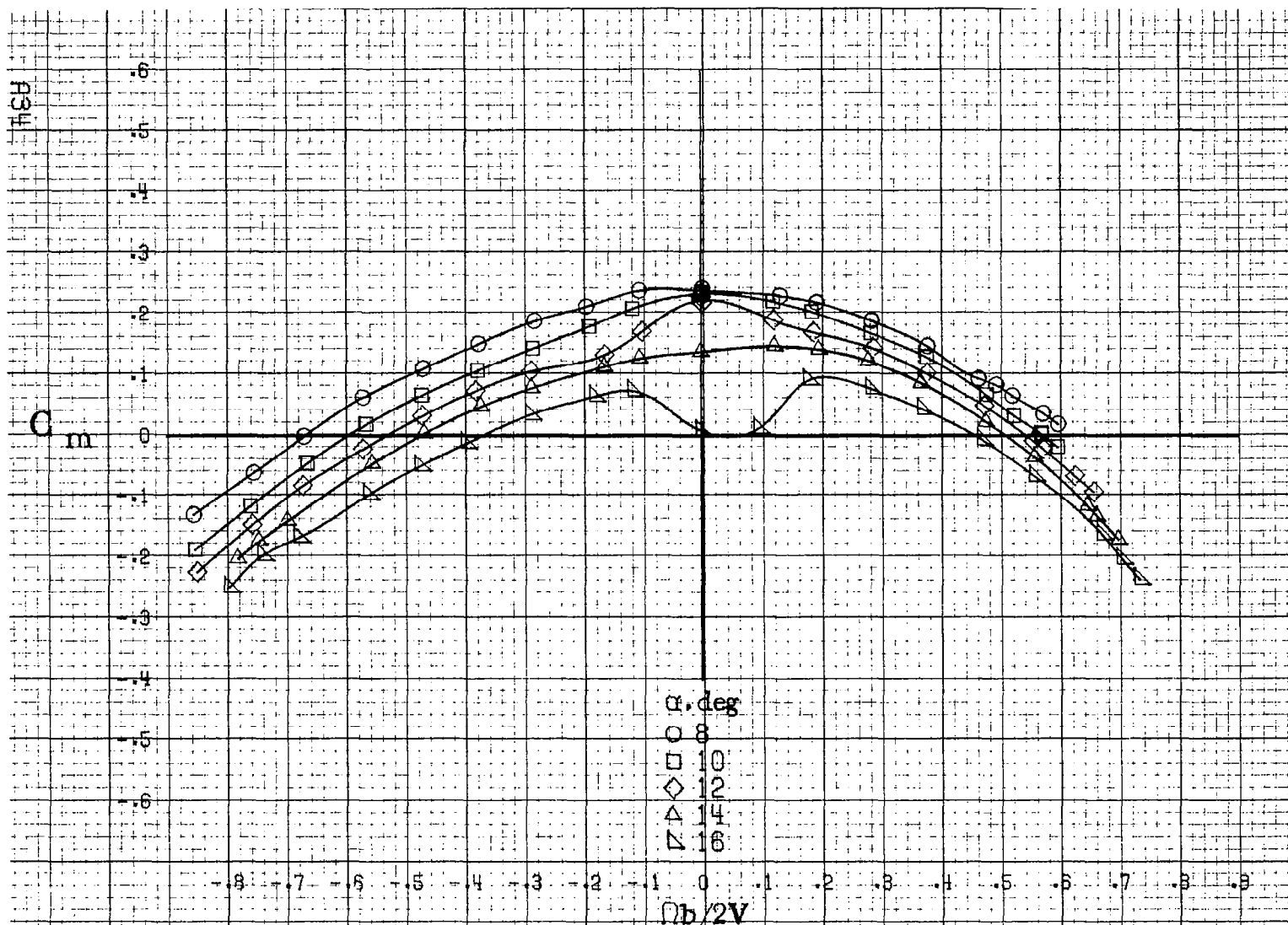
(a) $\alpha = 8$ to 16° , $SR = 91 \text{ cm (36 in.)}$.

Figure A-8. Effect of rotation rate and angle of attack on rolling-moment coefficient for basic configuration. $\delta_e = -20^\circ$, $\delta_a = 20^\circ$, $\delta_r = -28^\circ$, $\beta = 0^\circ$.



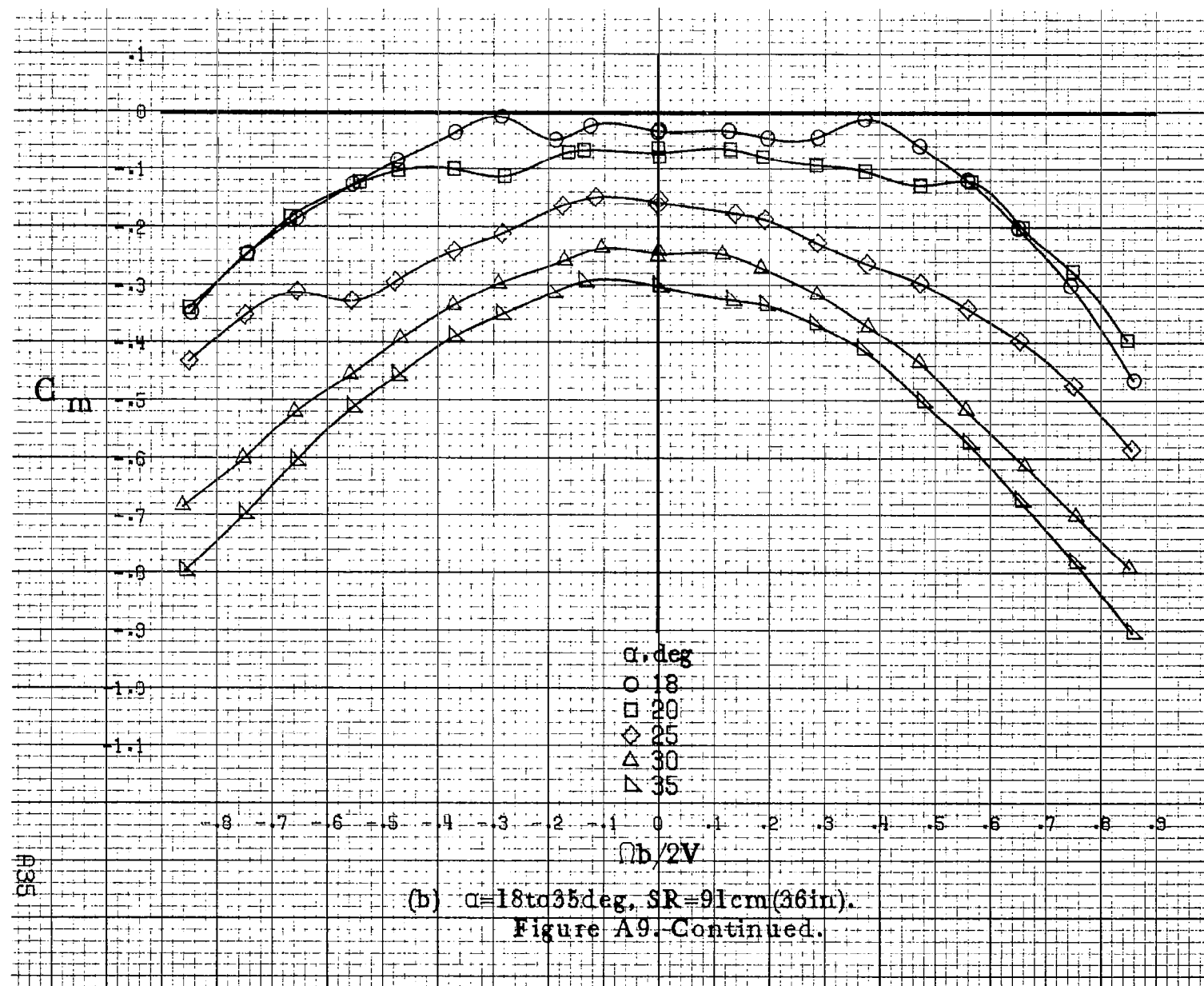


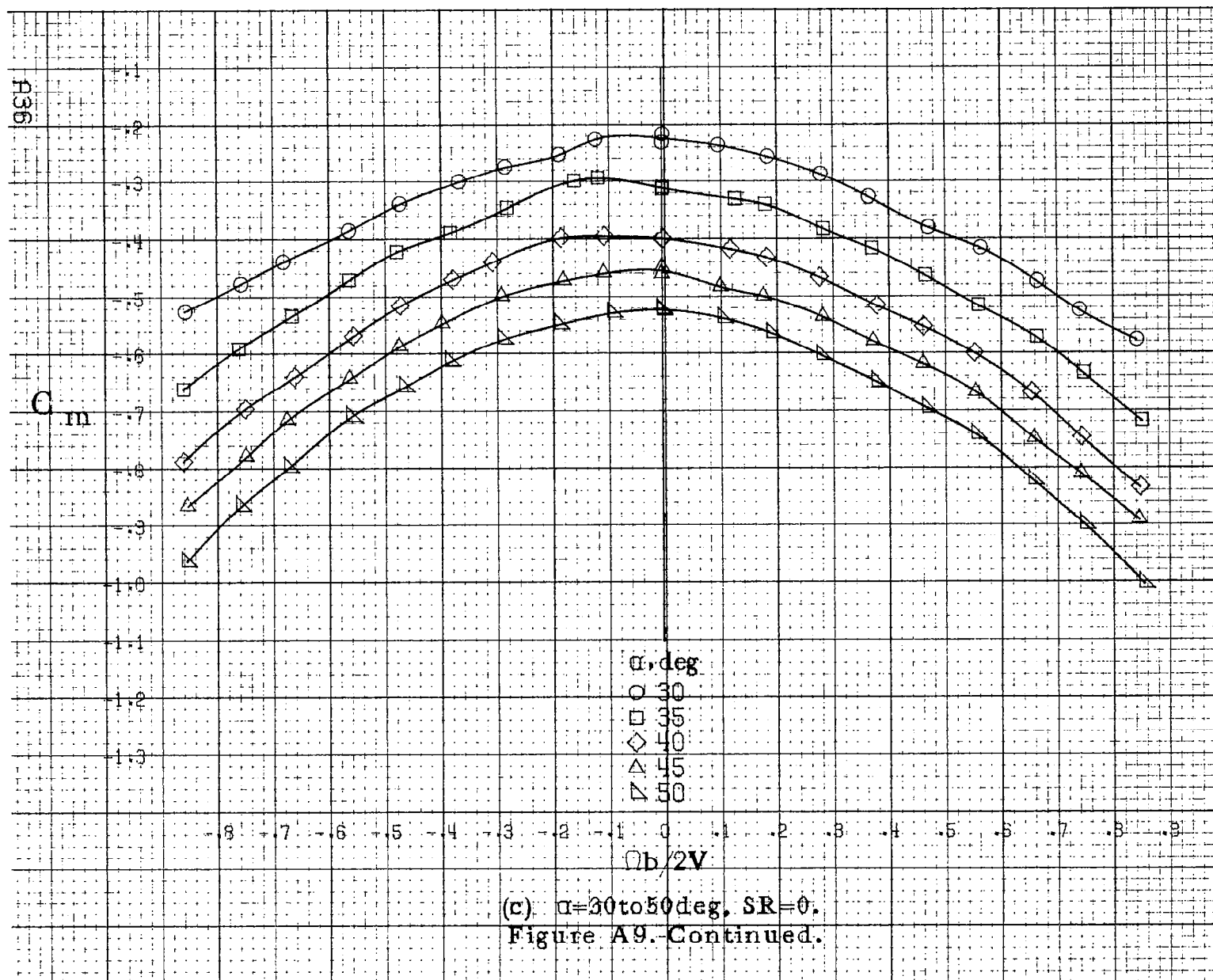


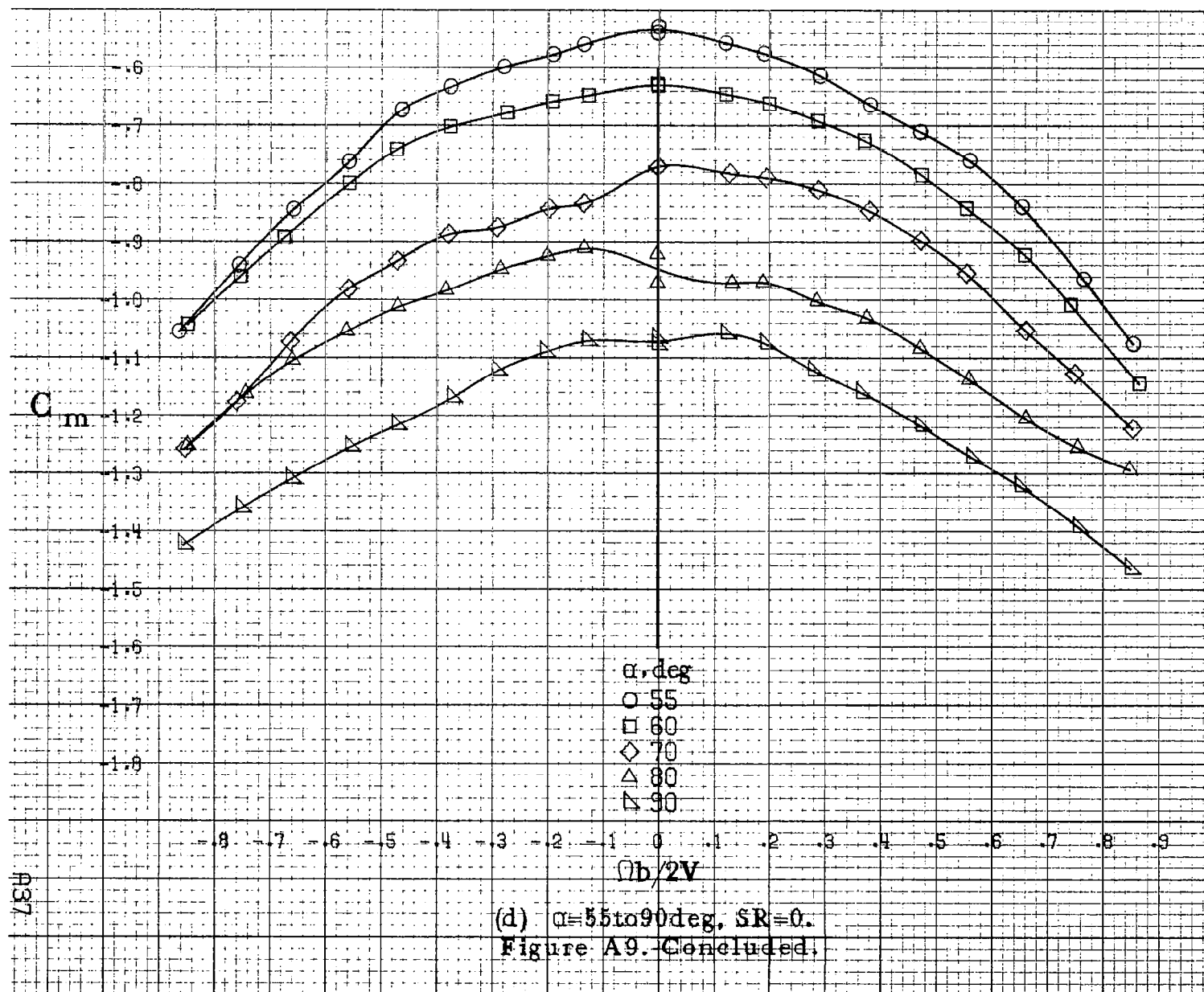


(a) $\alpha = 8$ to 16° , $SR = 91\text{cm (36in)}$.

Figure A9. Effect of rotation rate and angle of attack on pitching-moment coefficient for basic configuration. $\delta_e = 20^\circ$, $\delta_a = 20^\circ$, $\delta_r = 28^\circ$, $\beta = 0^\circ$.







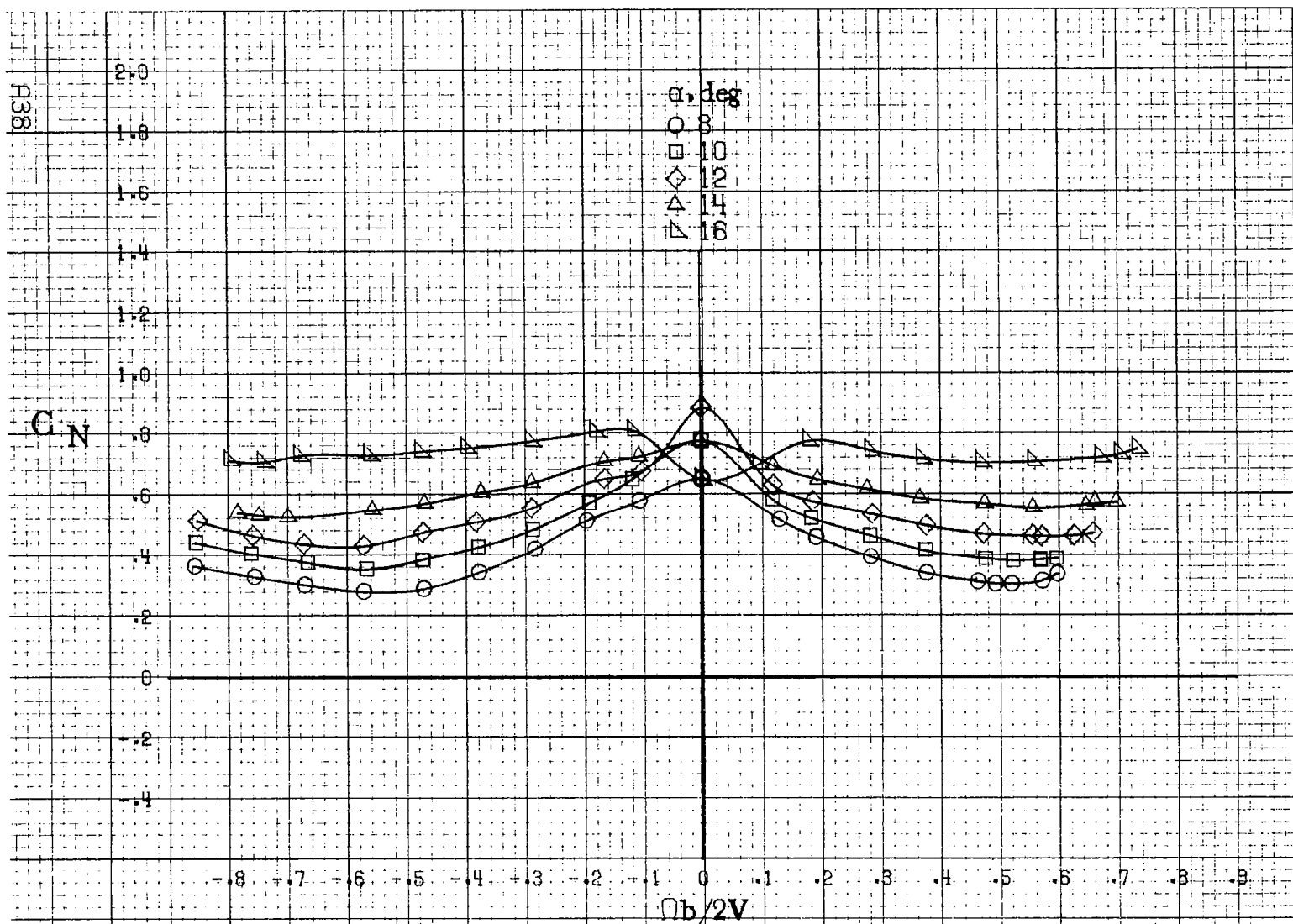
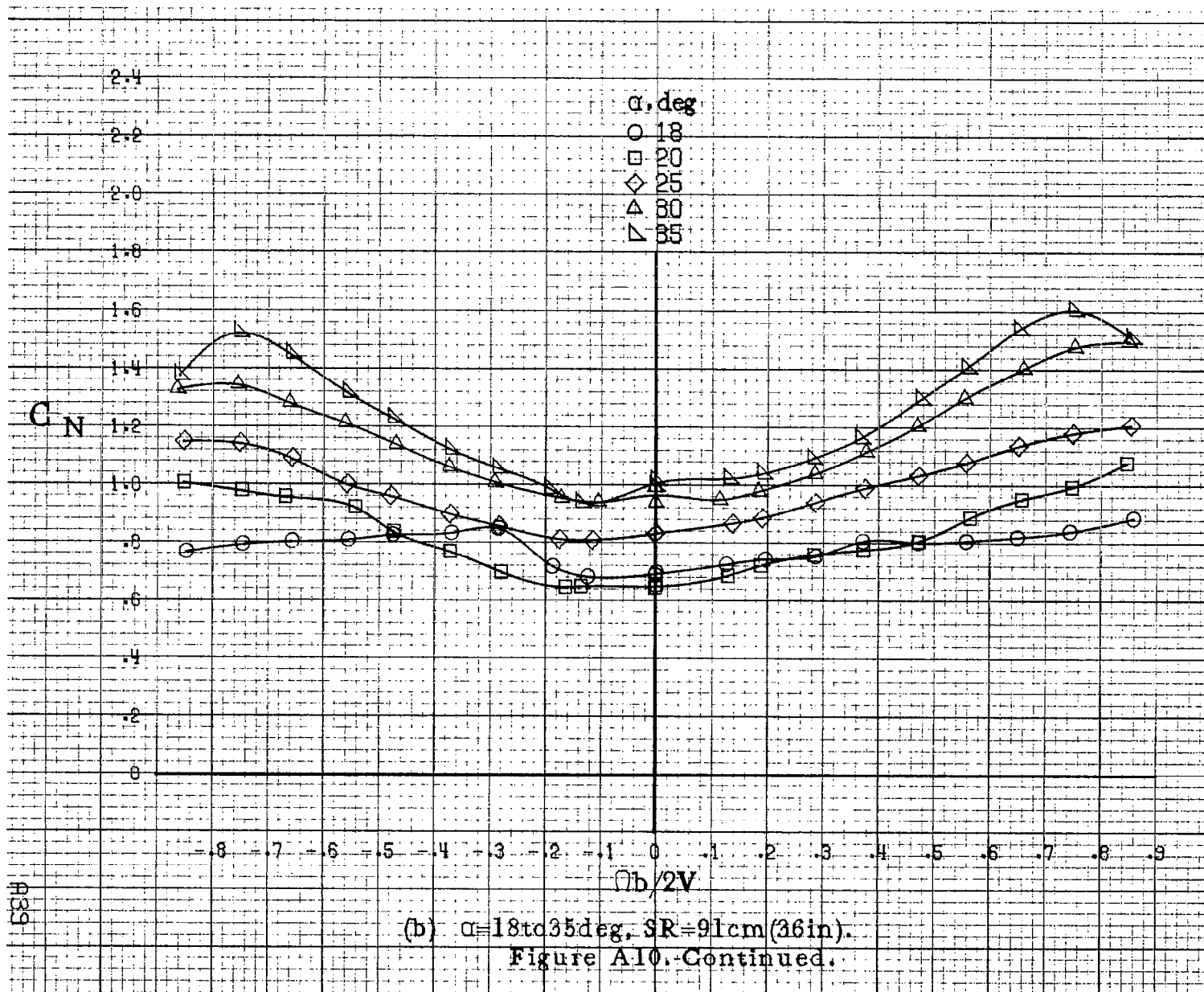
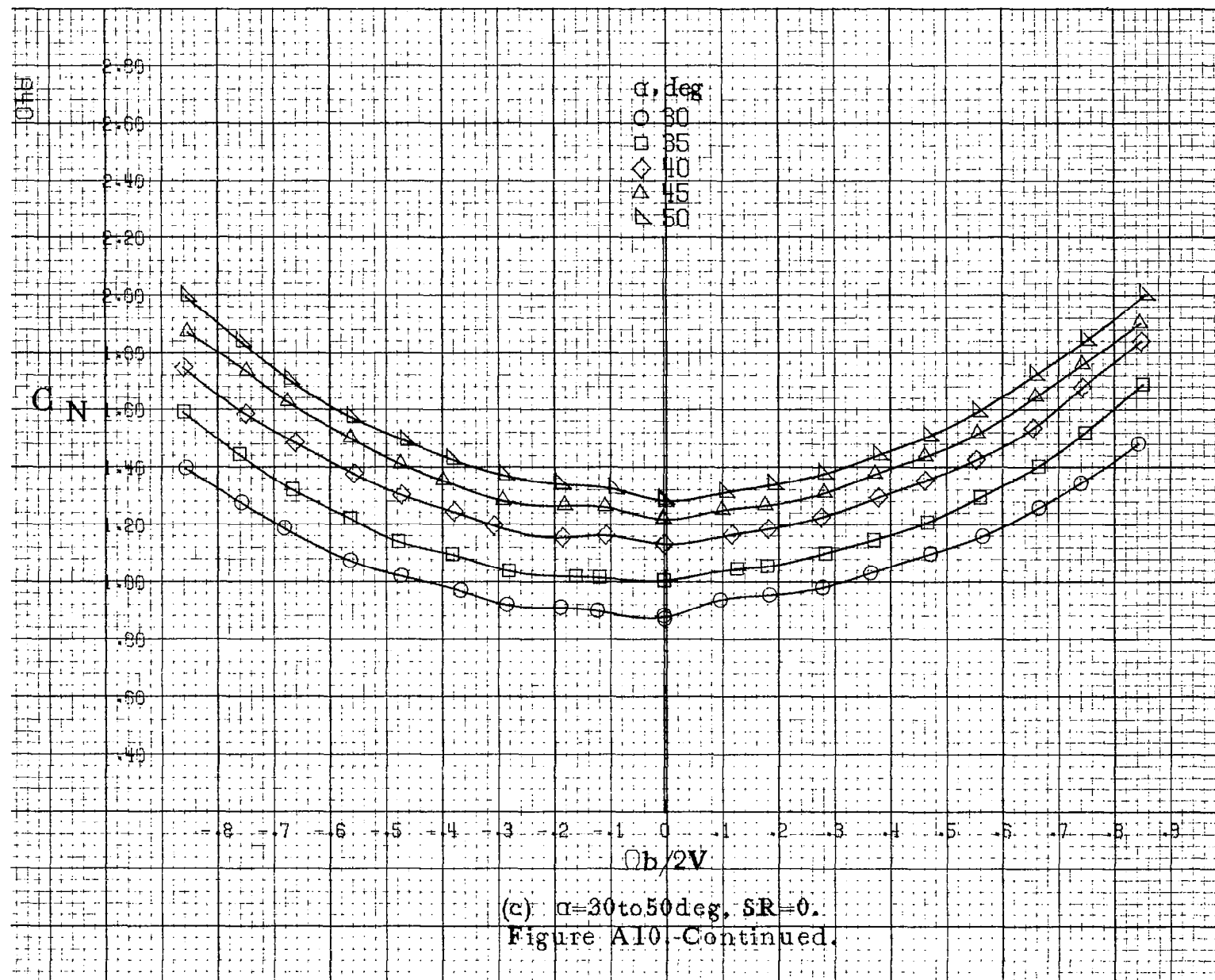
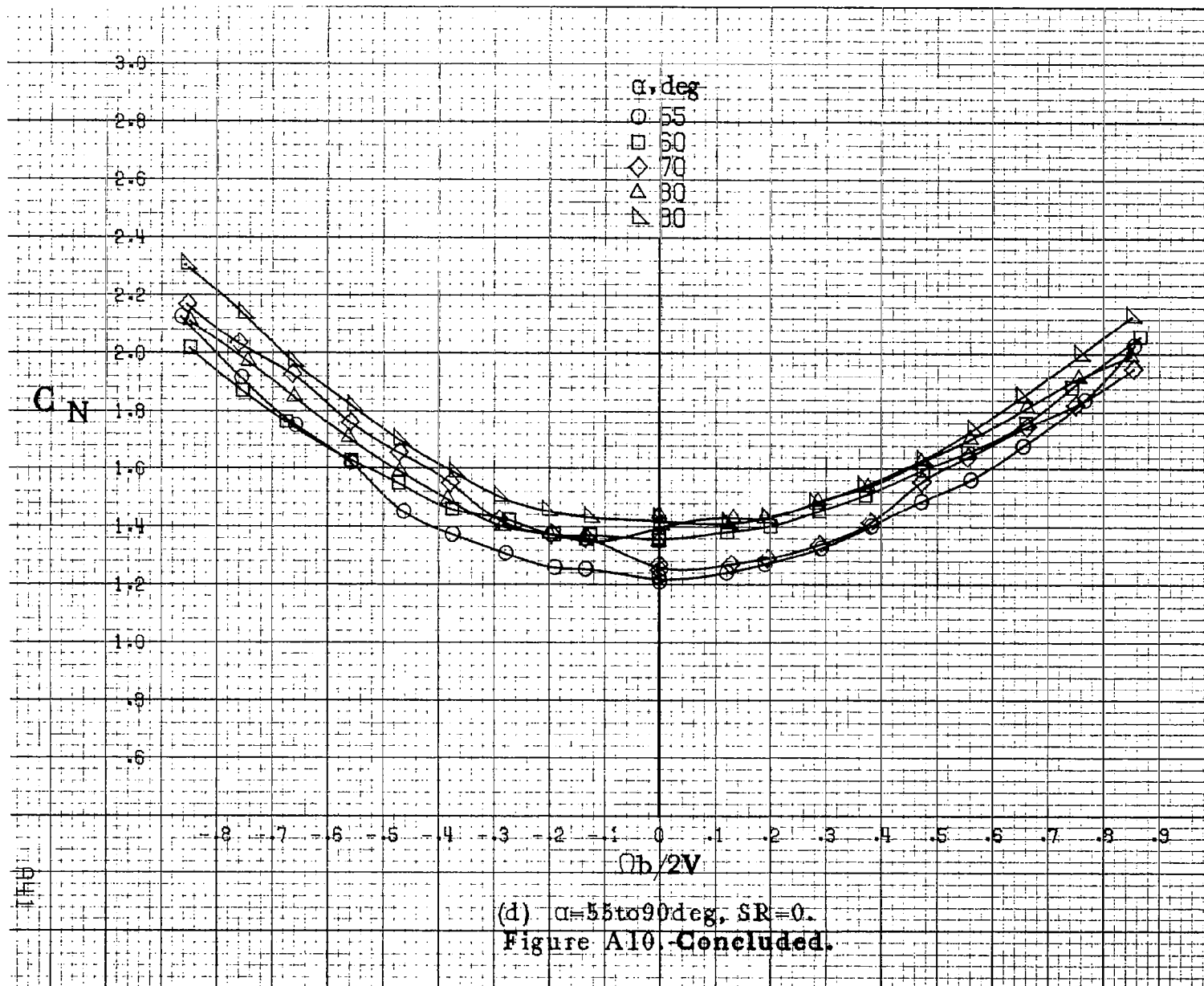
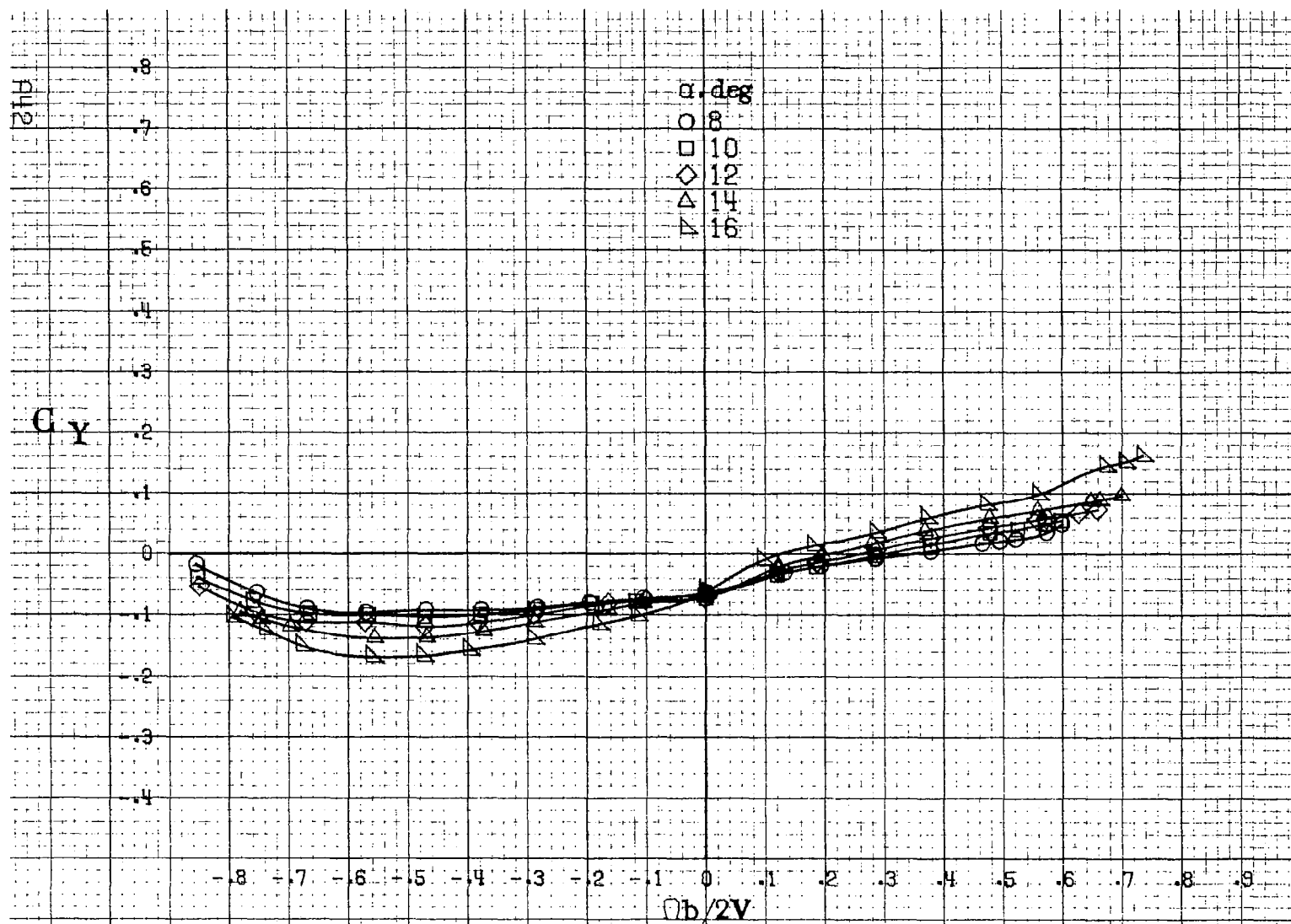


Figure A10. Effect of rotation rate and angle of attack on normal force coefficient for basic configuration. $\delta_e = -20^\circ$, $\delta_a = 20^\circ$, $\delta_r = -28^\circ$, $\beta = 0^\circ$.



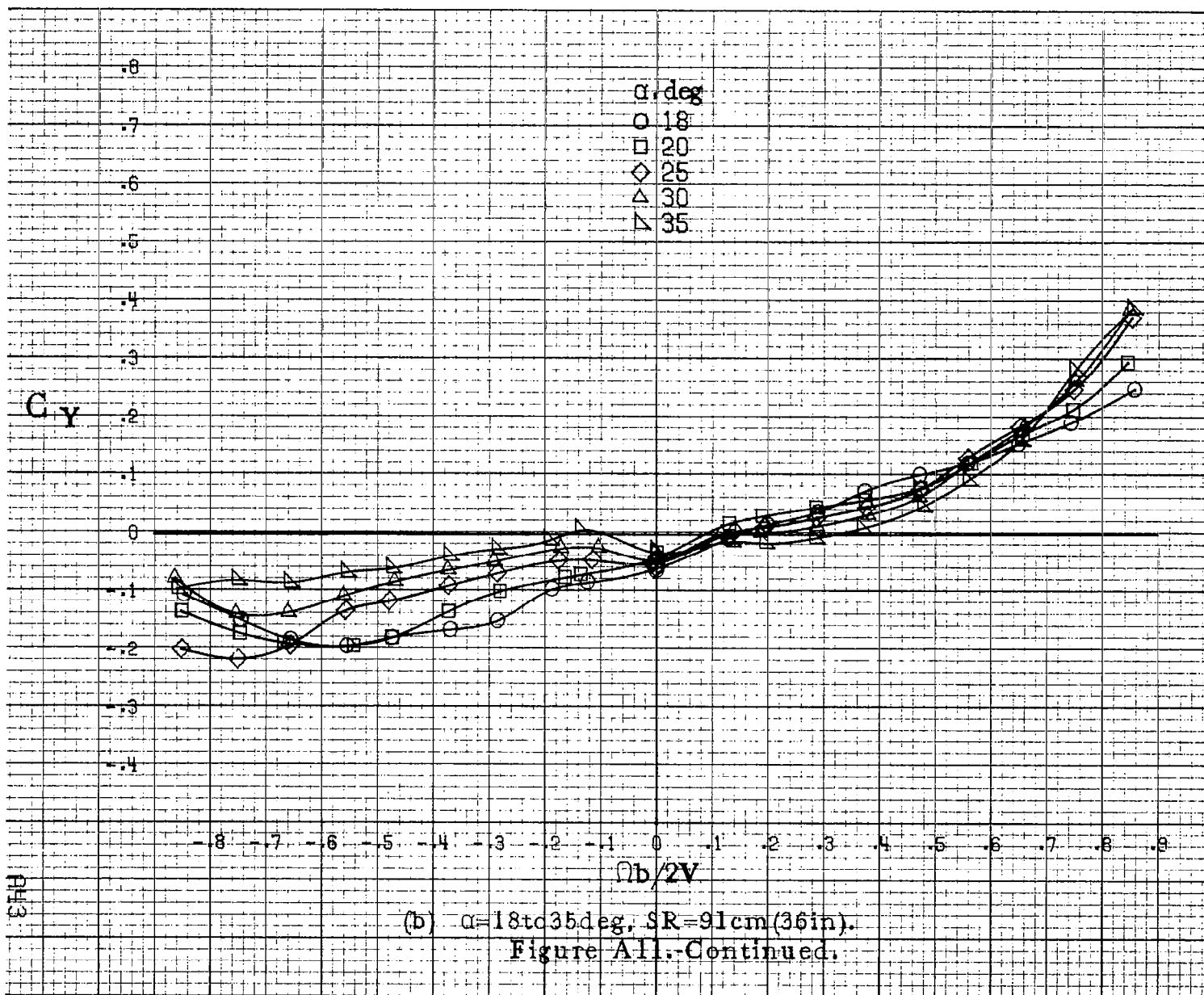


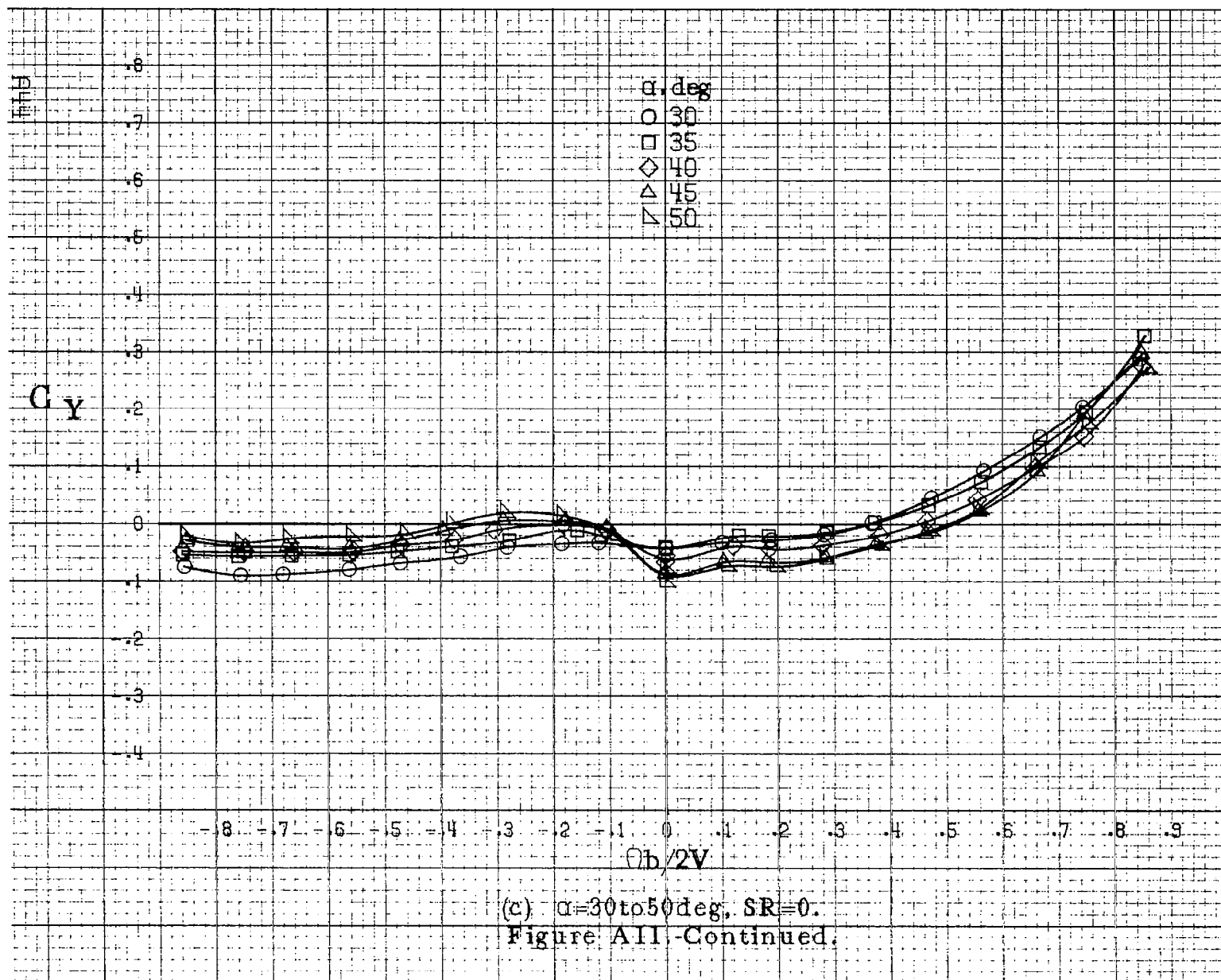


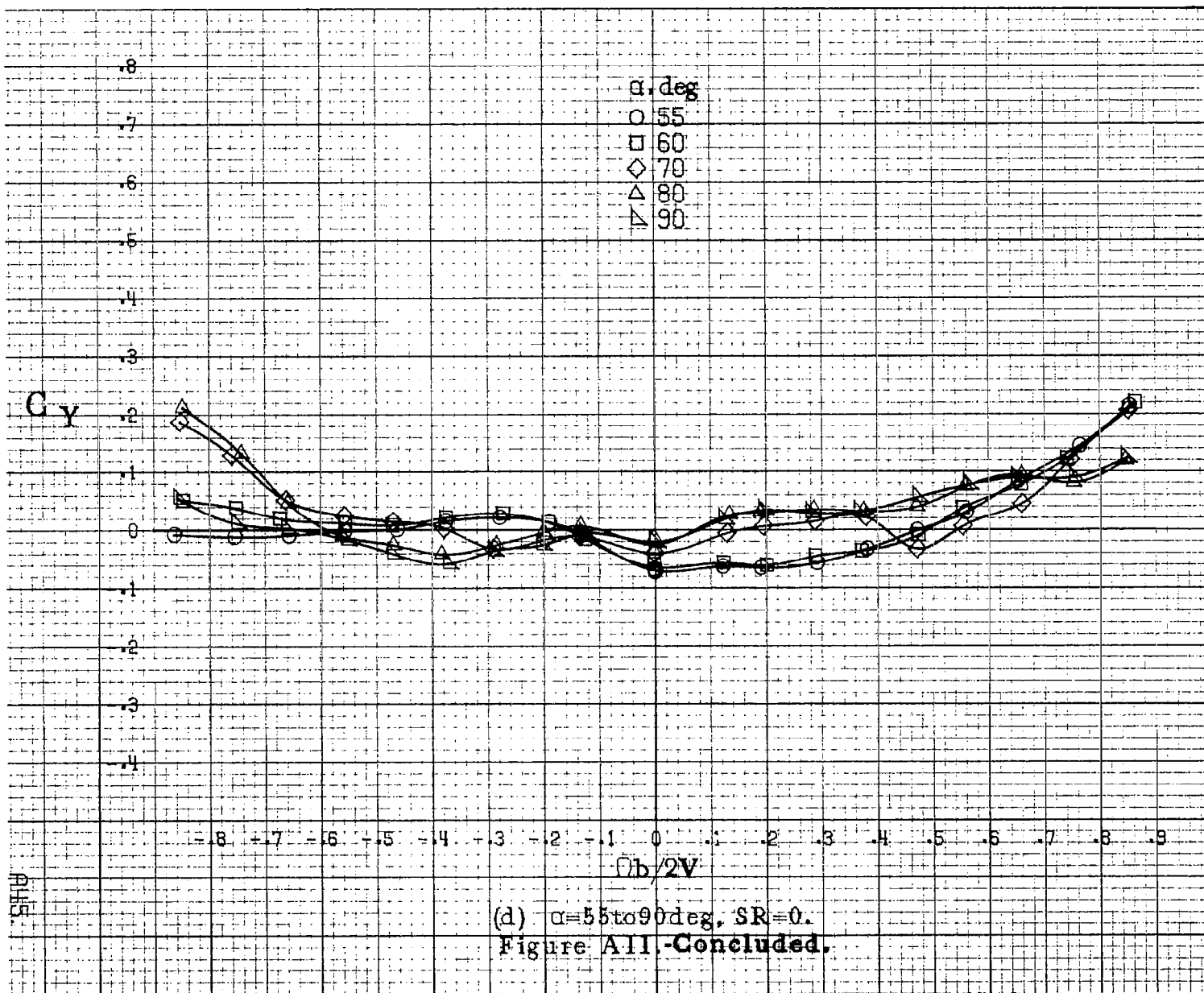


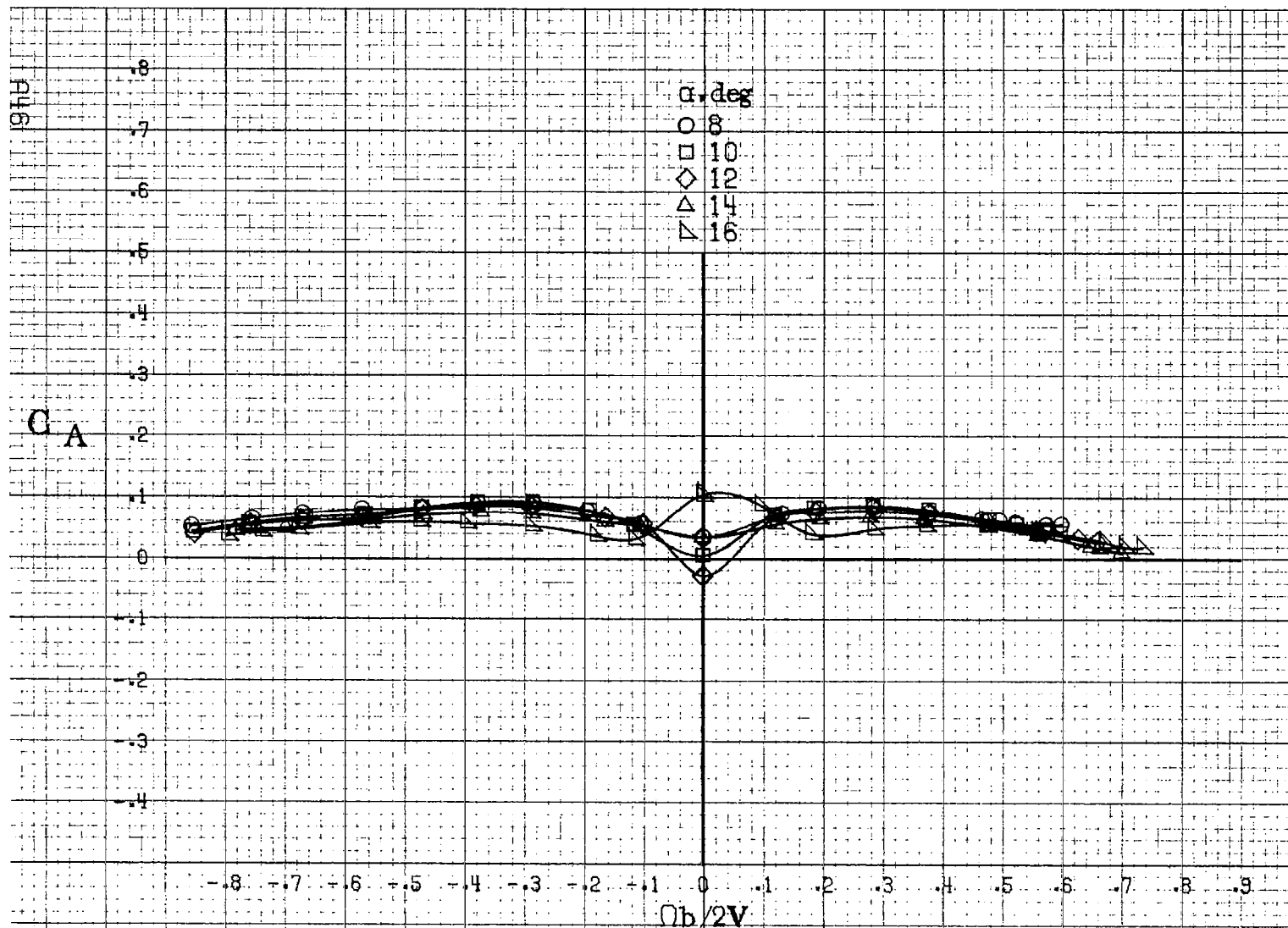
(a) $\alpha = 8$ to 16° , $SR = 91\text{cm}(36\text{in})$.

Figure A11. Effect of rotation rate and angle of attack on side force coefficient for basic configuration. $\delta_e = -20^\circ$, $\delta_a = 20^\circ$, $\delta_r = -28^\circ$, $\beta = 0^\circ$.



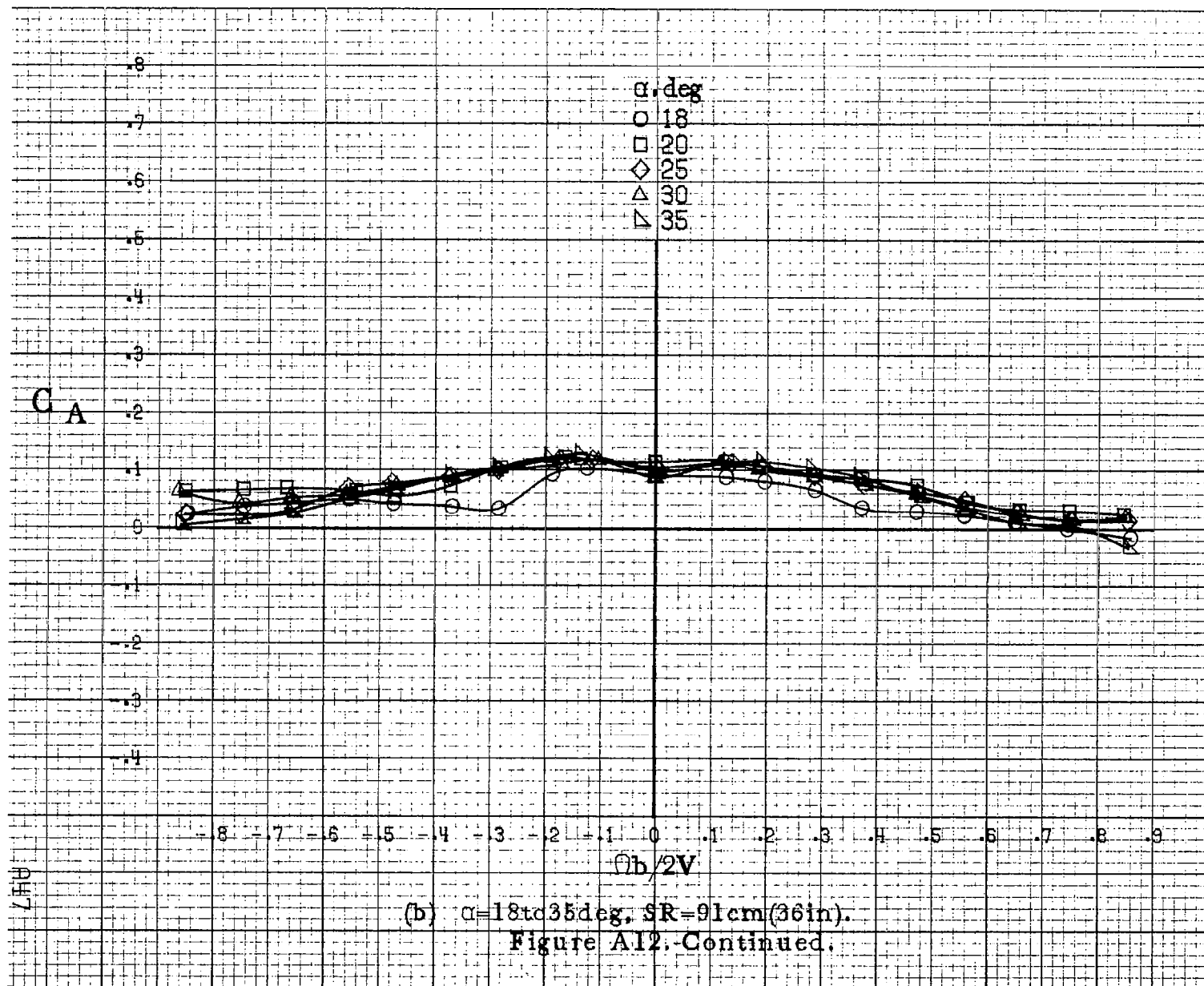


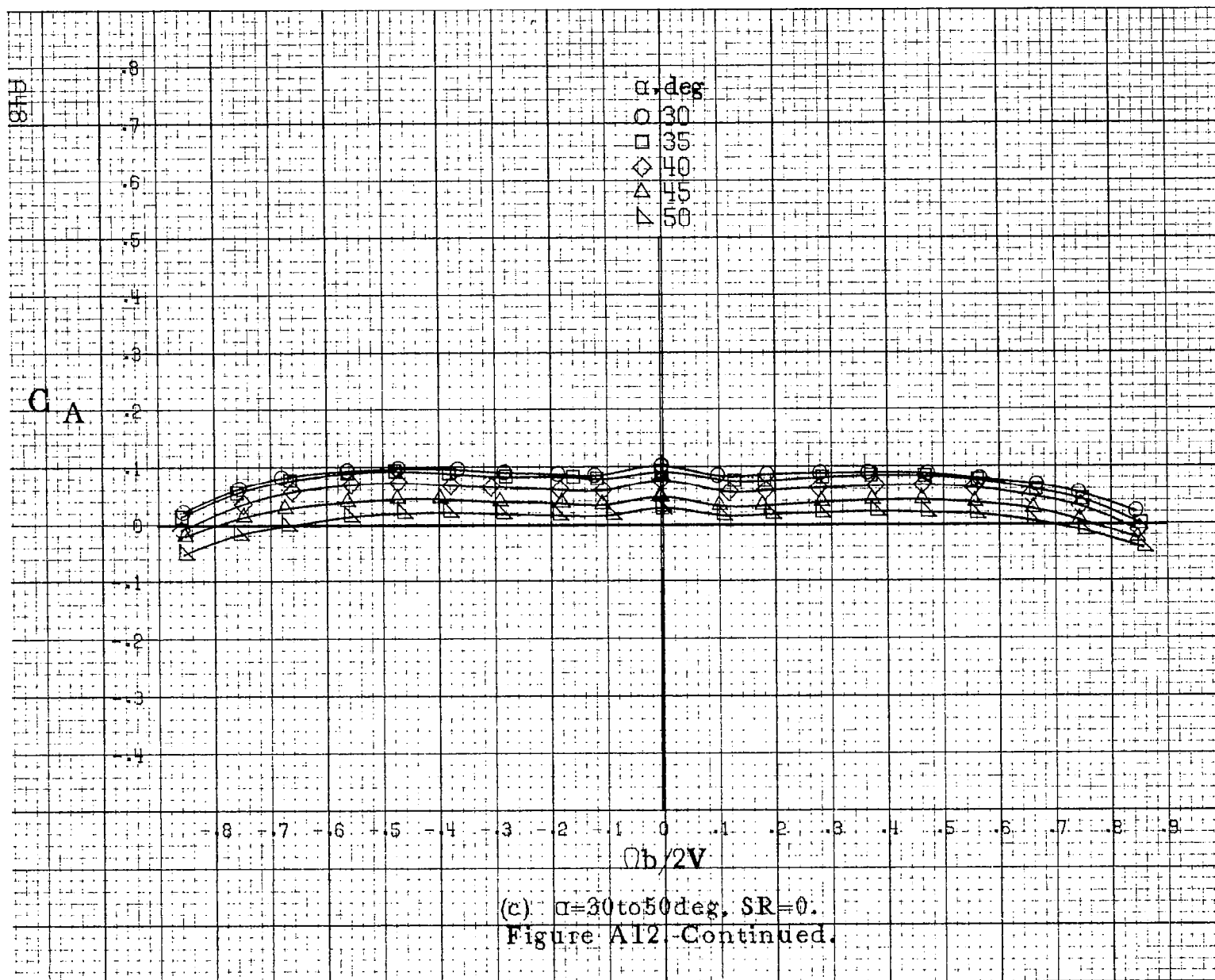


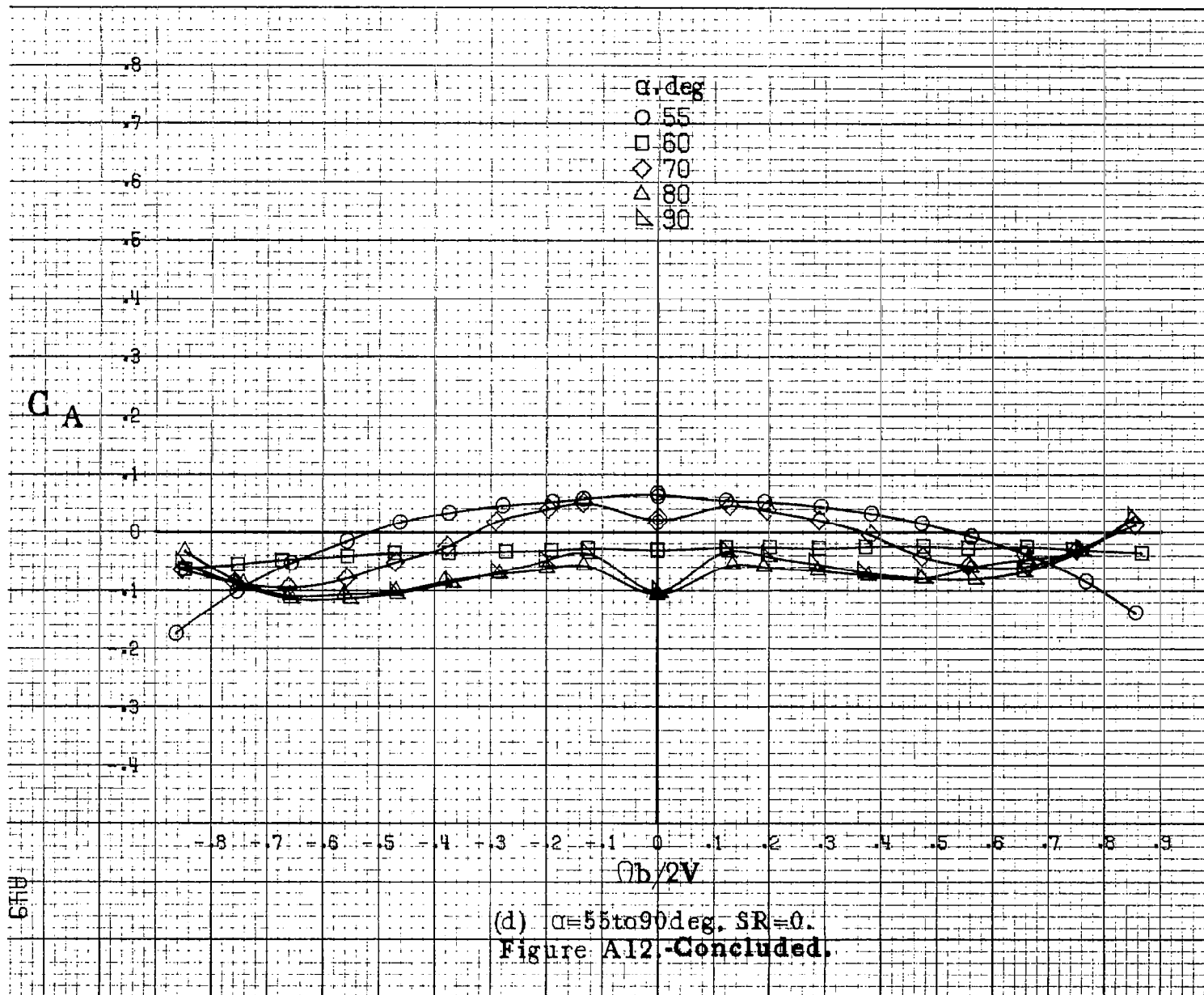


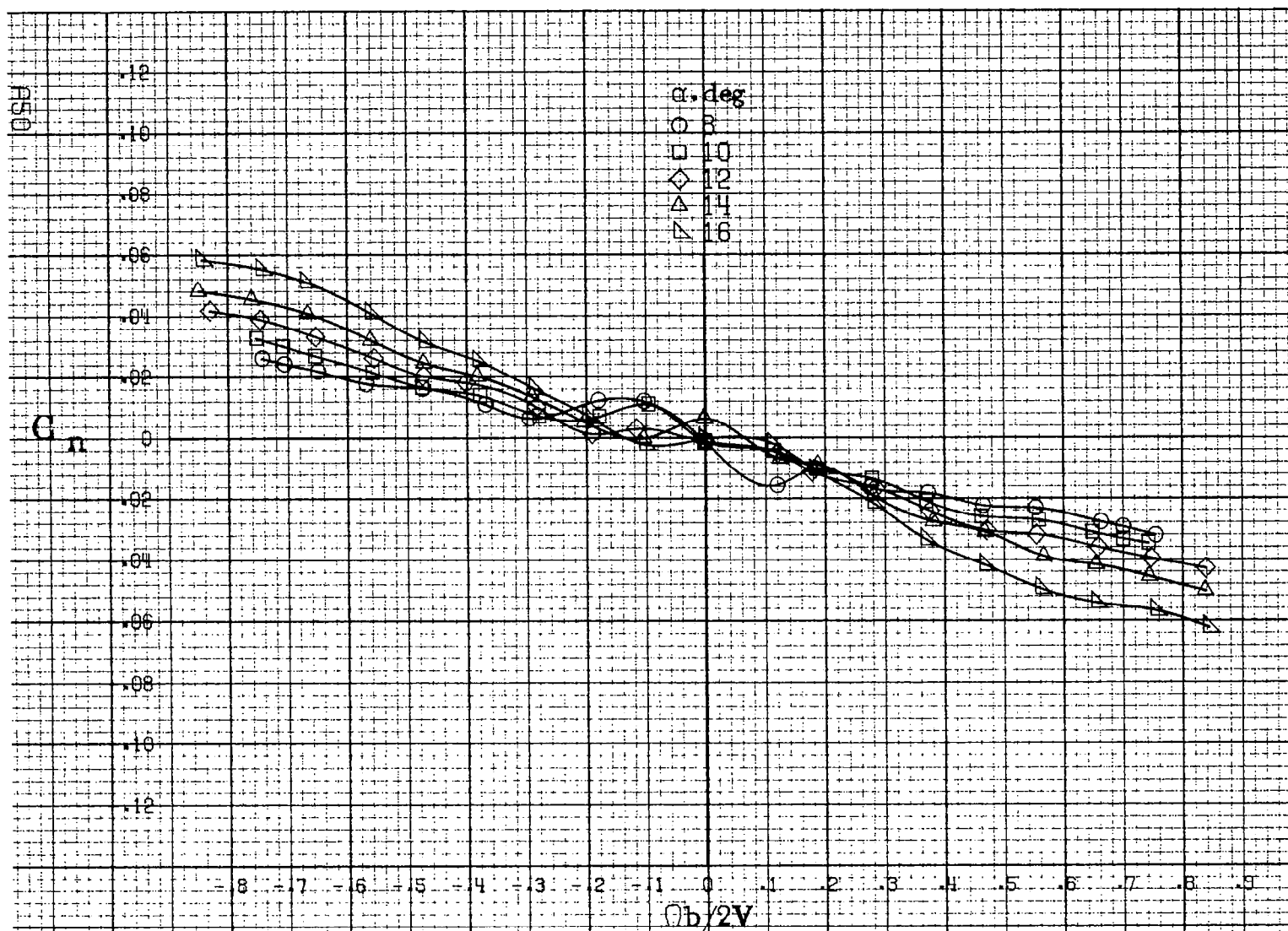
(a) $\alpha = 8$ to 16° , $SR = 91 \text{ cm (36 in)}$.

Figure A12. Effect of rotation rate and angle of attack on axial force coefficient for basic configuration. $\delta_e = -20^\circ$, $\delta_a = 20^\circ$, $\delta_r = -28^\circ$, $\beta = 0^\circ$.



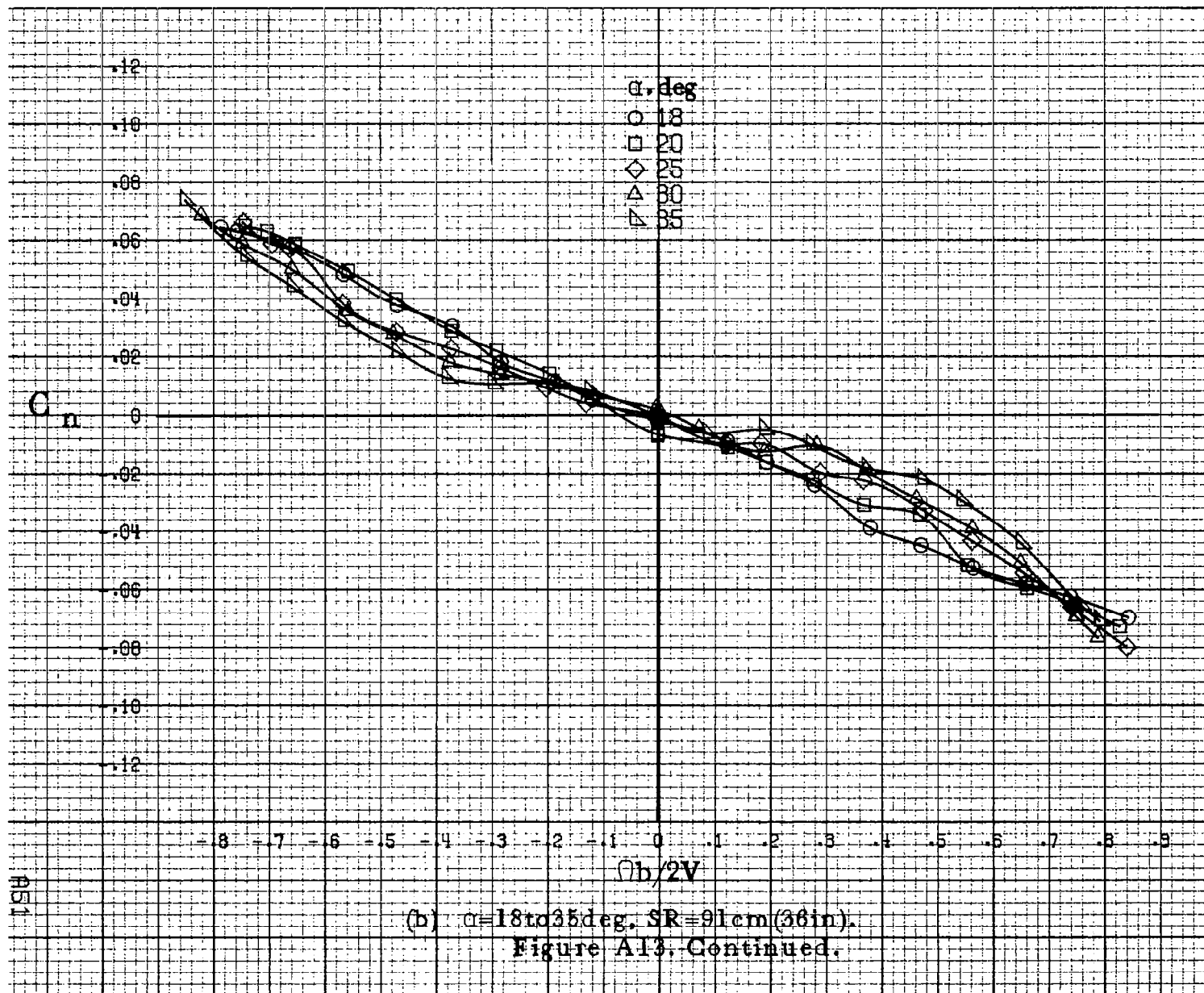


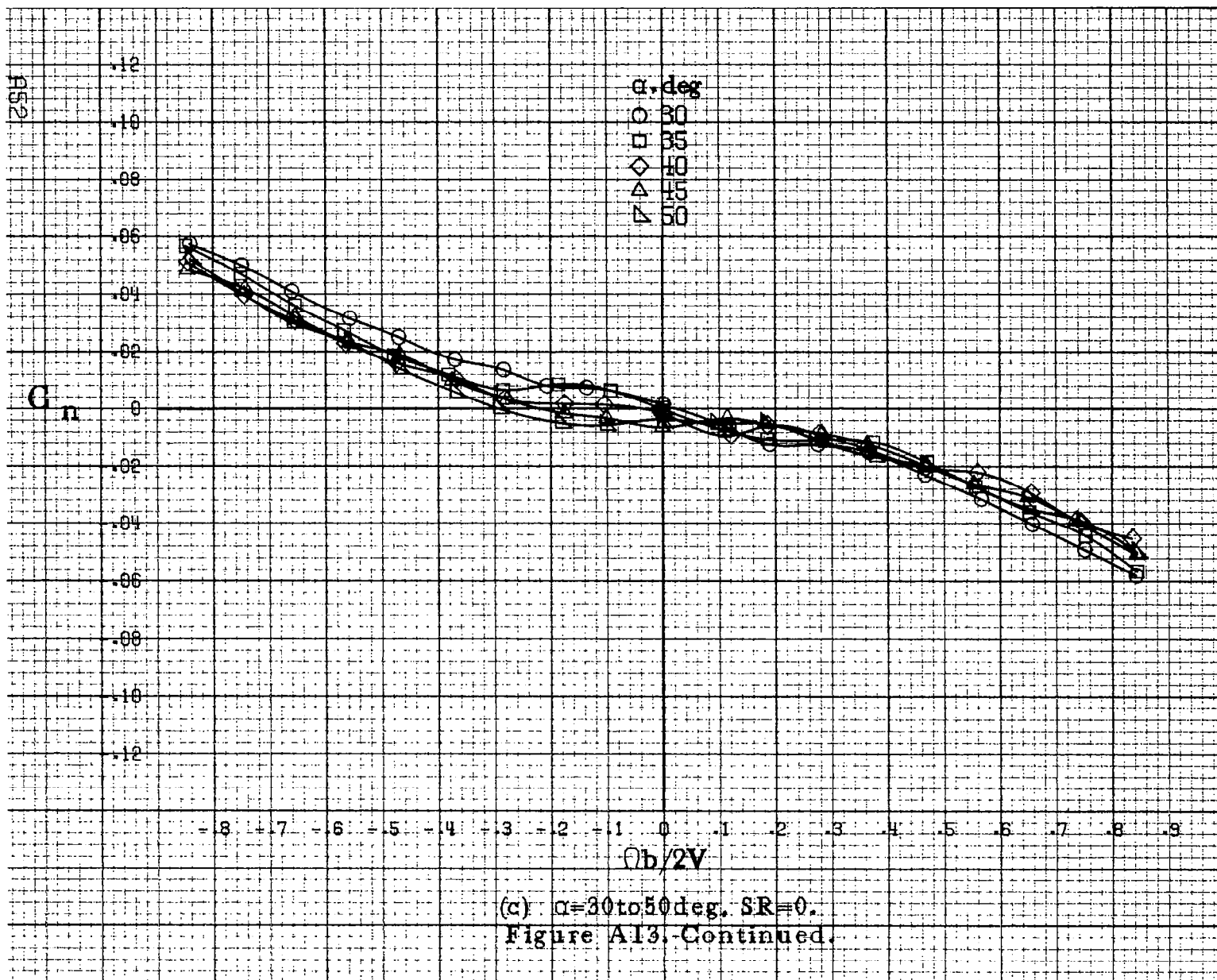


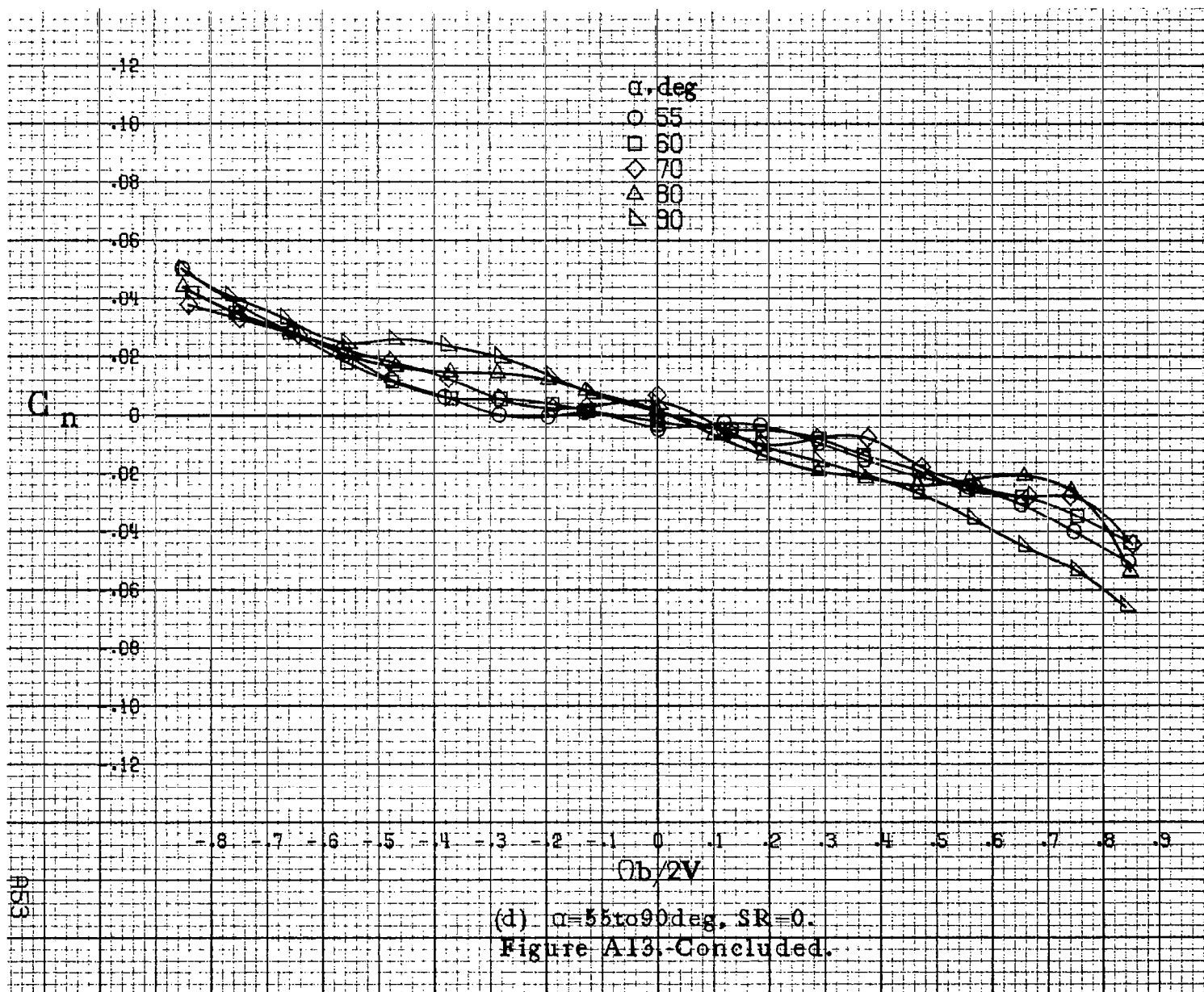


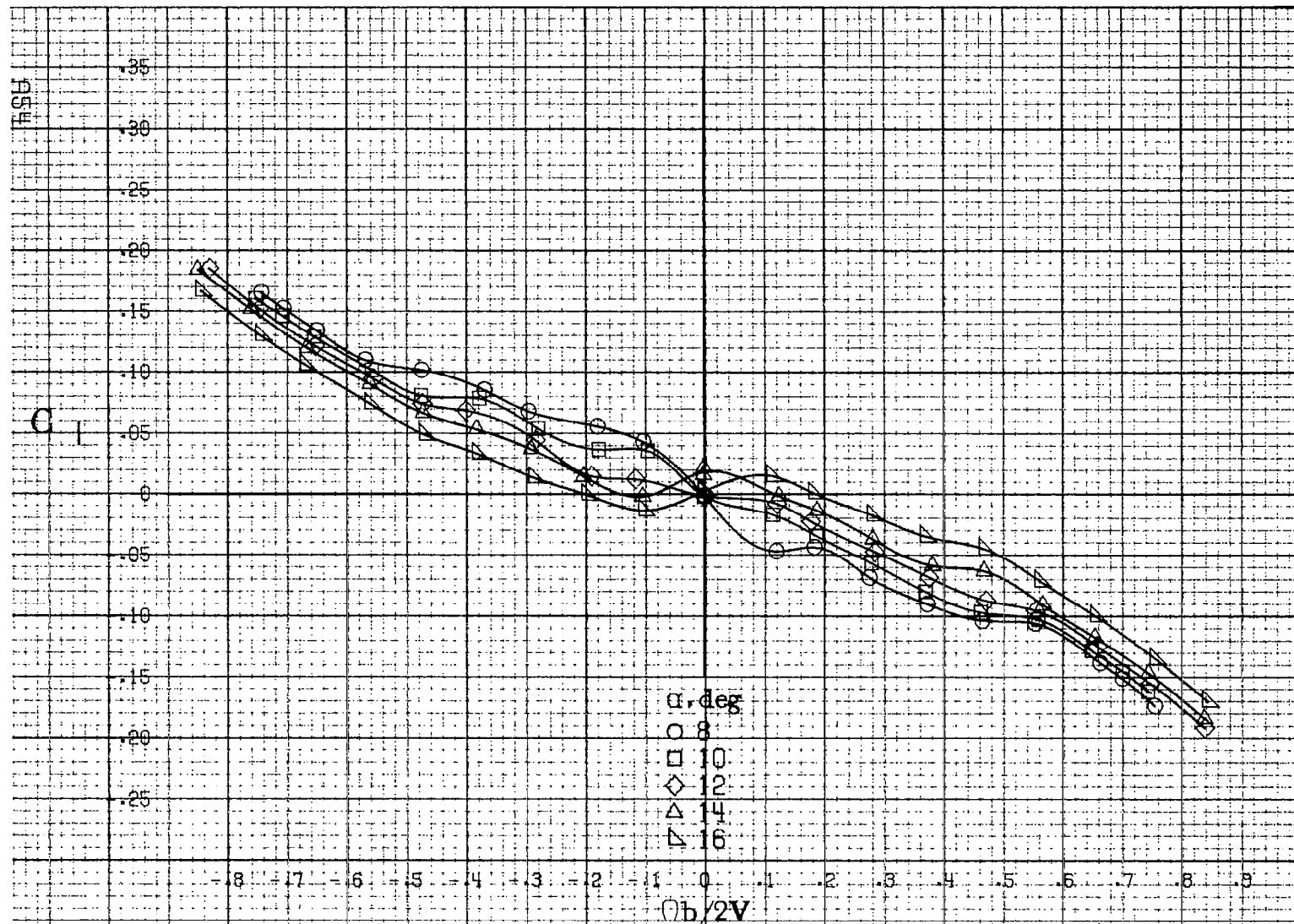
(a) $\alpha = 8$ to 16° , $SR = 91\text{cm} (36\text{in})$.

Figure A13. Effect of rotation rate and angle of attack on yawing moment coefficient for configuration having outboard LE wing droop. $\delta_e = 0^\circ$, $\delta_a = 0^\circ$, $\delta_r = 0^\circ$, $\beta = 0^\circ$.



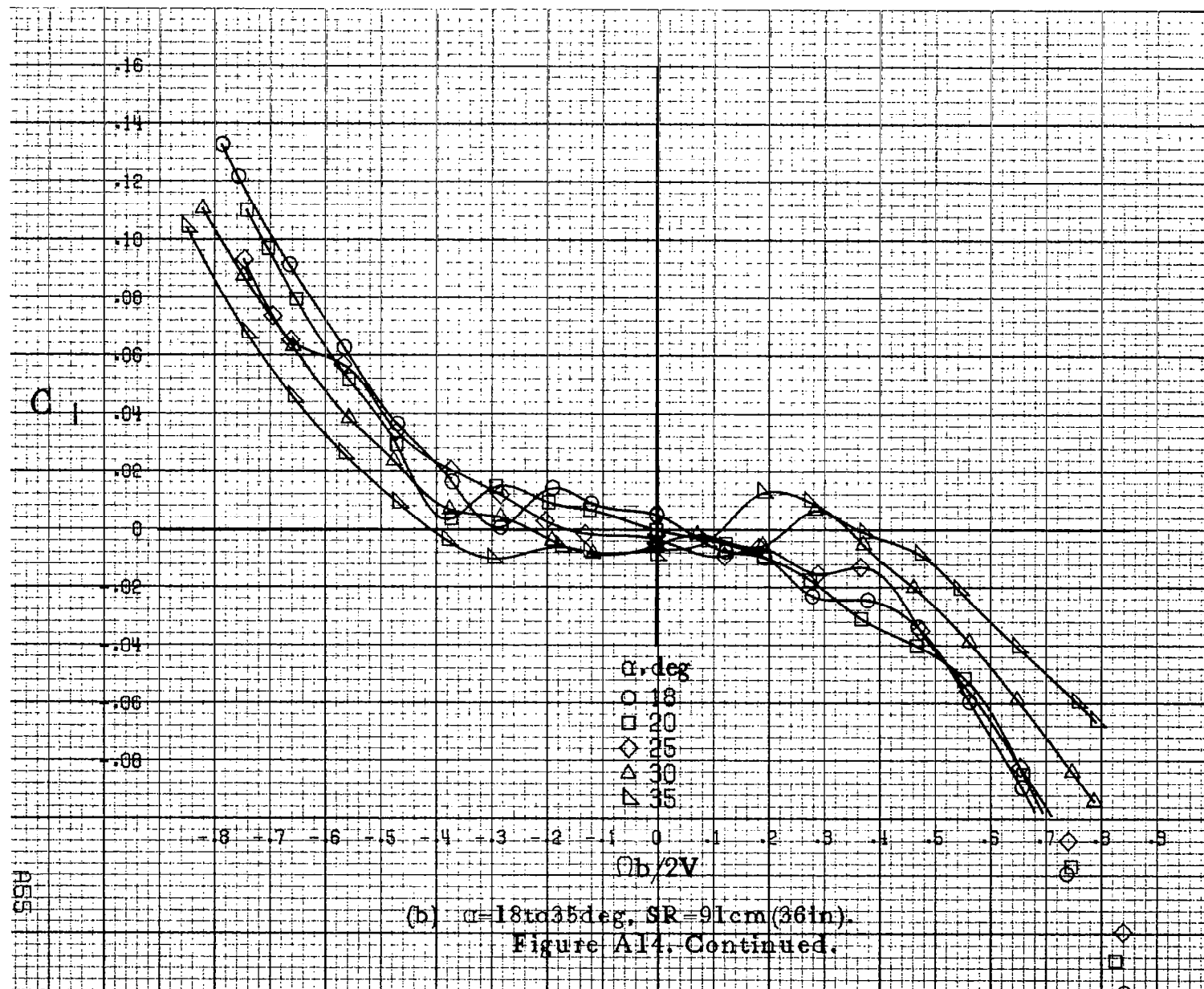


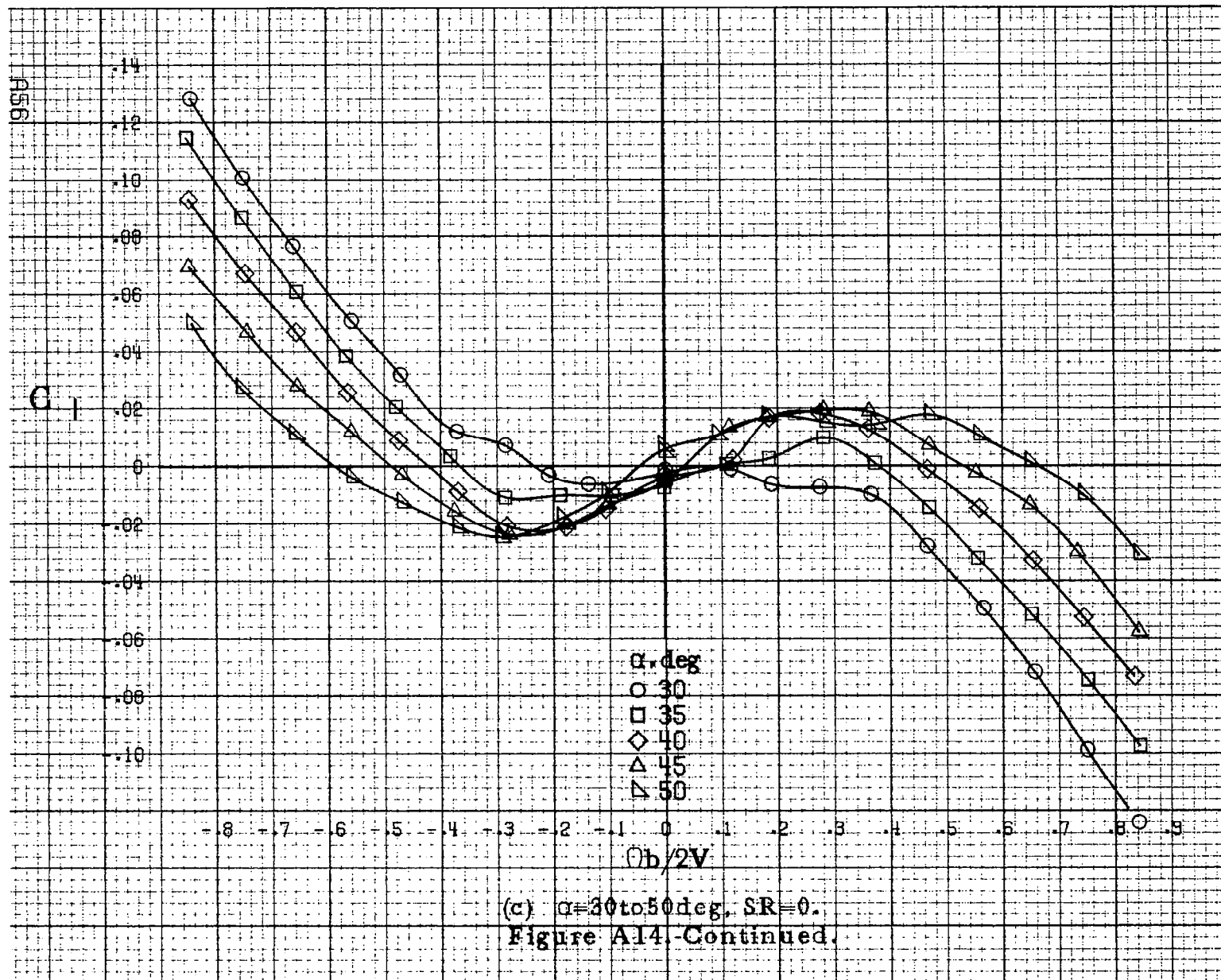


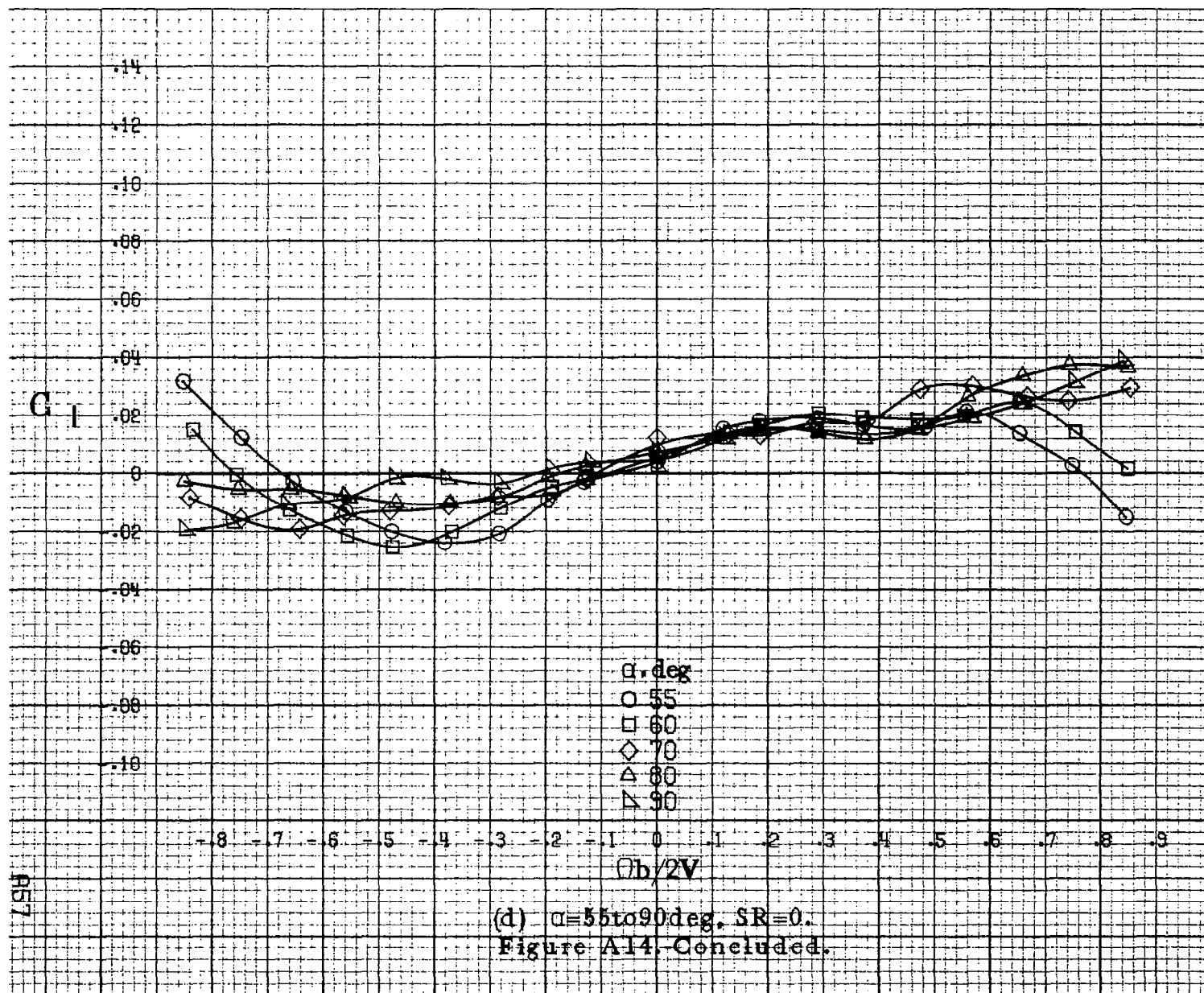


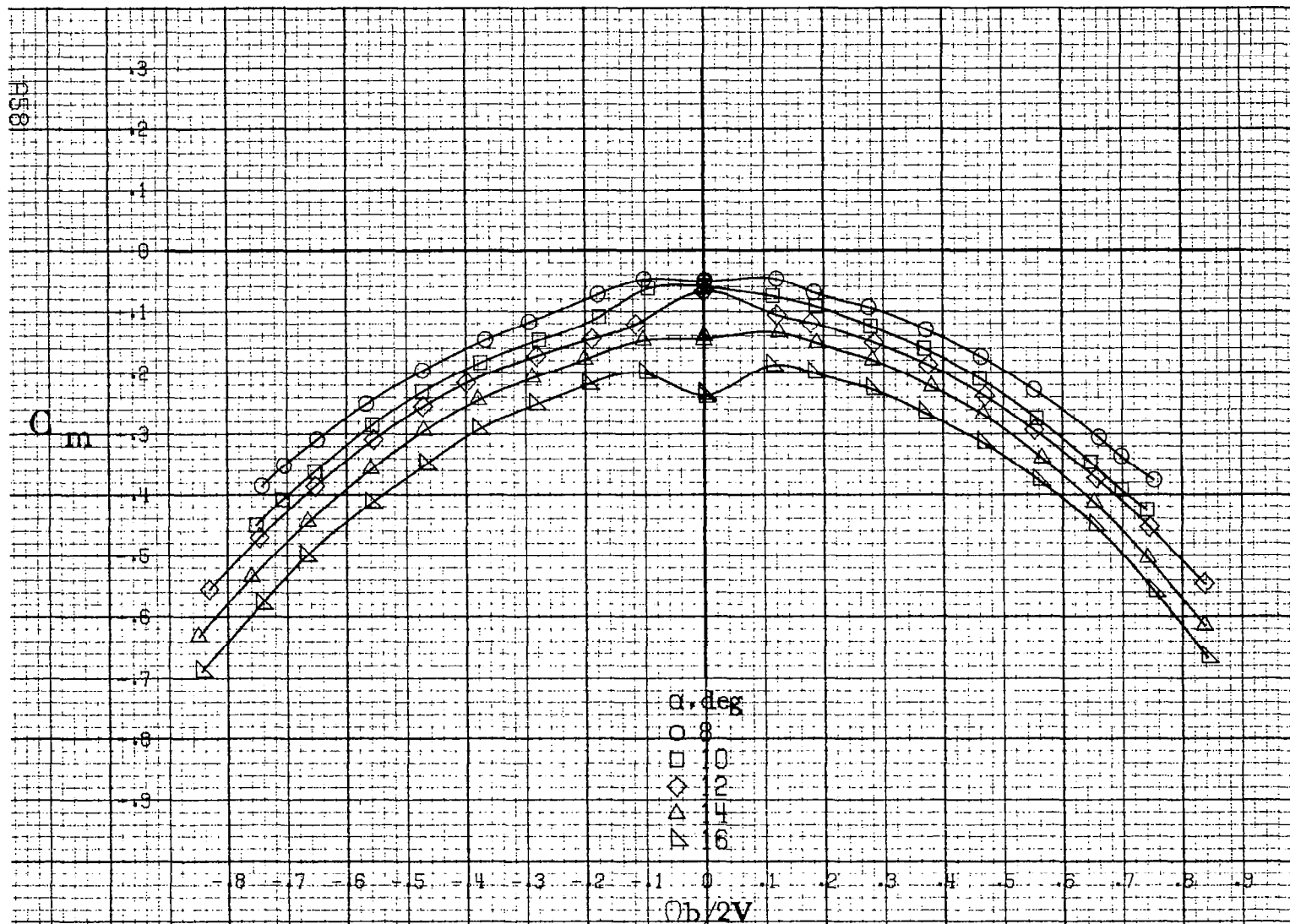
(a) $\alpha = 8$ to 16° , $SR = 91\text{cm (36in)}$.

Figure A14. Effect of rotation rate and angle of attack on rolling-moment coefficient for configuration having outboard LE wing droop. $\delta_e = 0^\circ$, $\delta_a = 0^\circ$, $\delta_r = 0^\circ$, $\beta = 0^\circ$.



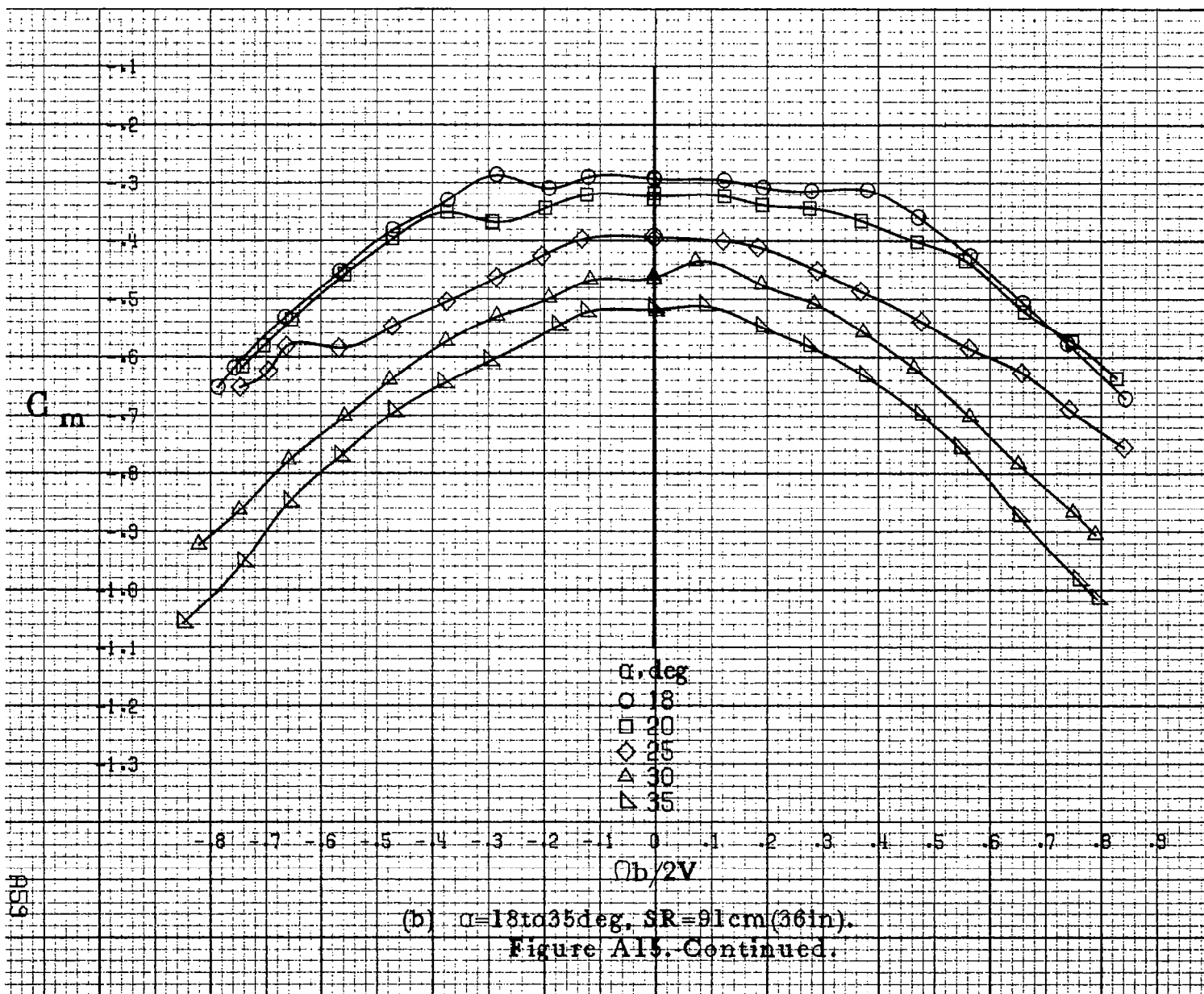


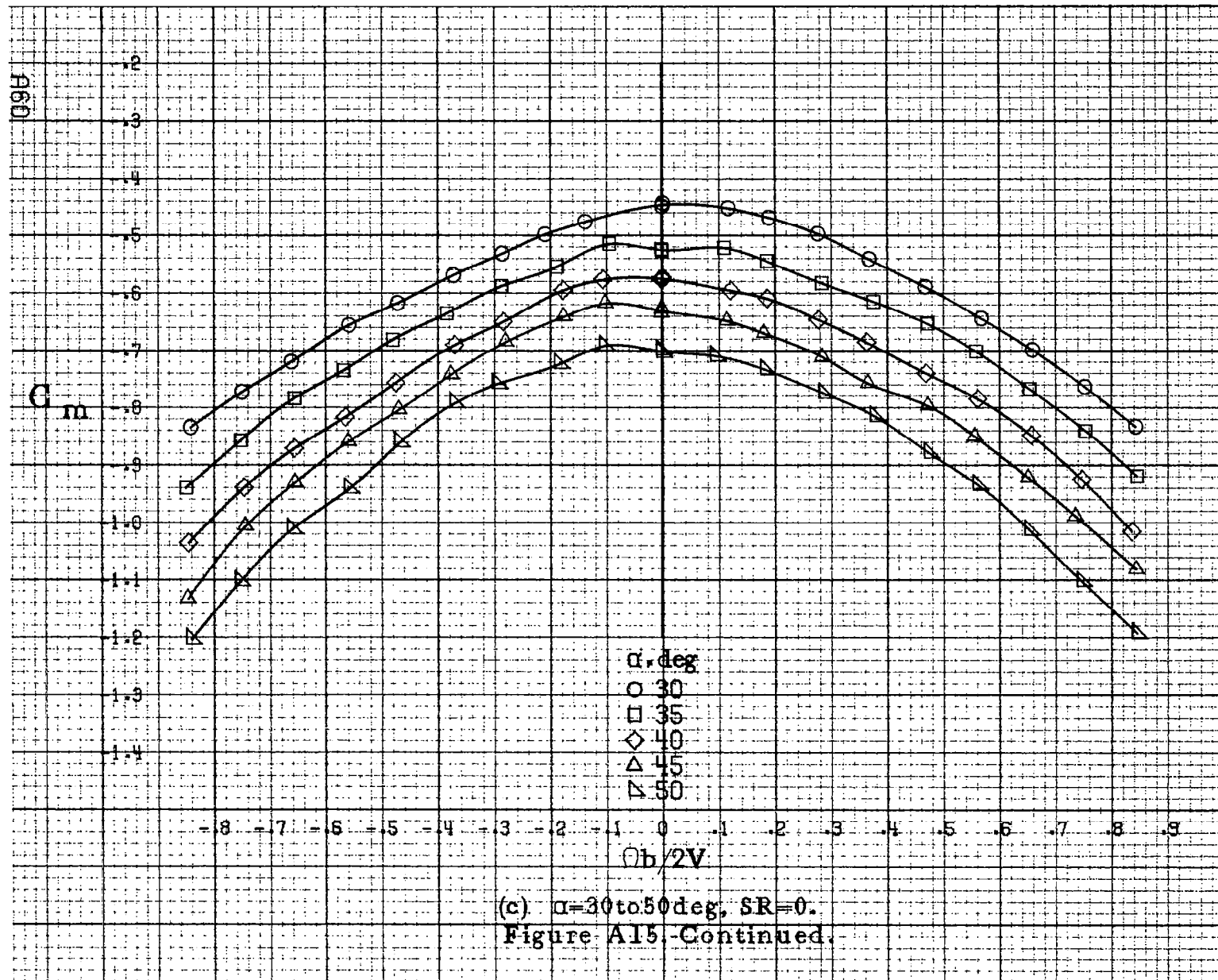


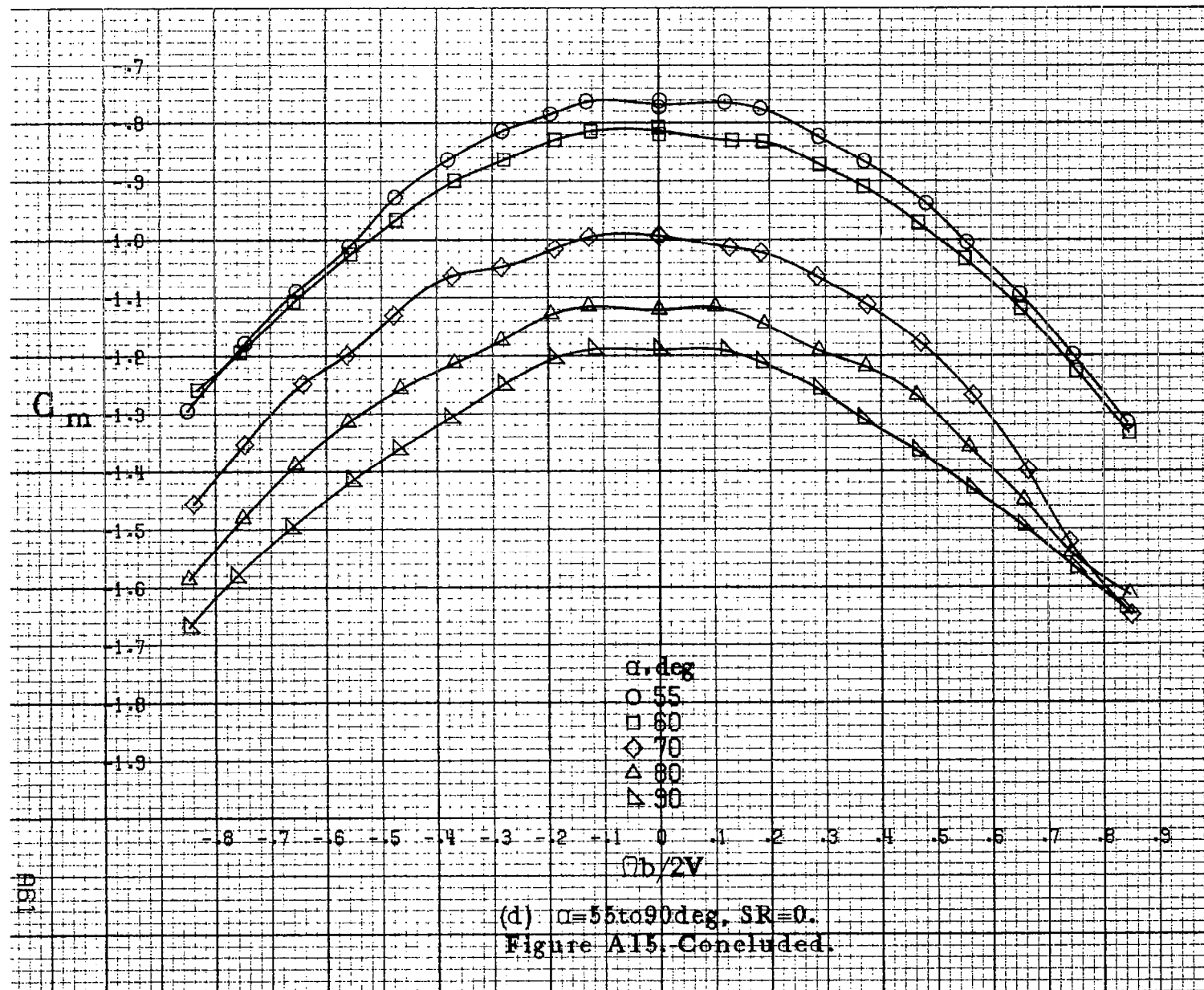


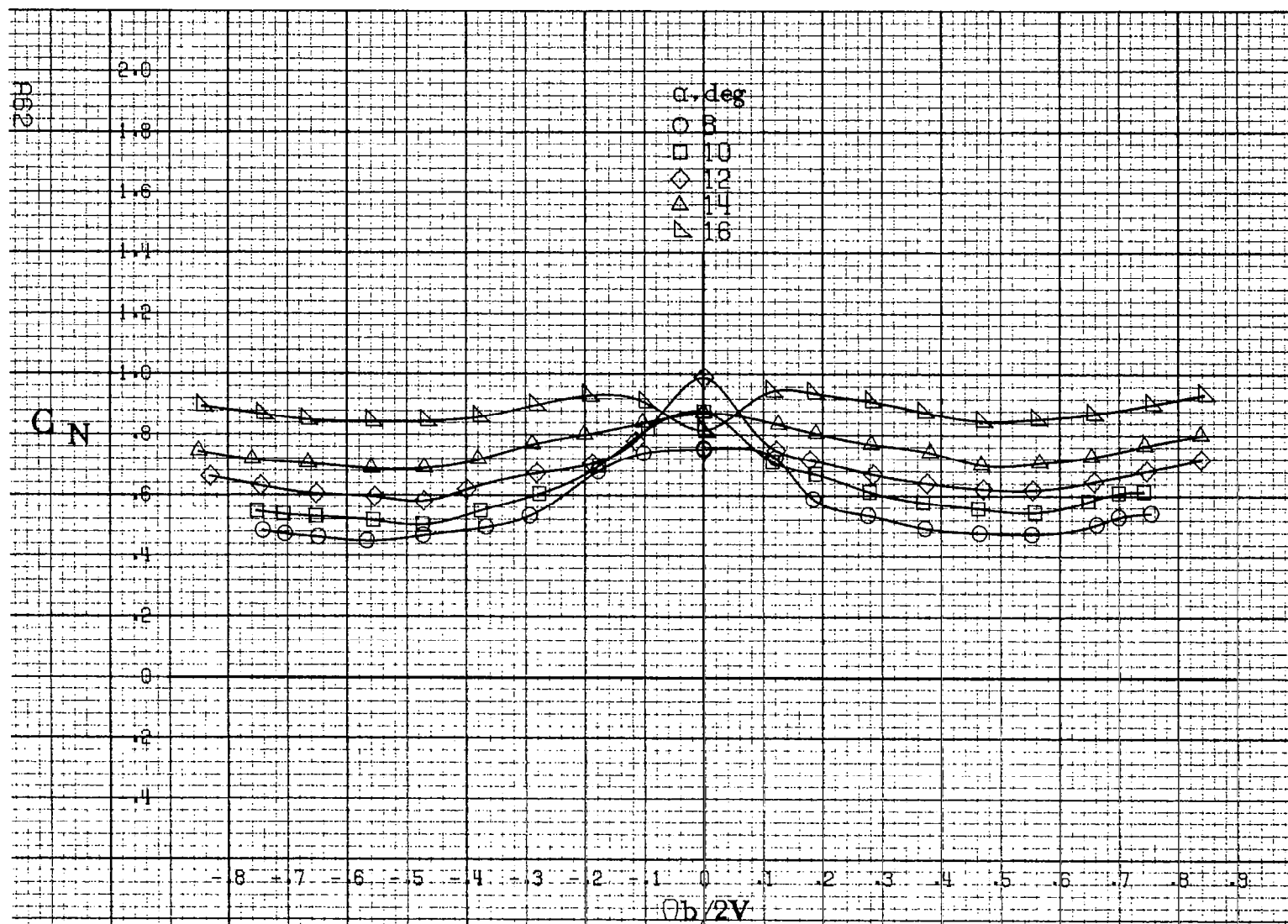
(a) $\alpha = 8$ to 16 deg, $SR = 91$ cm (36 in).

Figure A15. Effect of rotation rate and angle of attack on pitching moment coefficient for configuration having outboard LE wing droop. $\delta_a = 0^\circ$, $\delta_a = 0^\circ$, $\delta_r = 0^\circ$, $\delta = 0^\circ$.



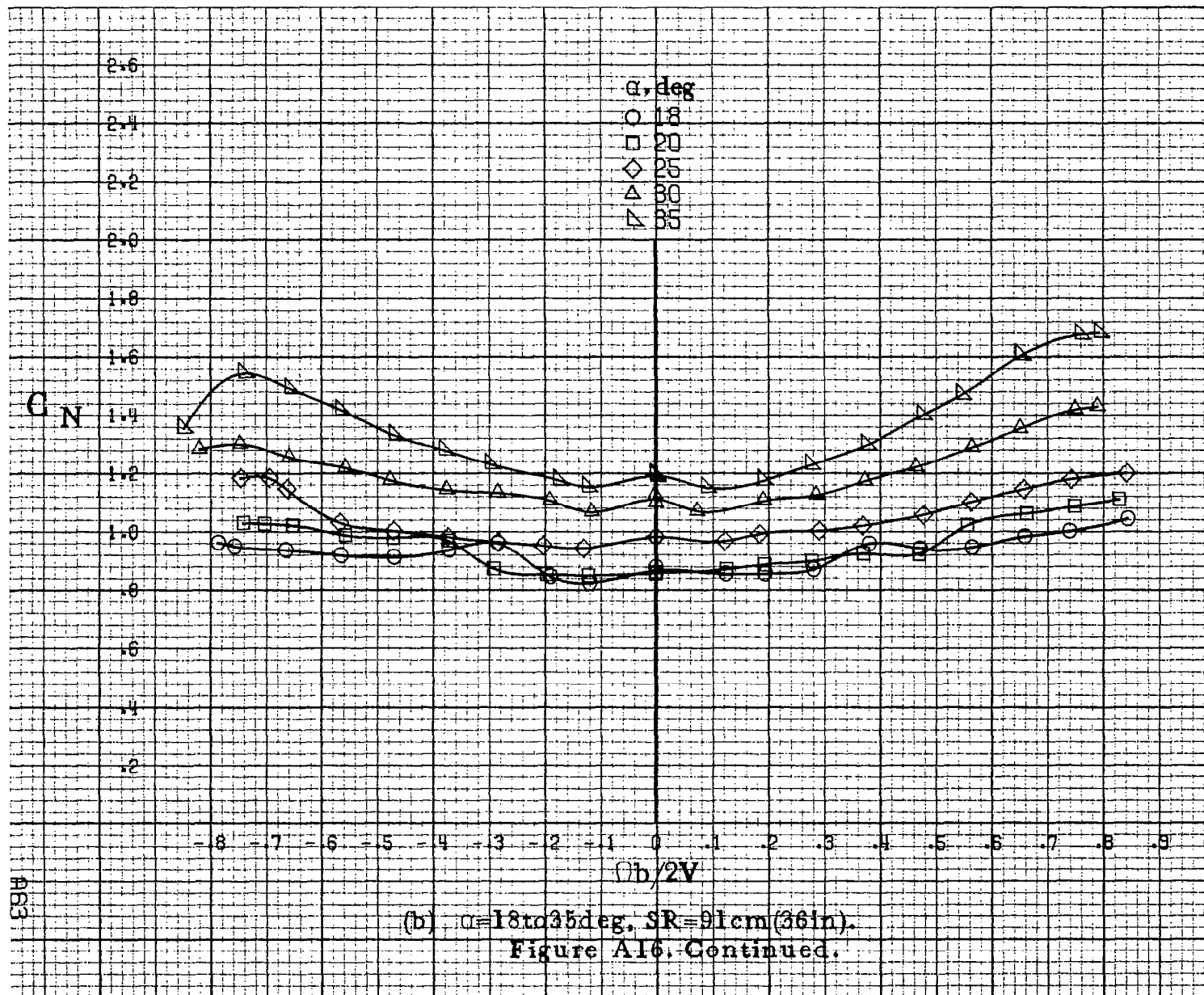


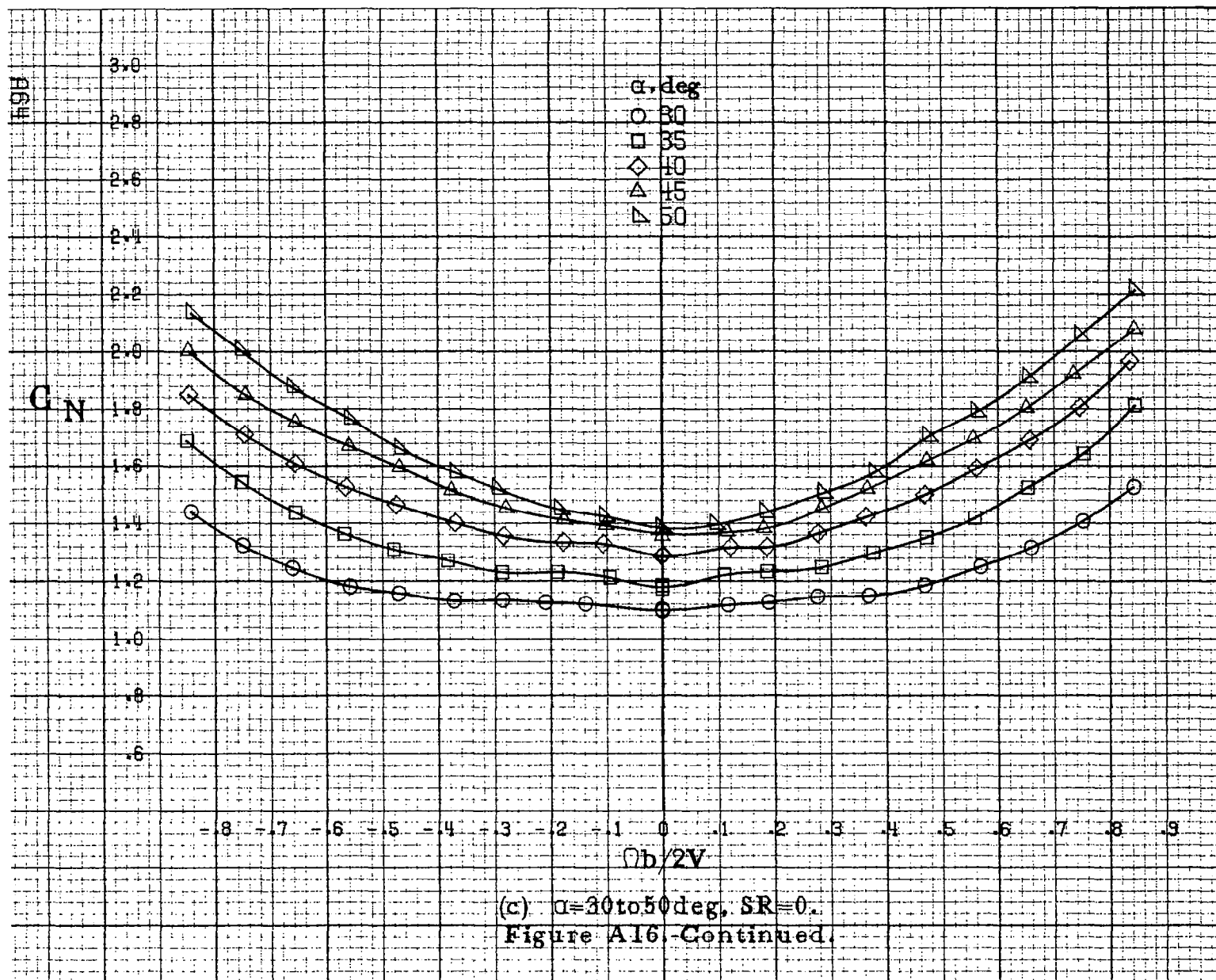


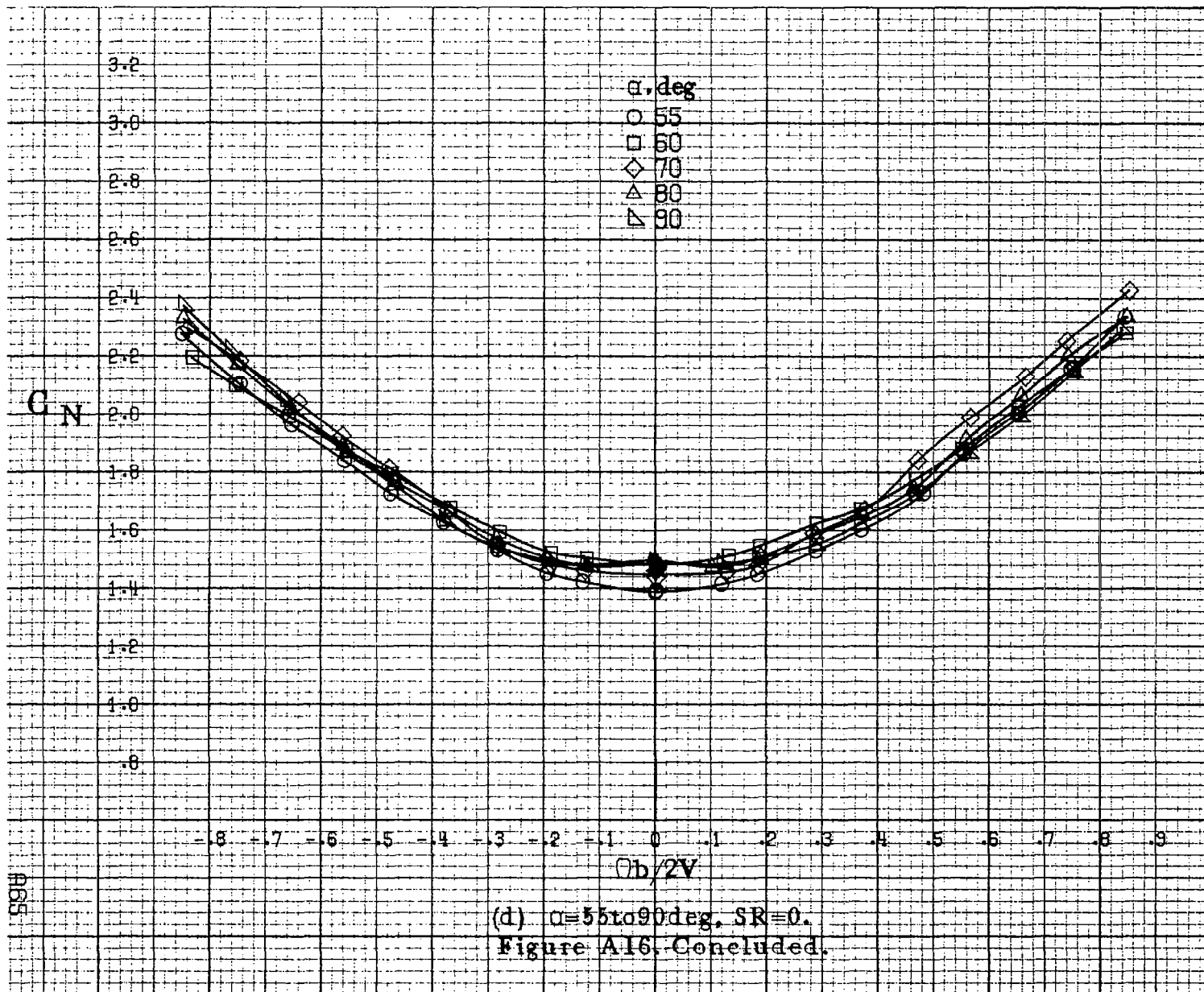


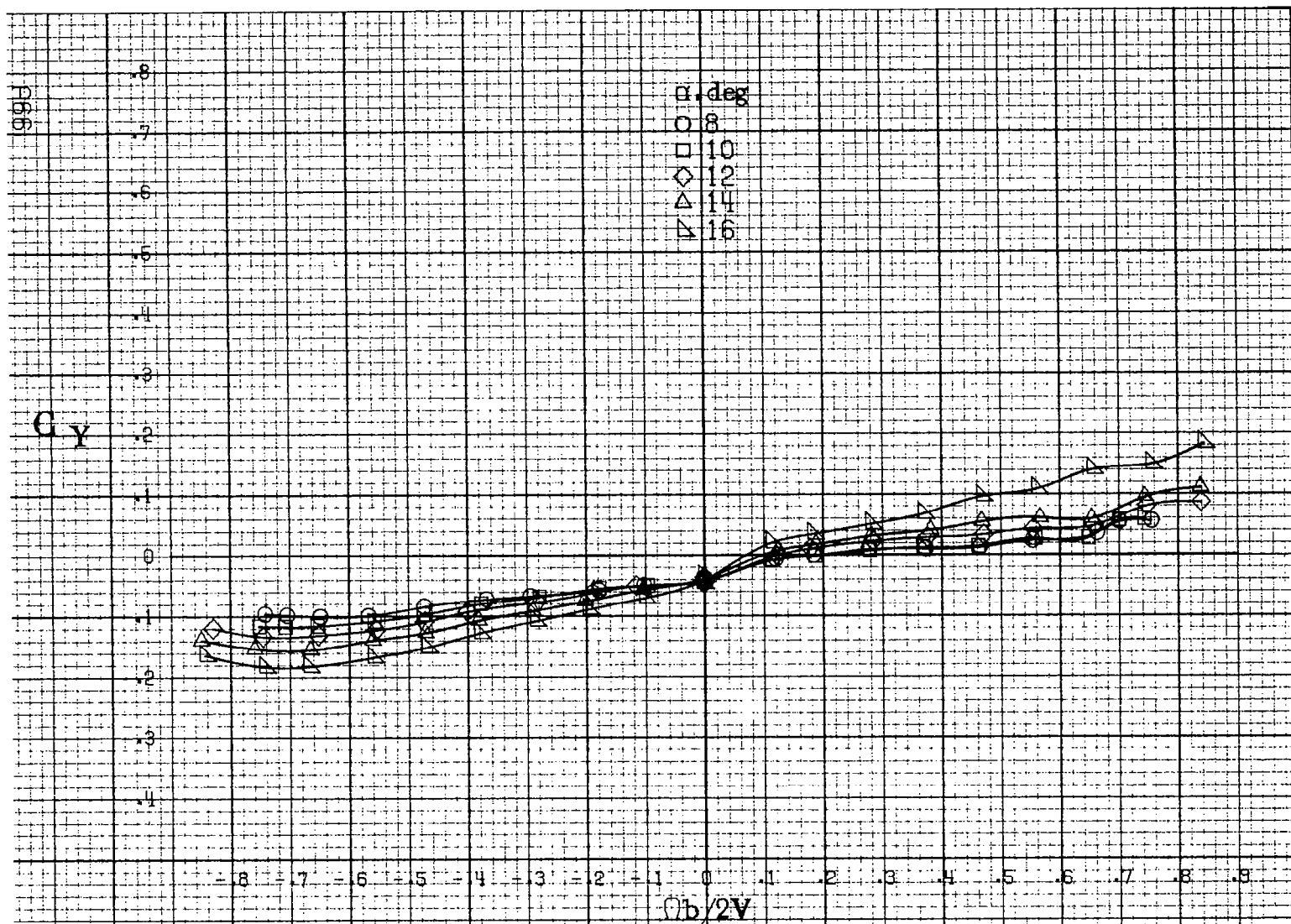
(a) $\alpha=8$ to 16° , $SR=91\text{cm}(36\text{in})$.

Figure A16. Effect of rotation rate and angle of attack on normal-force coefficient for configuration having outboard LE wing droop. $\delta_e=0^\circ$, $\delta_a=0^\circ$, $\delta_r=0^\circ$, $\beta=0^\circ$.



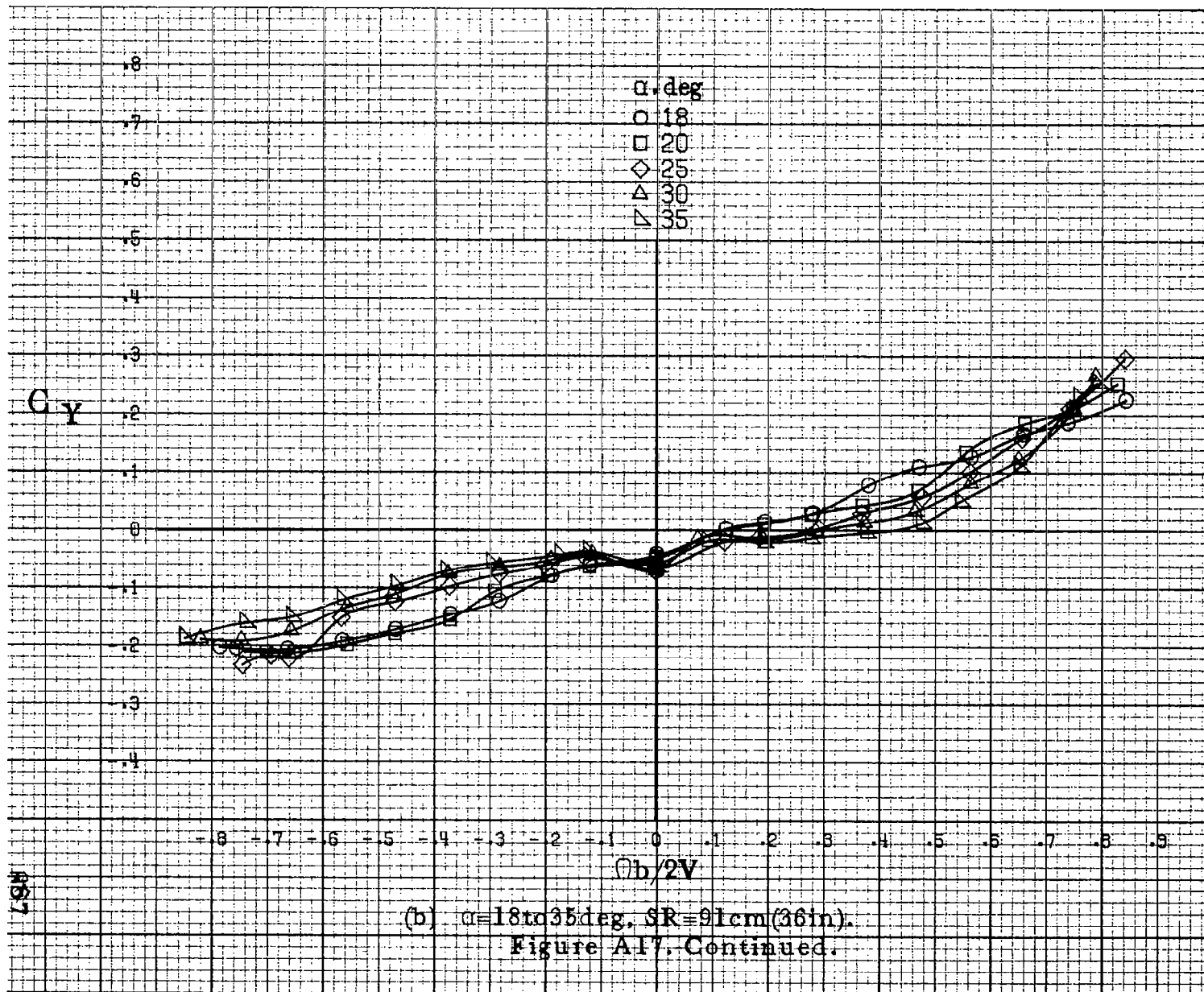


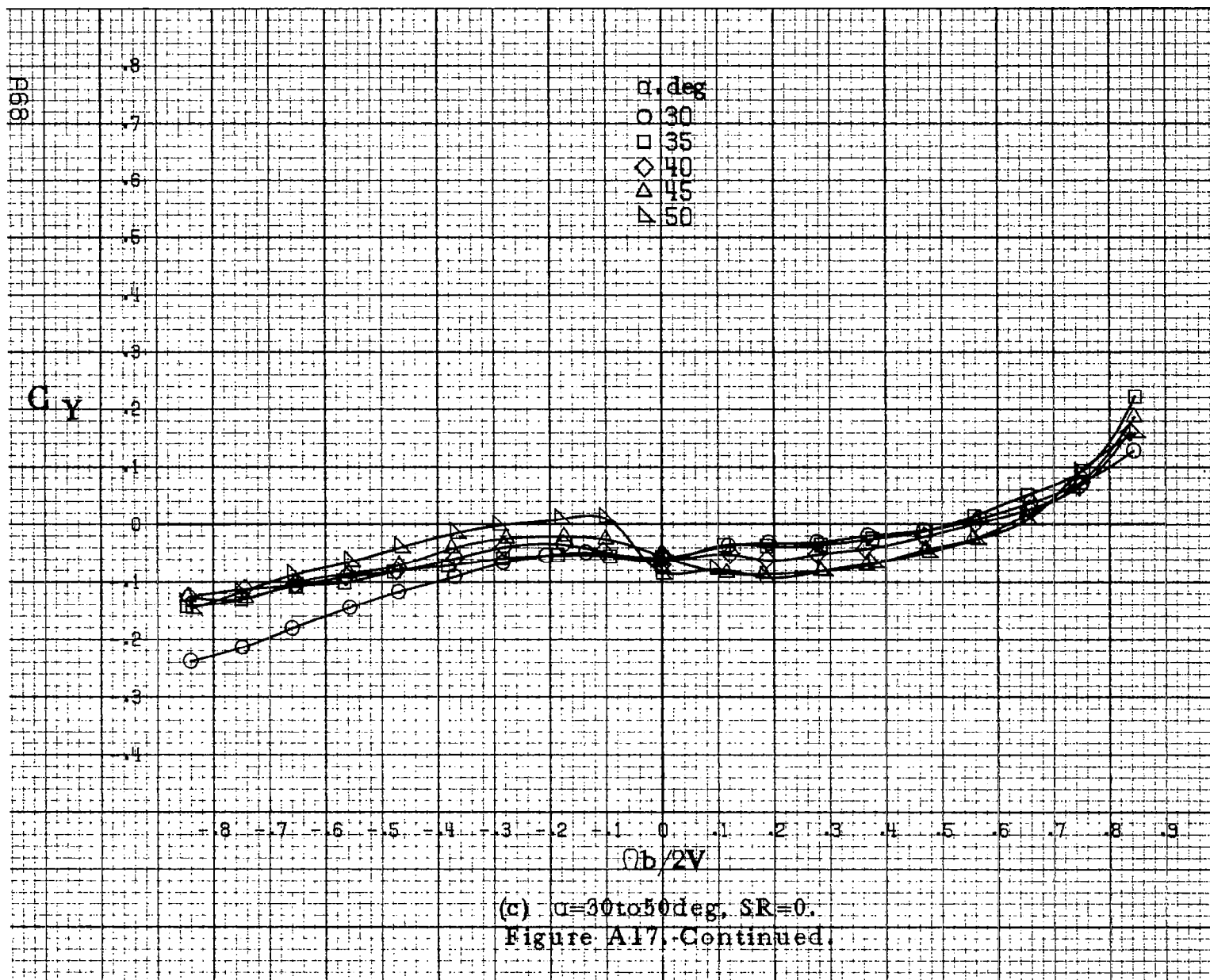


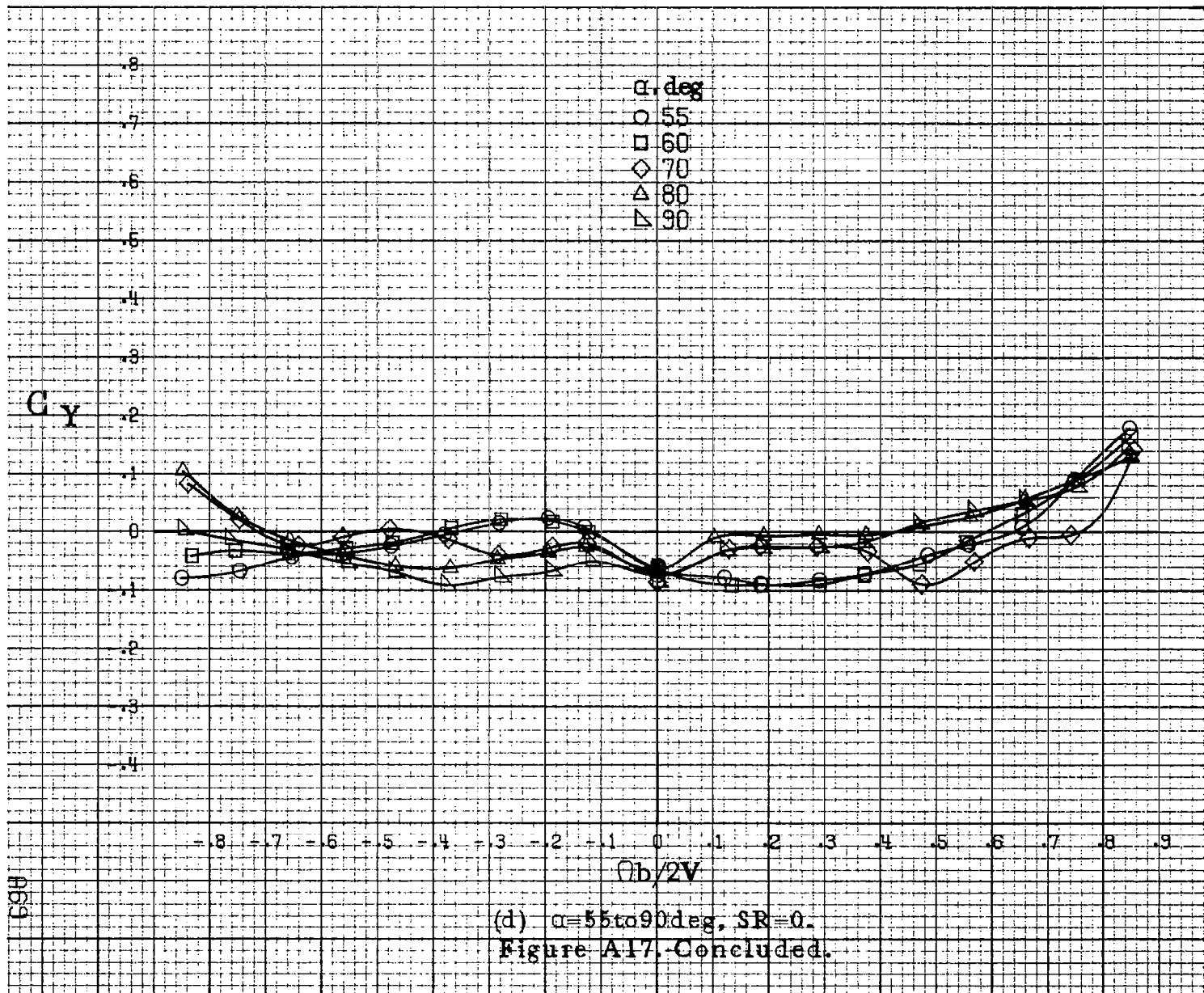


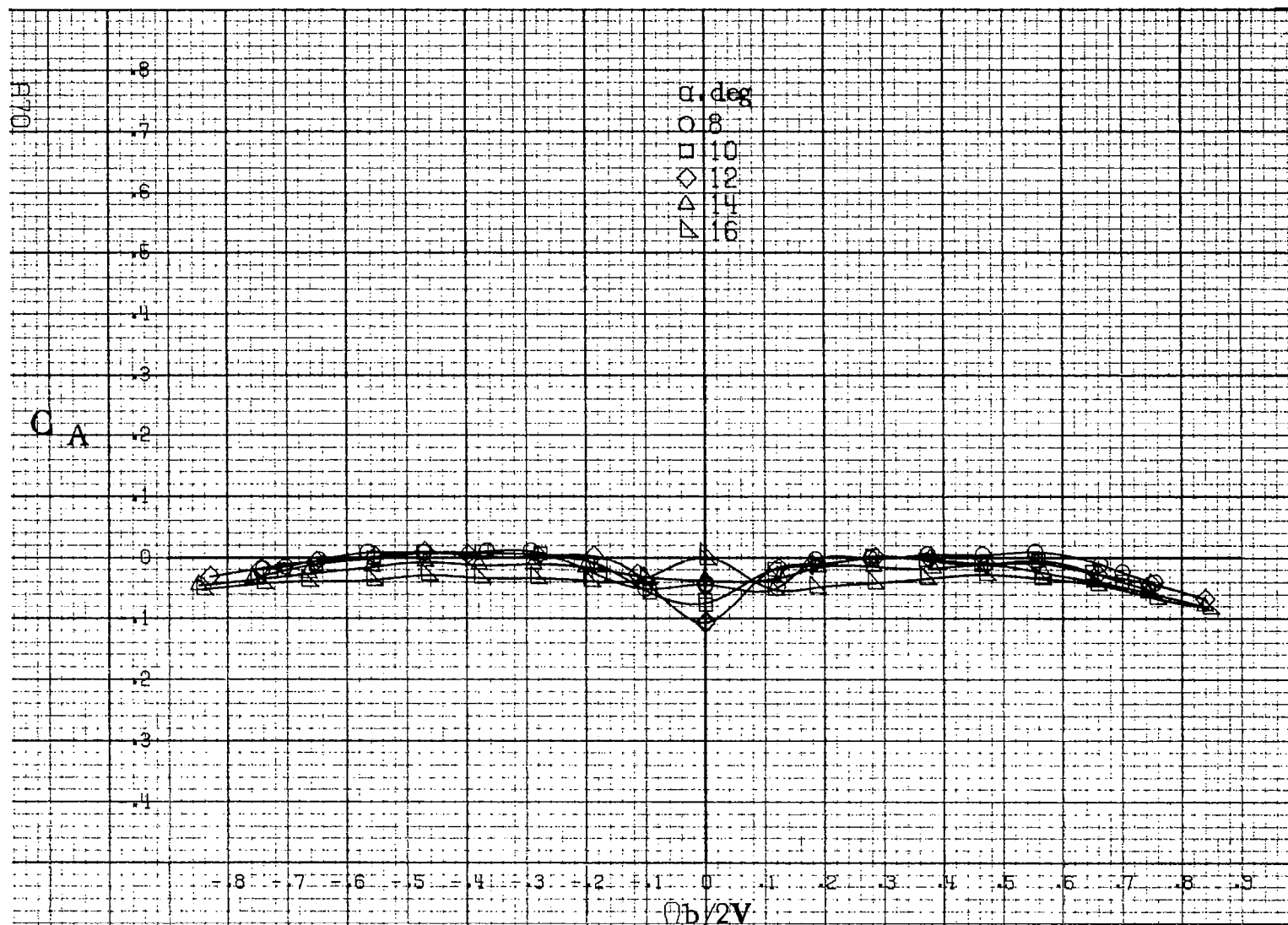
(a) $\alpha = 8$ to 16° , $SR = 91\text{cm}(36\text{in})$.

Figure A17. Effect of rotation rate and angle of attack on side-force coefficient for configuration having outboard LE wing droop. $\delta_e = 0^\circ$, $\delta_a = 0^\circ$, $\delta_r = 0^\circ$, $\beta = 0^\circ$.



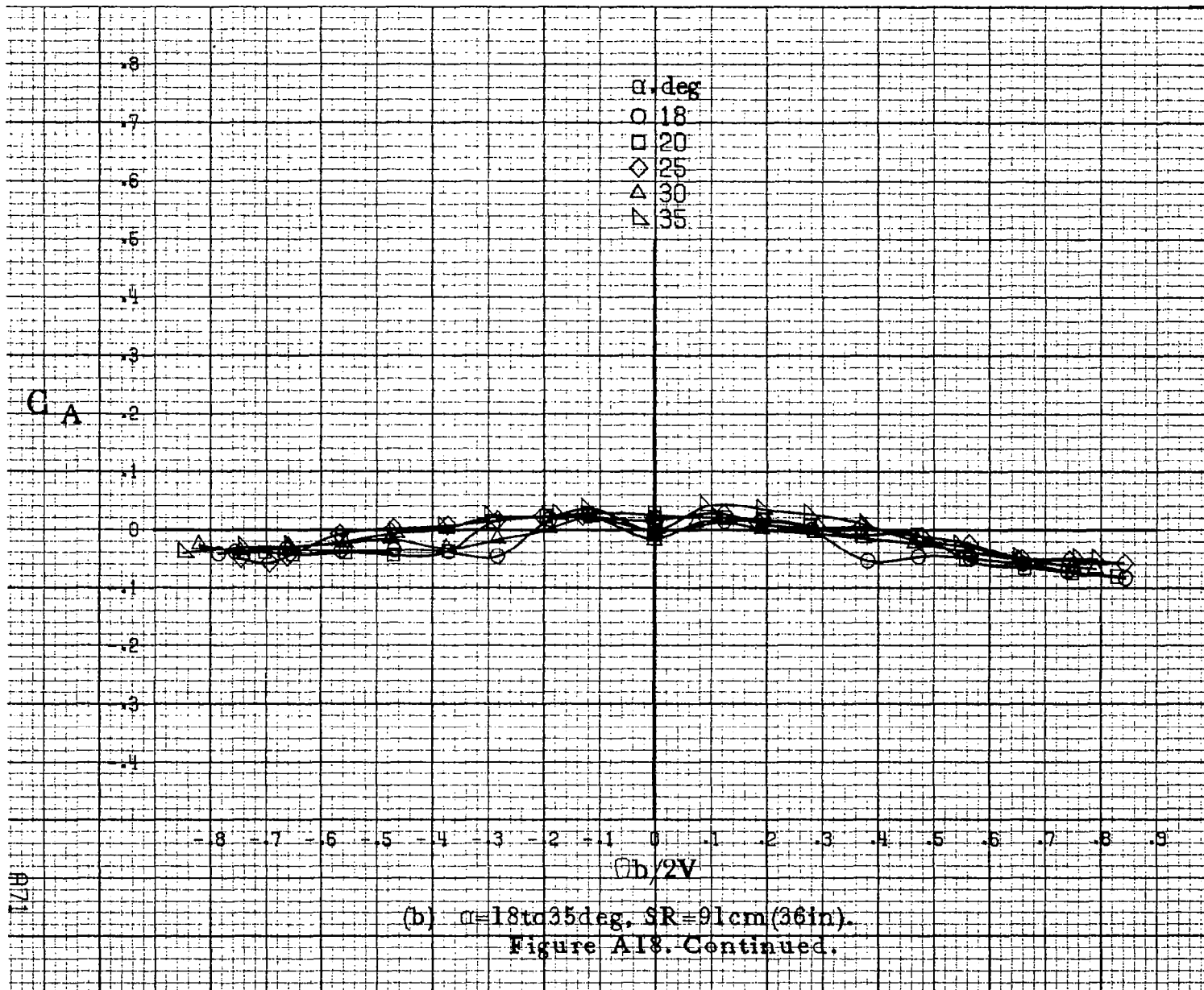


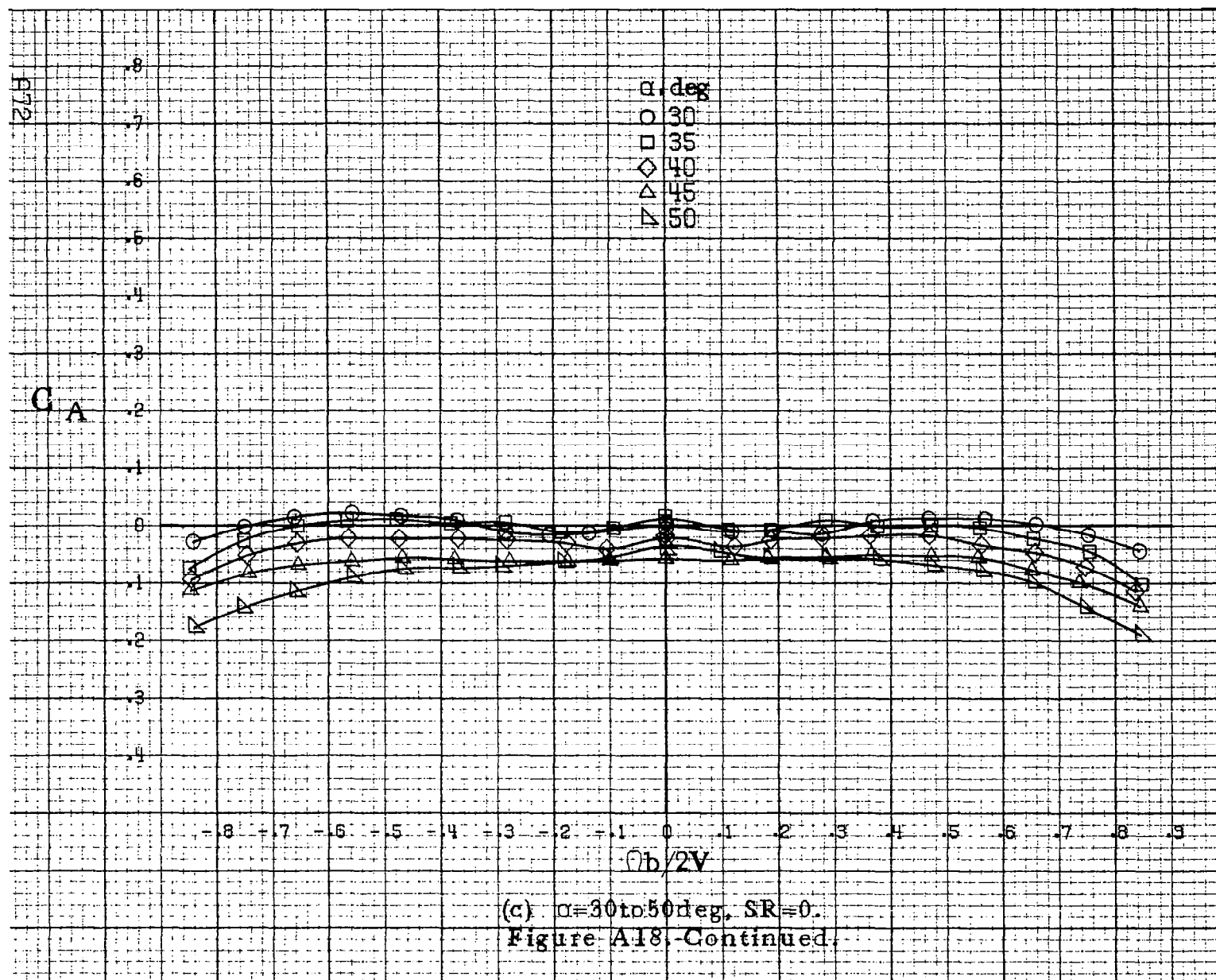


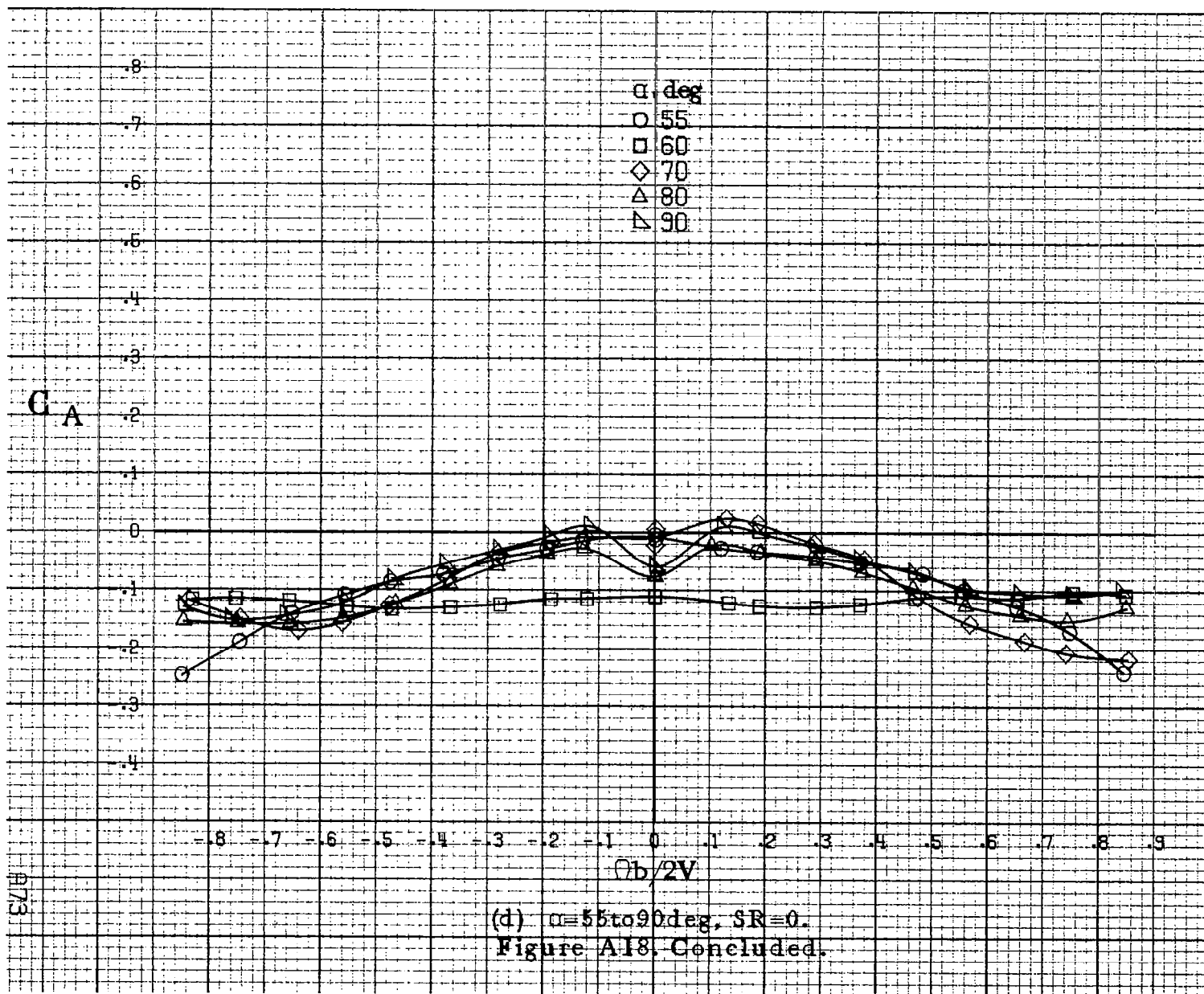


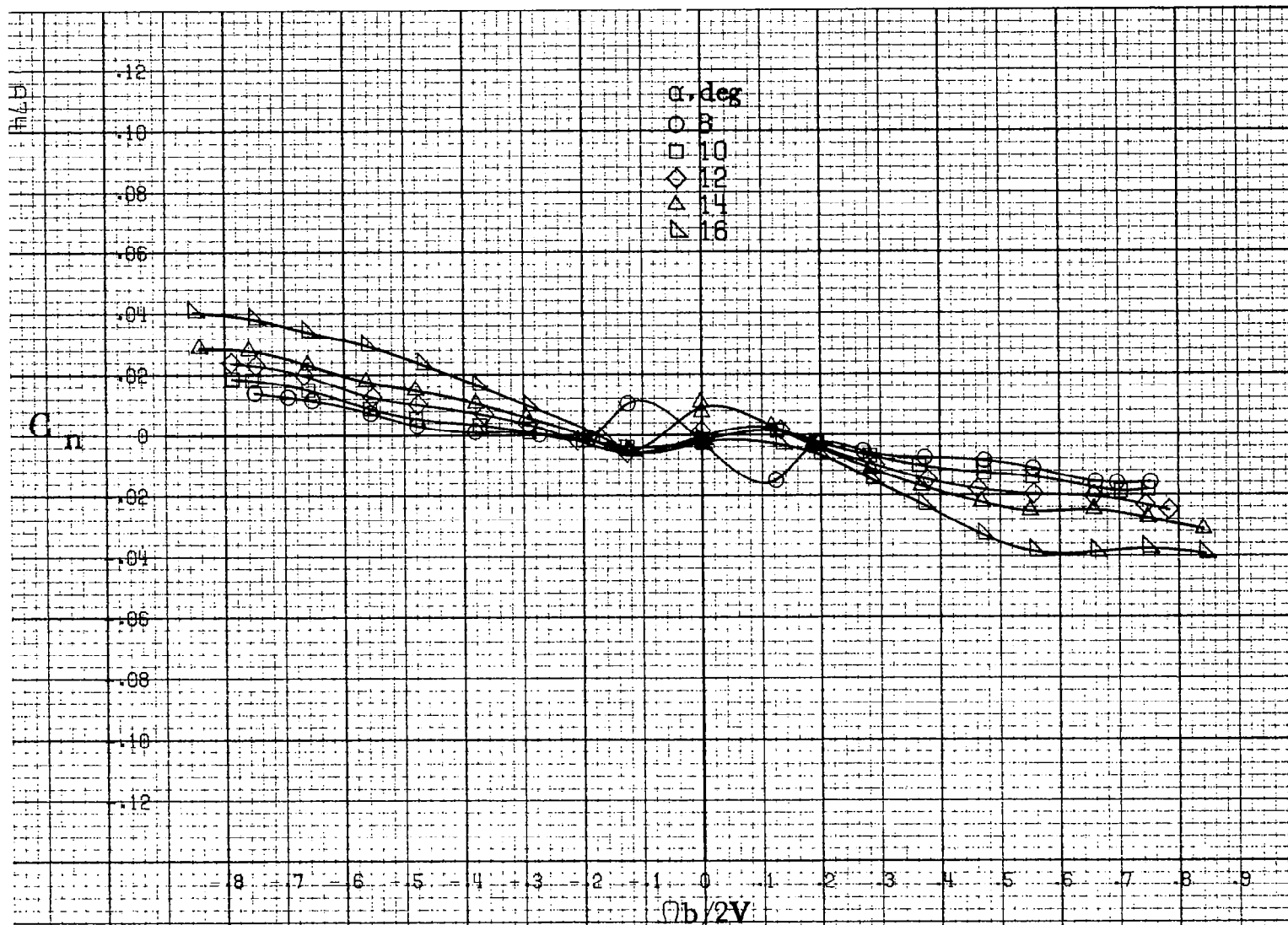
(a) $\alpha=8$ to 16 deg, $SR=91$ cm (36 in).

Figure A18. Effect of rotation rate and angle of attack on axial force coefficient for configuration having outboard LE wing droop. $\delta_e=0^\circ$, $\delta_a=0^\circ$, $\delta_r=0^\circ$, $B=0^\circ$.



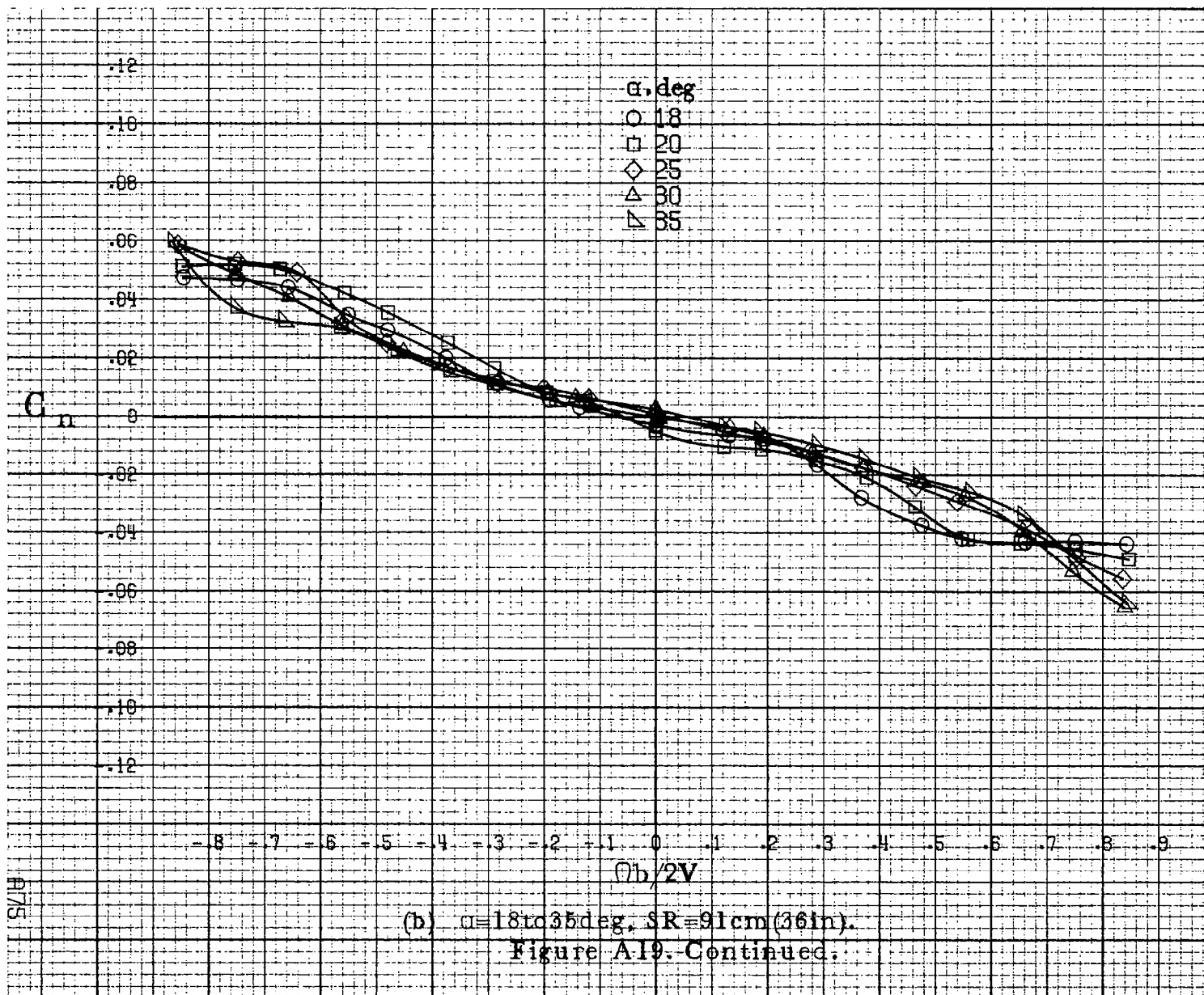


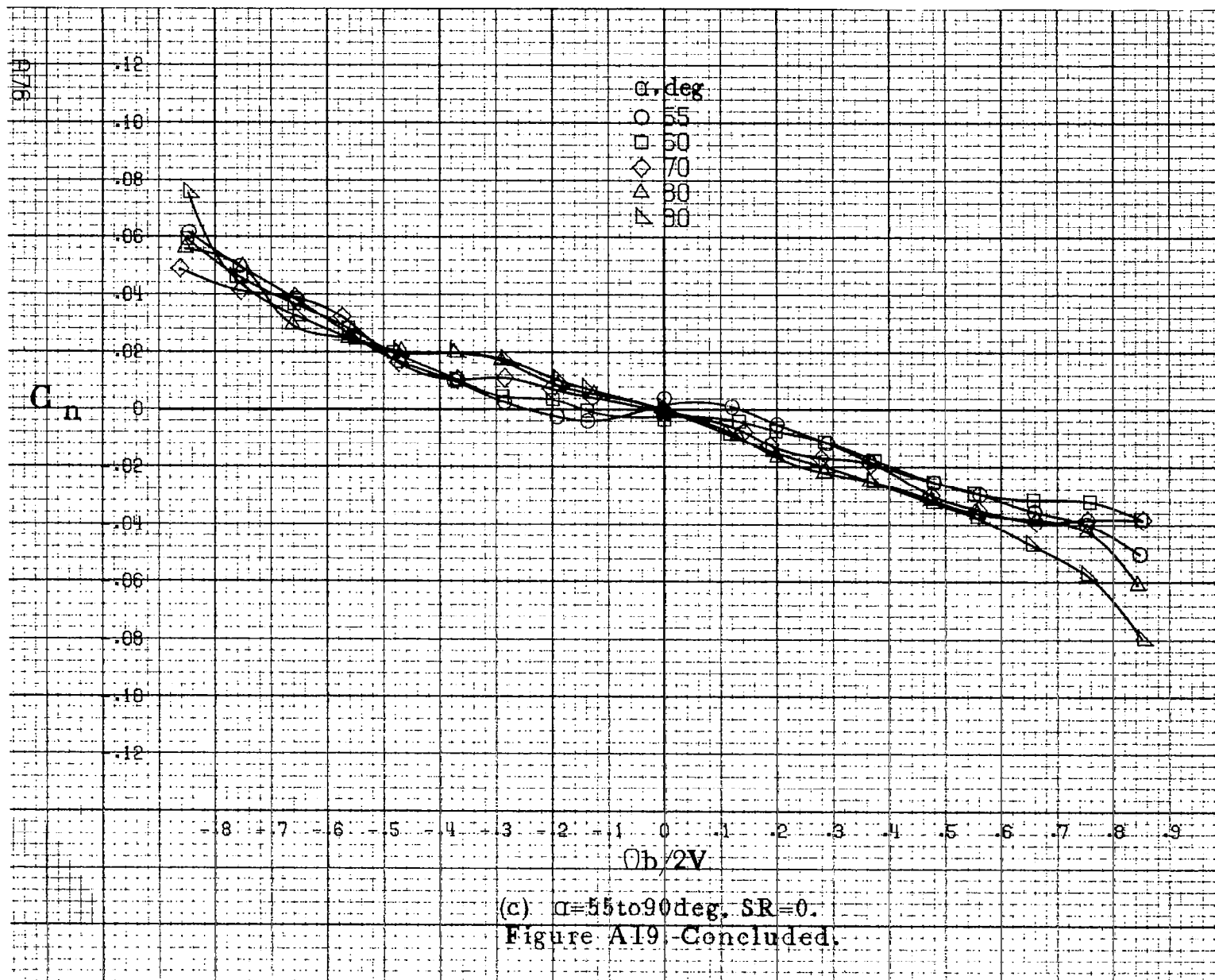


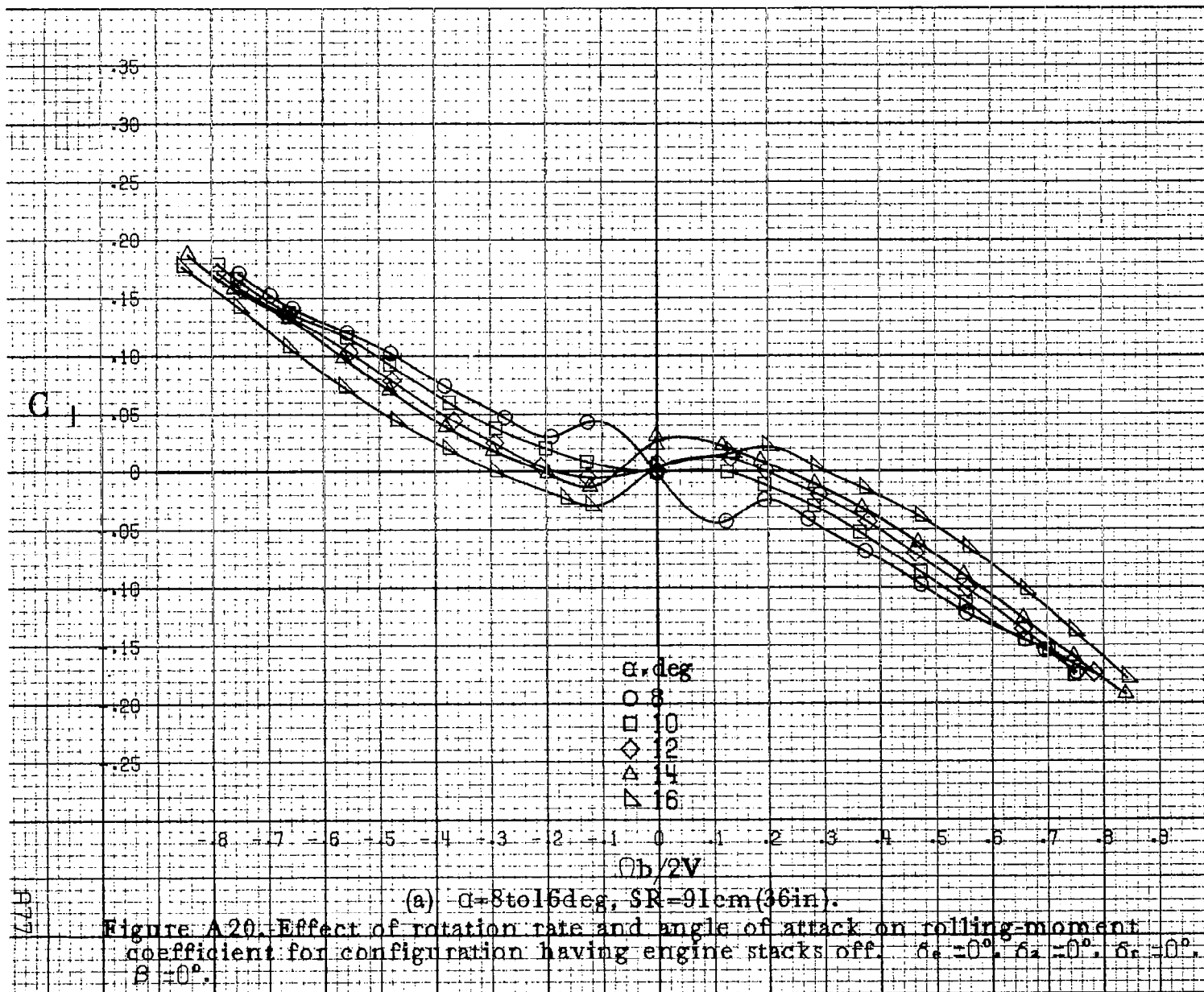


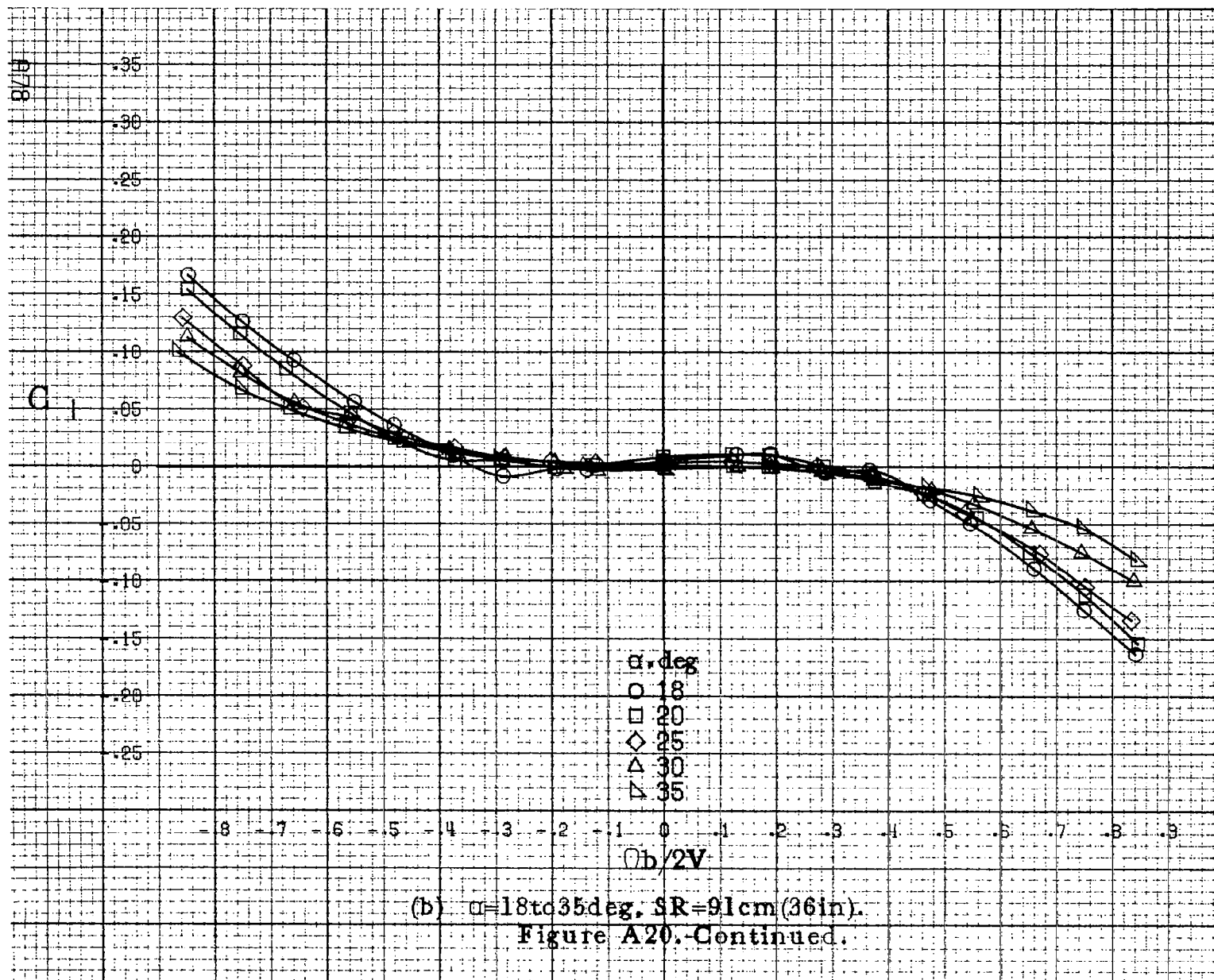
(a) $\alpha=8$ to 16° , $SR=91\text{cm}(36\text{in})$.

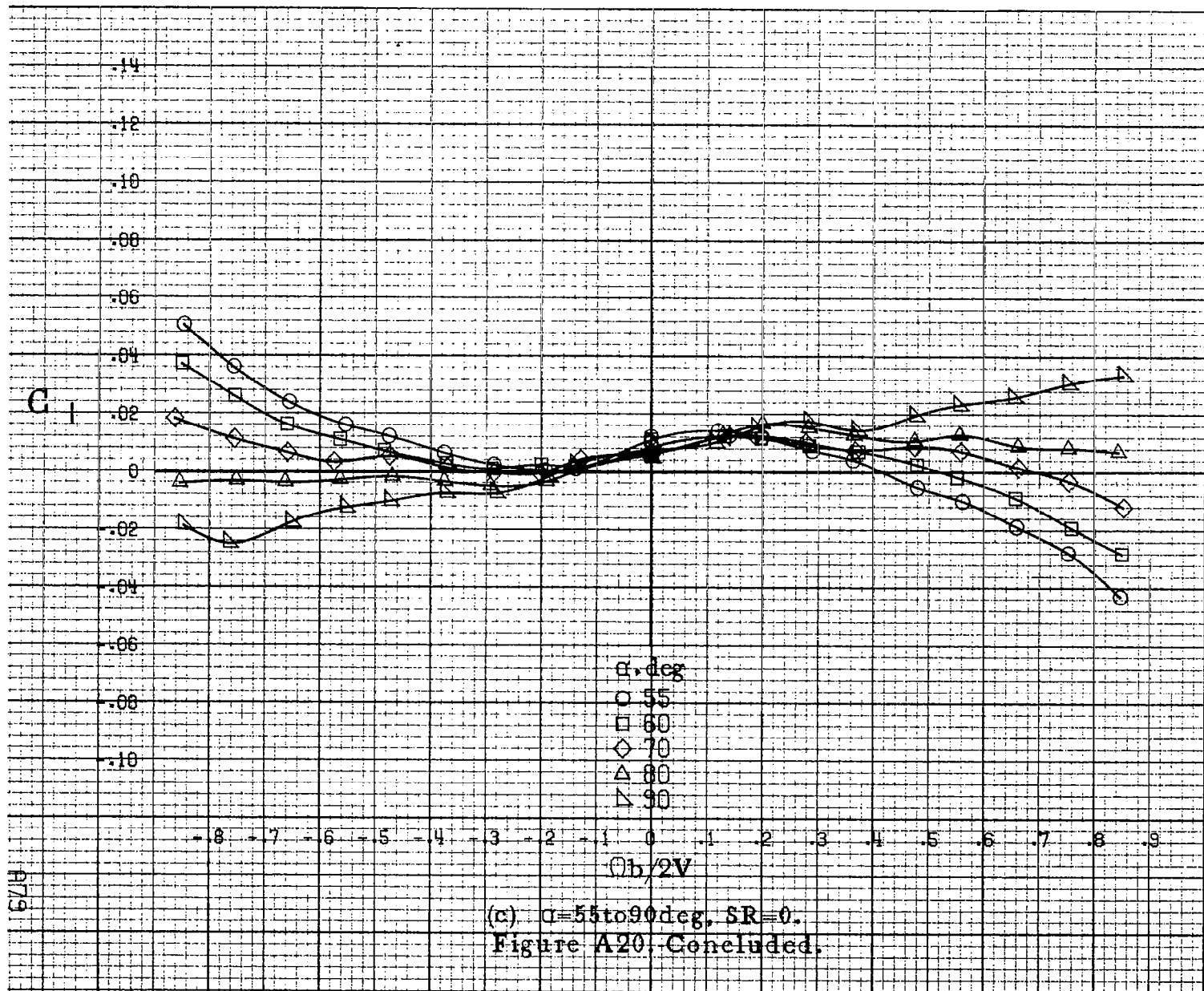
Figure A19: Effect of rotation rate and angle of attack on yawing moment coefficient for configuration having engine stacks off. $\delta_a=0^\circ$, $\delta_s=0^\circ$, $\delta_r=0^\circ$, $\beta=0^\circ$.

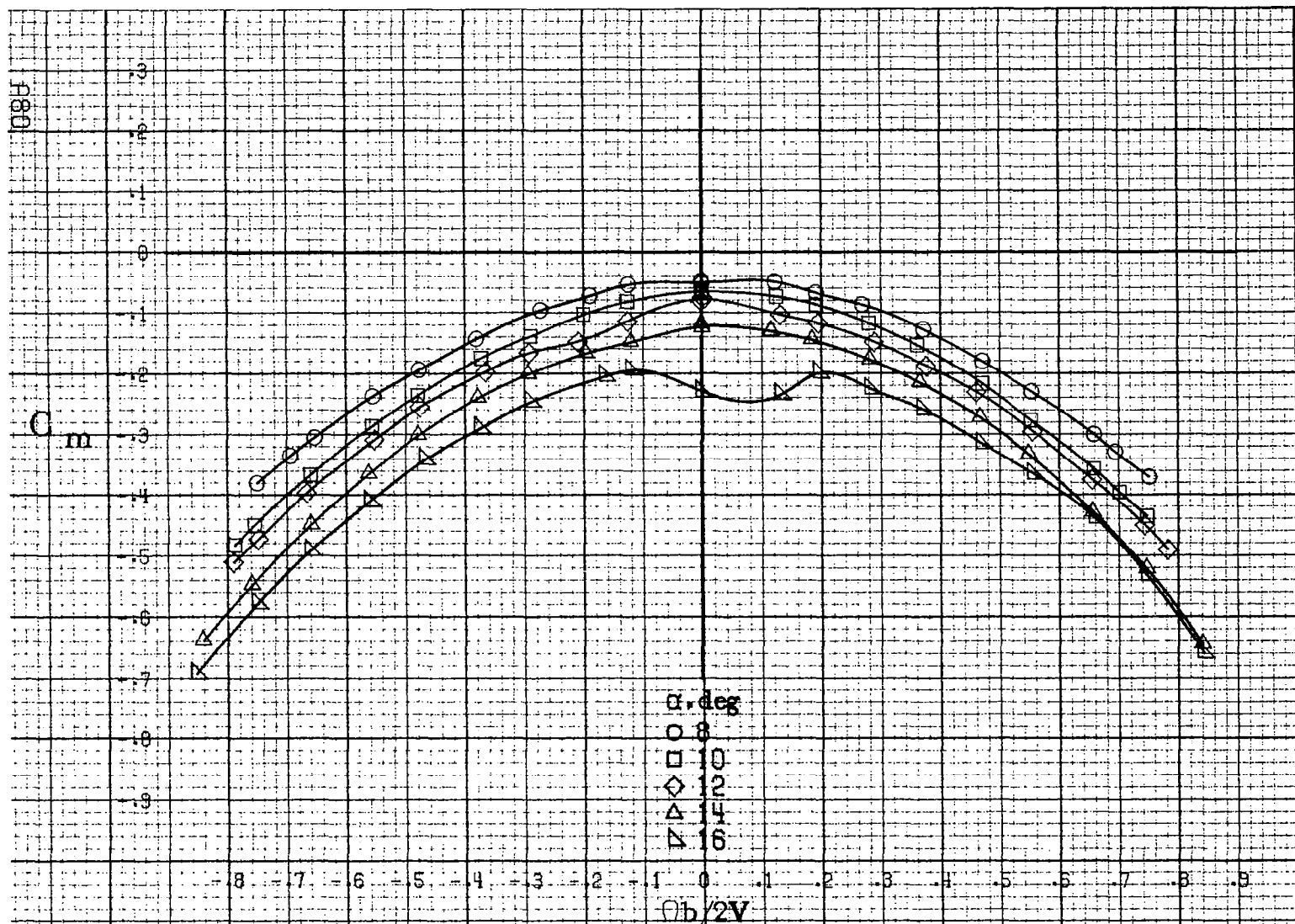






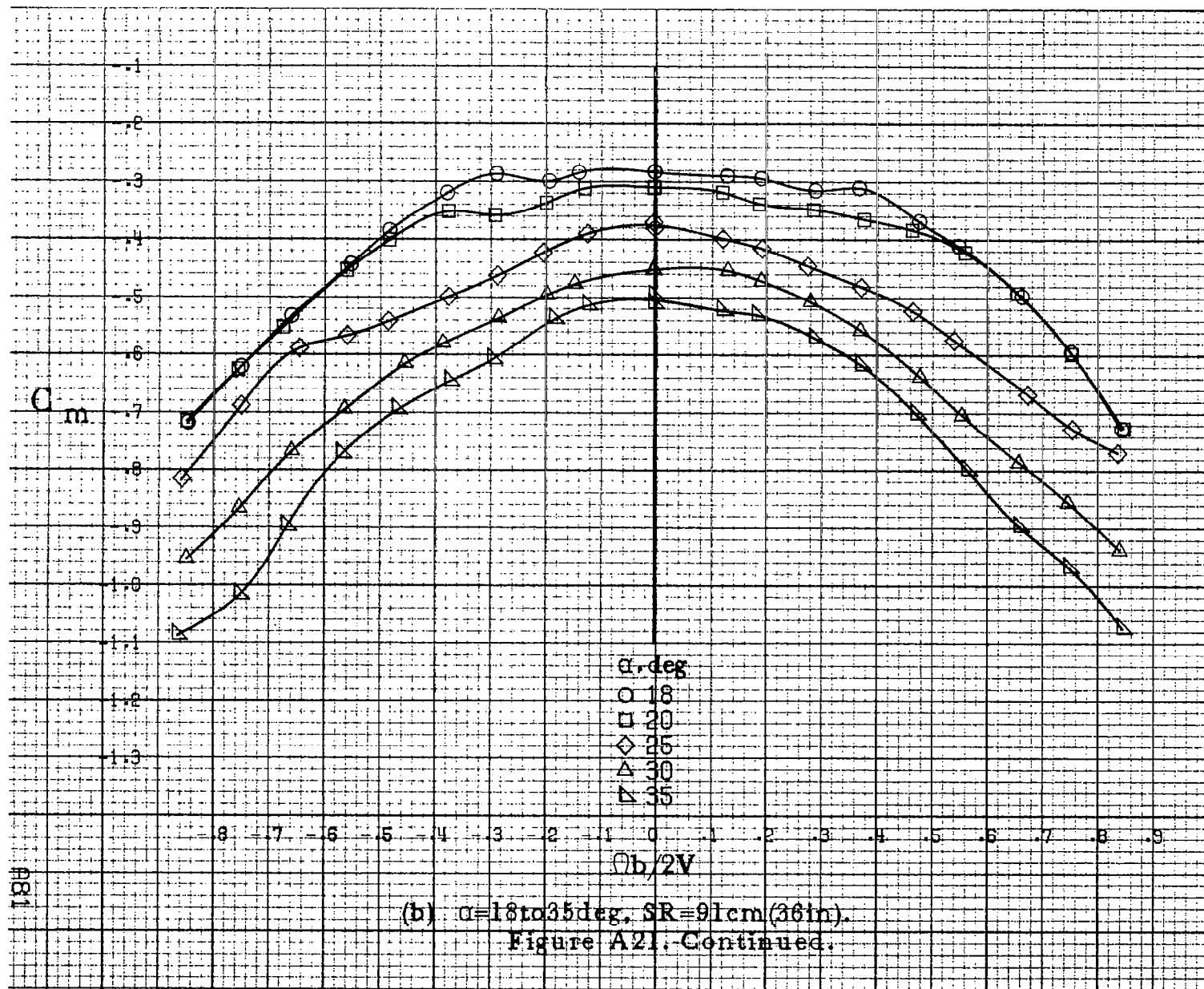


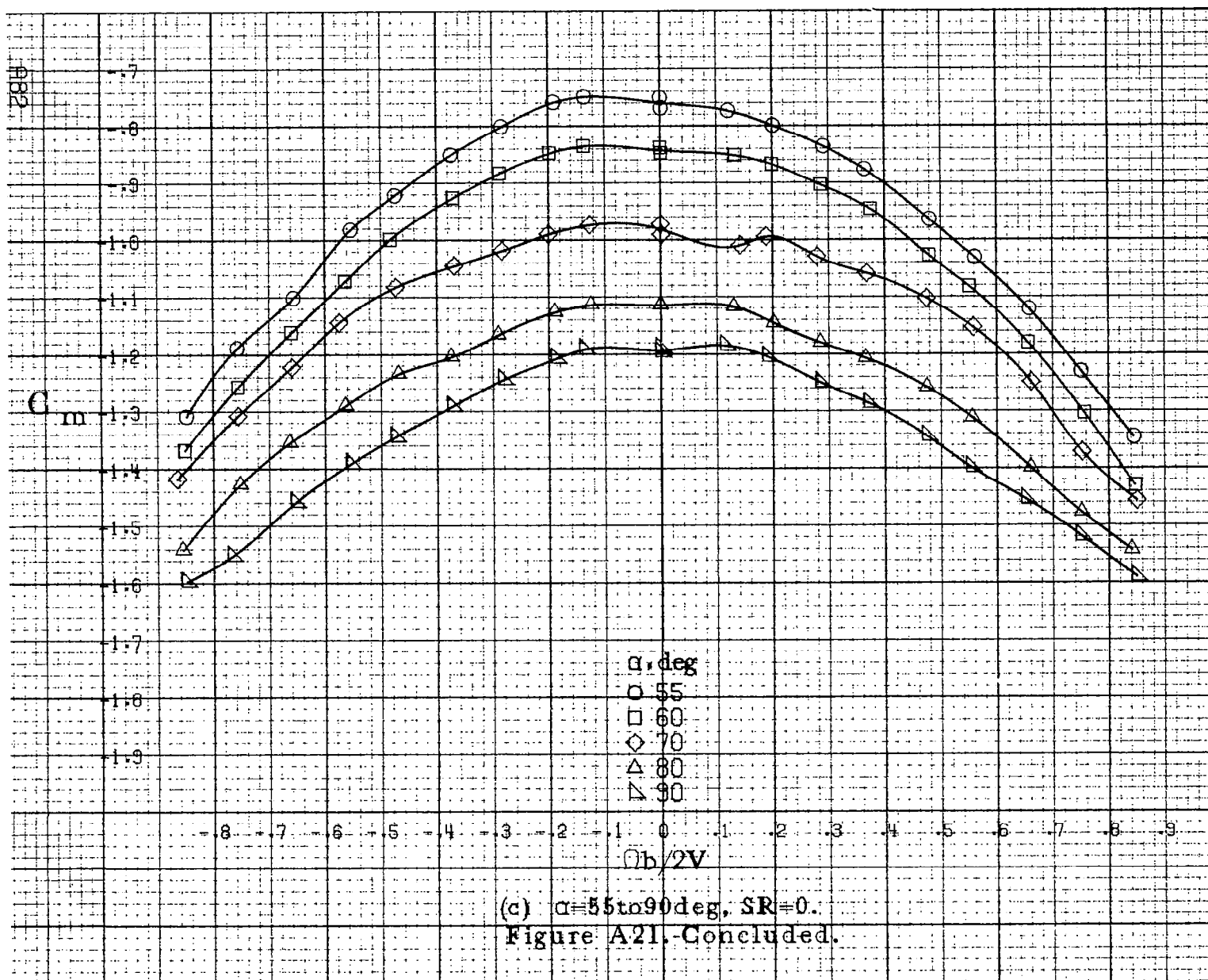


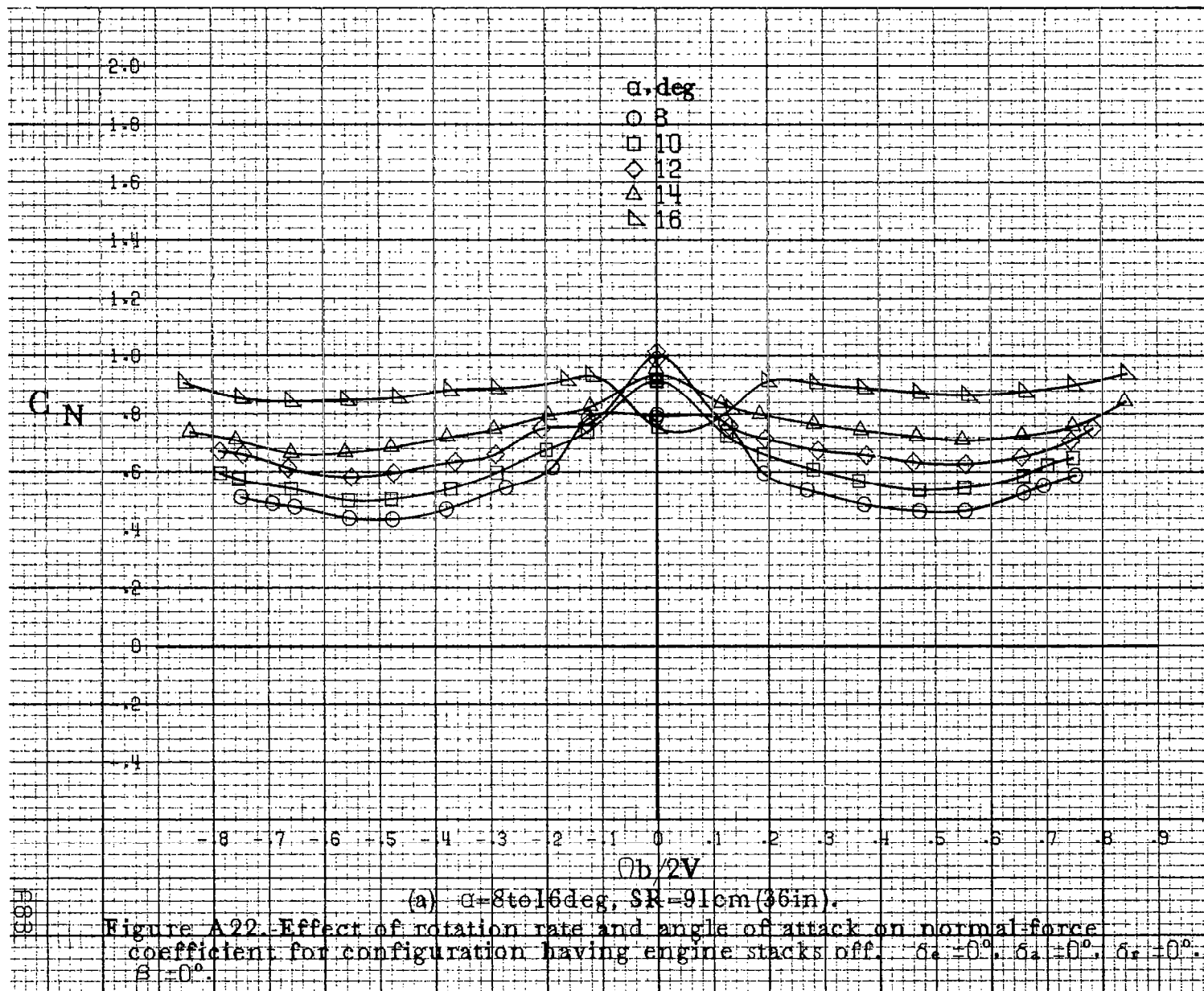


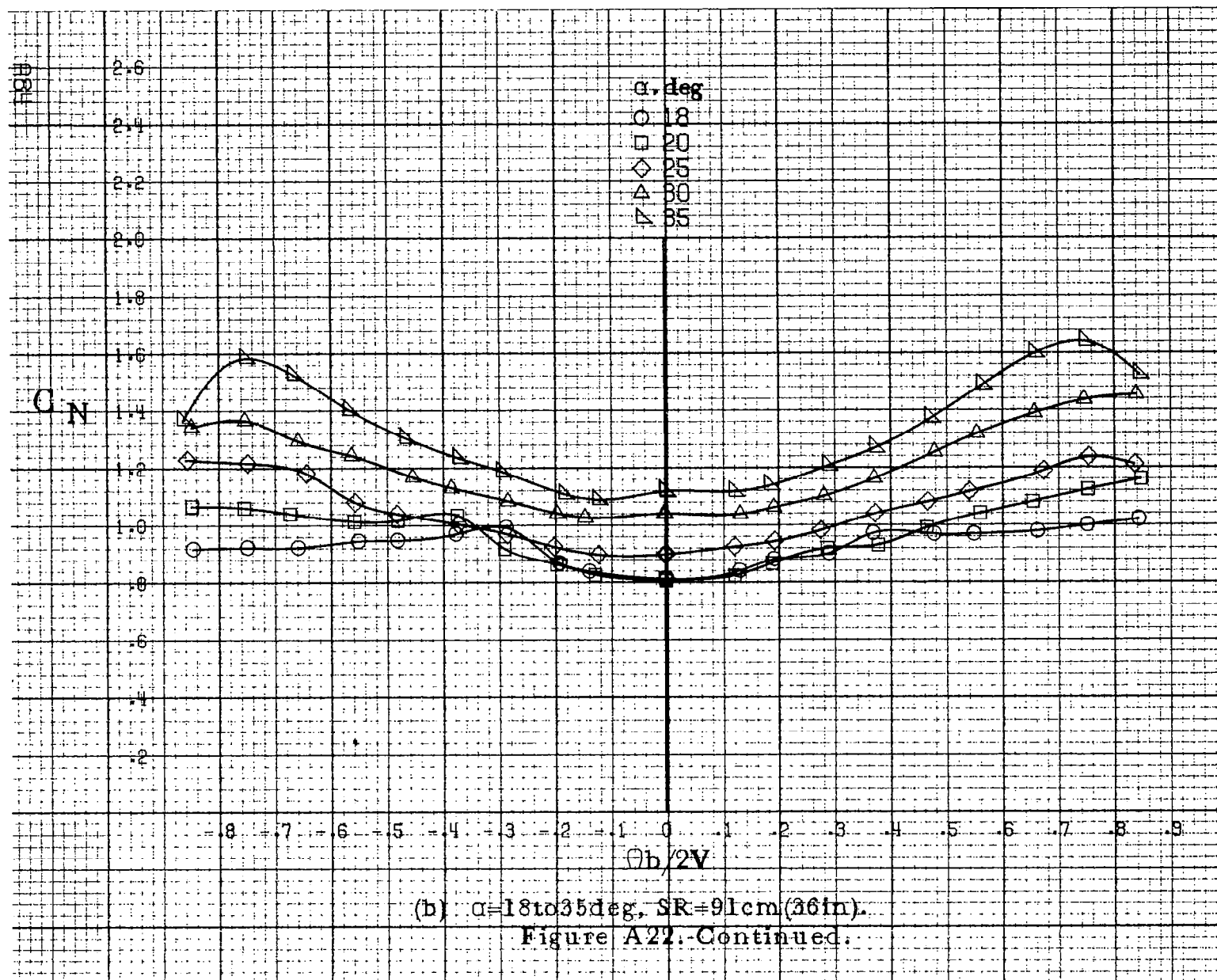
(a) $\alpha = 8$ to 16° , $SR = 91 \text{ cm (36 in)}$.

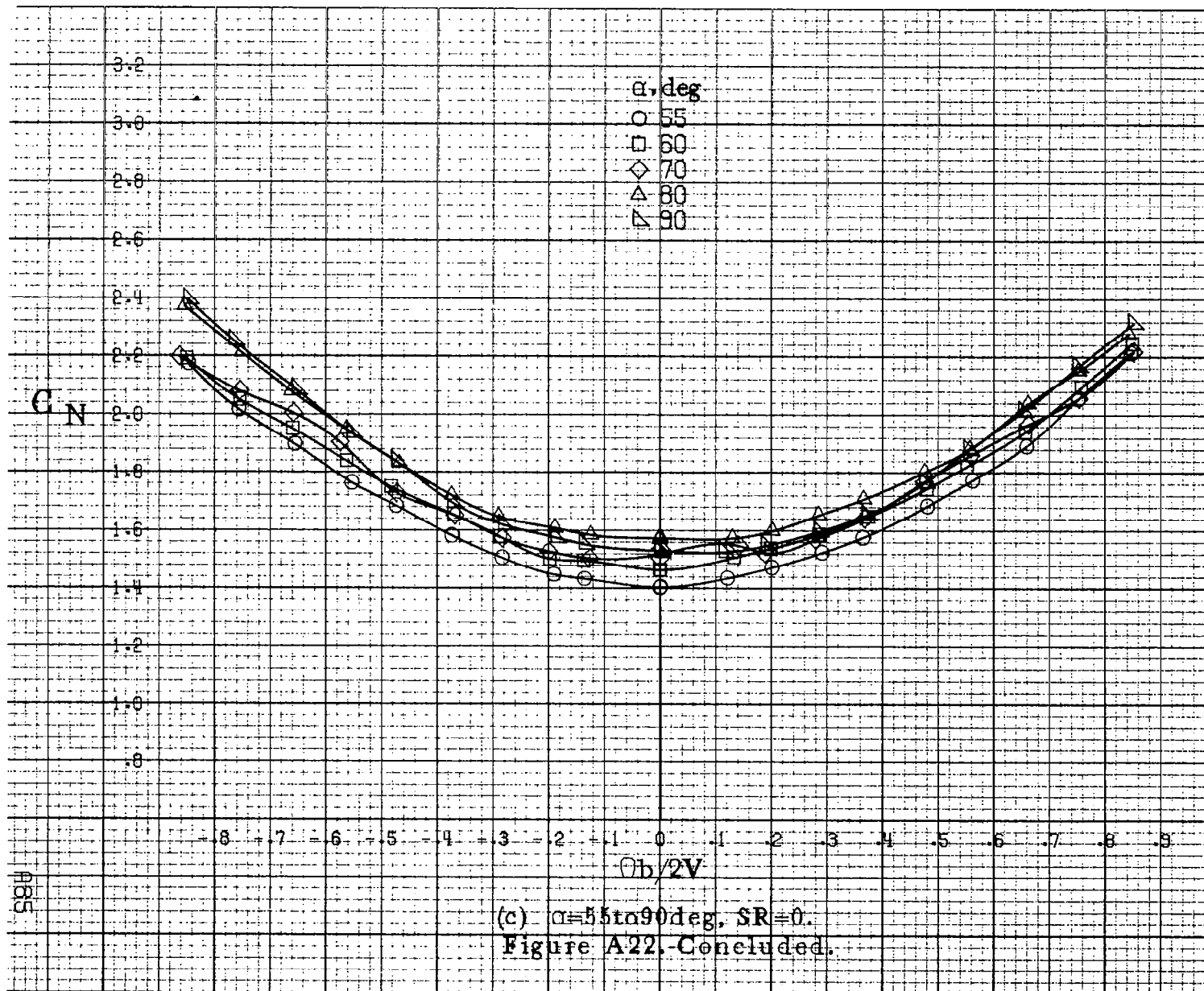
Figure A21. Effect of rotation rate and angle of attack on pitching moment coefficient for configuration having engine stacks off. $\delta_a = 0^\circ$, $\delta_s = 0^\circ$, $\delta_z = 0^\circ$, $\beta = 0^\circ$.

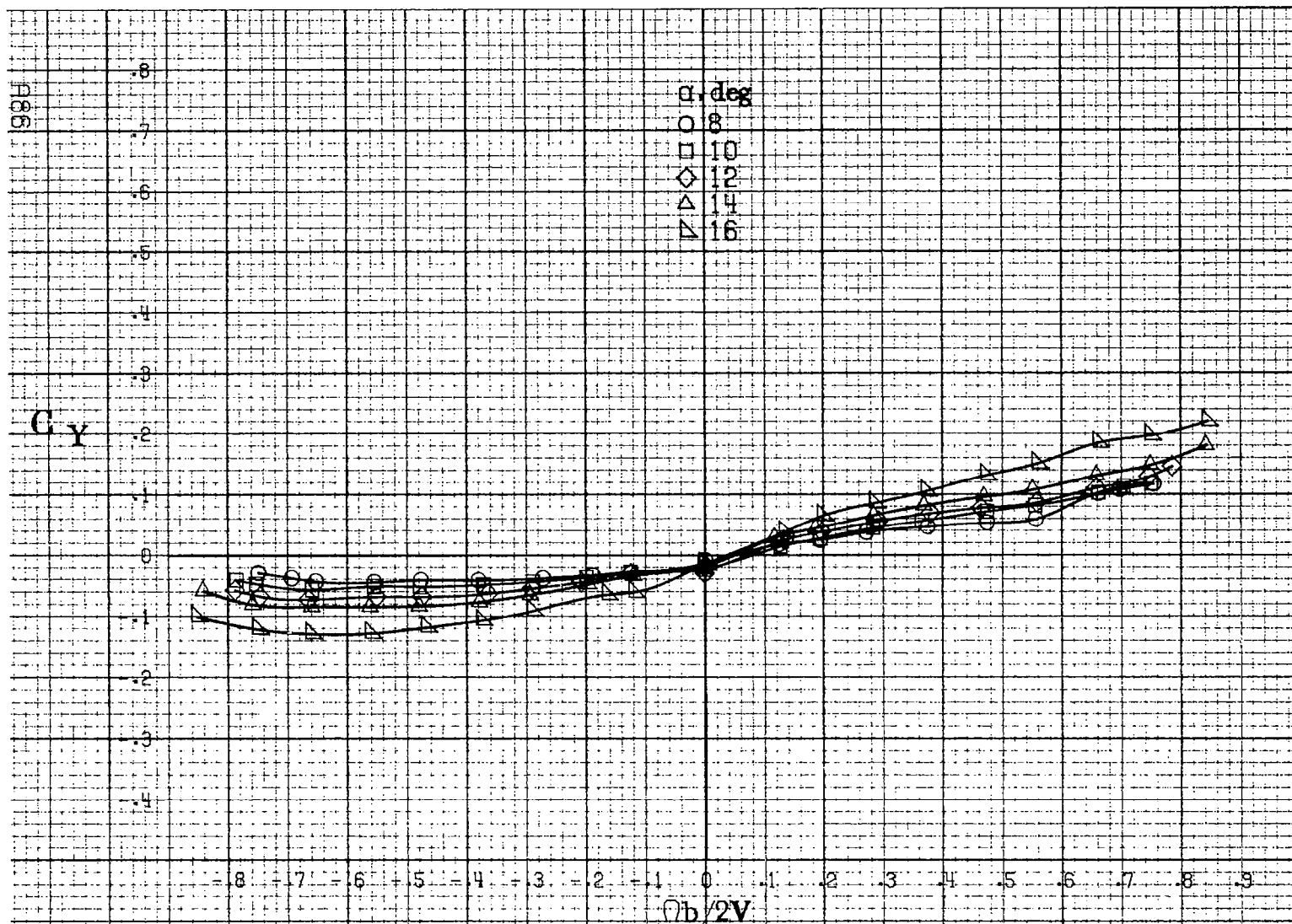






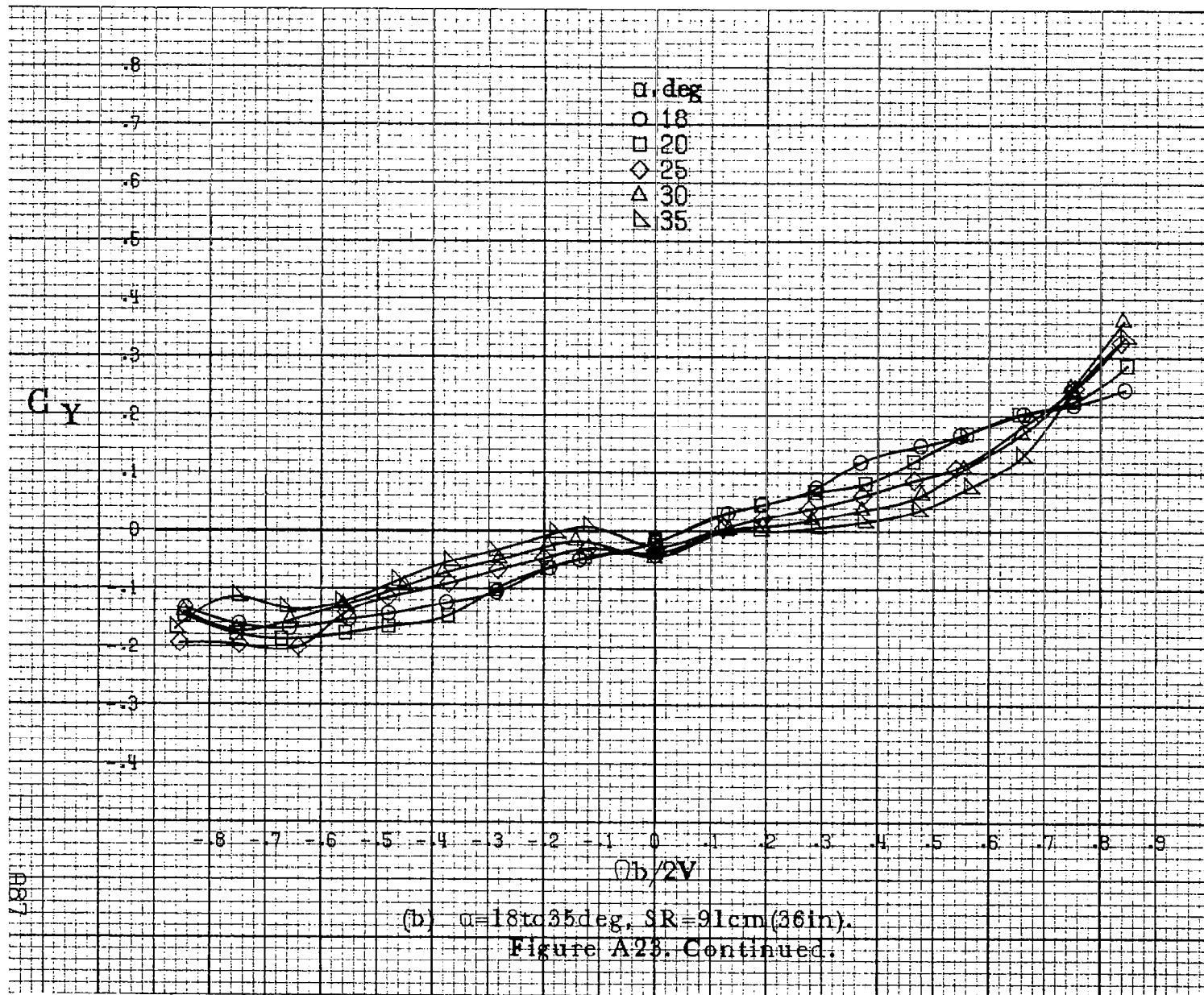


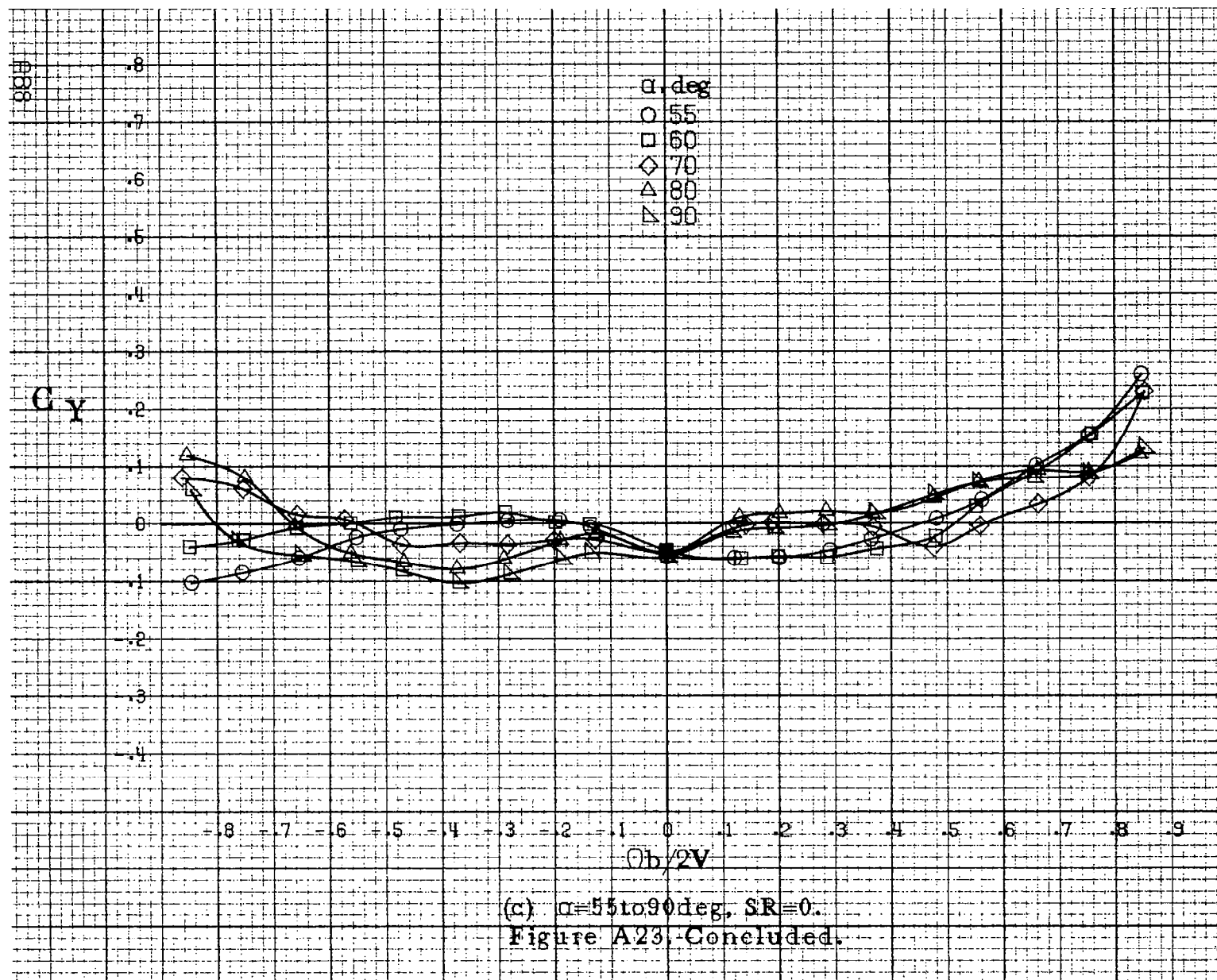


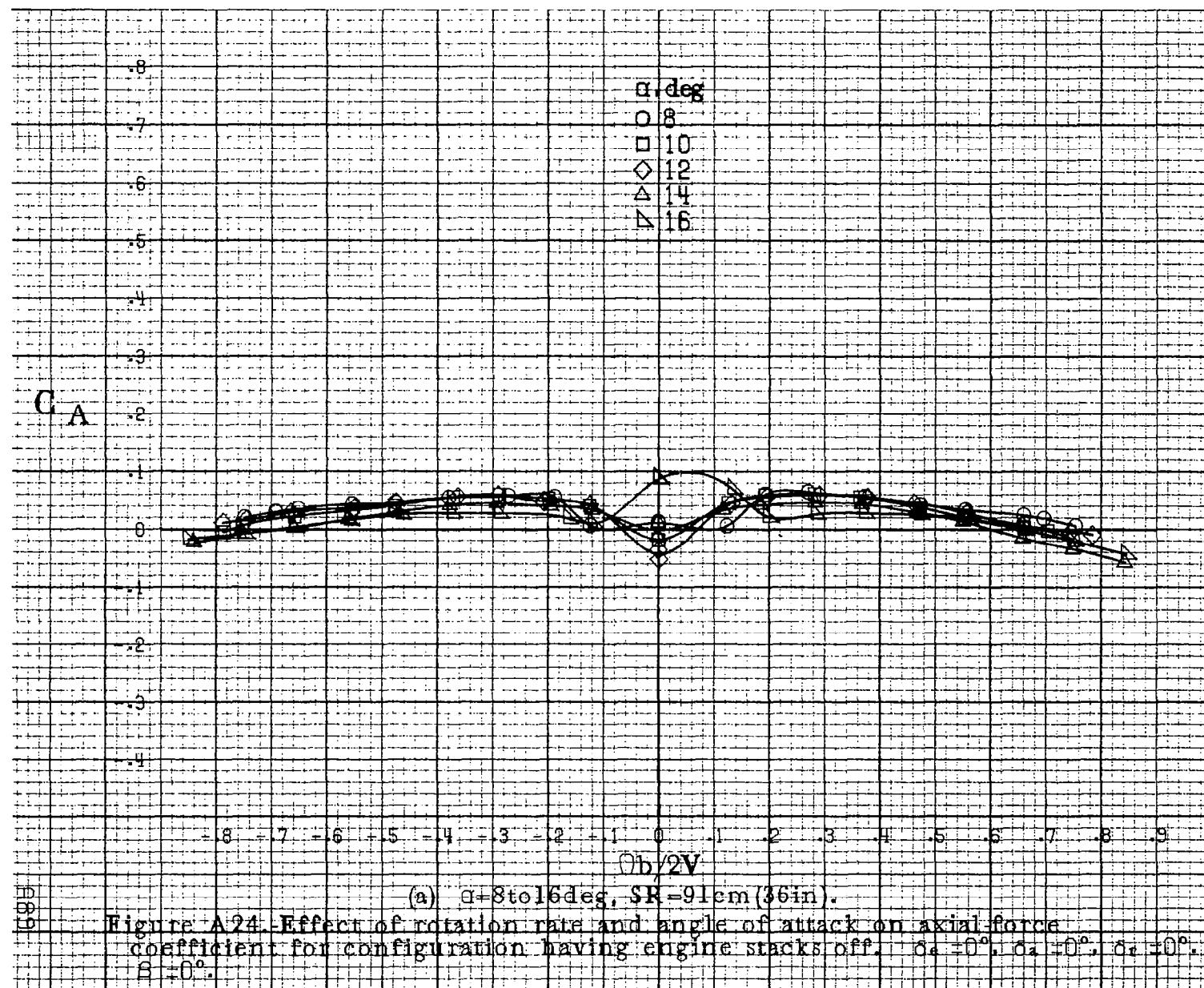


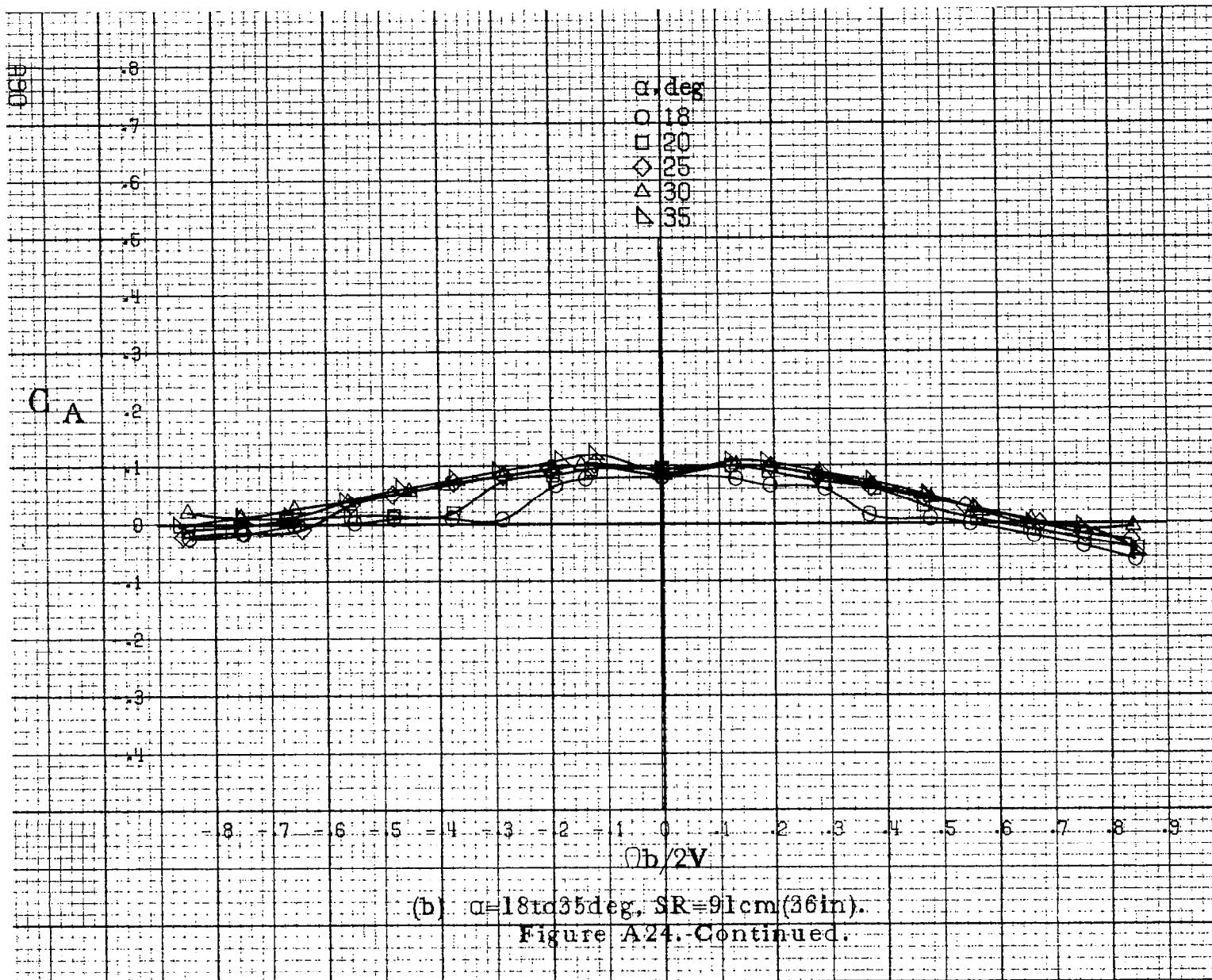
(a) $\alpha = 8 \text{ to } 16 \text{ deg}$, $SR = 91 \text{ cm (36 in)}$.

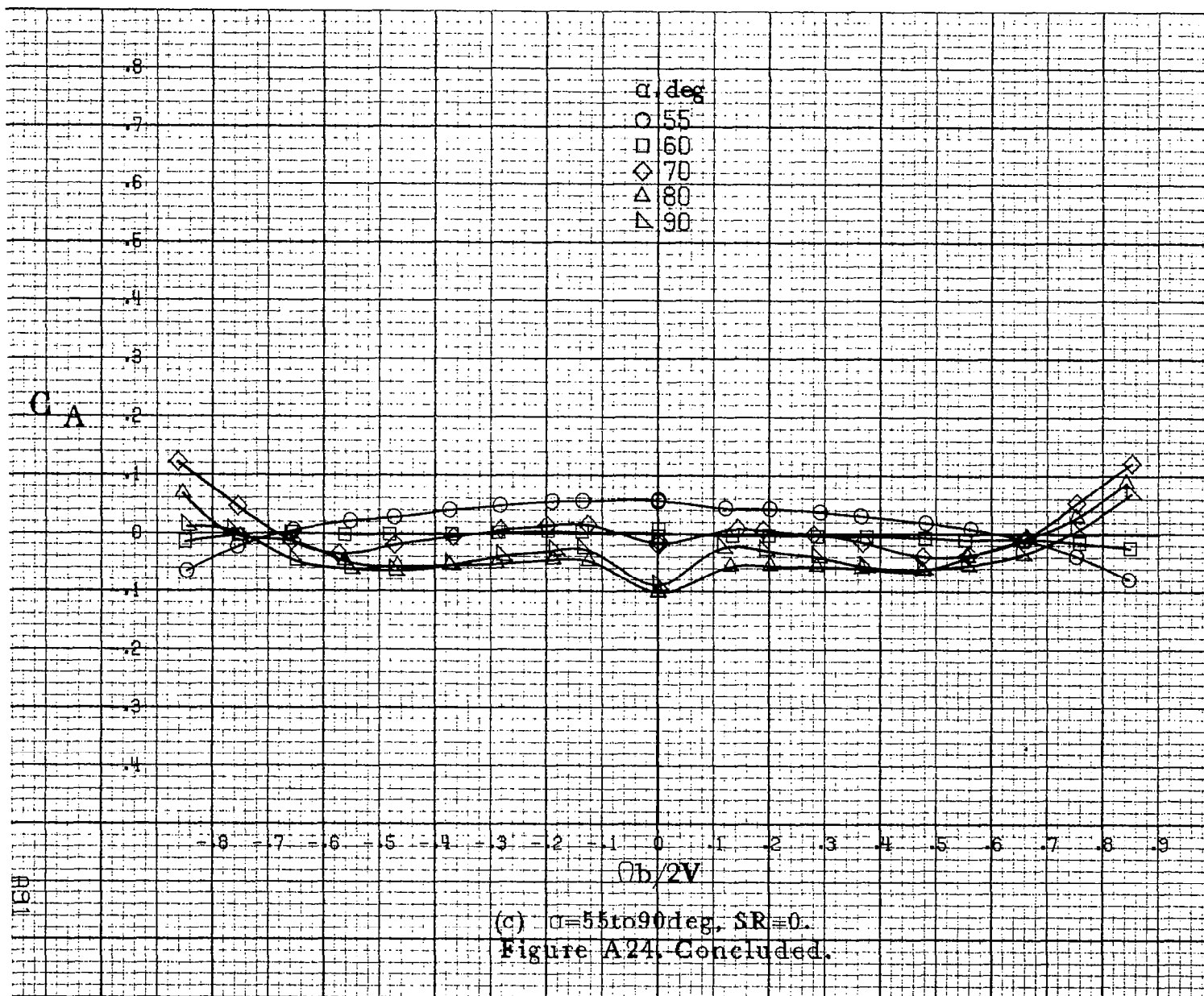
Figure A23. Effect of rotation rate and angle of attack on side force coefficient for configuration having engine stacks off. $\delta_e = 0^\circ$, $\delta_a = 0^\circ$, $\delta_r = 0^\circ$, $\beta = 0^\circ$.

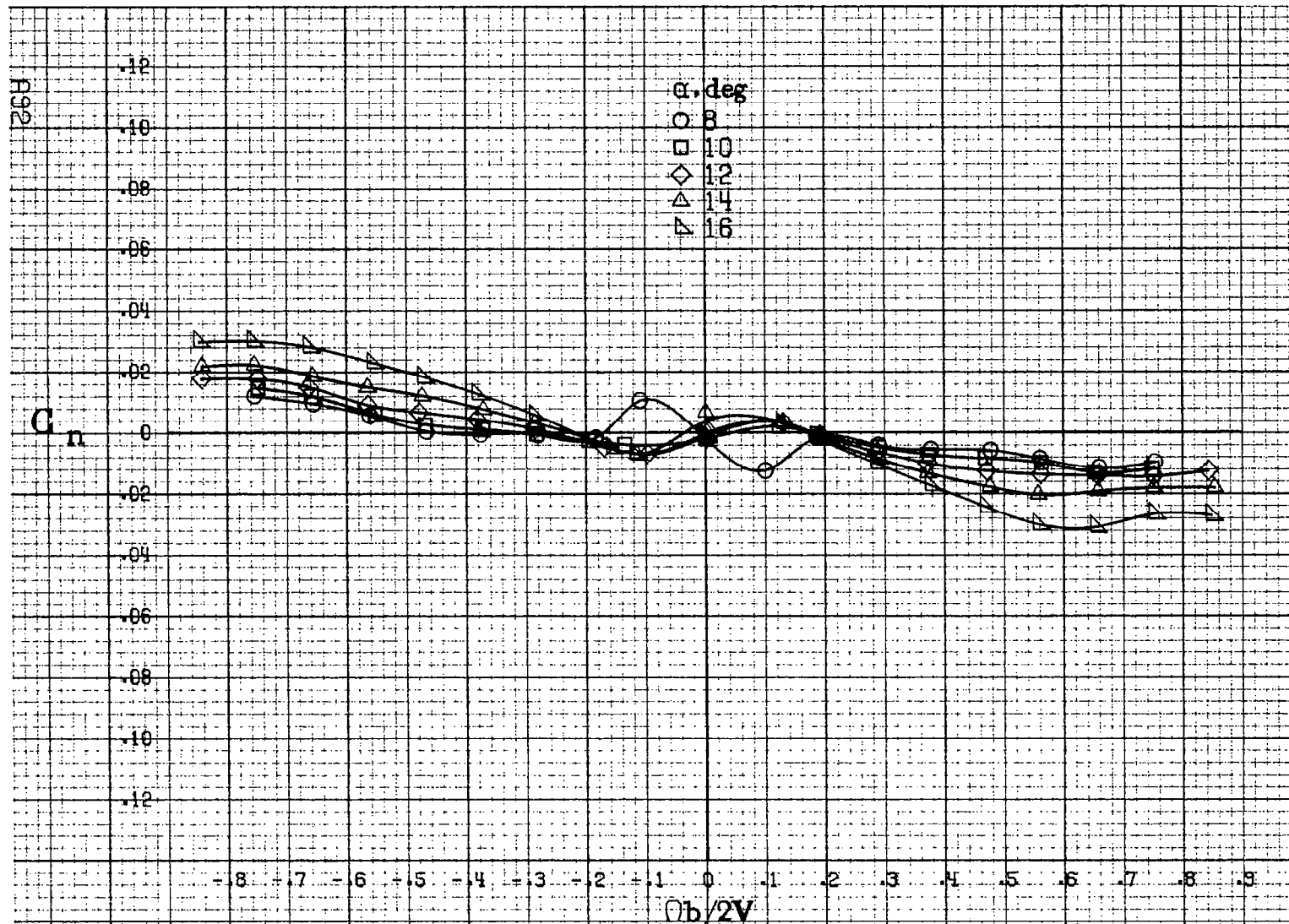






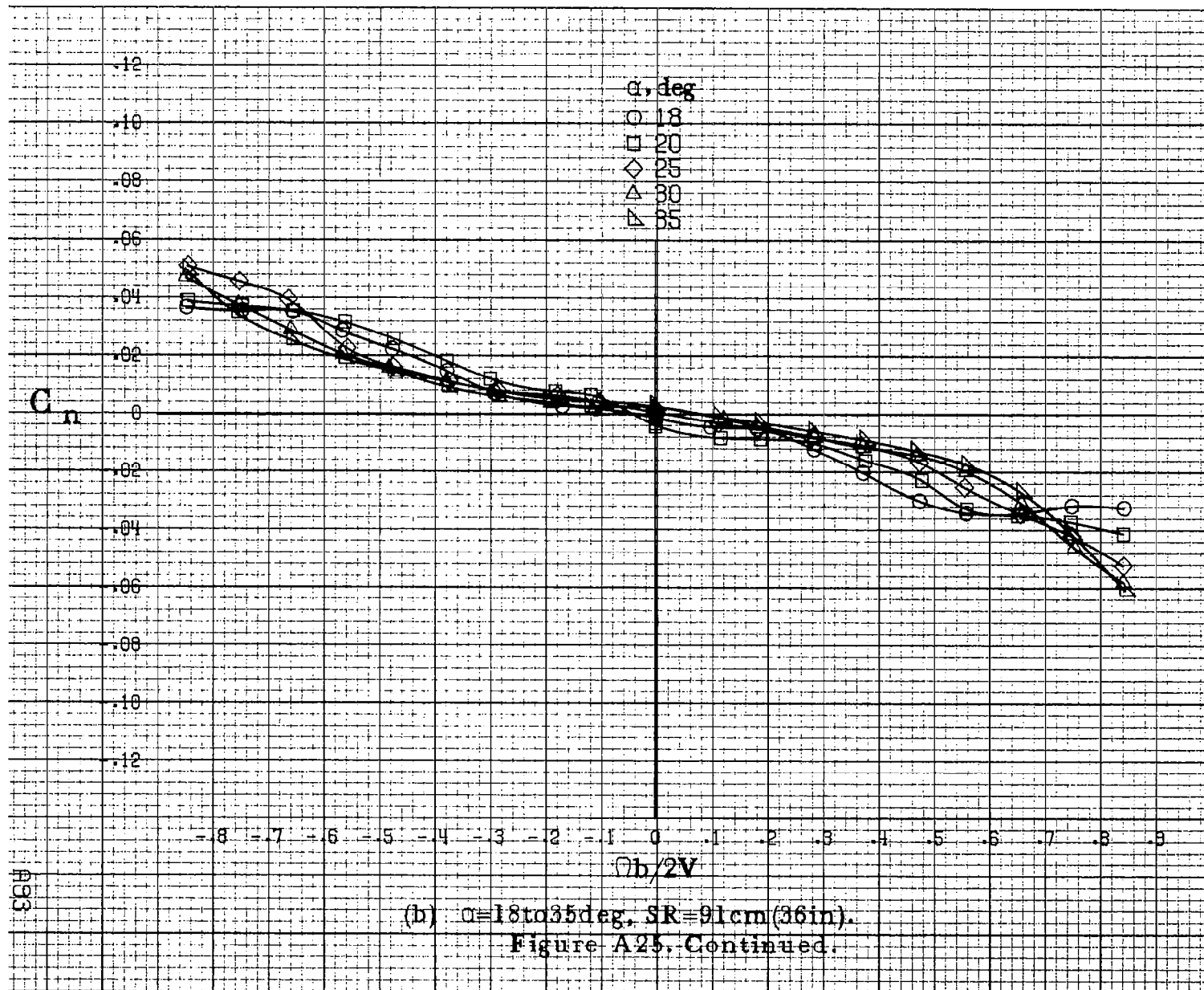


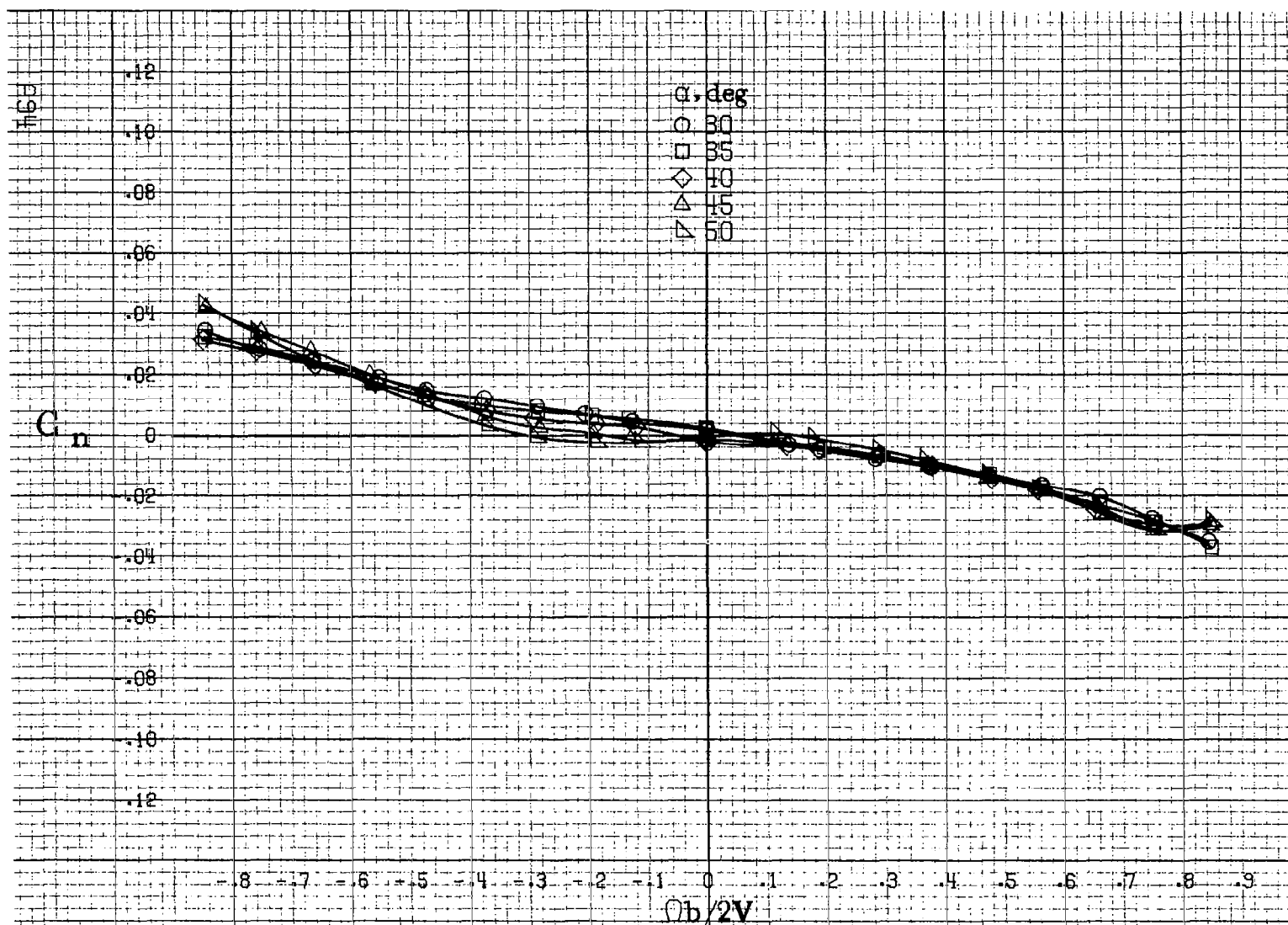




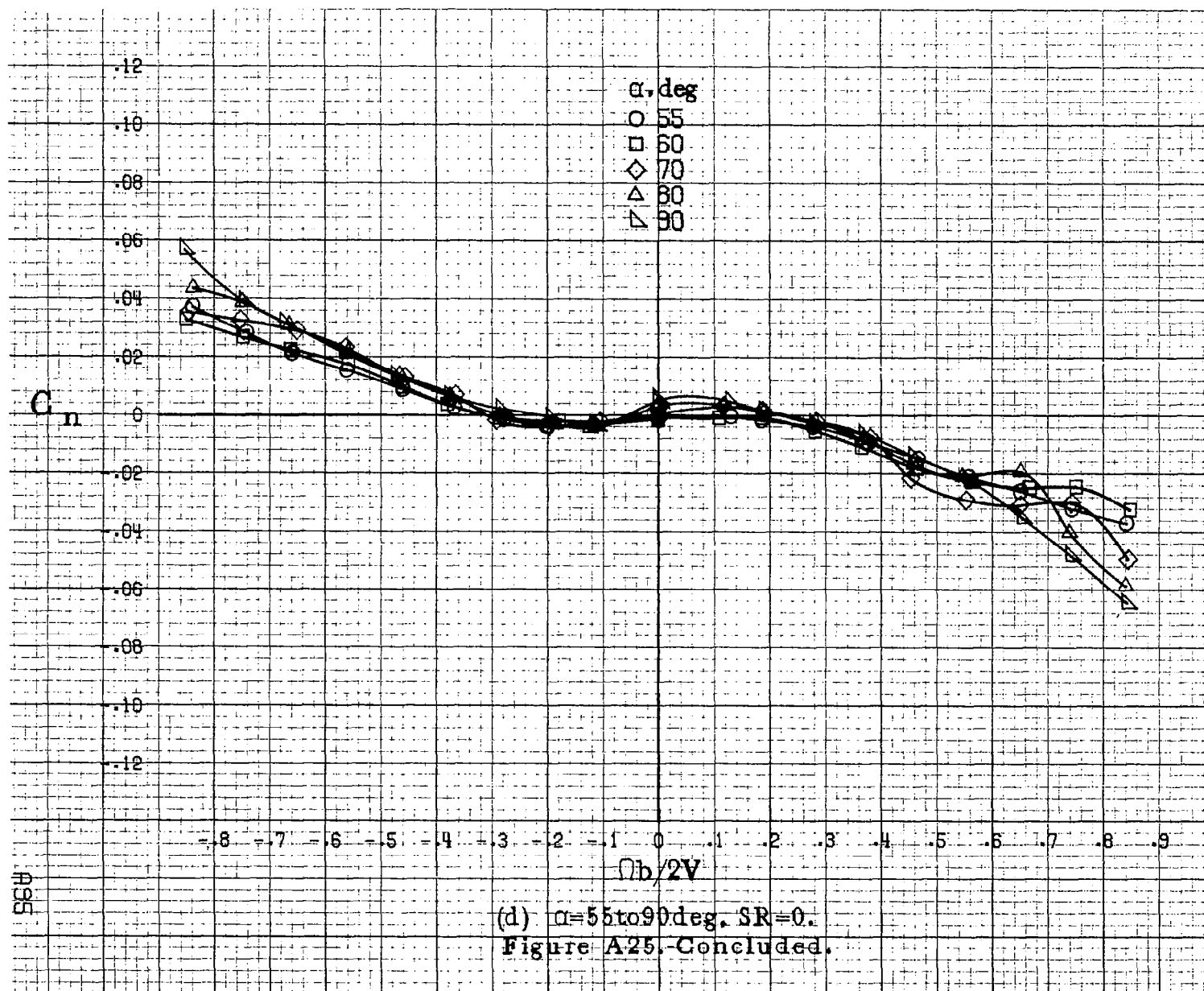
(a) $\alpha=8\text{ to }16\text{deg}$, $SR=91\text{cm}(36\text{in})$.

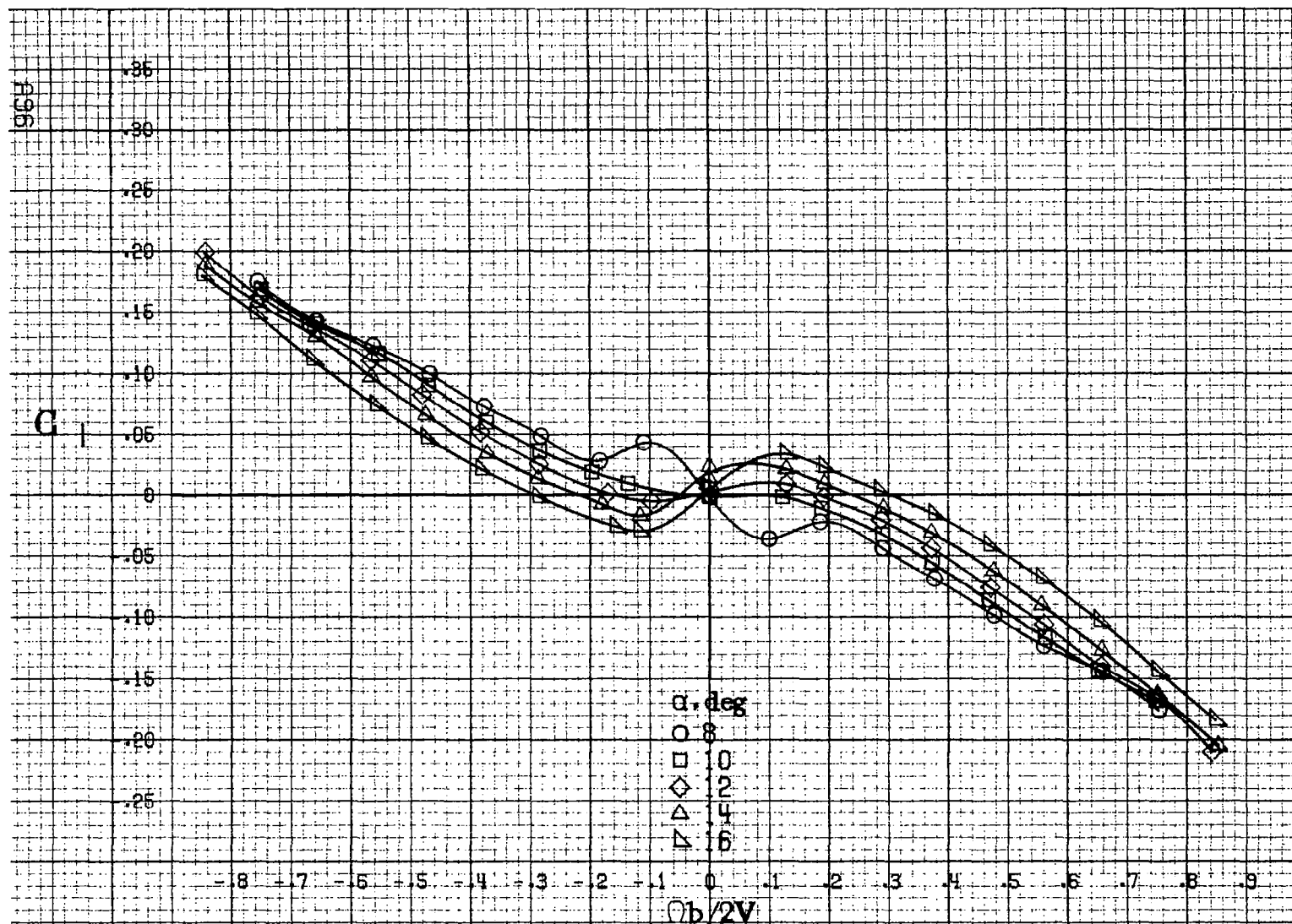
Figure A25. Effect of rotation rate and angle of attack on yawing-moment coefficient for configuration having ventrals and strakes off. $\delta_e=0^\circ$, $\delta_a=0^\circ$, $\delta_r=0^\circ$, $\beta=0^\circ$.





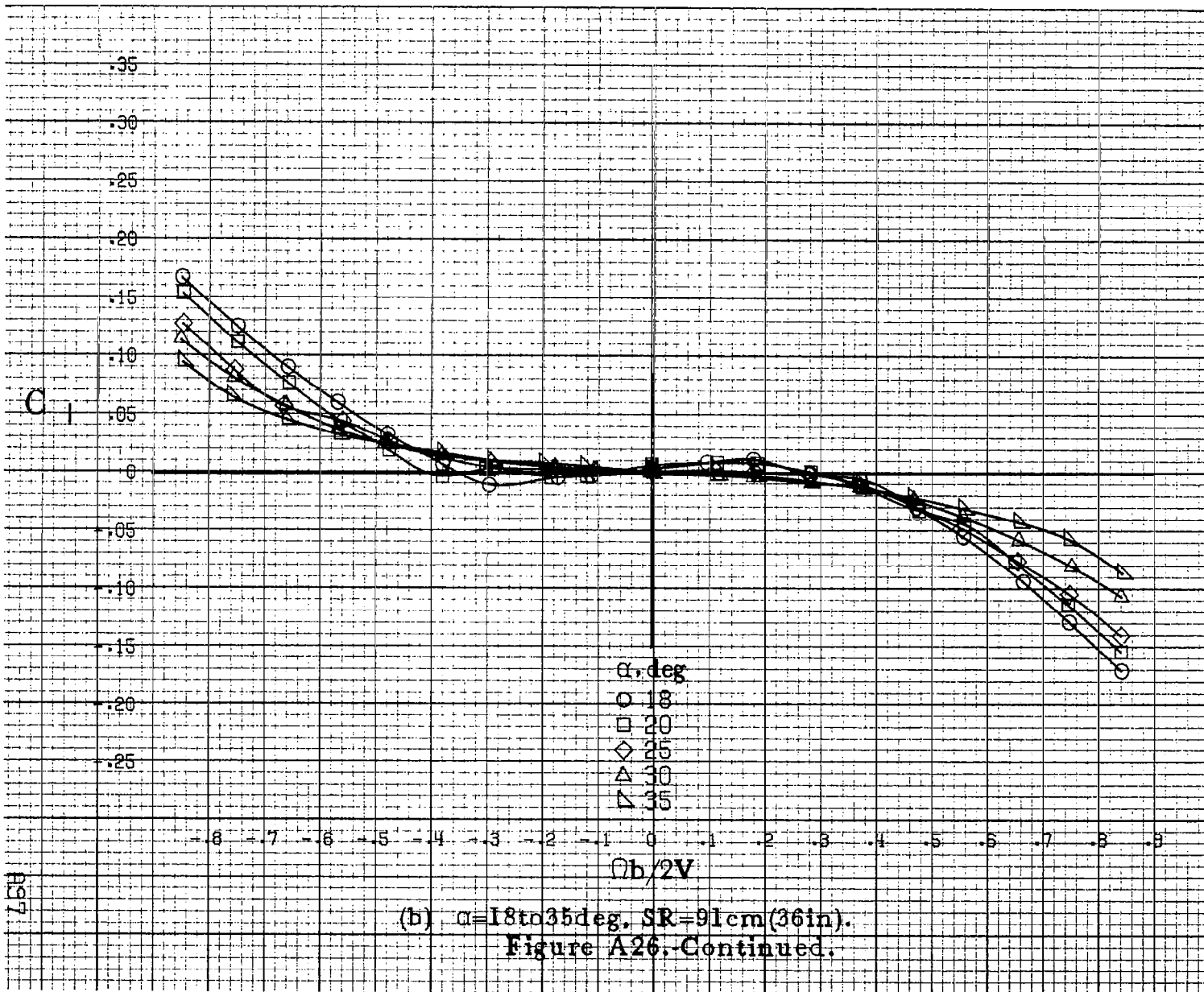
(c) $\alpha=30$ to 50° , $SR=0$.
Figure A25 -Continued.

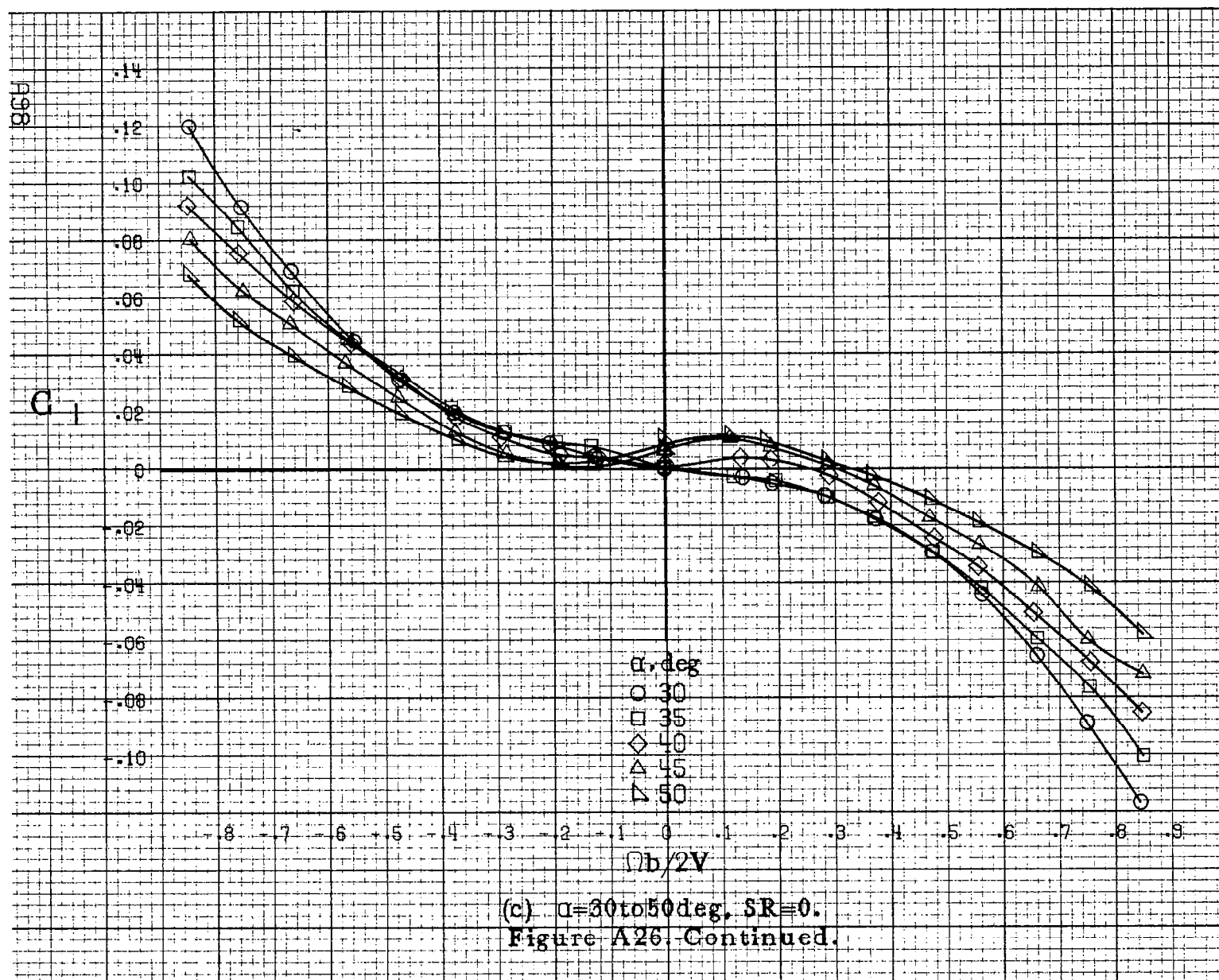


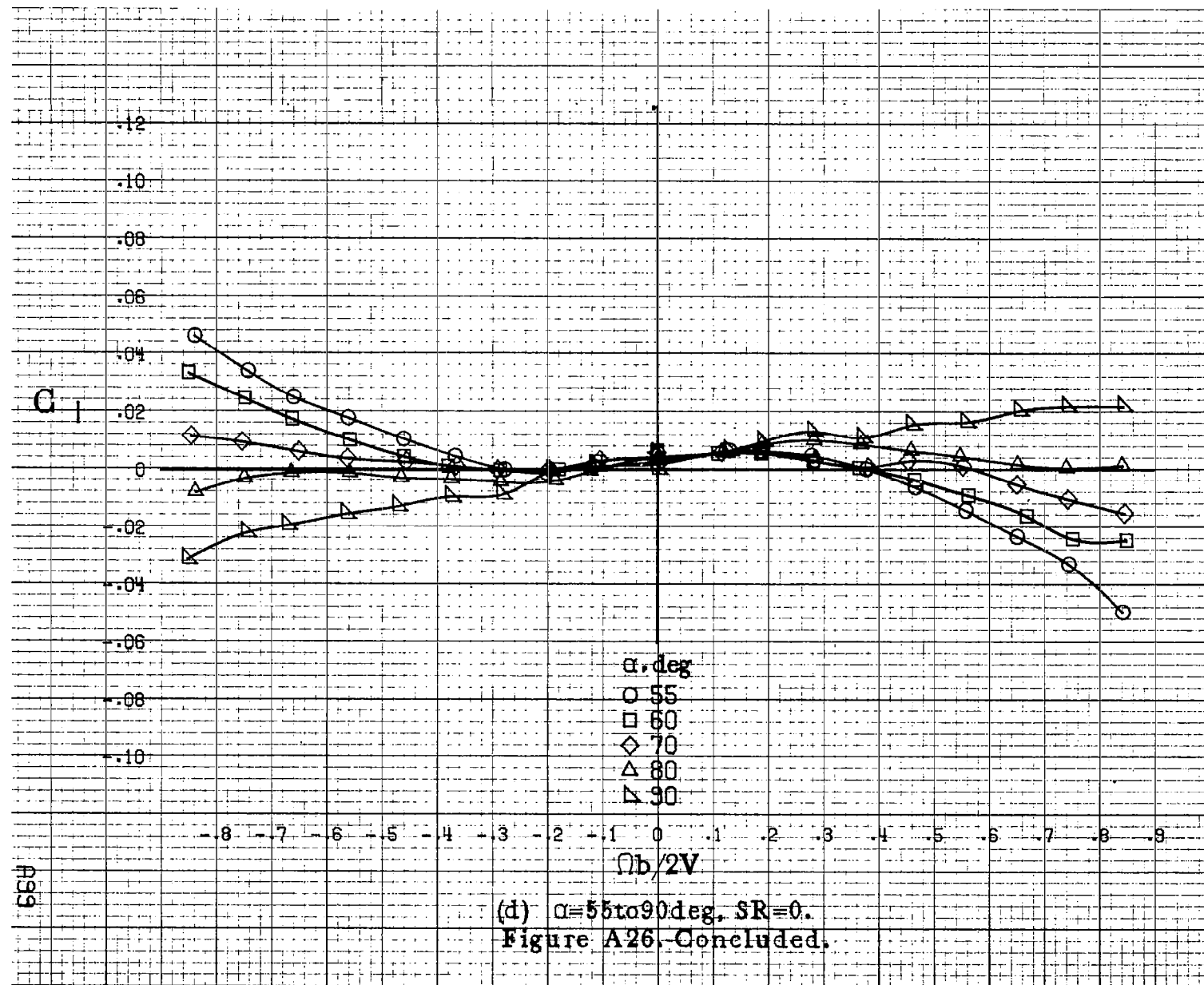


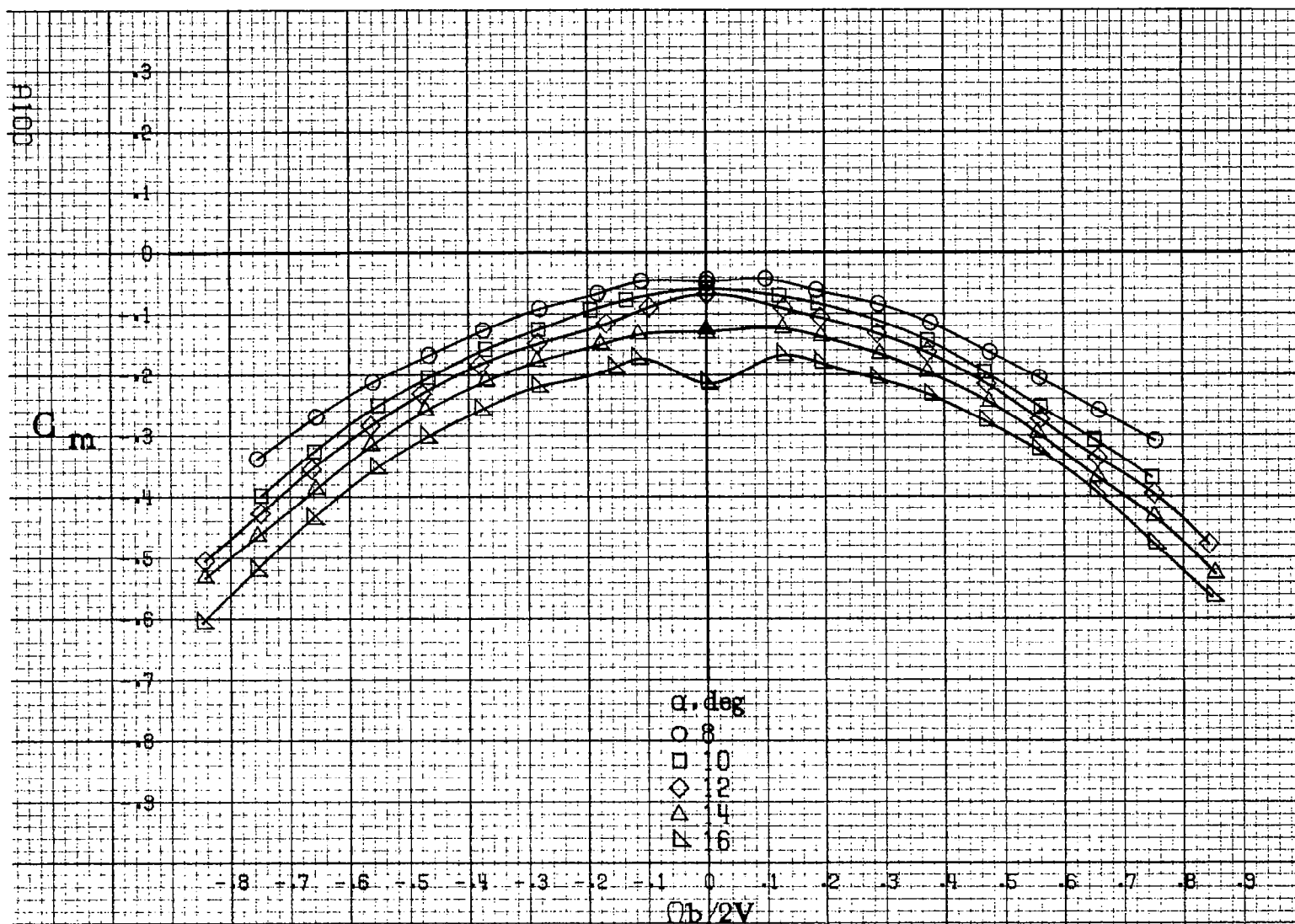
(a) $\alpha = 8$ to 16 deg, $SR = 91$ cm (35 in).

Figure A26. Effect of rotation rate and angle of attack on rolling-moment coefficient for configuration having ventrals and strakes off. $\delta_e = 0^\circ$, $\delta_a = 0^\circ$, $\delta_r = 0^\circ$, $\beta = 0^\circ$.



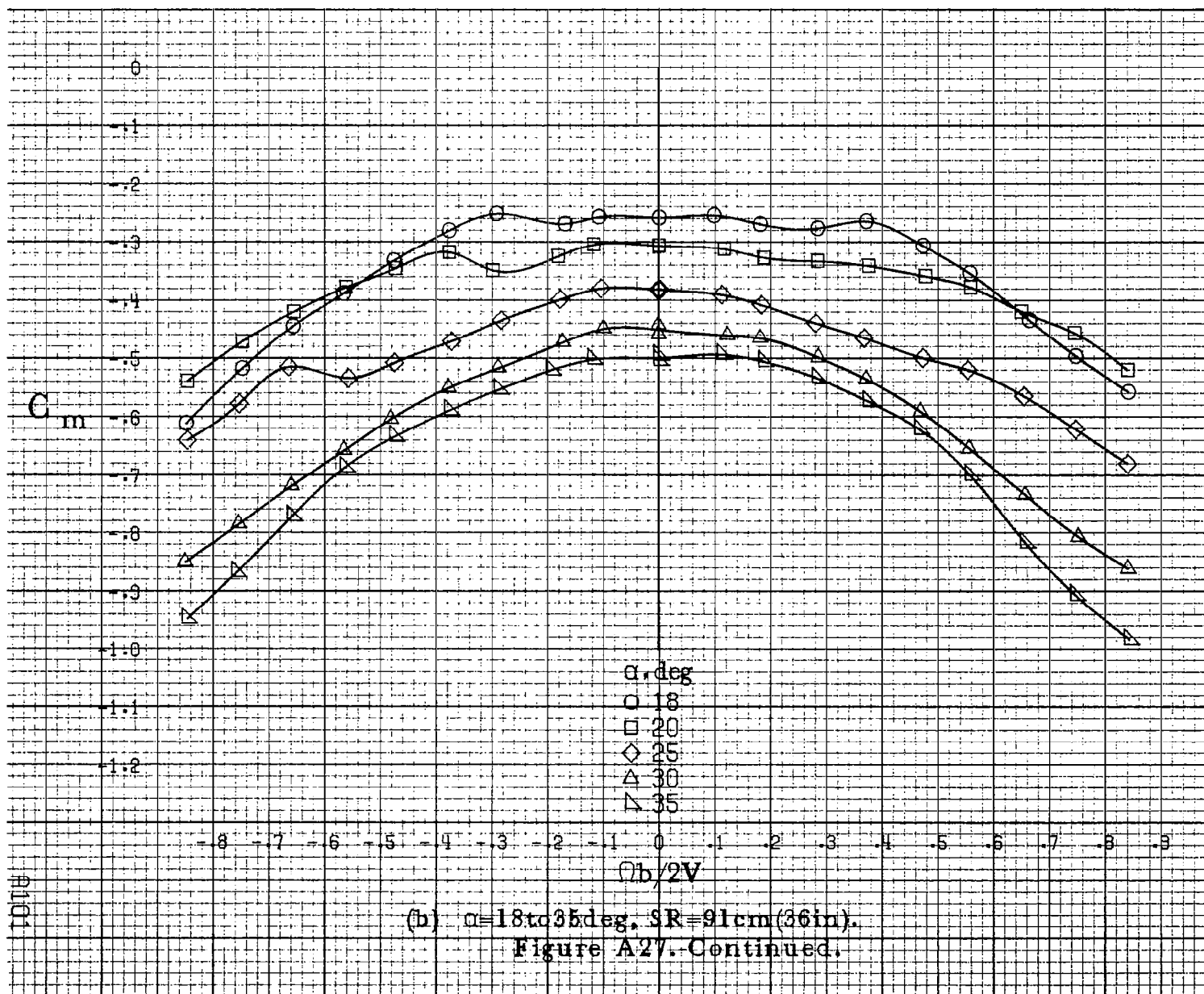


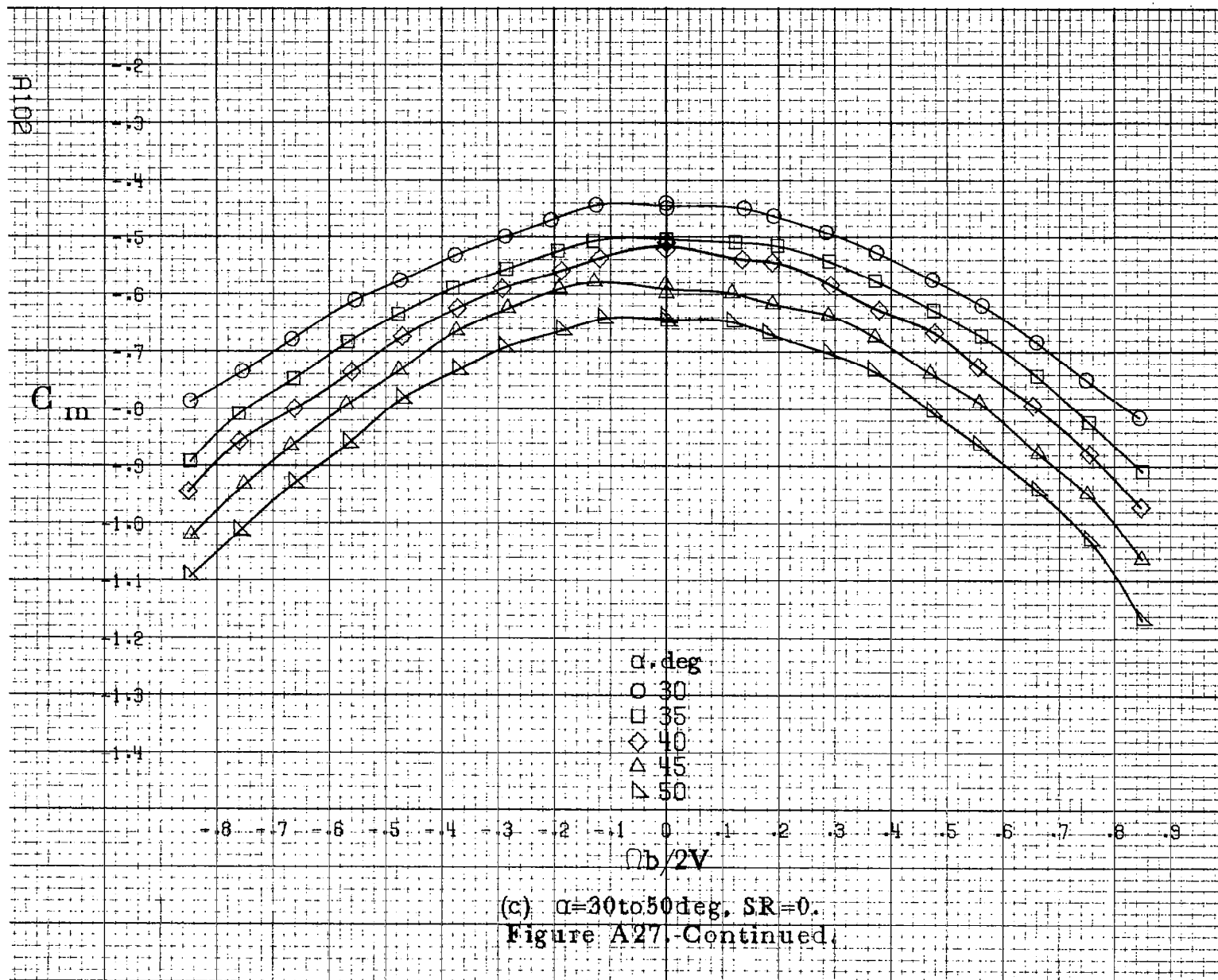


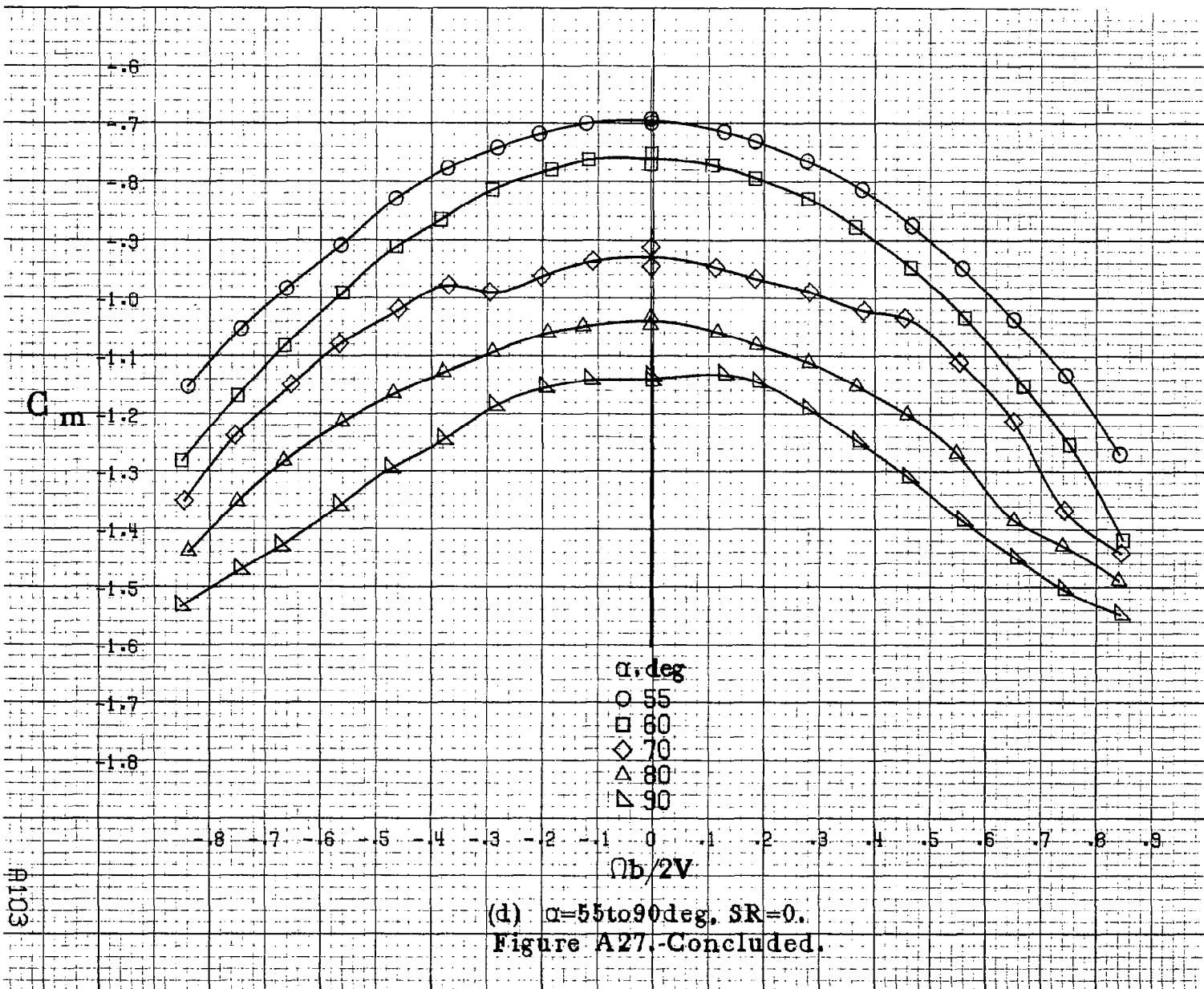


(a) $\alpha = 8$ to 16° , $SR = 91\text{cm (36in.)}$.

Figure A27. Effect of rotation rate and angle of attack on pitching moment coefficient for configuration having ventrals and strakes off. $\delta_a = 0^\circ$, $\delta_s = 0^\circ$, $\delta_r = 0^\circ$, $\beta = 0^\circ$.

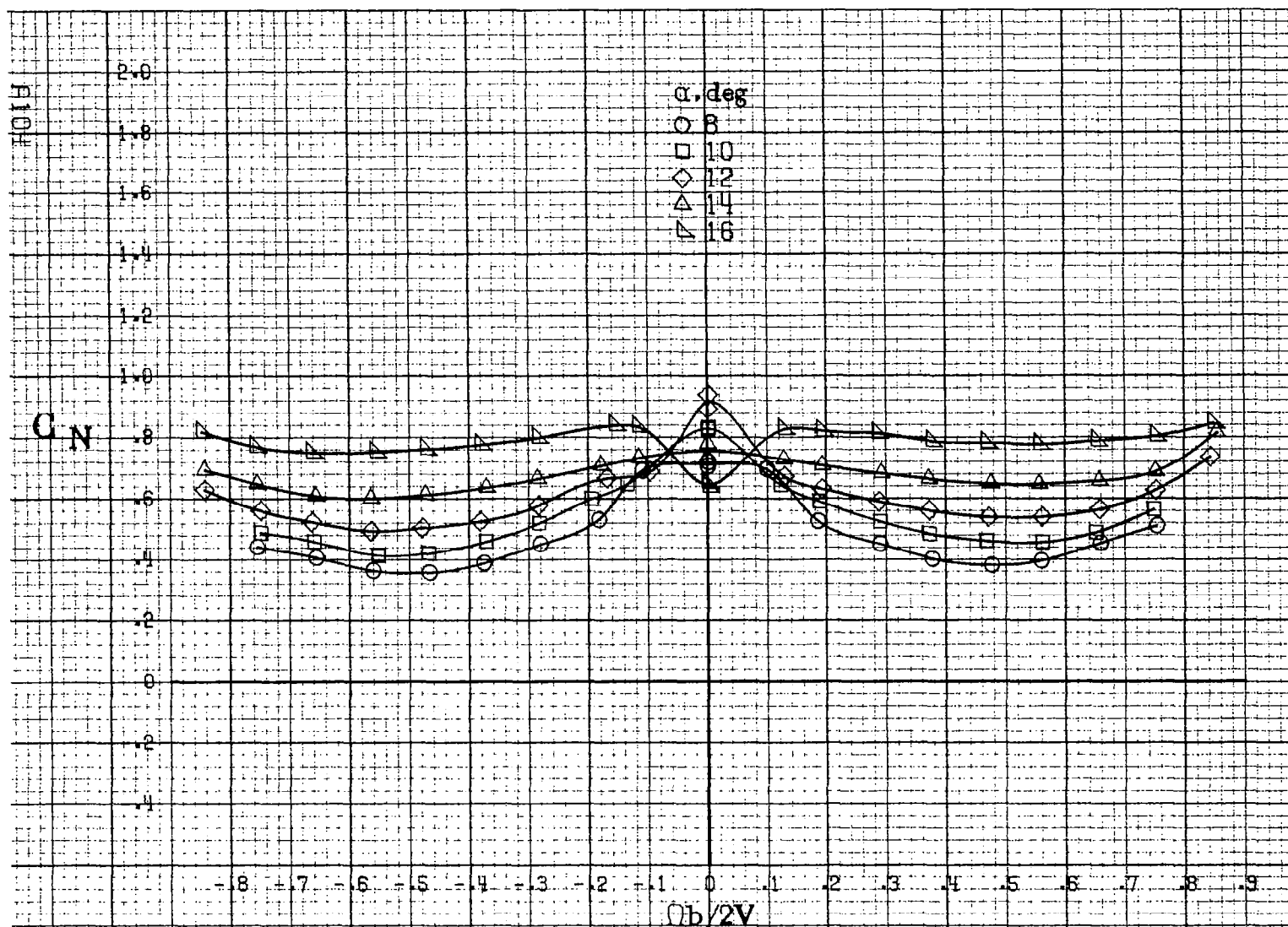






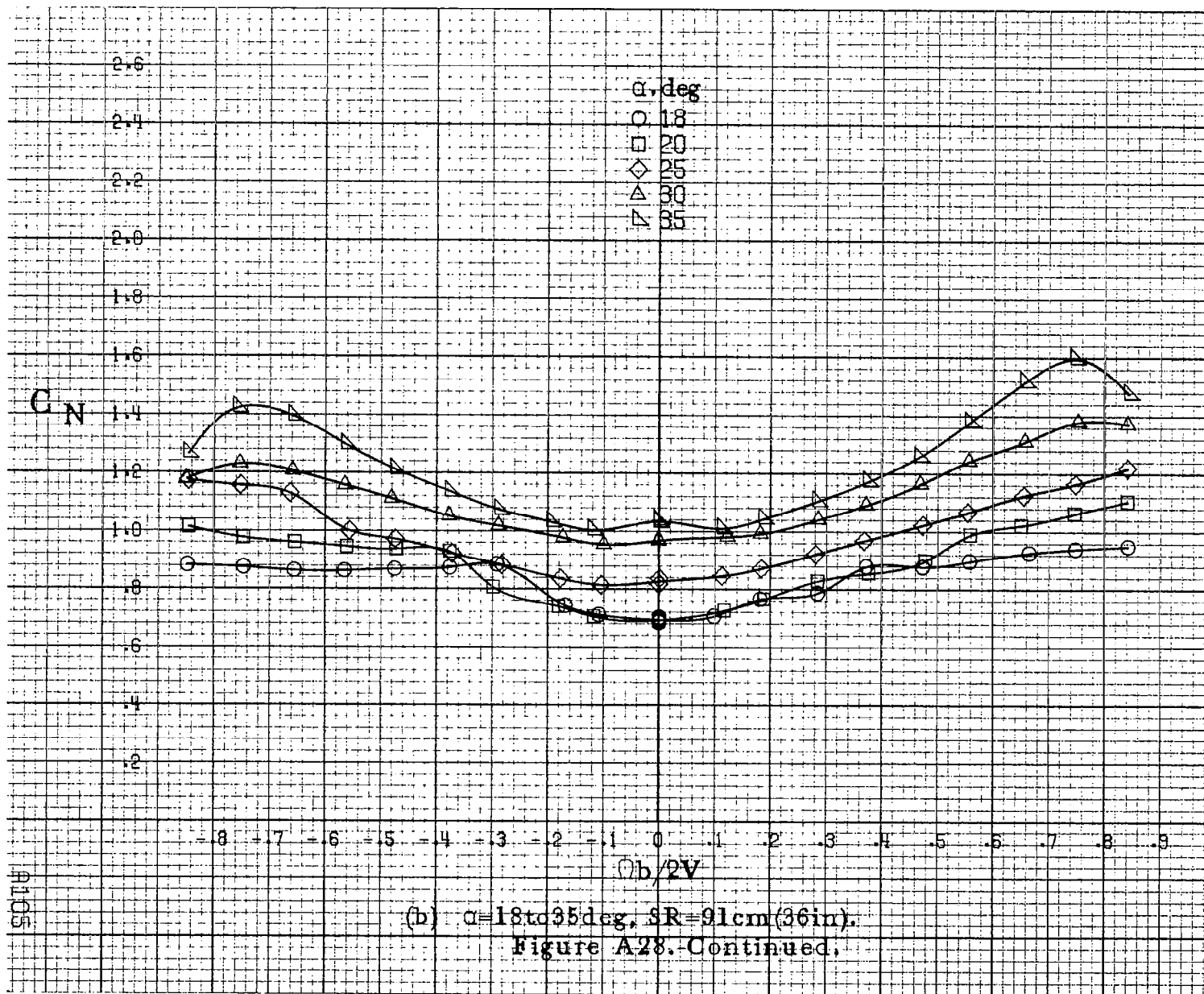
(d) $\alpha=55$ to 90° , $SR=0$.
 Figure A27. Concluded.

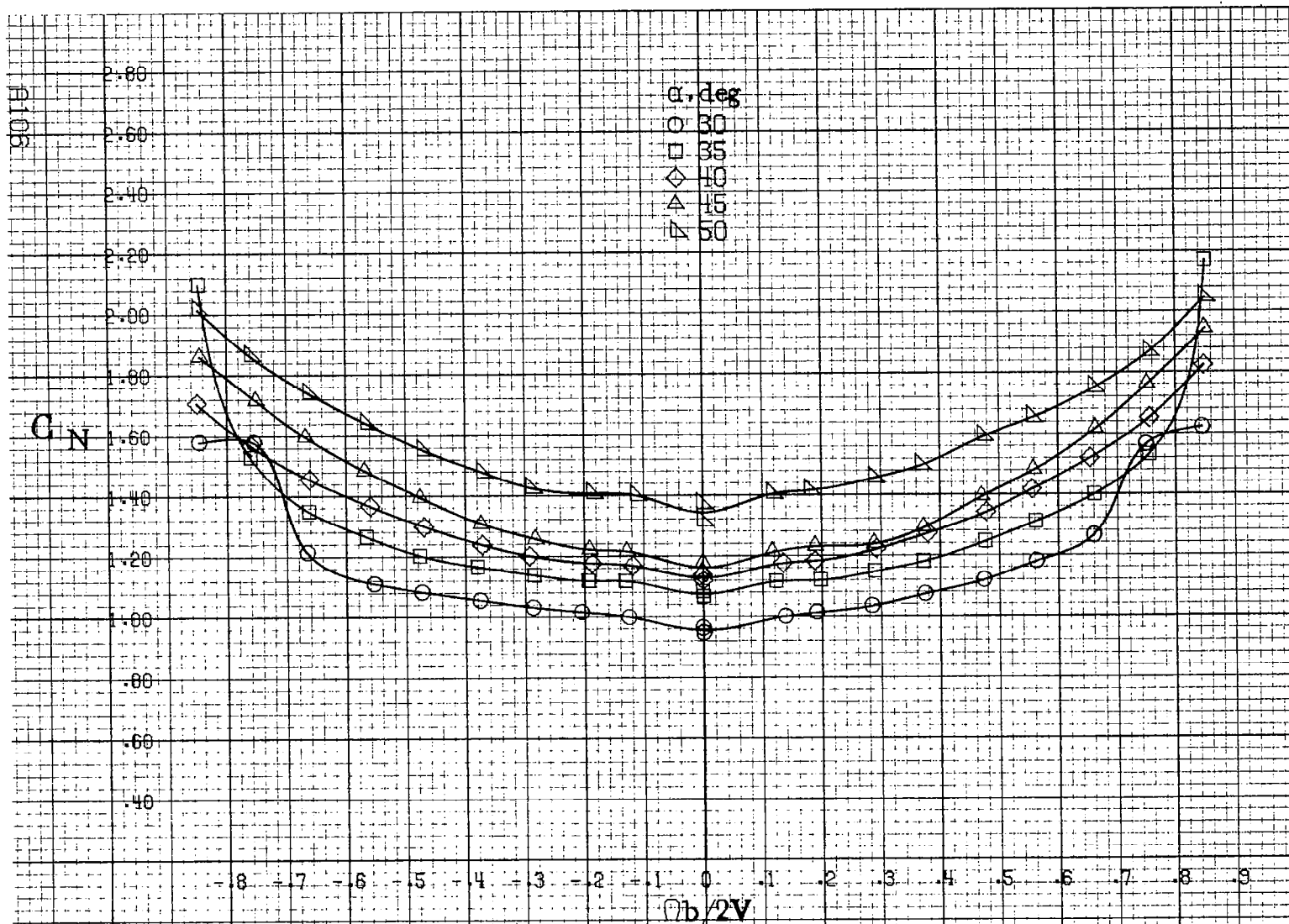
#103



(a) $\alpha = 8$ to 16 deg, $SR = 91$ cm (36 in).

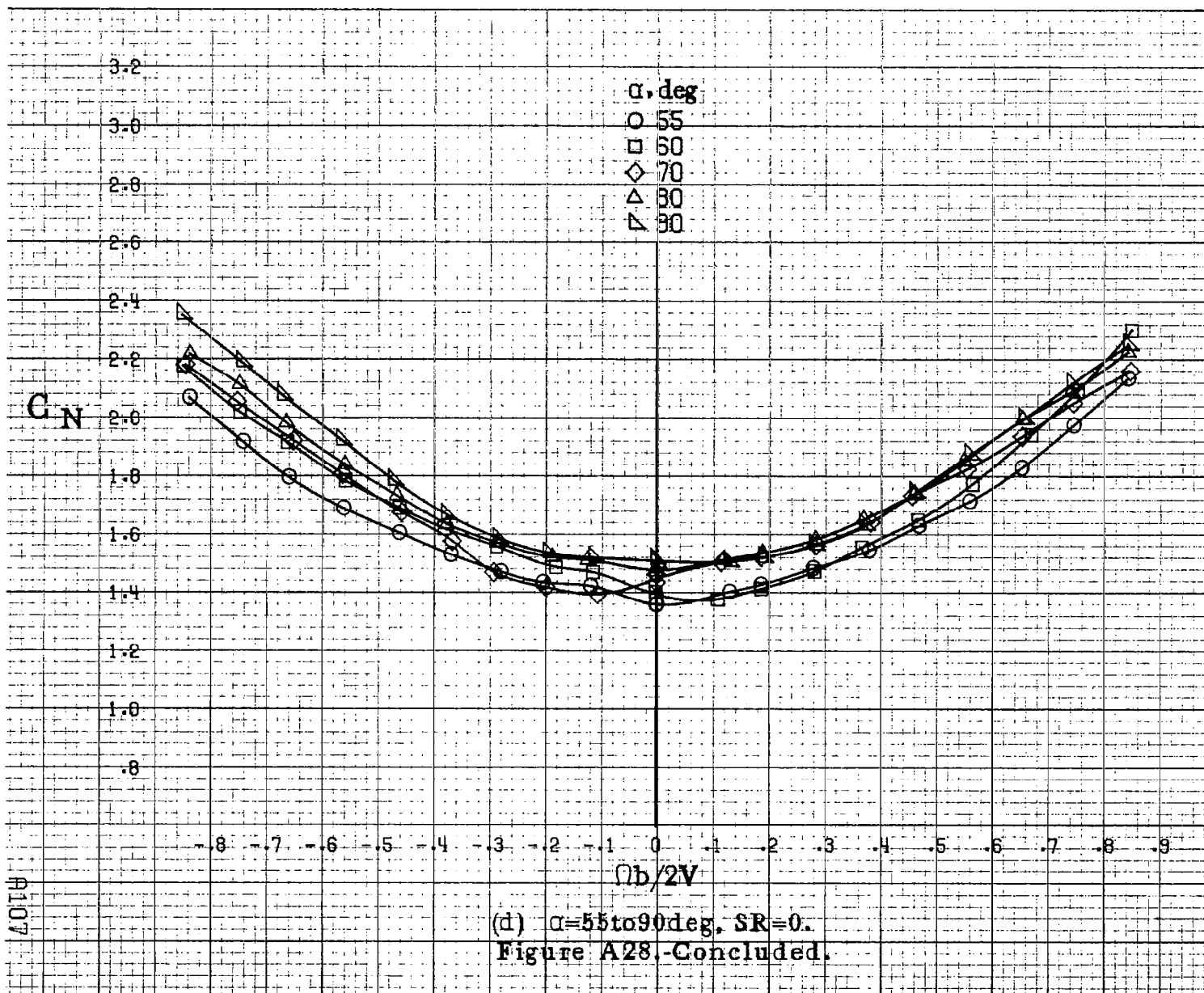
Figure A28. Effect of rotation rate and angle of attack on normal force coefficient for configuration having ventrals and strakes off. $\delta_a = 0^\circ$, $\delta_s = 0^\circ$, $\delta_r = 0^\circ$, $\beta = 0^\circ$.

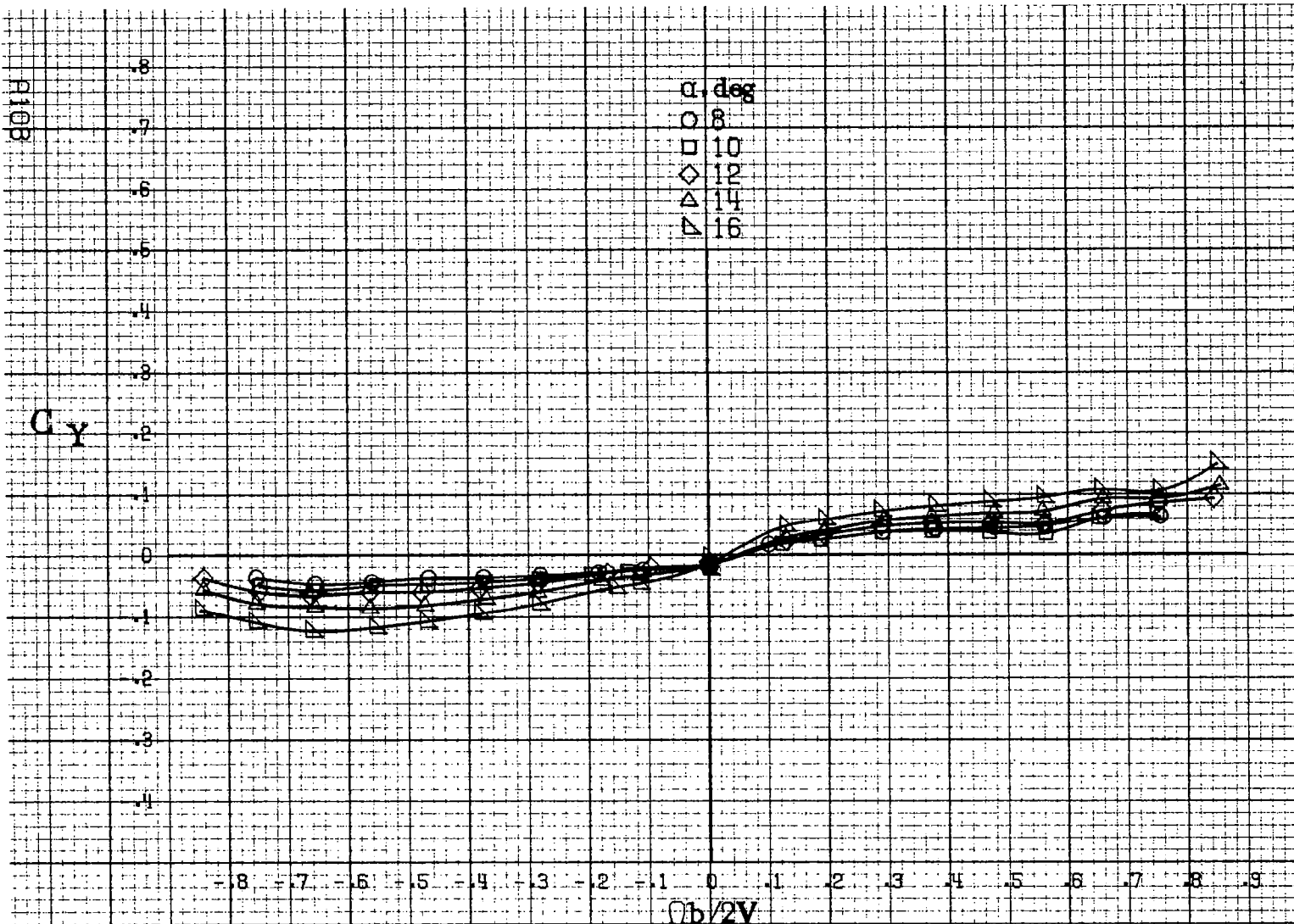




(c) $\alpha = 30$ to 50° , $SR = 0$.

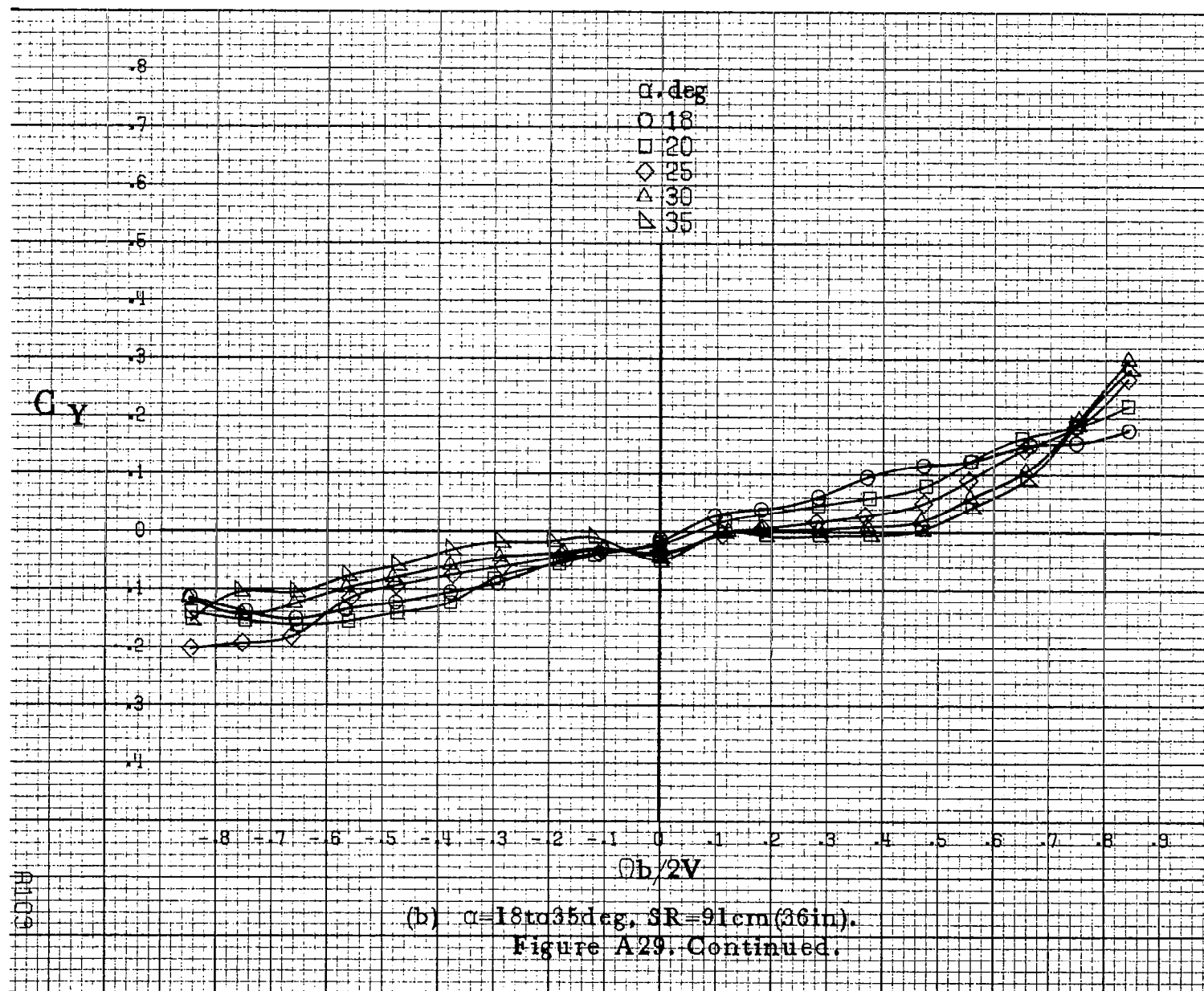
Figure A28. Continued.

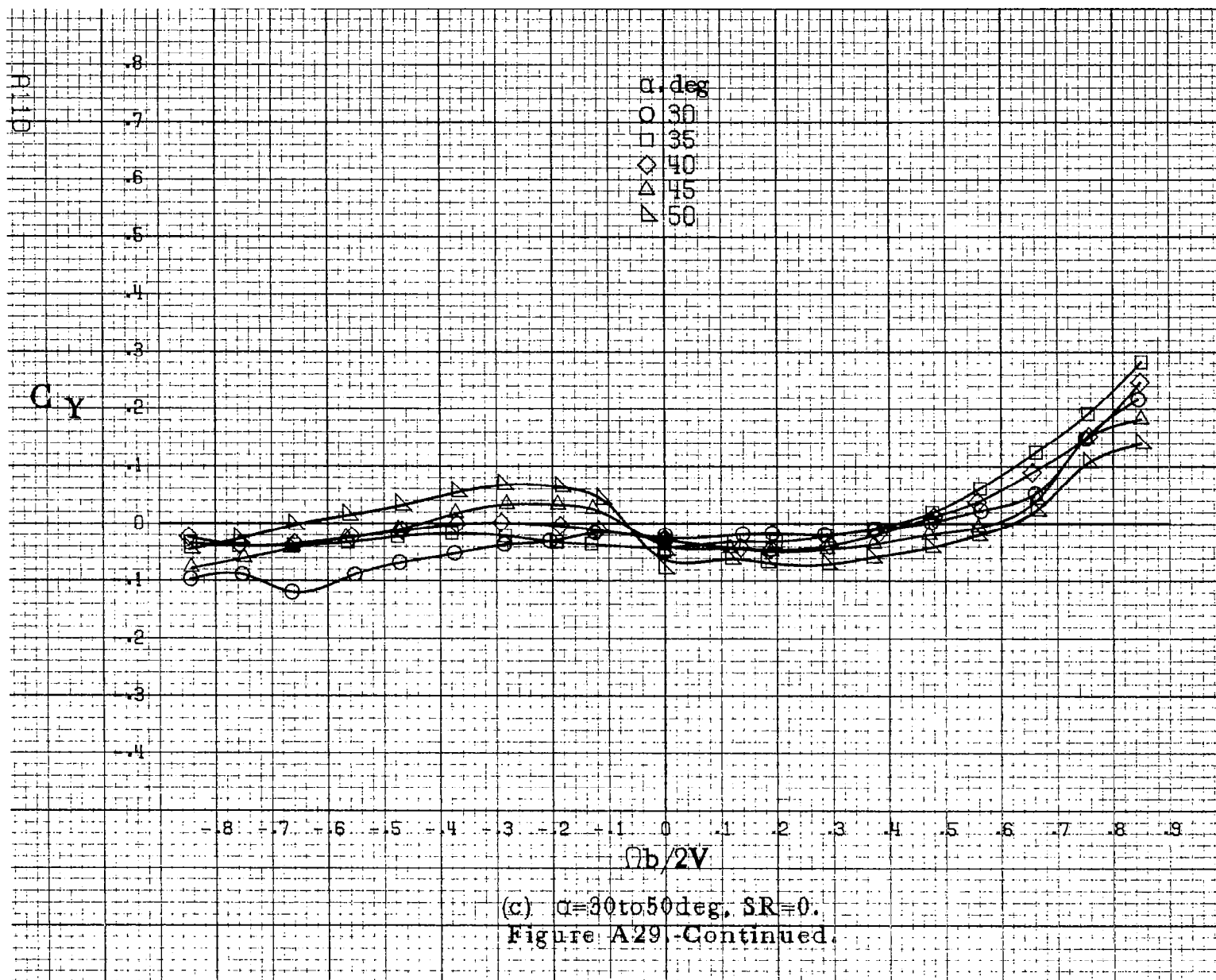


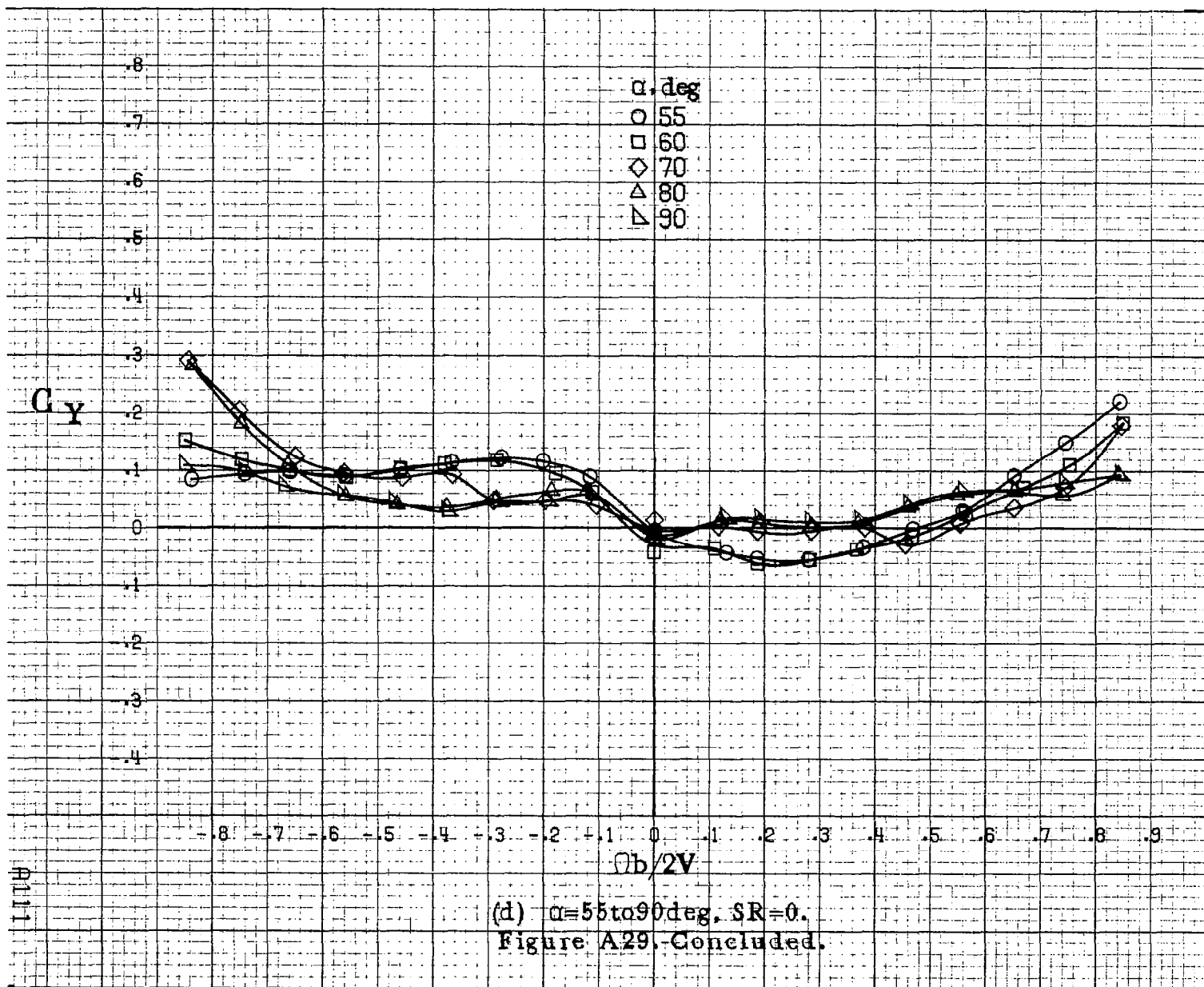


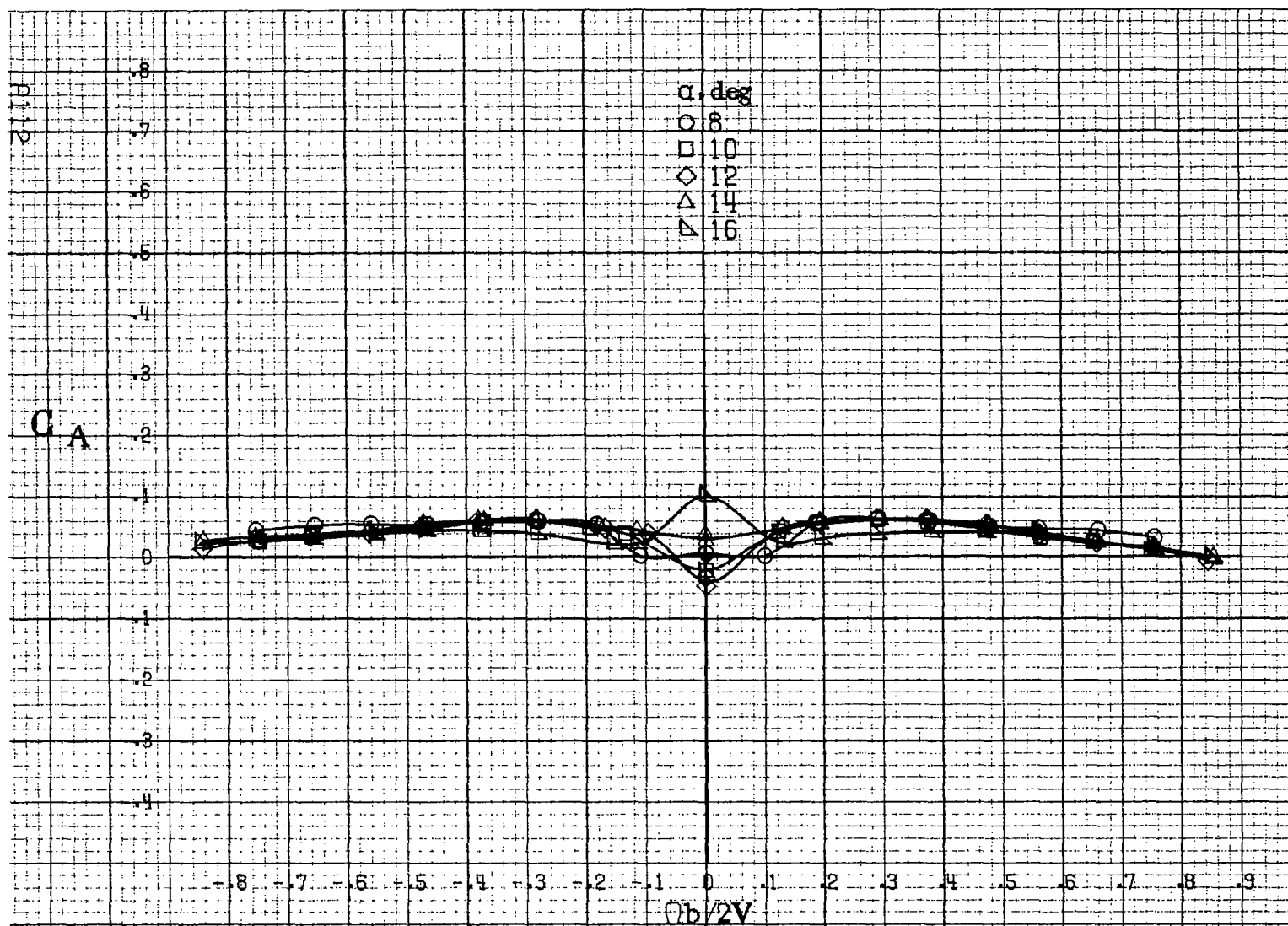
(a) $\alpha=8$ to 16° , $SR=91\text{cm}$ (35in).

Figure A29. Effect of rotation rate and angle of attack on side force coefficient for configuration having ventrals and strakes off. $\delta_1=0^\circ$, $\delta_2=0^\circ$, $\beta=0^\circ$.



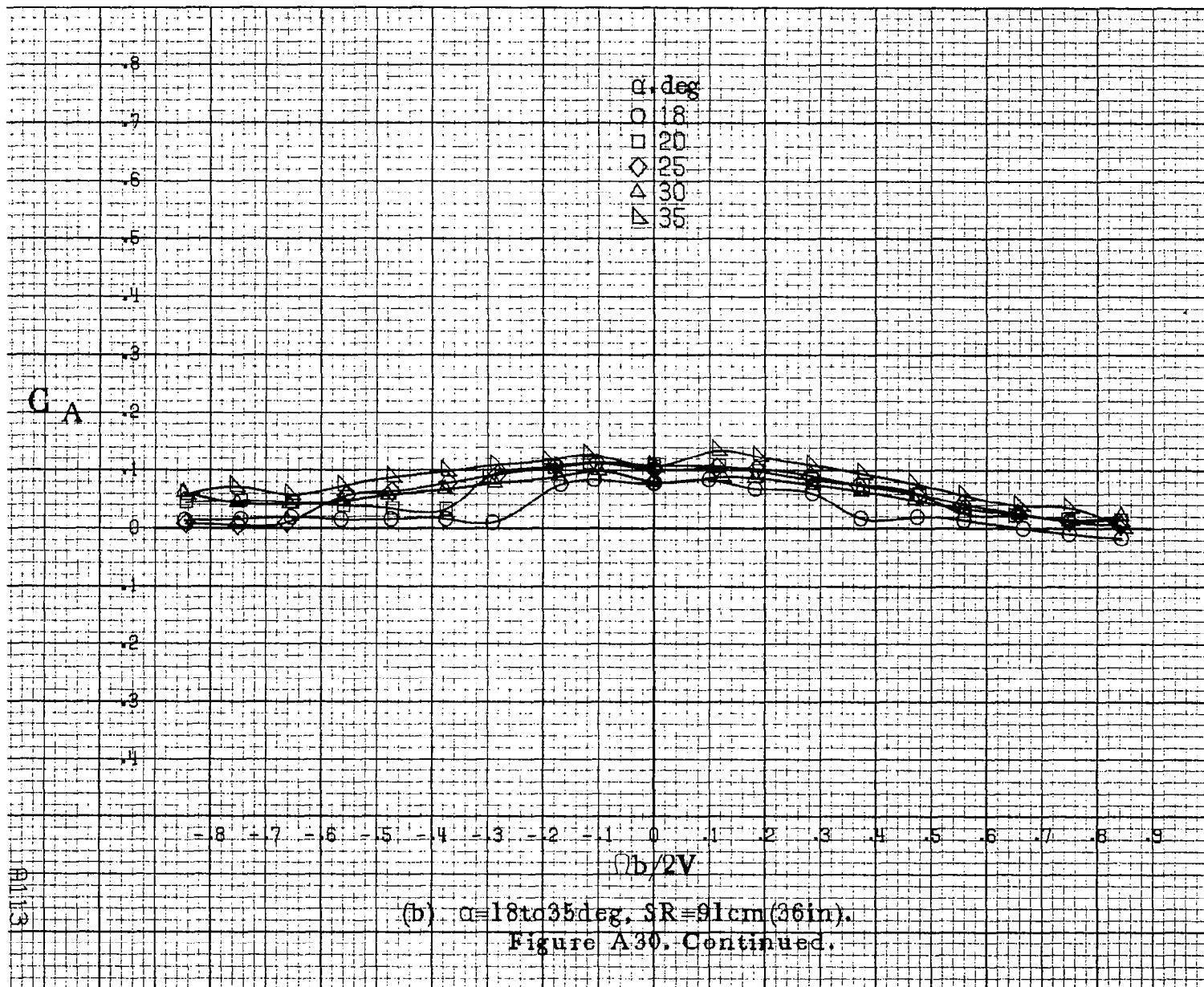


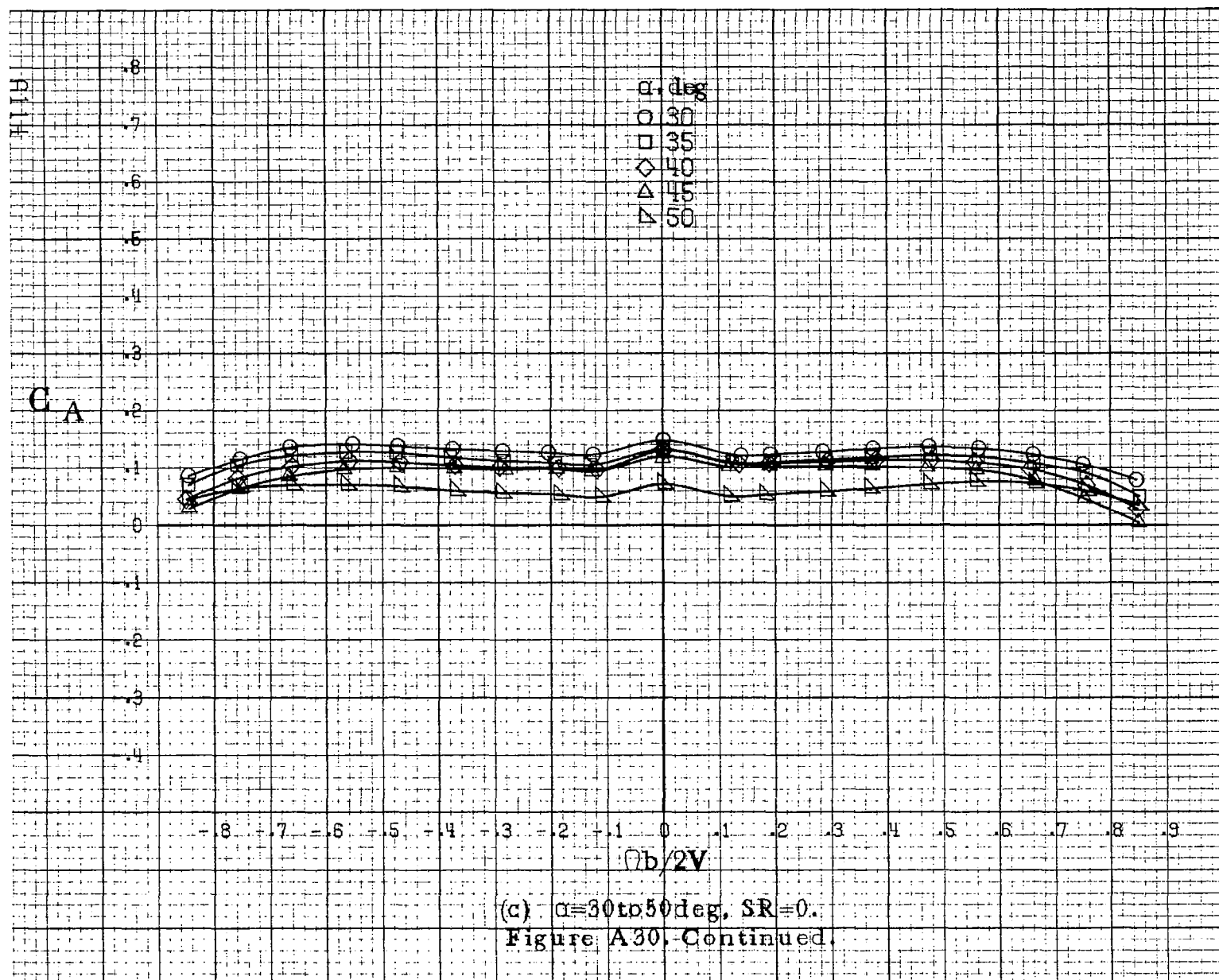


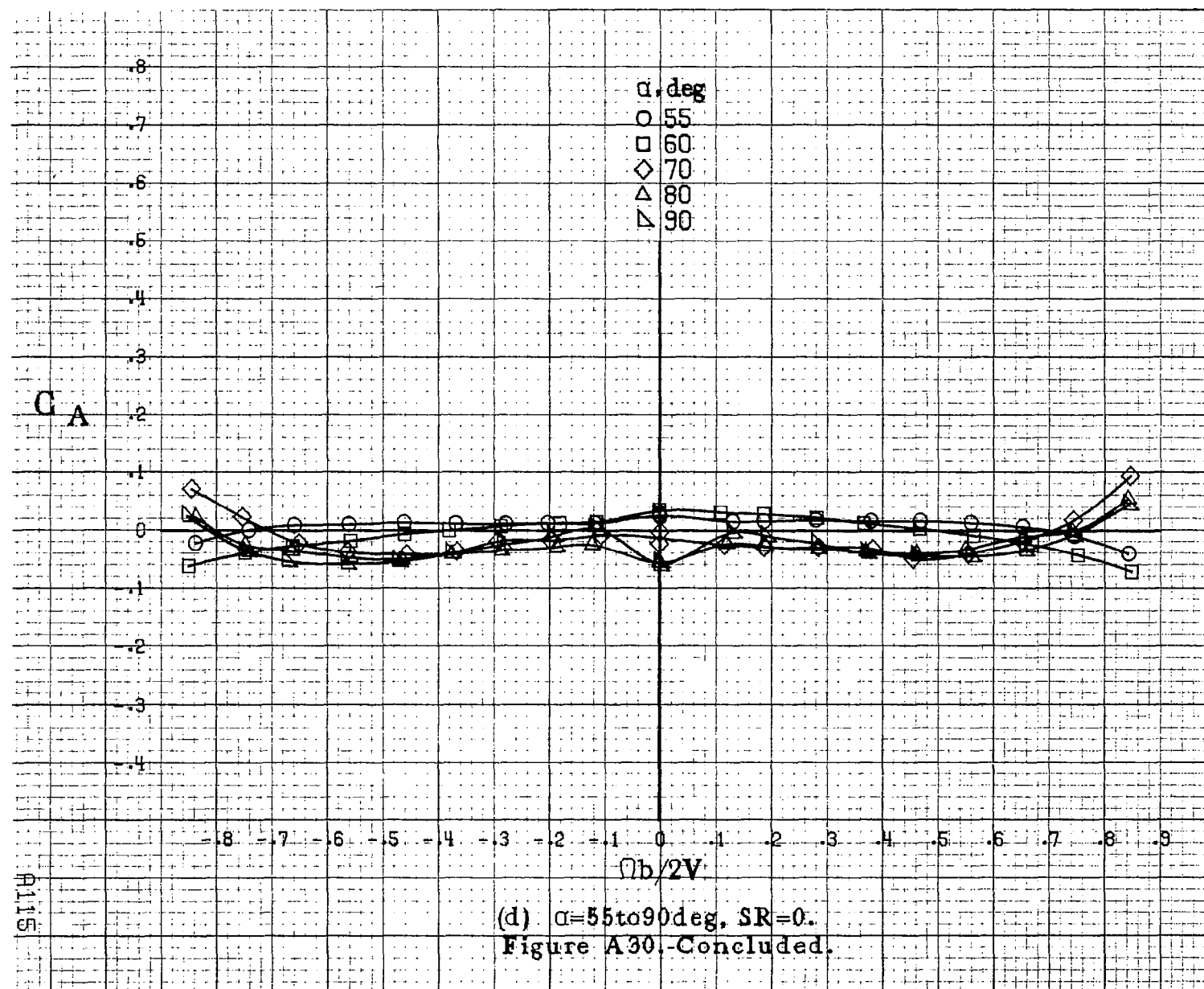


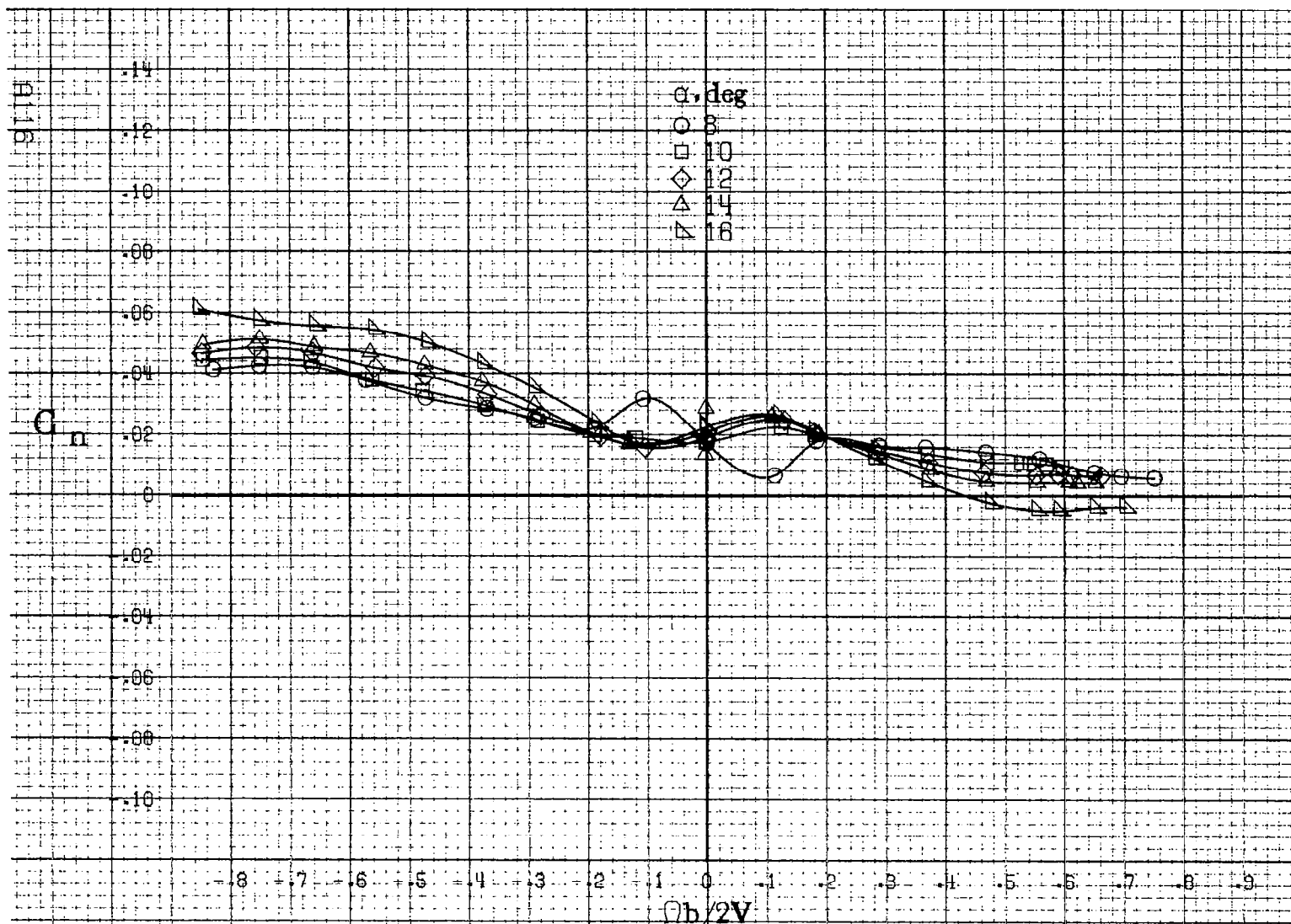
(a) $\alpha = 8$ to 16° , $SR = 91 \text{ cm (36 in.)}$.

Figure A30. Effect of rotation rate and angle of attack on axial force coefficient for configuration having ventrals and strakes off. $\delta_s = 0^\circ$, $\delta_a = 0^\circ$, $\delta_r = 0^\circ$, $\beta = 0^\circ$.



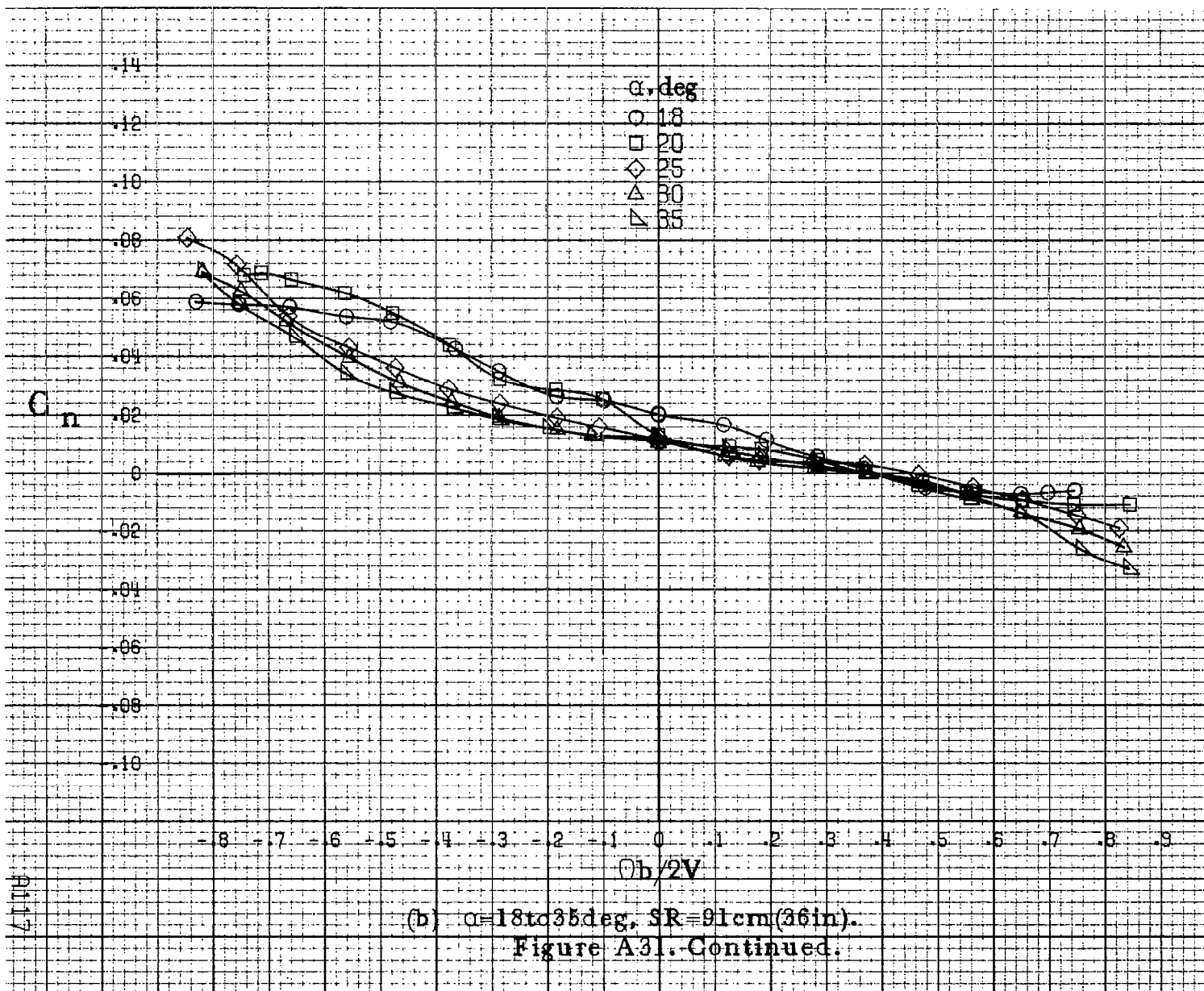


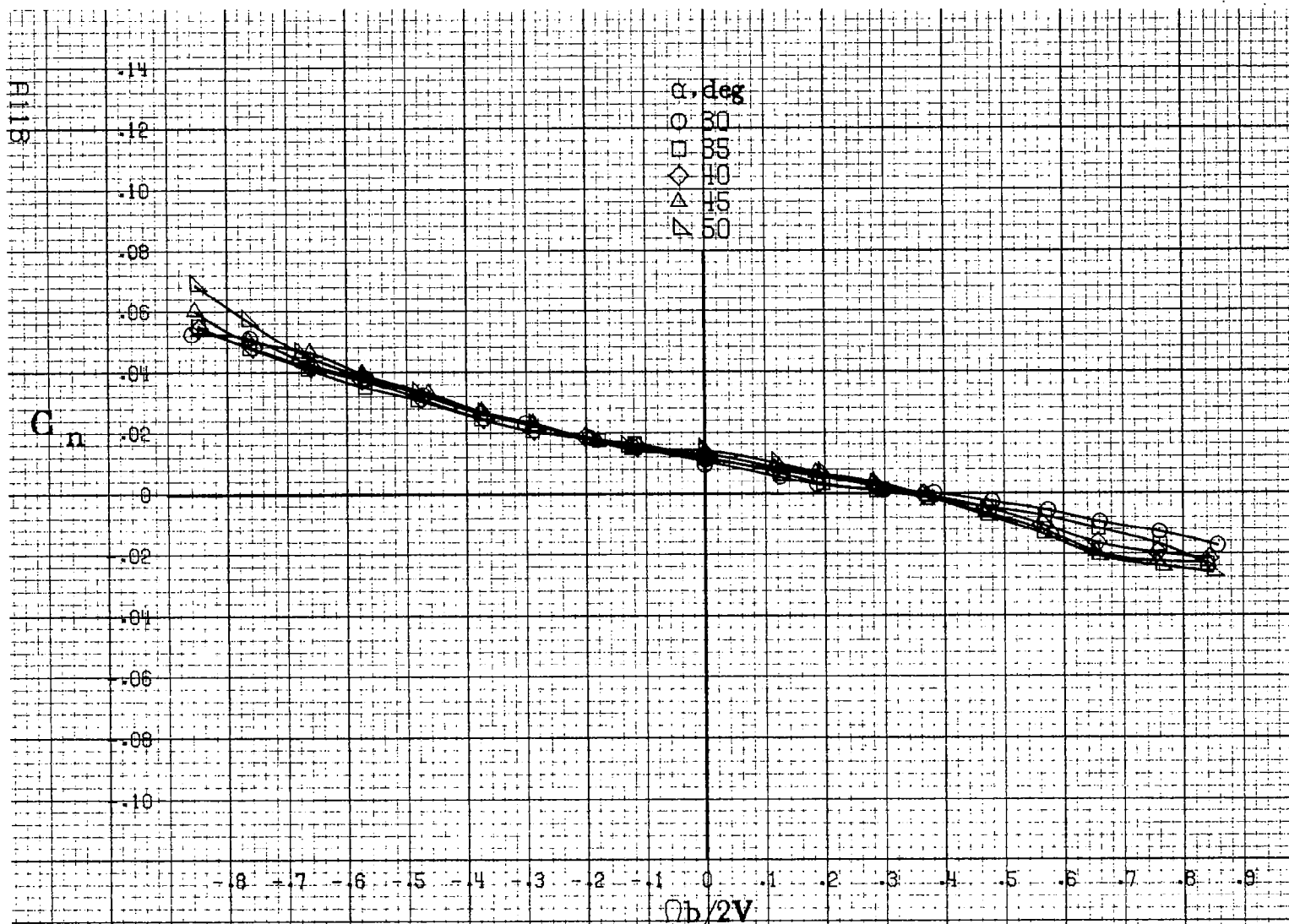




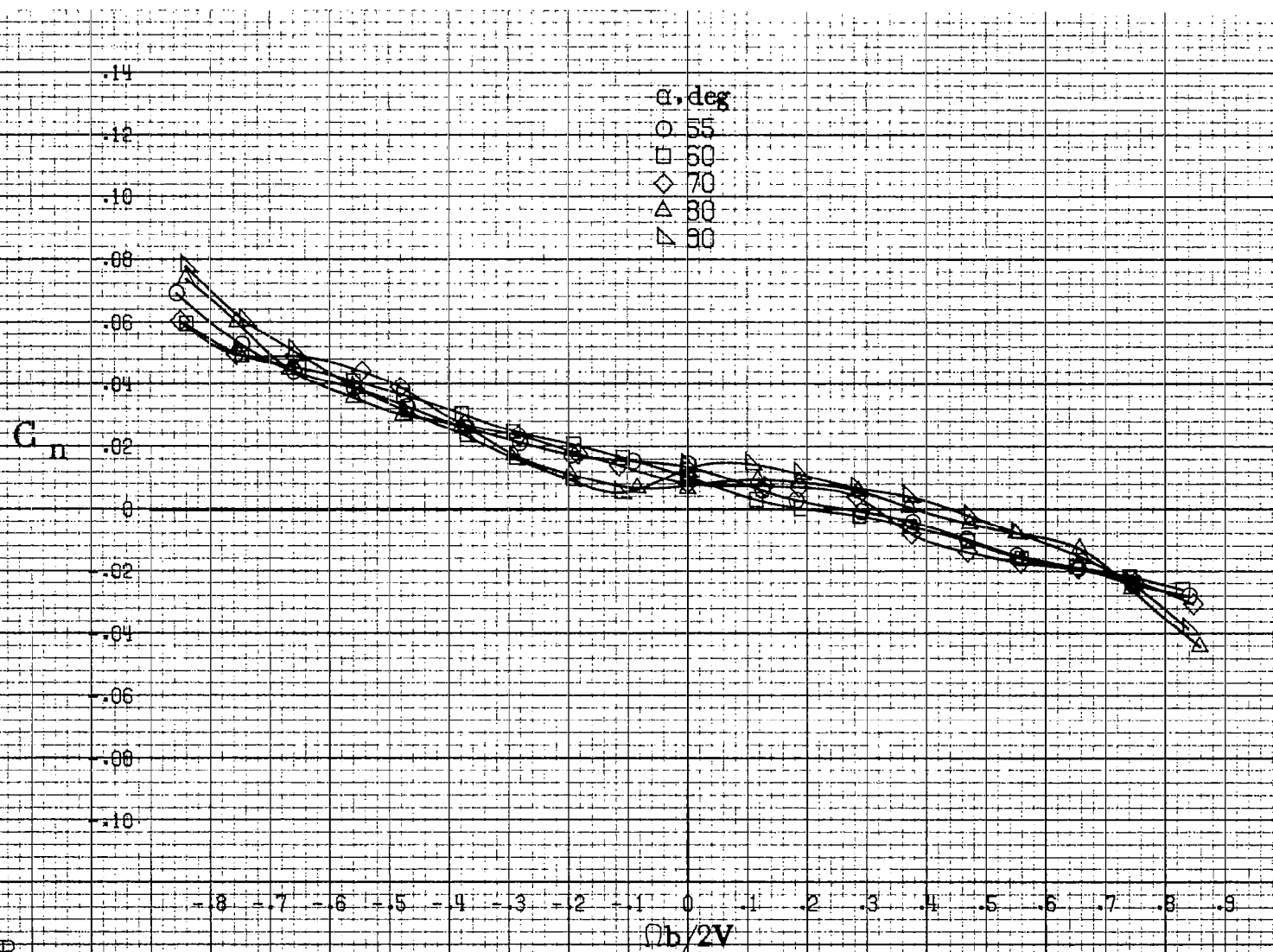
(a) $\alpha = 8$ to 16° , $SR = 91\text{cm}(36\text{in})$.

Figure A31. Effect of rotation rate and angle of attack on yawing-moment coefficient for configuration having ventrals and strakes off. $\delta_e = -20^\circ$, $\delta_a = -20^\circ$, $\delta_r = -28^\circ$, $\beta = 0^\circ$.



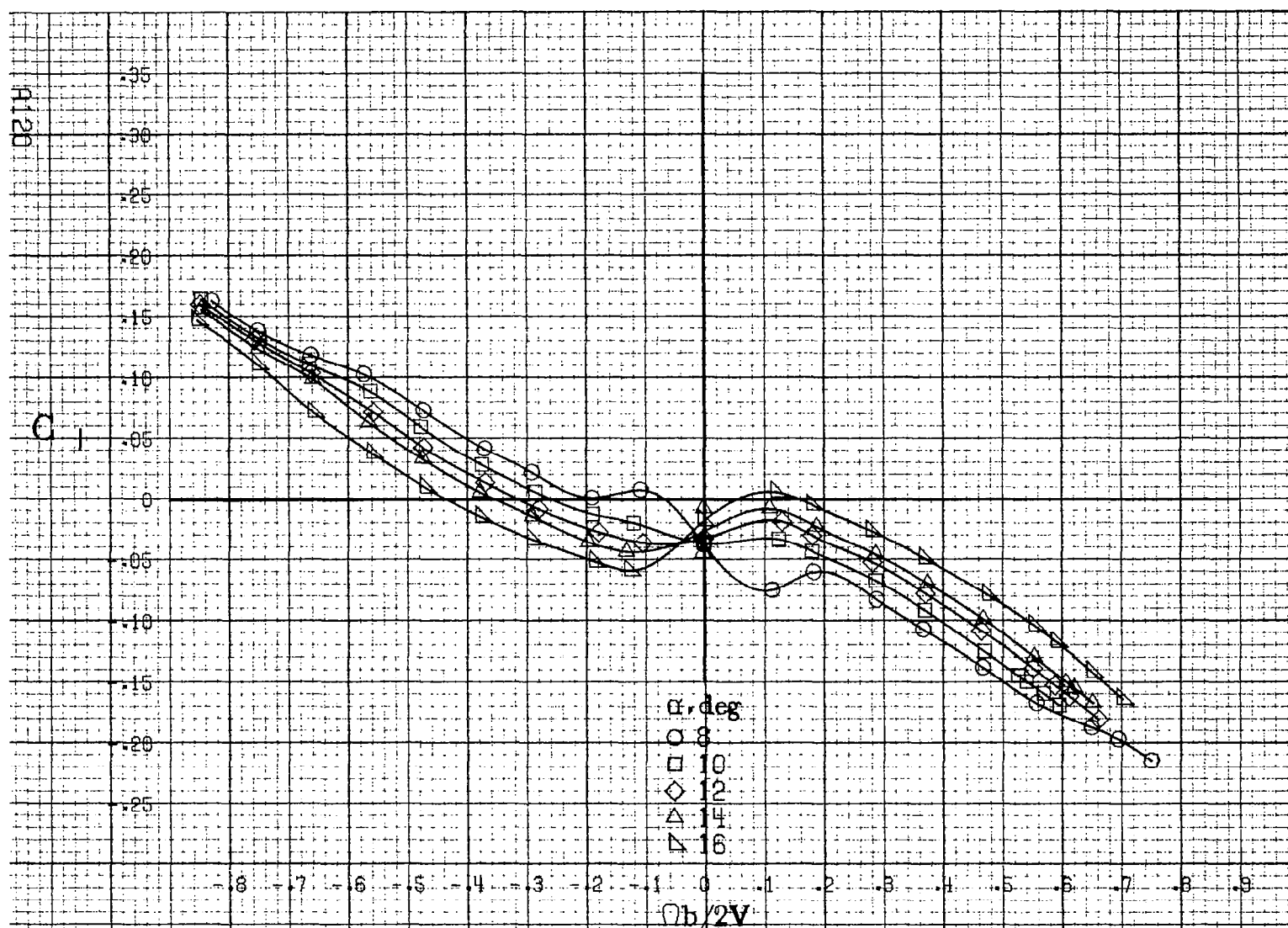


(c) $\alpha=30$ to 50° , $SR=0$.
Figure A31 -Continued.



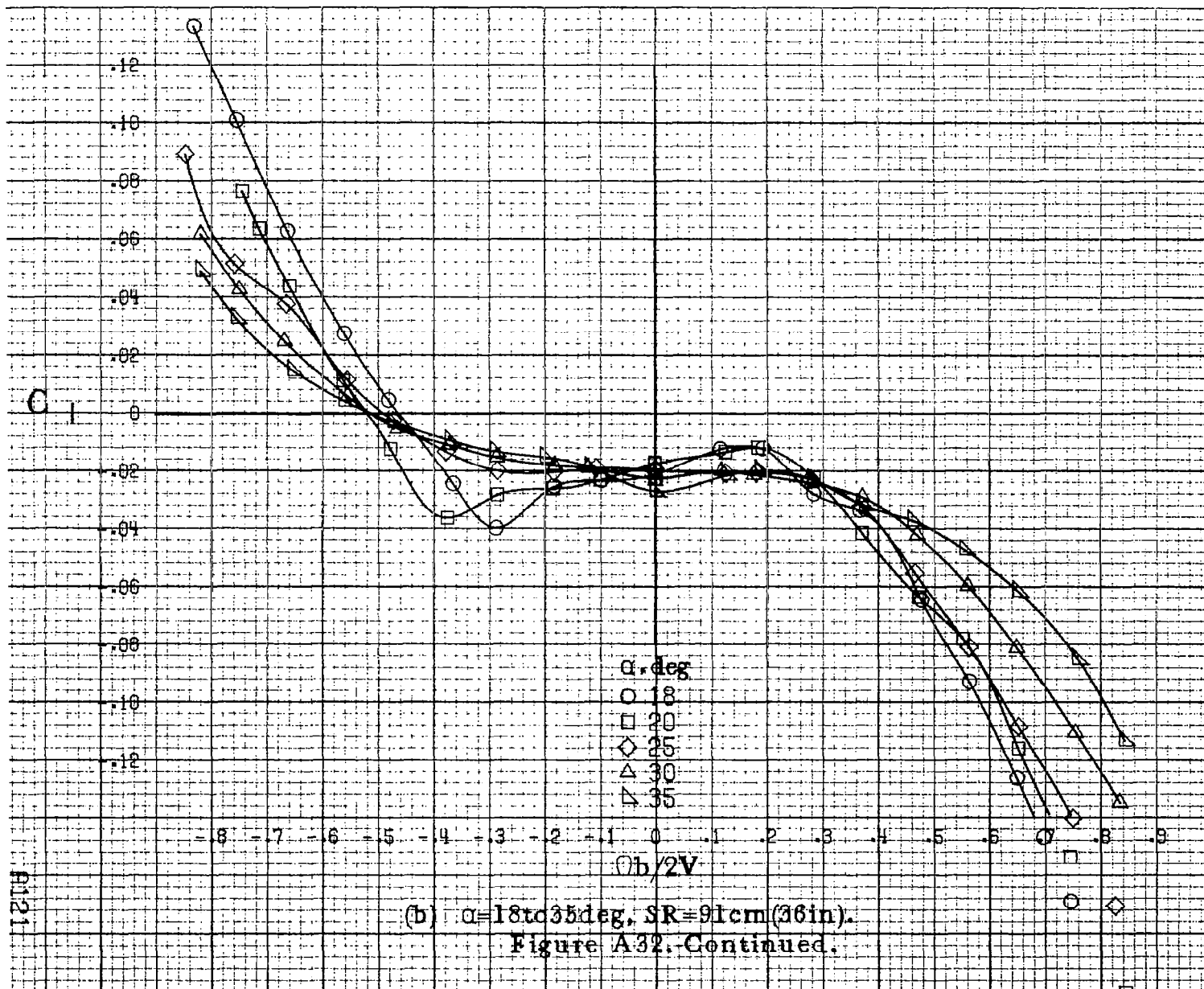
(d) $\alpha=55$ to 90° , $SR=0$.

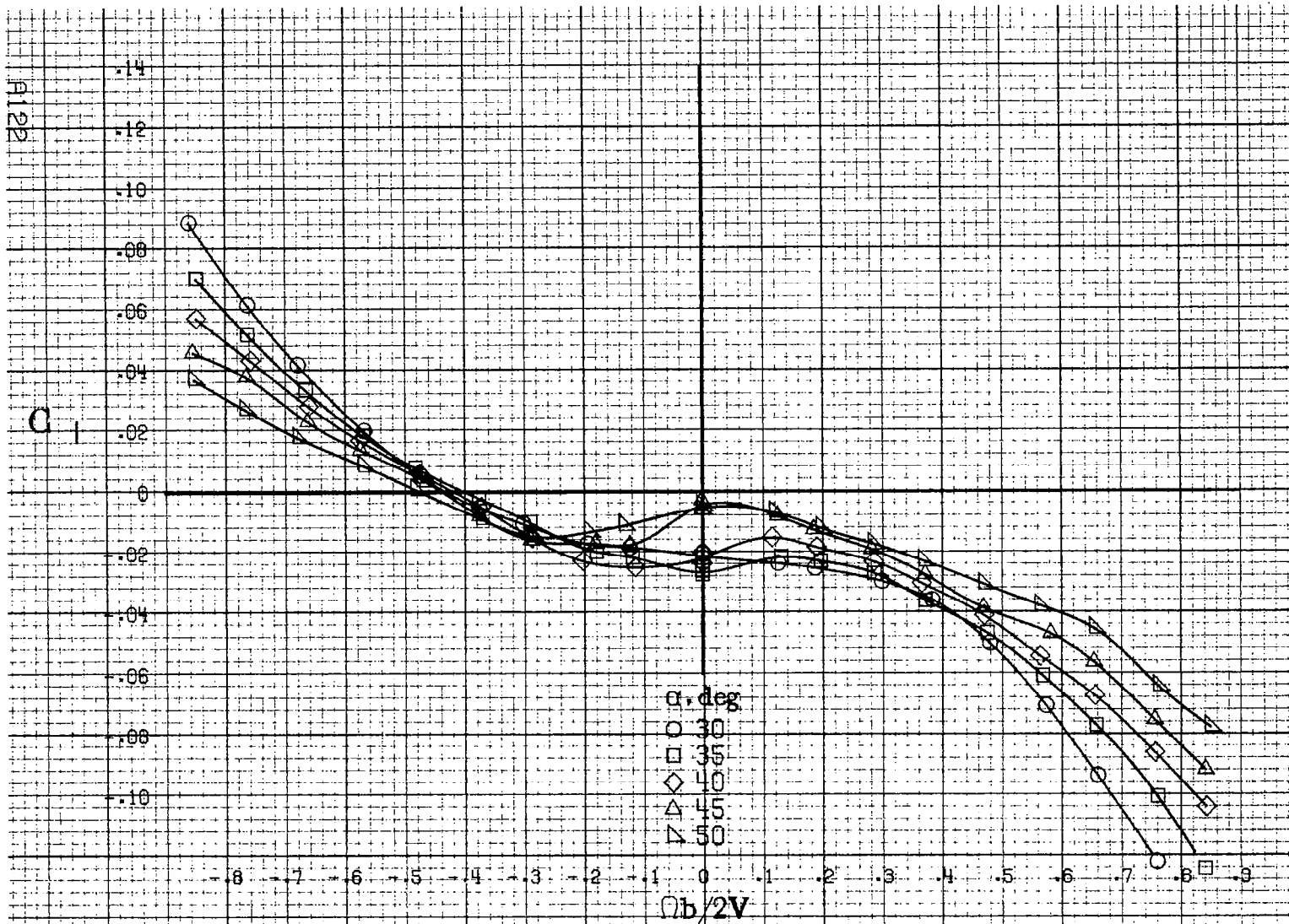
Figure A31. Concluded.



(a) $\alpha=8$ to 16° , $SR=91\text{cm}(36\text{in})$.

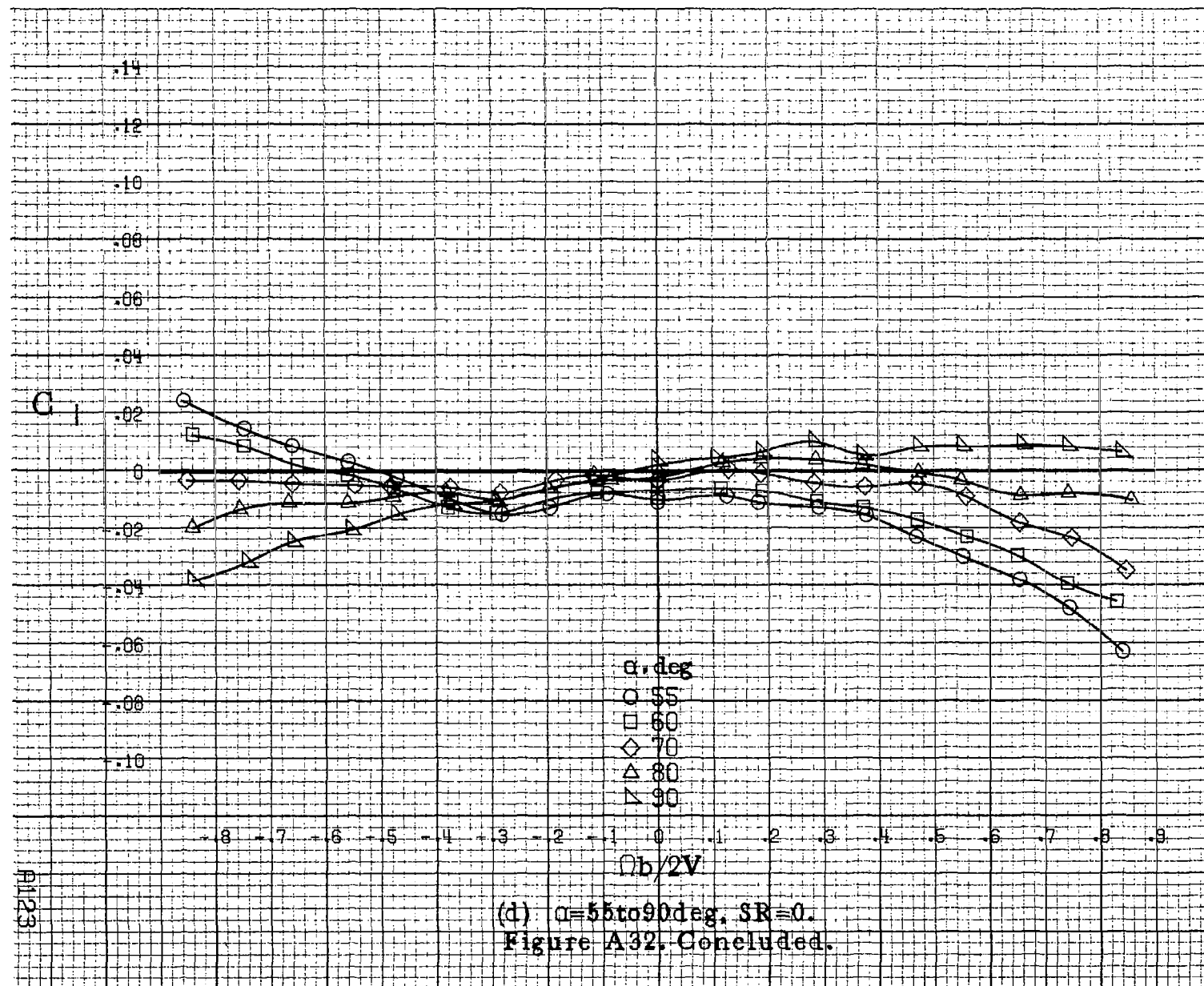
Figure A32. Effect of rotation rate and angle of attack on rolling moment coefficient for configuration having ventrals and strakes off. $\delta_a = -20^\circ$, $\delta_s = -20^\circ$, $\delta_r = -28^\circ$, $\beta = 0^\circ$.

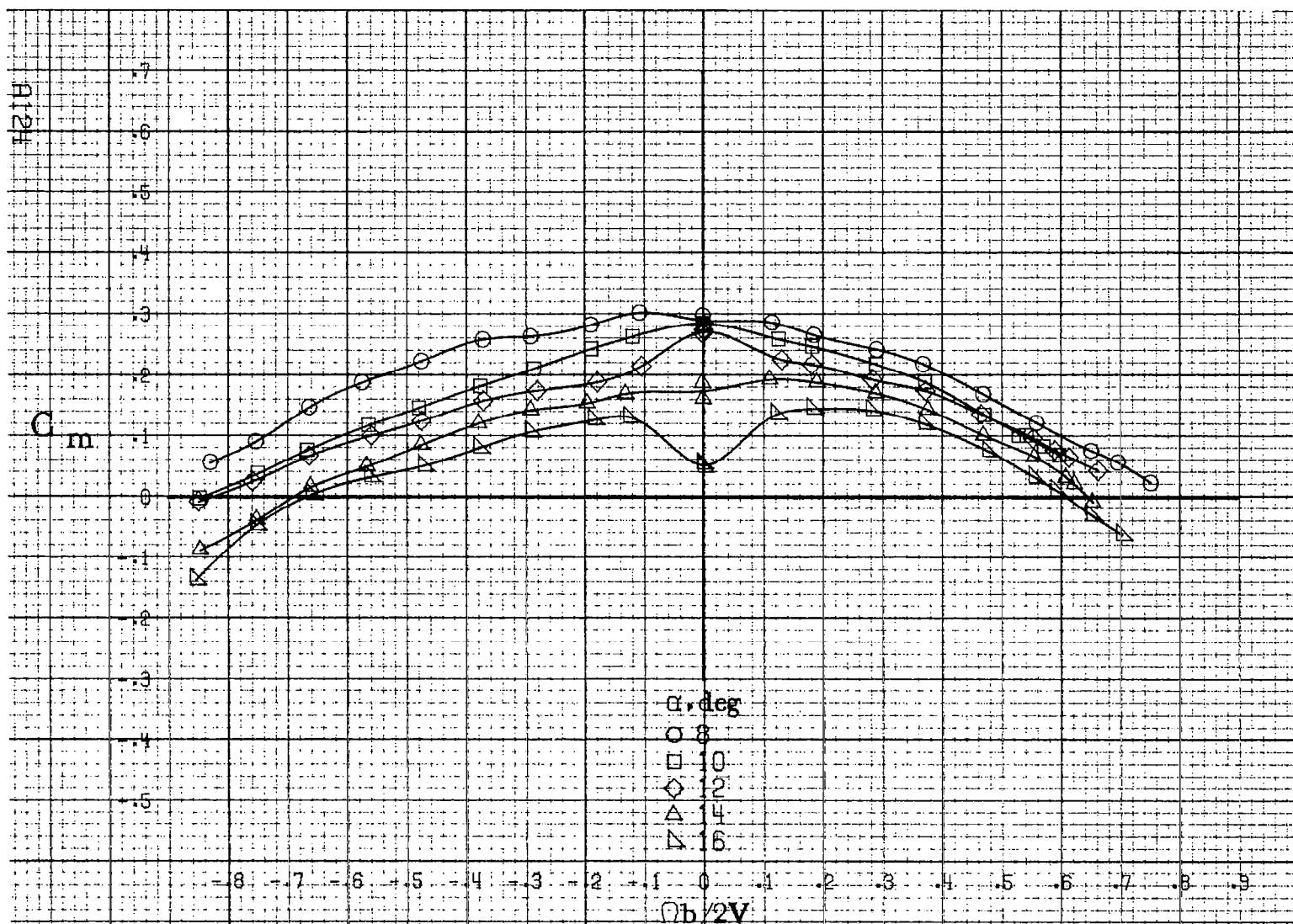




(c) $\alpha=30$ to 50 deg, $SR=0$.

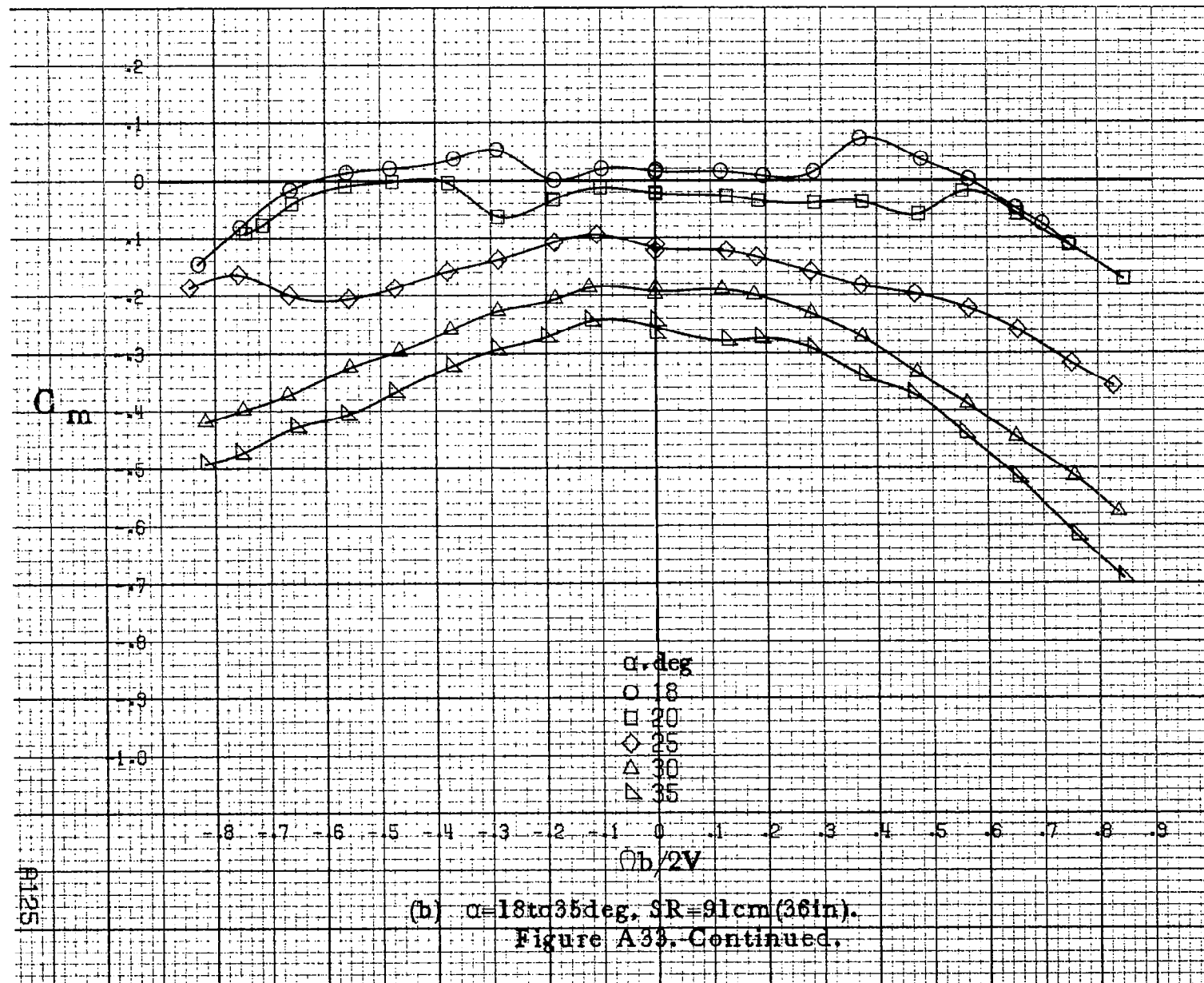
Figure A32.-Continued.

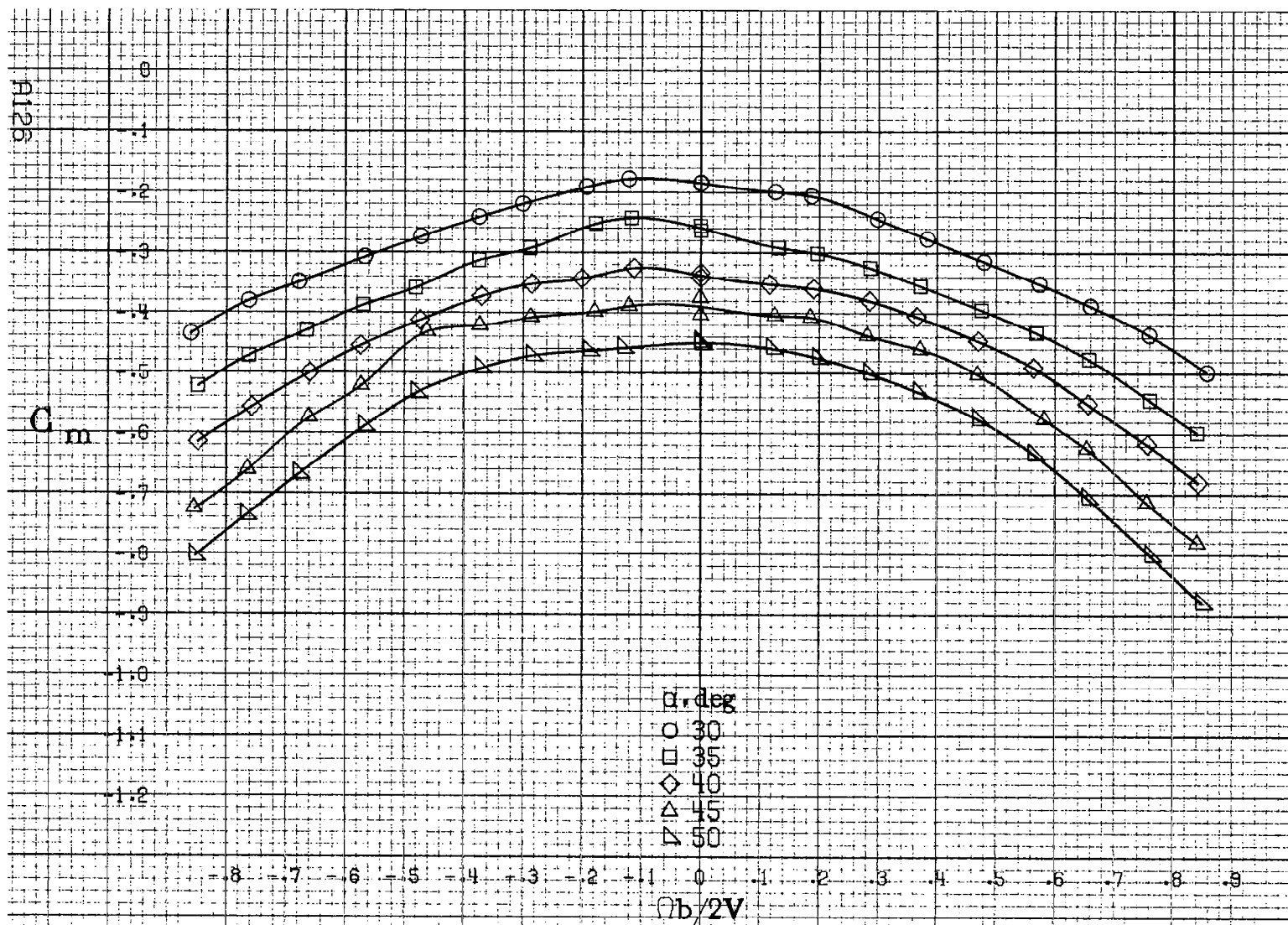




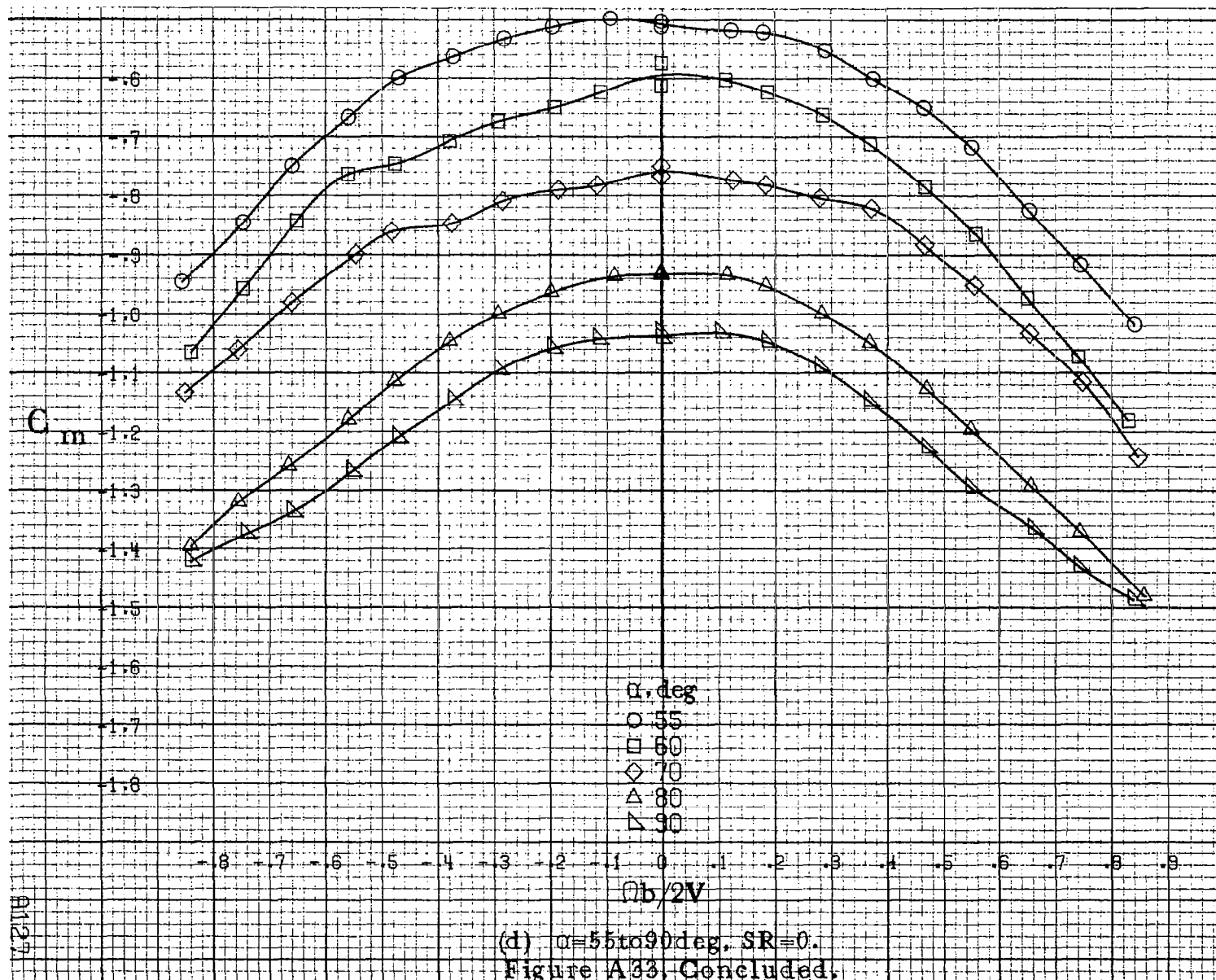
(a) $\alpha = 8 \text{ to } 16 \text{ deg}$, $SR = 91 \text{ cm (36 in)}$.

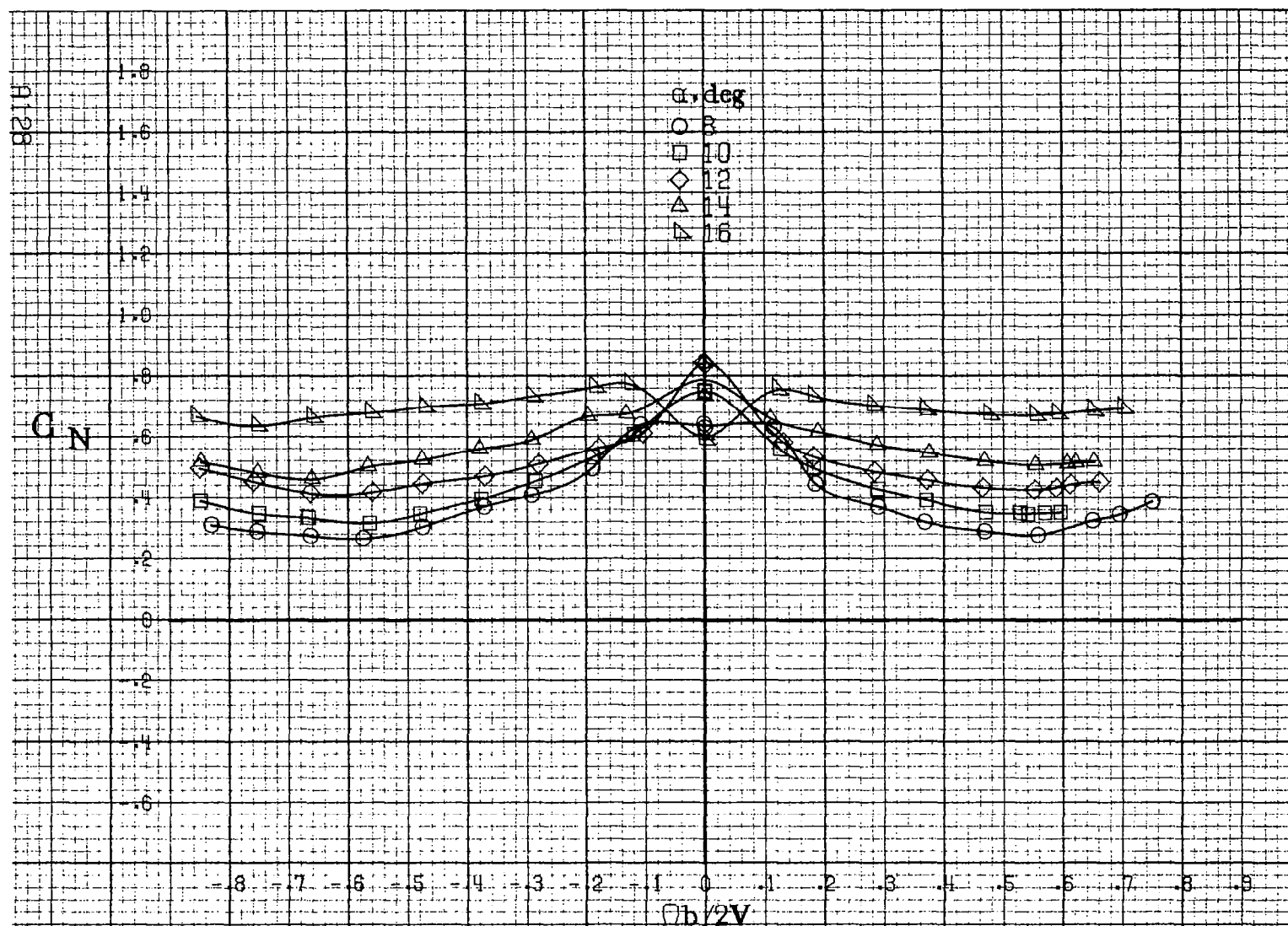
Figure A-33. Effect of rotation rate and angle of attack on pitching-moment coefficient for configuration having venturals and strakes off. $\delta_r = -20^\circ$, $\delta_a = 20^\circ$, $B = 0^\circ$.





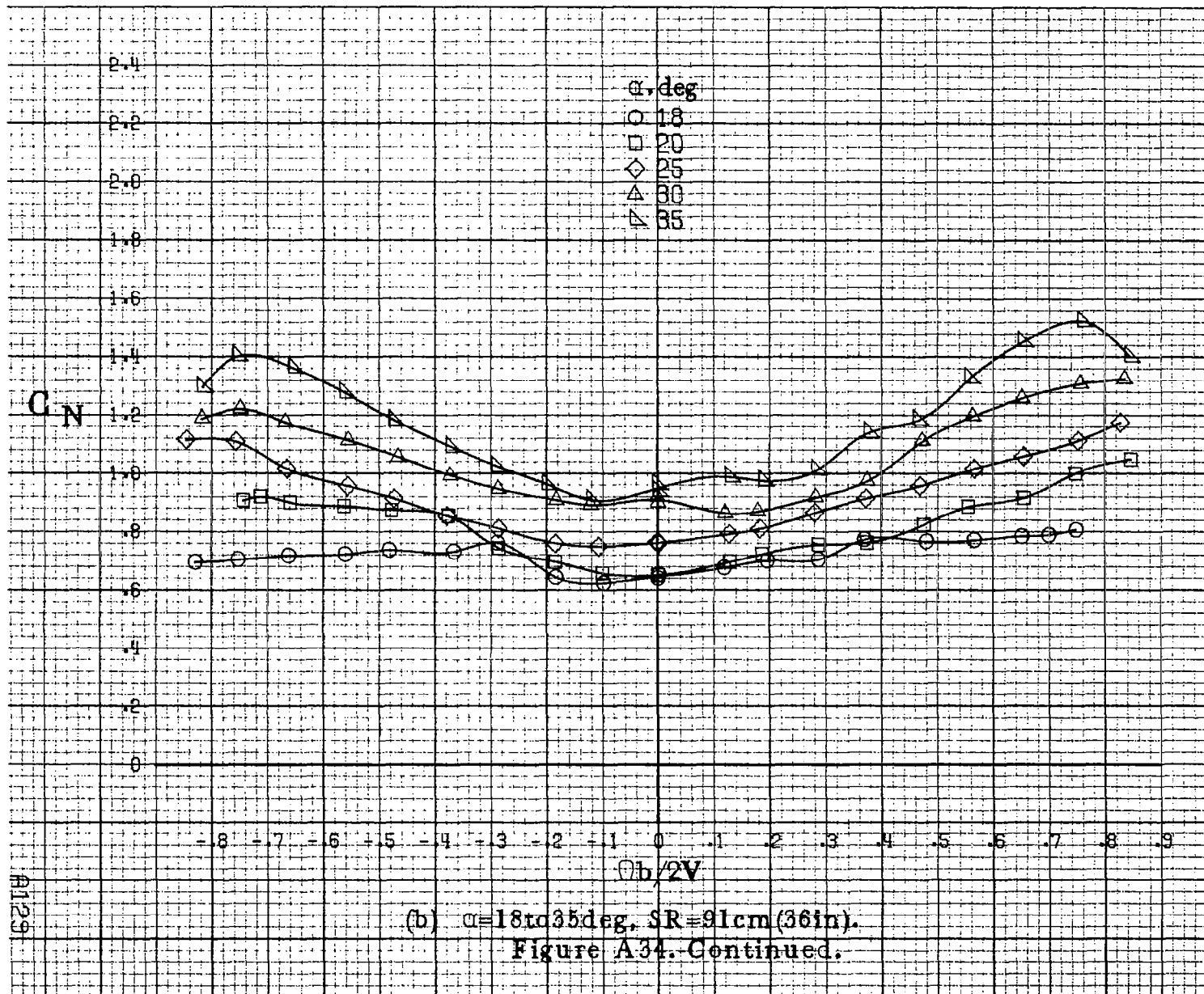
(c) $\alpha=30$ to 50° , $SR=0$.
 Figure A33. Continued.

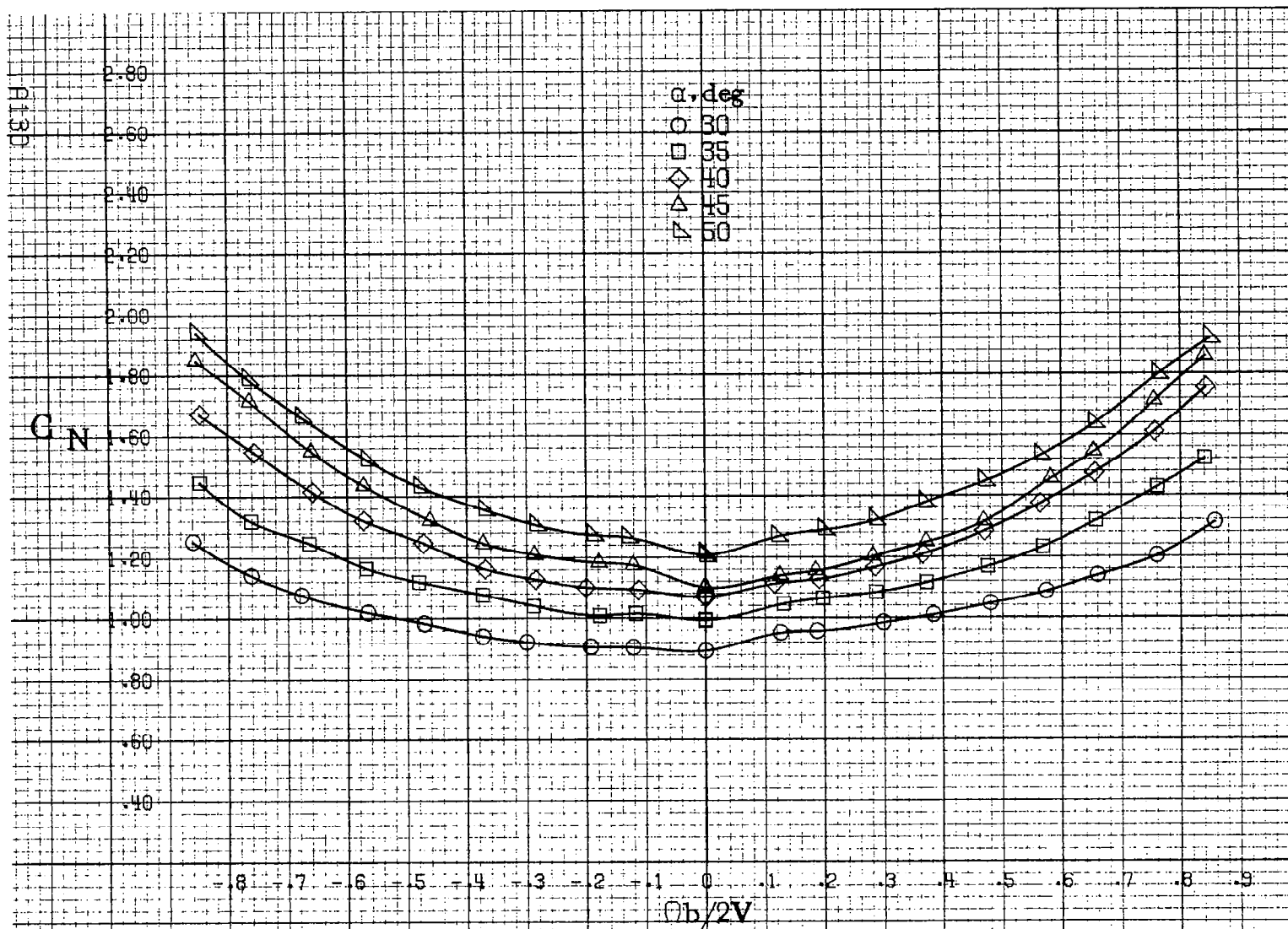




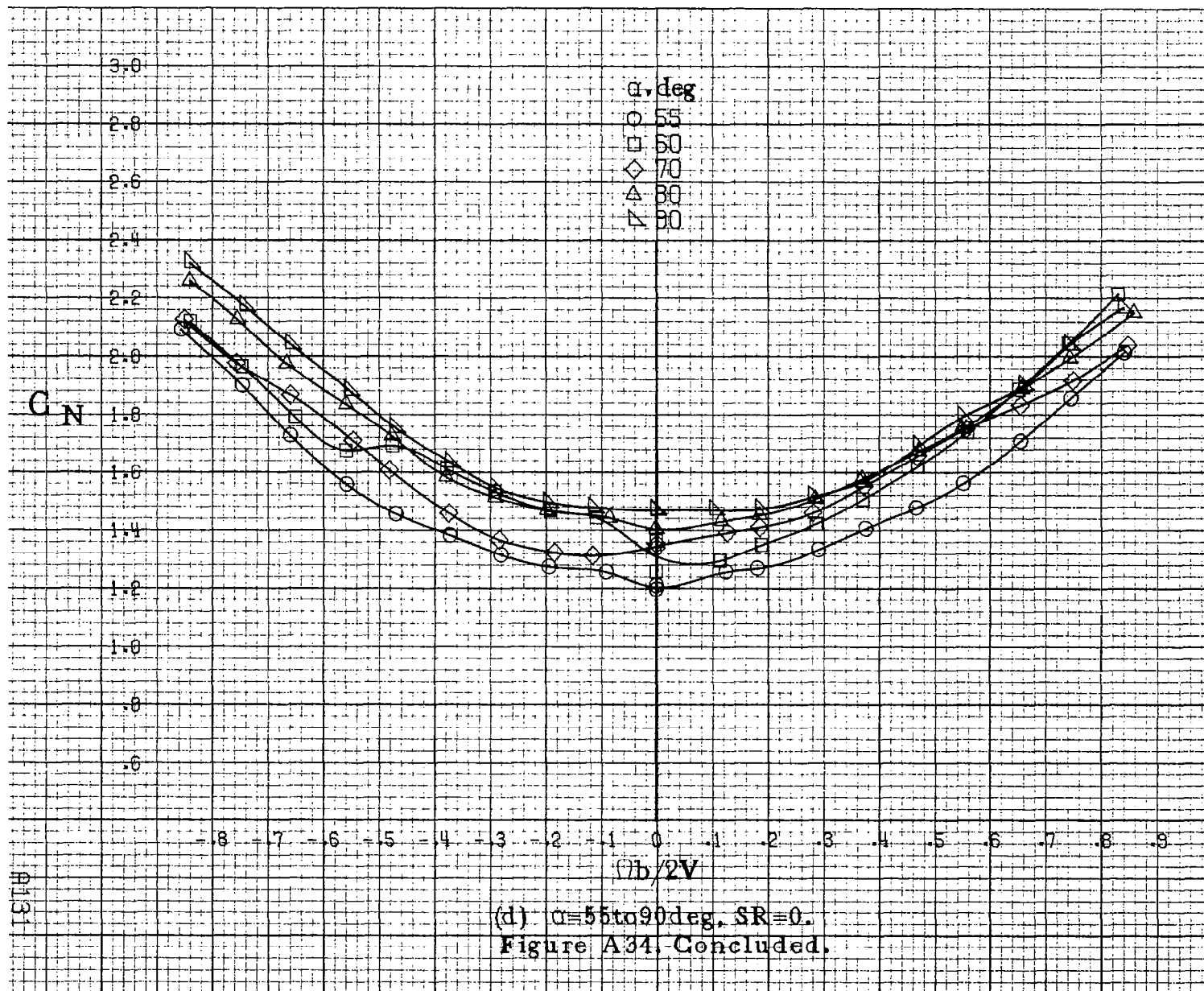
(a) $\alpha = 3$ to 16 deg, SR = 91 cm (36 in).

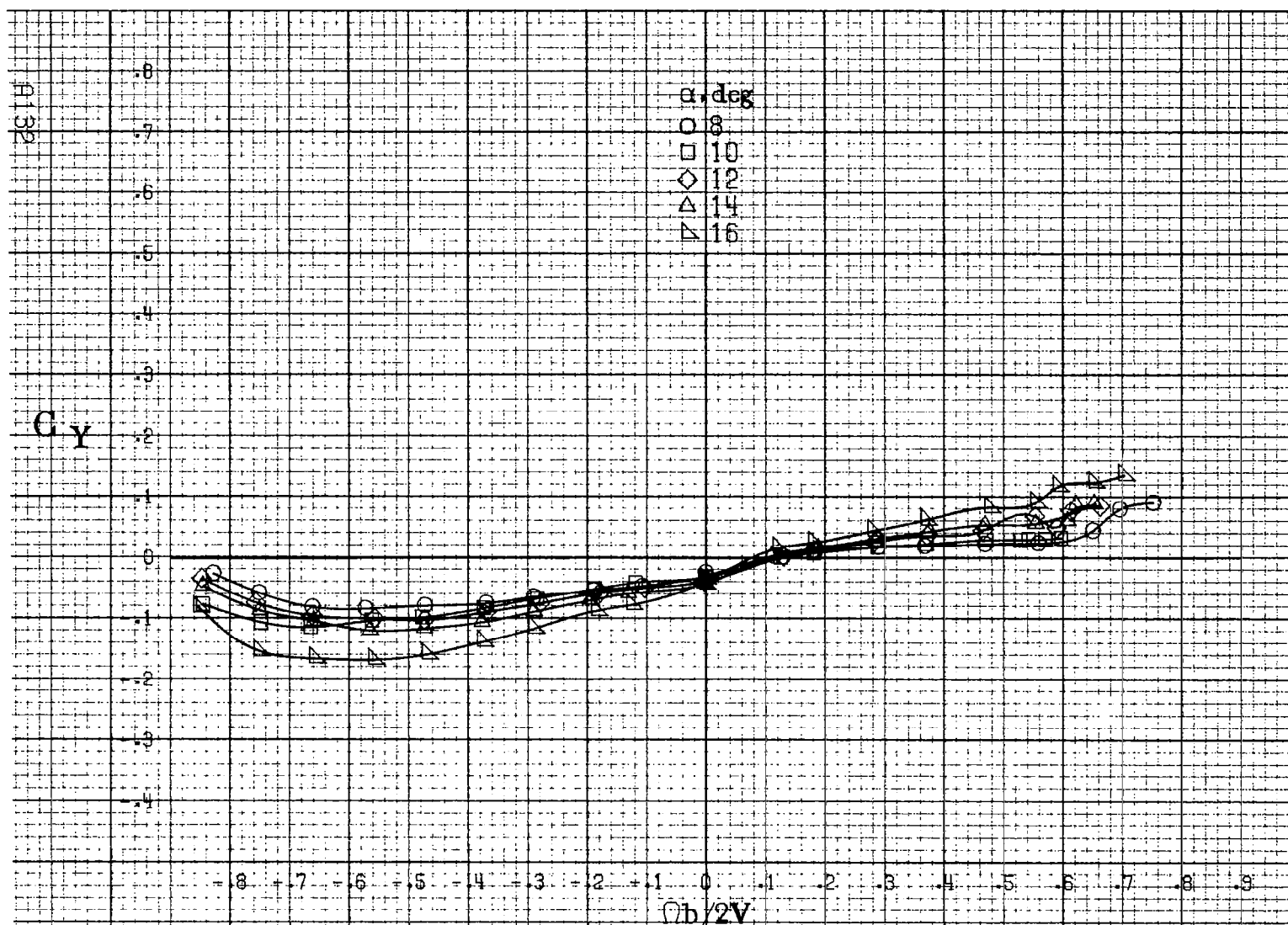
Figure A-34. Effect of rotation rate and angle of attack on normal force coefficient for configuration having ventrals and strakes off. $\delta_r = -28^\circ$, $\delta_s = 0^\circ$, $\delta_a = -20^\circ$, $\delta_e = 20^\circ$.





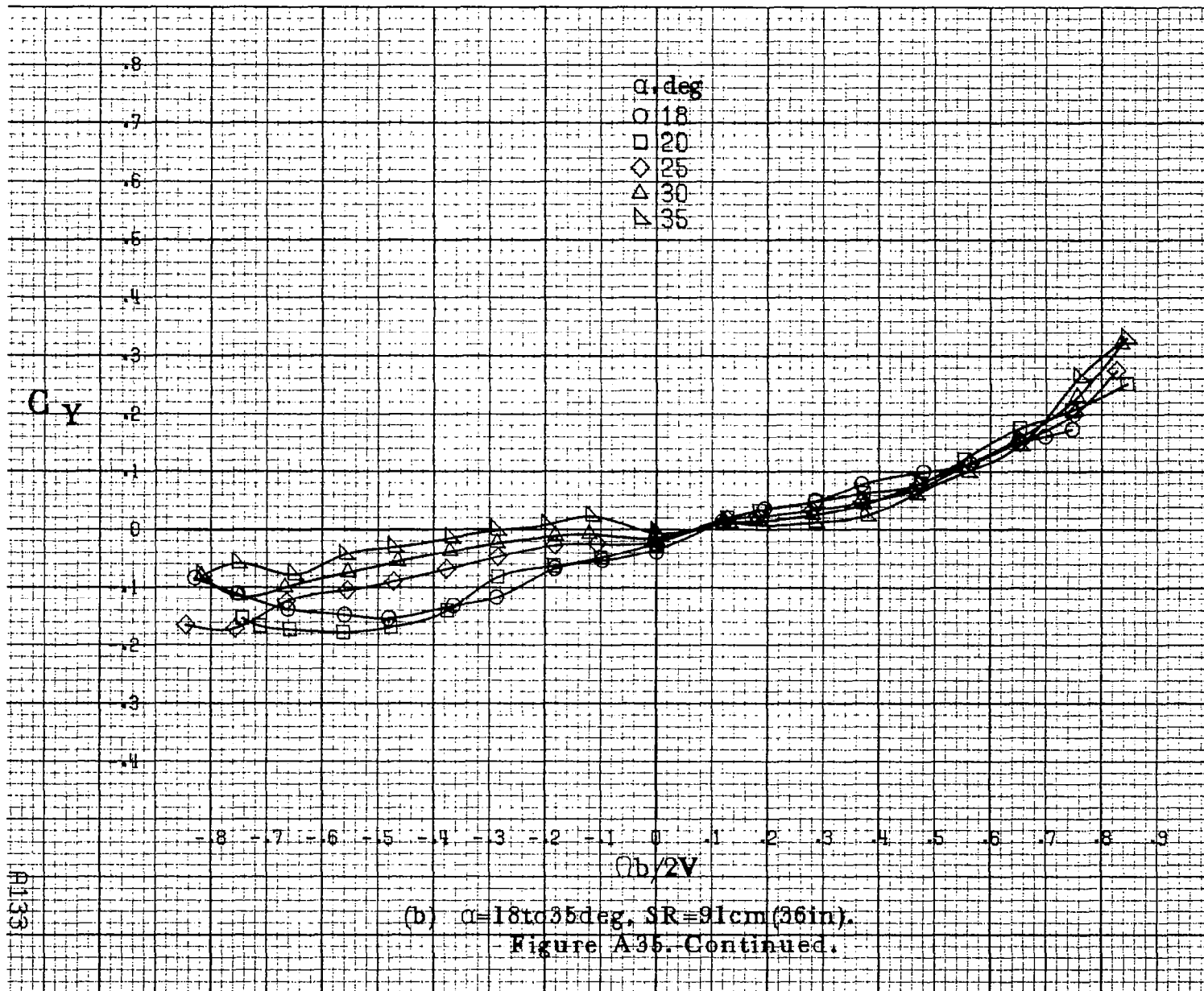
(c) $\alpha = 30$ to 50 deg, $SR = 0$.
Figure A34, Continued.

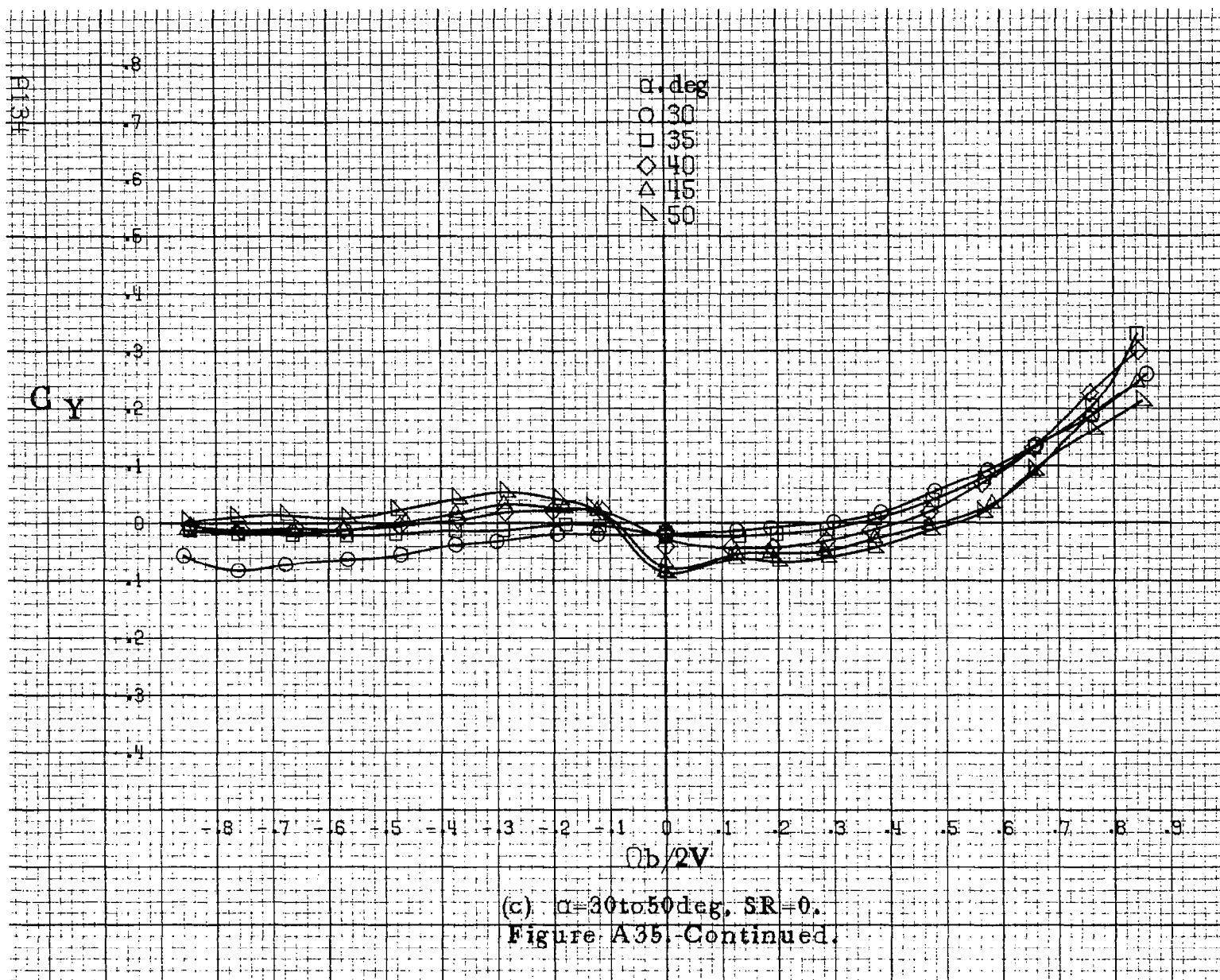


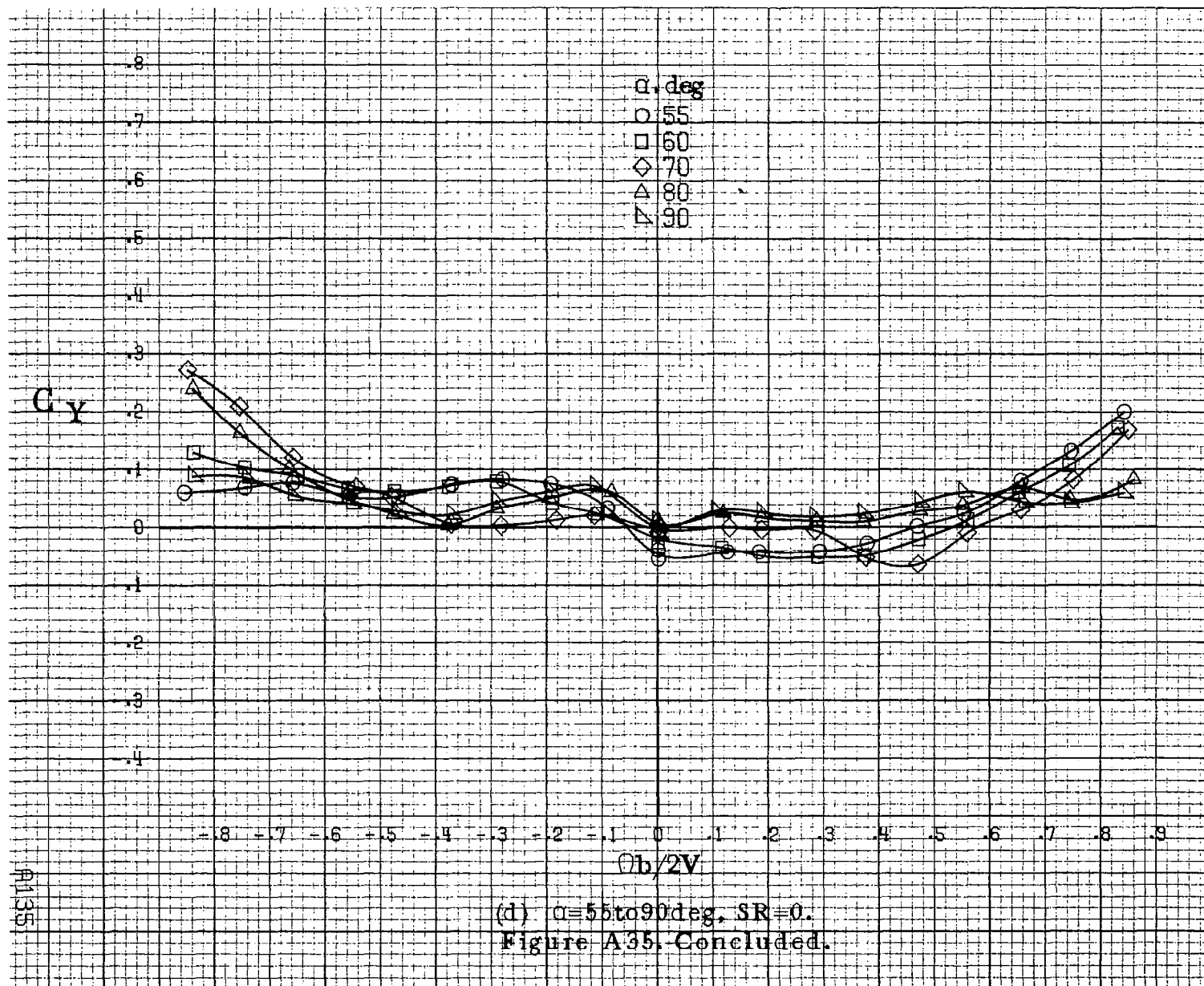


(a) $\alpha=8$ to 16° , $SR=91\text{cm}(36\text{in})$.

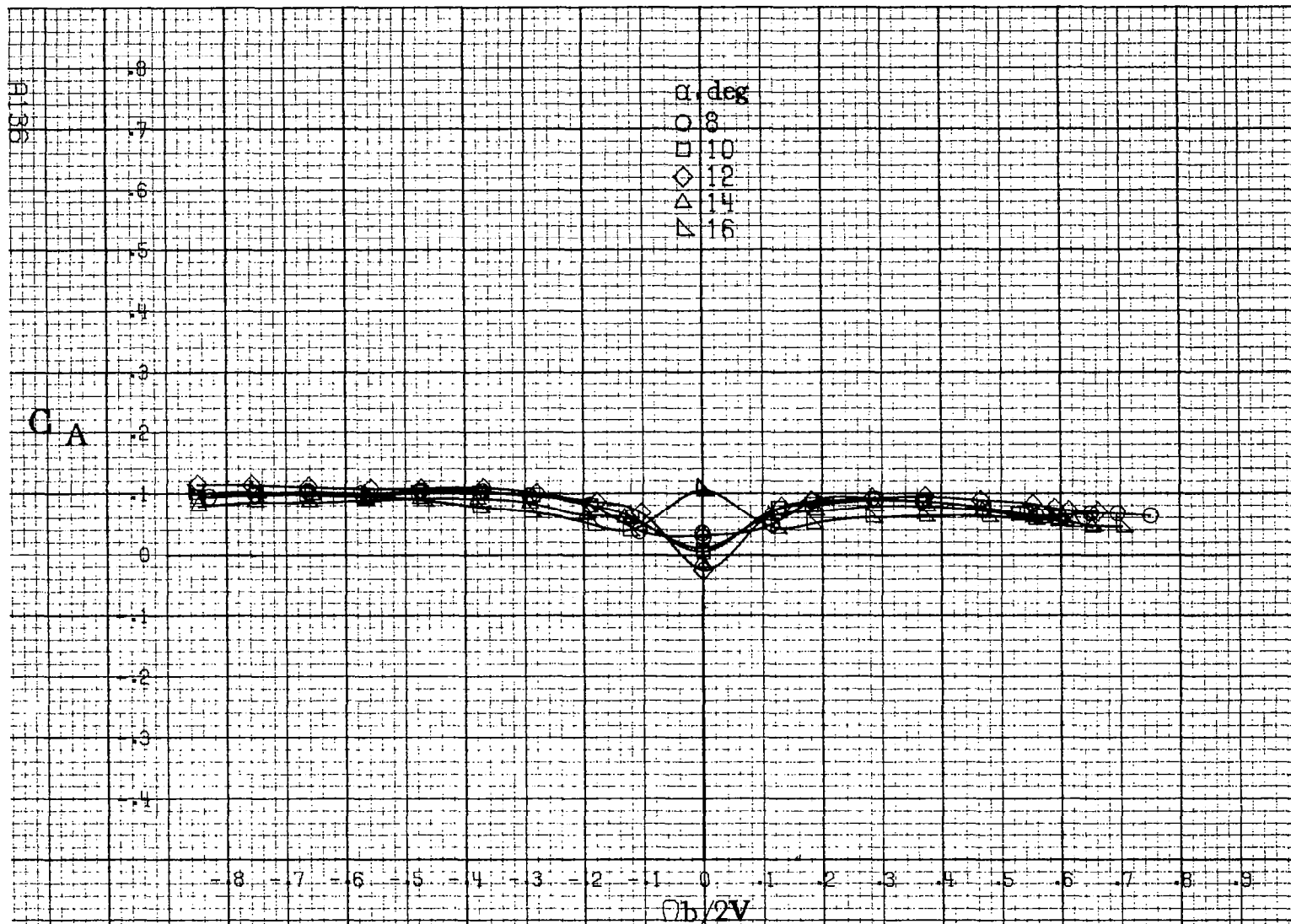
Figure A.35. Effect of rotation rate and angle of attack on side force coefficient for configuration having ventrals and strakes off. $\delta_r = +20^\circ$, $\delta_a = 20^\circ$, $\delta_r = -20^\circ$, $\delta_a = 0^\circ$.





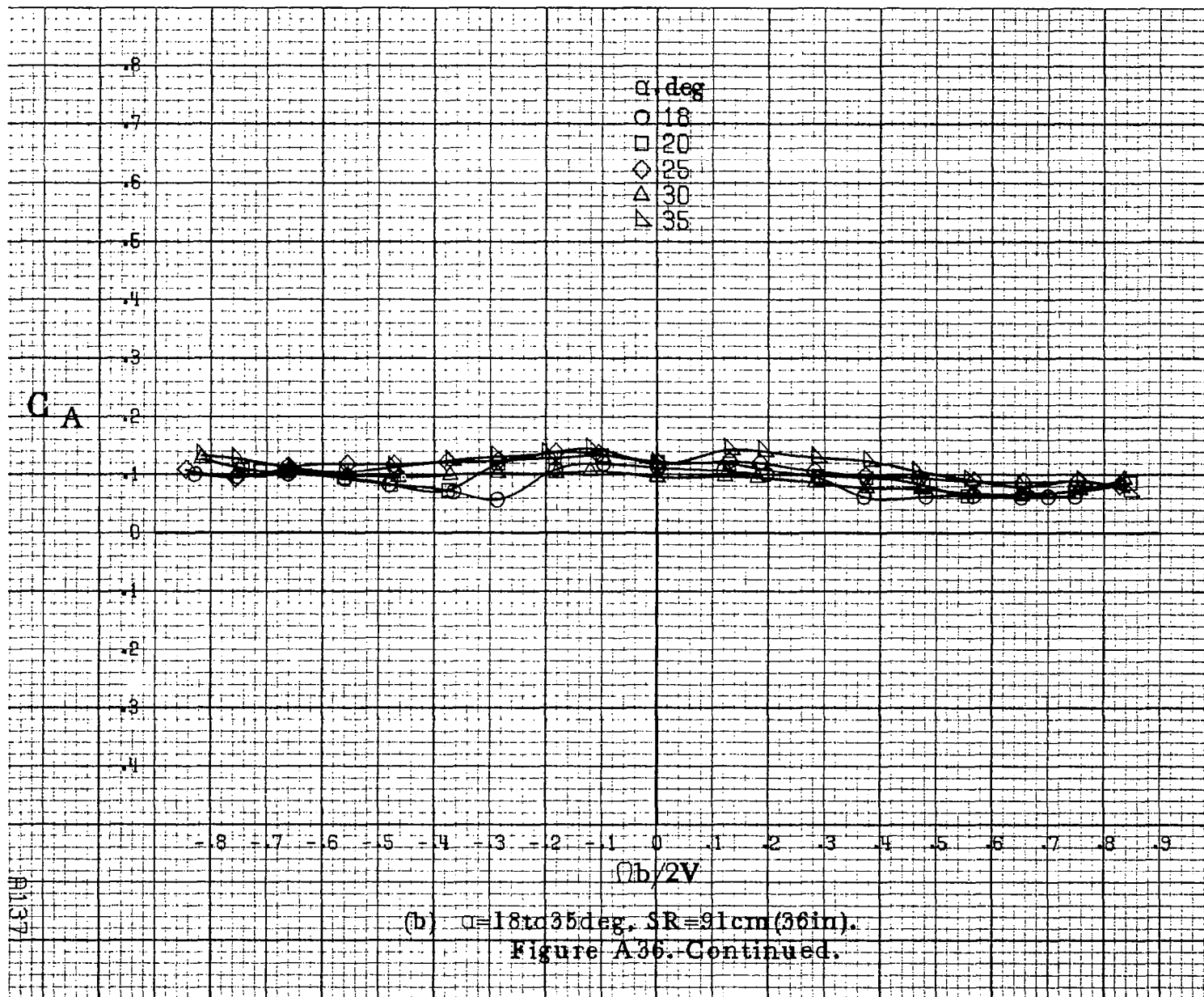


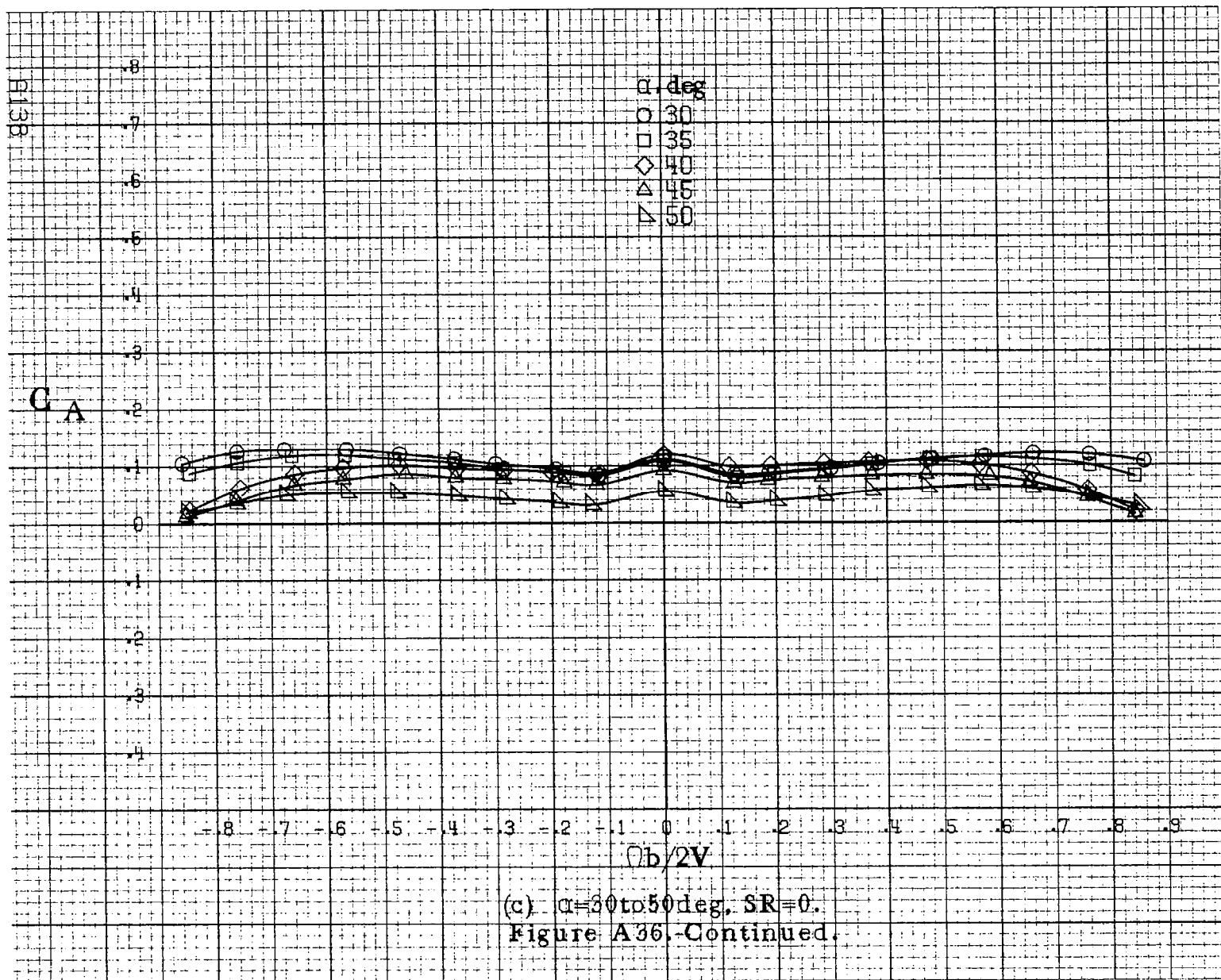
(d) $\alpha=55$ to 90° , $SR=0$.
Figure A35. Concluded.

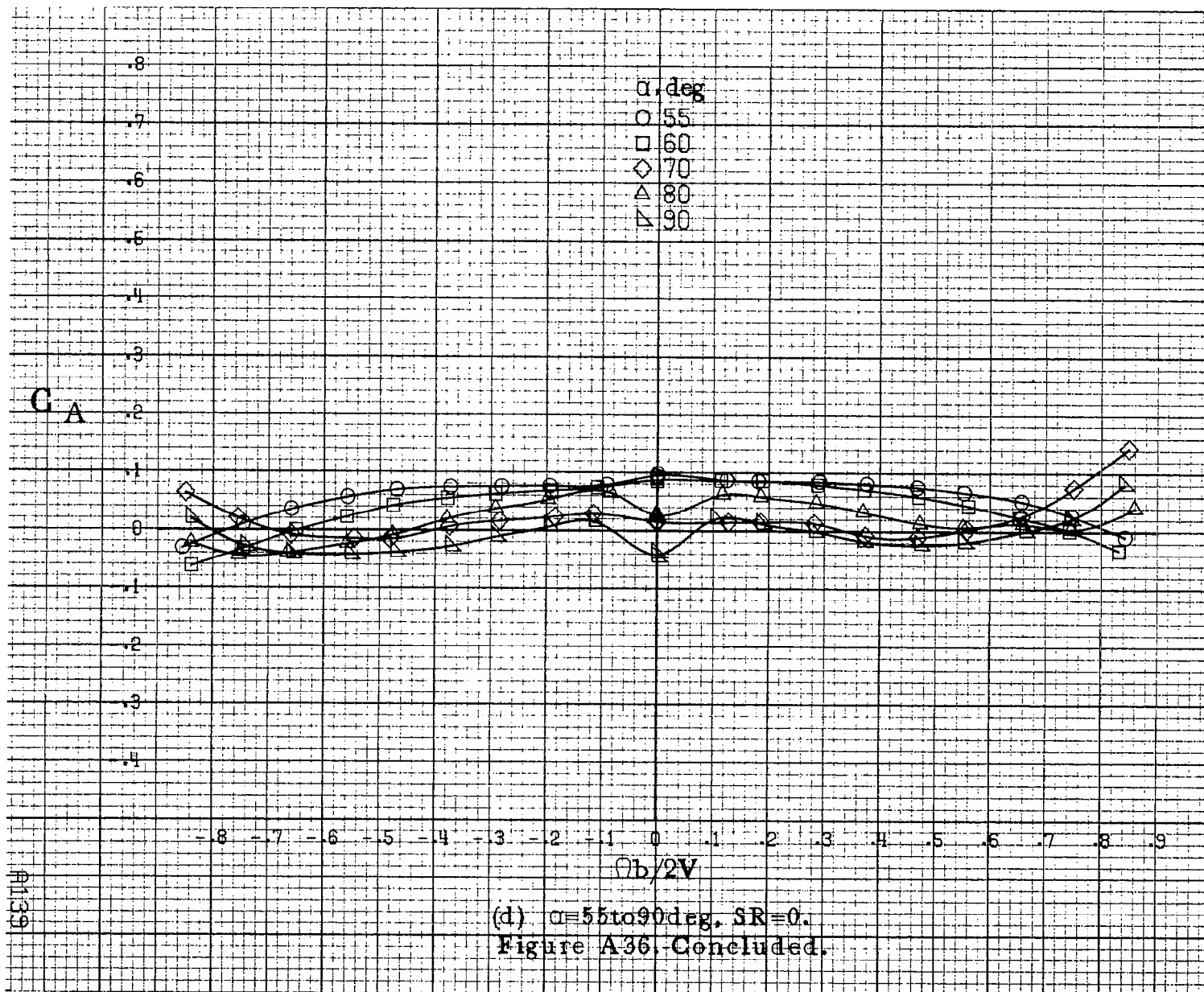


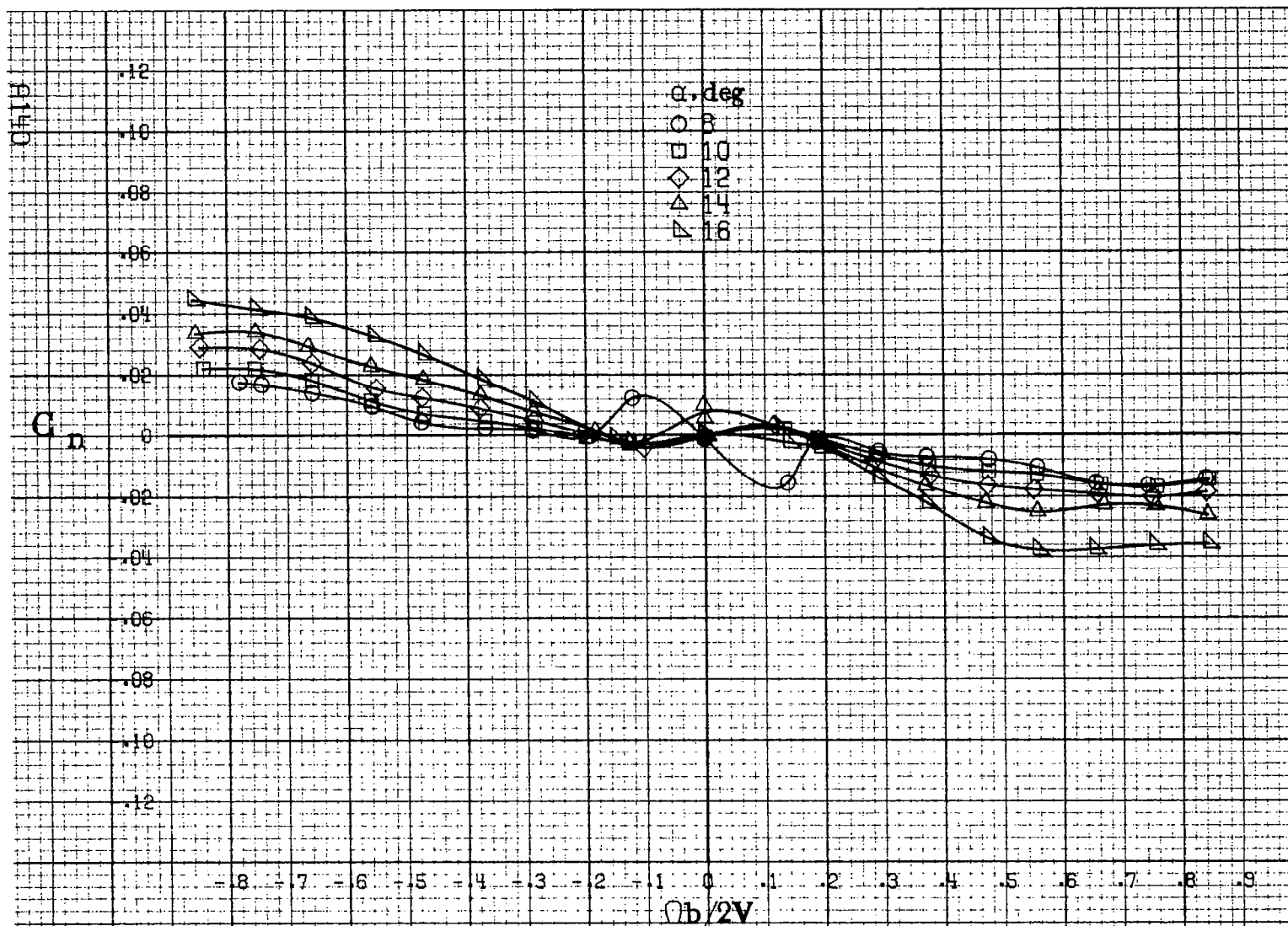
(a) $\alpha=8$ to 16° , $SR=91\text{cm}(36\text{in})$.

Figure A36. Effect of rotation rate and angle of attack on axial force coefficient for configuration having ventrals and strakes off. $\delta_r = -20^\circ$, $\delta_a = -20^\circ$, $\delta_r = -25^\circ$, $\delta = 0^\circ$.



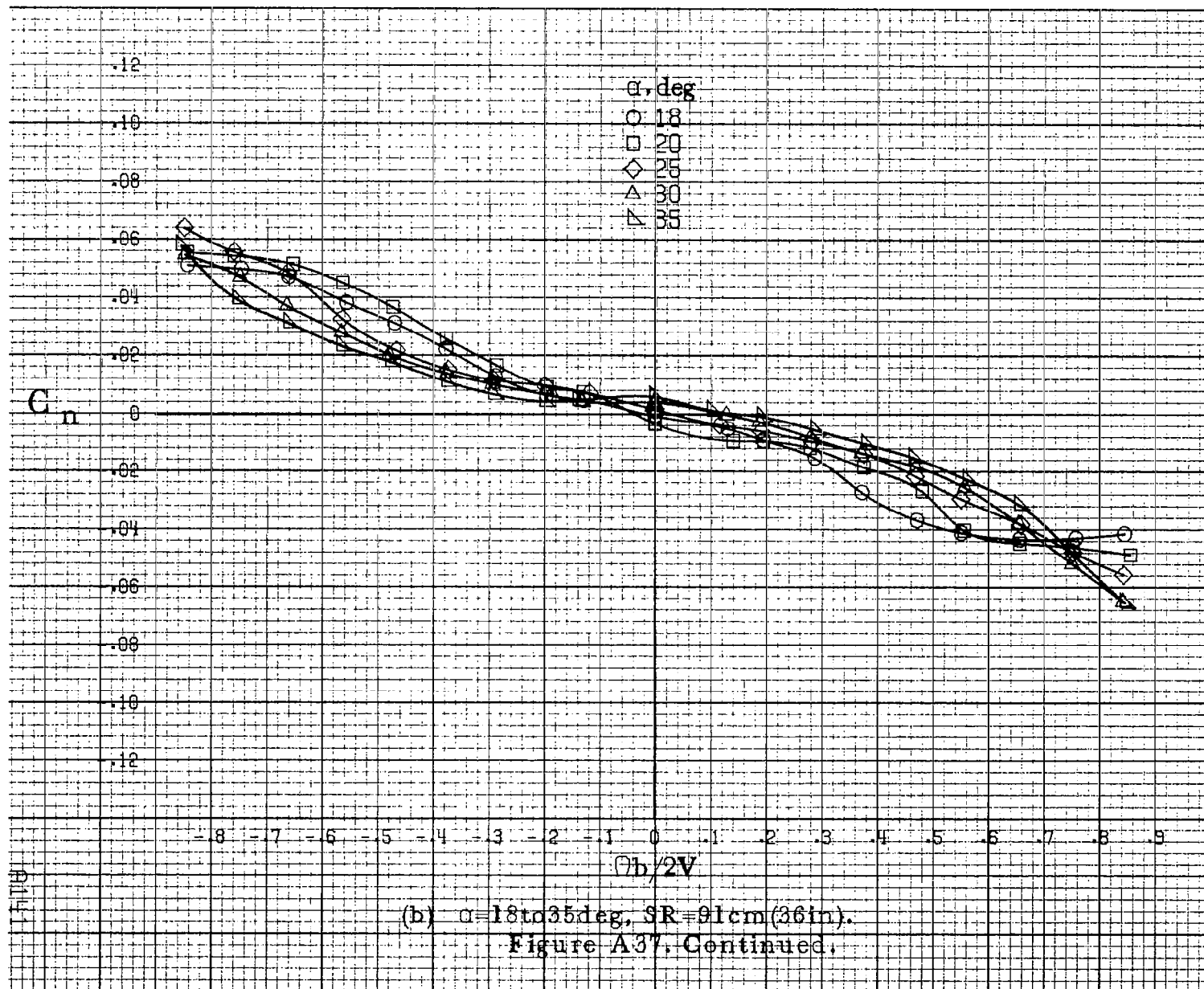


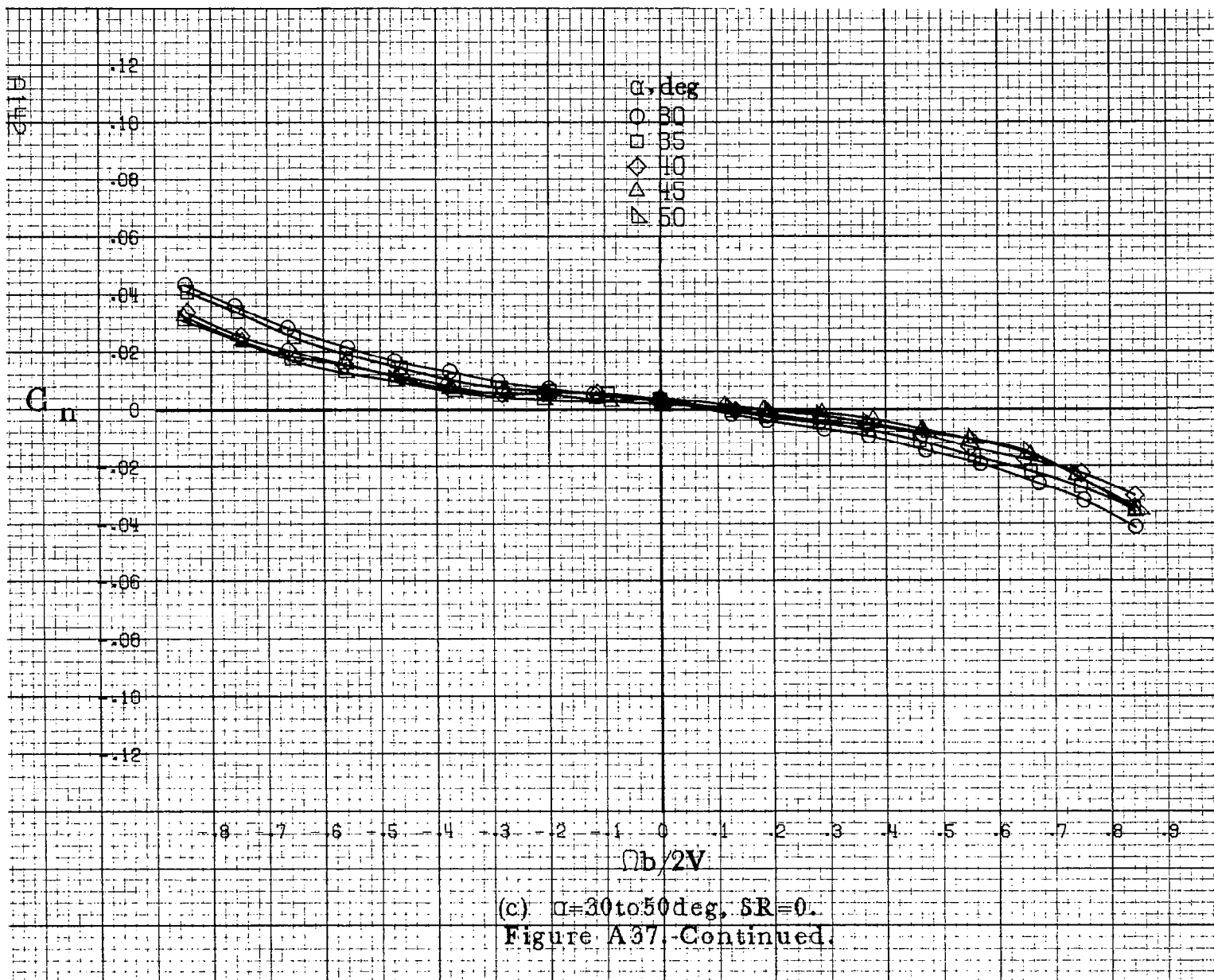


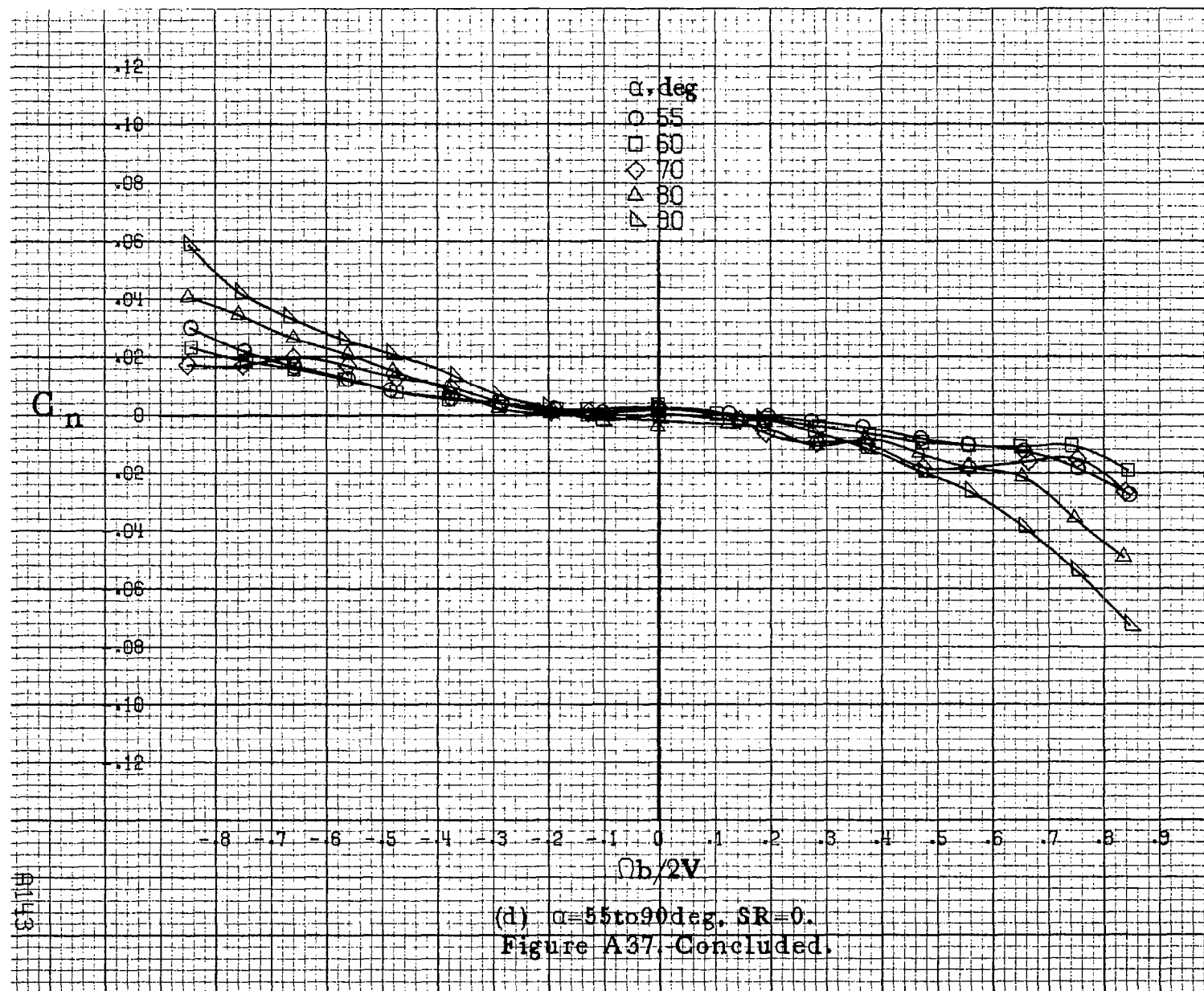


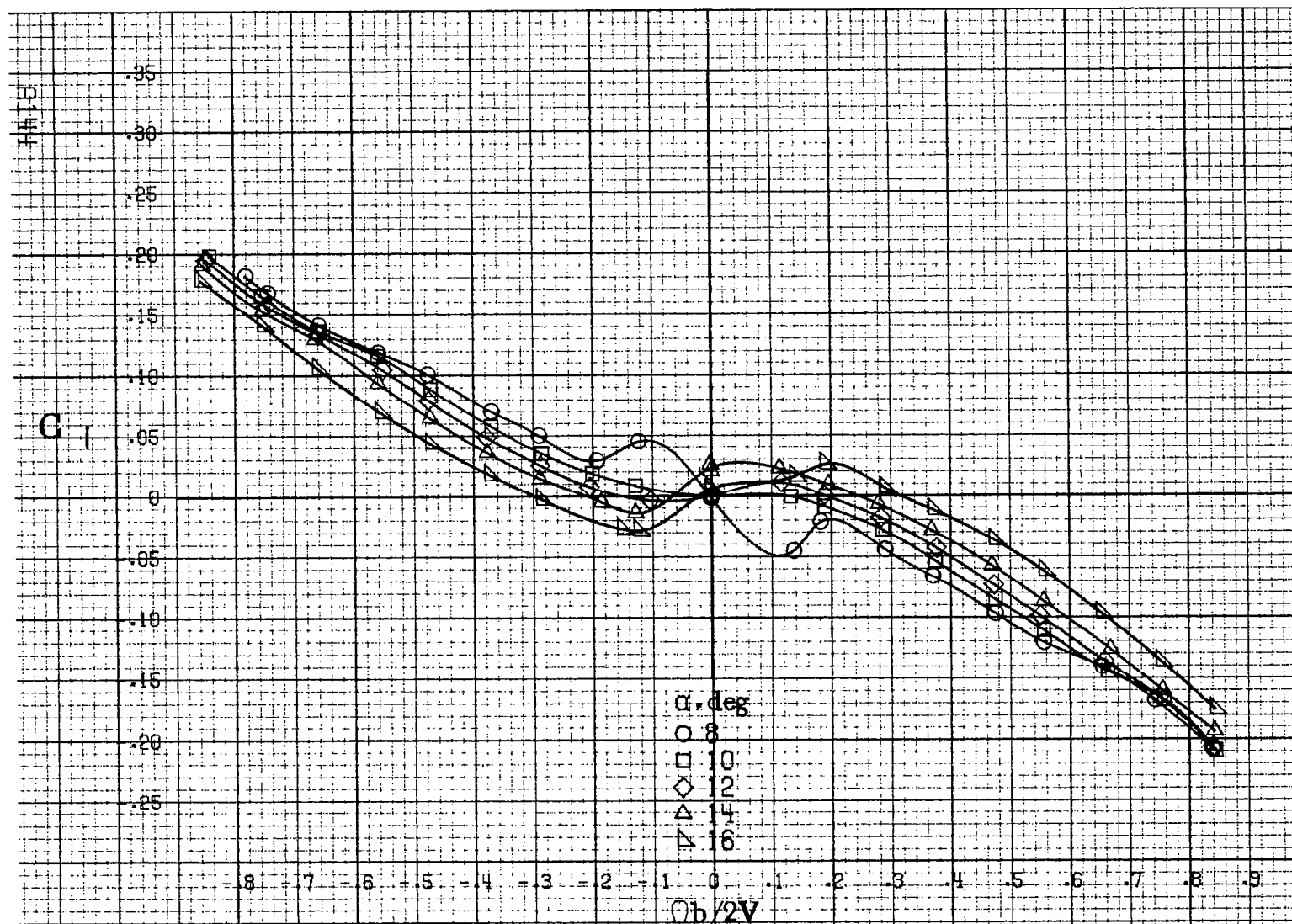
(a) $\alpha=8$ to 16° , $SR=91$ cm (36 in).

Figure A37. Effect of rotation rate and angle of attack on yawing moment coefficient for configuration having sharp-edged fuselage bottom. $\delta_a=0^\circ$, $\delta_s=0^\circ$, $\beta=0^\circ$.



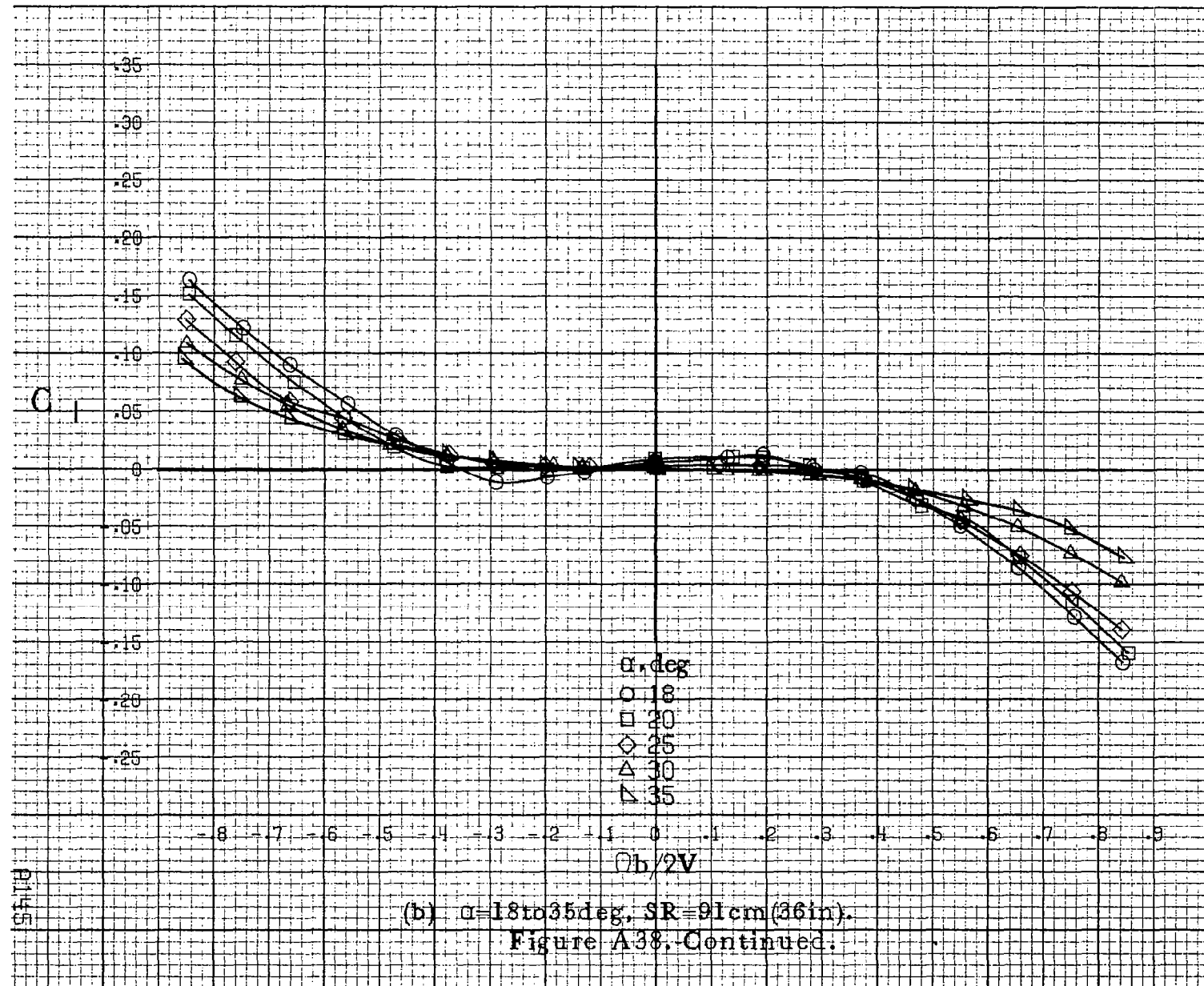


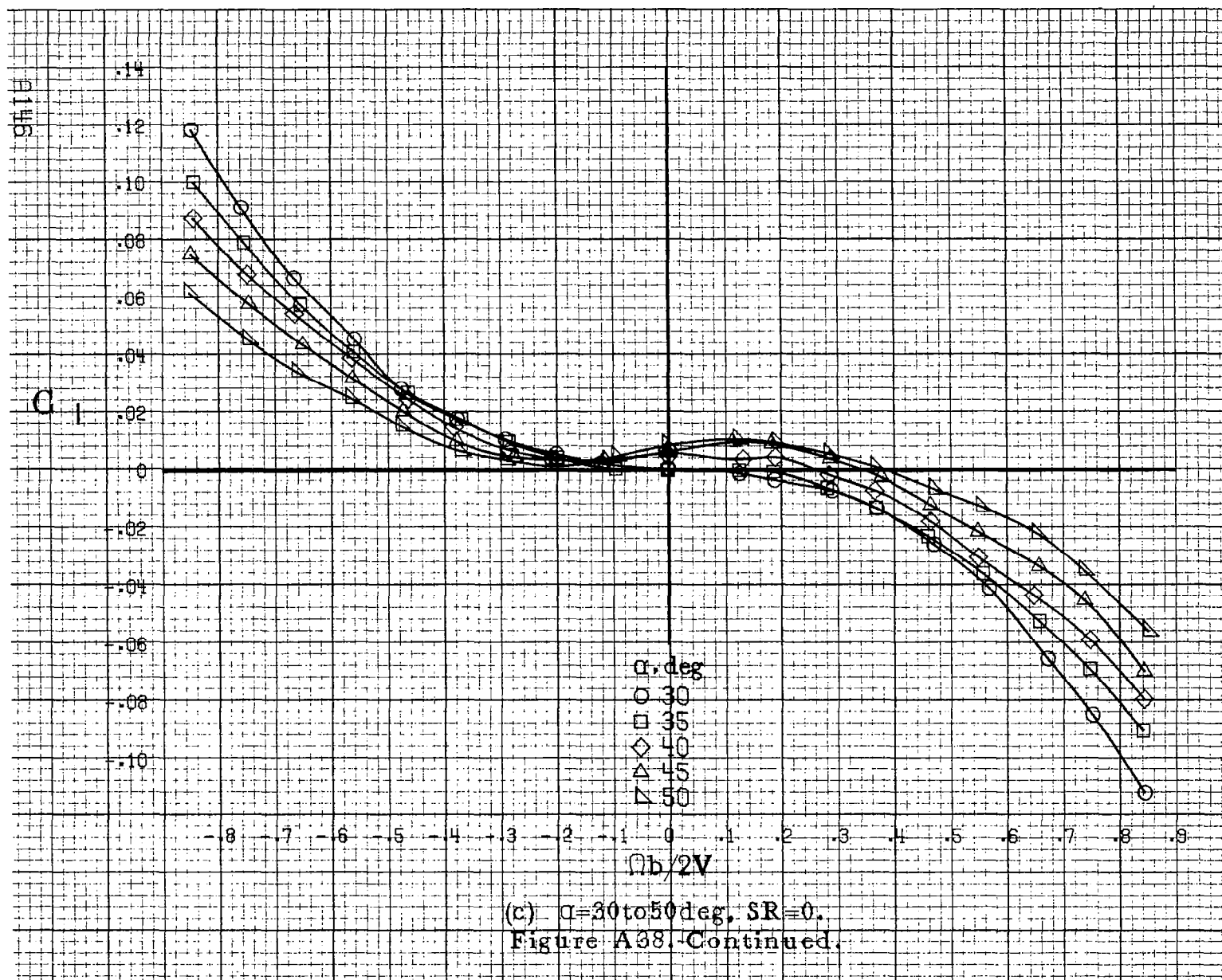


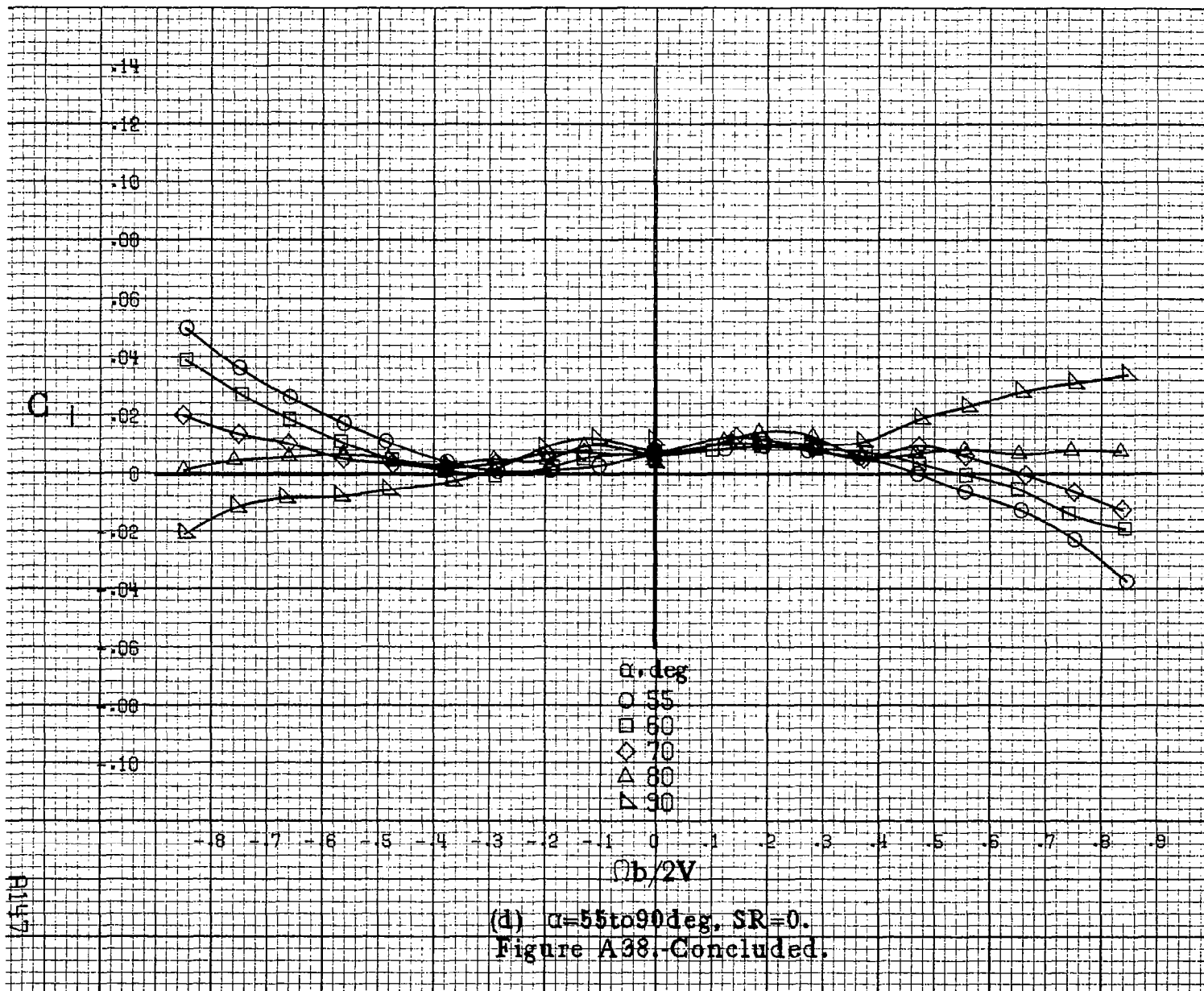


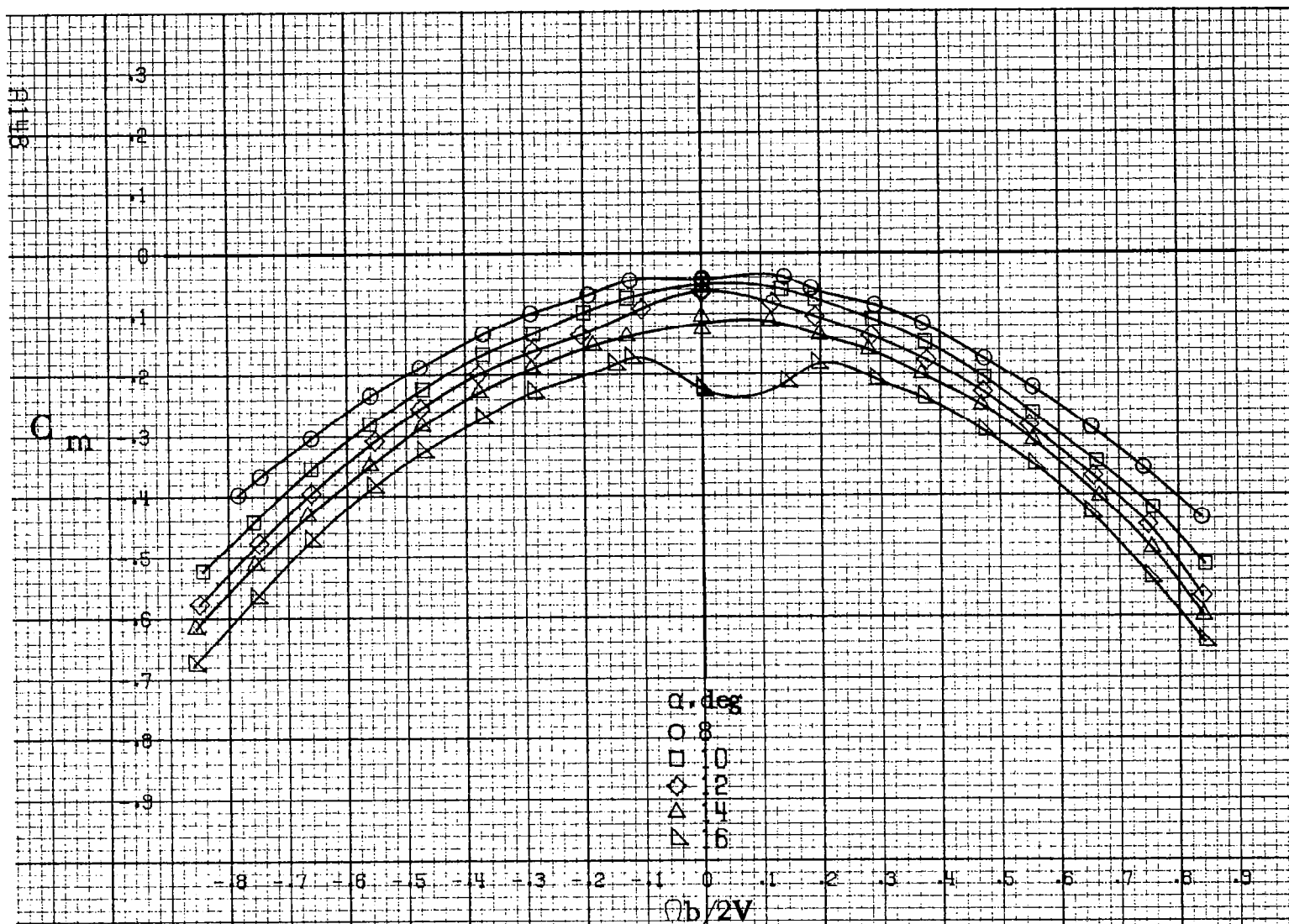
(a) $\alpha=8$ to 16° , $SR=91\text{cm}(36\text{in})$.

Figure A38. Effect of rotation rate and angle of attack on rolling-moment coefficient for configuration having sharp-edged fuselage bottom. $\delta_a=0^\circ$, $\delta_r=0^\circ$, $\beta=0^\circ$.



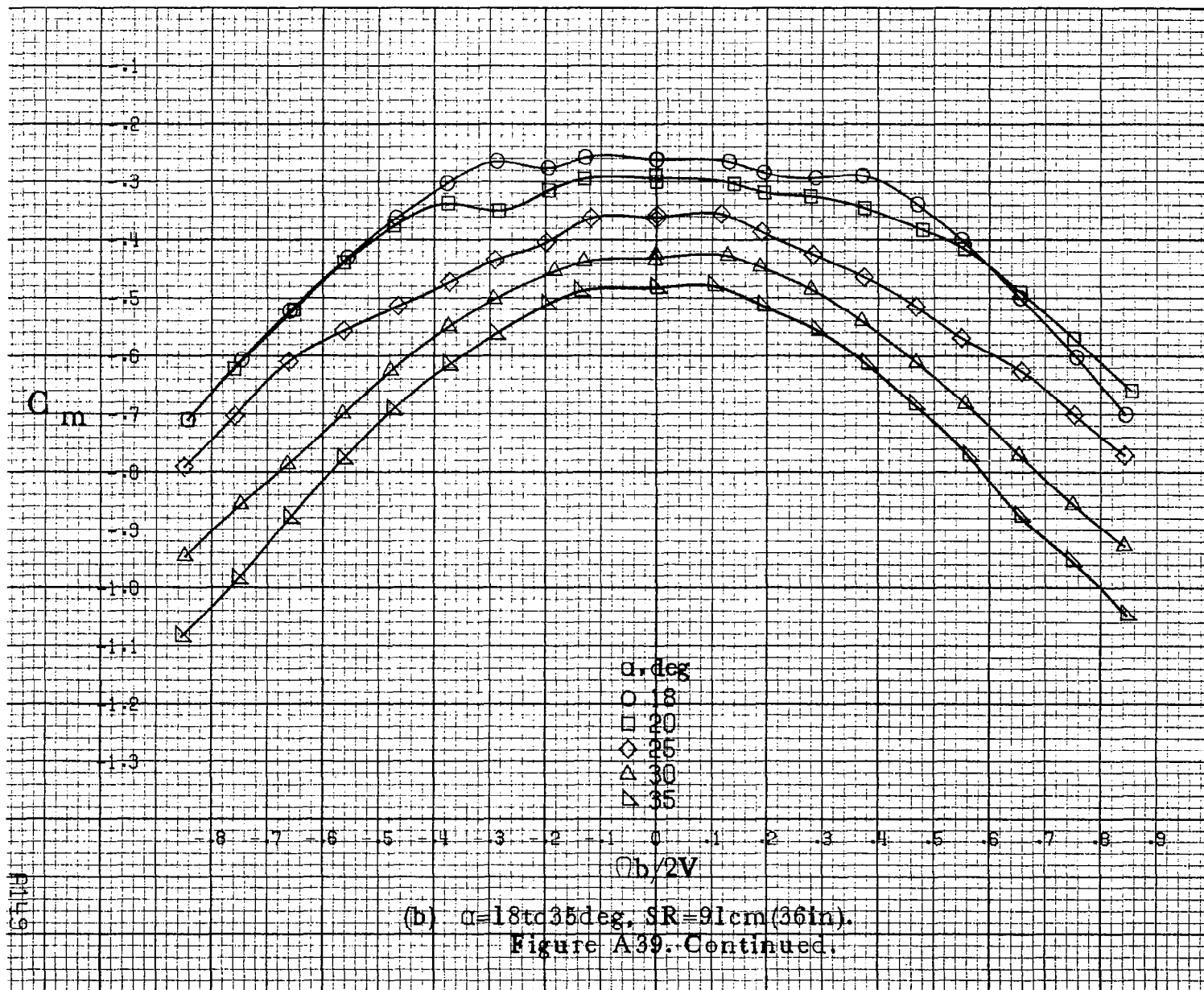


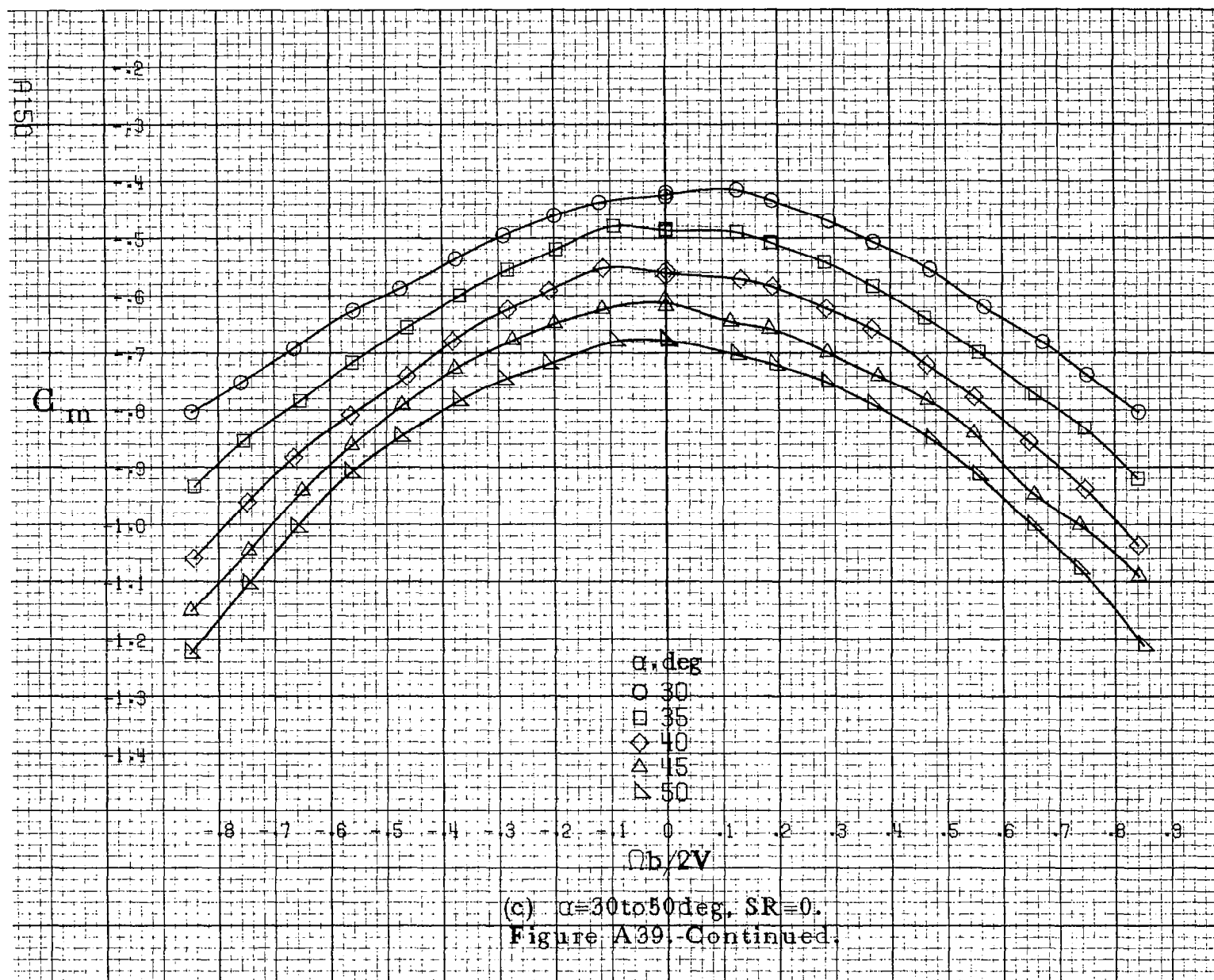


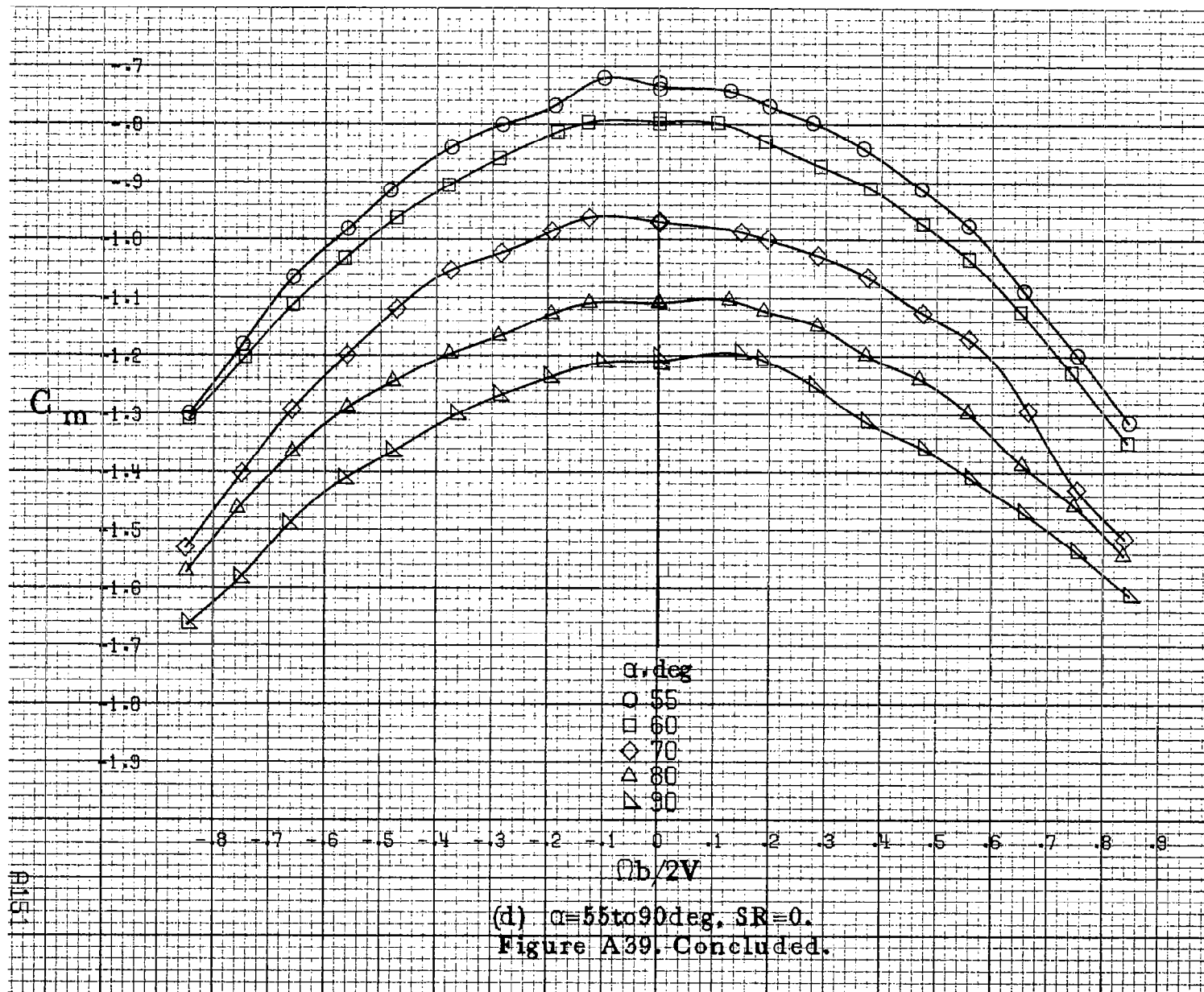


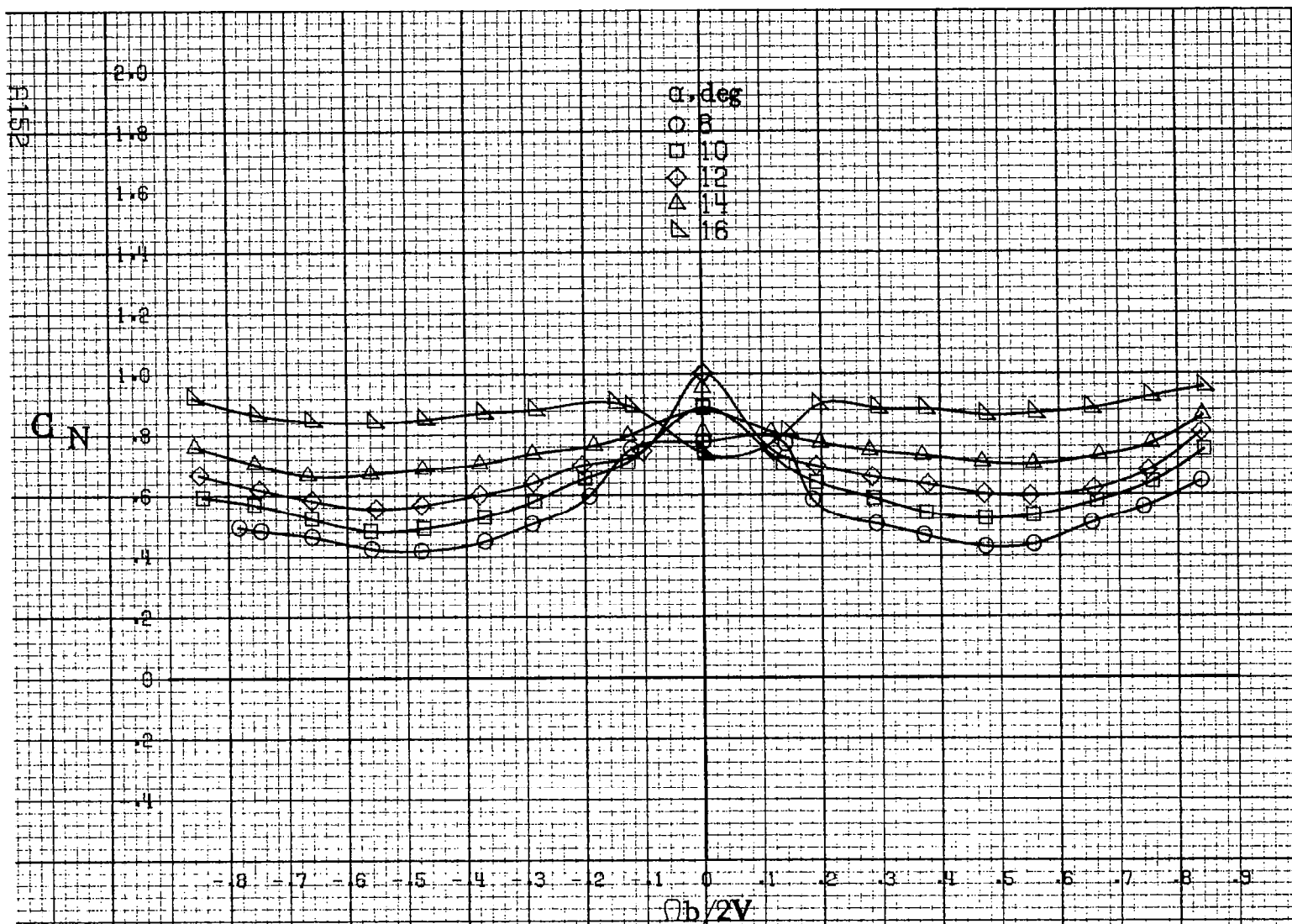
(a) $\alpha = 8$ to 16° , $SR = 91 \text{ cm (36 in.)}$.

Figure A39. Effect of rotation rate and angle of attack on pitching moment coefficient for configuration having sharp-edged fuselage bottom. $\delta_a = 0^\circ$, $\delta_c = 0^\circ$, $\beta = 0^\circ$.



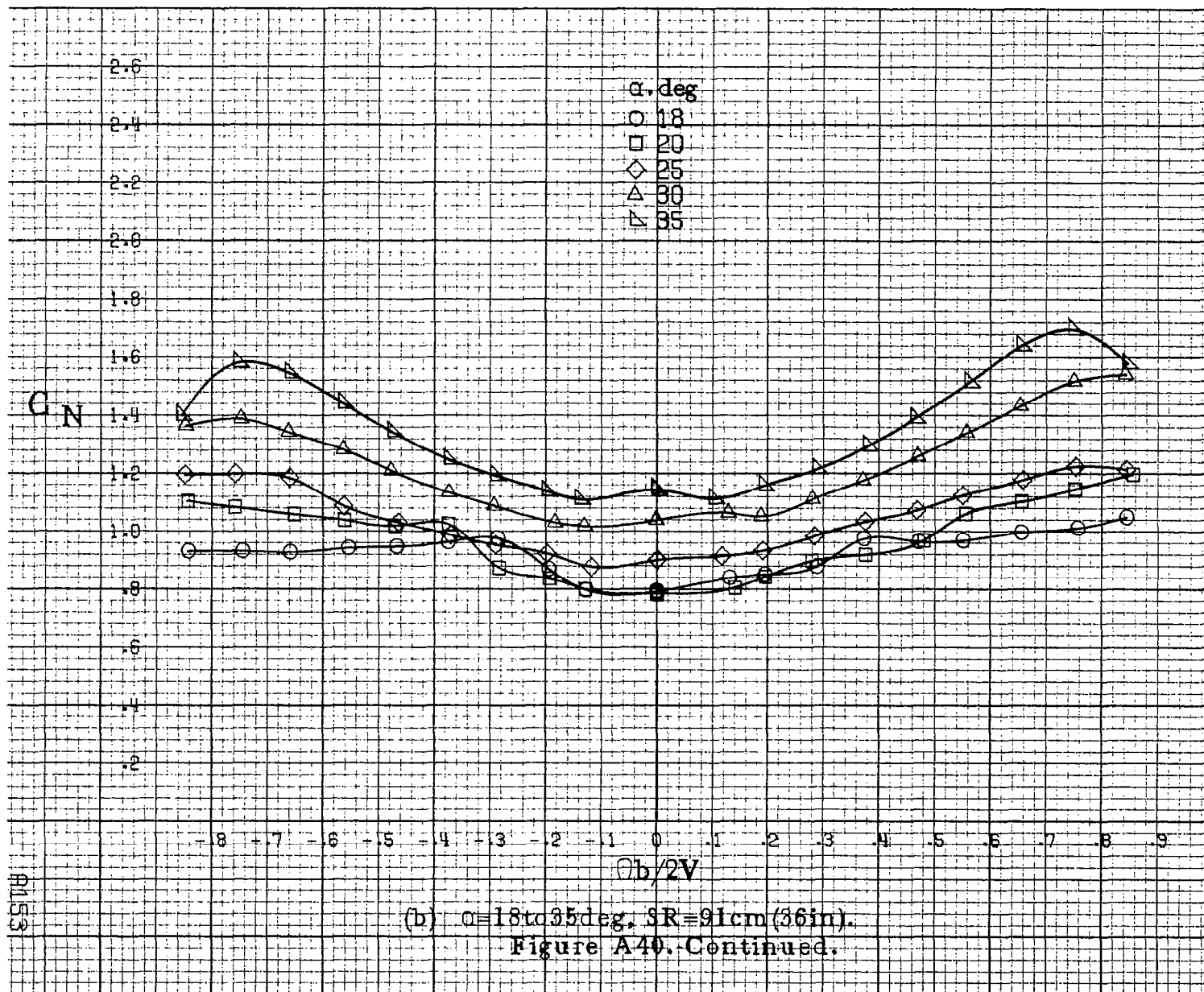


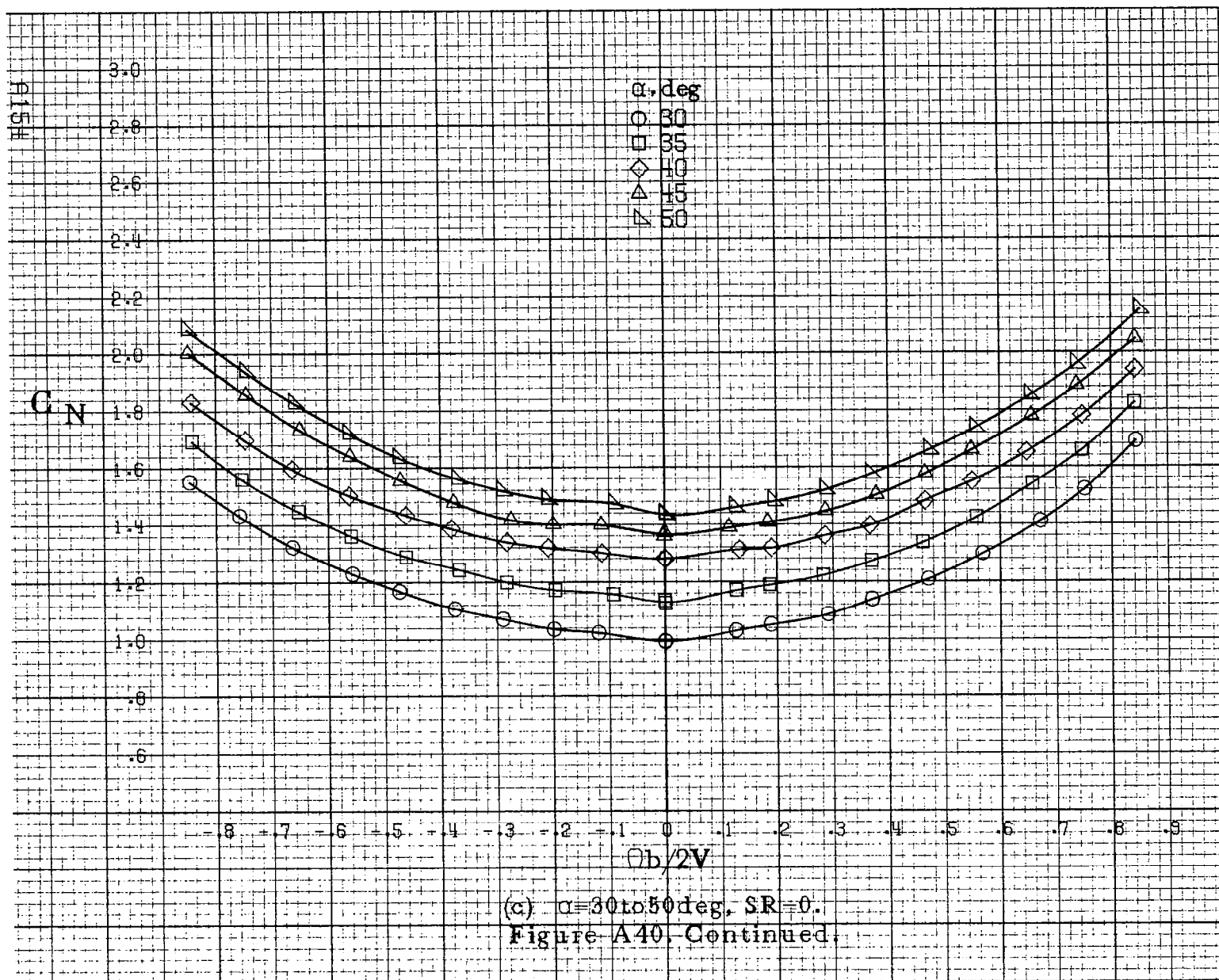


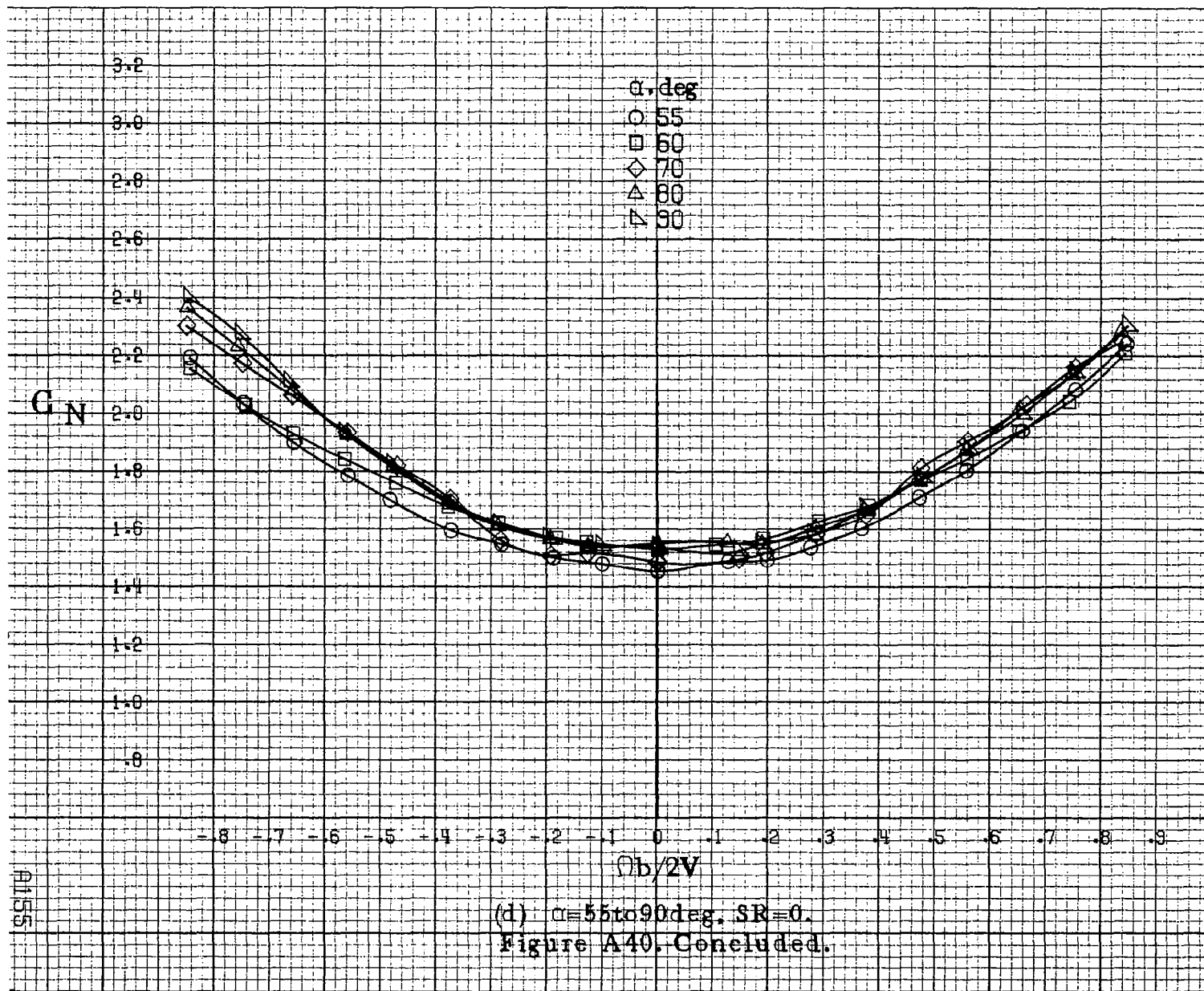


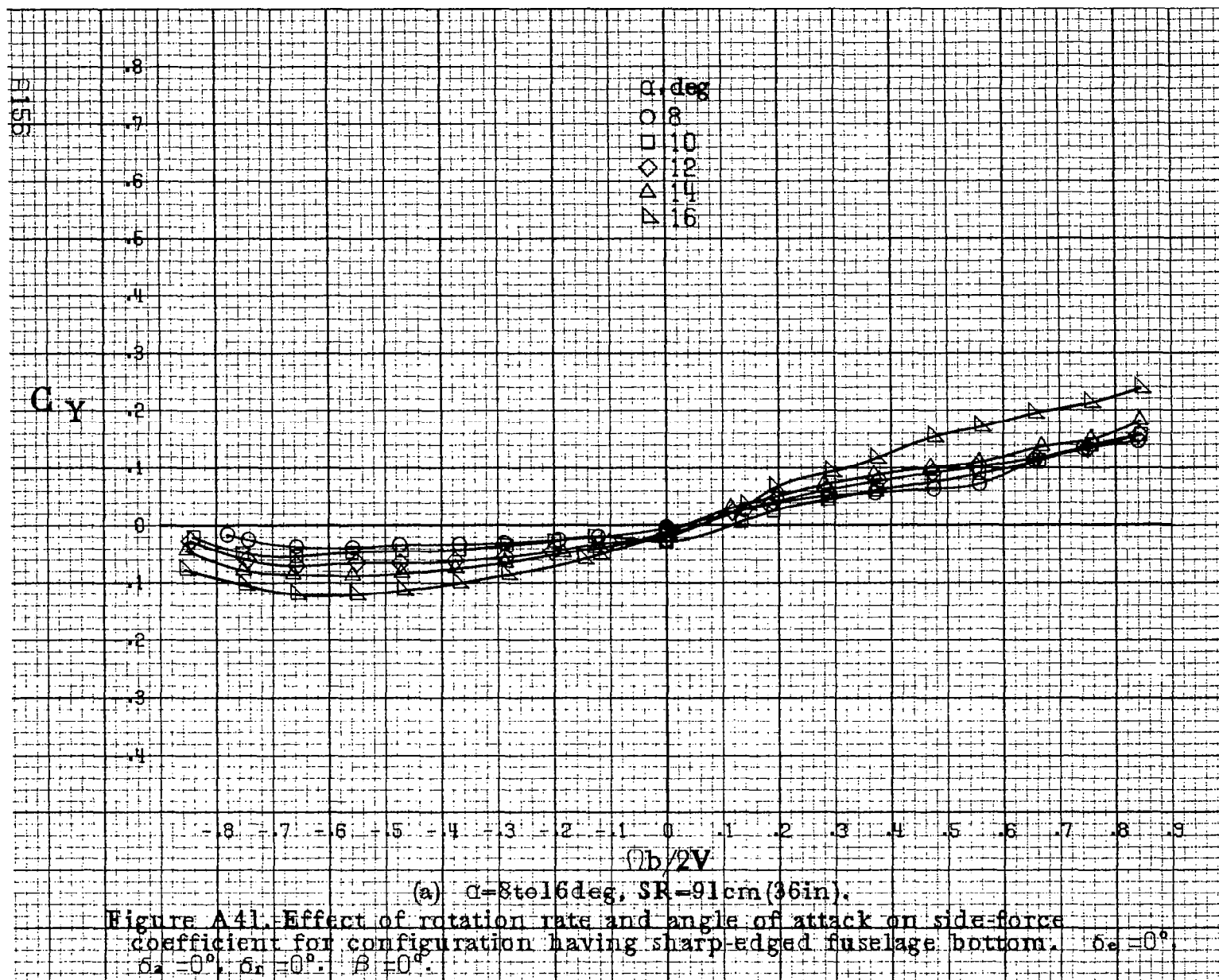
(a) $\alpha=8$ to 16° , $SR=91\text{cm}(36\text{in})$.

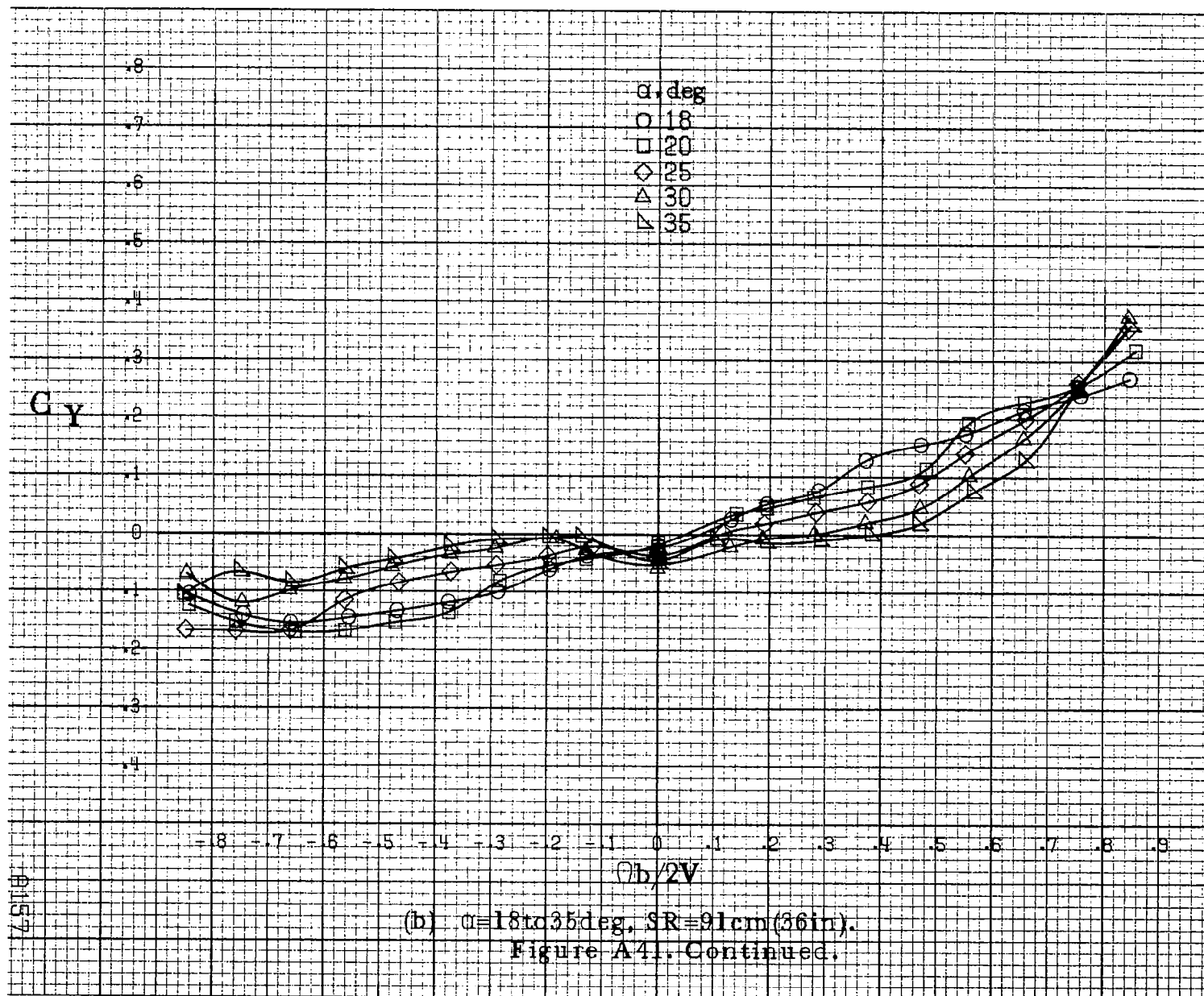
Figure A40. Effect of rotation rate and angle of attack on normal-force coefficient for configuration having sharp-edged fuselage bottom. $\delta_e=0^\circ$; $\delta_a=0^\circ$; $\delta_r=0^\circ$; $\beta=0^\circ$.

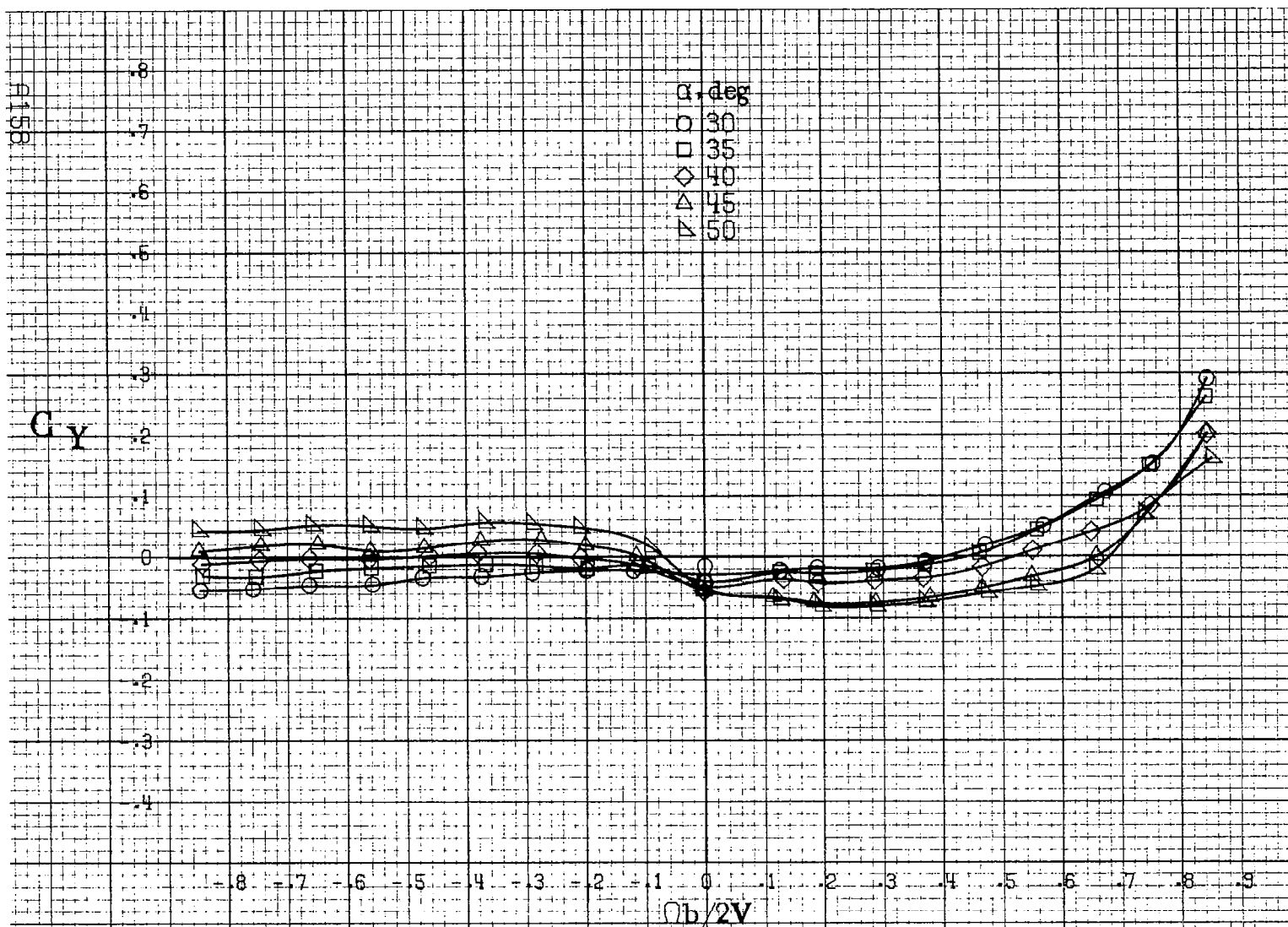




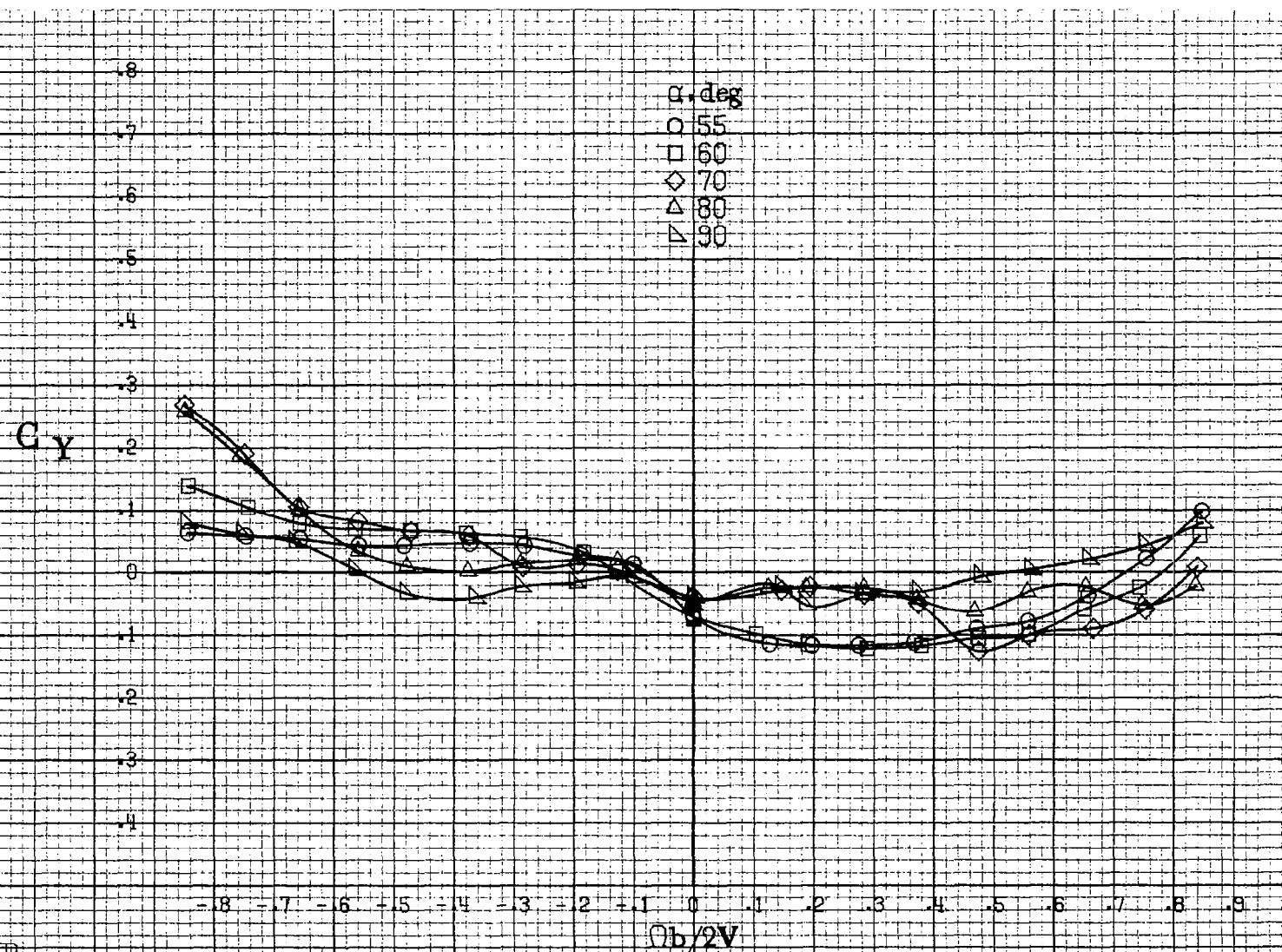




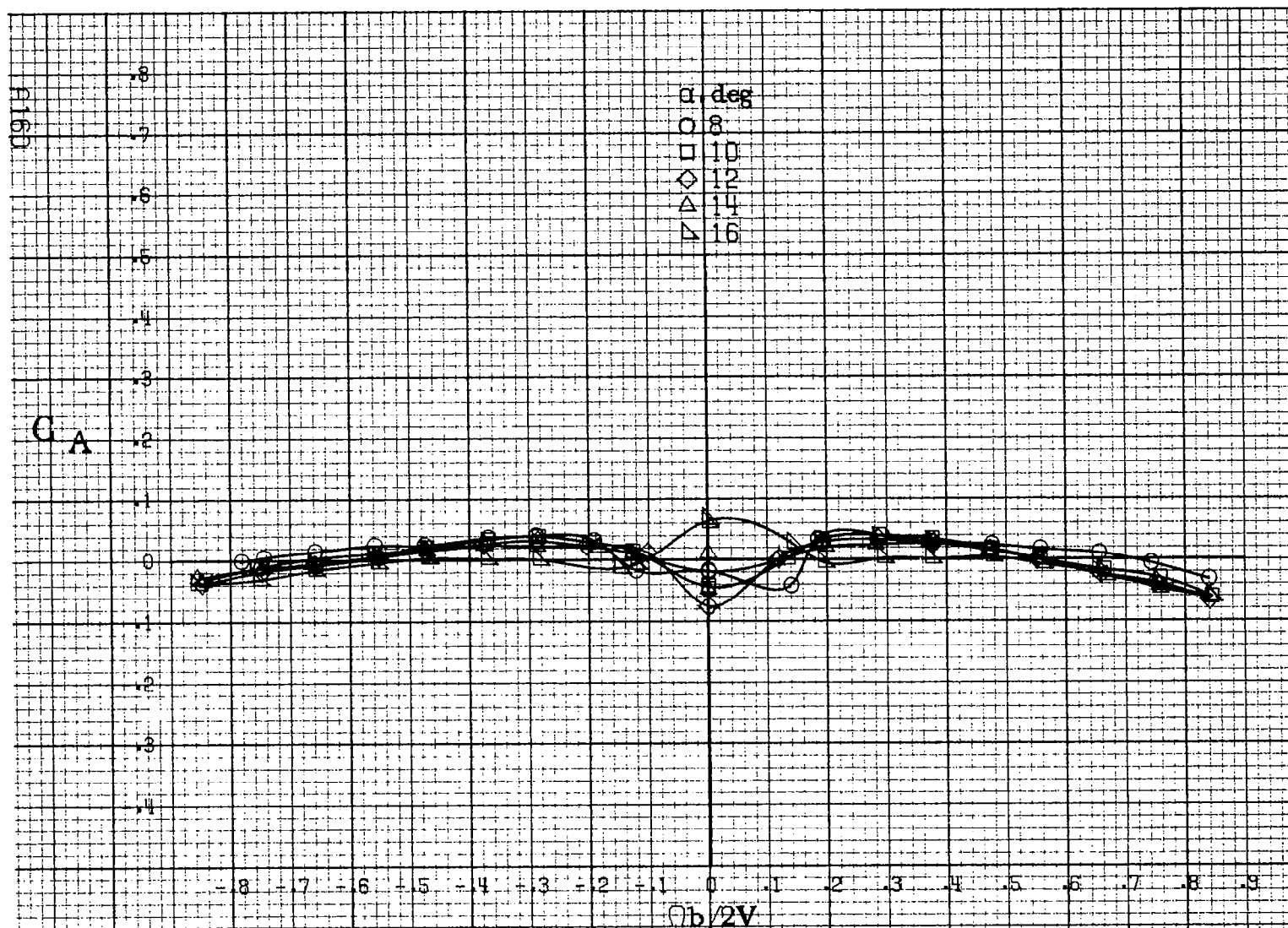




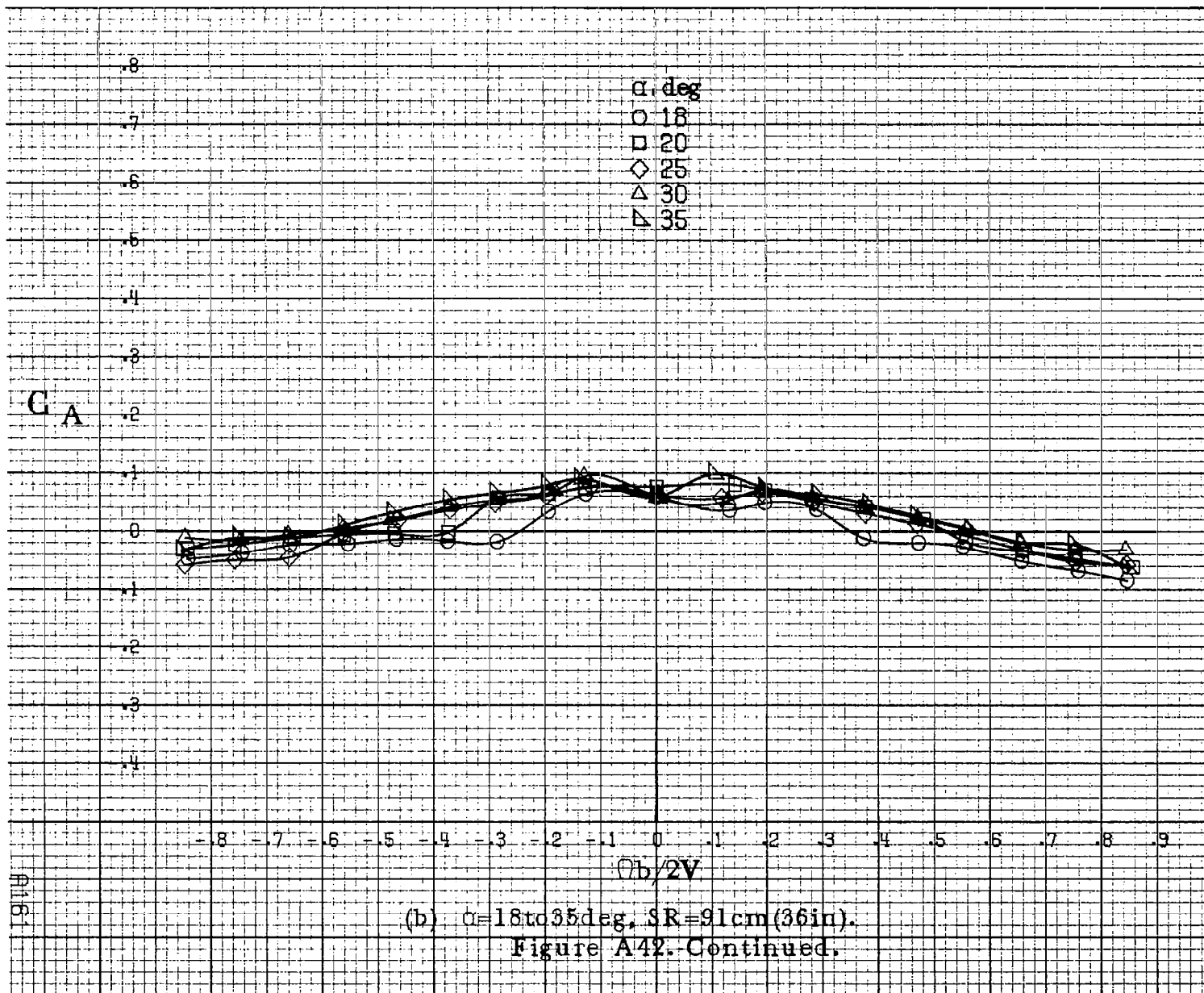
(c) $\alpha=30$ to 50° , $SR=0$.
Figure A41 - Continued.

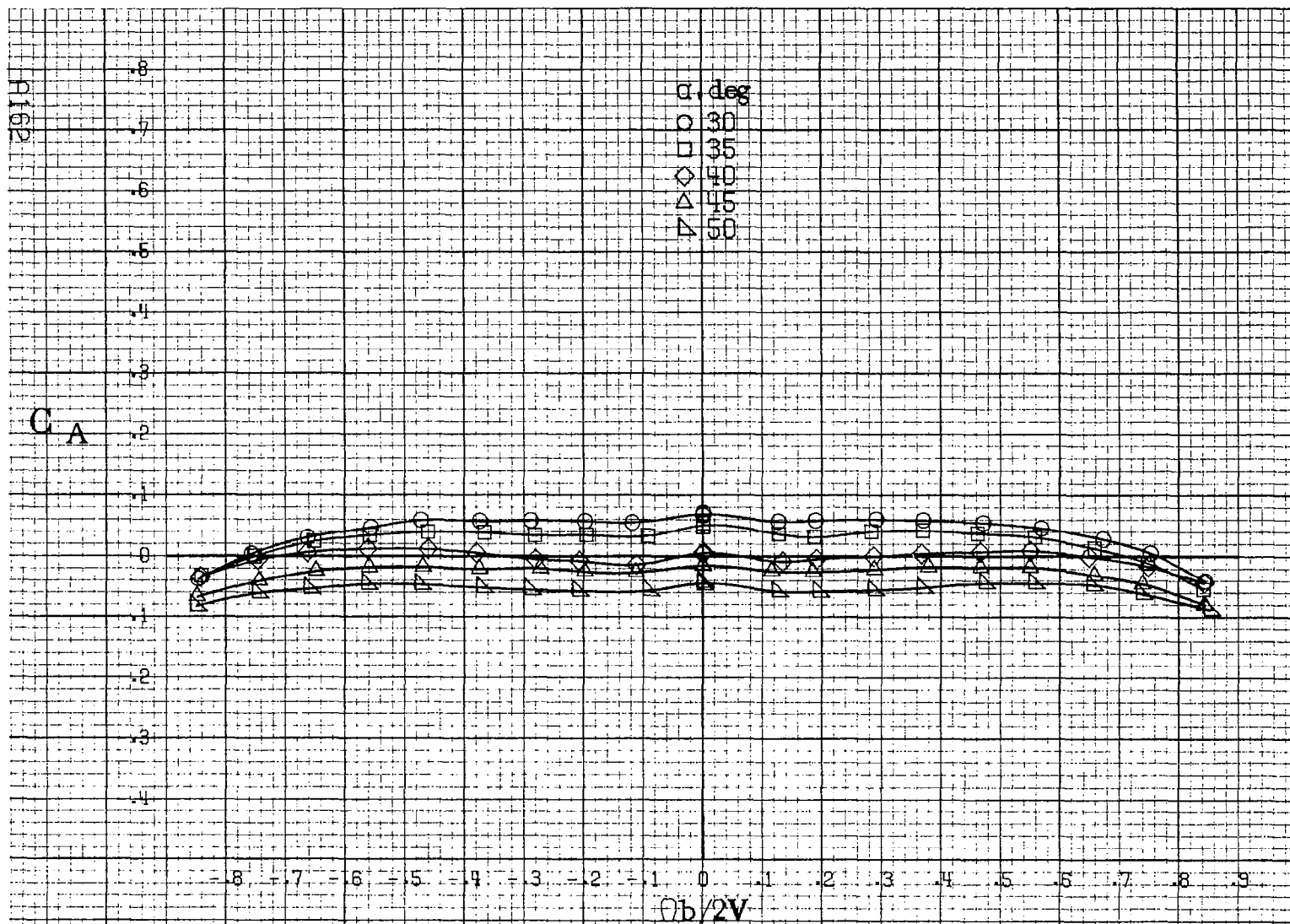


(d) $\alpha=55$ to 90 deg, $SR=0$.
Figure A41. Concluded.



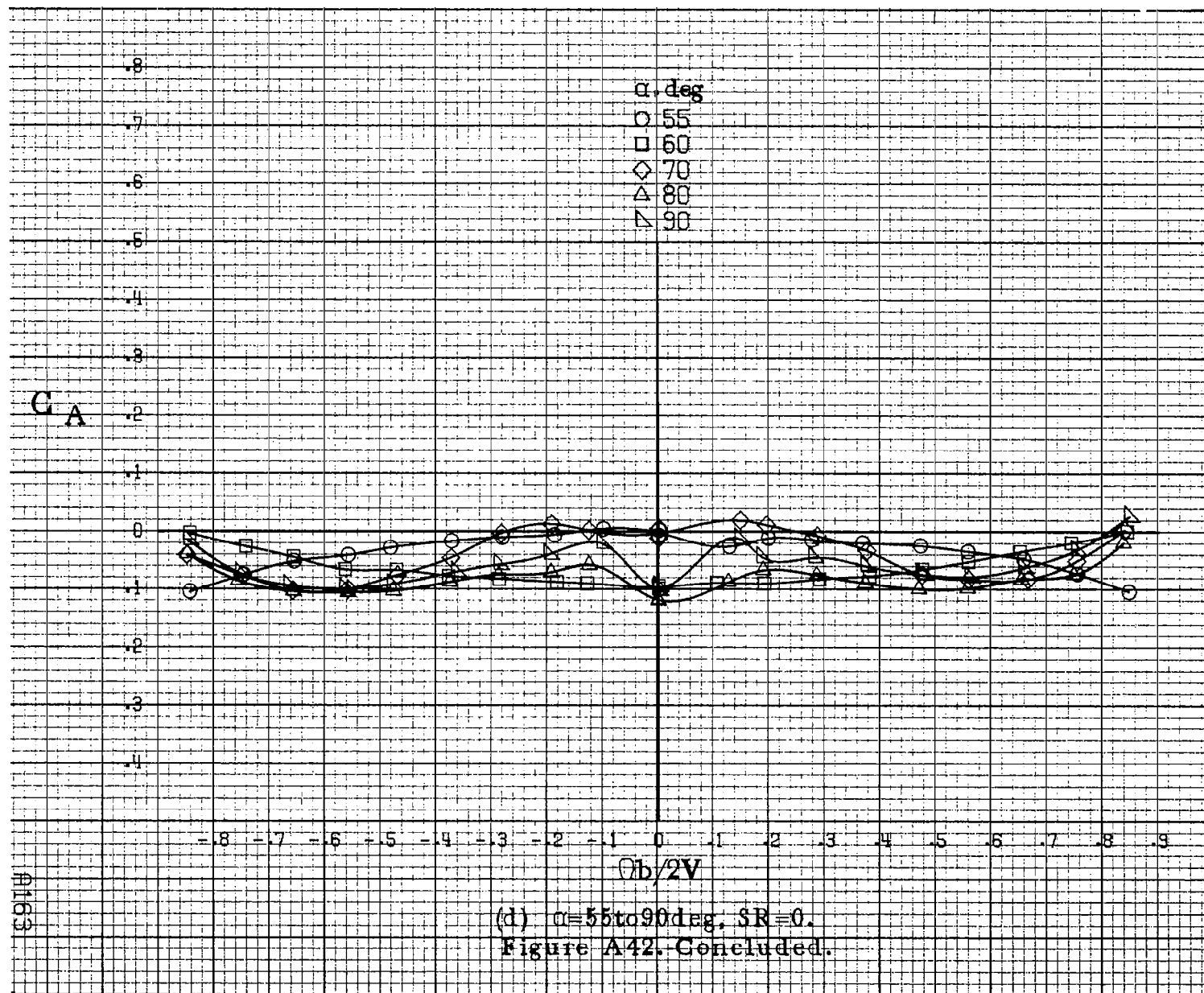
(a) $\alpha = 8$ to 16° , $SR = 91 \text{ cm (36 in.)}$.
 Figure A42. Effect of rotation rate and angle of attack on axial force coefficient for configuration having sharp-edged fuselage bottom. $\delta_a = 0^\circ$, $\delta_r = 0^\circ$, $\beta = 0^\circ$.

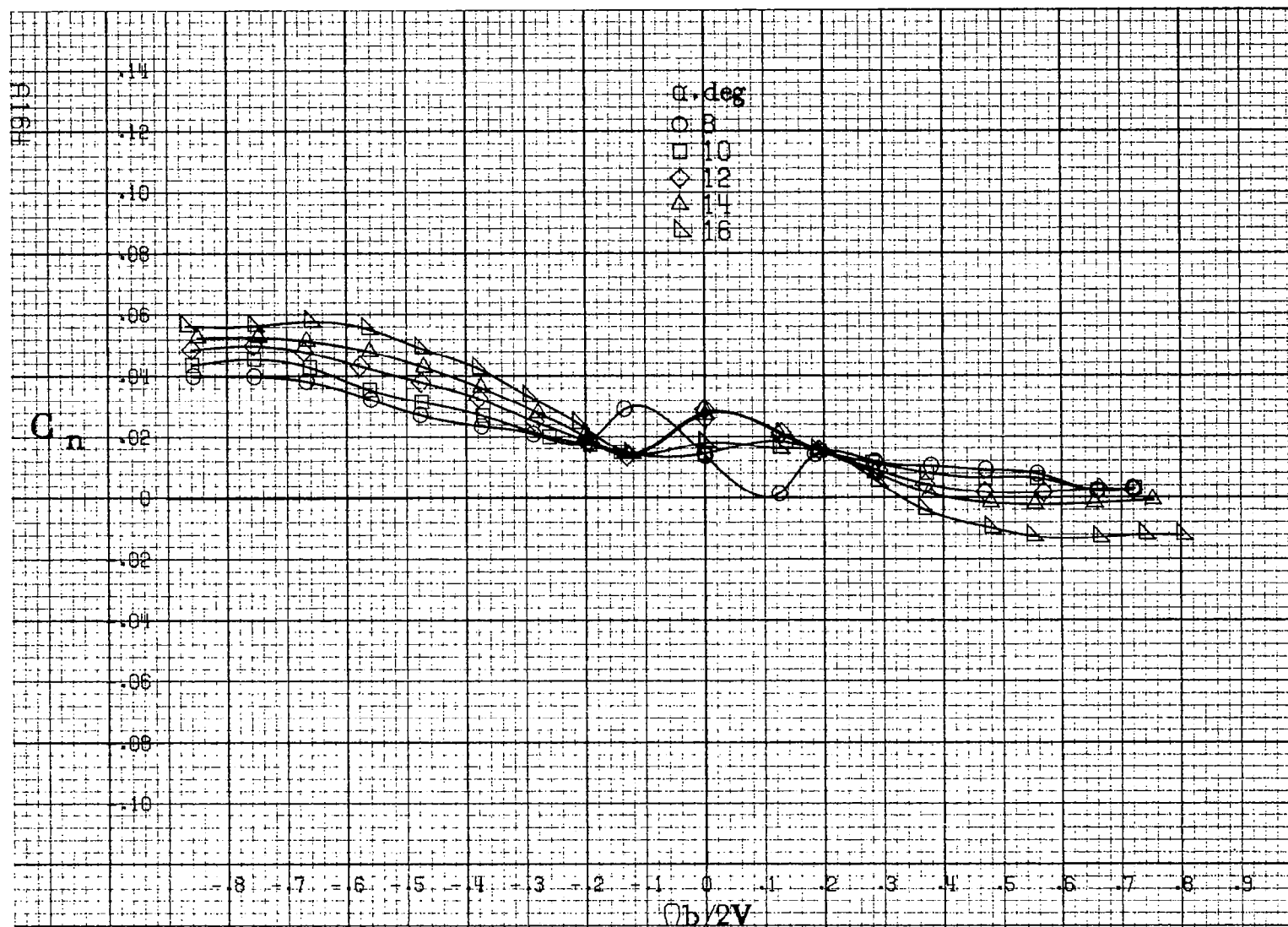




(c) $\alpha=30$ to 50 deg, $SR=0$.

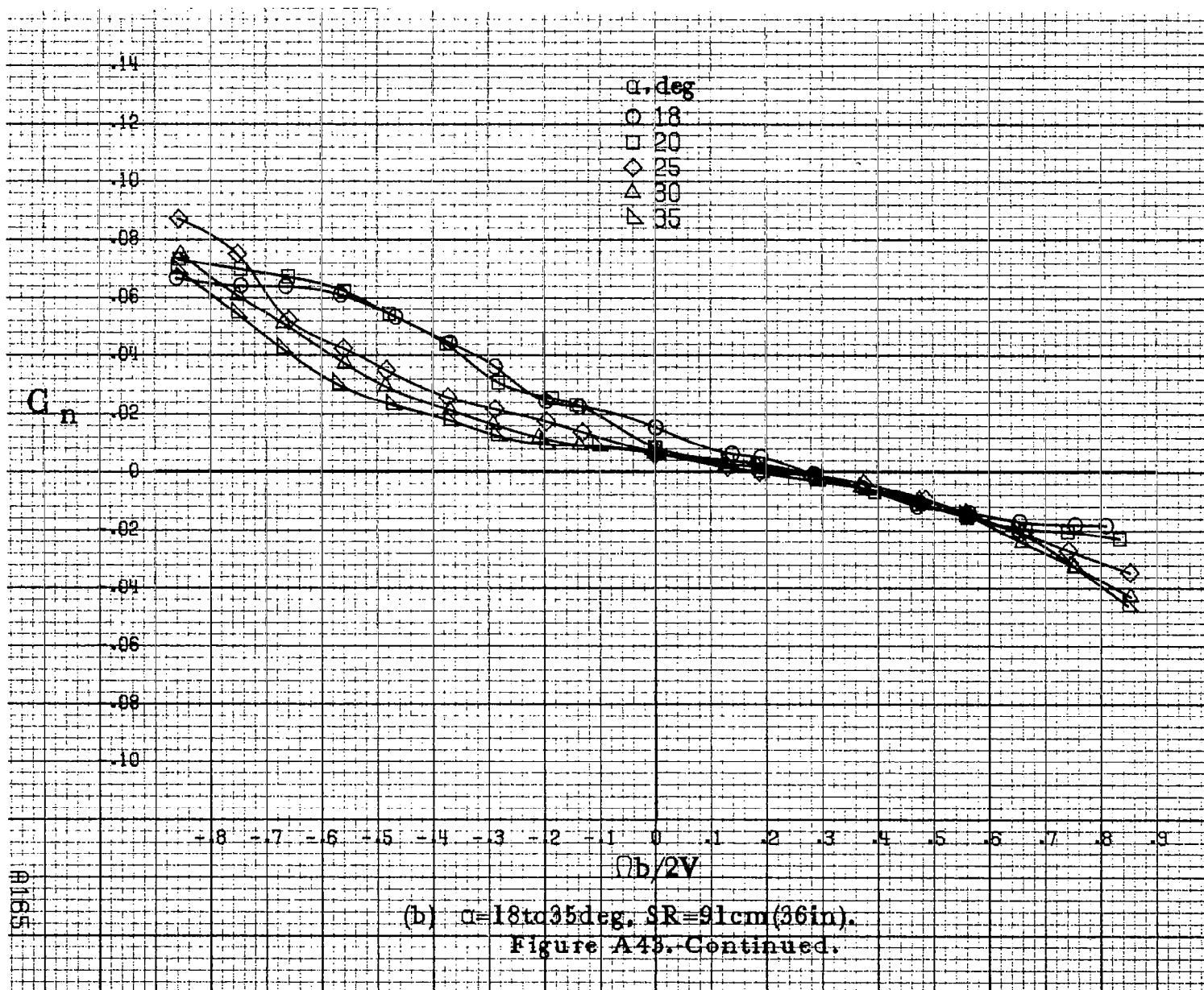
Figure A42. Continued.

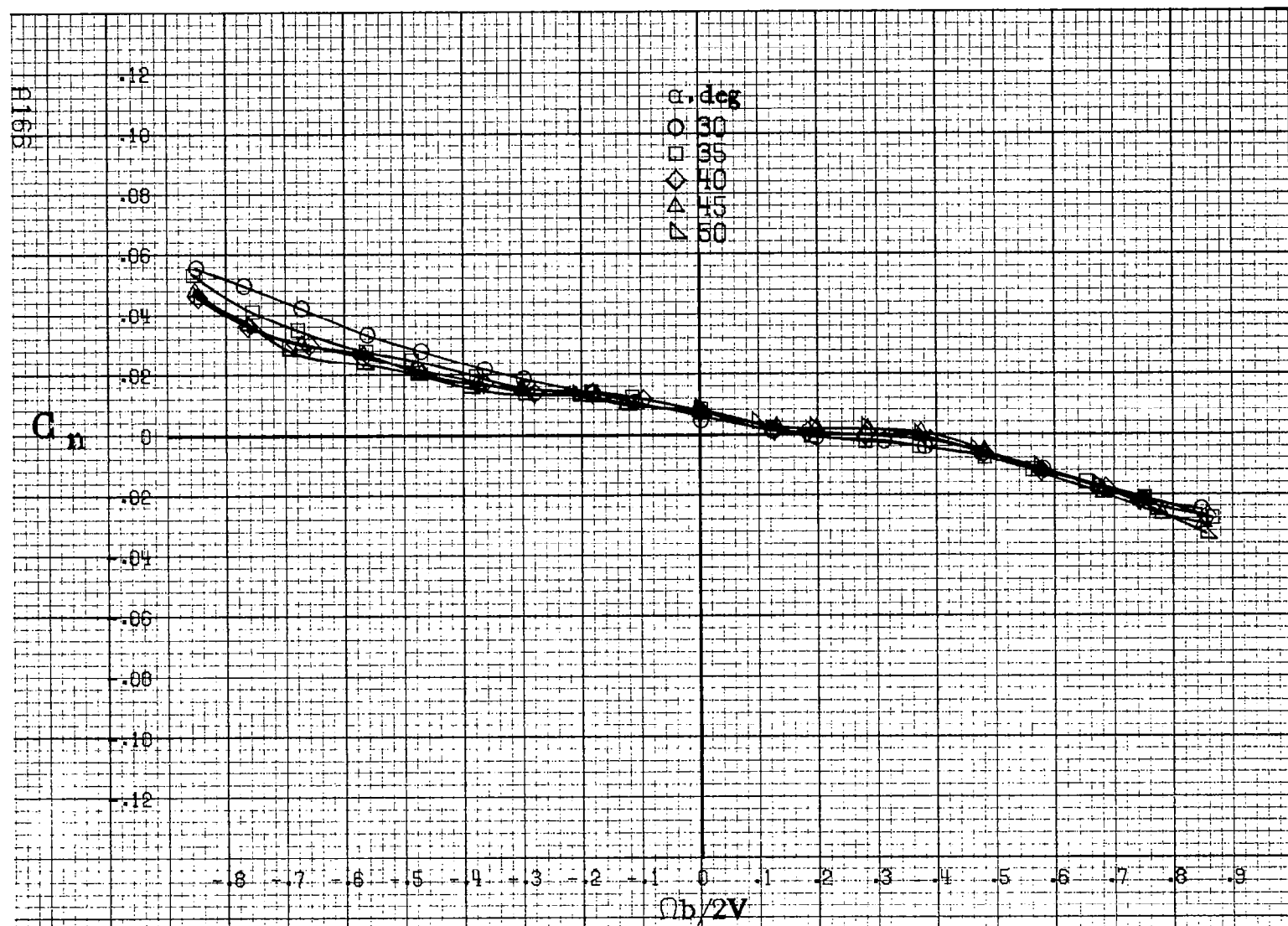




(a) $\alpha=8$ to 16° , $SR=91\text{cm}(36\text{in})$.

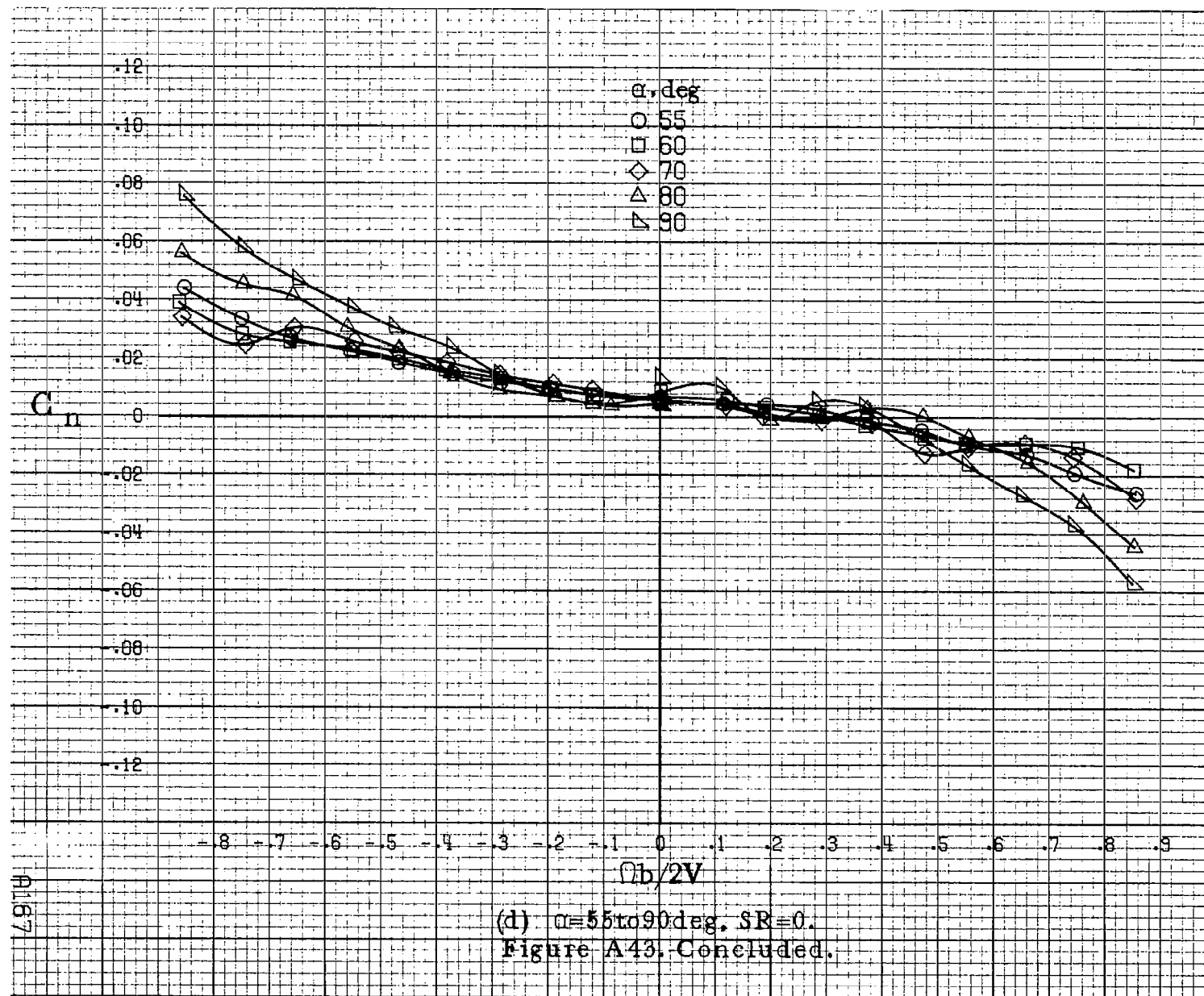
Figure A43. Effect of rotation rate and angle of attack on yawing moment coefficient for configuration having sharp-edged fuselage bottom. $\delta_e = -20^\circ$, $\delta_a = -20^\circ$, $\delta_r = -28^\circ$, $\beta = 0^\circ$.

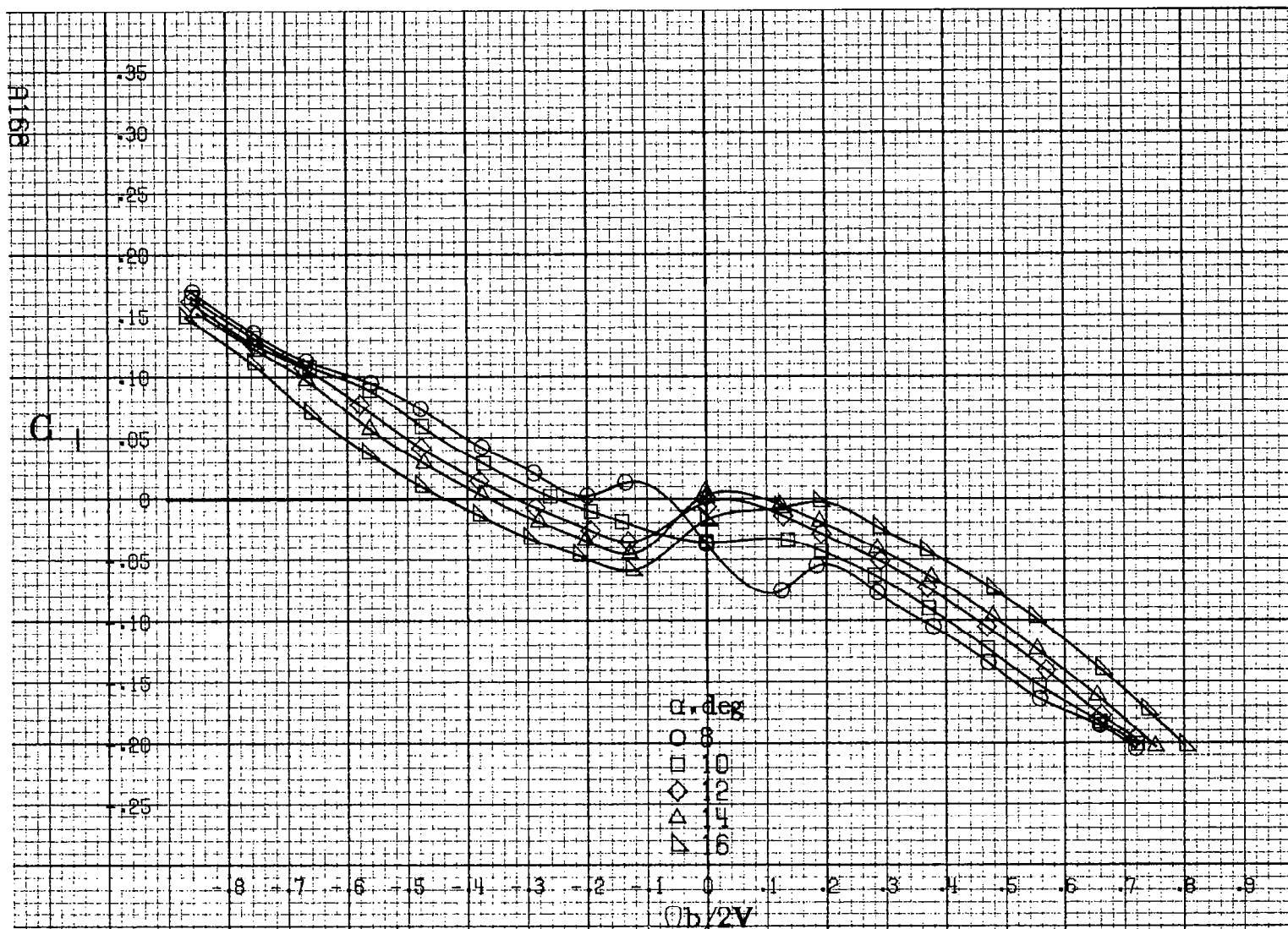




(c) $\alpha=30$ to 50 deg, $SR=0$.

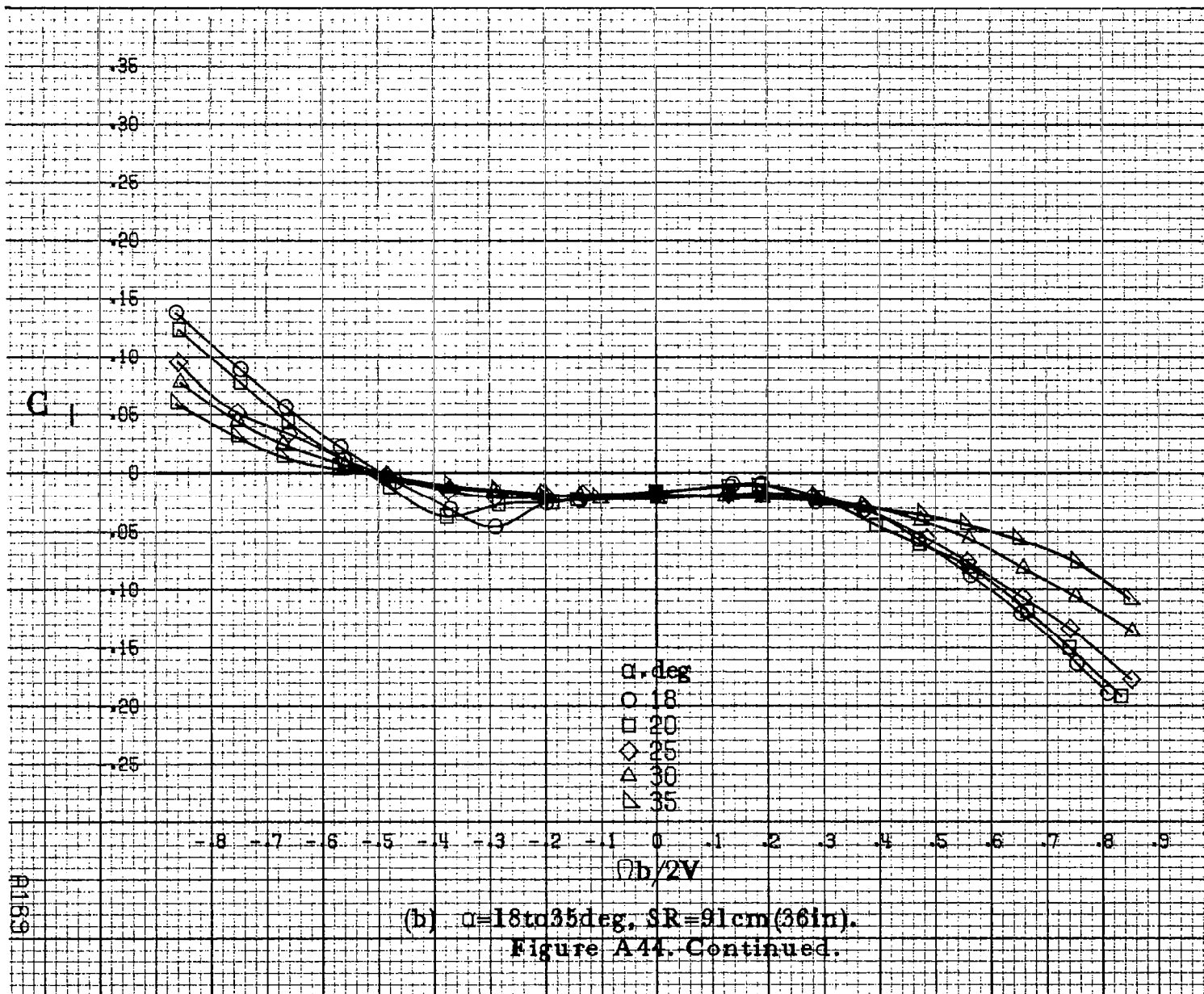
Figure A43. Continued.

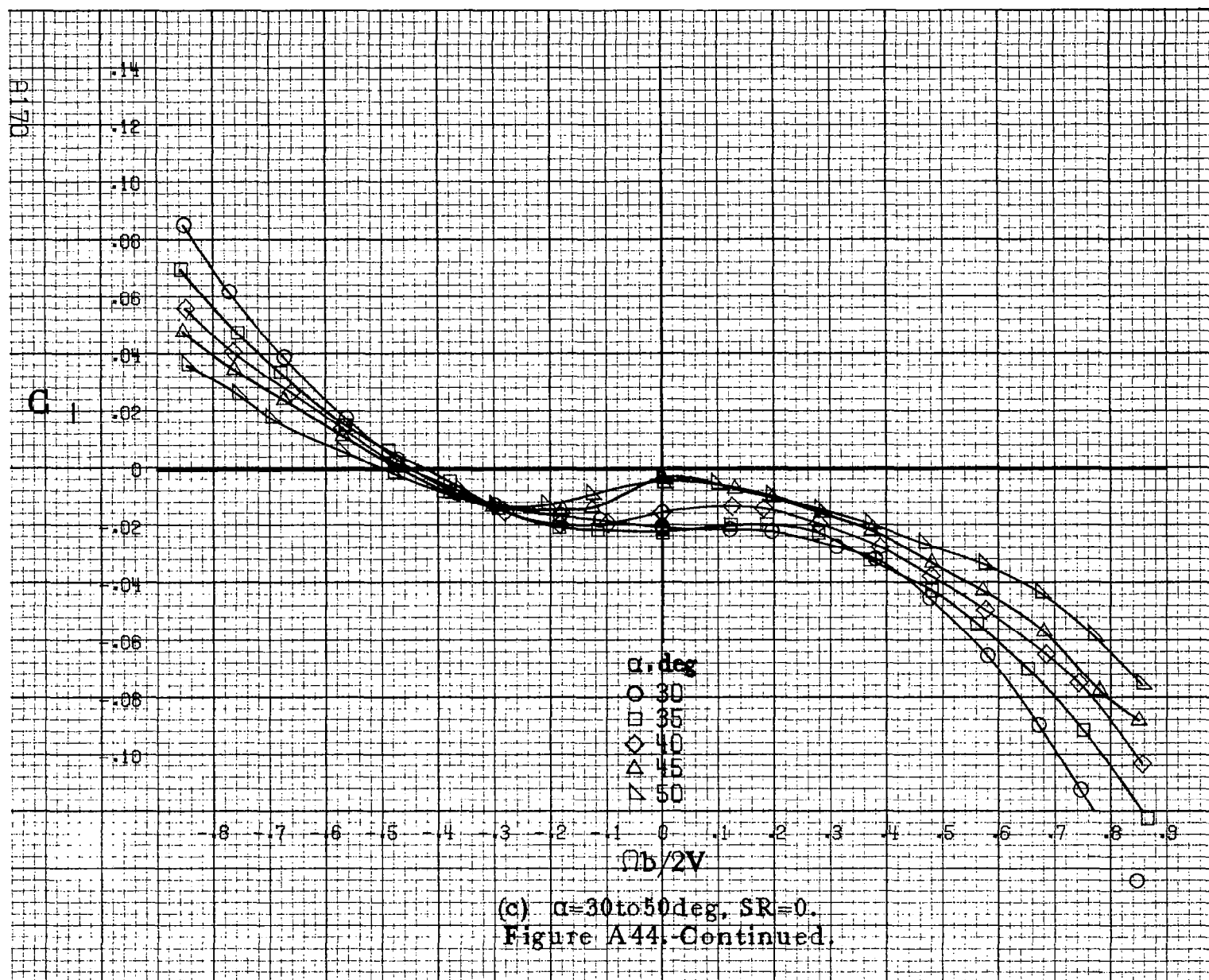


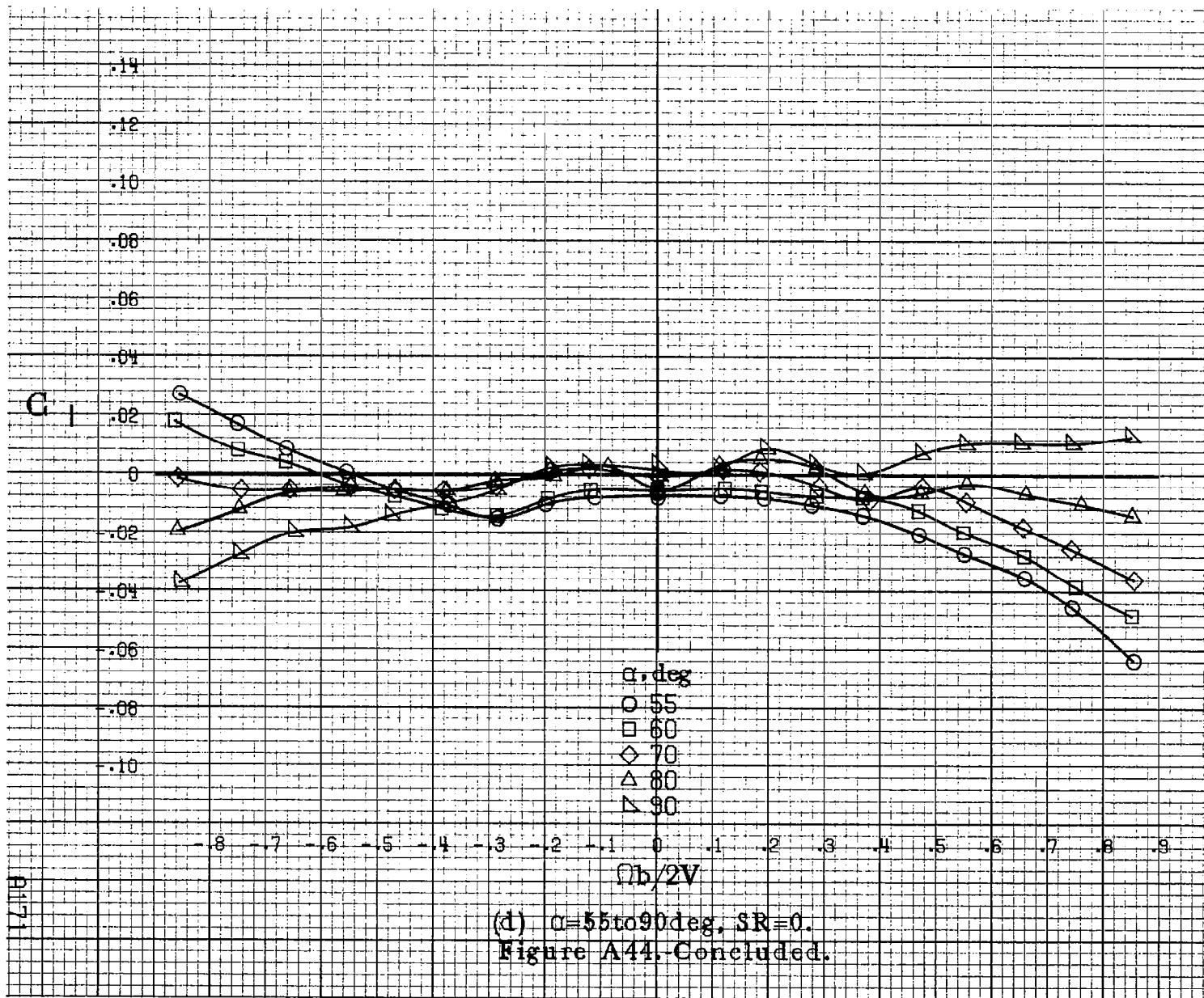


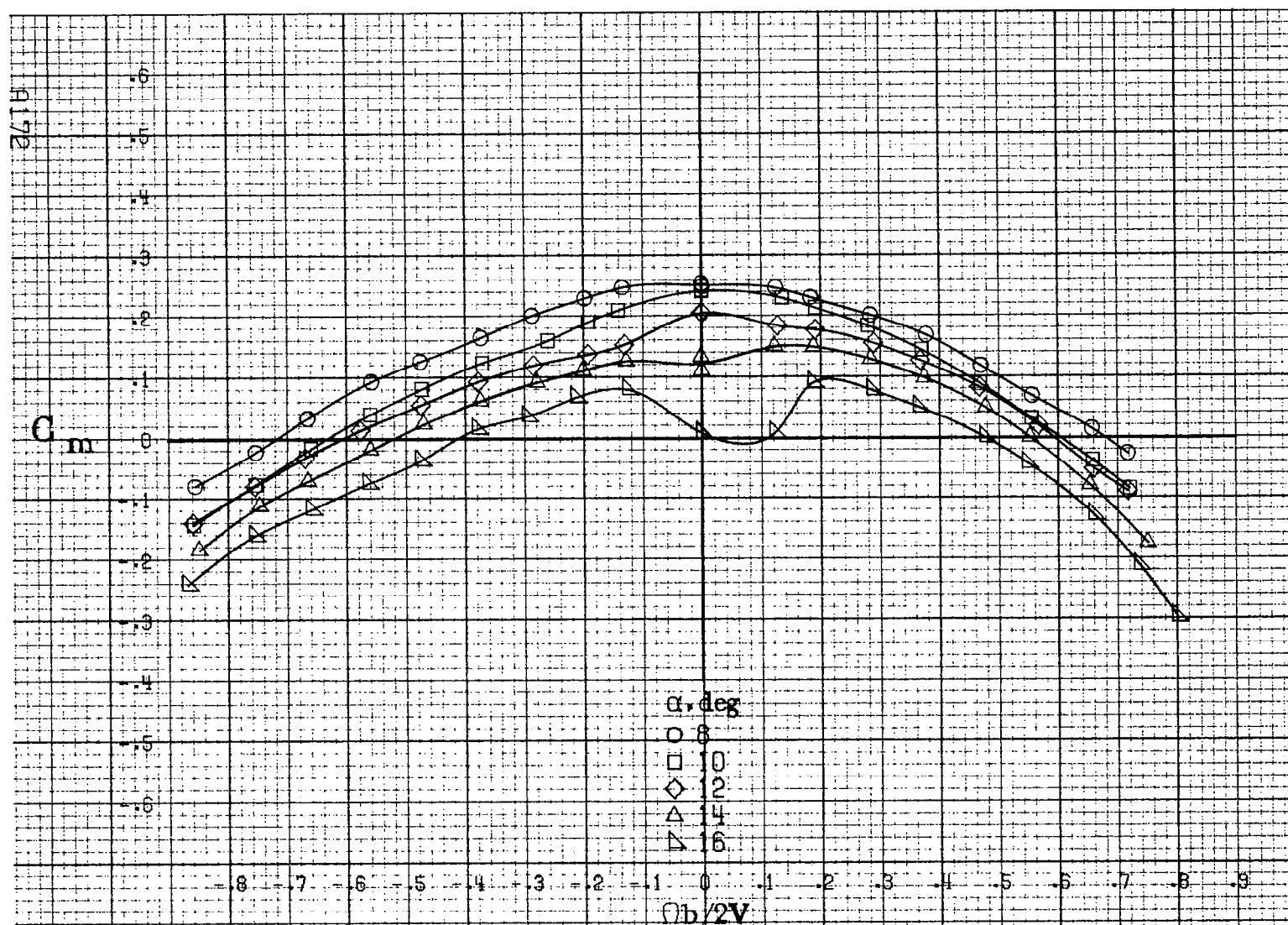
(a) $\alpha = 8$ to 16° , $SR = 91$ cm (36 in).

Figure A-44. Effect of rotation rate and angle of attack on rolling-moment coefficient for configuration having sharp-edged fuselage bottom. $\delta_a = -20^\circ$, $\delta_s = -28^\circ$, $\beta = 0^\circ$.



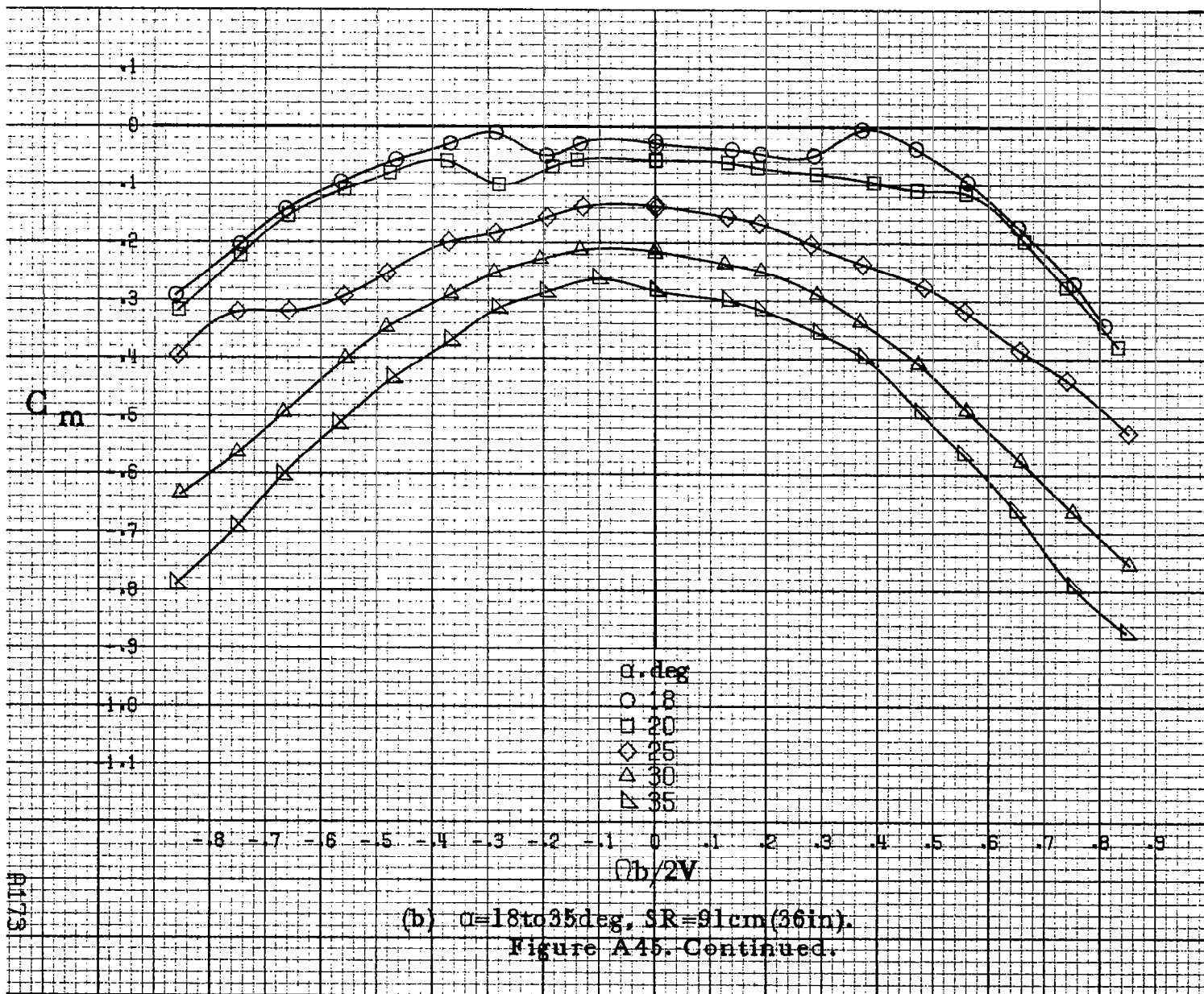


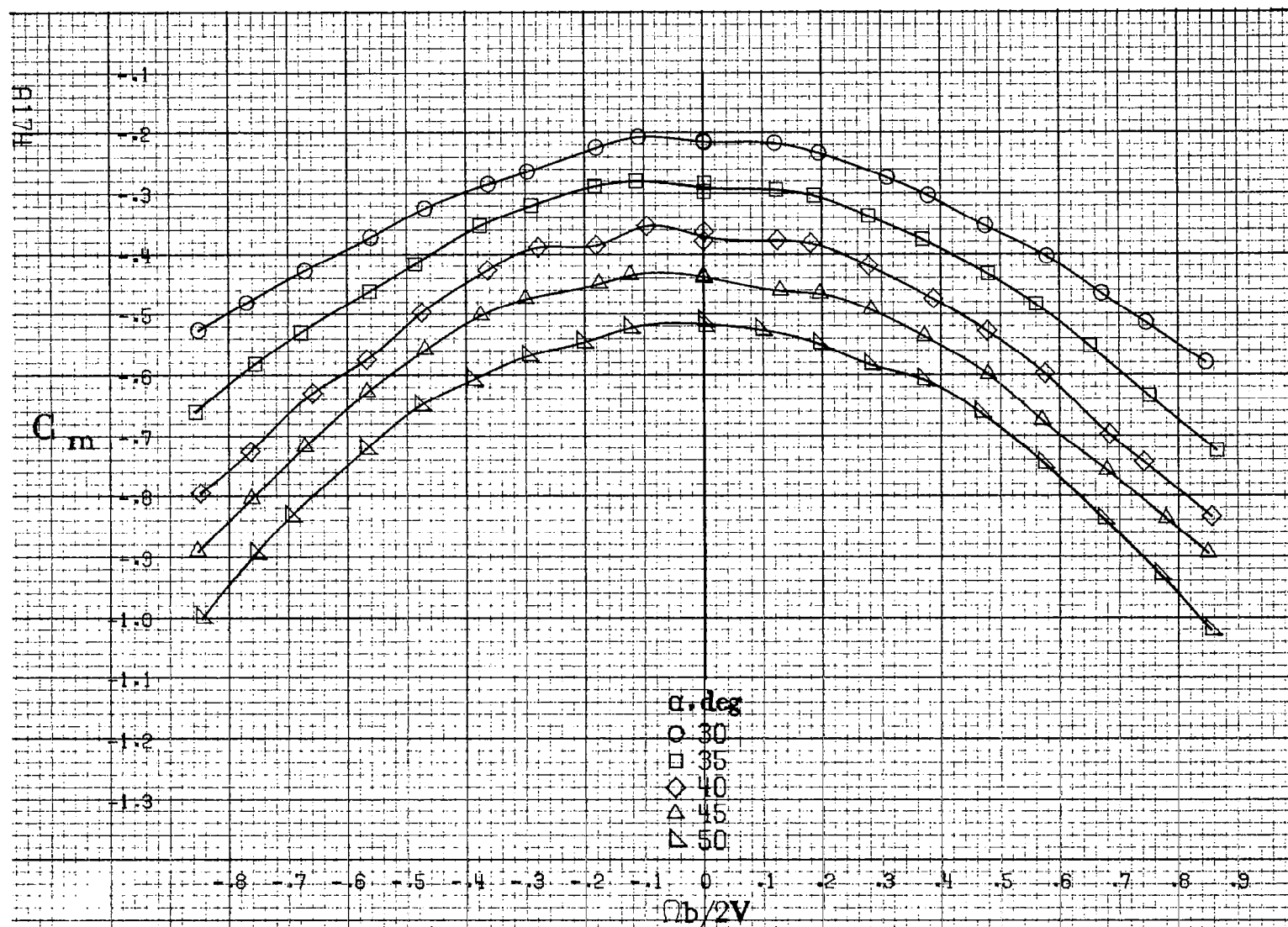




(a) $\alpha = 8$ to 16 deg, $SR = 91$ cm (36 in).

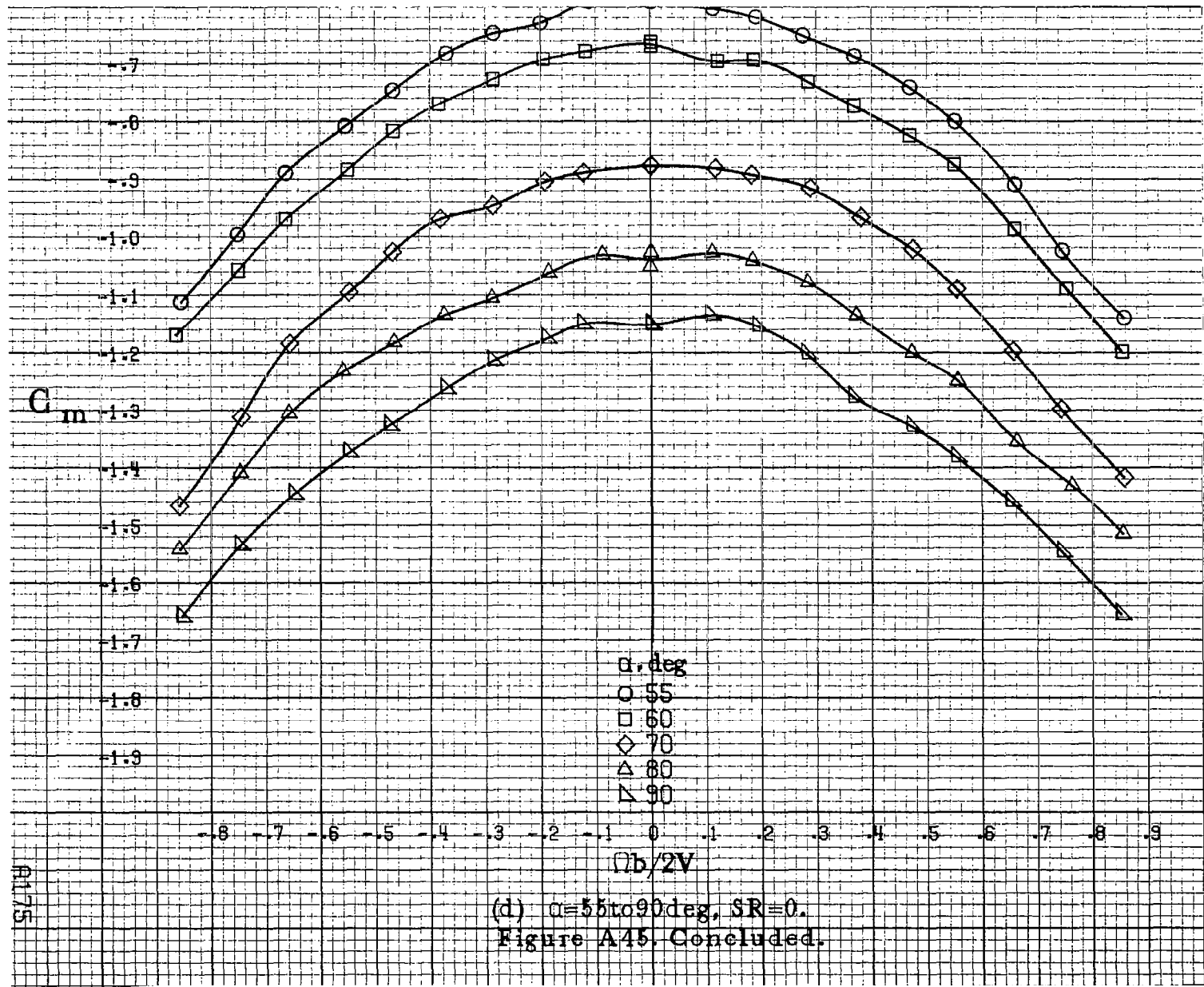
Figure A.45. Effect of rotation rate and angle of attack on pitching moment coefficient for configuration having sharp-edged fuselage bottom. $\delta_a = -20^\circ$, $\delta_r = \pm 28^\circ$, $\beta = 0^\circ$.

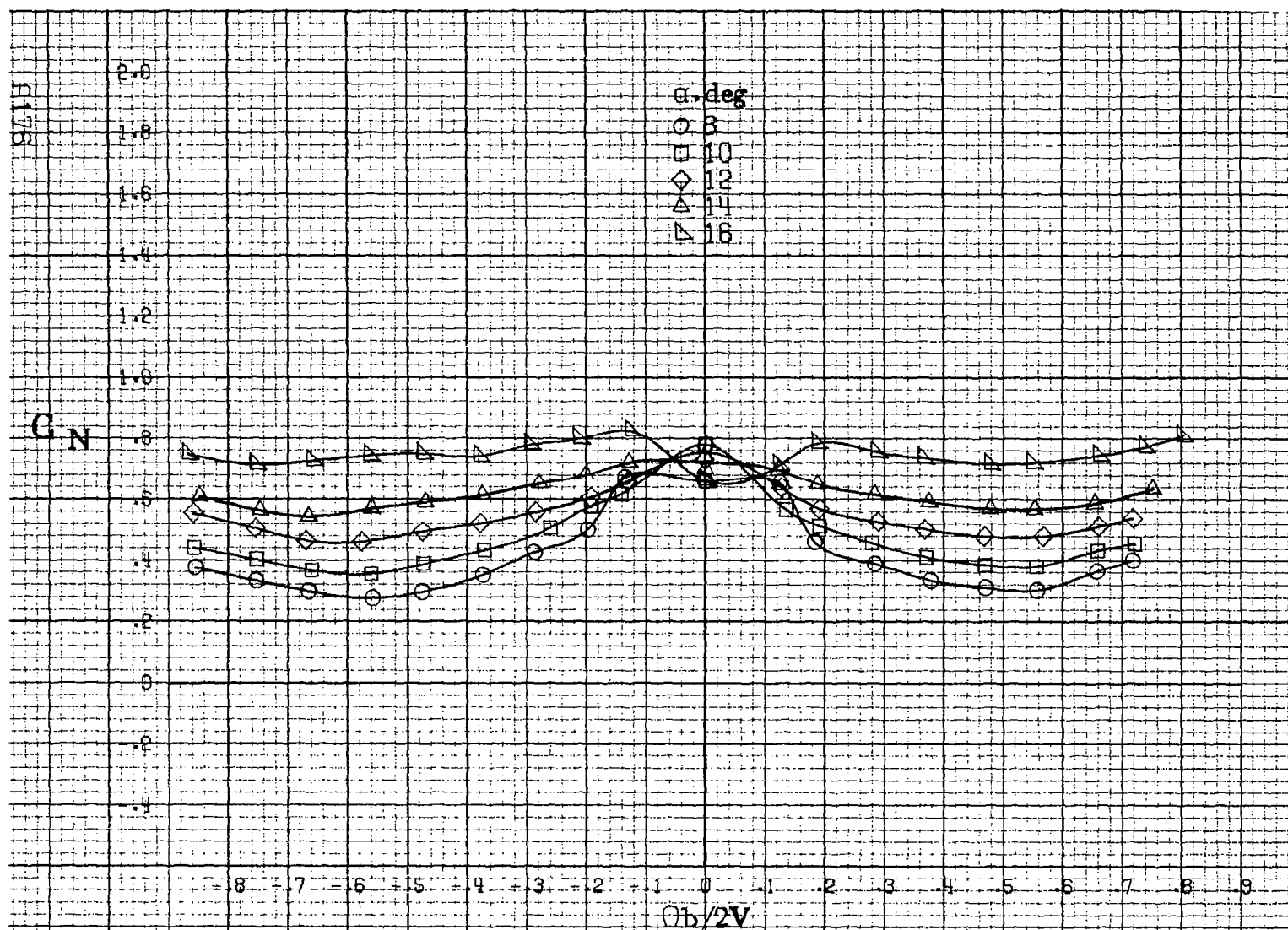




(c) $\alpha=30$ to 50 deg. $SR=0$.

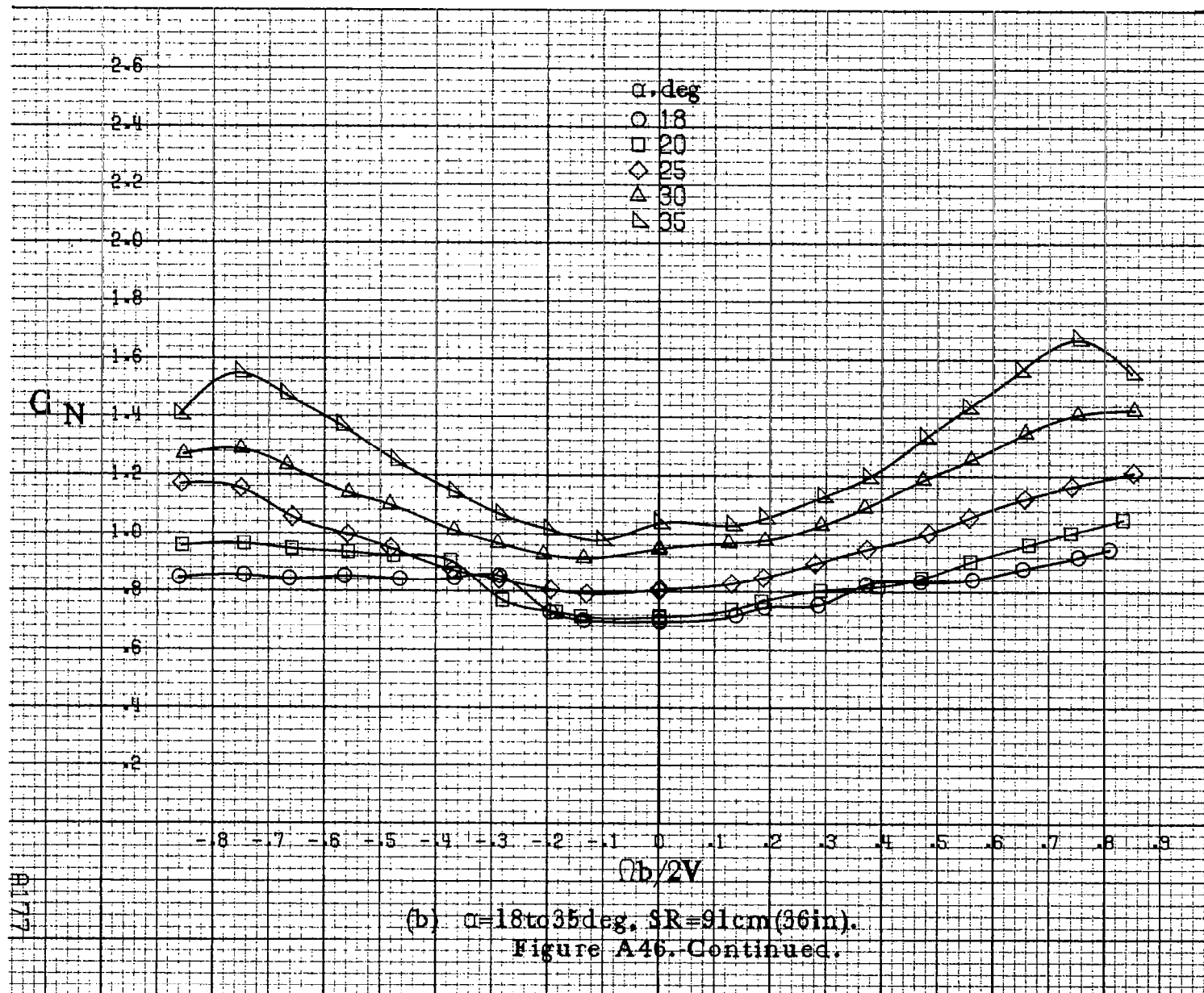
Figure A45.-Continued.

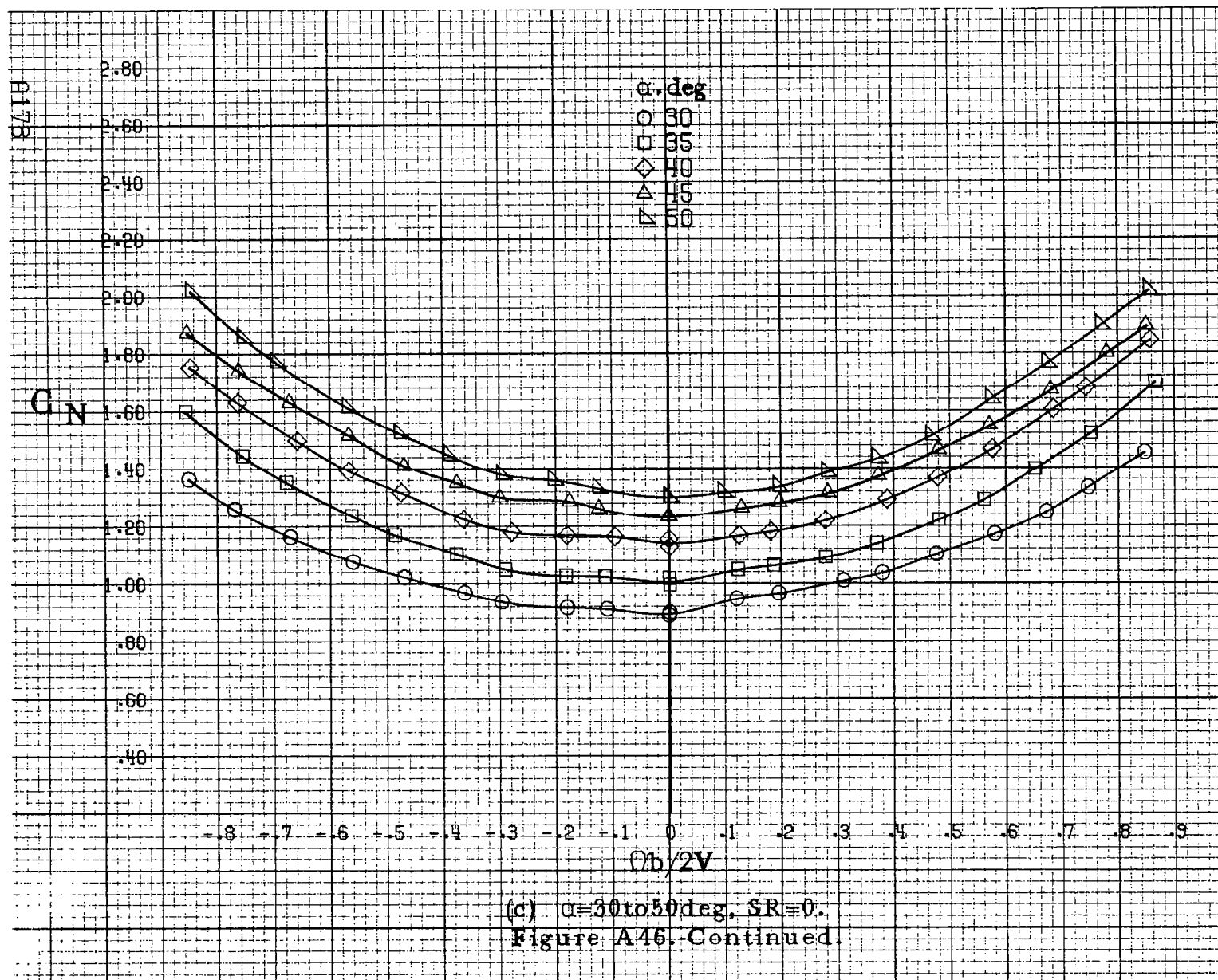


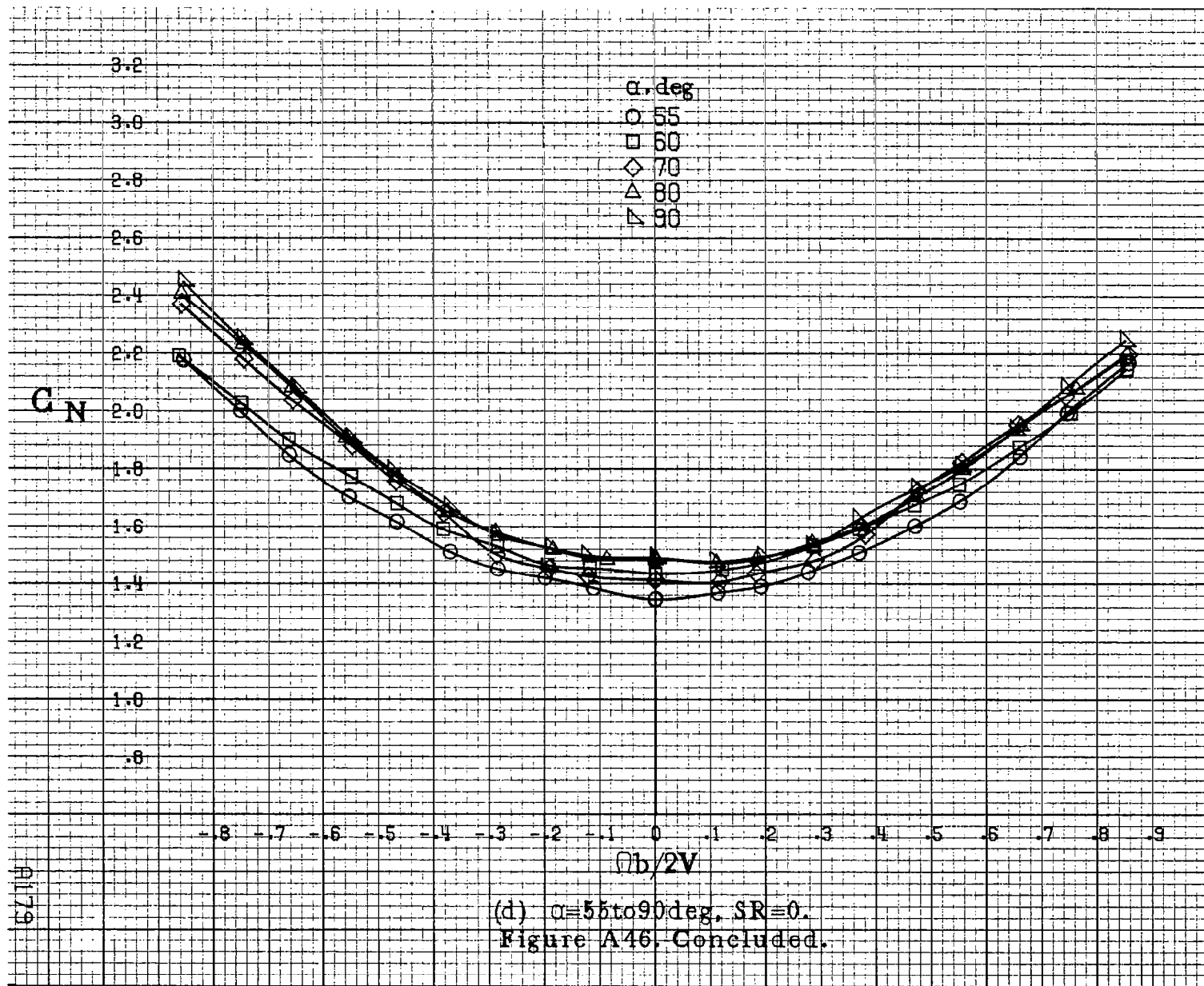


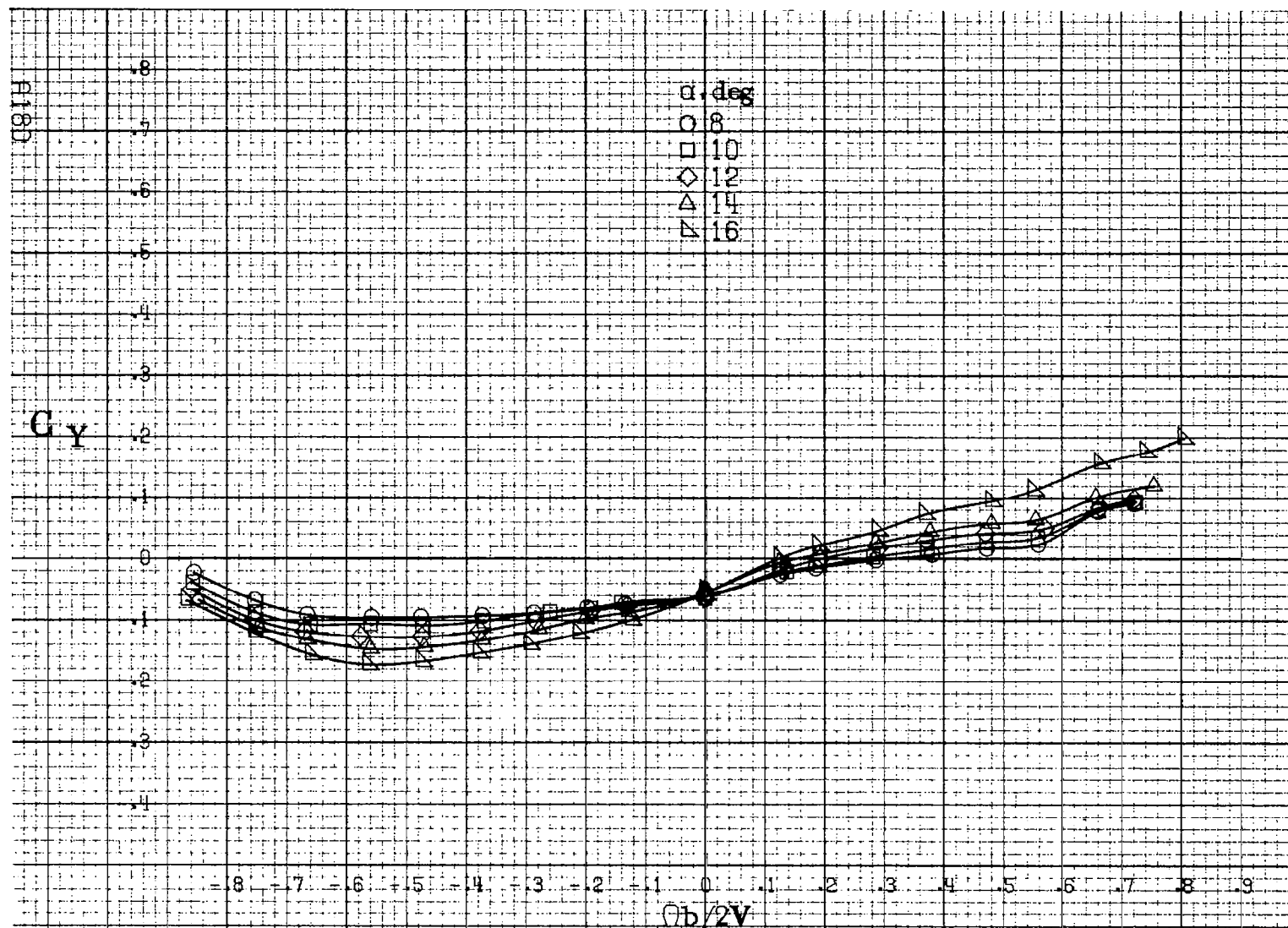
(a) $\alpha = 8$ to 16 deg, $SR = 91$ cm (36 in).

Figure A46. Effect of rotation rate and angle of attack on normal force coefficient for configuration having sharp-edged fuselage bottom. $\delta_a = -20^\circ$, $\delta_r = -28^\circ$, $\beta = 0^\circ$.



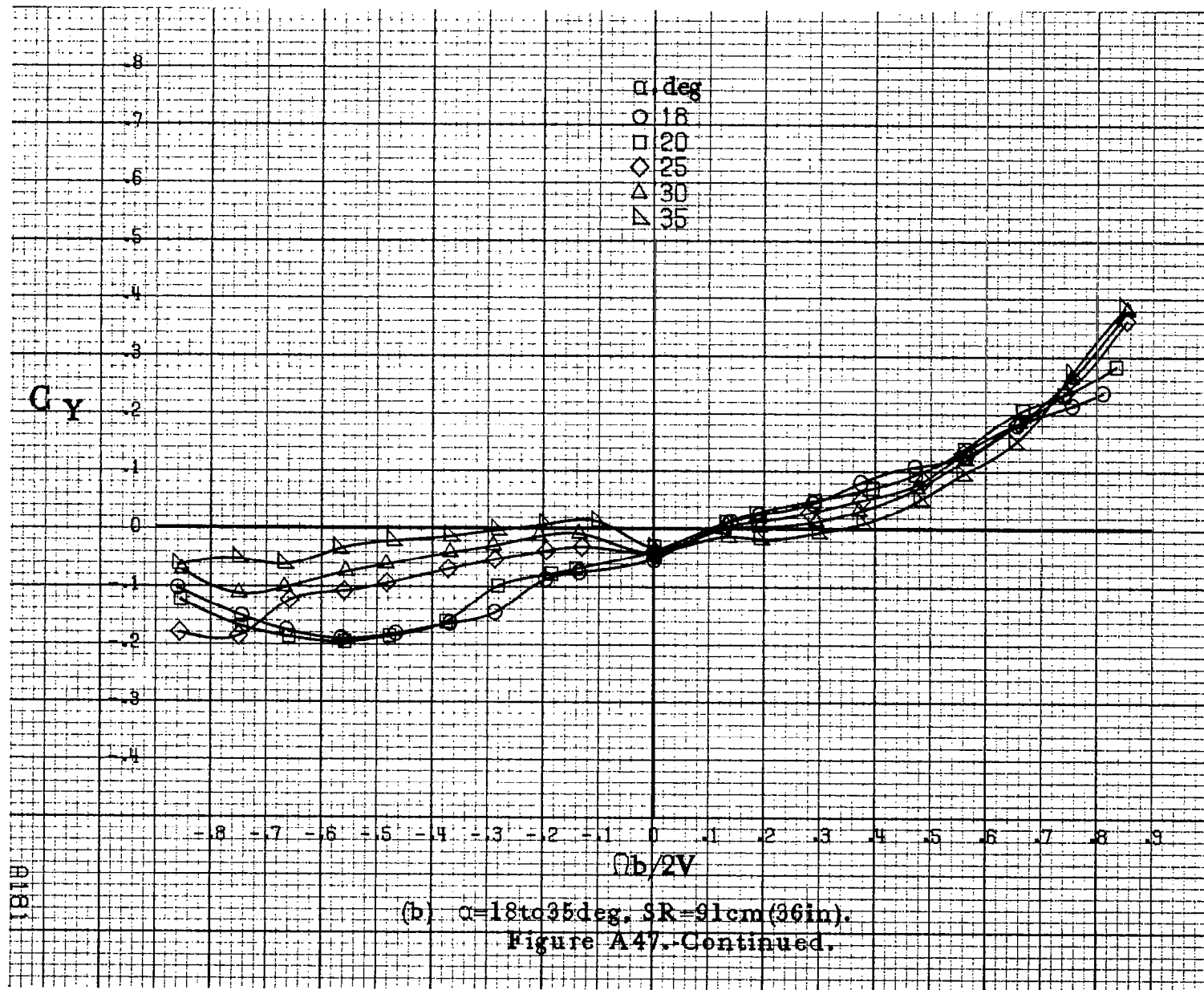


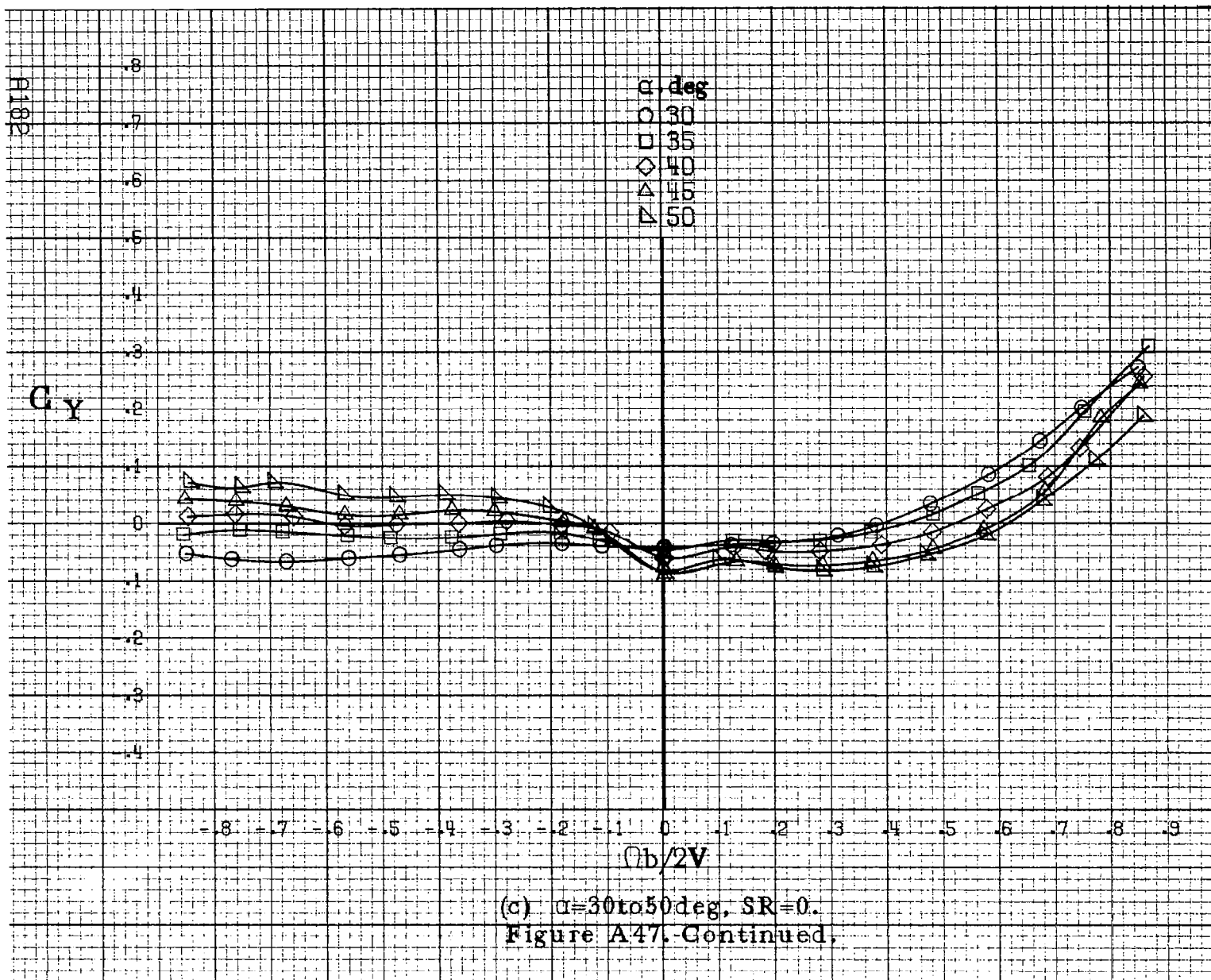


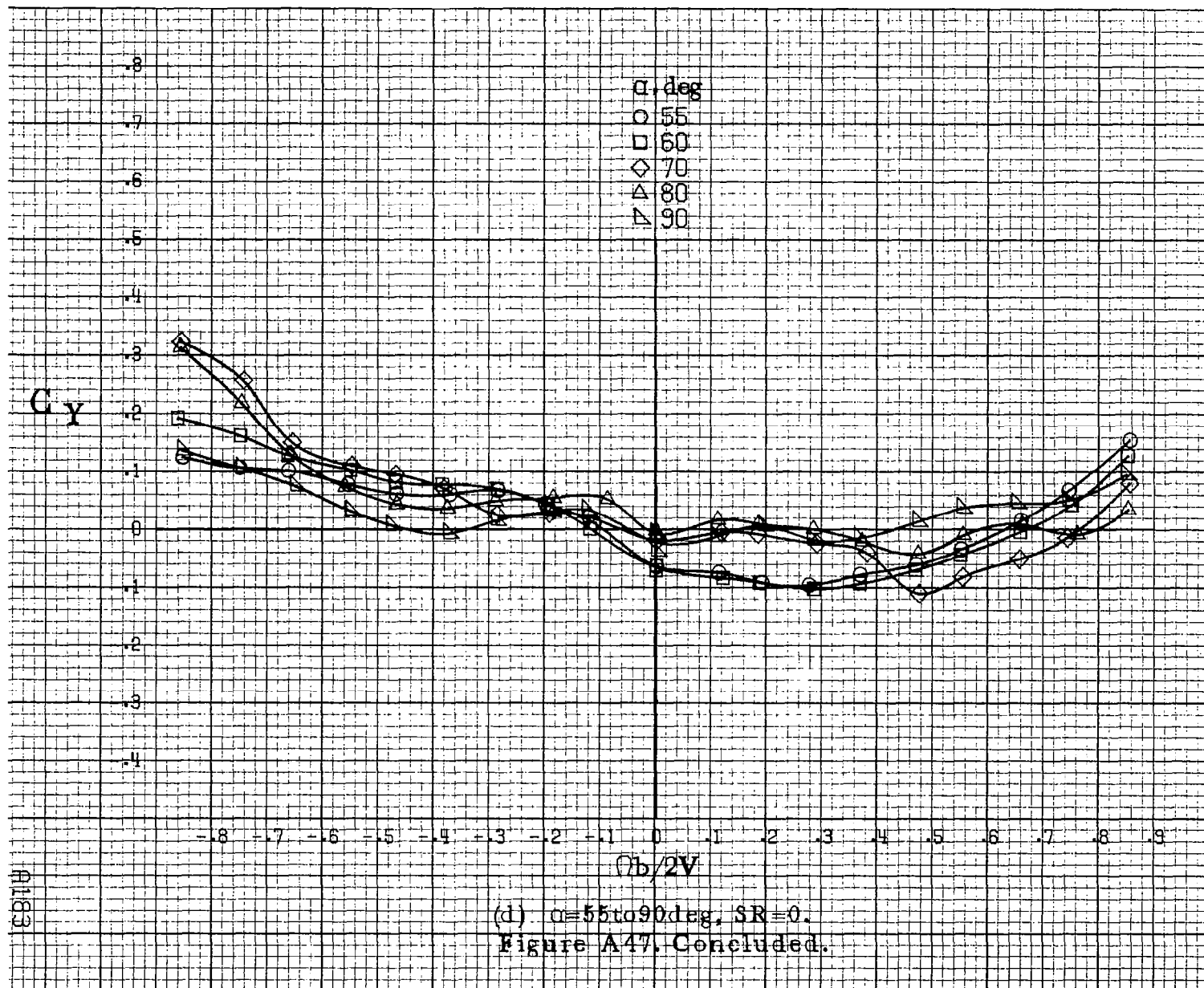


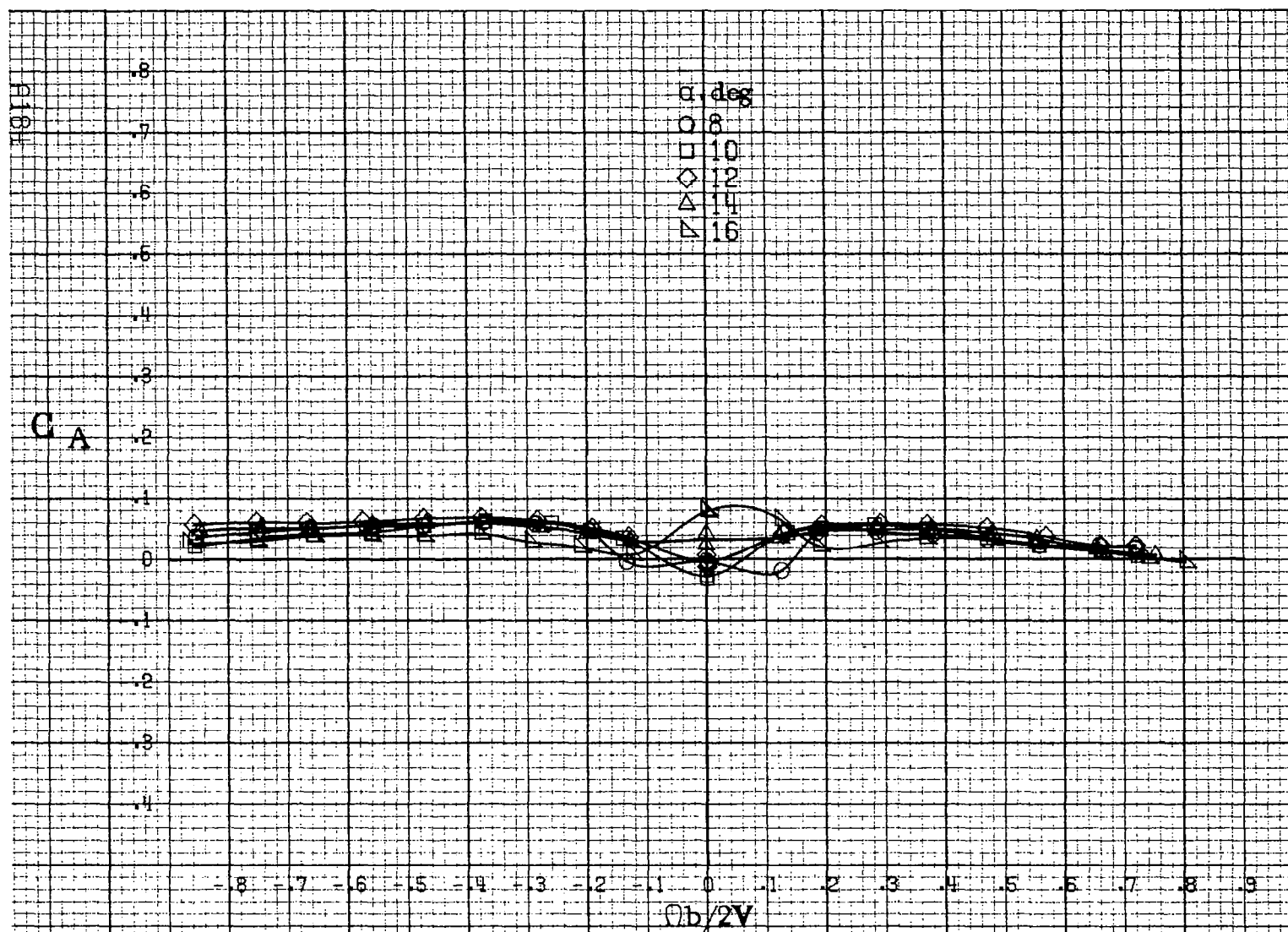
(a) $\alpha = 8$ to 16 deg, $SR = 91$ cm (36 in).

Figure A47. Effect of rotation rate and angle of attack on side force coefficient for configuration having sharp-edged fuselage bottom. $\delta_a = -20^\circ$, $\delta_r = -28^\circ$, $\beta = 0^\circ$.



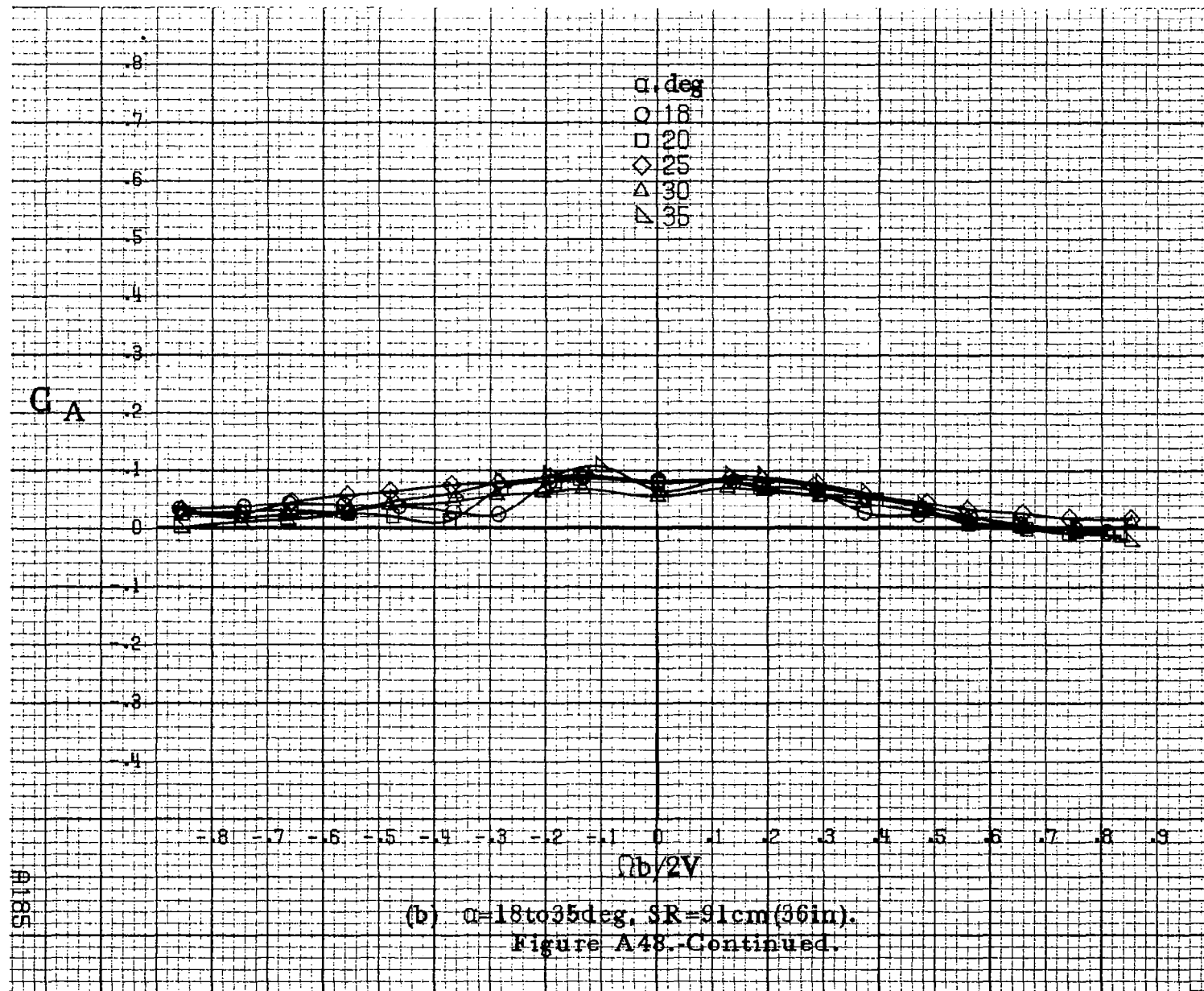






(a) $\alpha = 8$ to 16° , $SR = 91\text{cm (36in)}$.

Figure A48. Effect of rotation rate and angle of attack on axial force coefficient for configuration having sharp-edged fuselage bottom. $\delta_e = -20^\circ$, $\delta_a = -20^\circ$, $\delta_r = -28^\circ$, $\beta = 0^\circ$.



H106

C_A

.8
.7
.6
.5
.4
.3
.2
.1
0
-.1
-.2
-.3
-.4

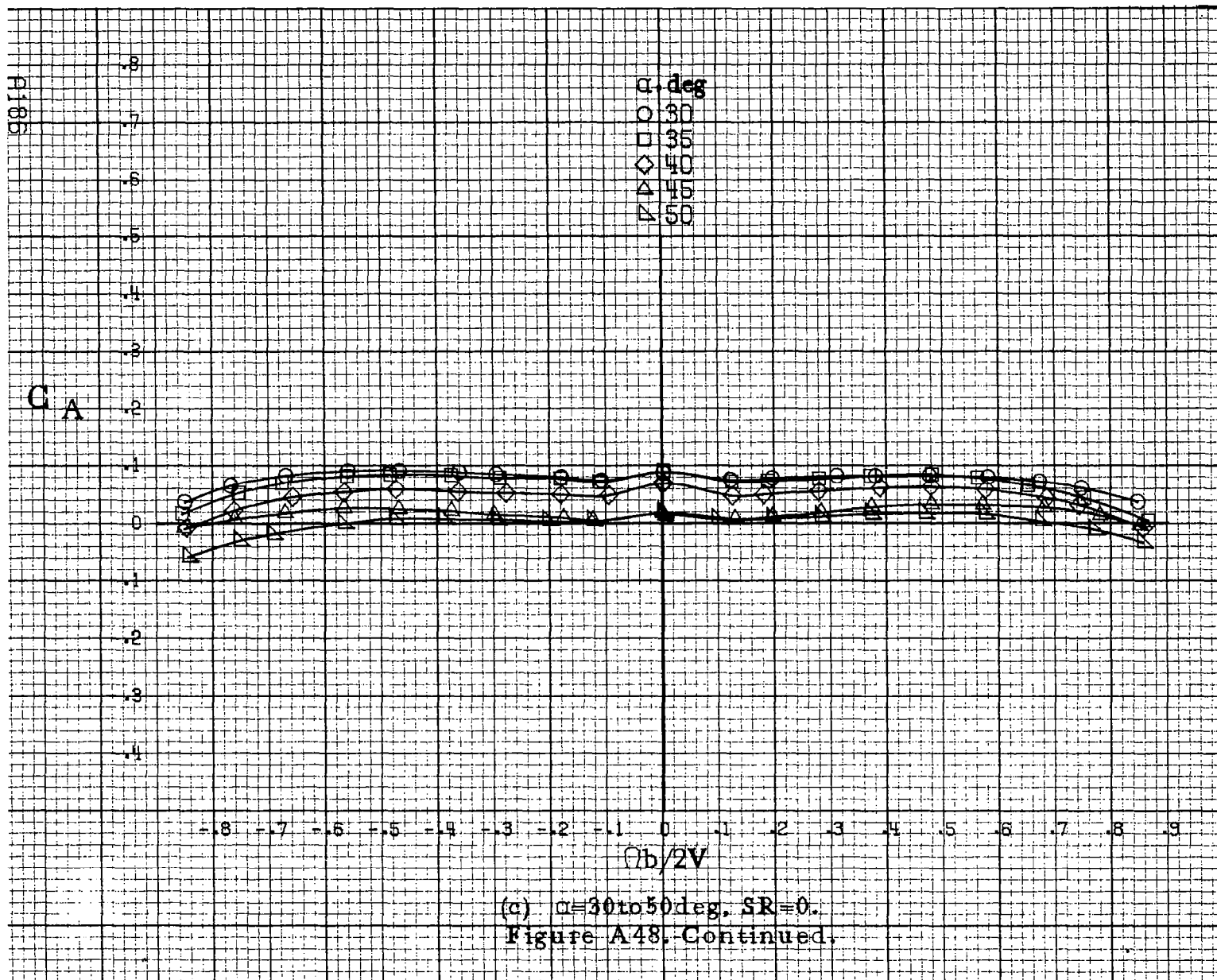
α , deg
○ 30
□ 35
◇ 40
△ 45
▽ 50

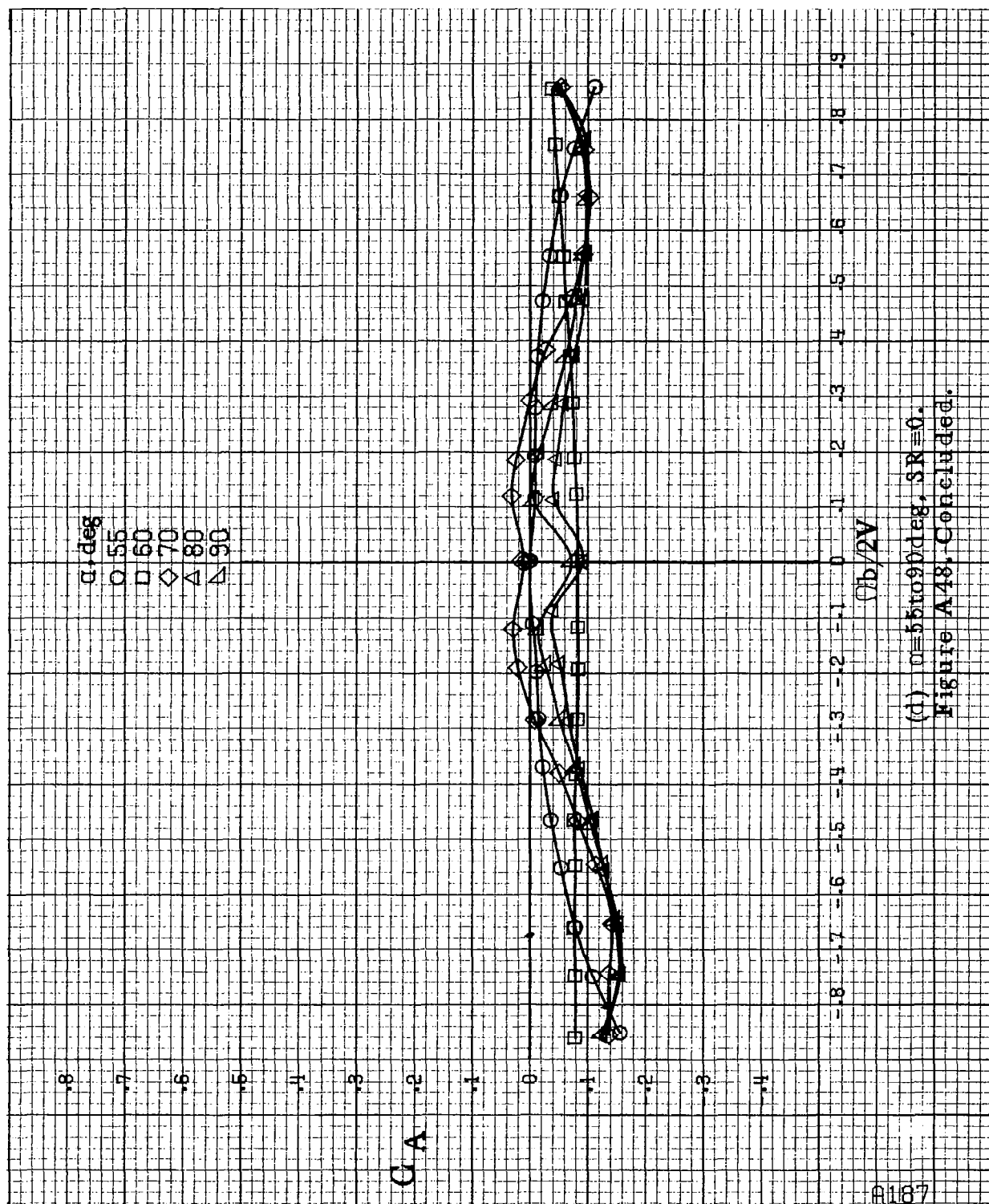
-.8 -.7 -.6 -.5 -.4 -.3 -.2 -.1 0 .1 .2 .3 .4 .5 .6 .7 .8 .9

$b/2V$

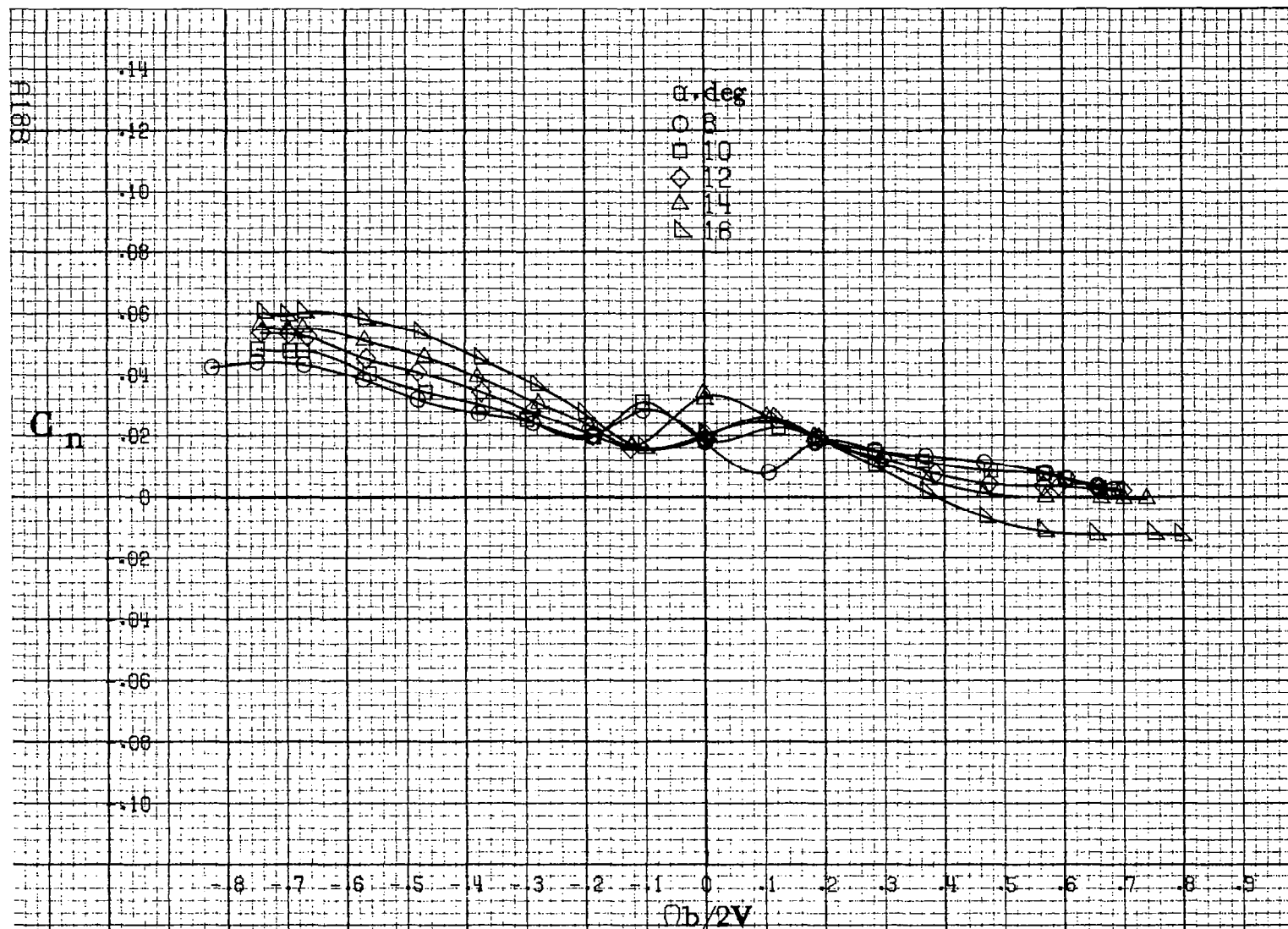
(a) $\alpha=30$ to 50 deg, $SR=0$.

Figure A48. Continued.



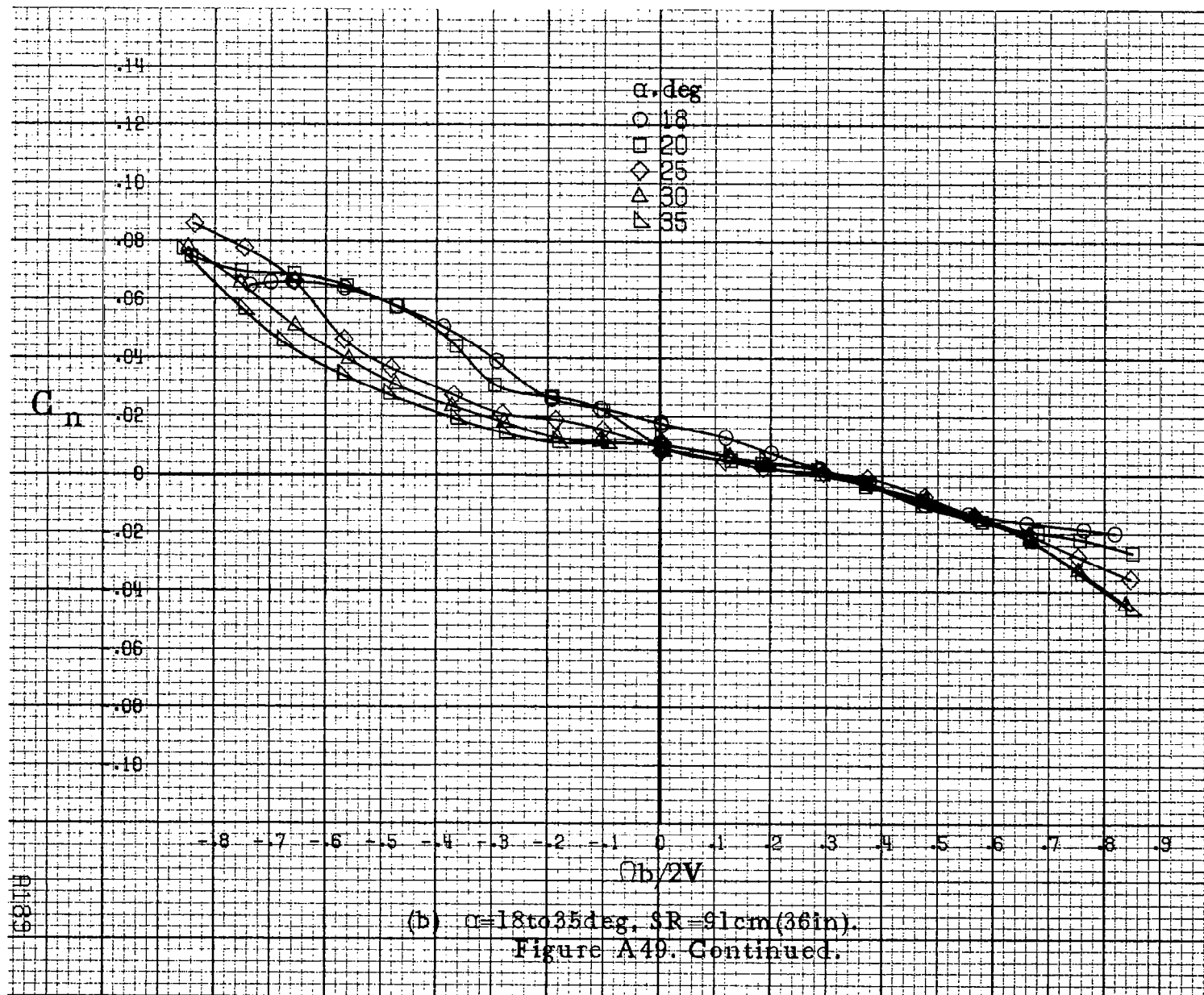


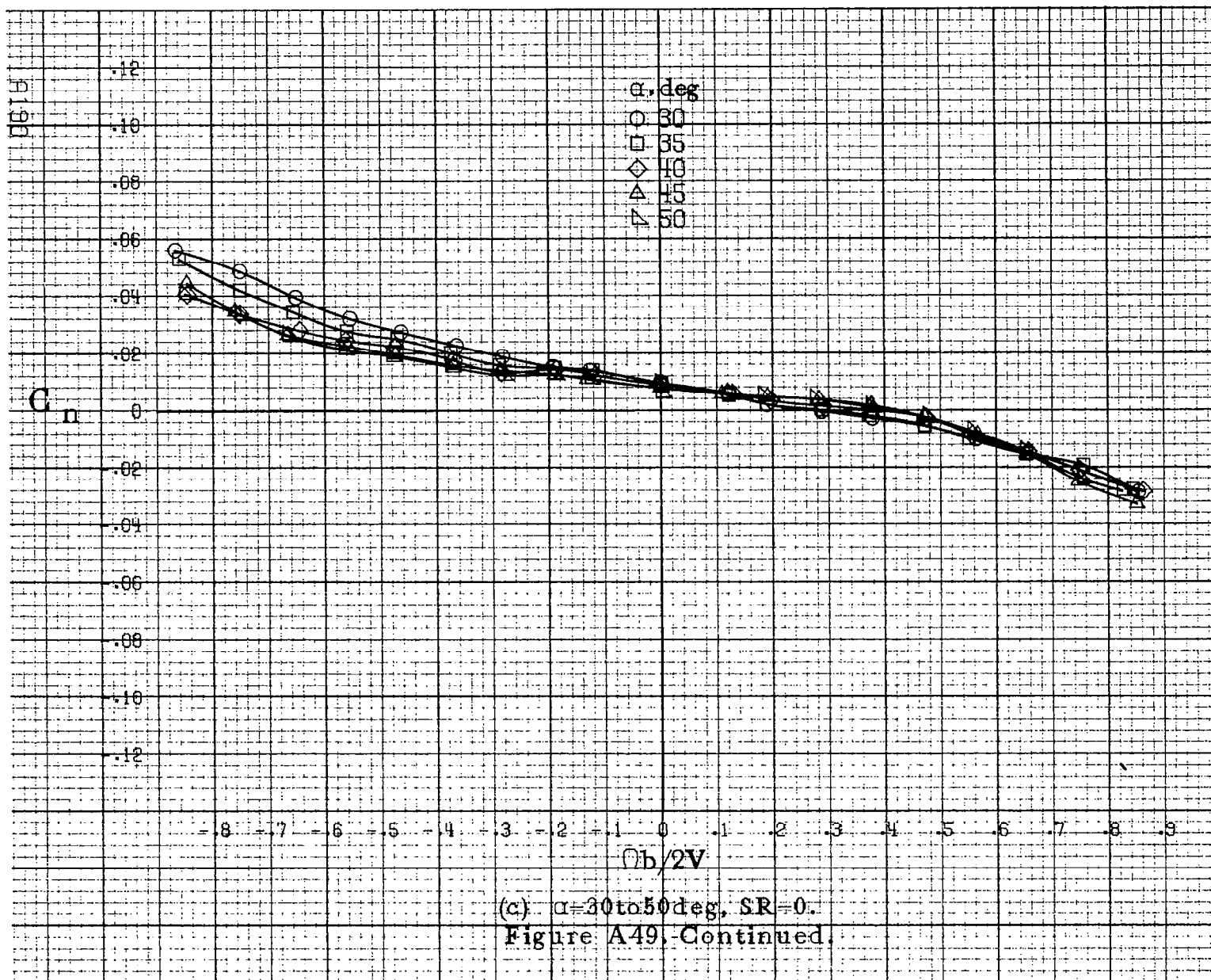
(d) $\alpha = 55$ to 90° deg, $SR = 0$.
Figure A48. Concluded.

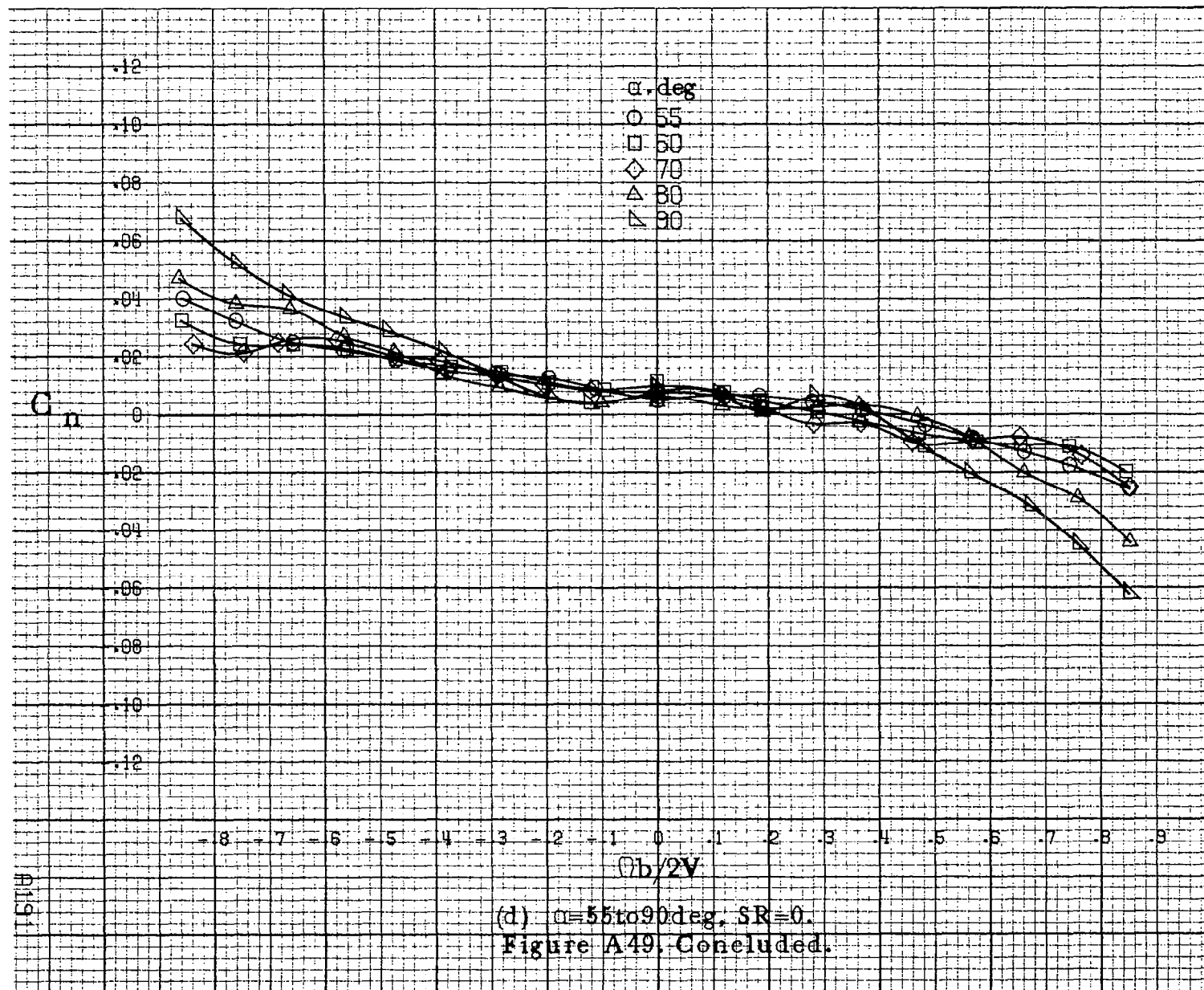


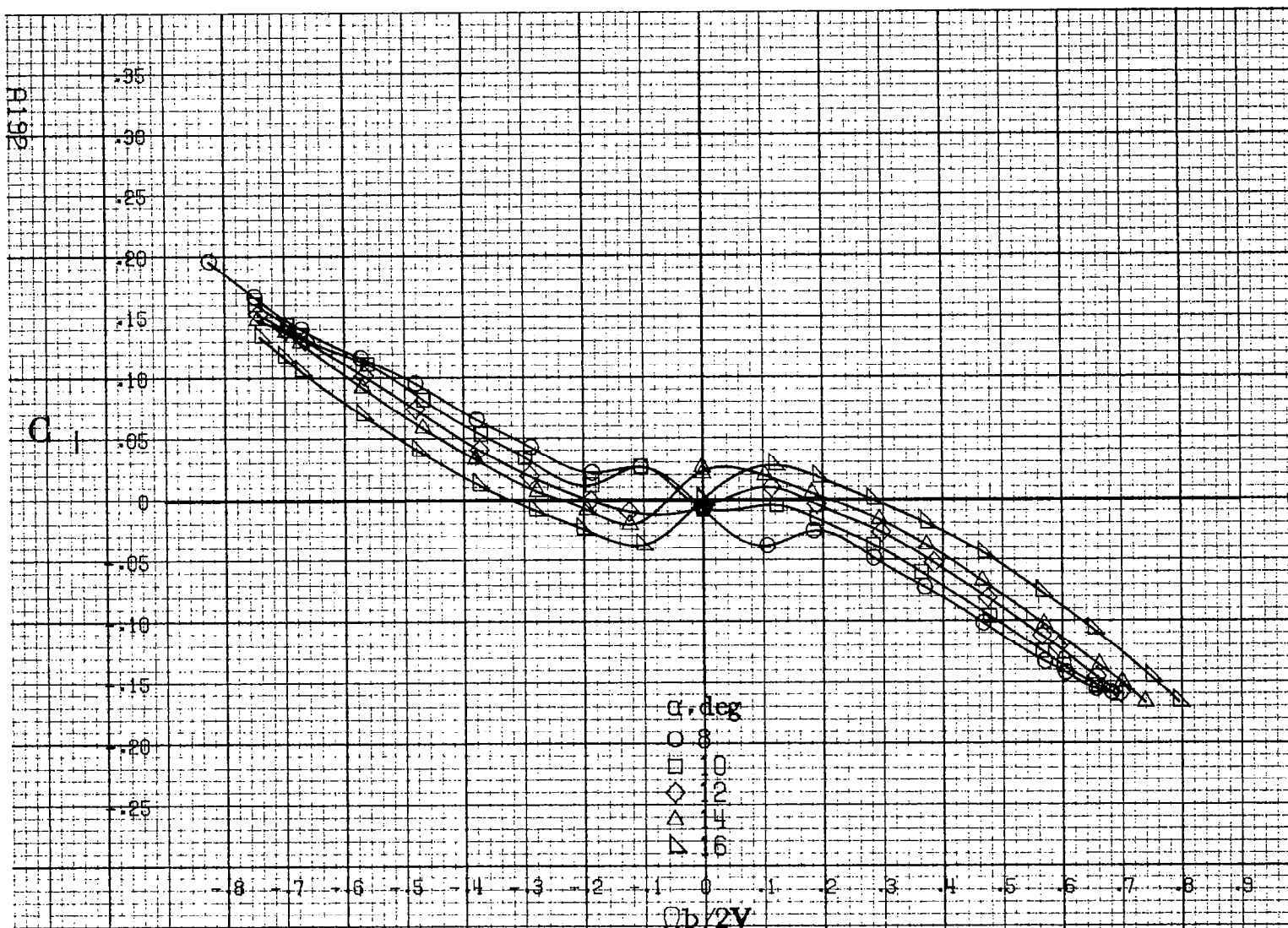
(a) $\alpha = 8$ to 16° , $SR = 91\text{cm (36in)}$.

Figure A49. Effect of rotation rate and angle of attack on yawing-moment coefficient for configuration having sharp-edged fuselage bottom. $\delta_a = -20^\circ$, $\delta_s = 0^\circ$, $\delta_r = -28^\circ$, $B = 0^\circ$.



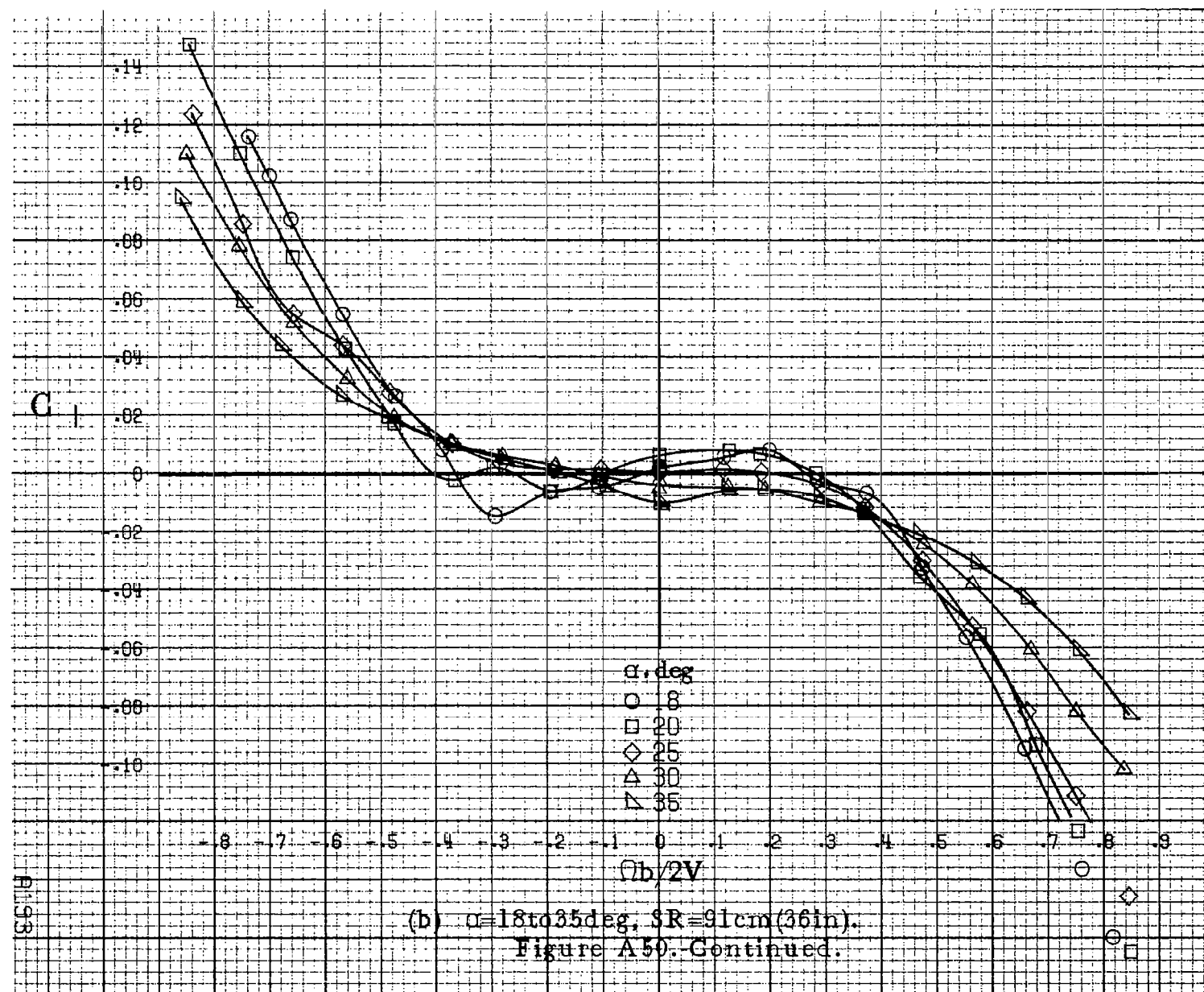


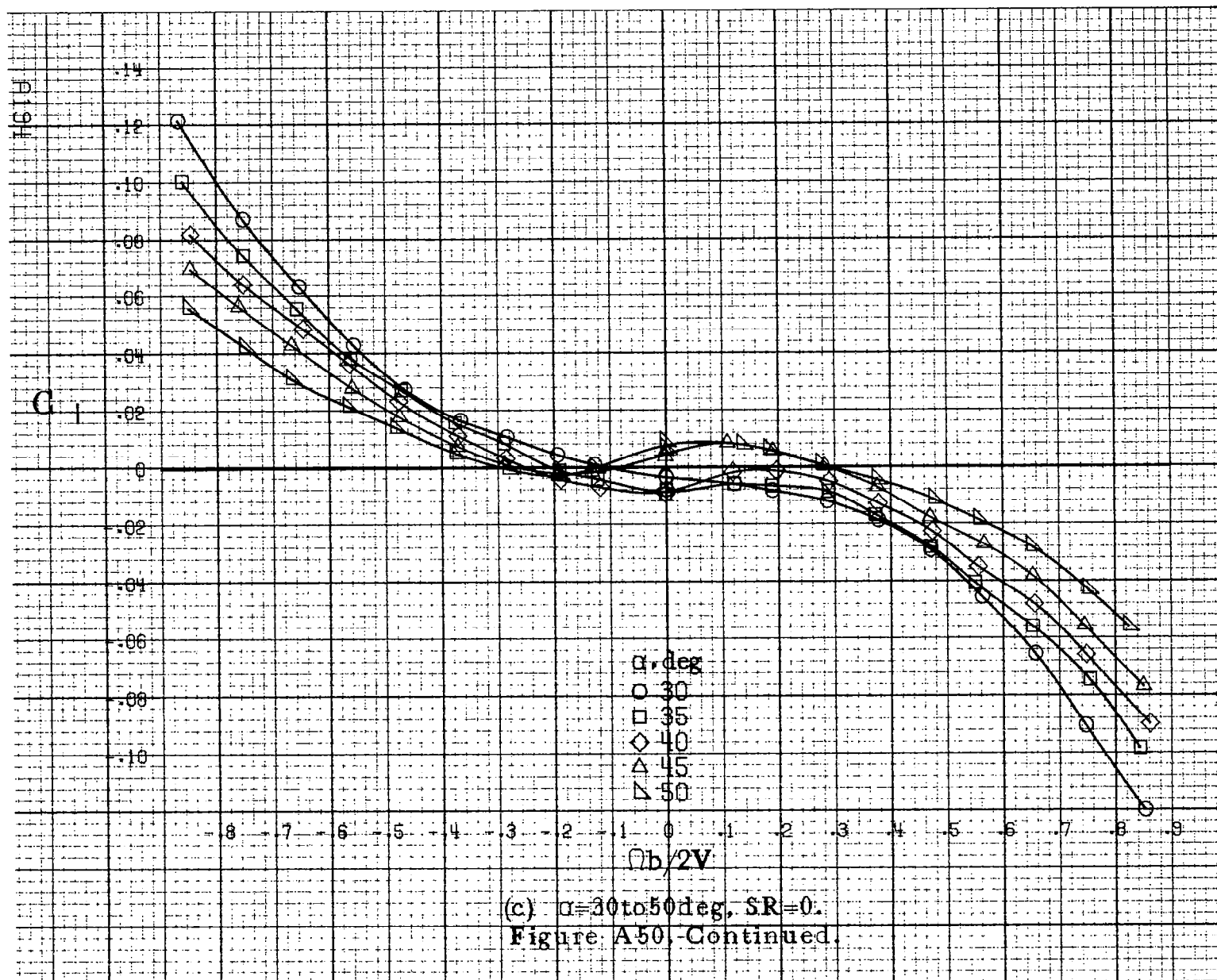


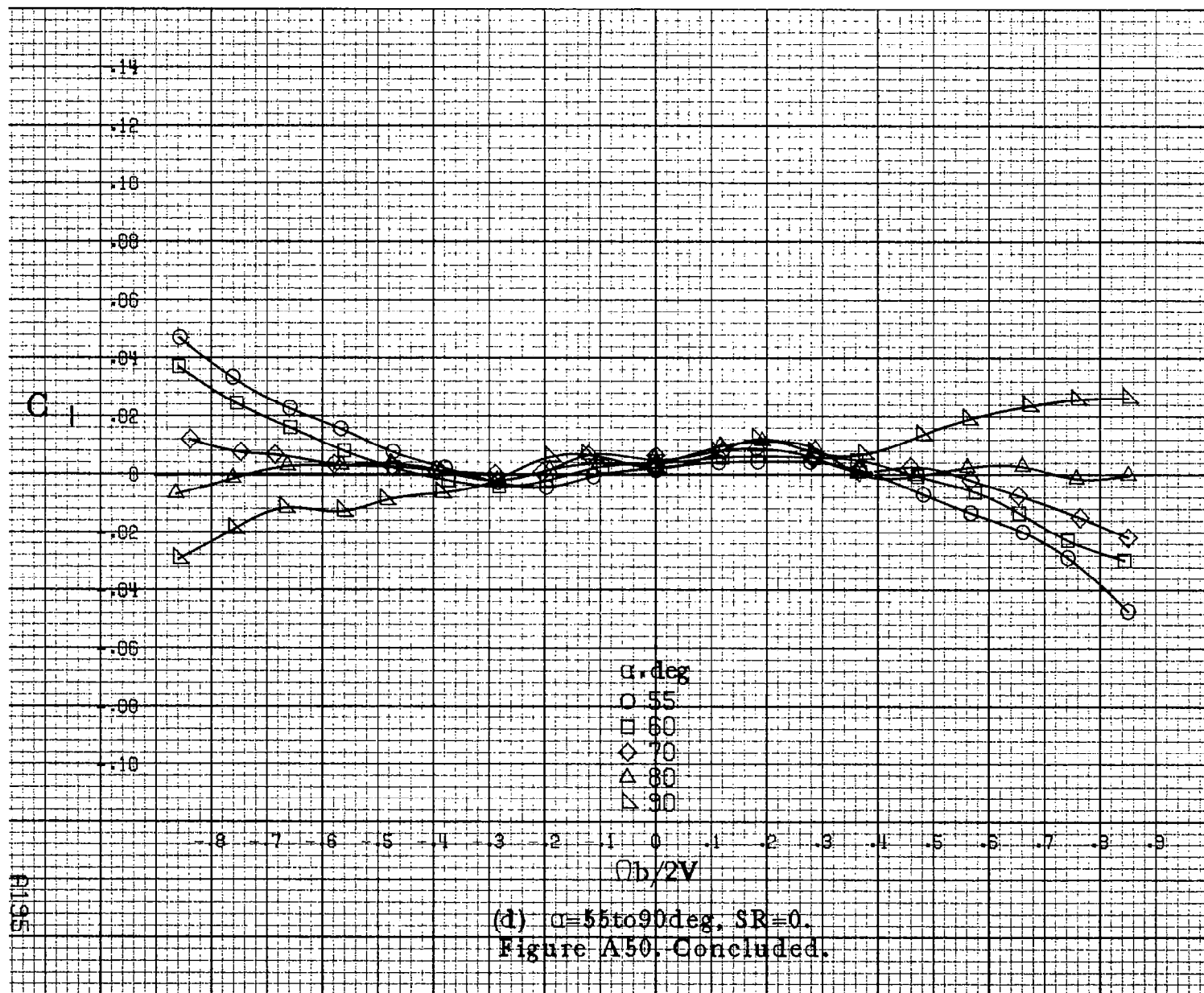


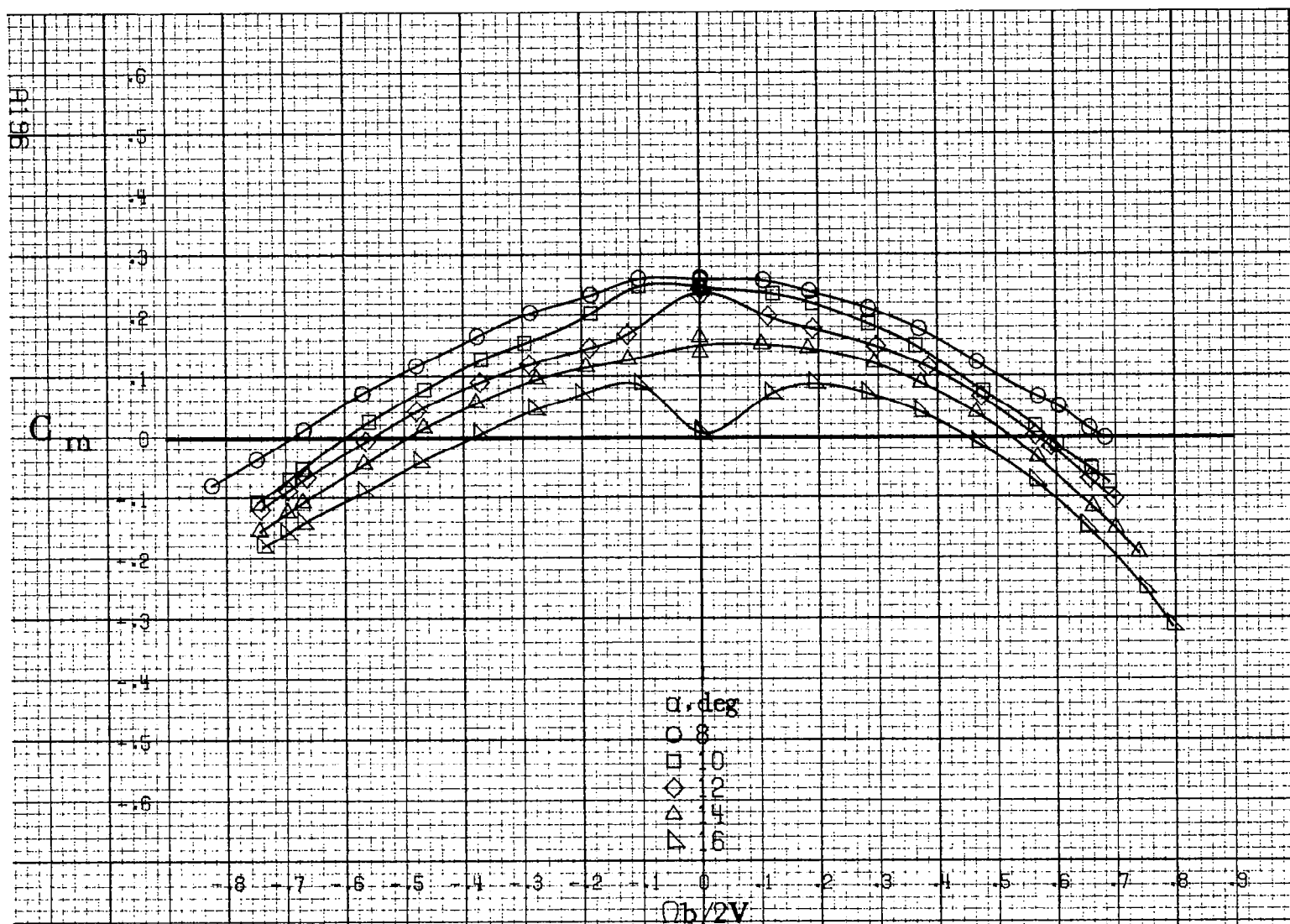
(a) $\alpha=8$ to 16 deg, $SR=91$ cm (36 in).

Figure A.50 Effect of rotation rate and angle of attack on rolling-moment coefficient for configuration having sharp-edged fuselage bottom. $\delta_a = 20^\circ$, $\delta_r = 28^\circ$, $\beta = 10^\circ$.



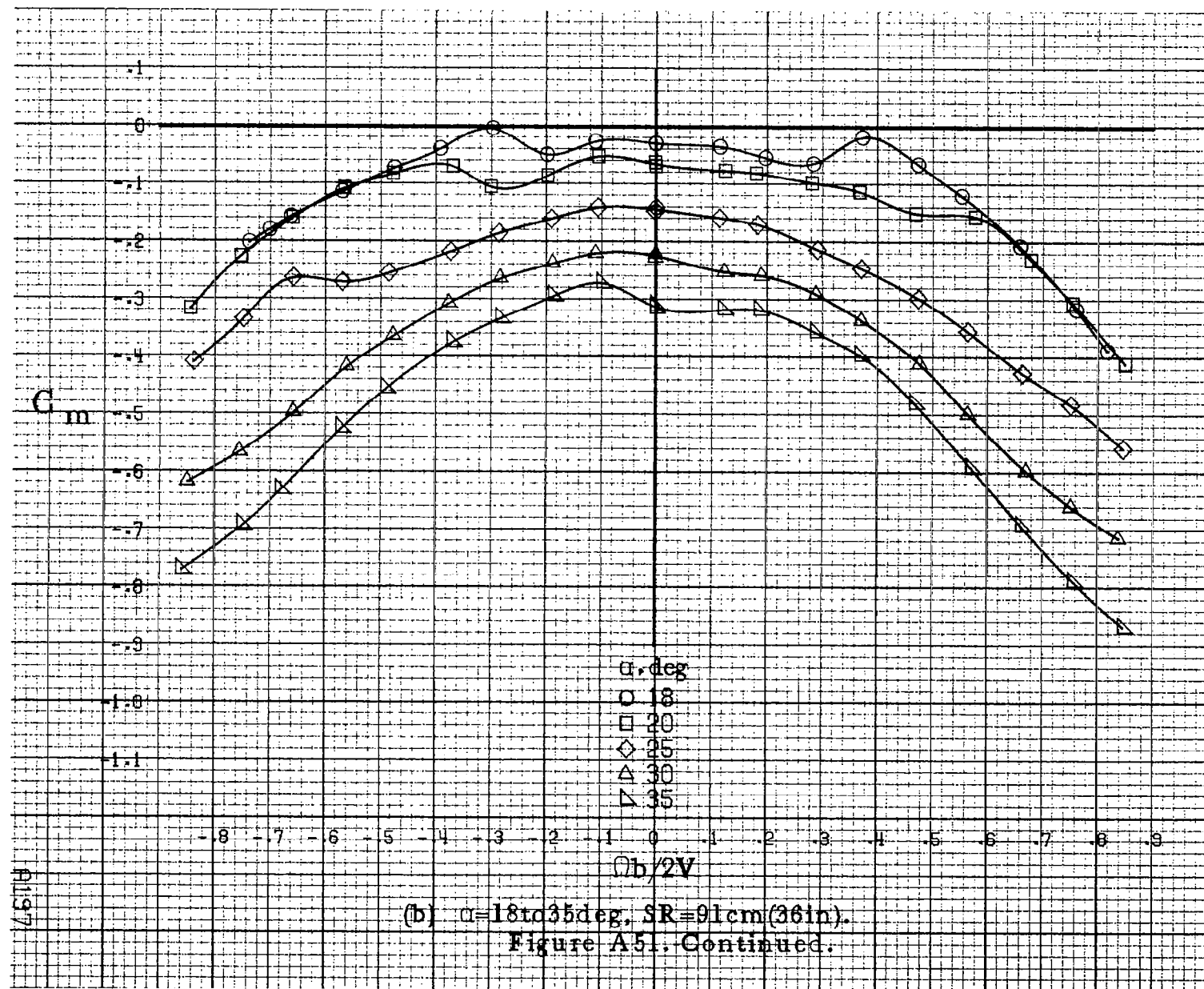


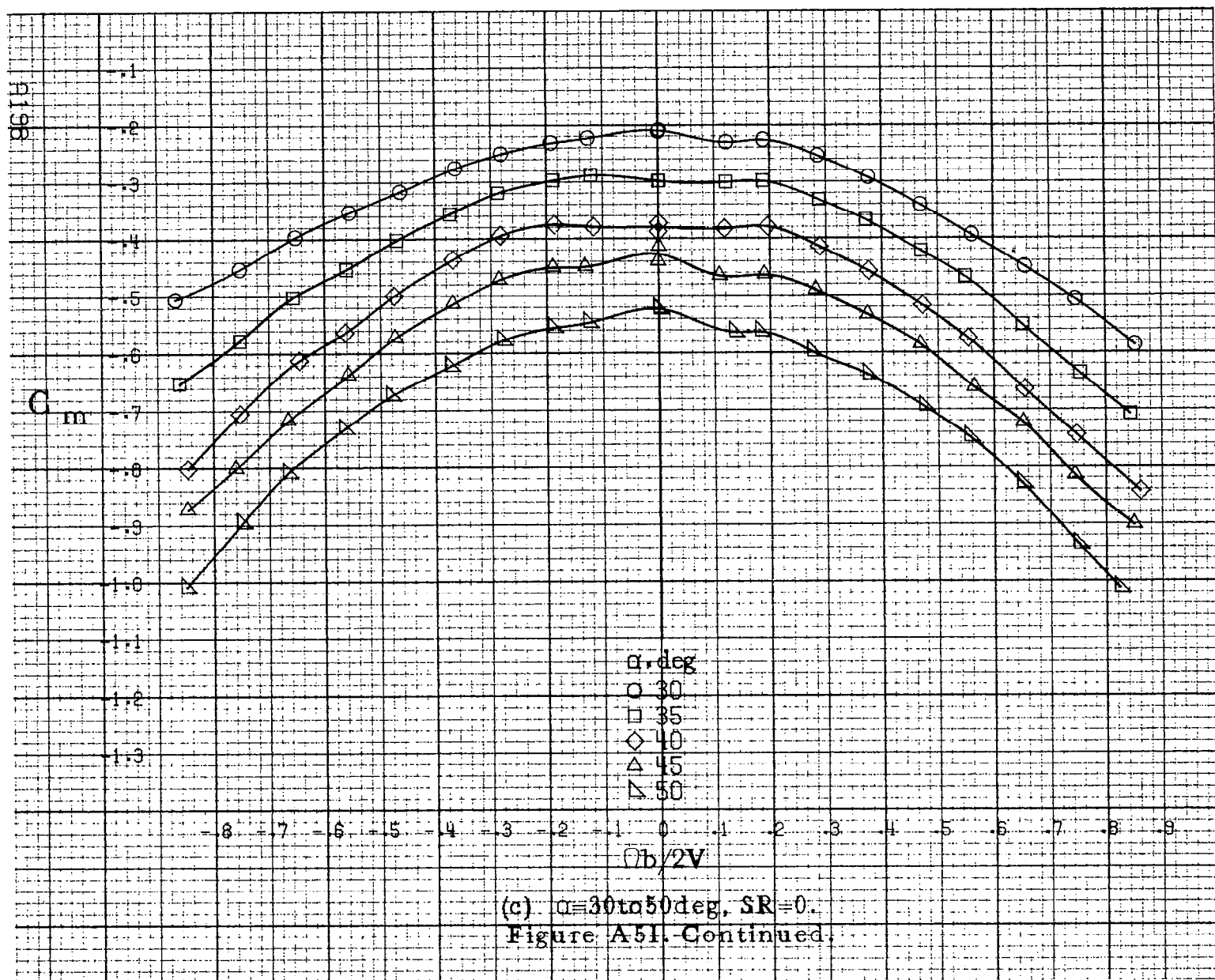


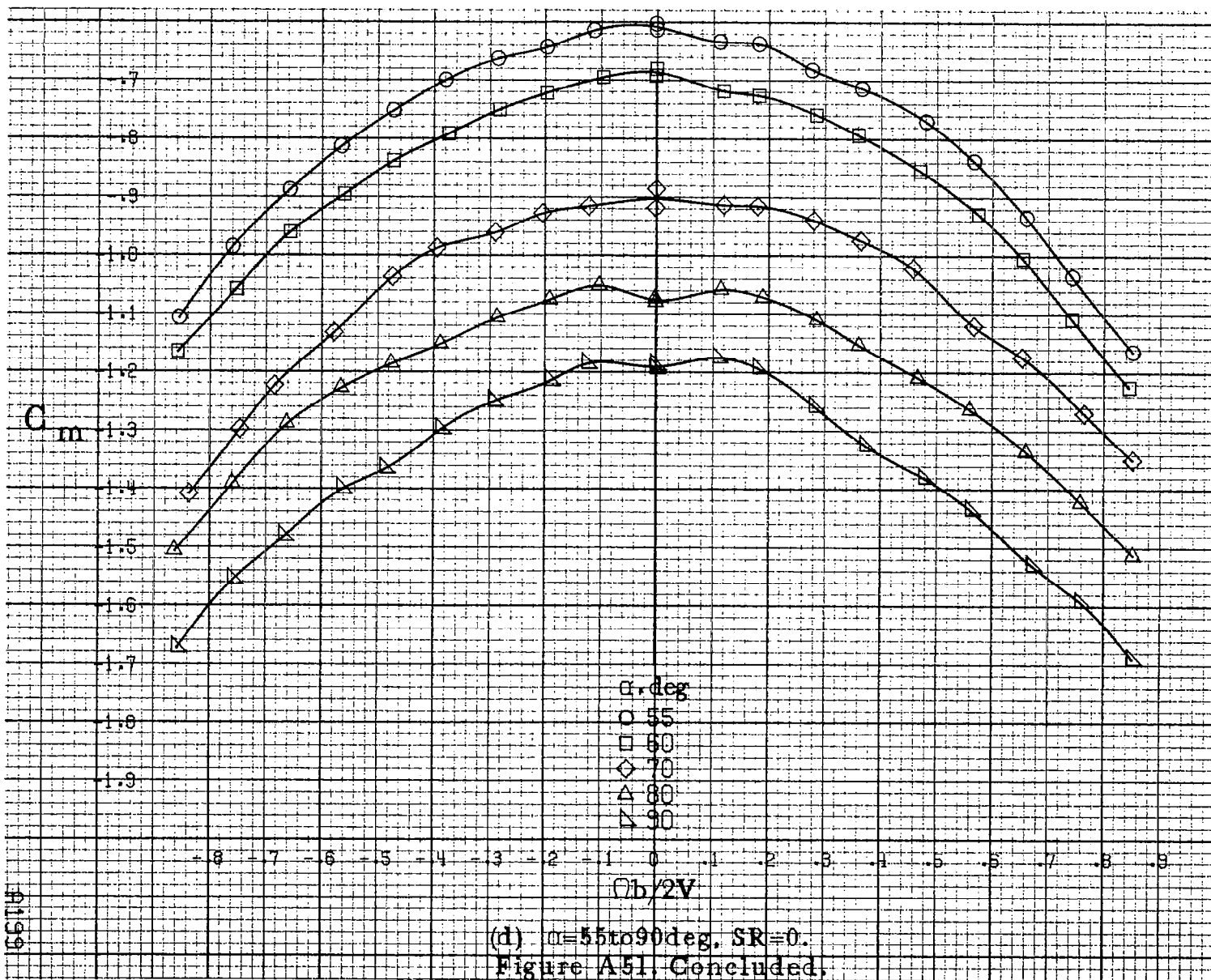


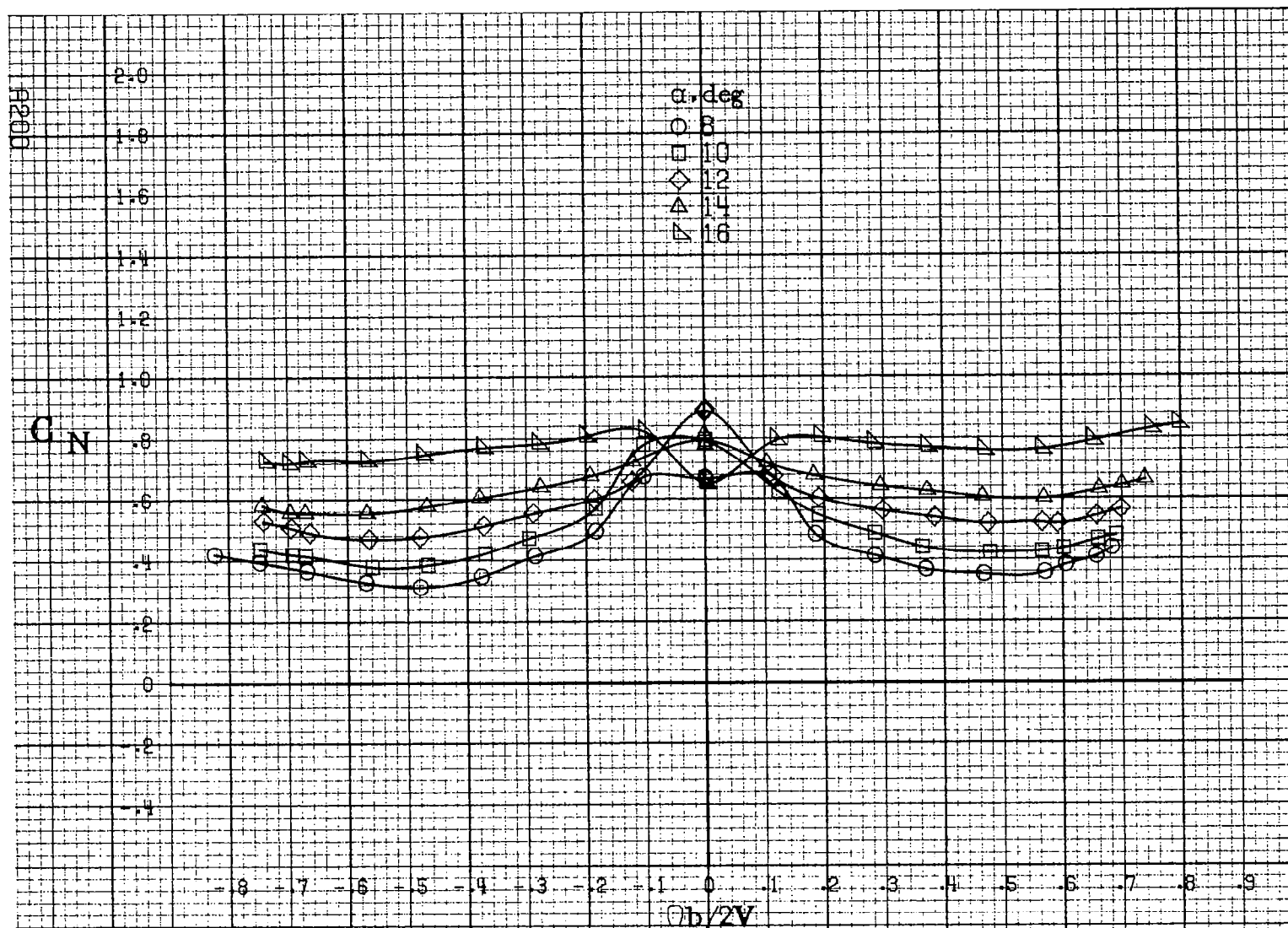
(a) $\alpha = 8$ to 16 deg, $SR = 91$ cm (36 in).

Figure A51. Effect of rotation rate and angle of attack on pitching moment coefficient for configuration having sharp-edged fuselage bottom. $\delta_a = 20^\circ$, $\delta_a = 0^\circ$, $\delta_c = -28^\circ$, $\beta = 0^\circ$.



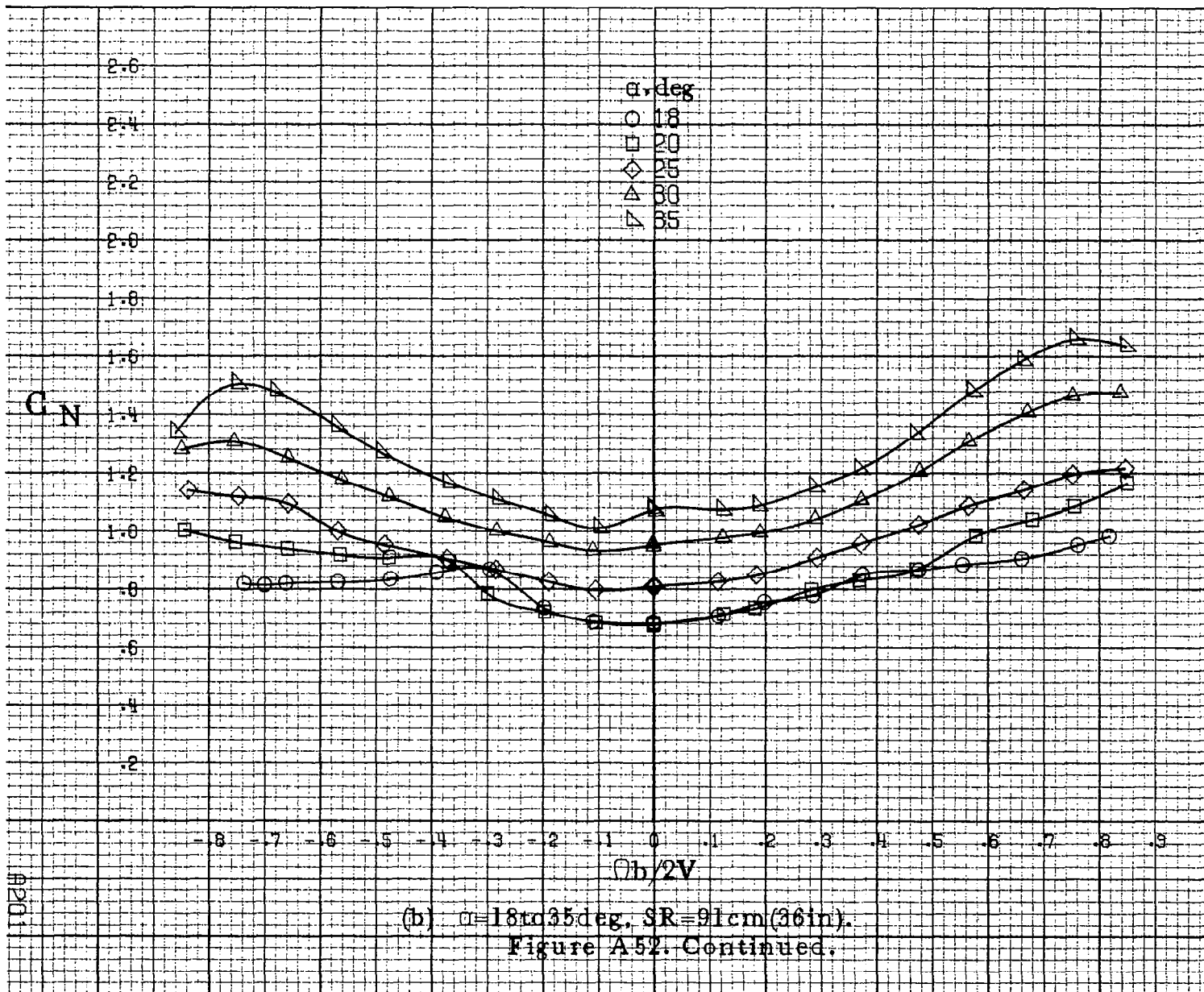


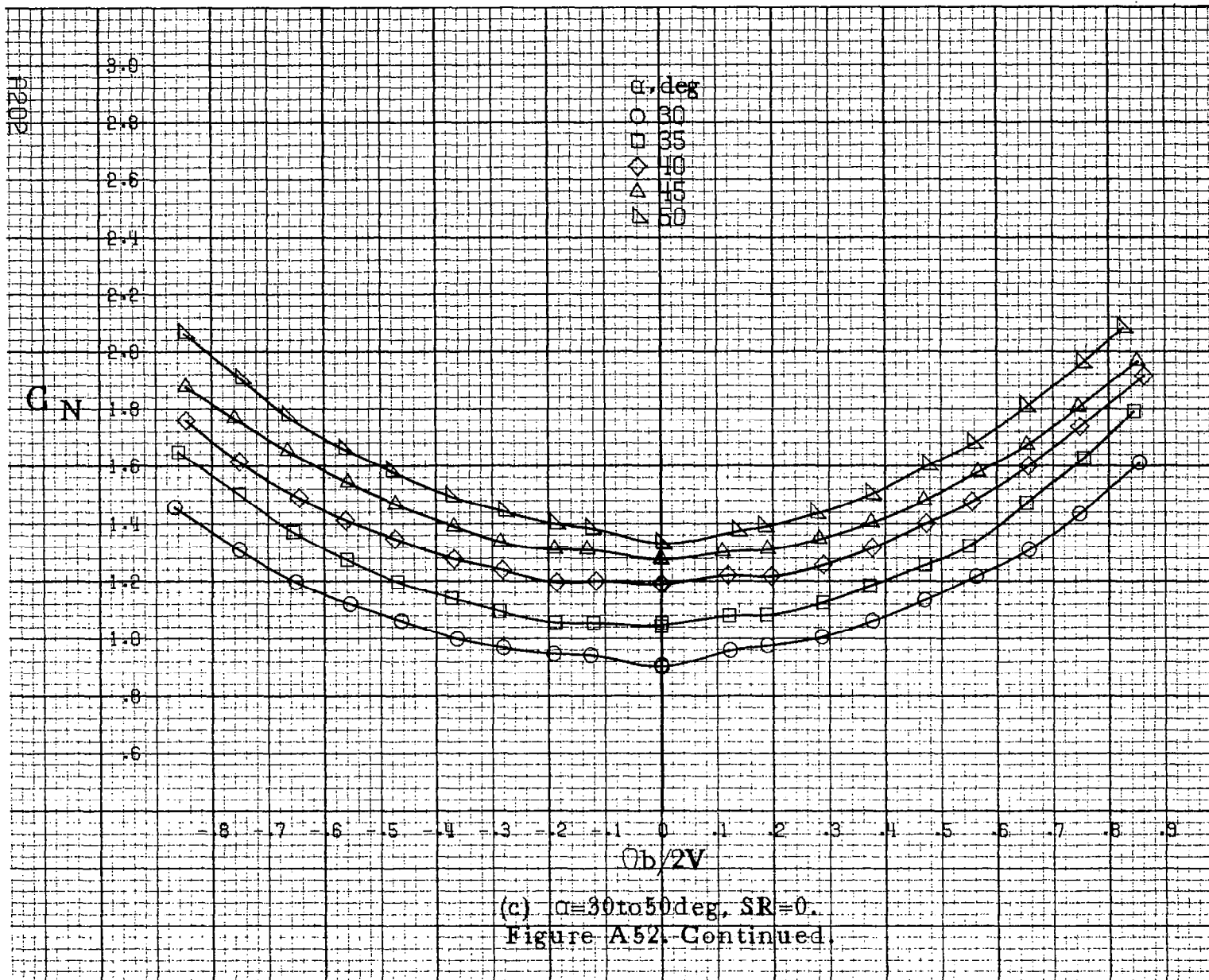


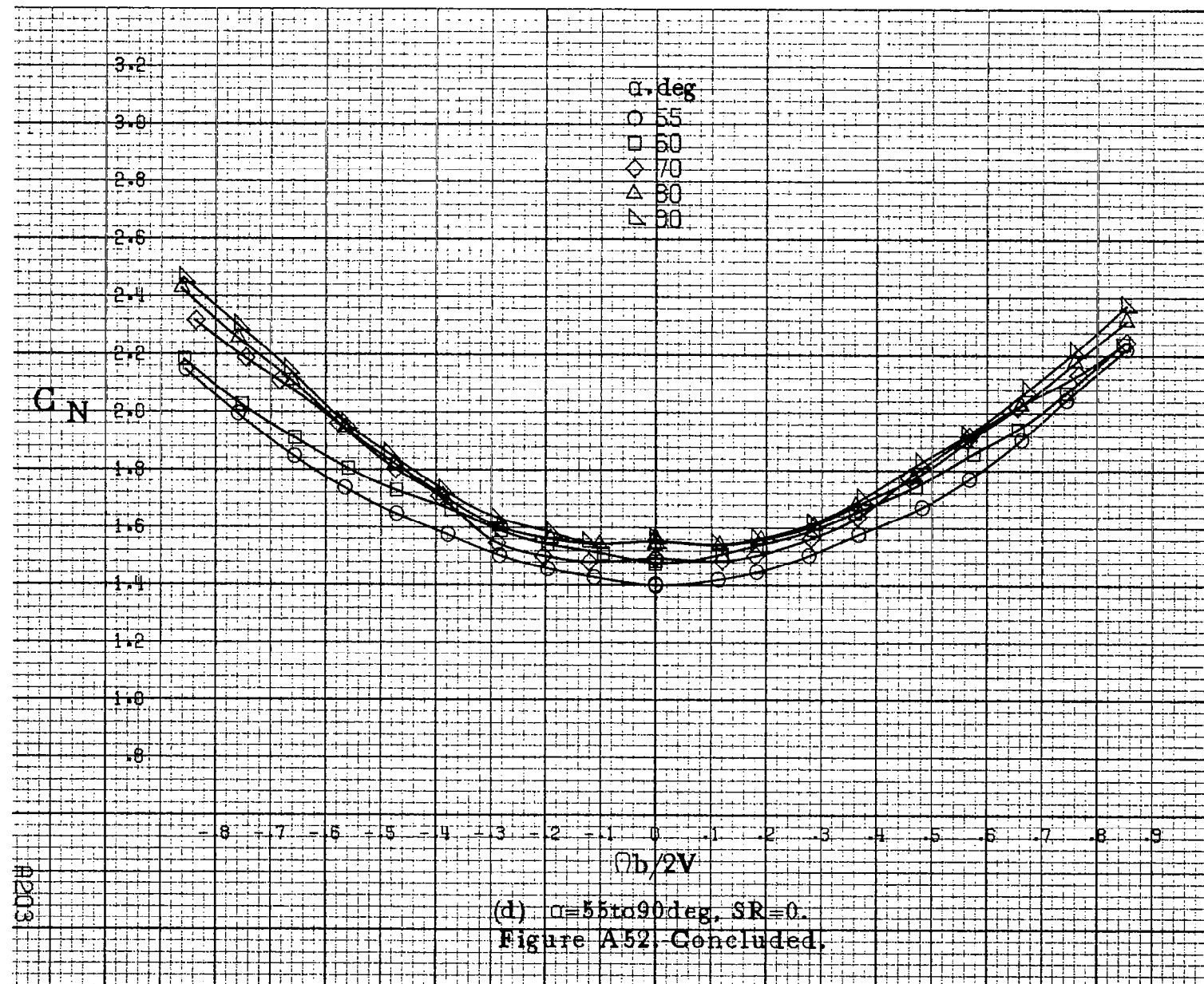


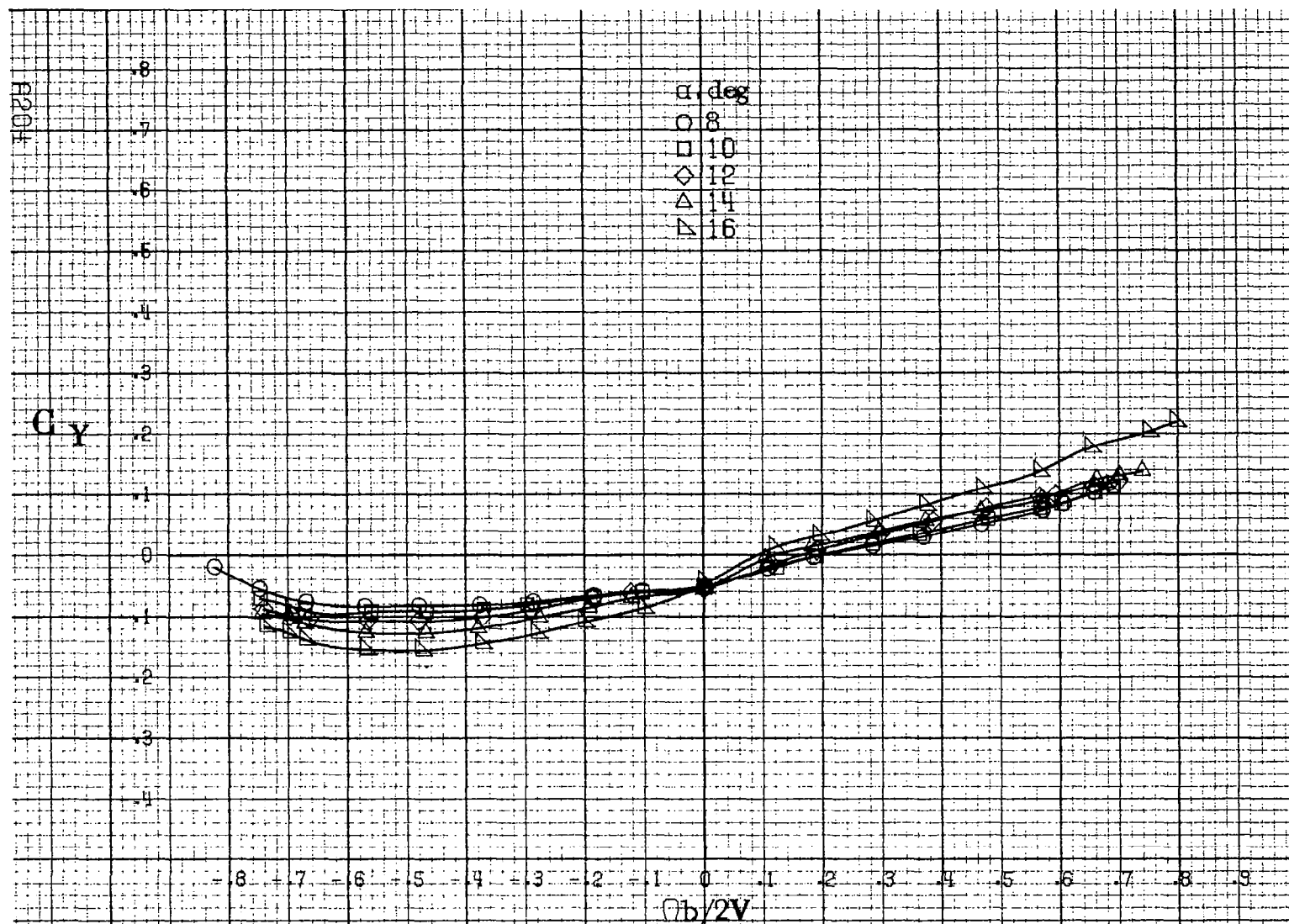
(a) $\alpha = 8$ to 16° , $SR = 91 \text{ cm (36 in.)}$.

Figure A52. Effect of rotation rate and angle of attack on normal force coefficient for configuration having sharp edged fuselage bottom. $\delta_a = 20^\circ$, $\delta_s = 0^\circ$, $\delta_r = -28^\circ$, $\beta = 0^\circ$.



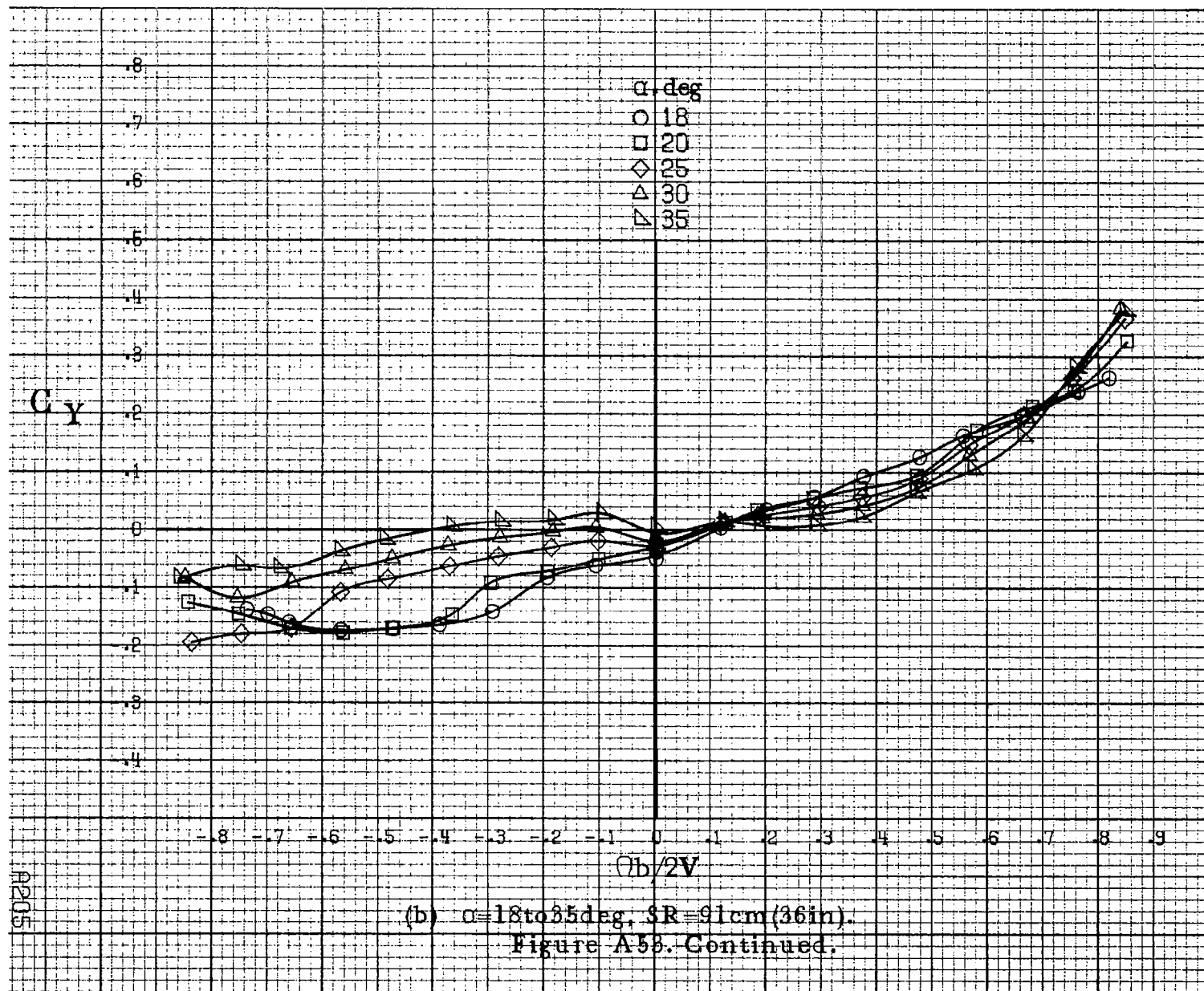


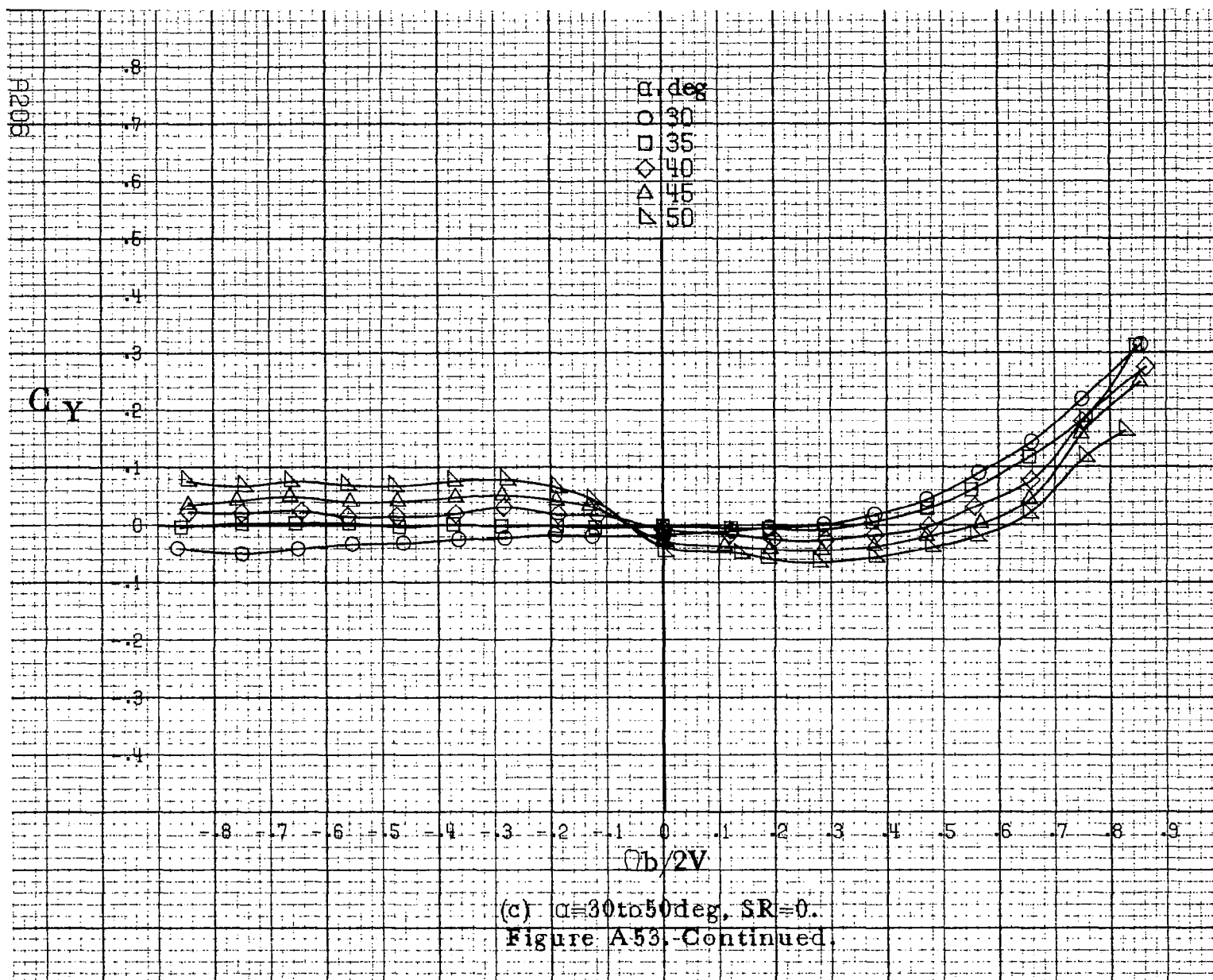


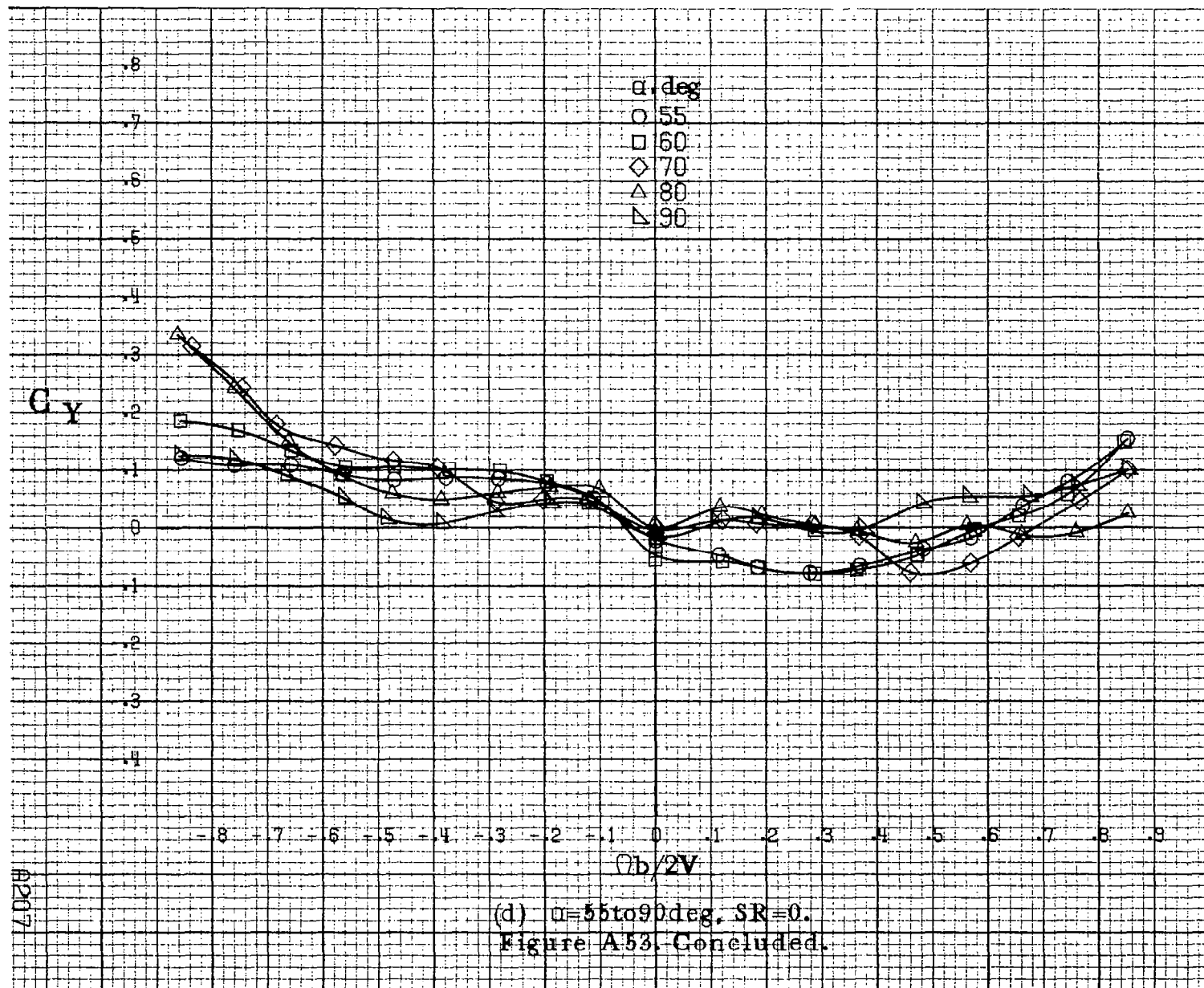


(a) $\alpha = 8$ to 16 deg, $SR = 91$ cm (36 in).

Figure A58. Effect of rotation rate and angle of attack on side-force coefficient for configuration having sharp-edged fuselage bottom. $\delta_a = -20^\circ$, $\delta_r = -28^\circ$, $\beta = 0^\circ$.







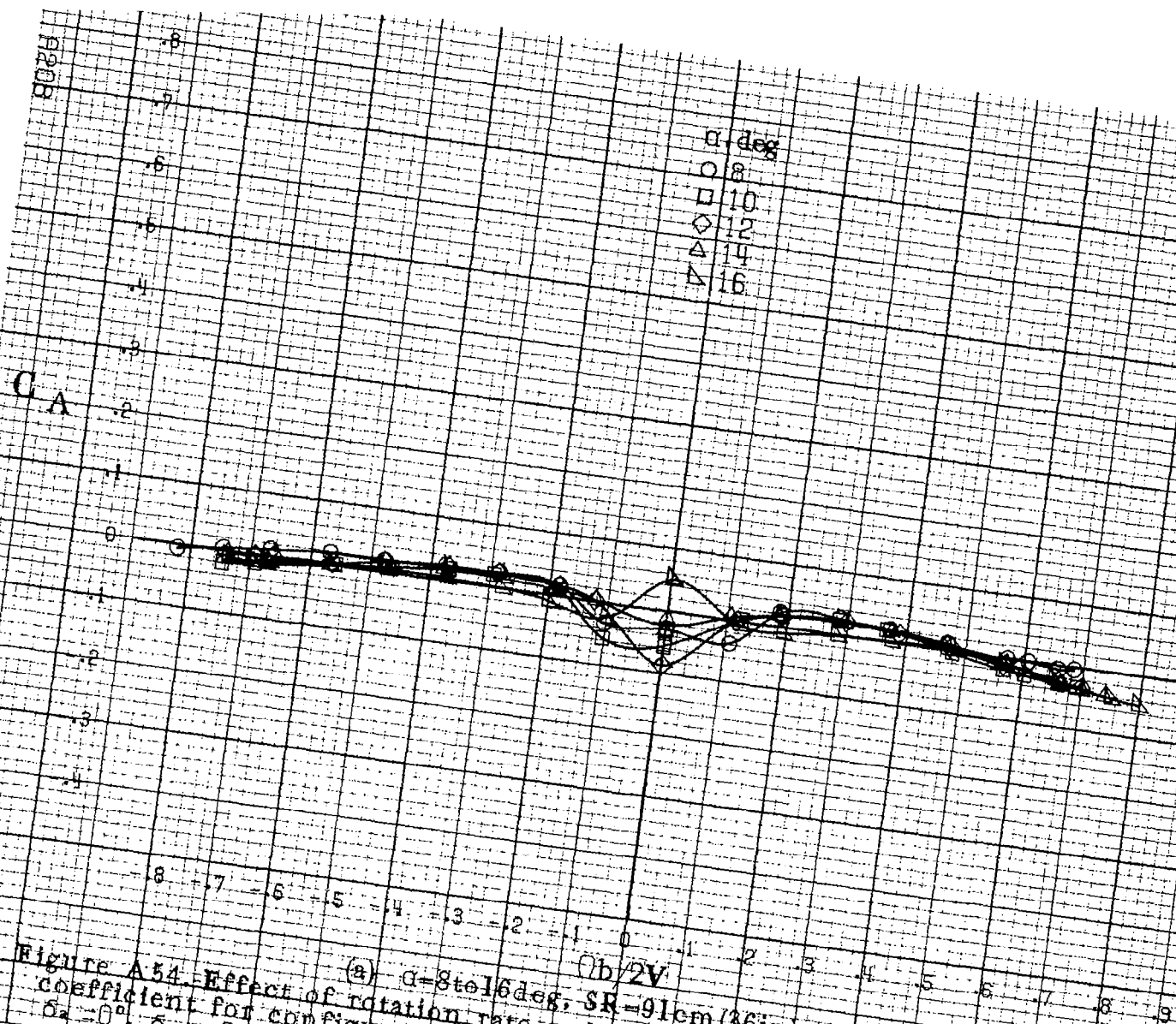
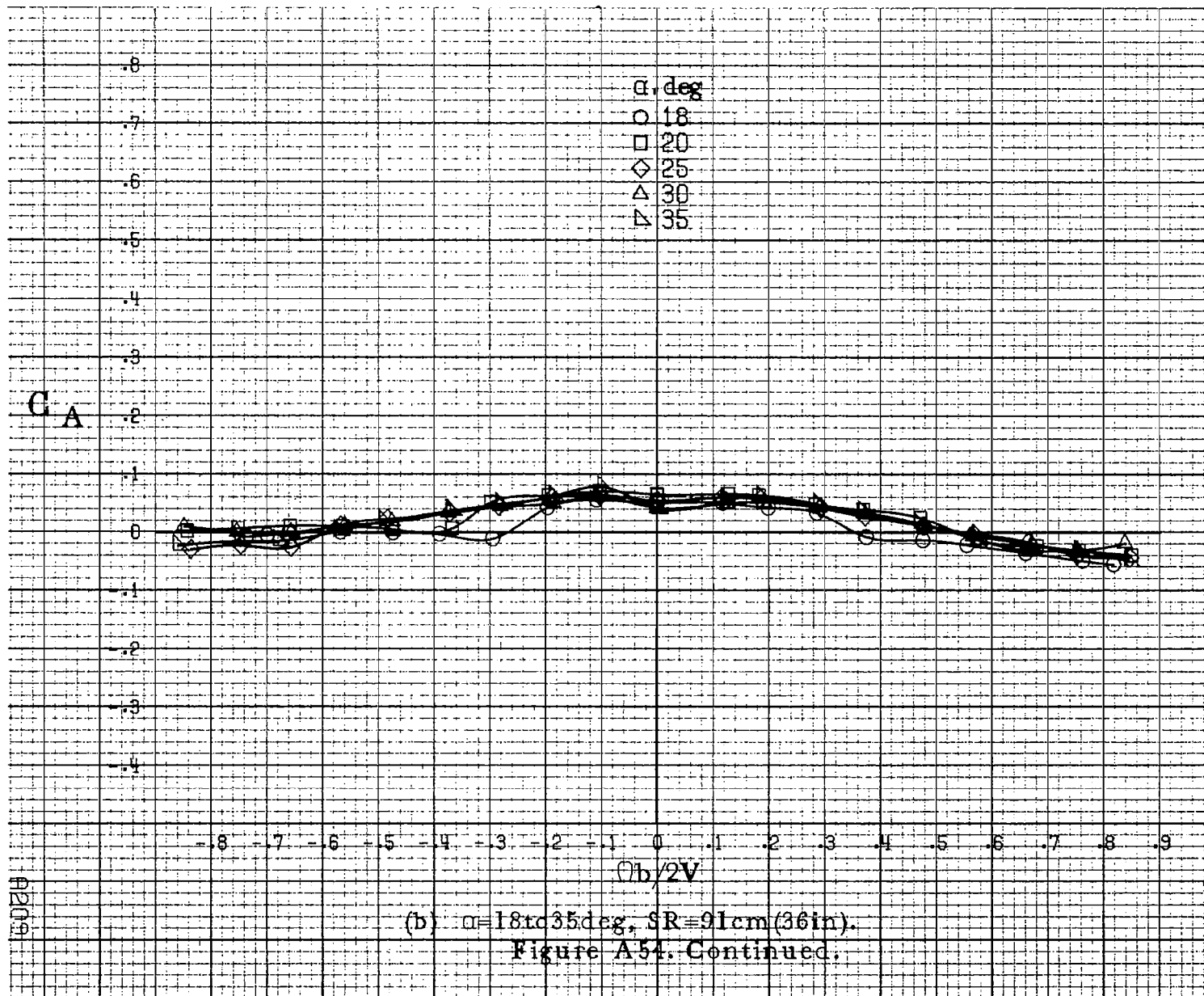
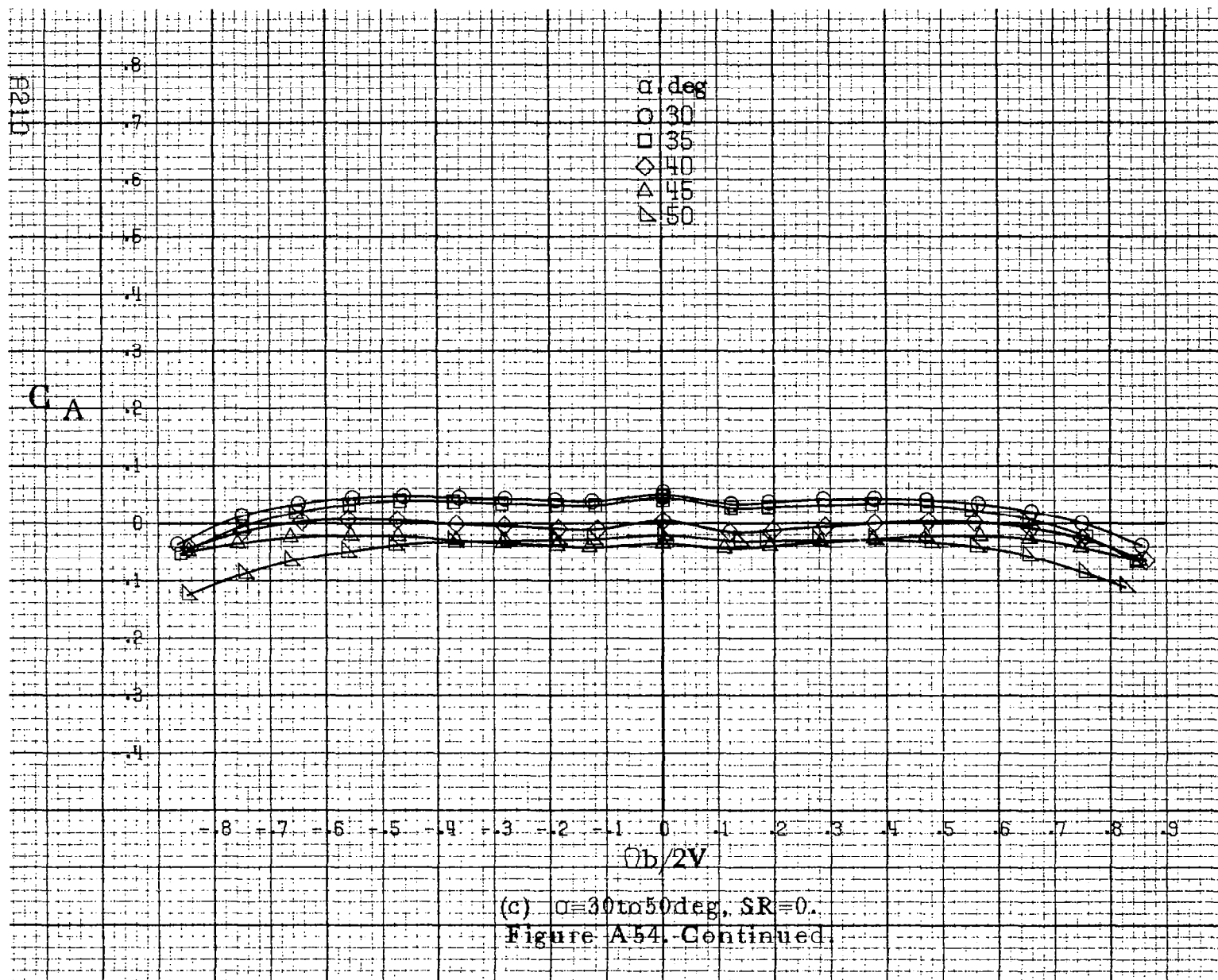
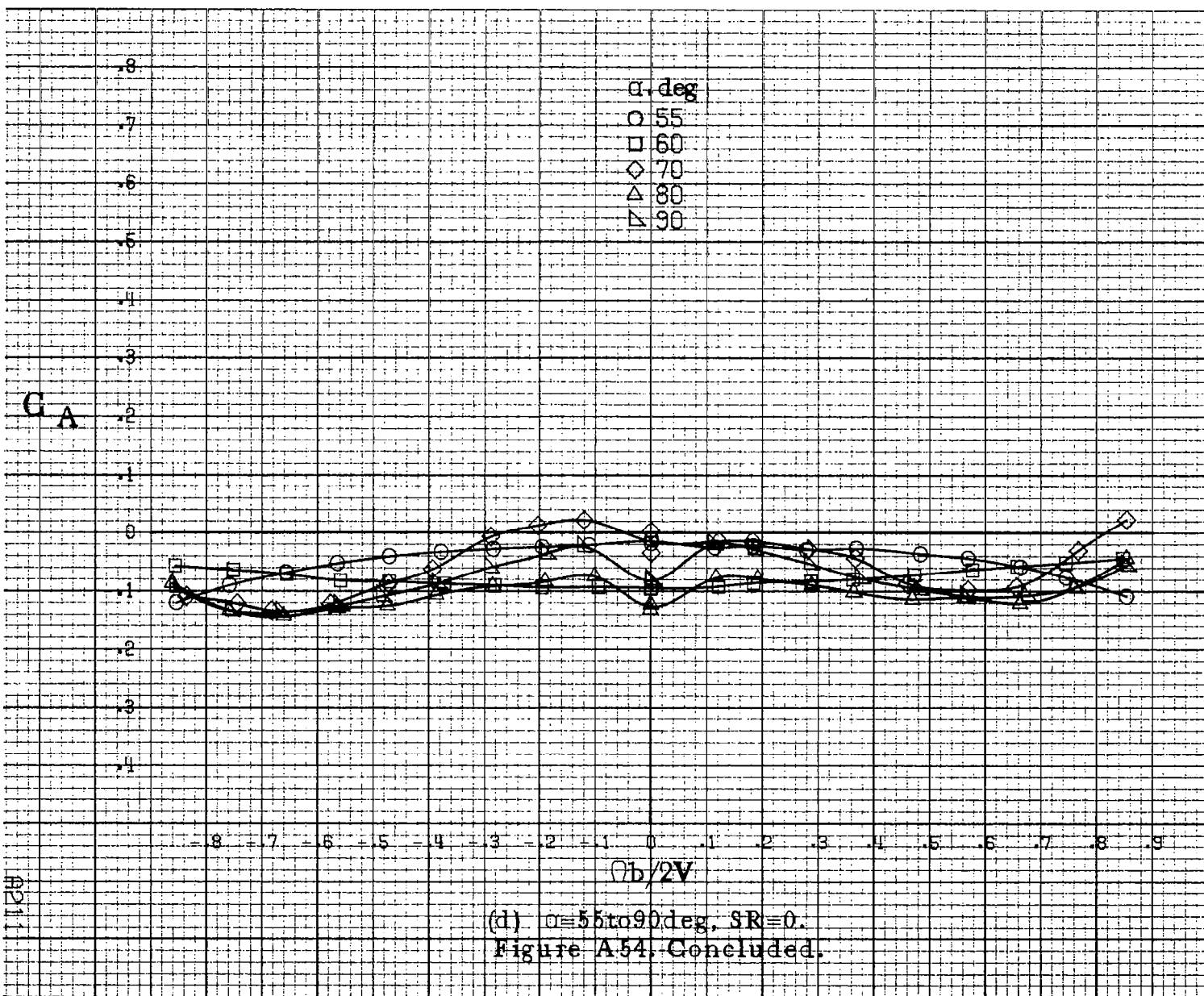
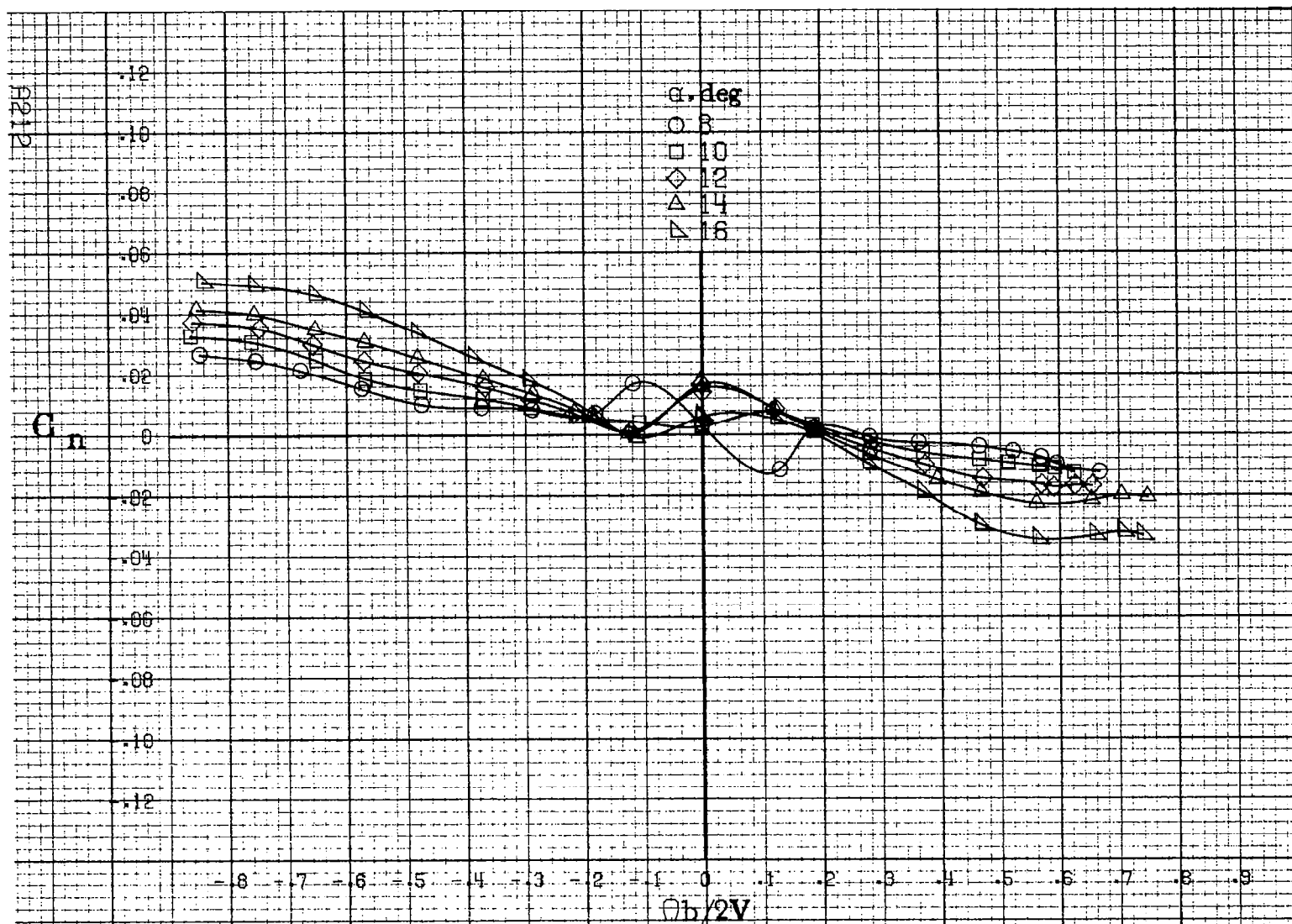


Figure A54. Effect of rotation rate and angle of attack on axial force coefficient for configuration having sharp edged fuselage bottom. $\delta_a = 0^\circ$, $\delta_c = -28^\circ$, $\beta = 0^\circ$. $\alpha = 8$ to 16 deg, $SR = 91$ cm (36 in). $\delta_a = -20^\circ$.



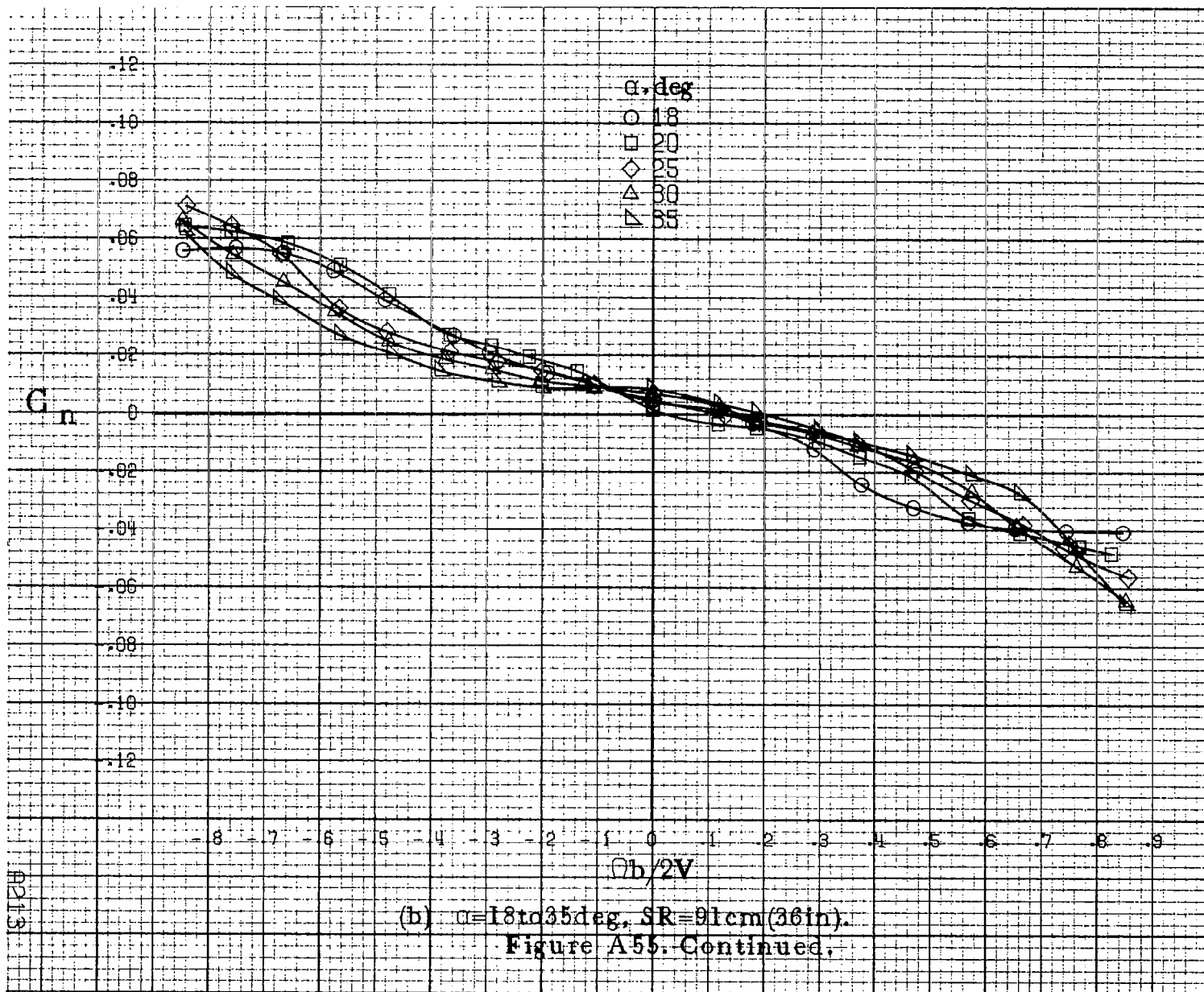


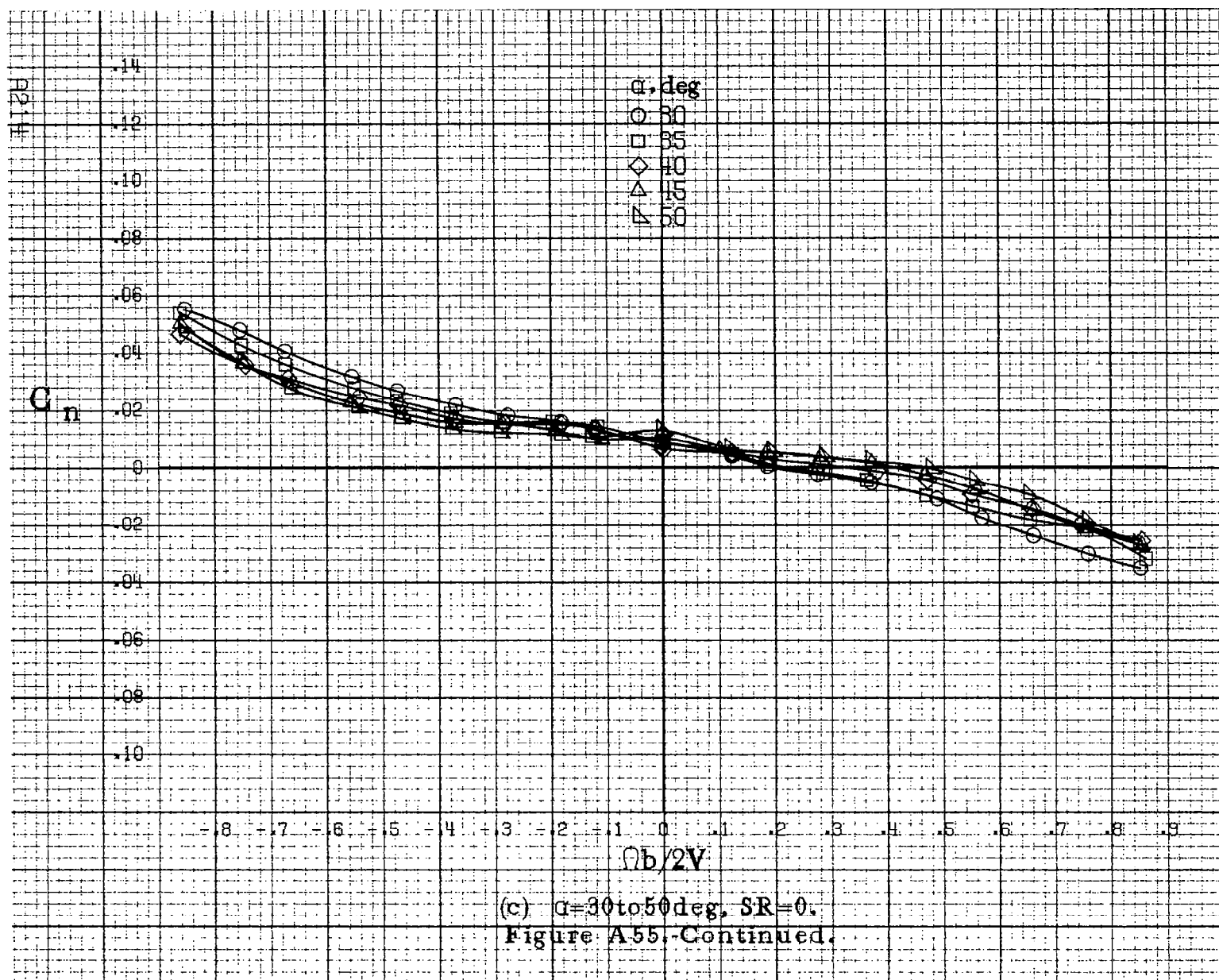


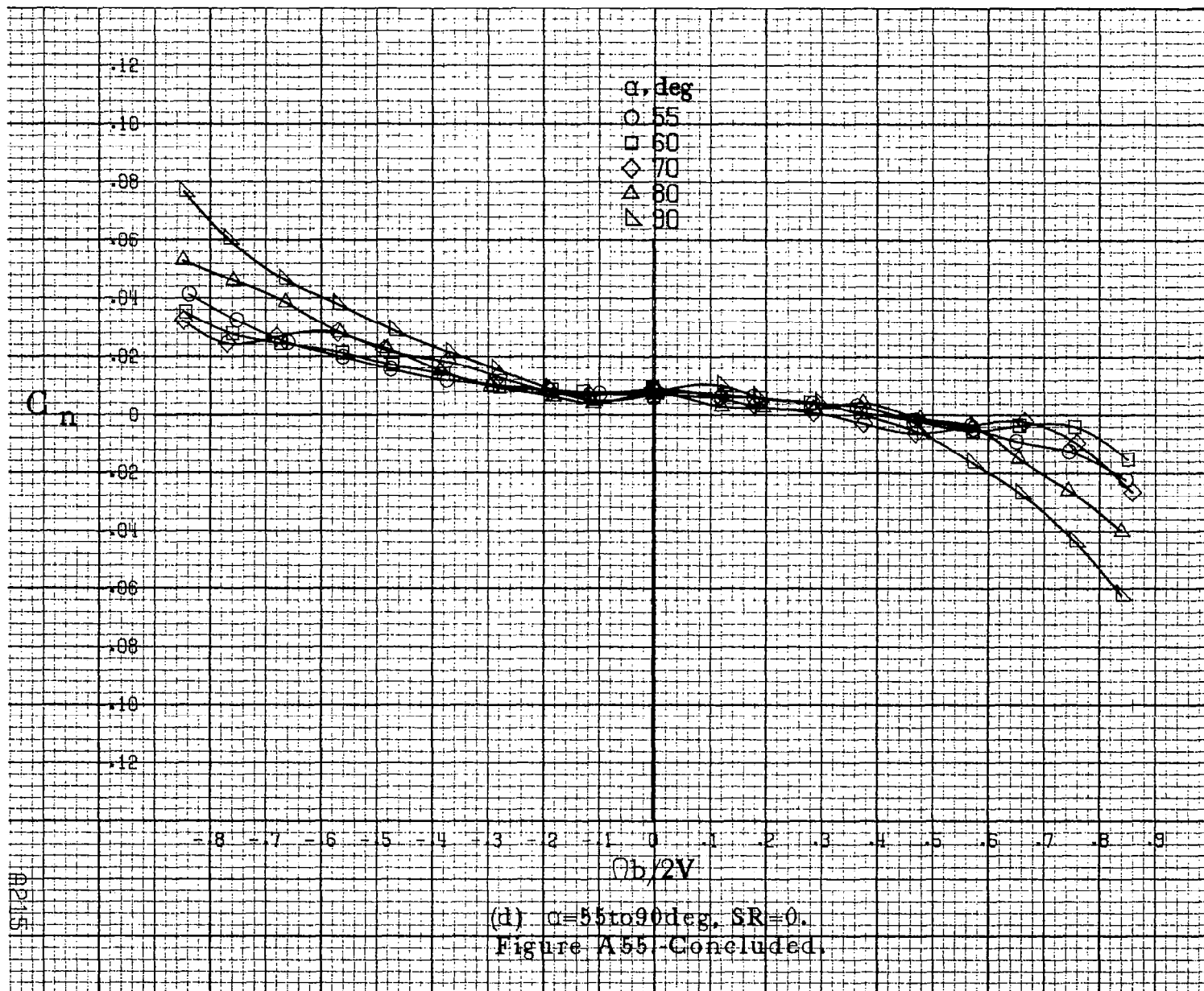


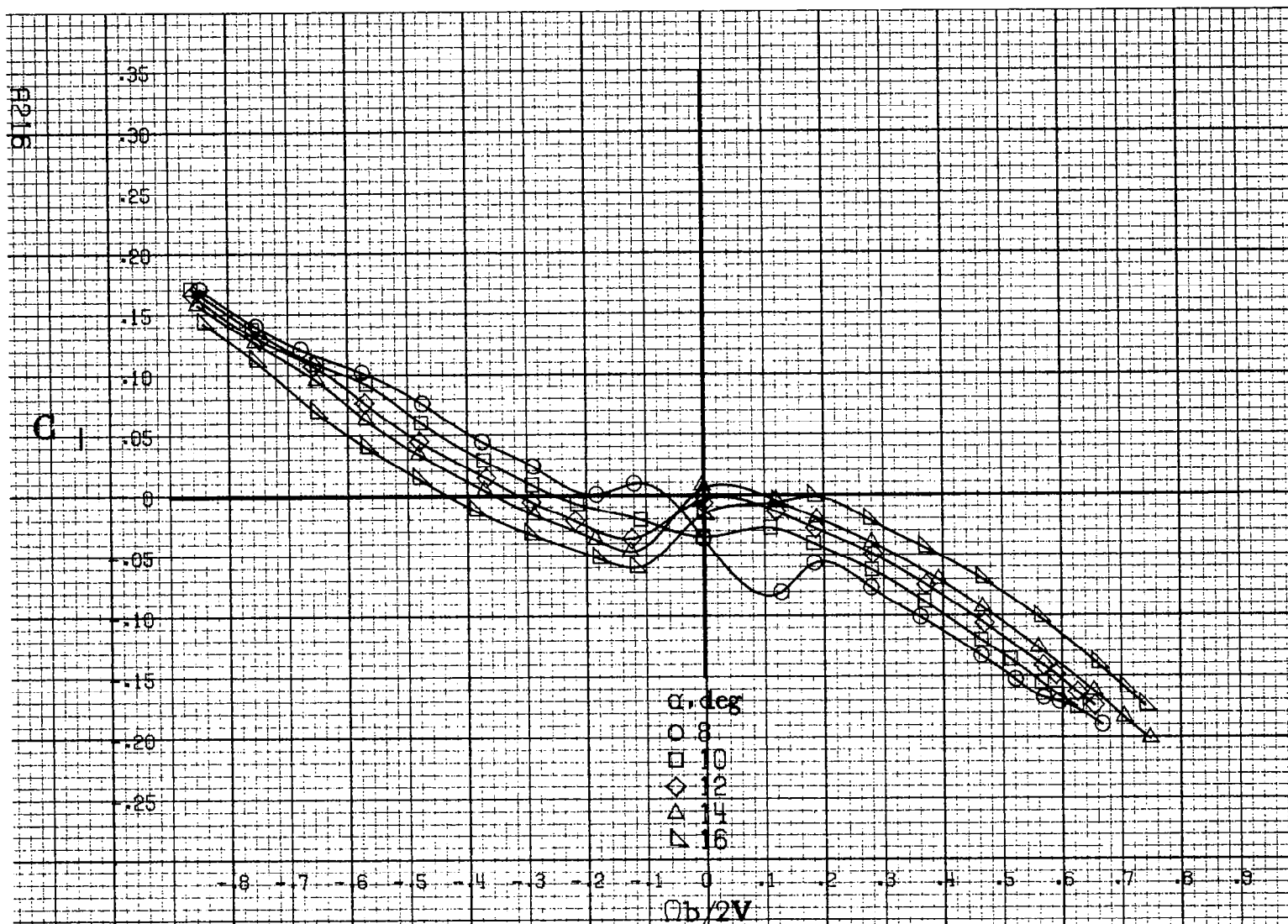
(a) $\alpha = 8$ to 16 deg, $SR = 91$ cm (36 in).

Figure A 55. Effect of rotation rate and angle of attack on yawing moment coefficient for configuration having sharp edged fuselage bottom. $\delta_a = 20^\circ$, $\delta_r = 0^\circ$, $\beta = 0^\circ$.



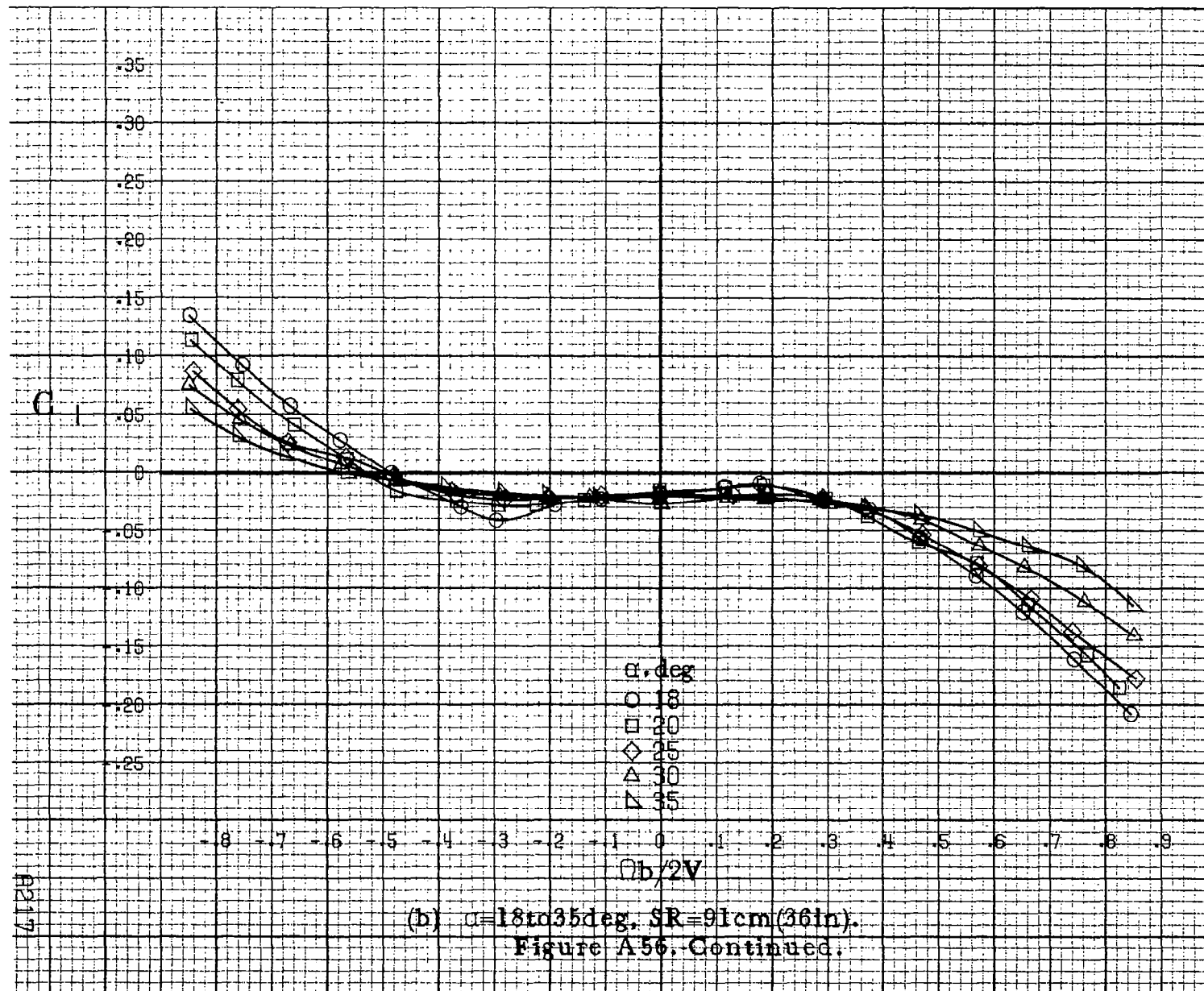


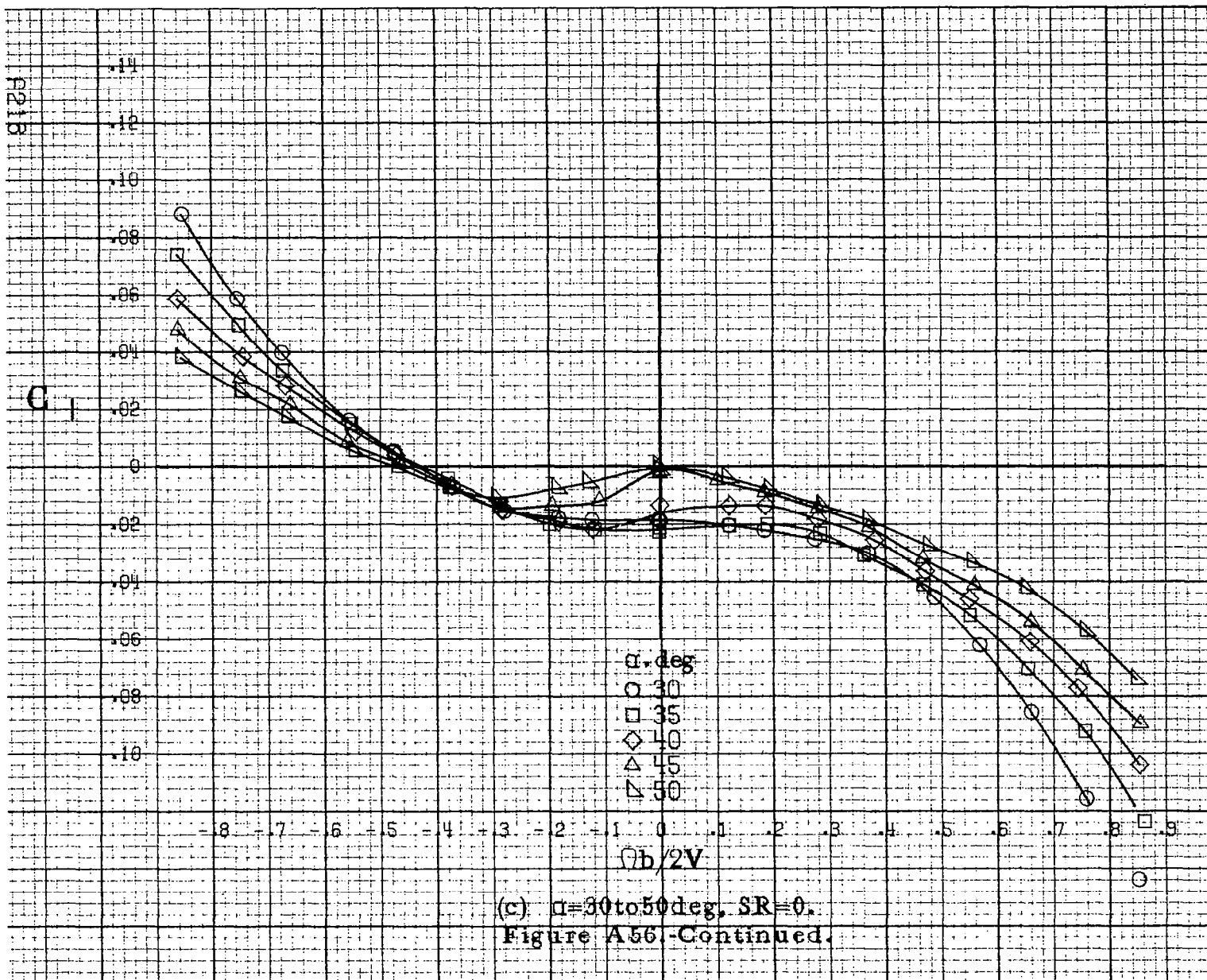


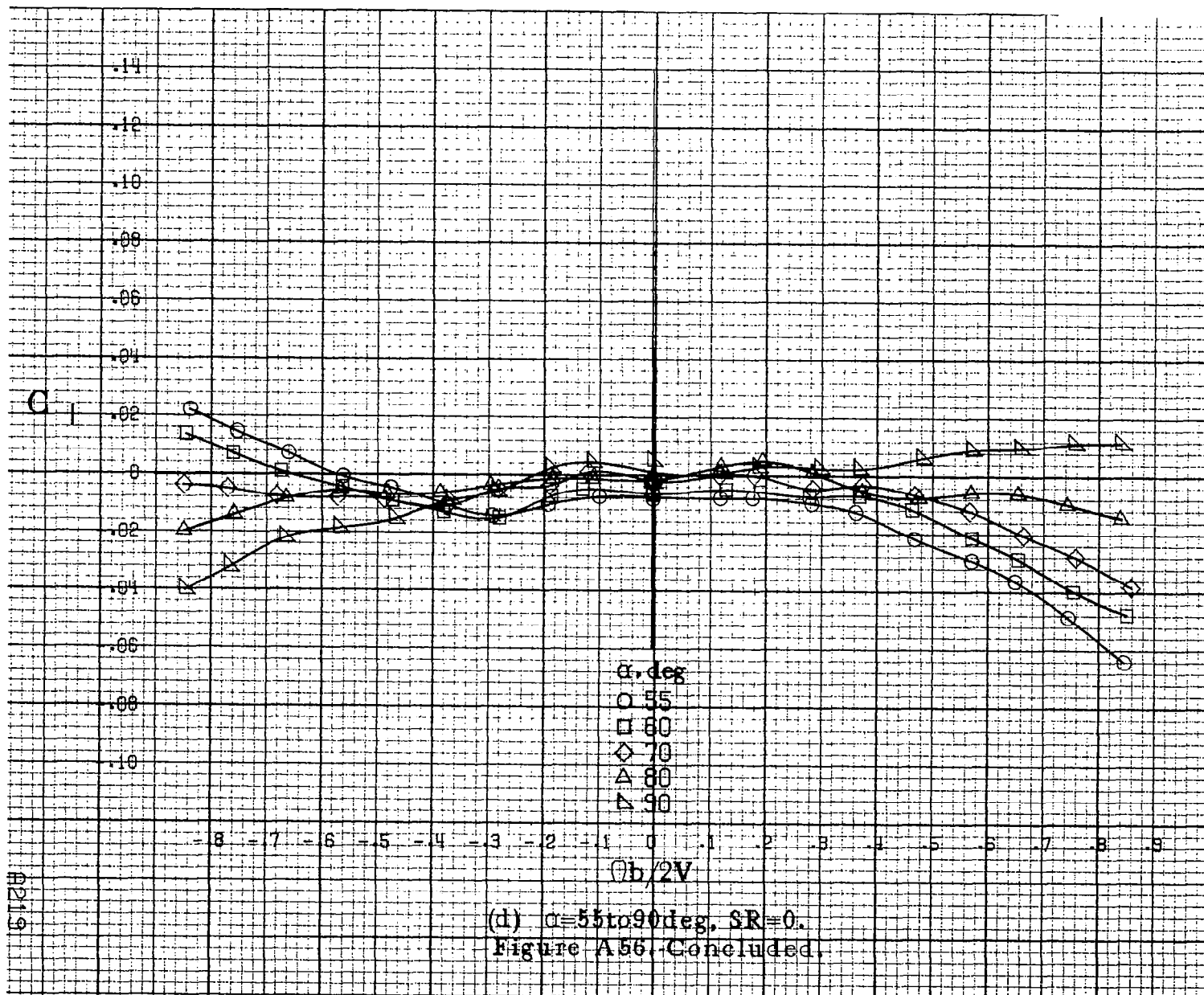


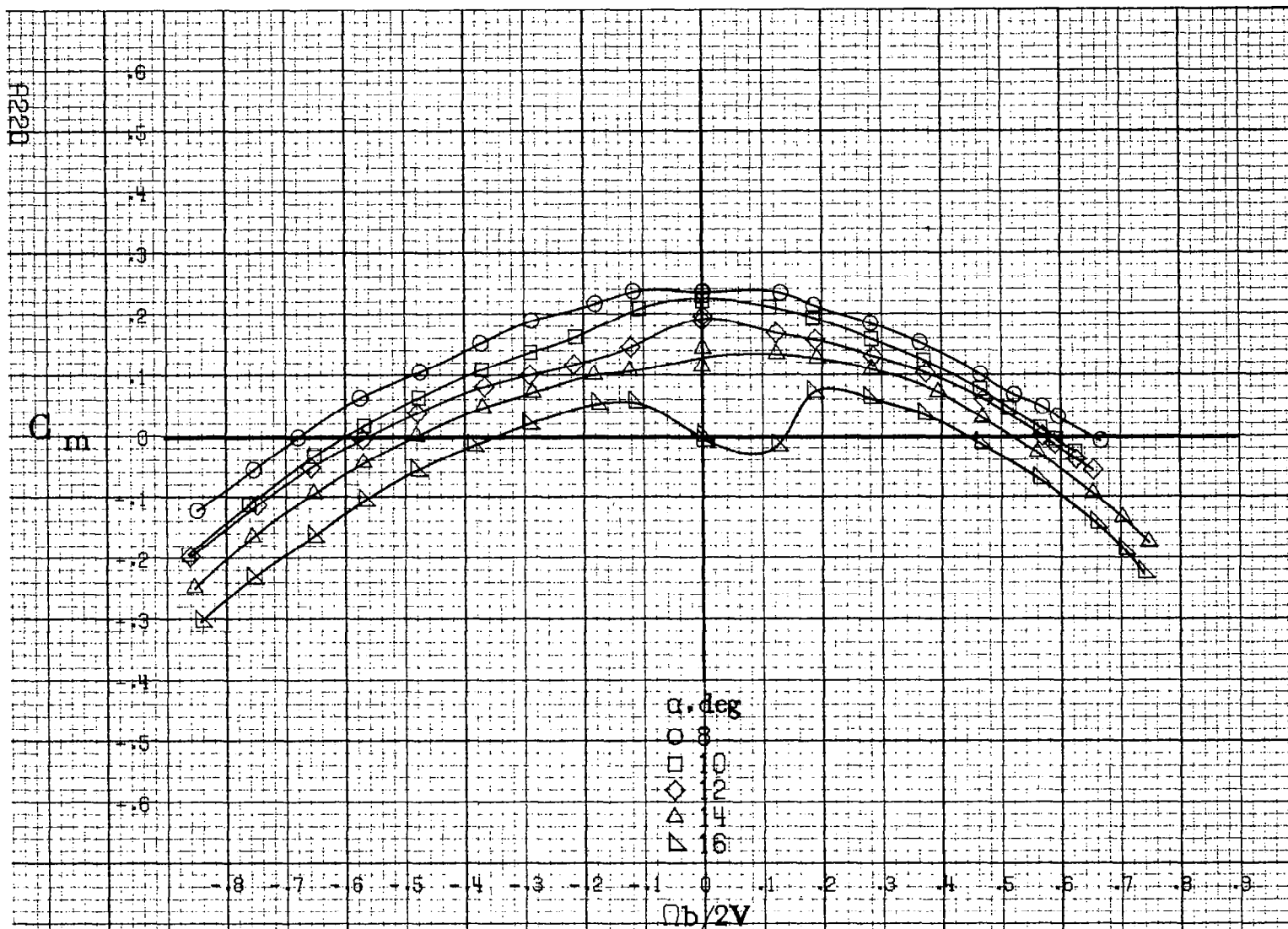
(a) $\alpha=8$ to 16 deg, SR-91cm (36in).

Figure A56. Effect of rotation rate and angle of attack on rolling-moment coefficient for configuration having sharp-edged fuselage bottom. $\delta_e = -20^\circ$, $\delta_a = 20^\circ$, $\delta_r = 0^\circ$, $\beta = 0^\circ$.



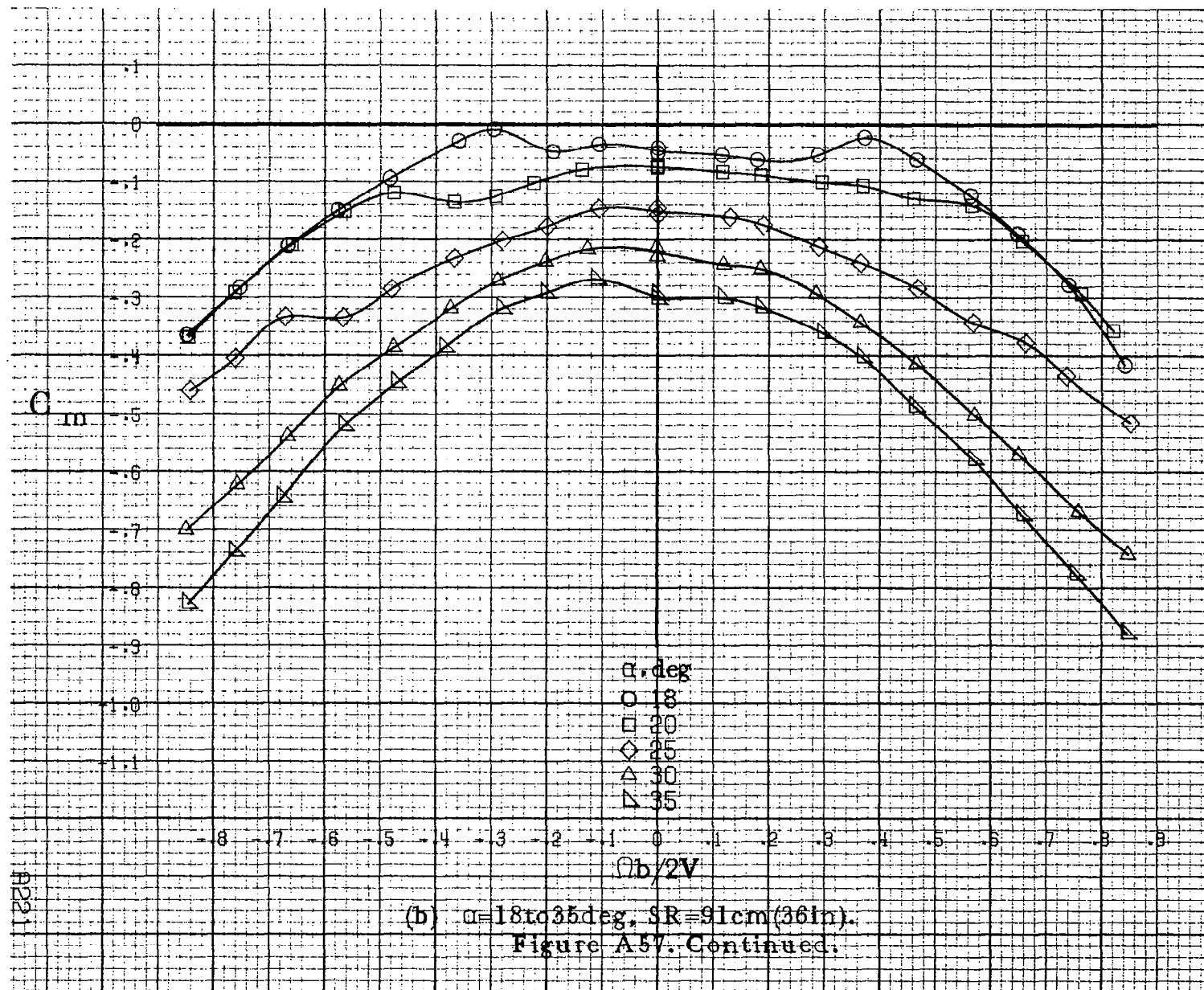




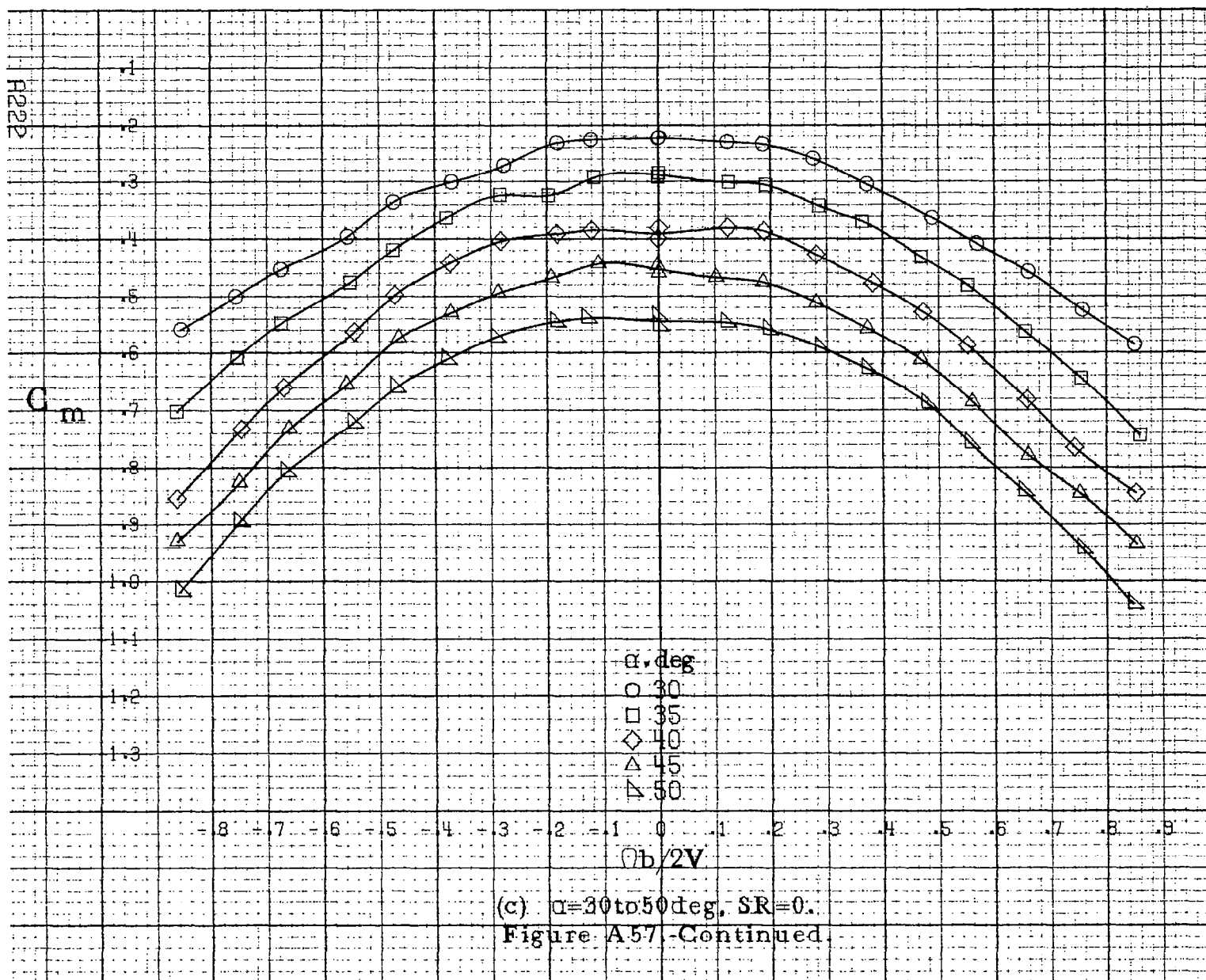


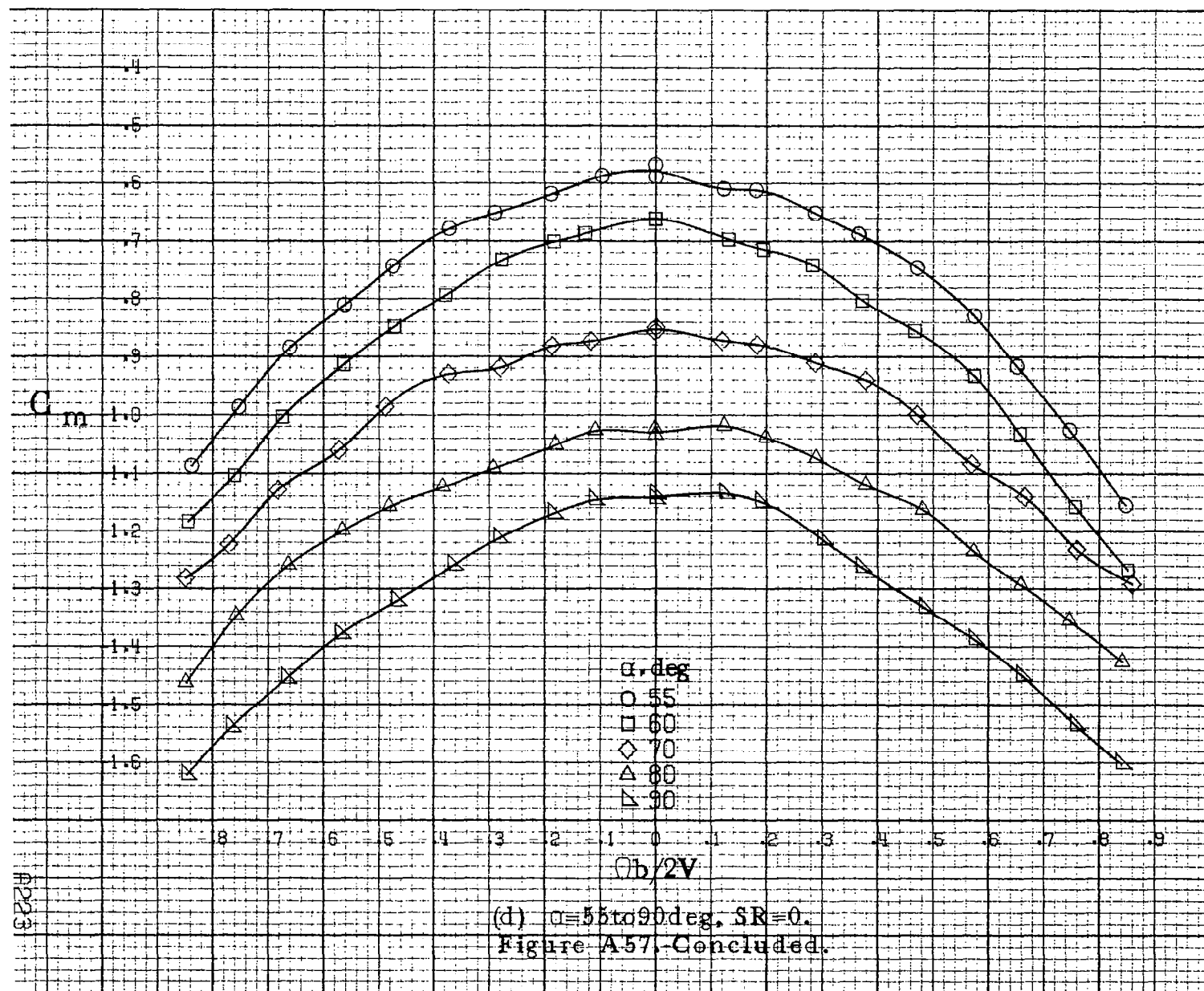
(a) $\alpha = 8 \text{ to } 16 \text{ deg}$, $SR = 91 \text{ cm (36 in.)}$.

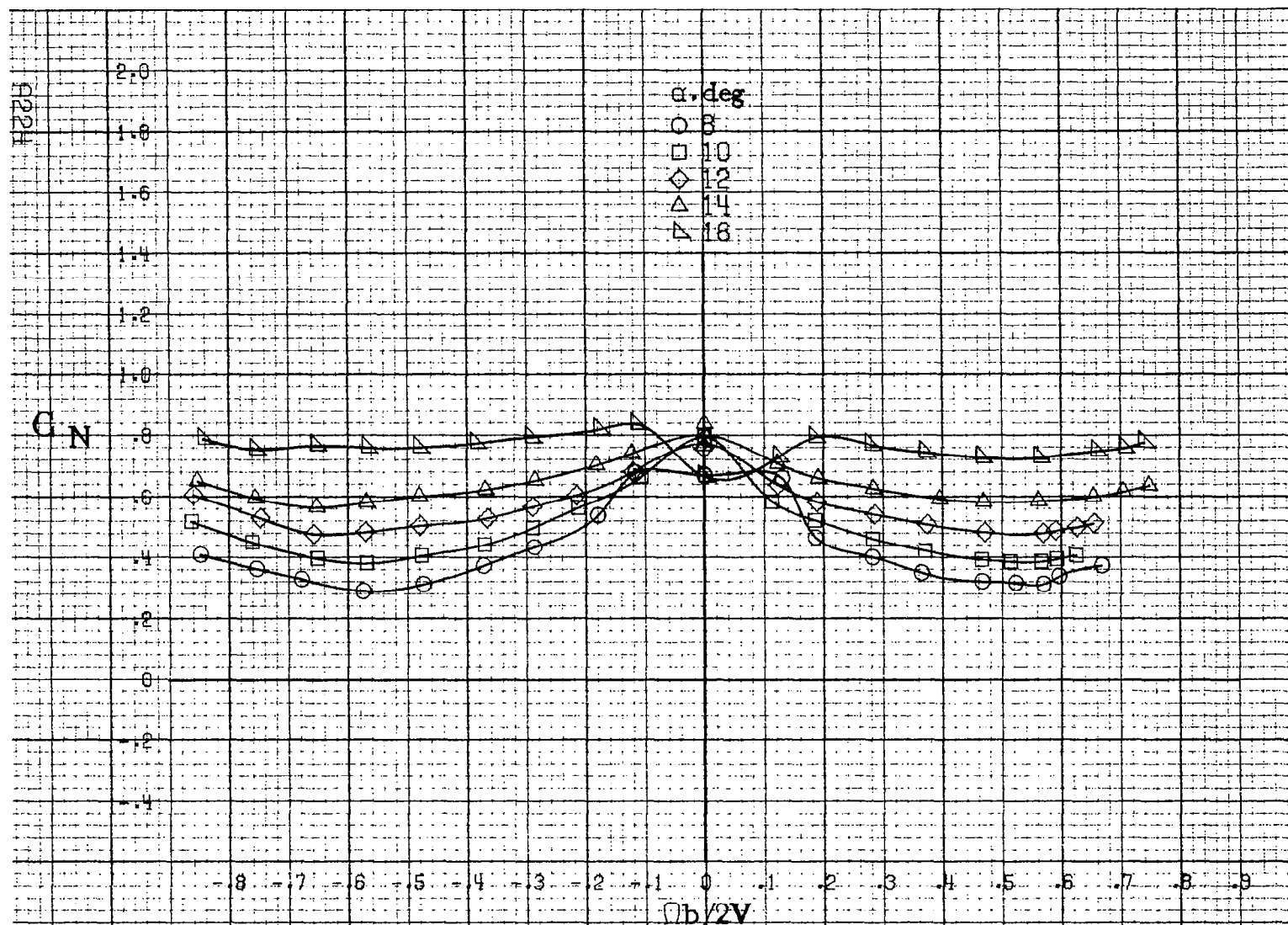
Figure A57. Effect of rotation rate and angle of attack on pitching-moment coefficient for configuration having sharp-edged fuselage bottom. $\delta_a = -20^\circ$, $\delta_s = 0^\circ$, $\beta = 0^\circ$.



H222

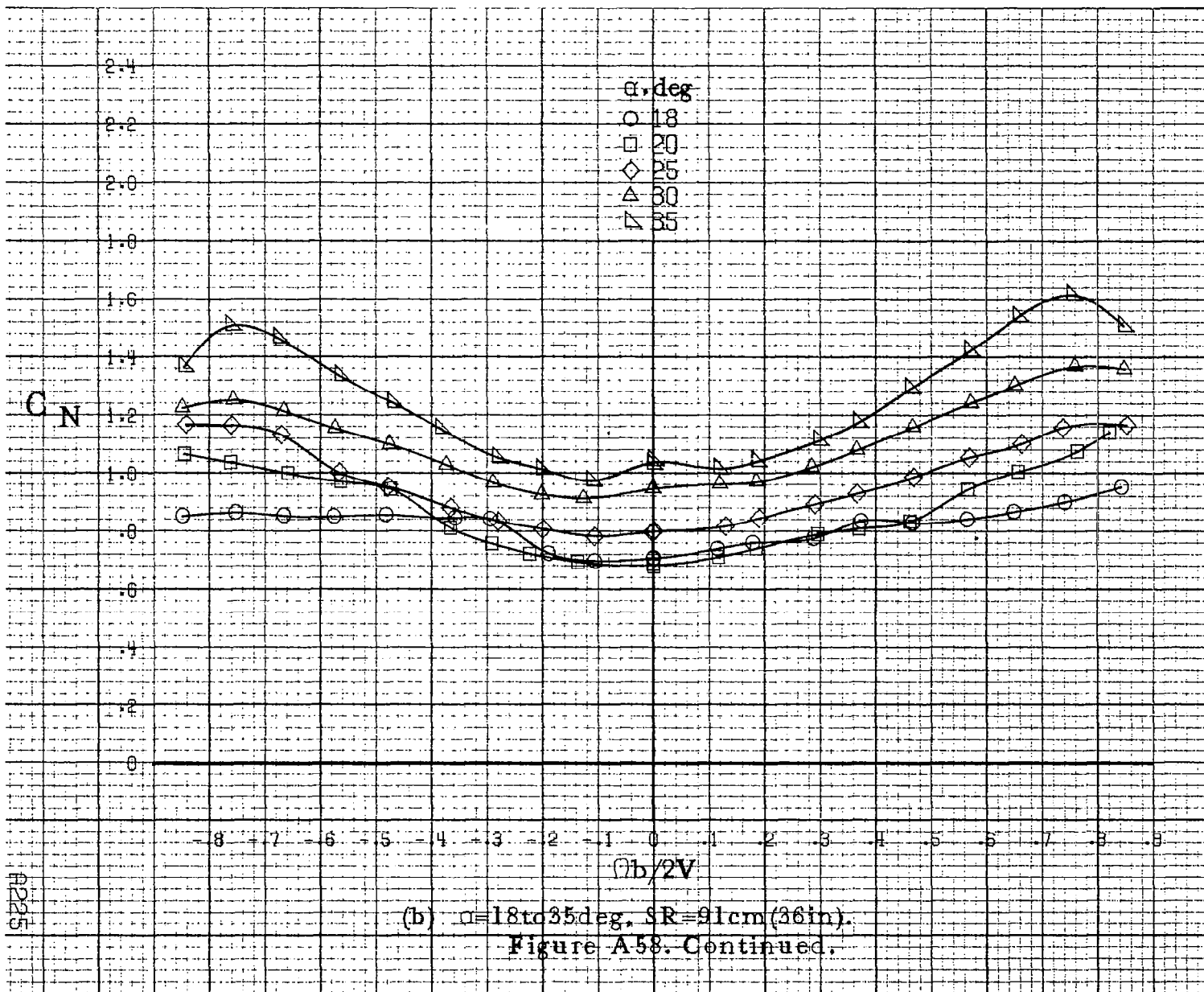


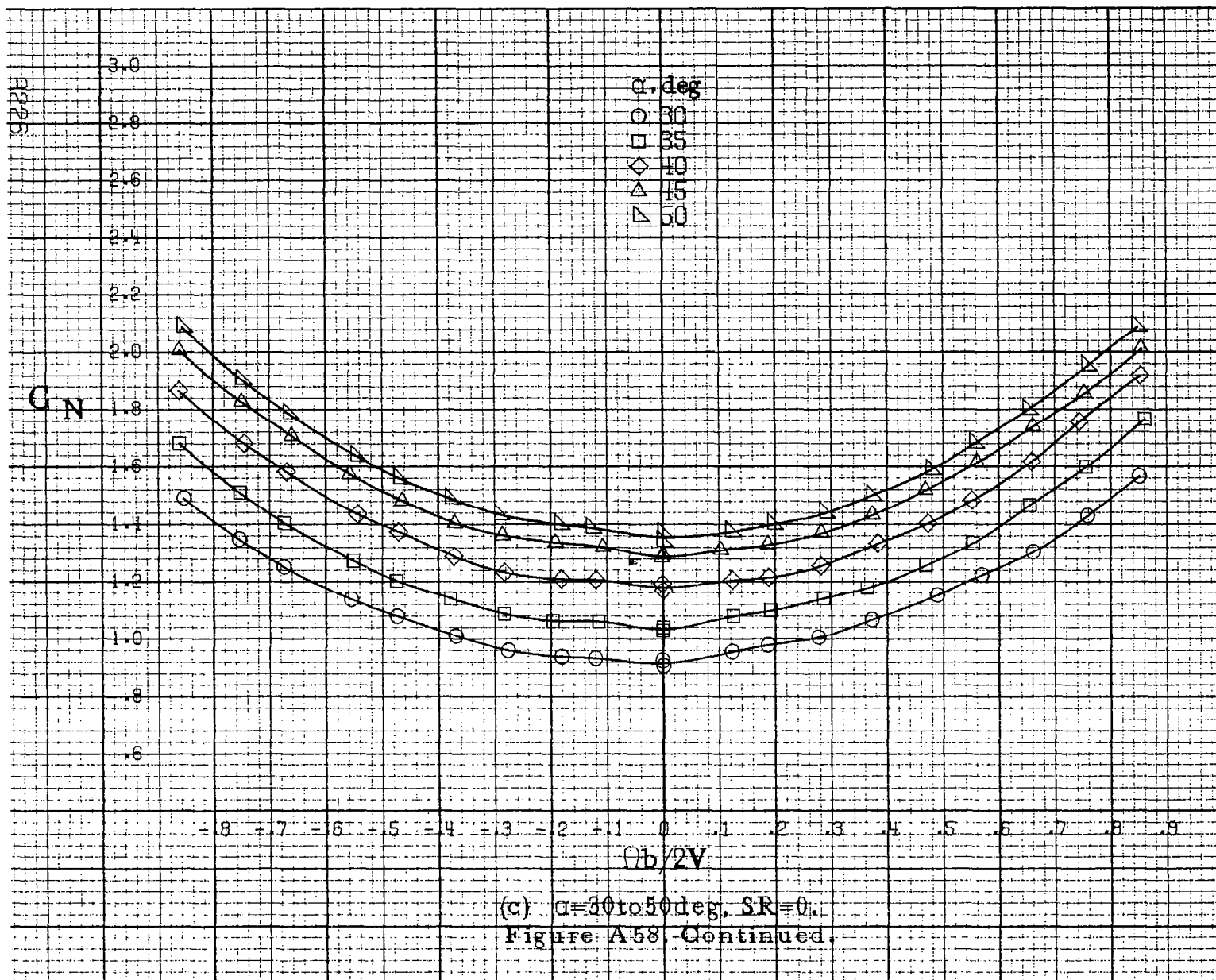


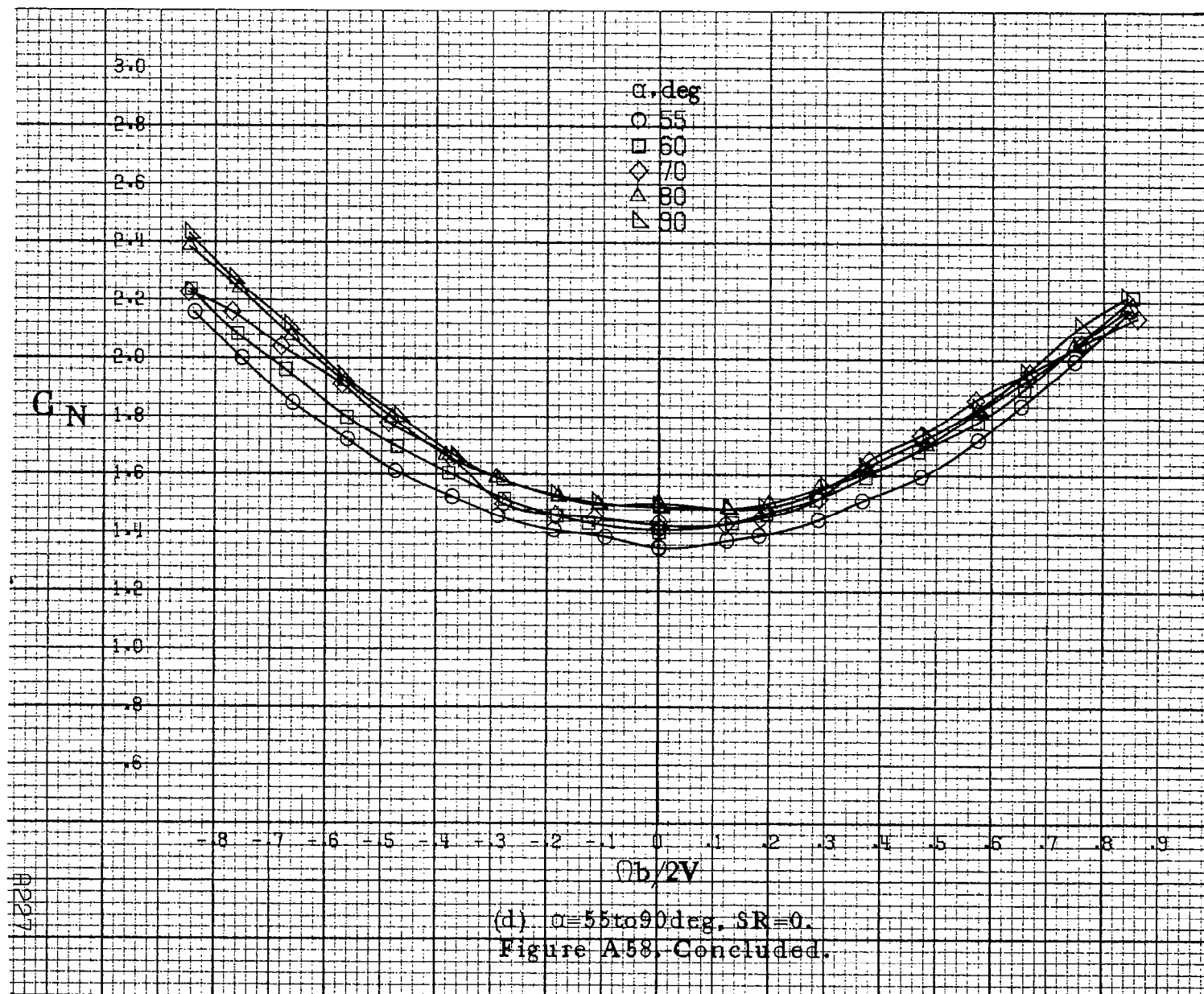


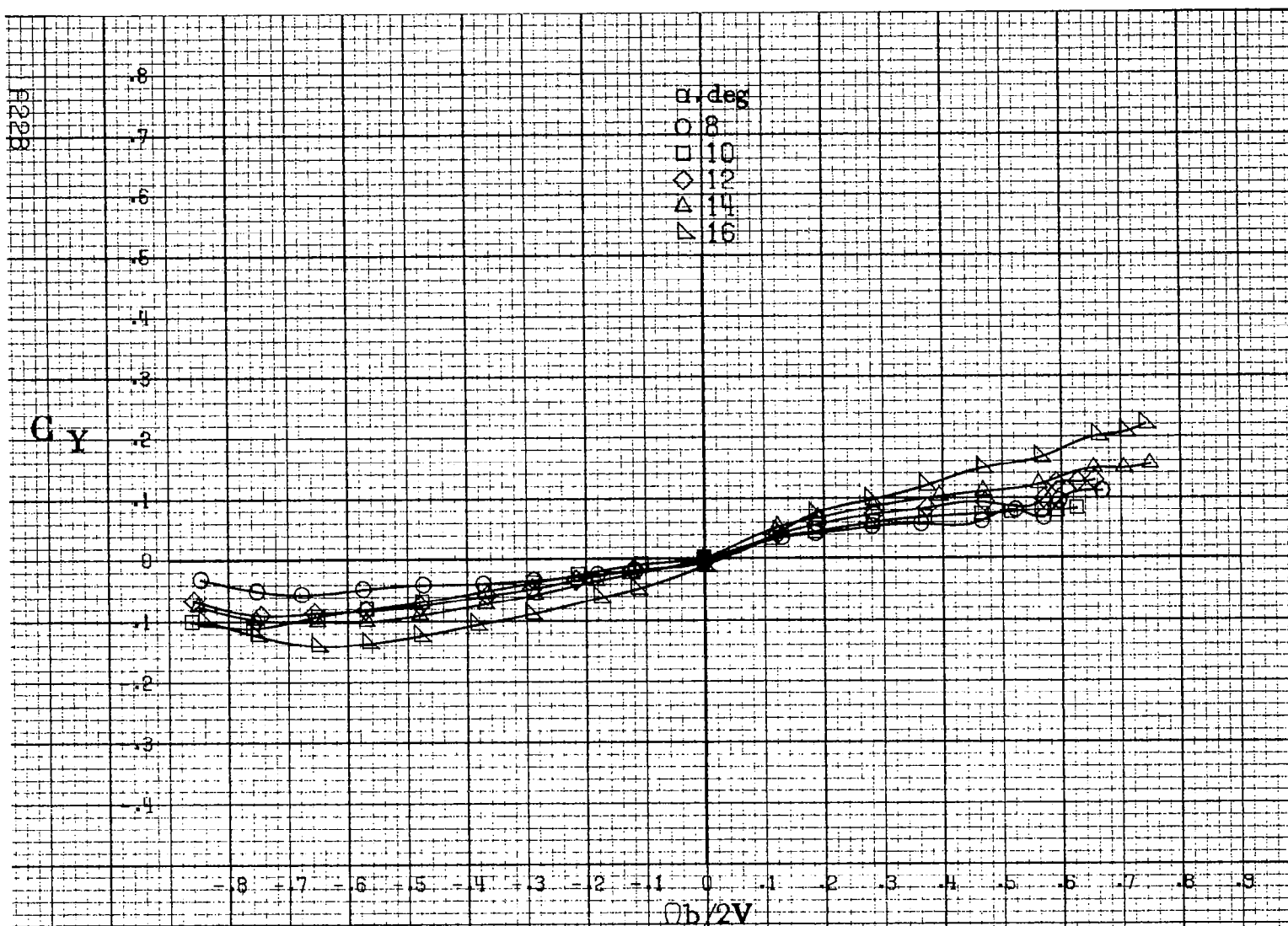
(a) $\alpha=8$ to 16 deg, $SR=91\text{cm}(36\text{in})$.

Figure A58. Effect of rotation rate and angle of attack on normal-force coefficient for configuration having sharp-edged fuselage bottom. $\delta_a = -20^\circ$, $\delta_r = 0^\circ$, $\delta_b = 0^\circ$.



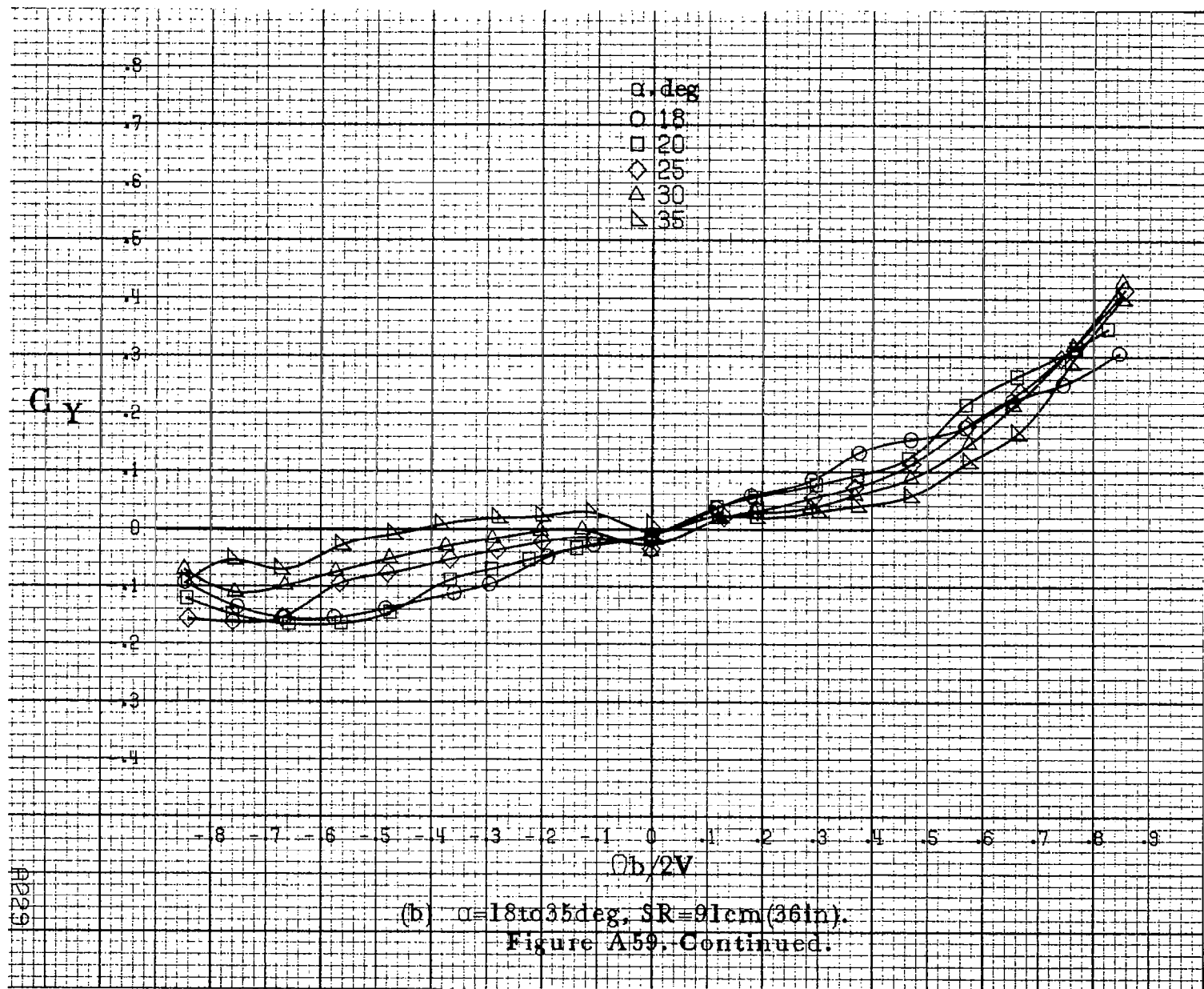


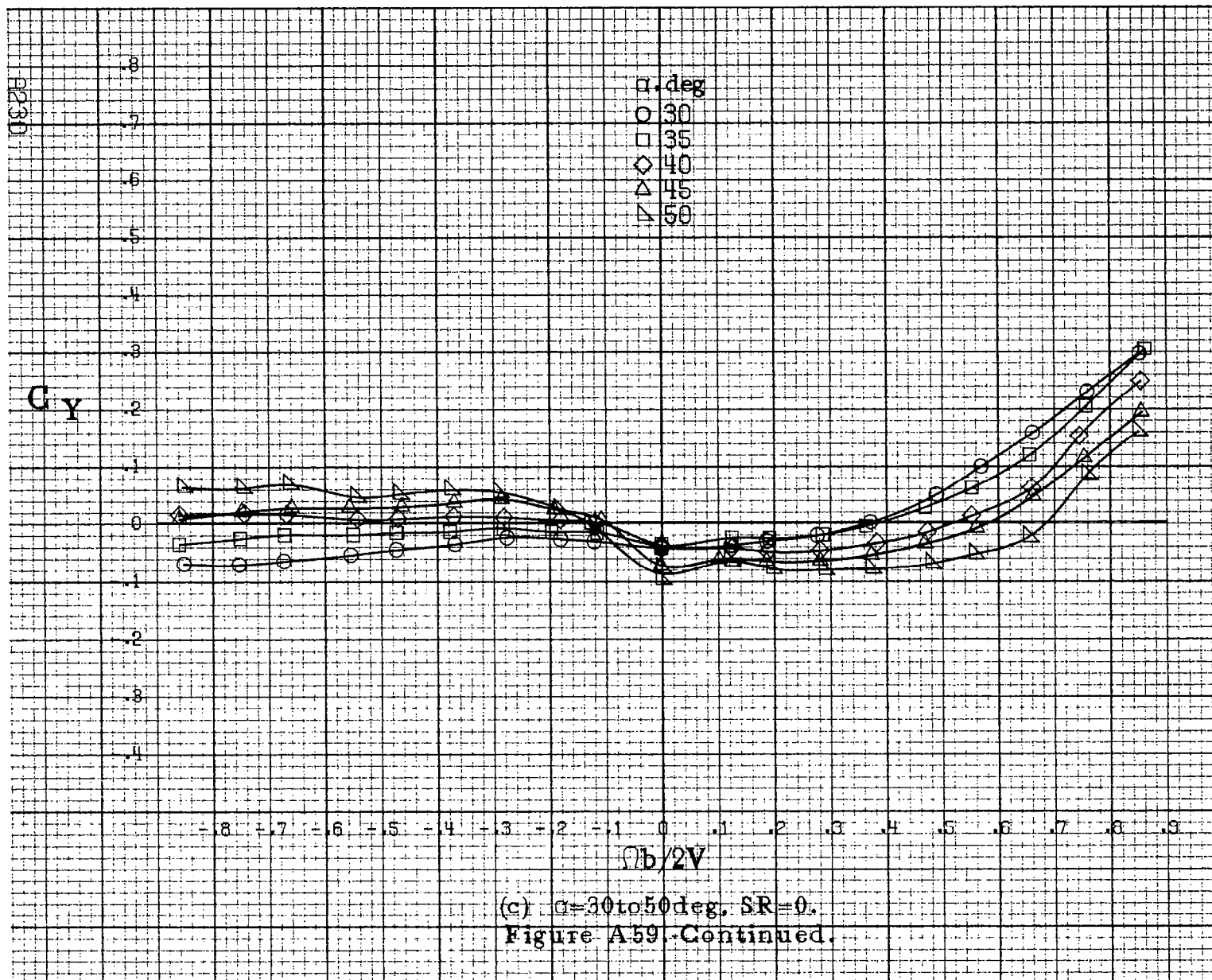


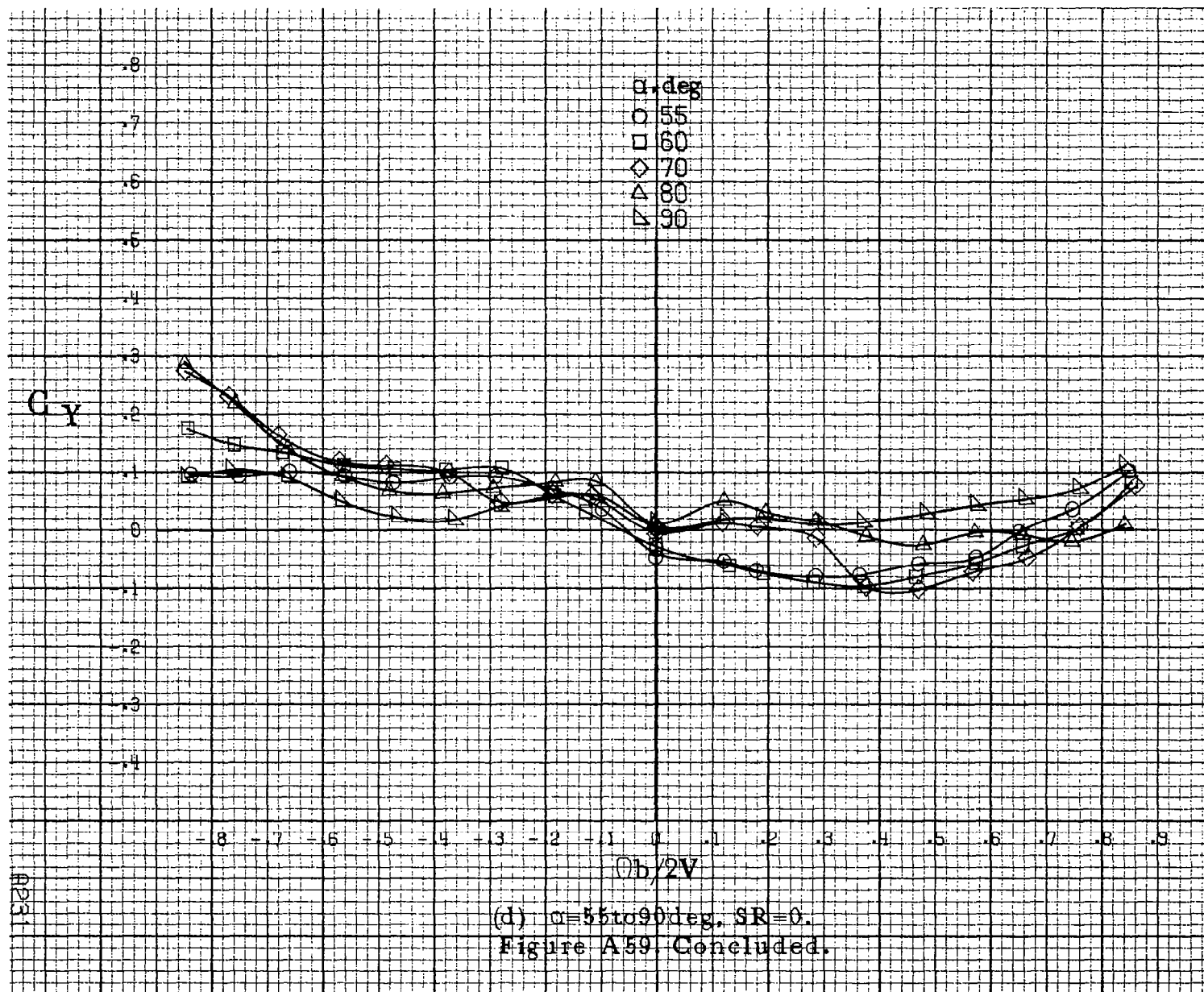


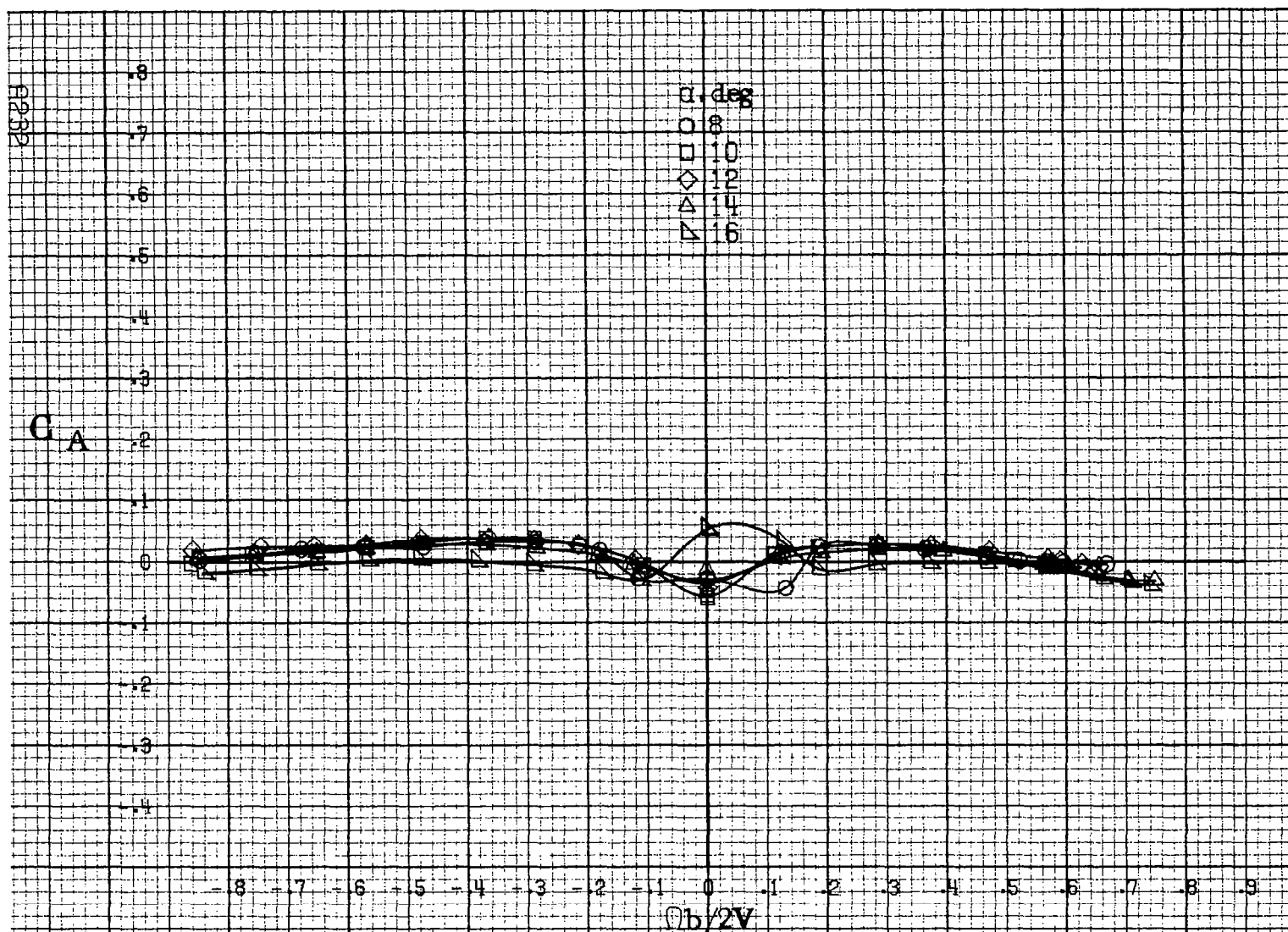
(a) $\alpha = 8$ to 16° , $SR = 91\text{cm (36in)}$.

Figure A59. Effect of rotation rate and angle of attack on side-force coefficient for configuration having sharp-edged fuselage bottom. $\delta_a = -20^\circ$, $\delta_r = 0^\circ$, $\delta = 0^\circ$.



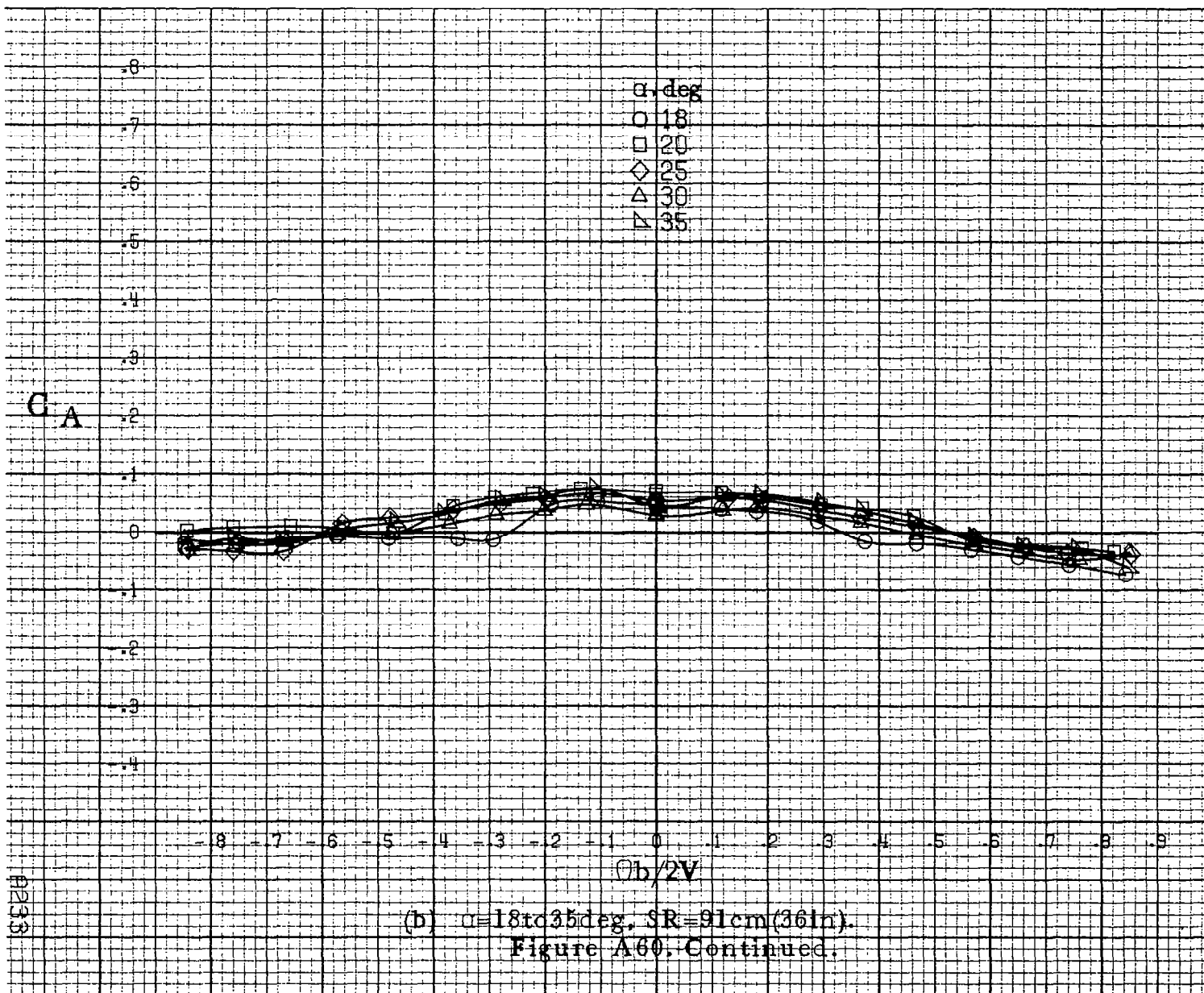


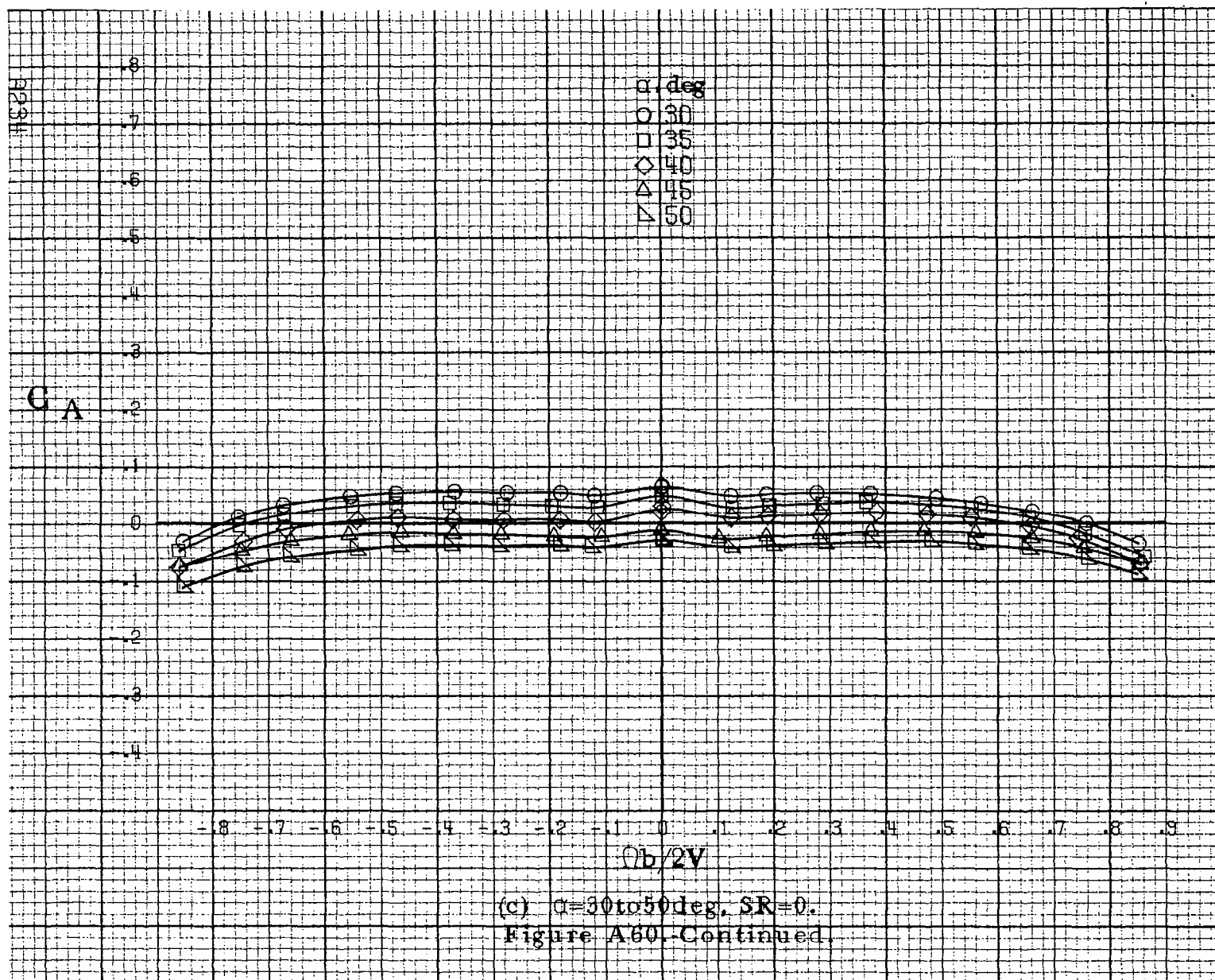


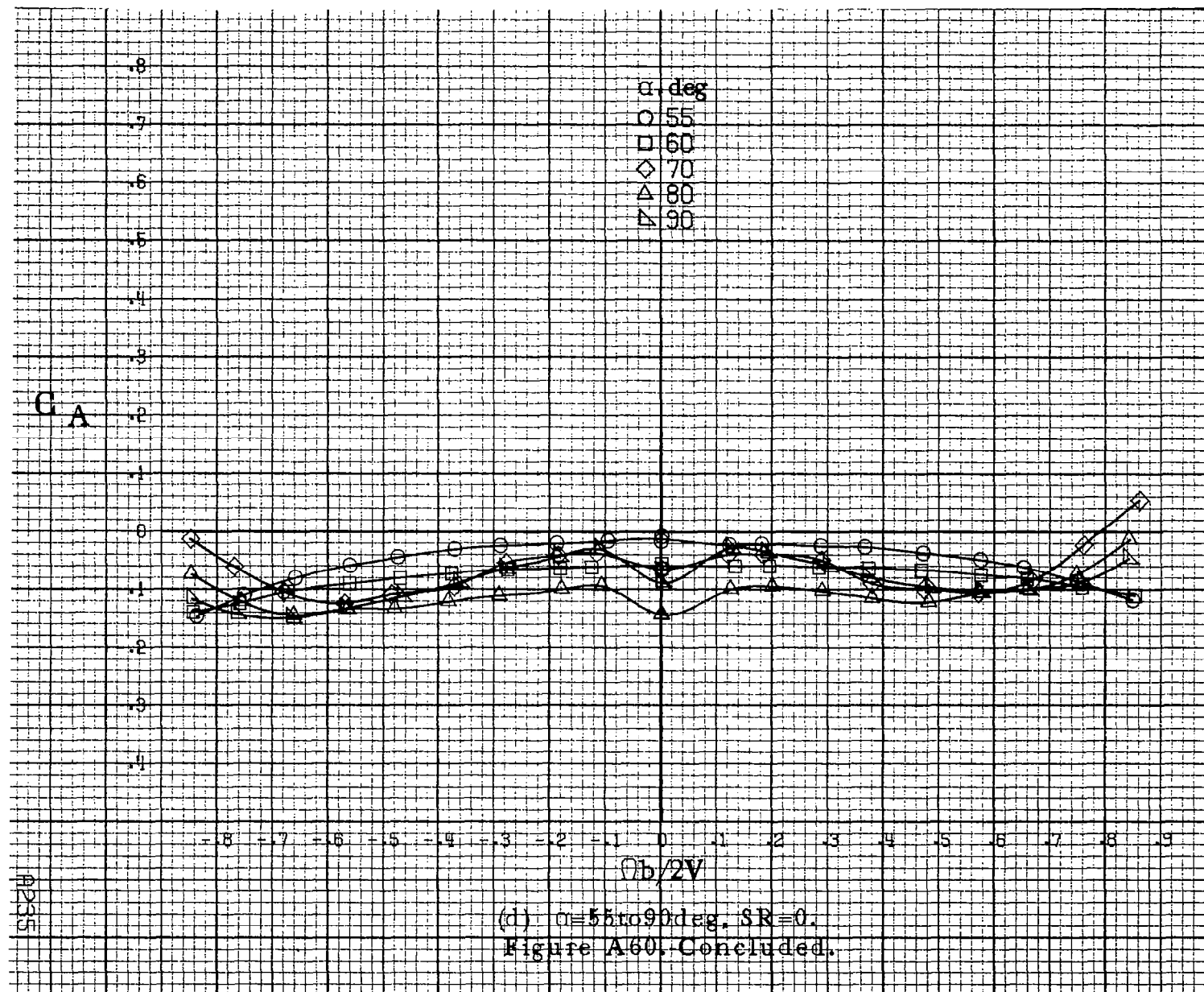


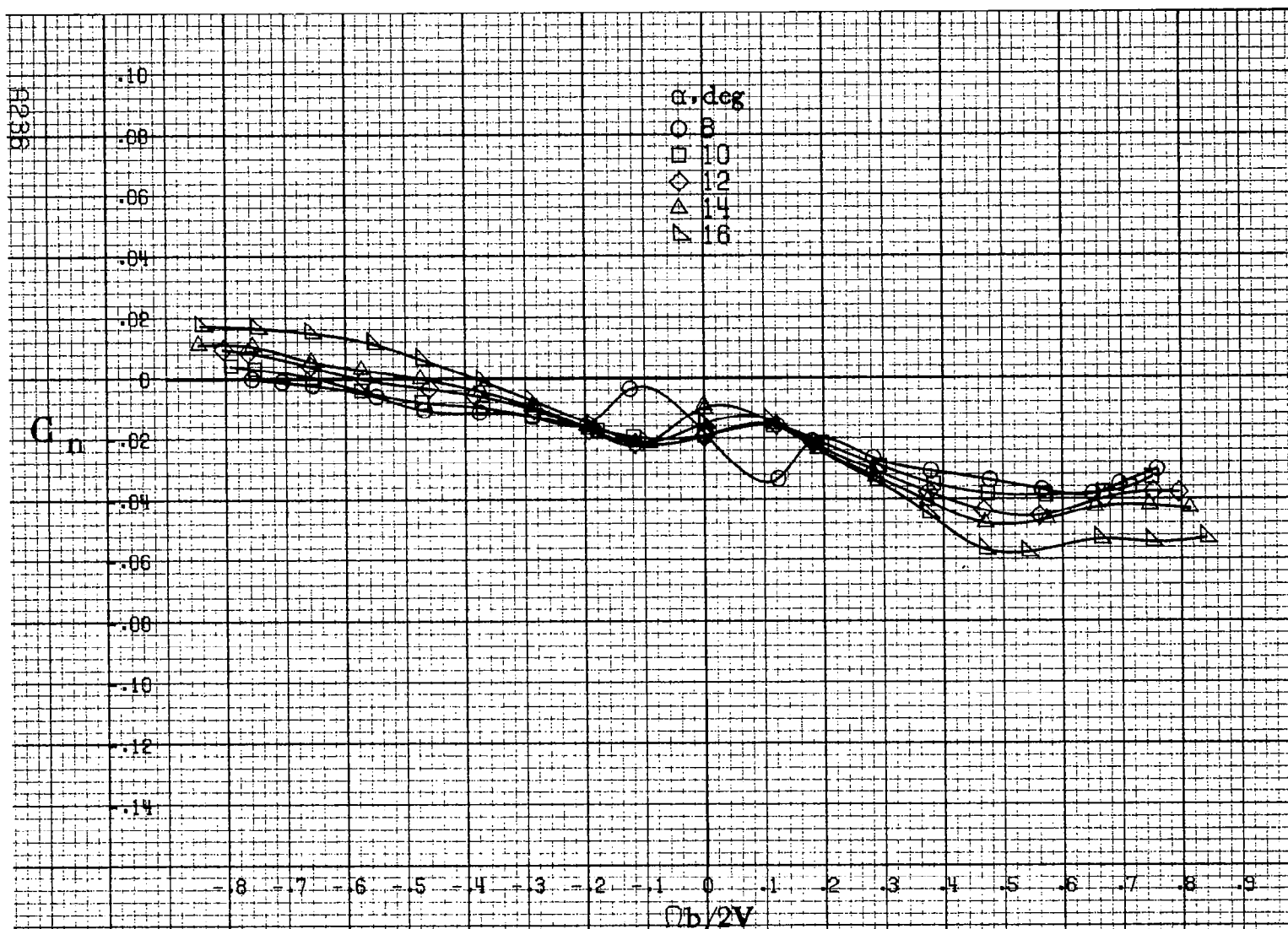
(a) $\alpha=8$ to 16 deg, $R=91$ cm (36 in).

Figure A60. Effect of rotation rate and angle of attack on axial force coefficient for configuration having sharp-edged fuselage bottom. $\delta_a = -20^\circ$, $\delta_s = -20^\circ$, $\delta_r = 0^\circ$, $\beta = 0^\circ$.



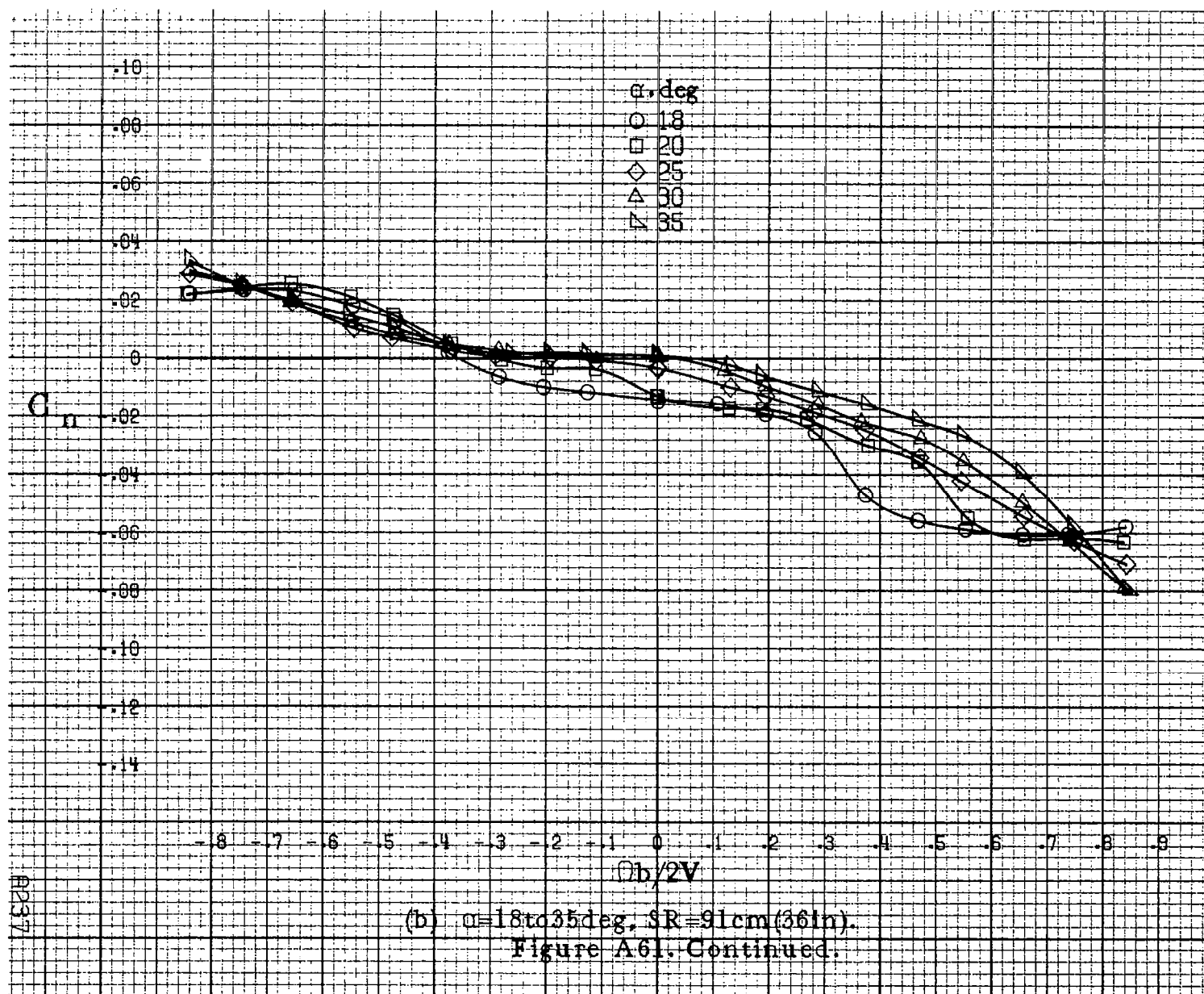


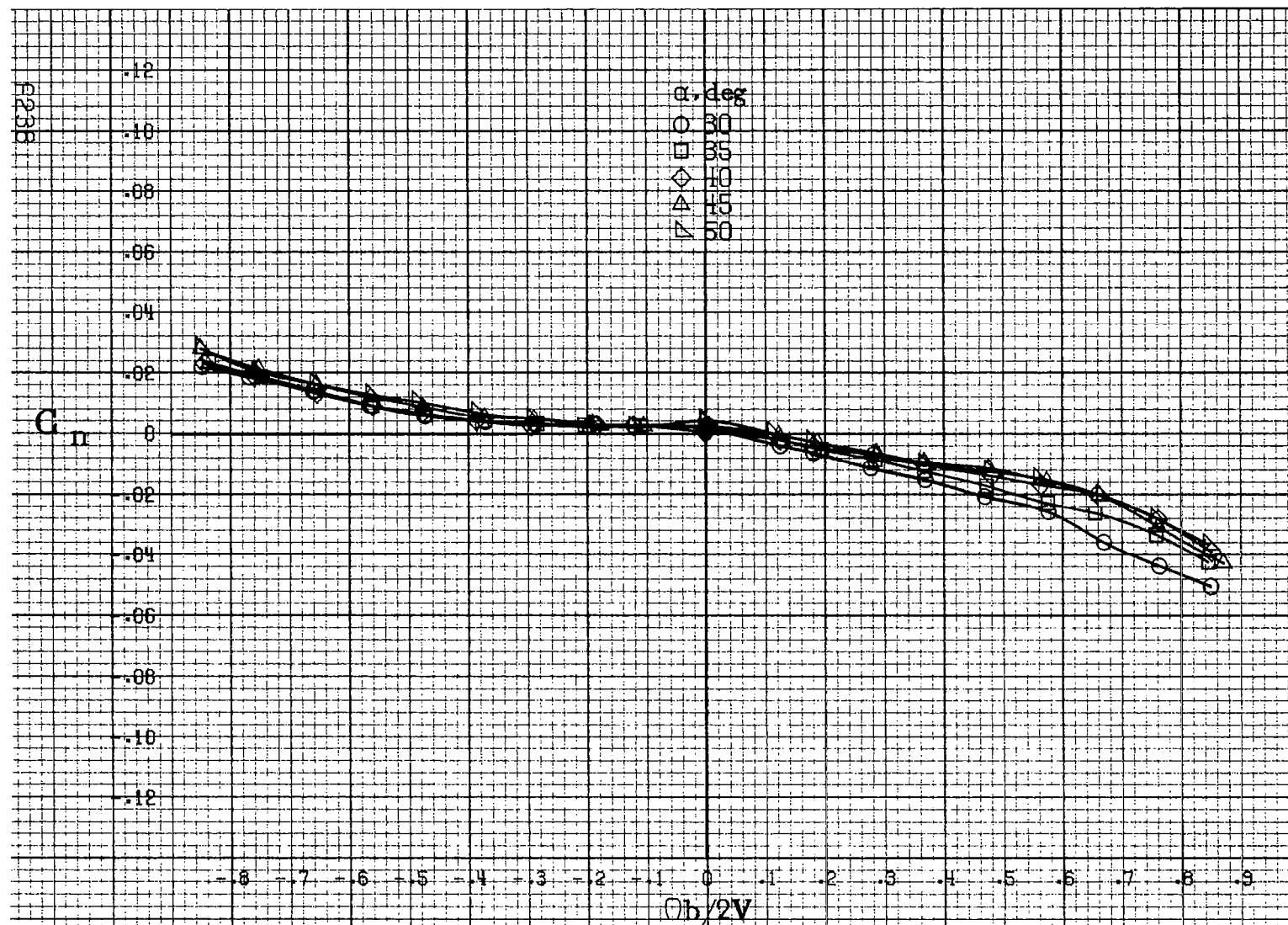




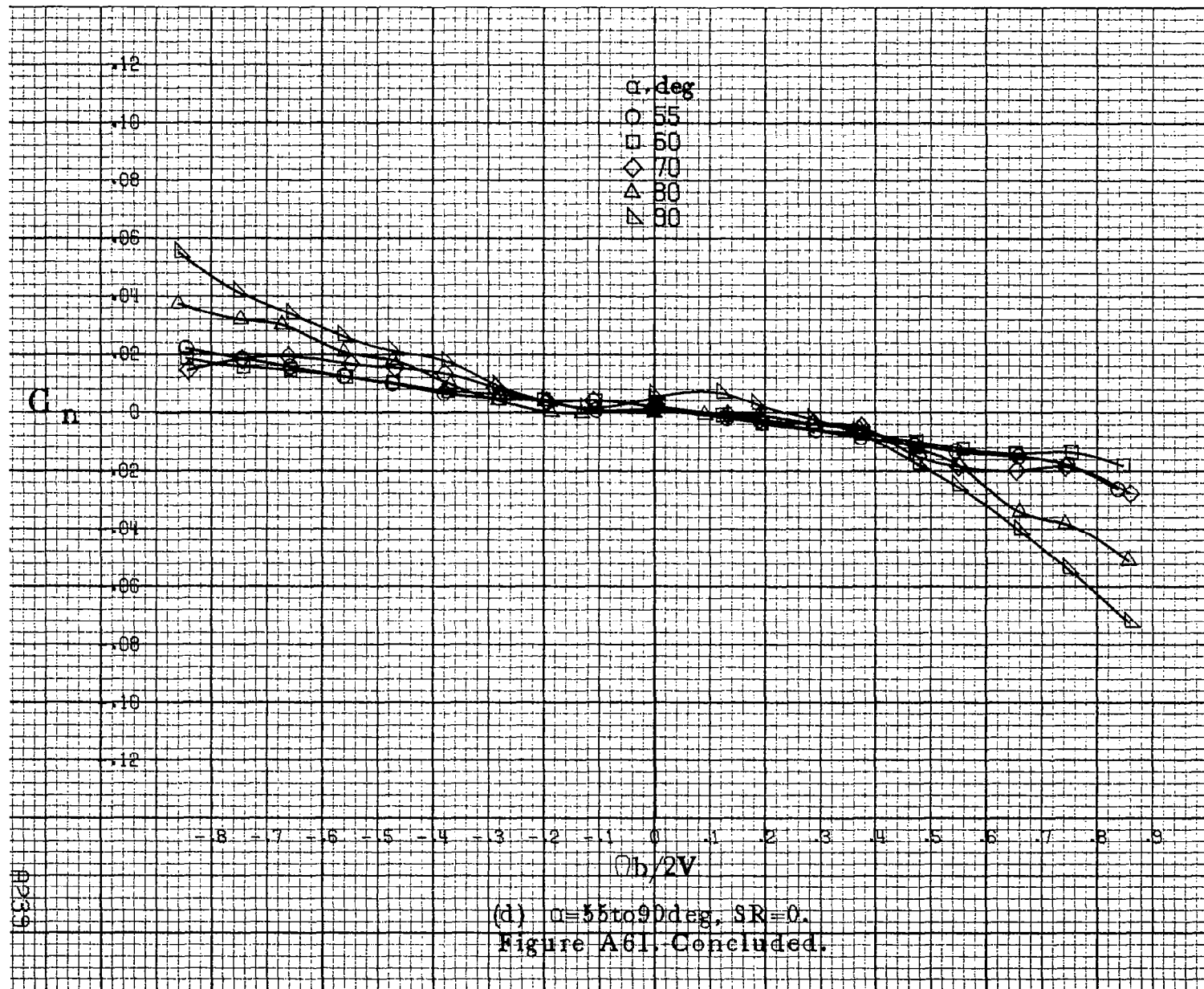
(a) $\alpha=8$ to 16 deg, $SR=91$ cm (36 in).

Figure A61. Effect of rotation rate and angle of attack on yawing-moment coefficient for configuration having sharp-edged fuselage bottom. $\delta_a=15^\circ$, $\delta_r=0^\circ$, $\delta_n=28^\circ$, $\beta=0^\circ$.



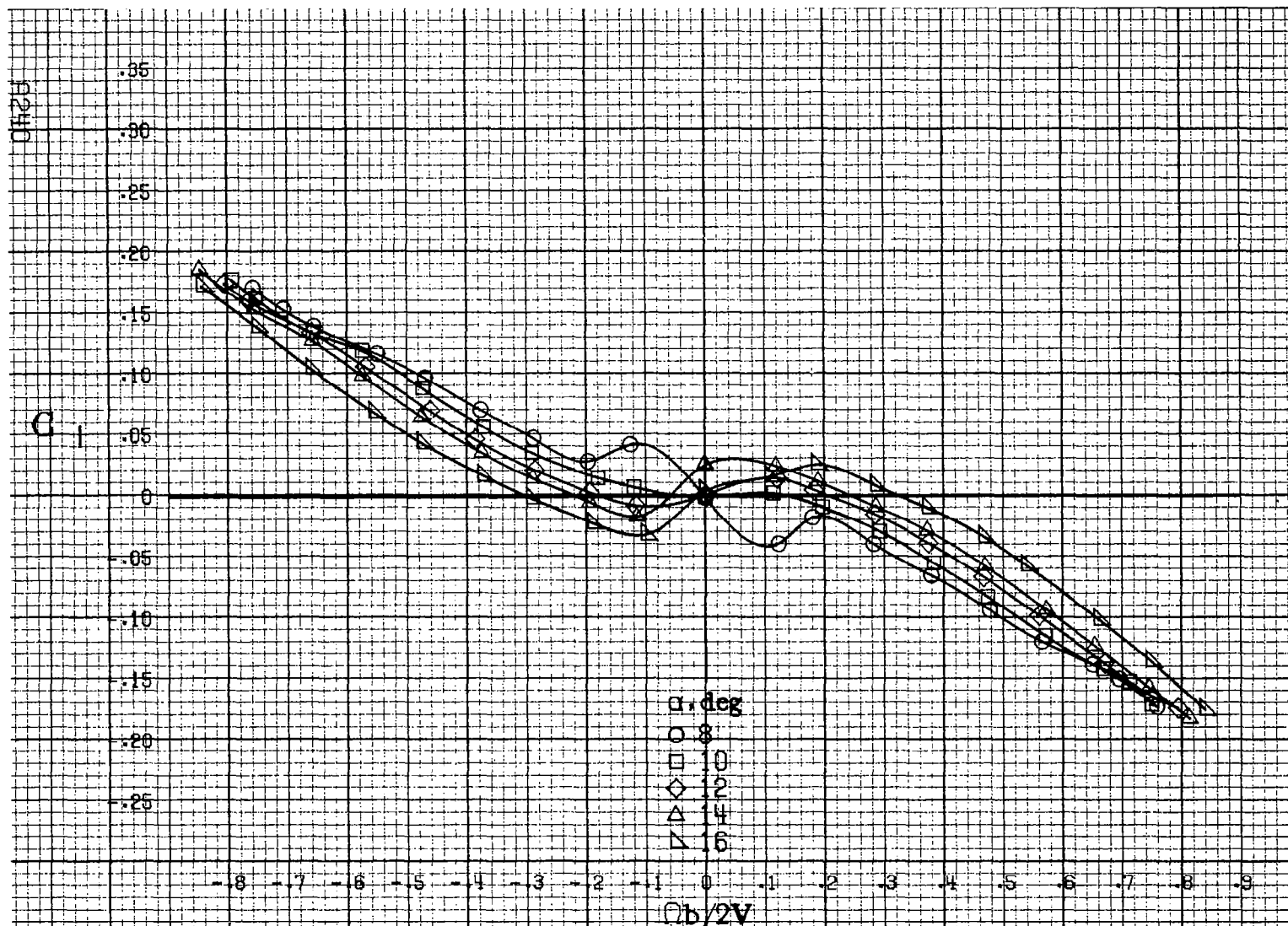


(c) $\alpha=30$ to 50° , $SR=0$.
Figure A61. Continued.



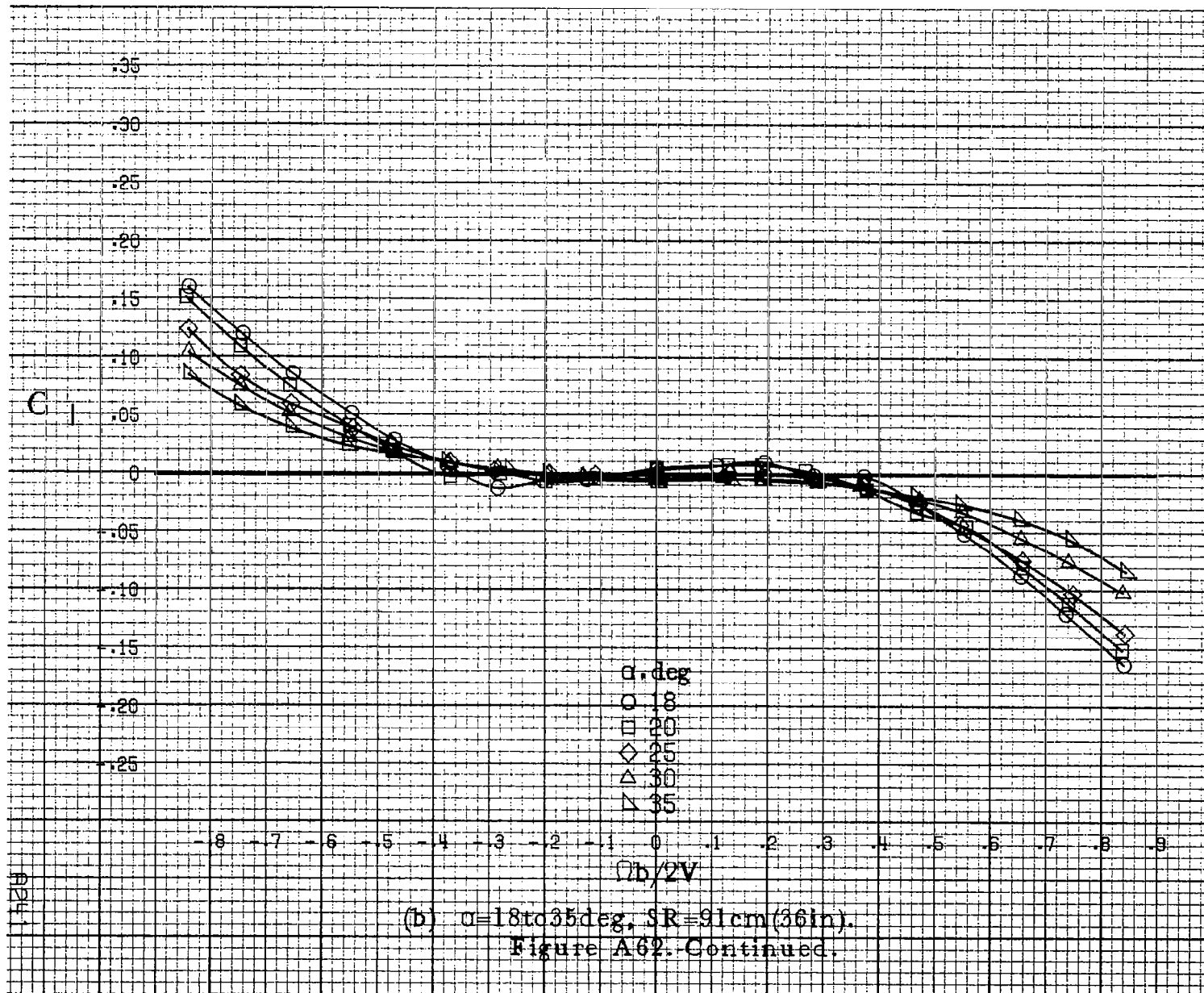
(d) $\alpha = 55$ to 90° , $SR = 0$.
Figure A61, Concluded.

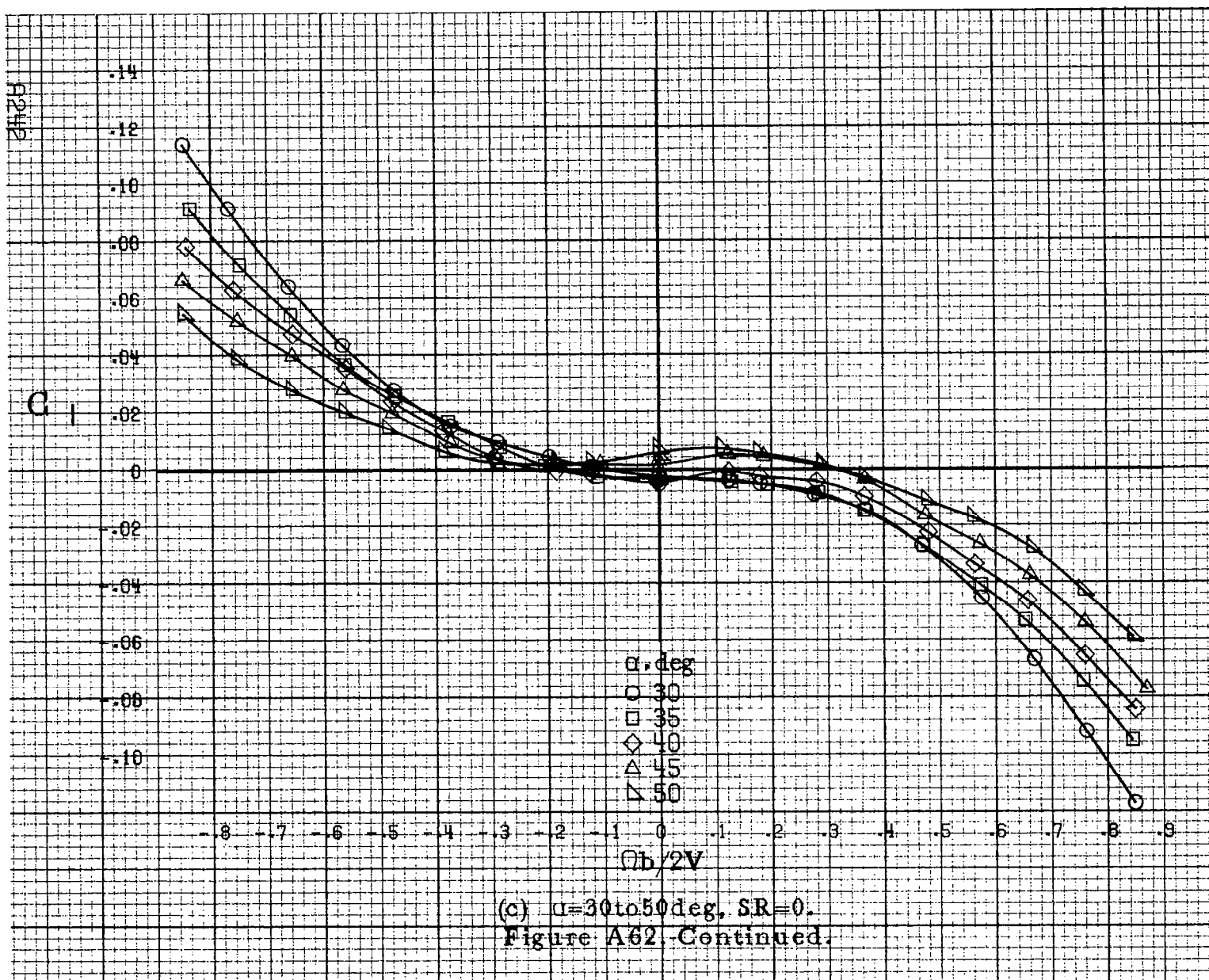
9239

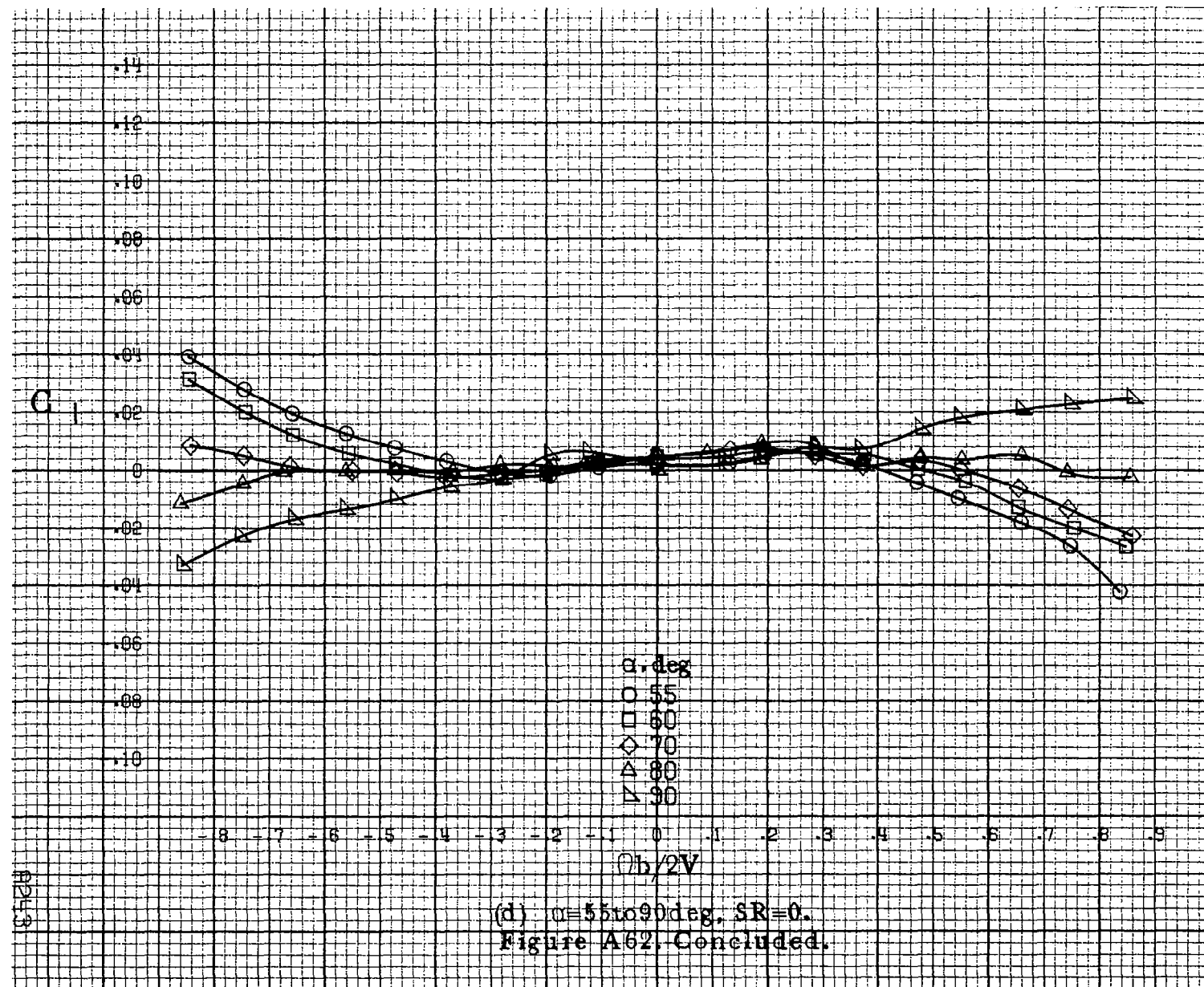


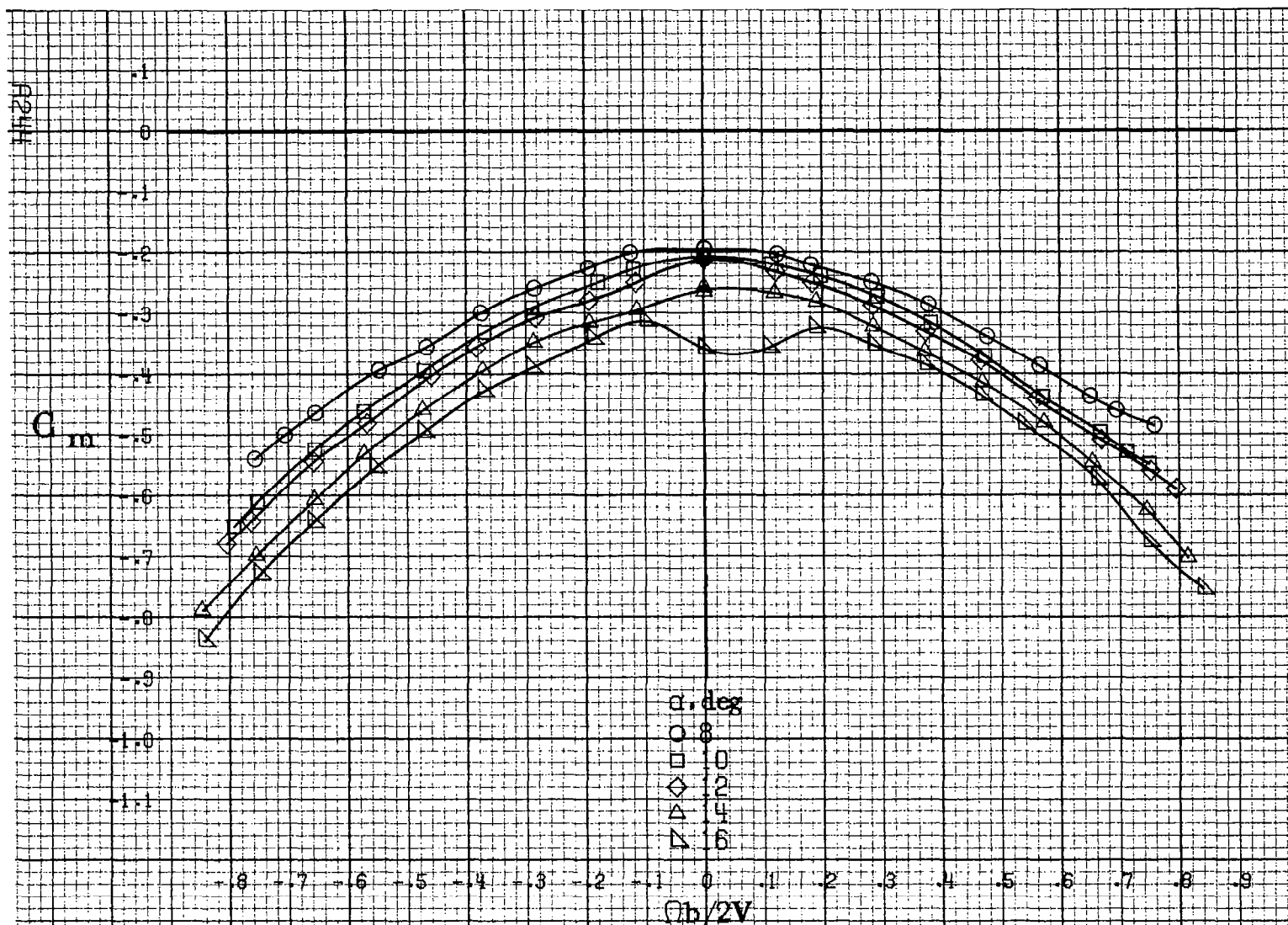
(a) $\alpha = 8$ to 16 deg, $SR = 91$ cm (36 in).

Figure A62. Effect of rotation rate and angle of attack on rolling moment coefficient for configuration having sharp-edged fuselage bottom. $\delta_a = 15^\circ$, $\delta_a = 0^\circ$, $\delta_r = 28^\circ$, $\beta = 0^\circ$.



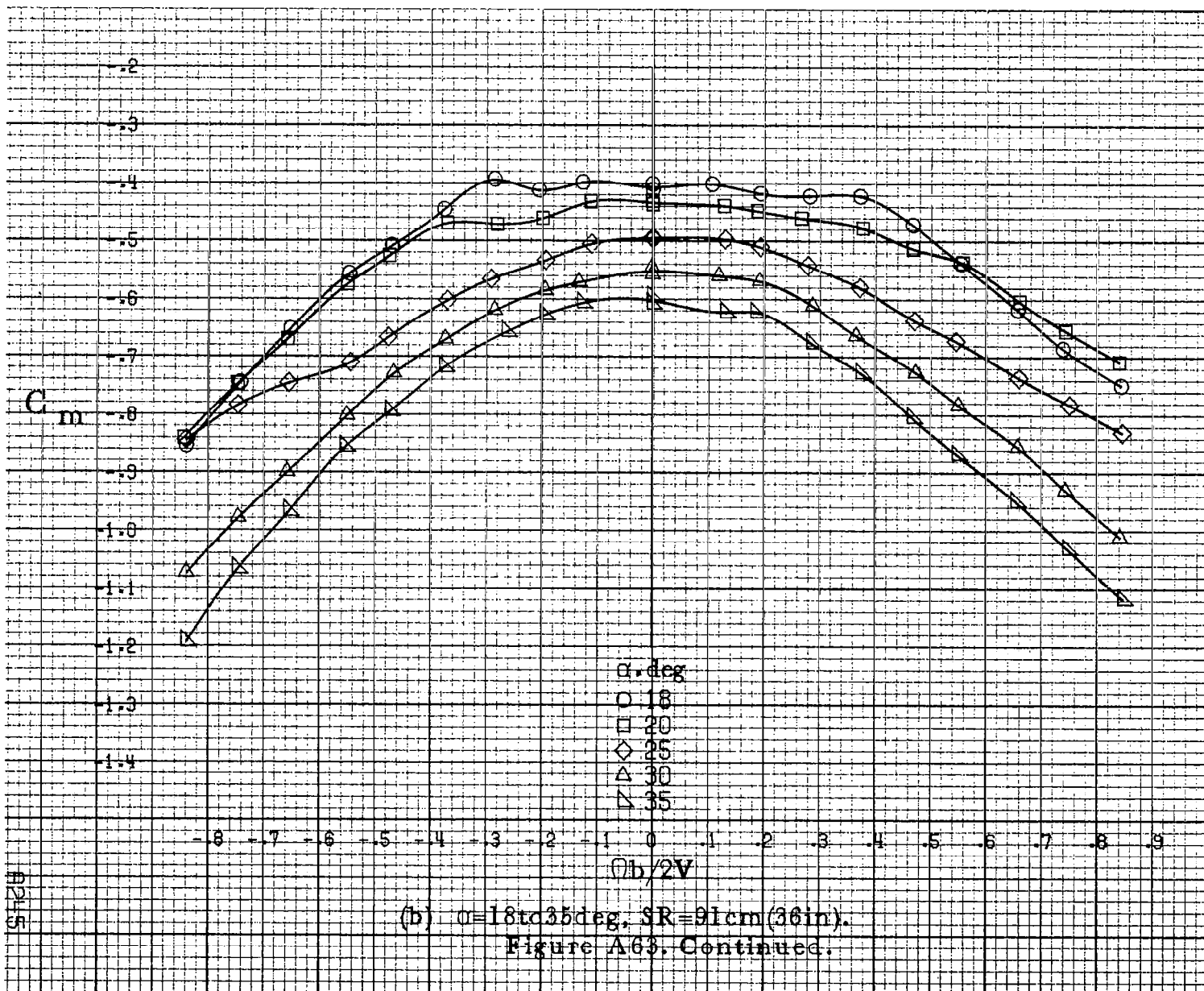






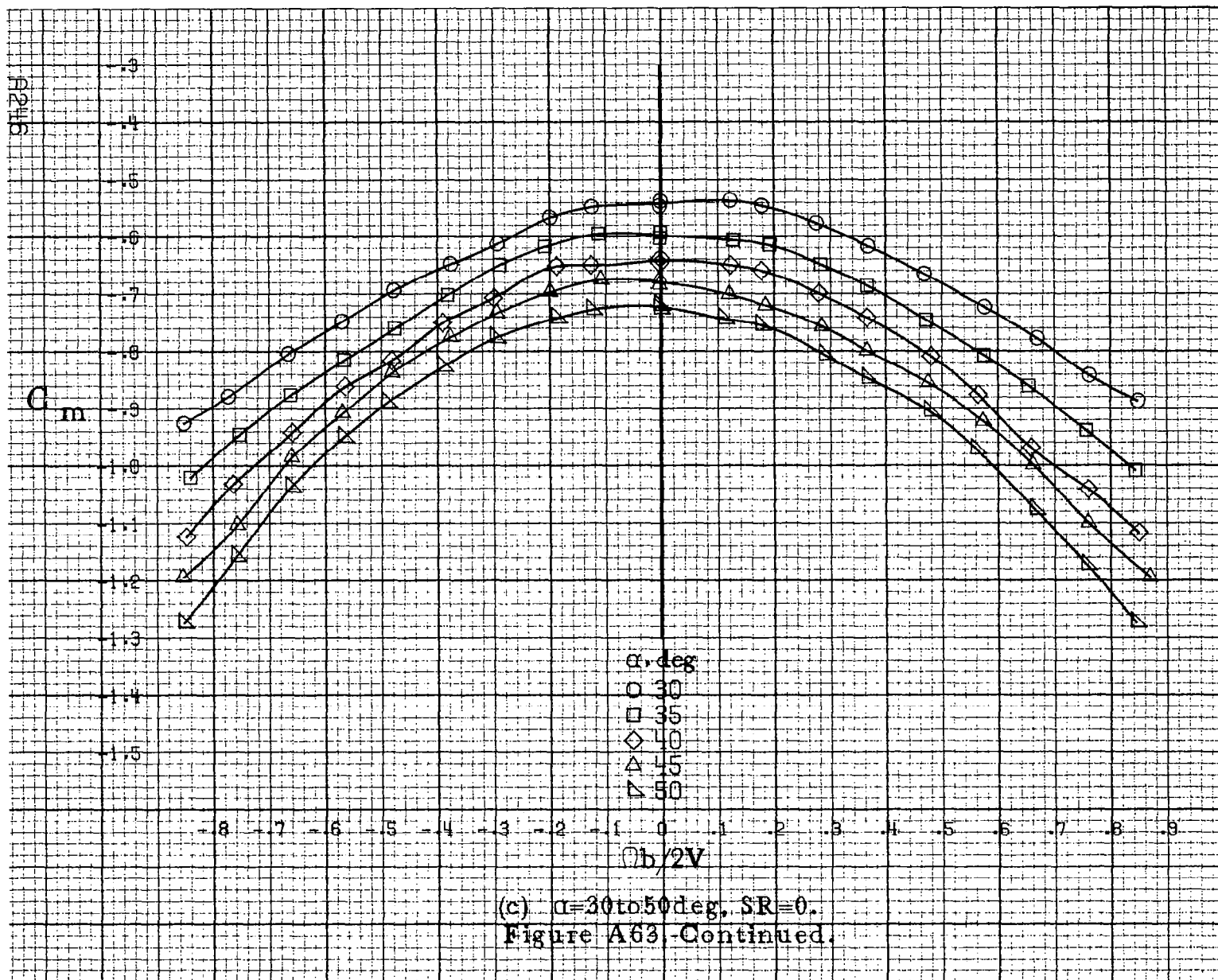
(a) $\alpha = 8$ to 16 deg, $SR = 91$ cm (36 in).

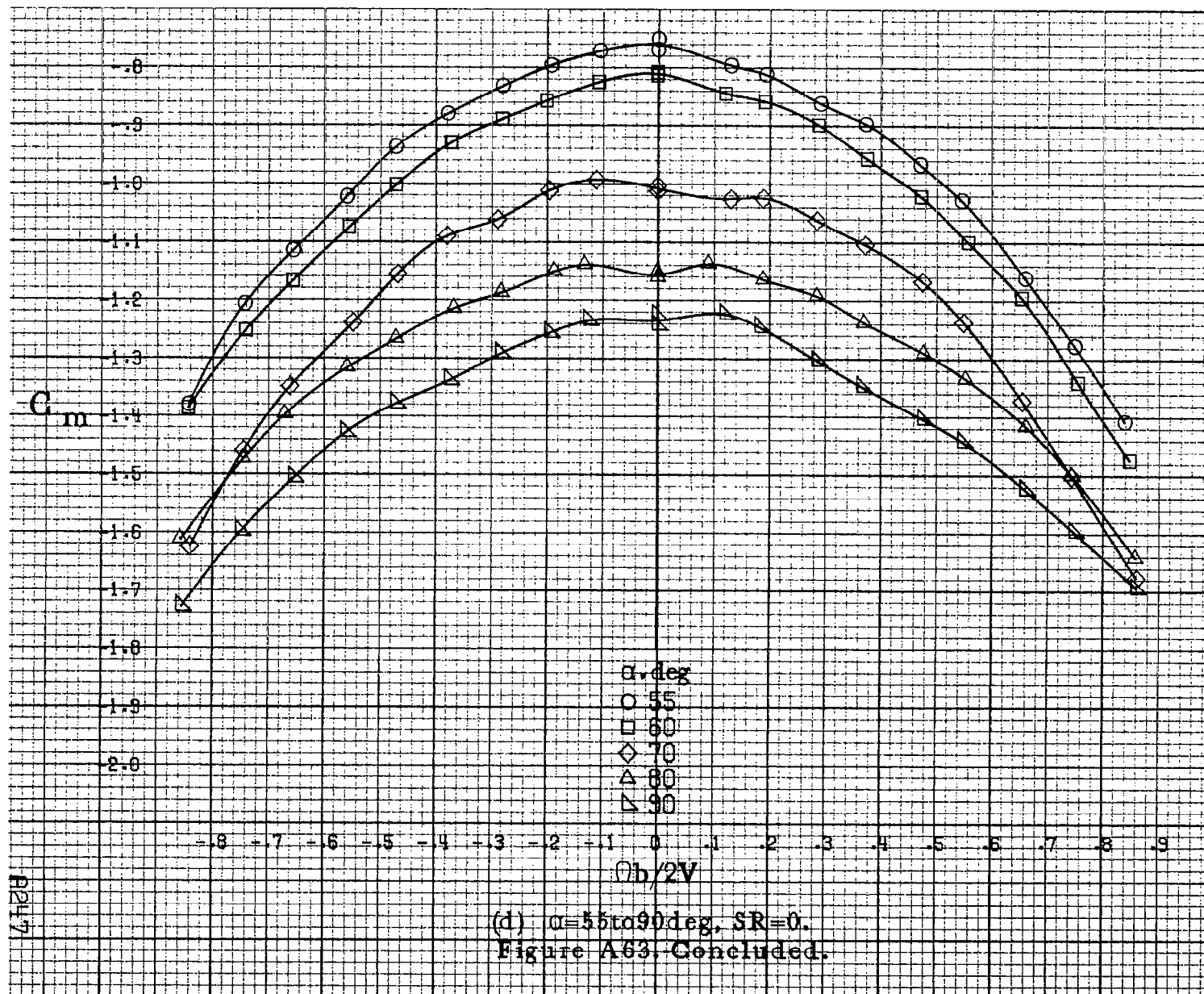
Figure A63. Effect of rotation rate and angle of attack on pitching moment coefficient for configuration having sharp-edged fuselage bottom. $\delta_a = 15^\circ$, $\delta_s = 0^\circ$, $\delta_r = 28^\circ$, $\beta = 0^\circ$.

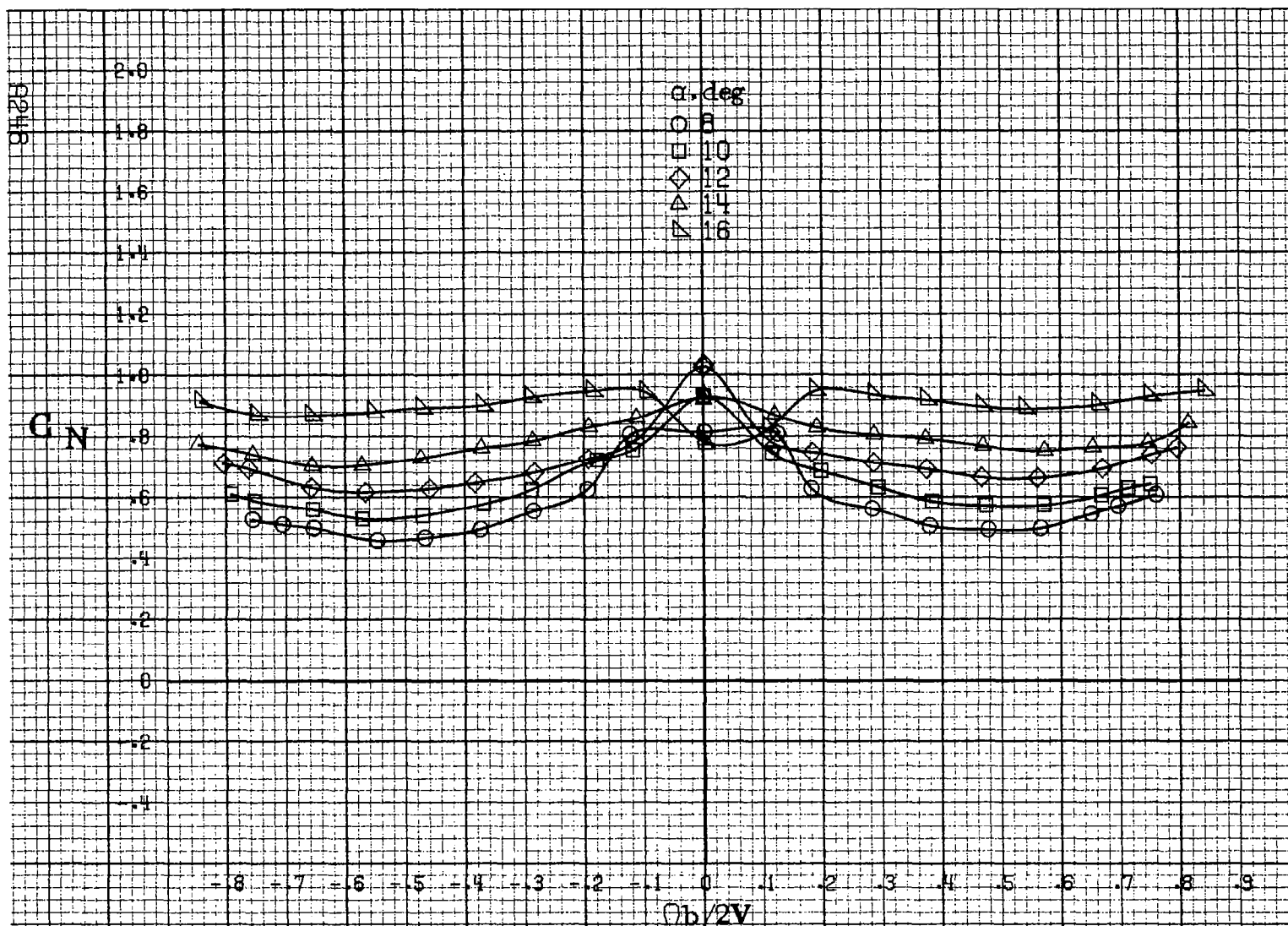


(b) $\alpha = 18$ to 35° , $SR = 91\text{cm}$ (36in).
Figure A63. Continued.

A245

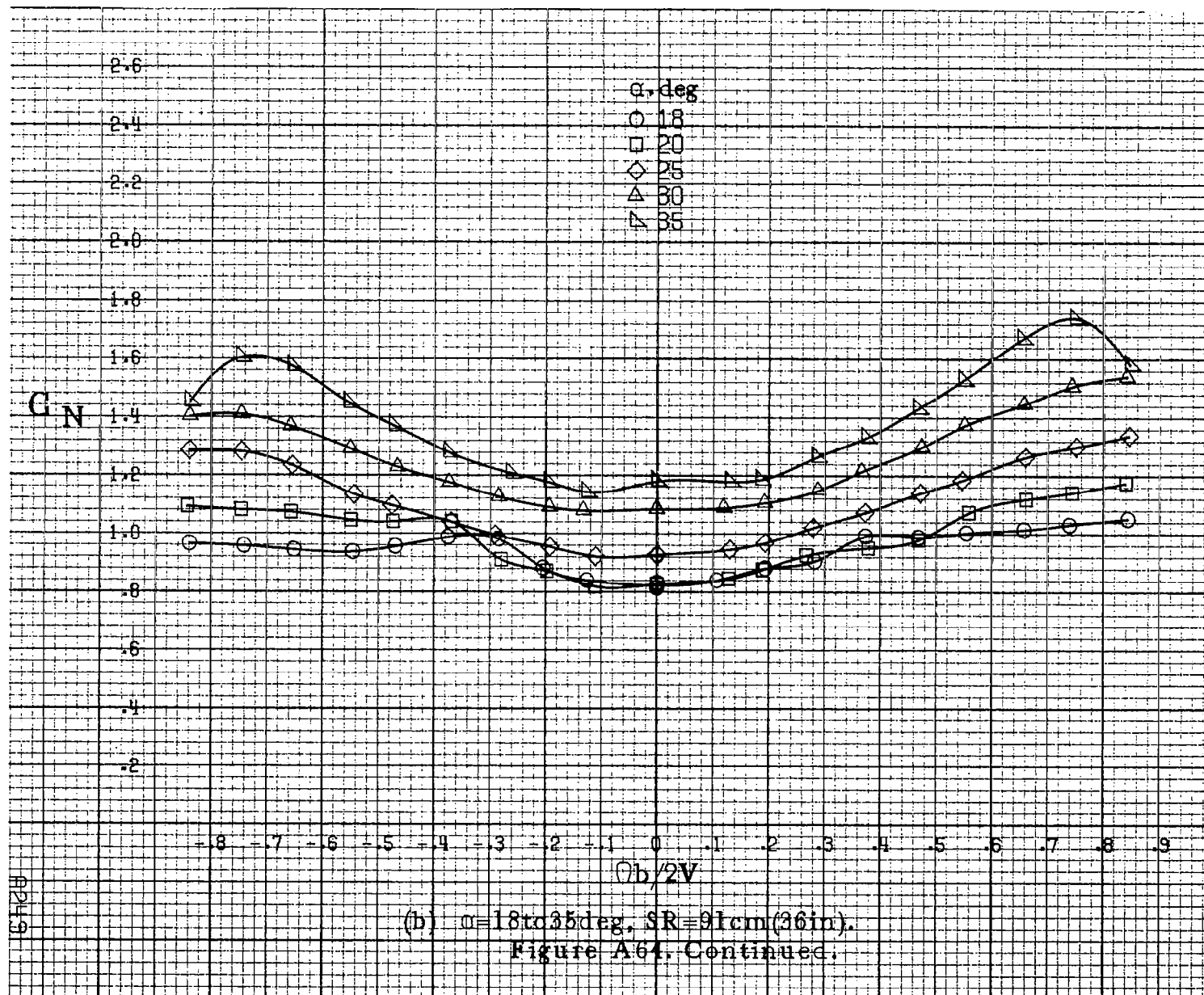


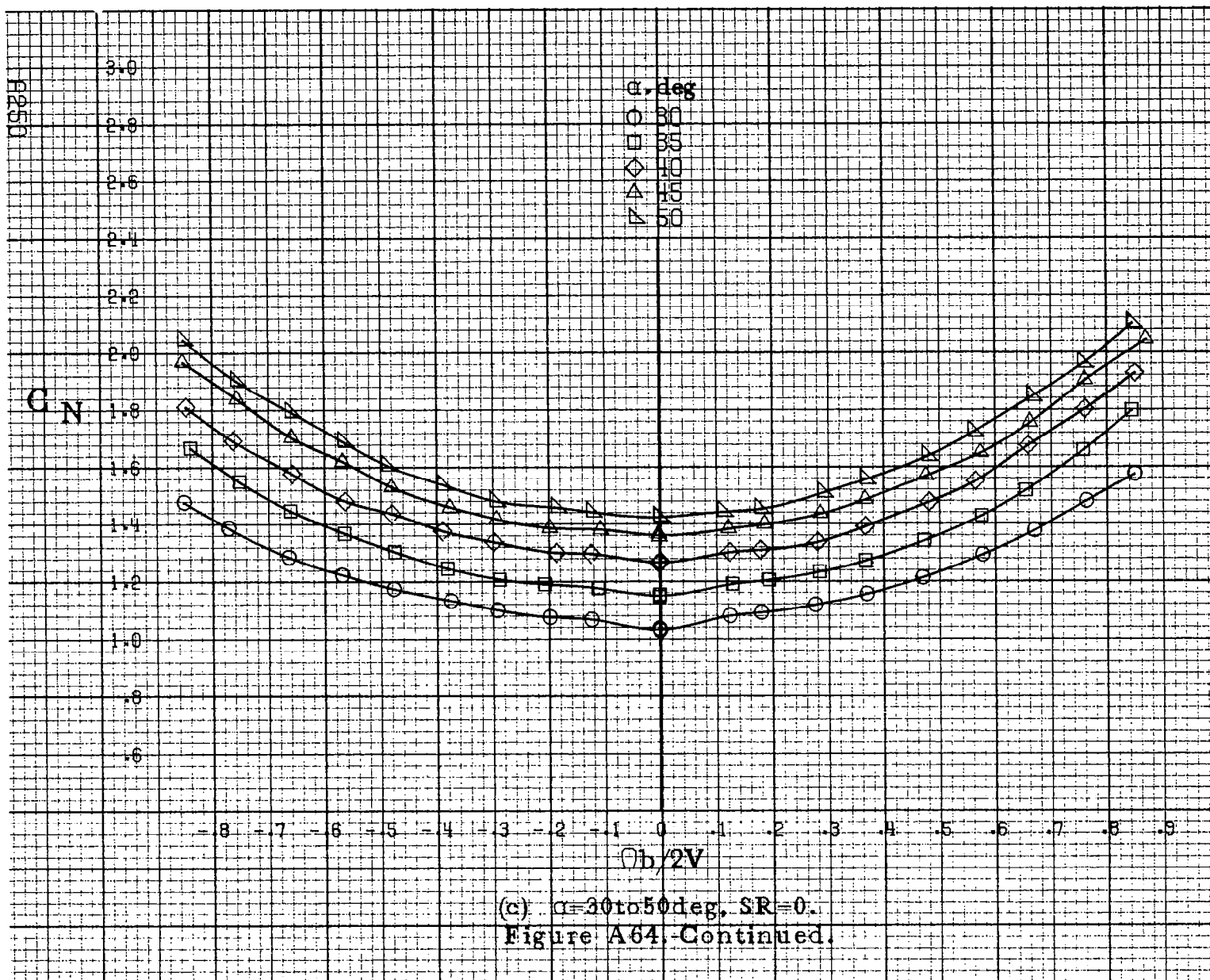


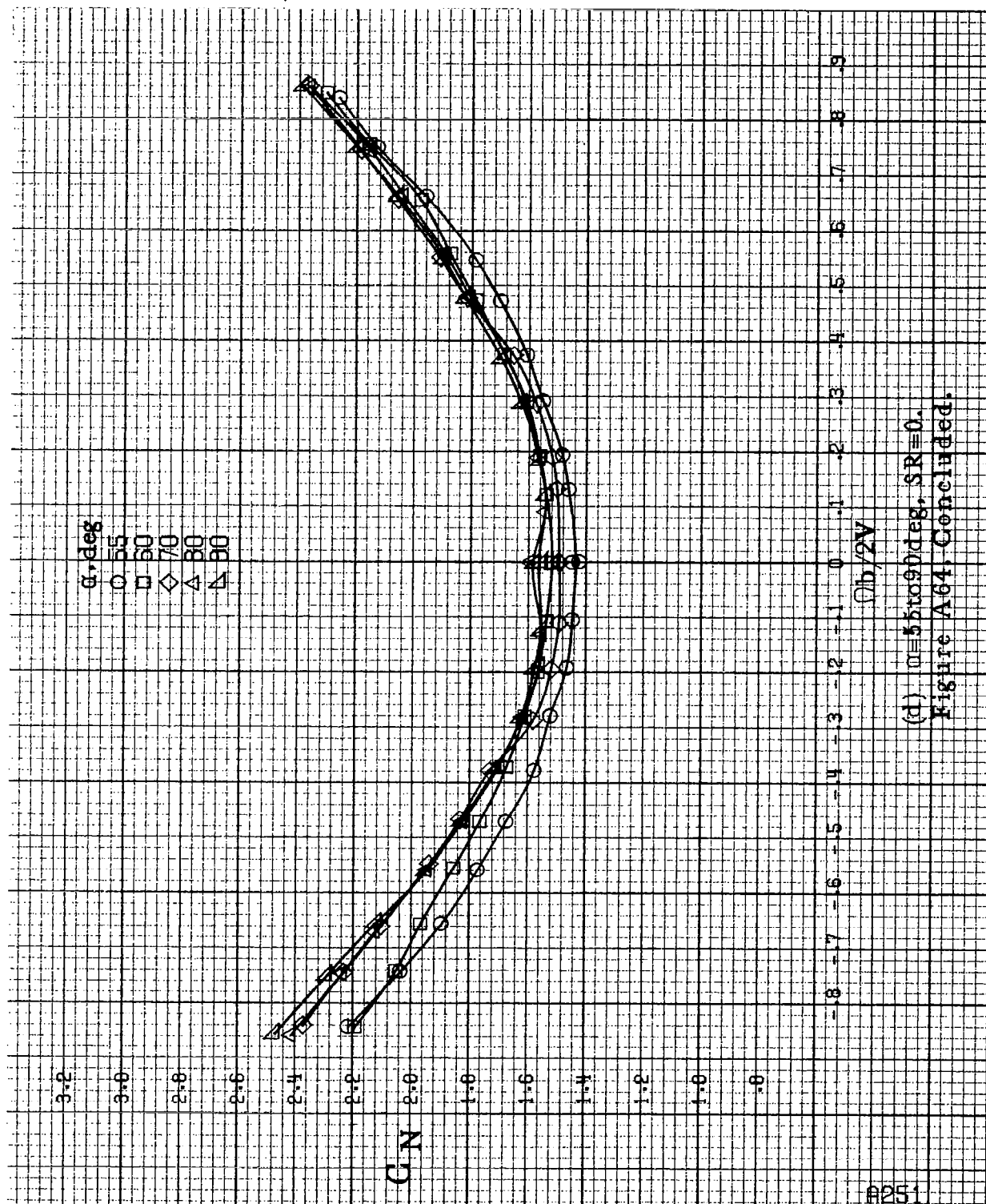


(a) $\alpha = 8 \text{ to } 16 \text{ deg}$, $SR = 91 \text{ cm (36 in)}$.

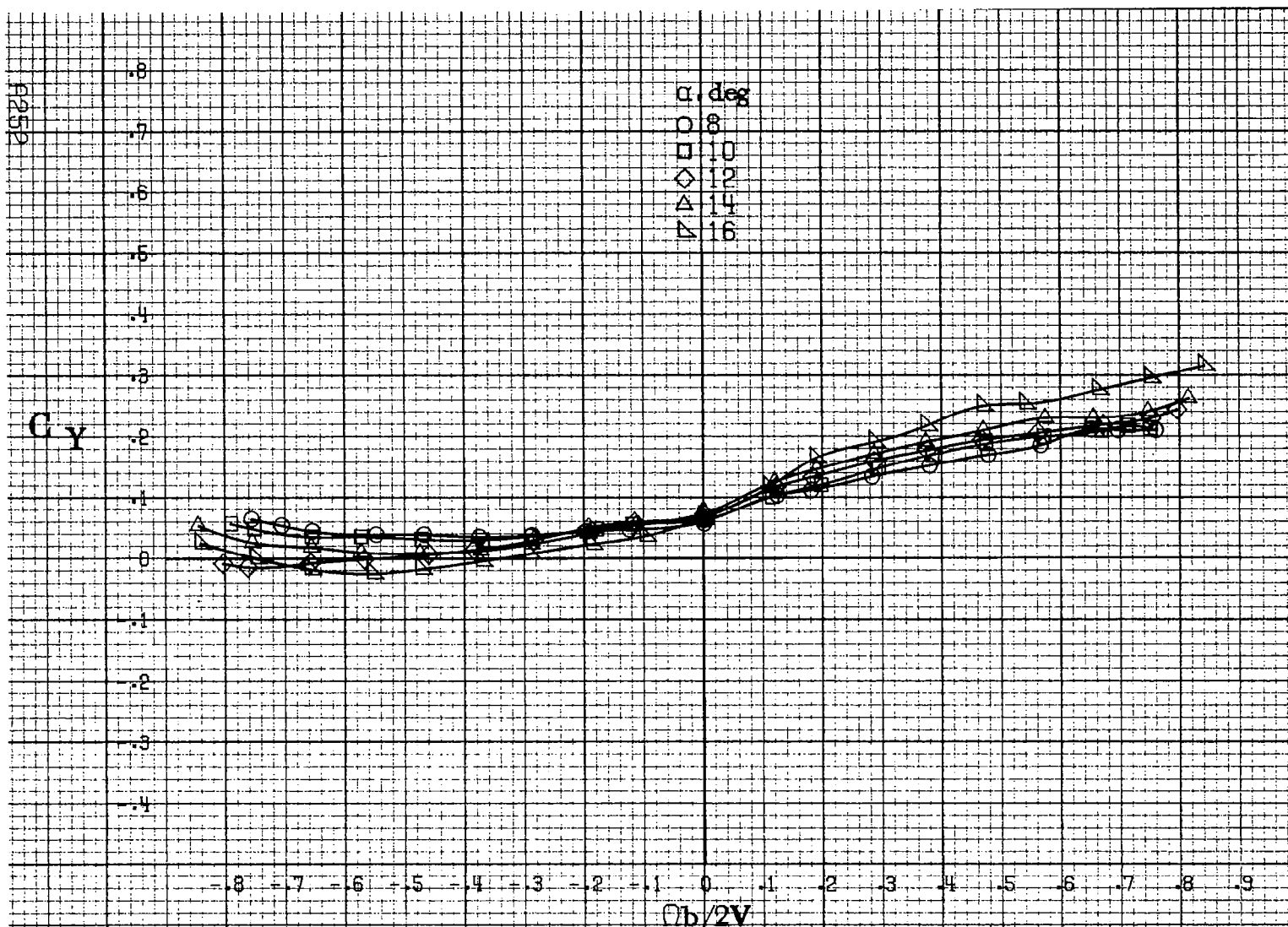
Figure A64. Effect of rotation rate and angle of attack on normal force coefficient for configuration having sharp edged fuselage bottom. $\delta_a = 15^\circ$, $\delta_a = 0^\circ$, $\delta_r = 28^\circ$, $\beta = 0^\circ$.





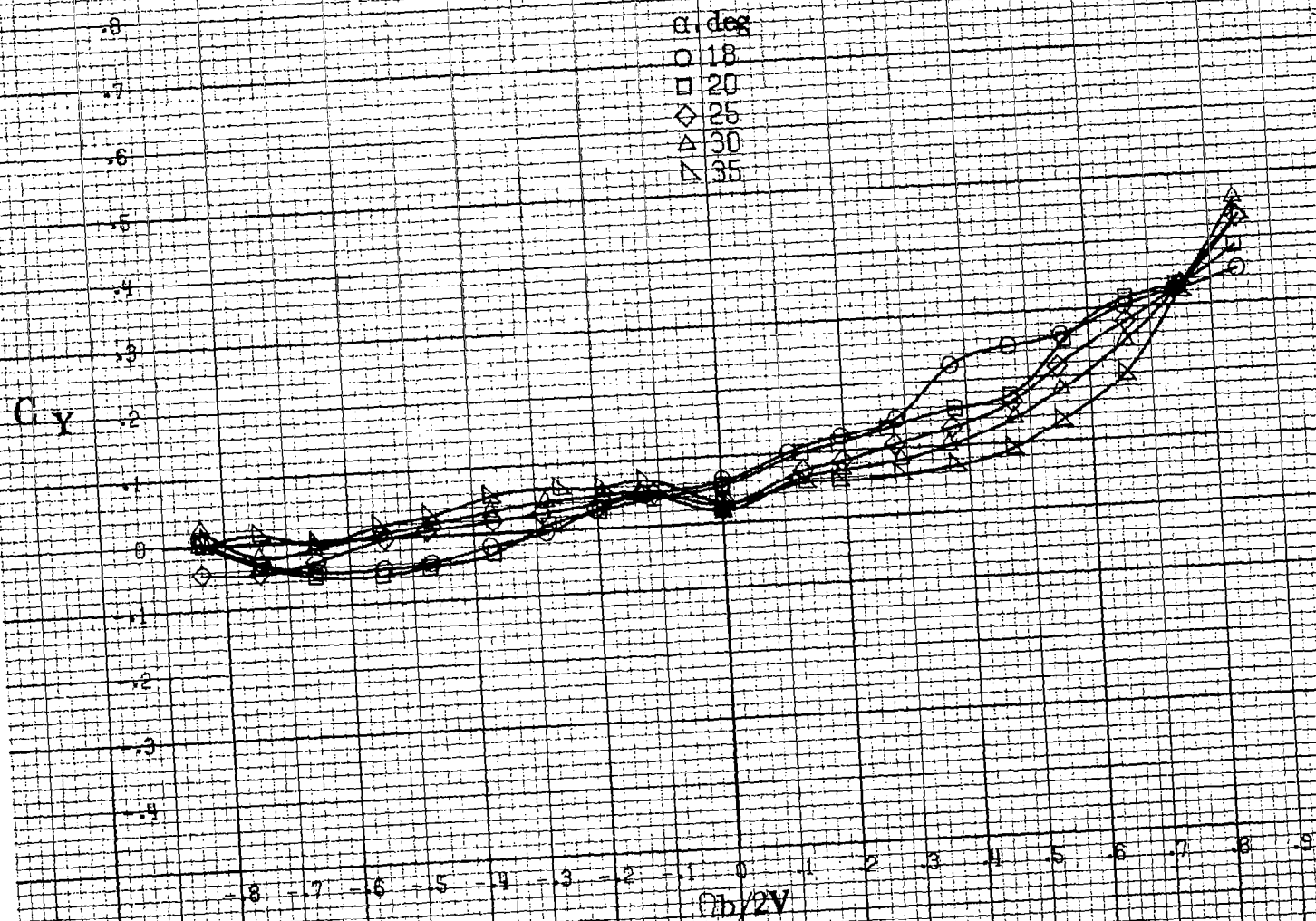


(d) $\alpha = 55$ to 90 deg, $SR = 0$.
Figure A64, Concluded.

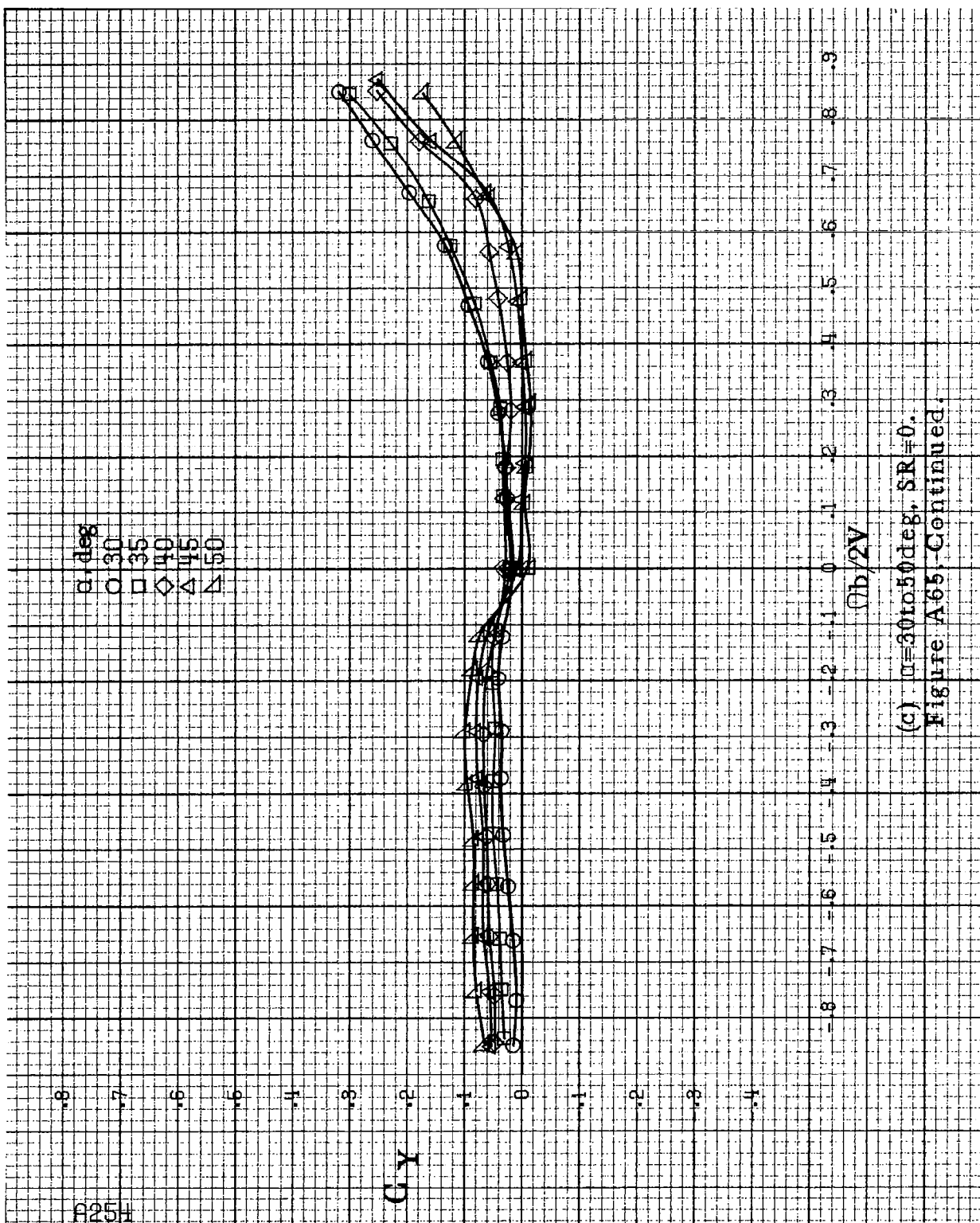


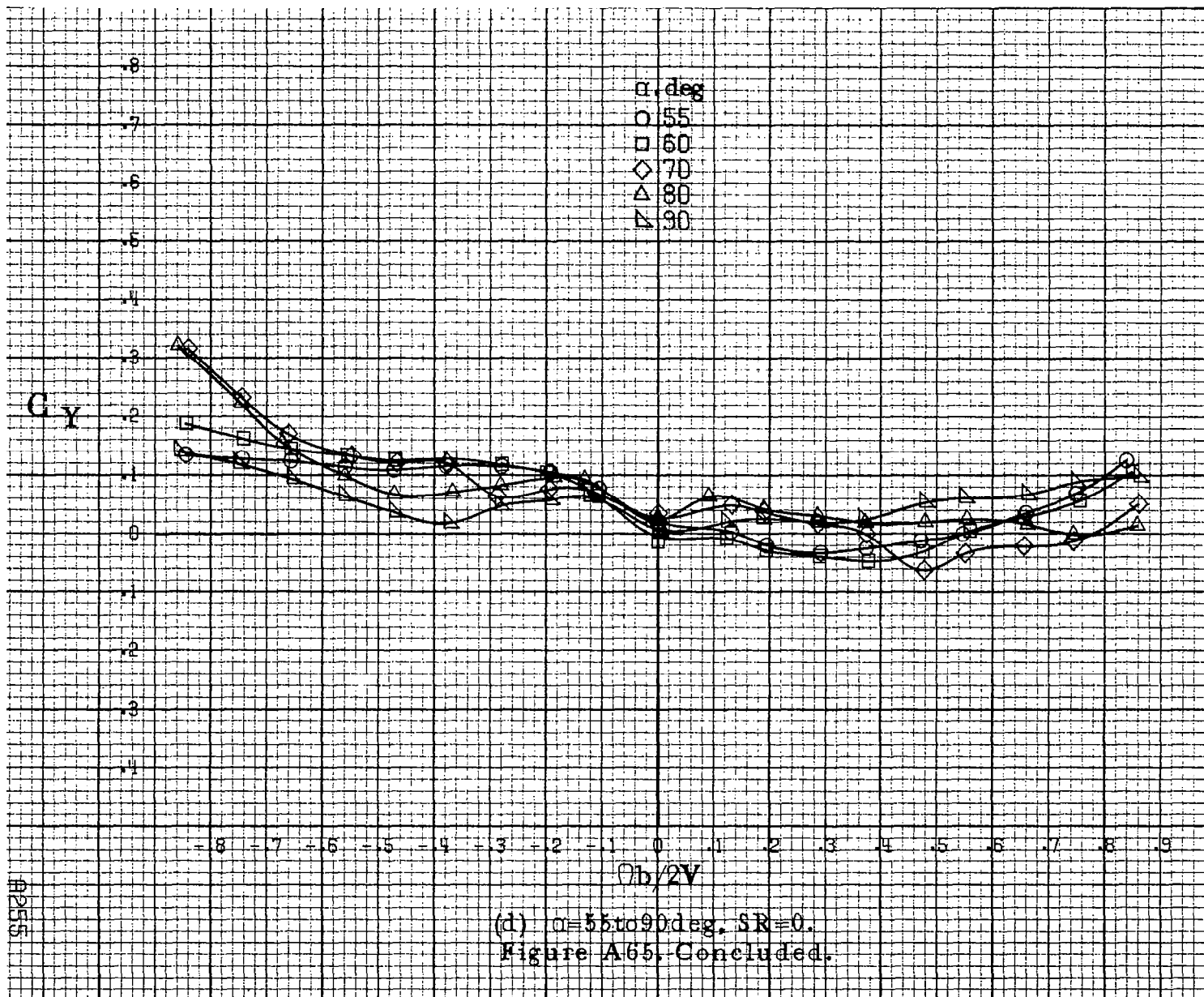
(a) $\alpha=8\text{ to }16\text{deg}$, $SR=91\text{cm}(36\text{in})$.

Figure A65.-Effect of rotation rate and angle of attack on side-force coefficient for configuration having sharp-edged fuselage bottom. $\delta_a=15^\circ$, $\delta_s=0^\circ$, $\delta_r=28^\circ$, $\beta=0^\circ$.

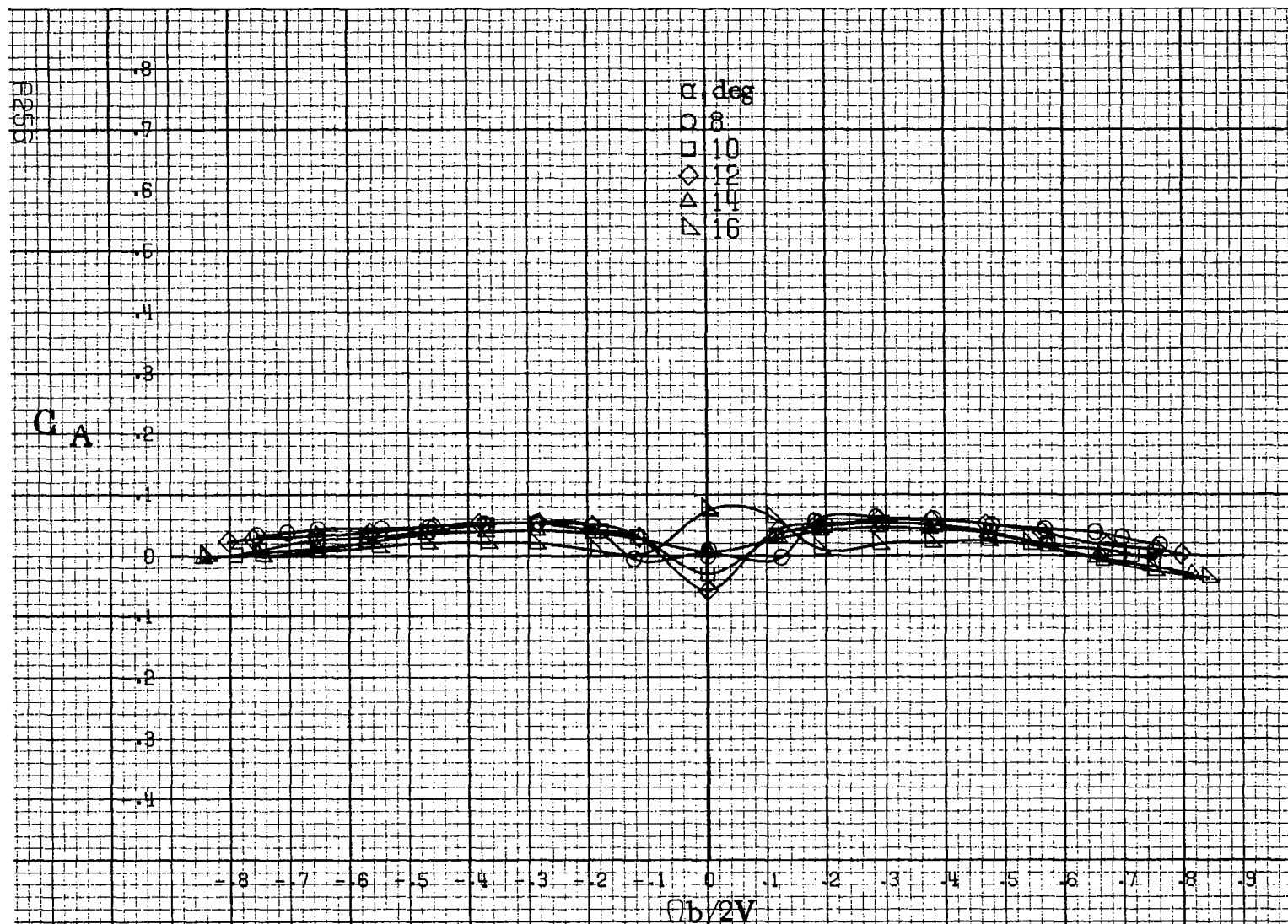


(b) $\alpha=18$ to 35° , $SR=91\text{cm}(36\text{in})$.
Figure A65. Continued.



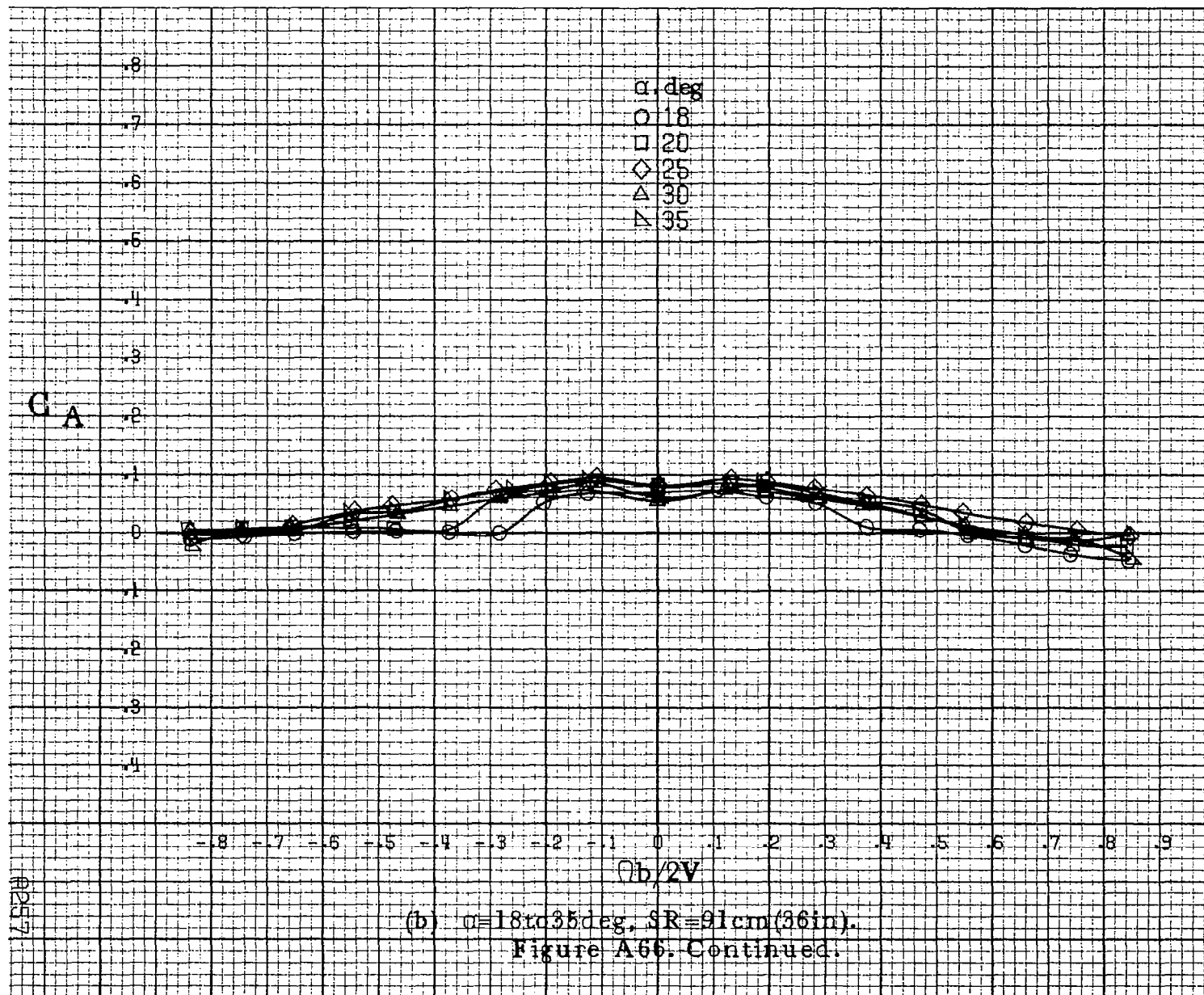


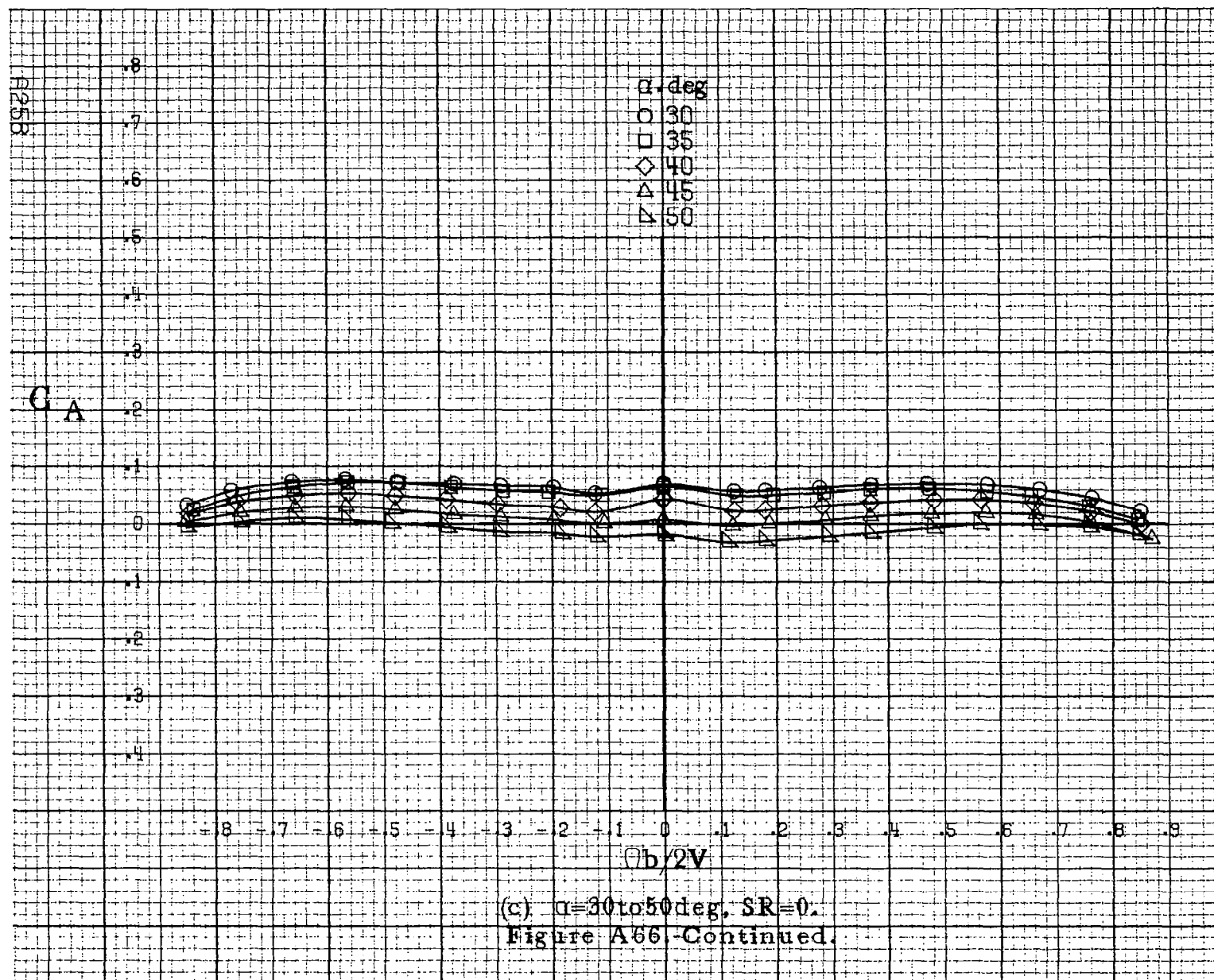
(d) $\alpha = 55$ to 90° , $SR = 0$.
Figure A65. Concluded.

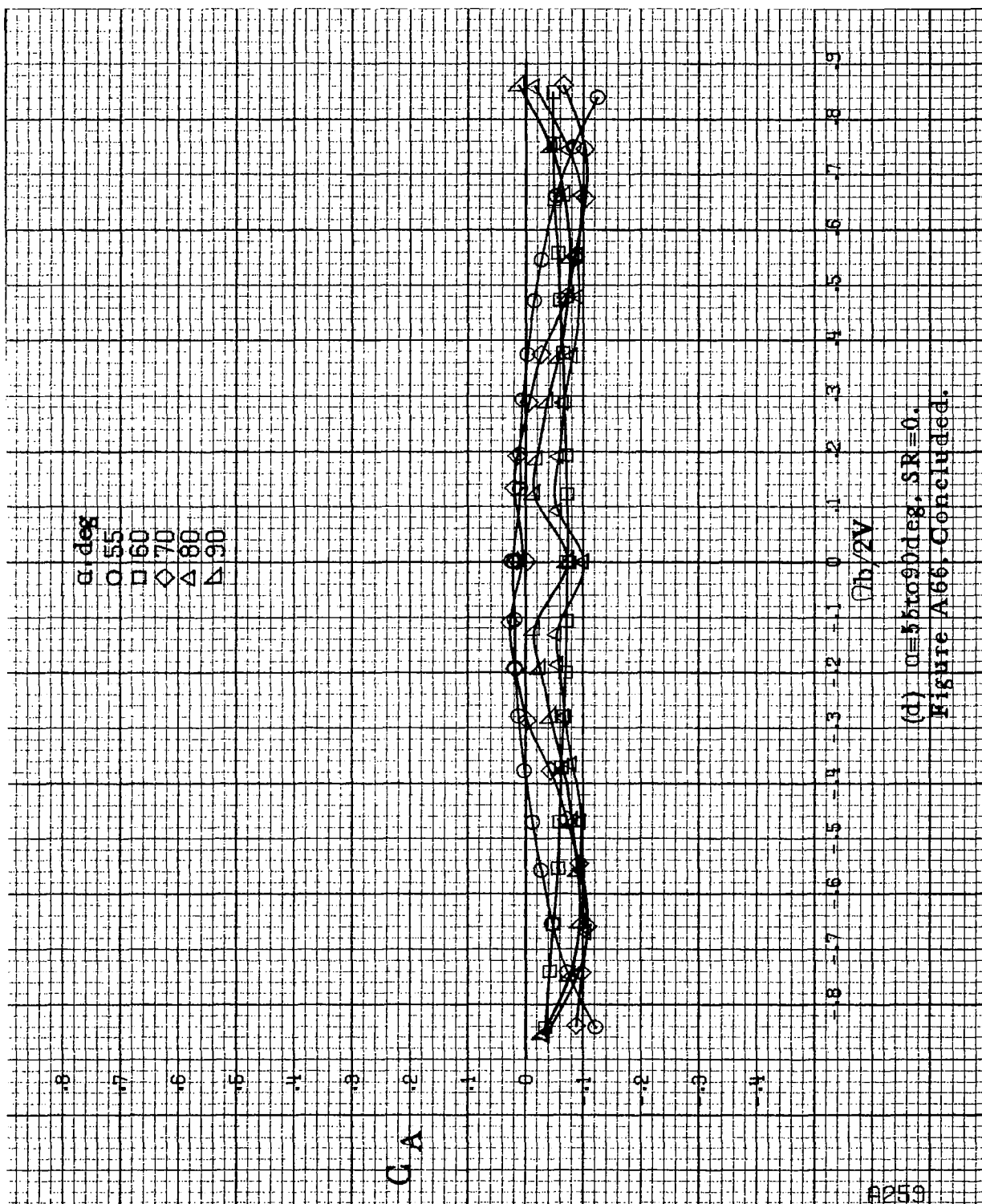


(a) $\alpha=8$ to 16° , $SR=91\text{cm}(36\text{in})$.

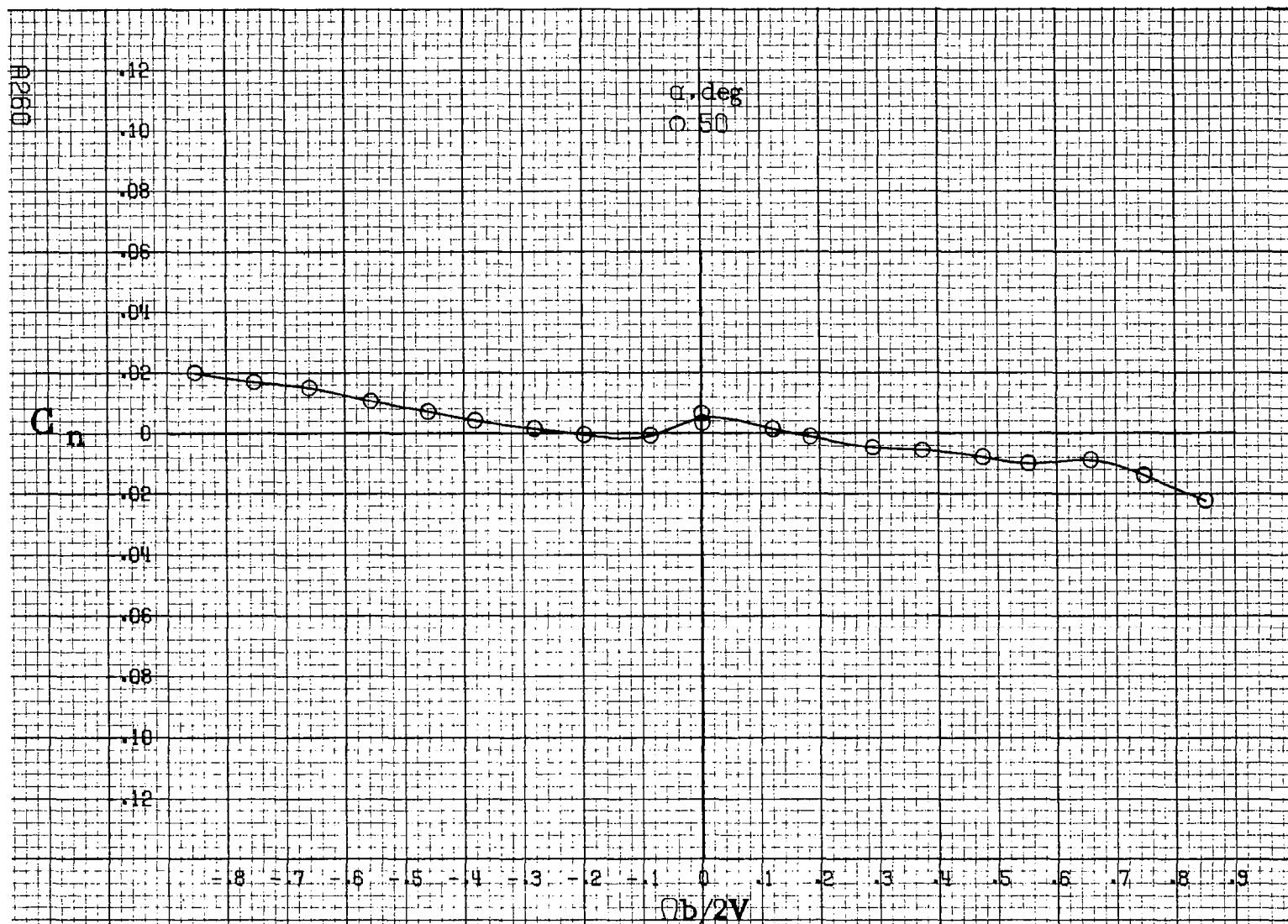
Figure A66. Effect of rotation rate and angle of attack on axial force coefficient for configuration having sharp-edged fuselage bottom. $\delta_a=15^\circ$, $\delta_s=0^\circ$, $\delta_r=28^\circ$, $\beta=0^\circ$.





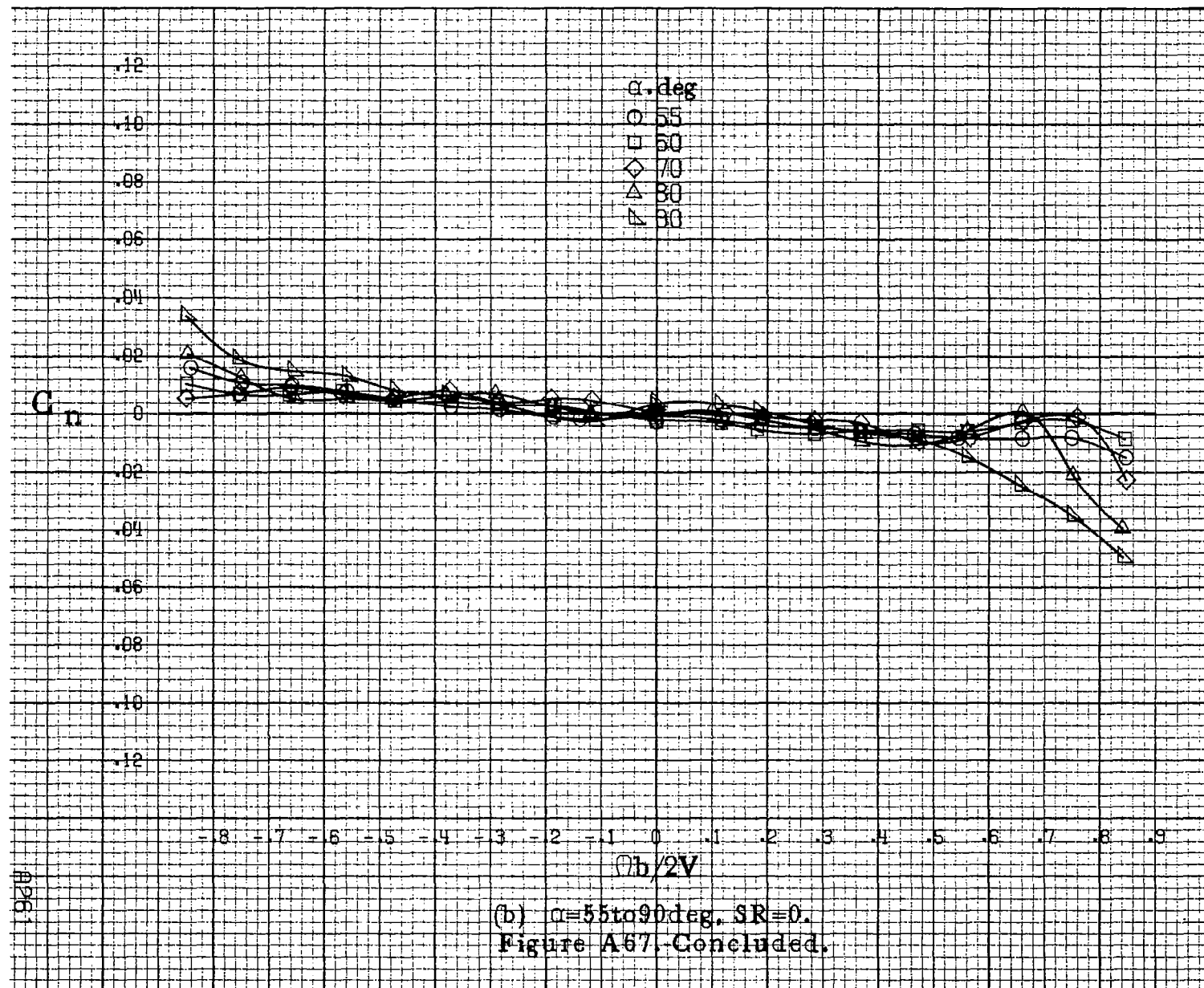


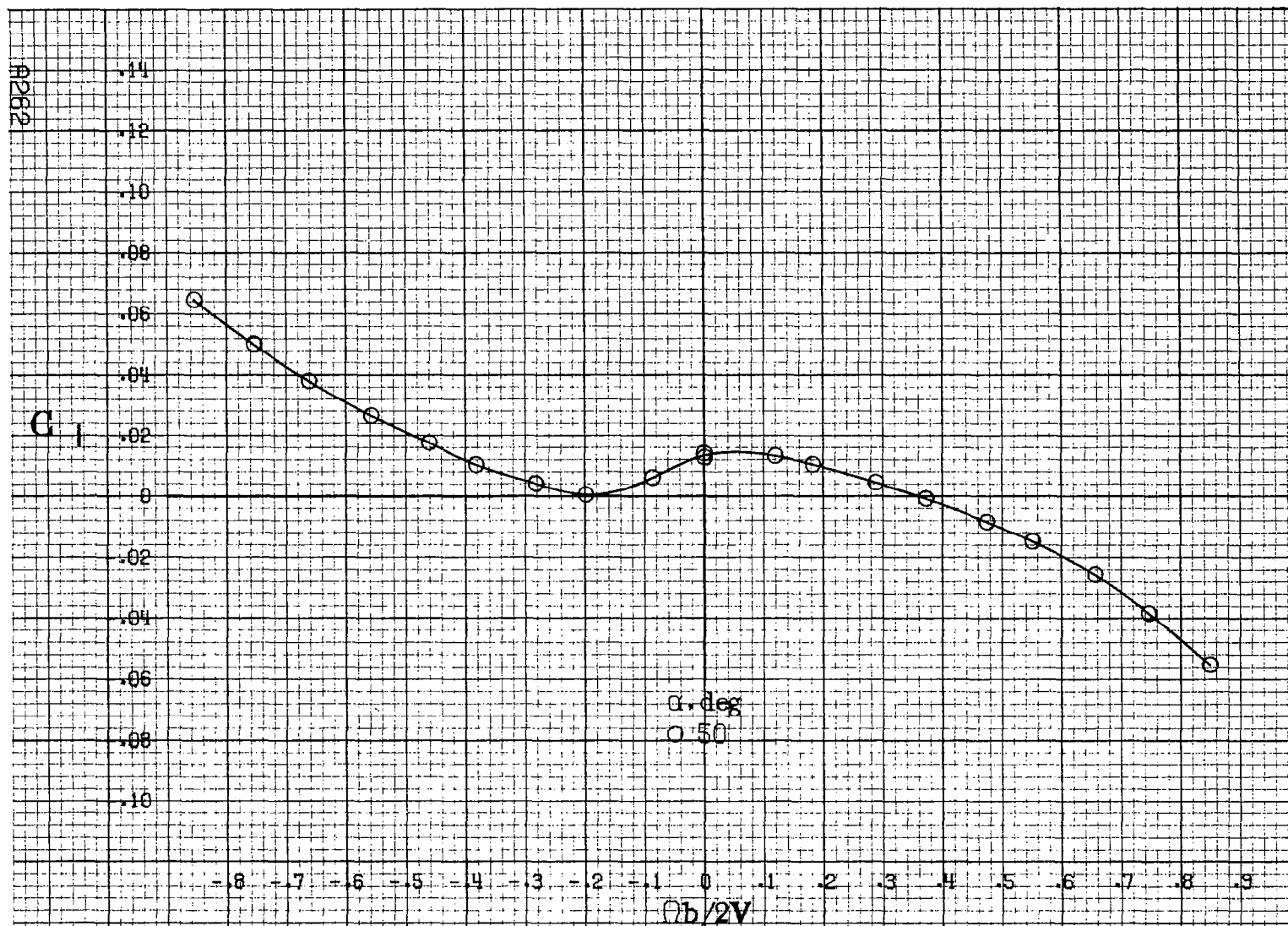
(d) $\alpha = 55$ to 90 deg, $SR = 0$.
Figure A66, Concluded.



(a) $\alpha = 50 \text{ deg}$, $SR=0$.

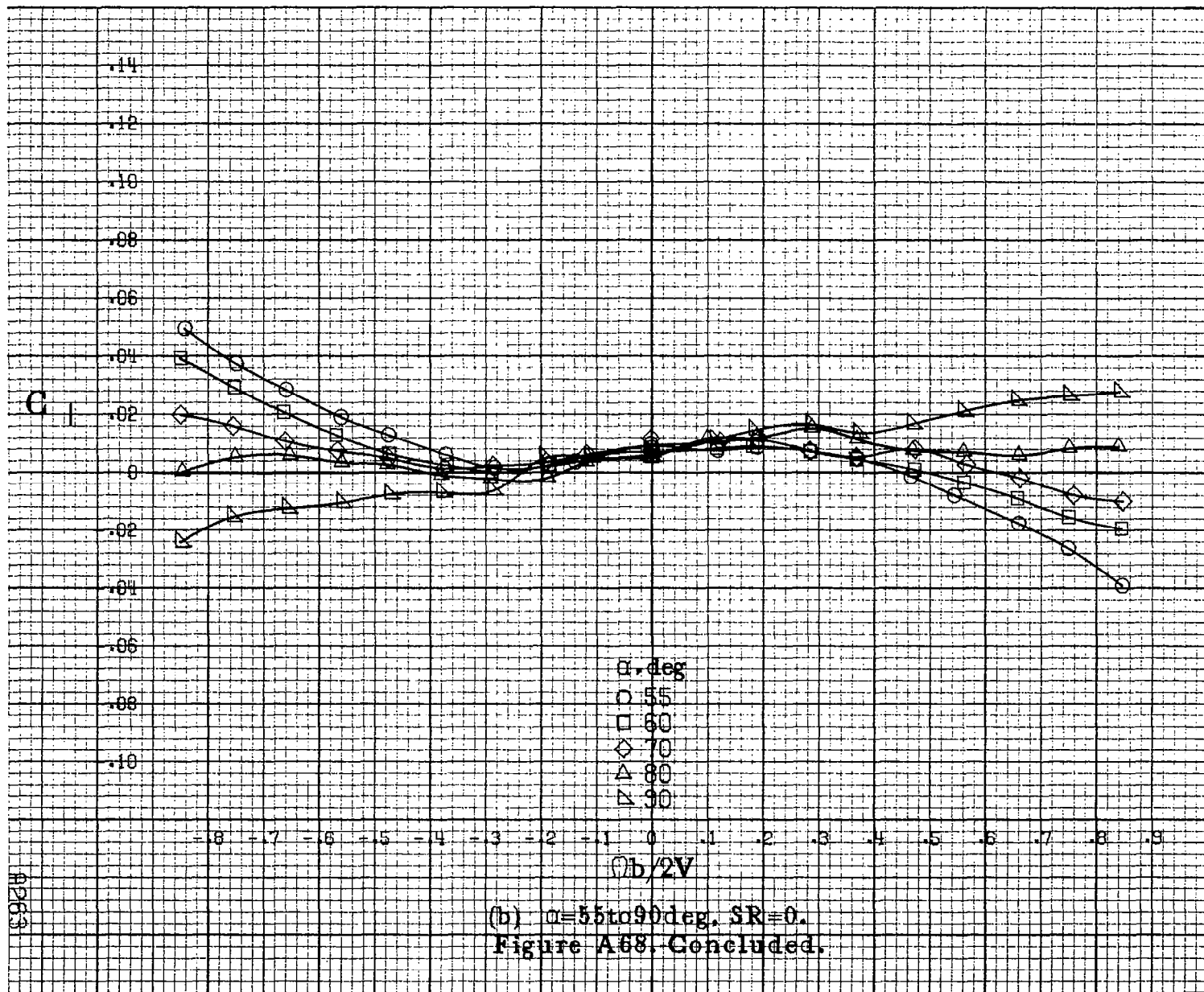
Figure A67. Effect of rotation rate and angle of attack on yawing-moment coefficient for configuration having sharp-edged fuselage bottom with ventrals and strakes off. $\delta_a = 0^\circ$, $\delta_s = 0^\circ$, $\delta_r = 0^\circ$, $\beta = 0^\circ$.

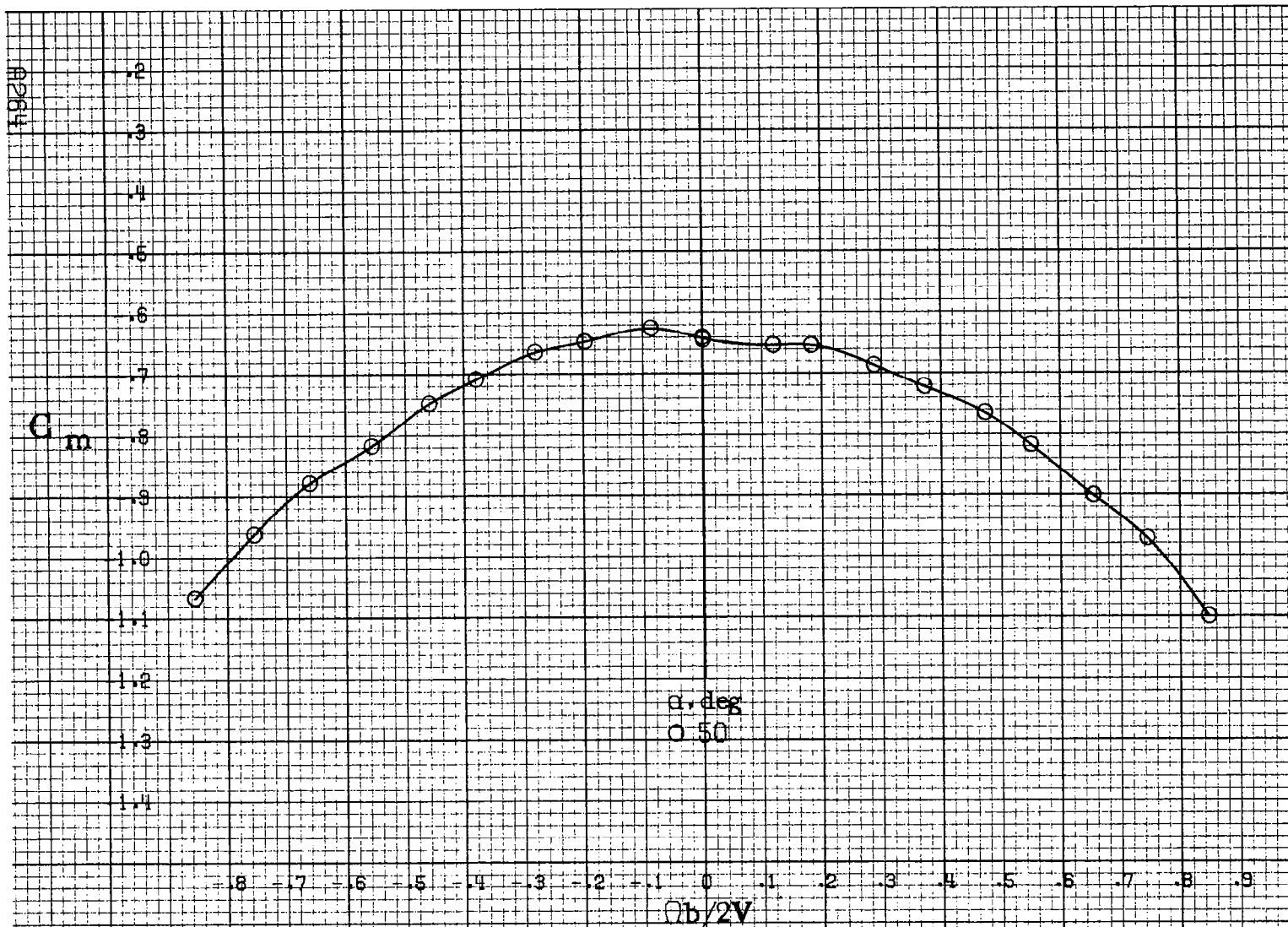




(a) $\alpha = 50^\circ$, $SR=0$.

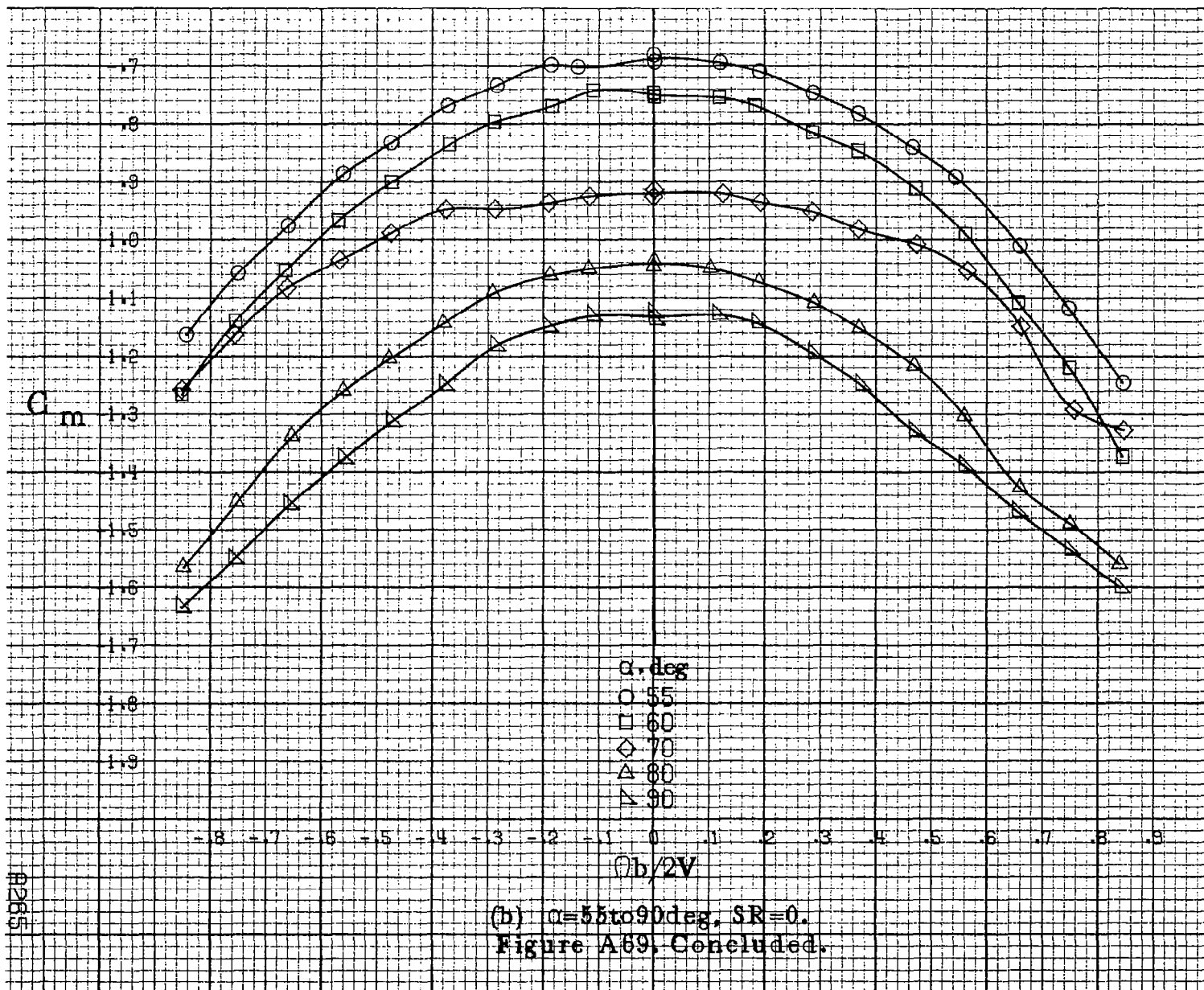
Figure A68. Effect of rotation rate and angle of attack on rolling-moment coefficient for configuration having sharp-edged fuselage bottom with ventrals and strakes off. $\delta_a = 0^\circ$, $\delta_s = 0^\circ$, $\delta_r = 0^\circ$, $\beta = 0^\circ$.

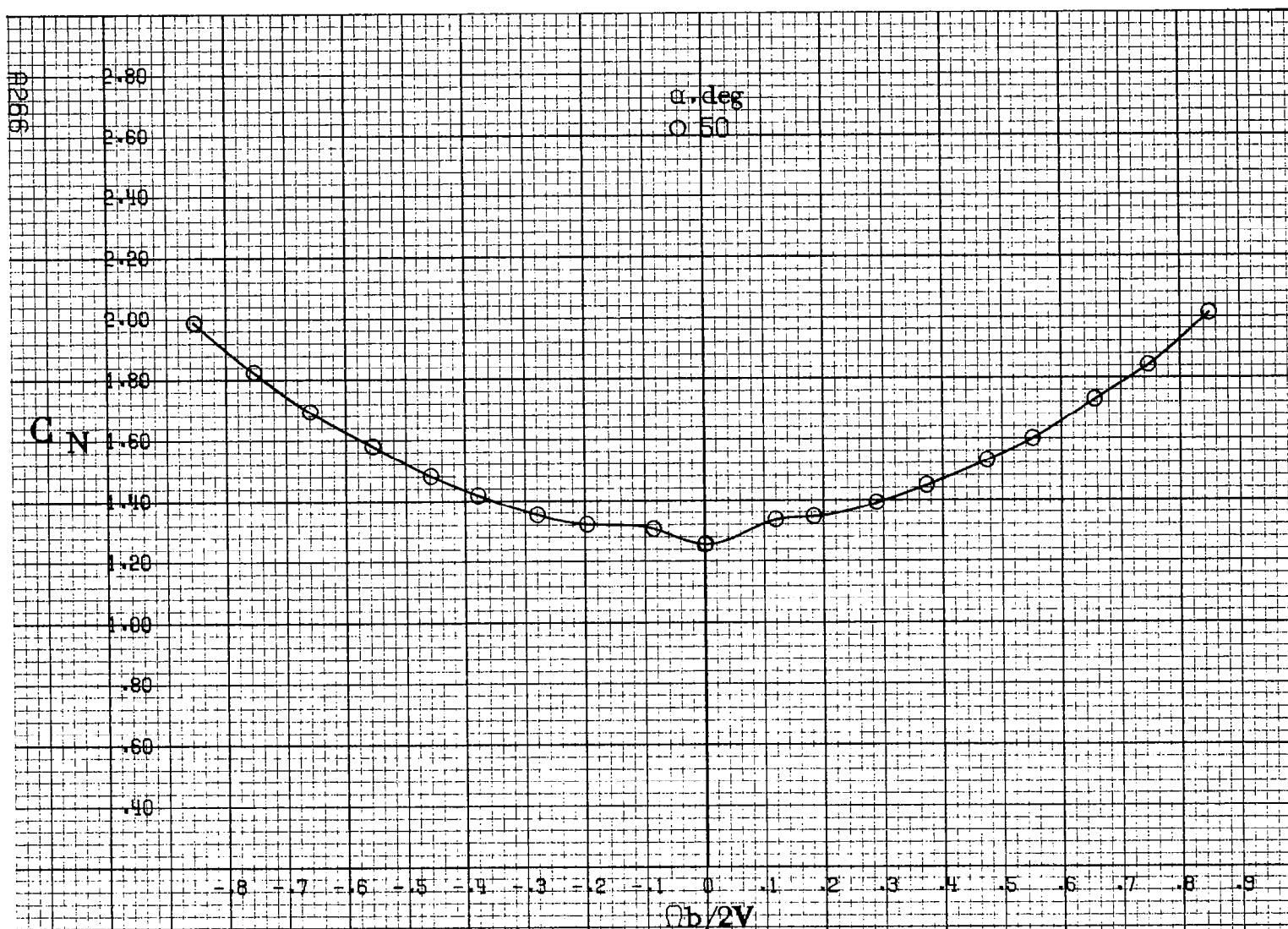




(a) $\alpha = 50^\circ$, $SR = 0$.

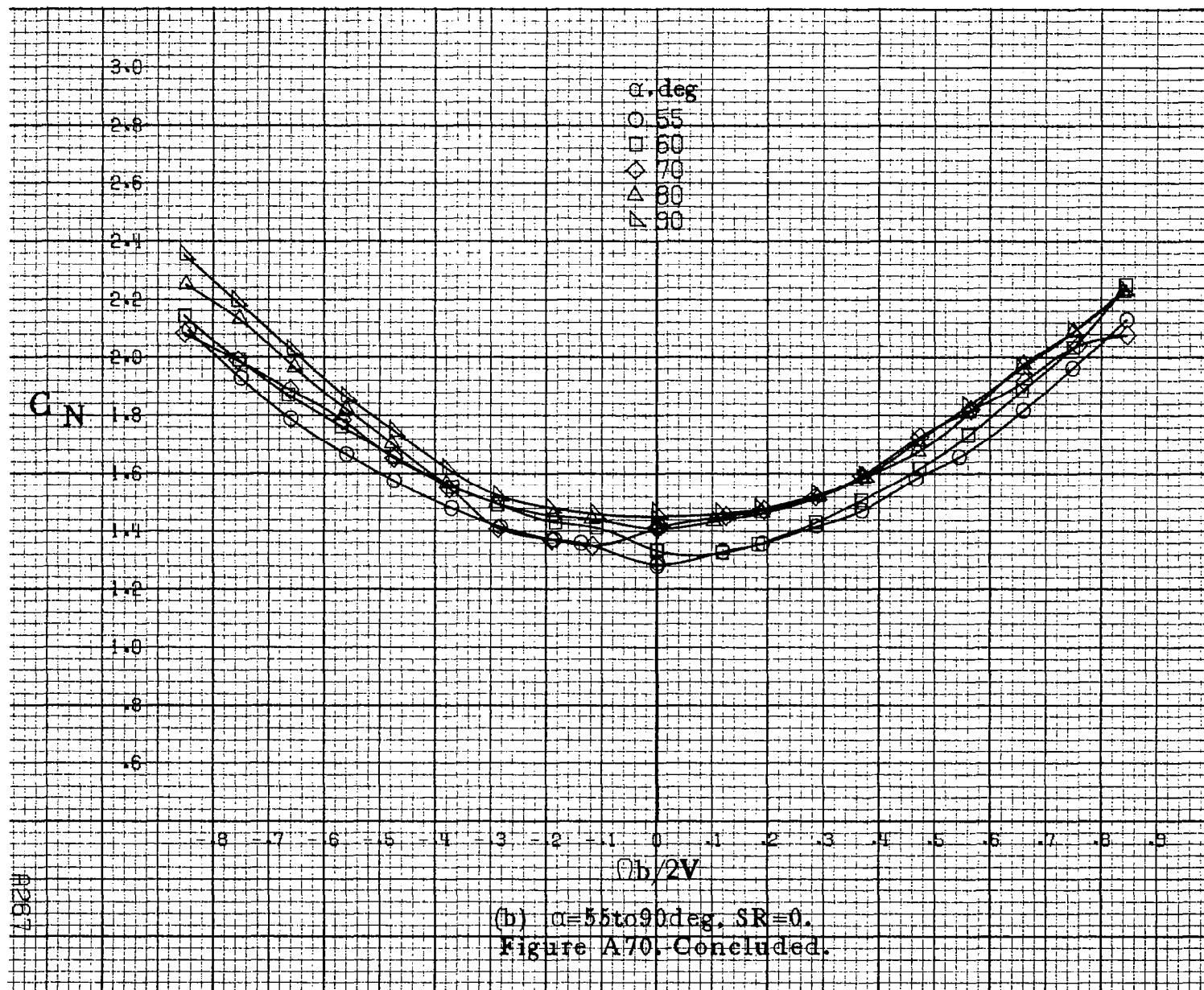
Figure A69.-Effect of rotation rate and angle of attack on pitching-moment coefficient for configuration having sharp-edged fuselage bottom with ventrals and strakes off. $\delta_a = 0^\circ$, $\delta_z = 0^\circ$, $\delta_r = 0^\circ$, $\beta = 0^\circ$.

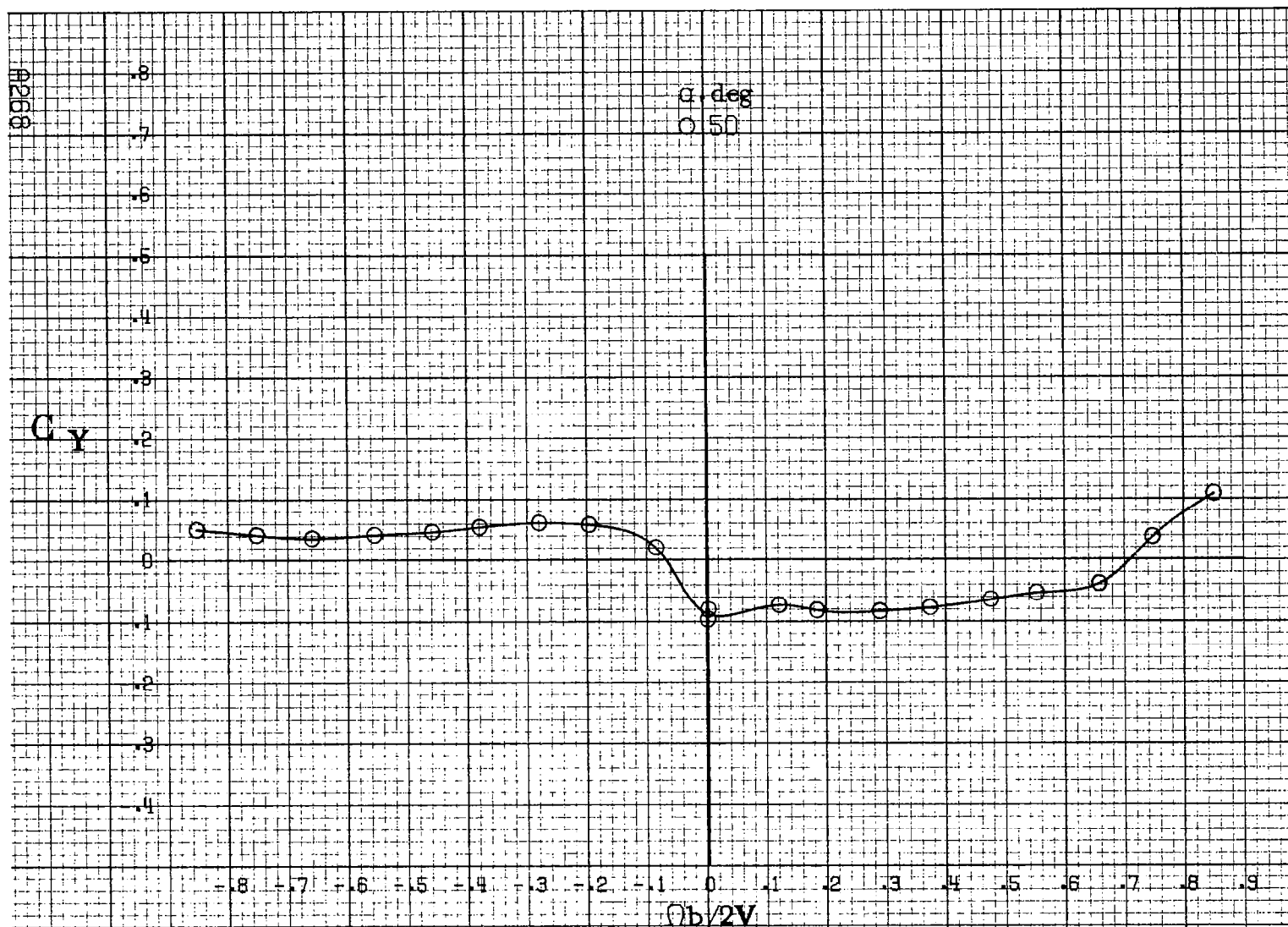




(a) $\alpha = 50^\circ$, $SR=0$.

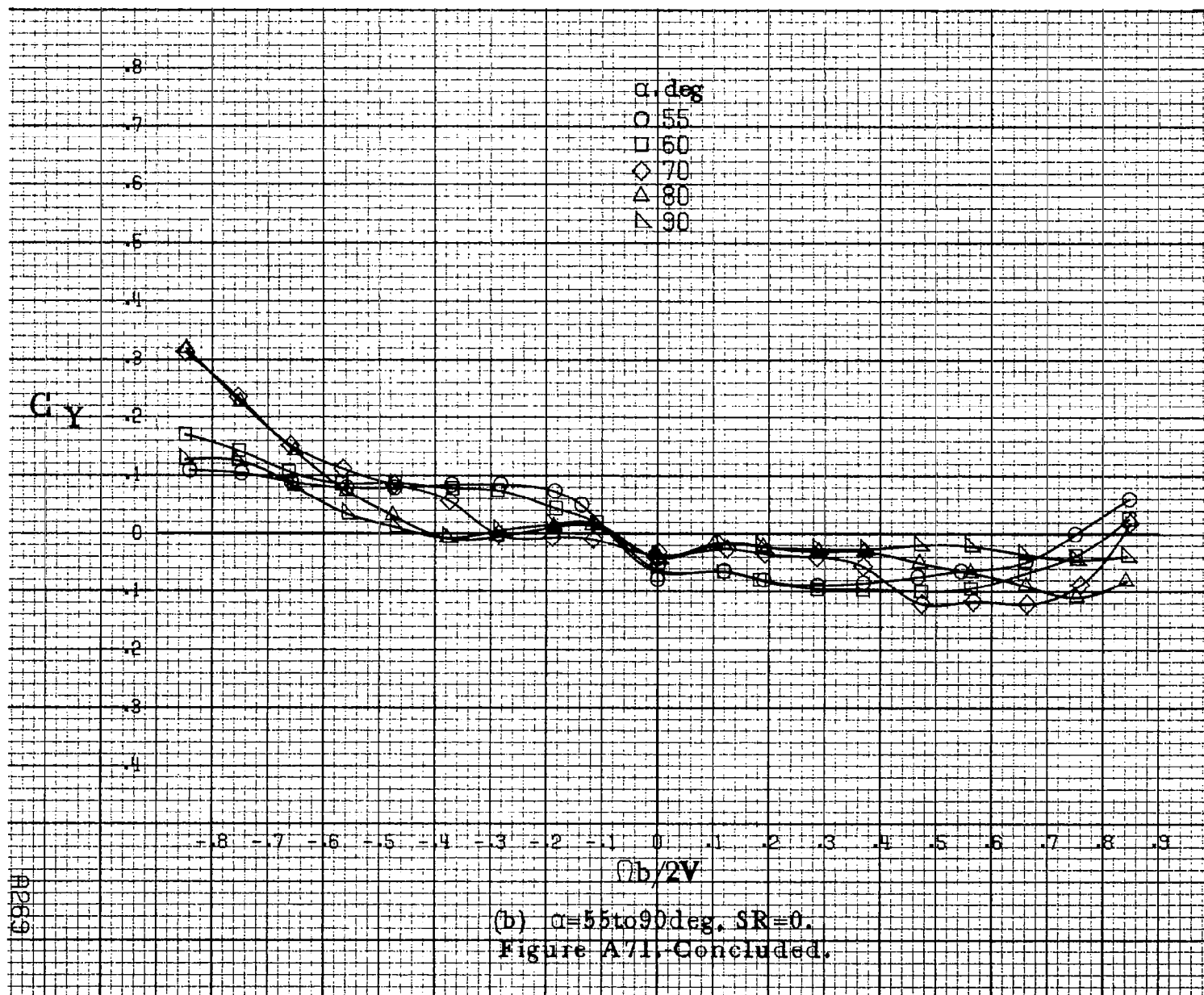
Figure A70. Effect of rotation rate and angle of attack on normal-force coefficient for configuration having sharp-edged fuselage bottom with ventrals and strakes off. $\delta_a = 0^\circ$, $\delta_s = 0^\circ$, $\delta_r = 0^\circ$, $\beta = 0^\circ$.

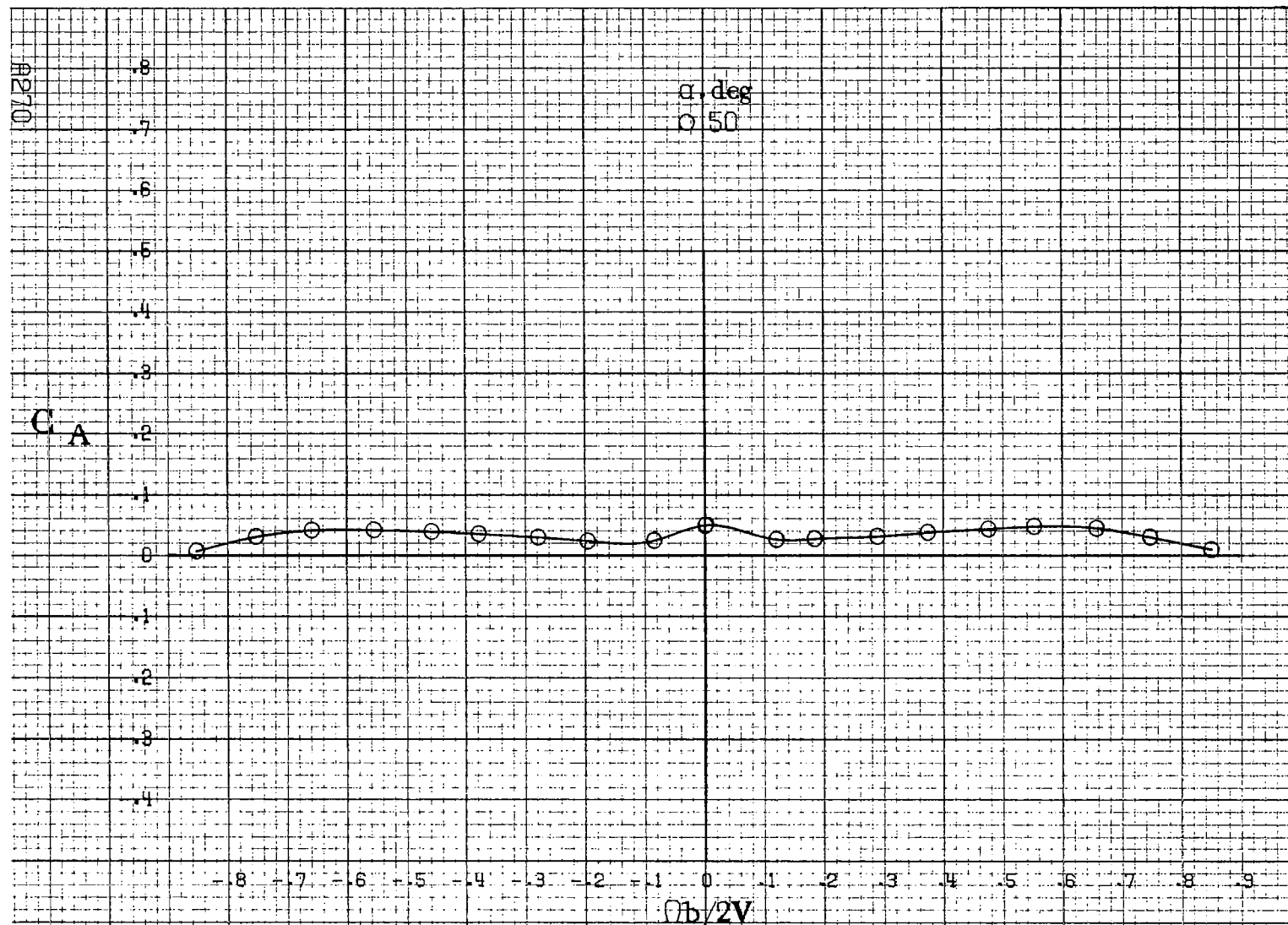




(a) $\alpha = 50$ deg, $SR=0$.

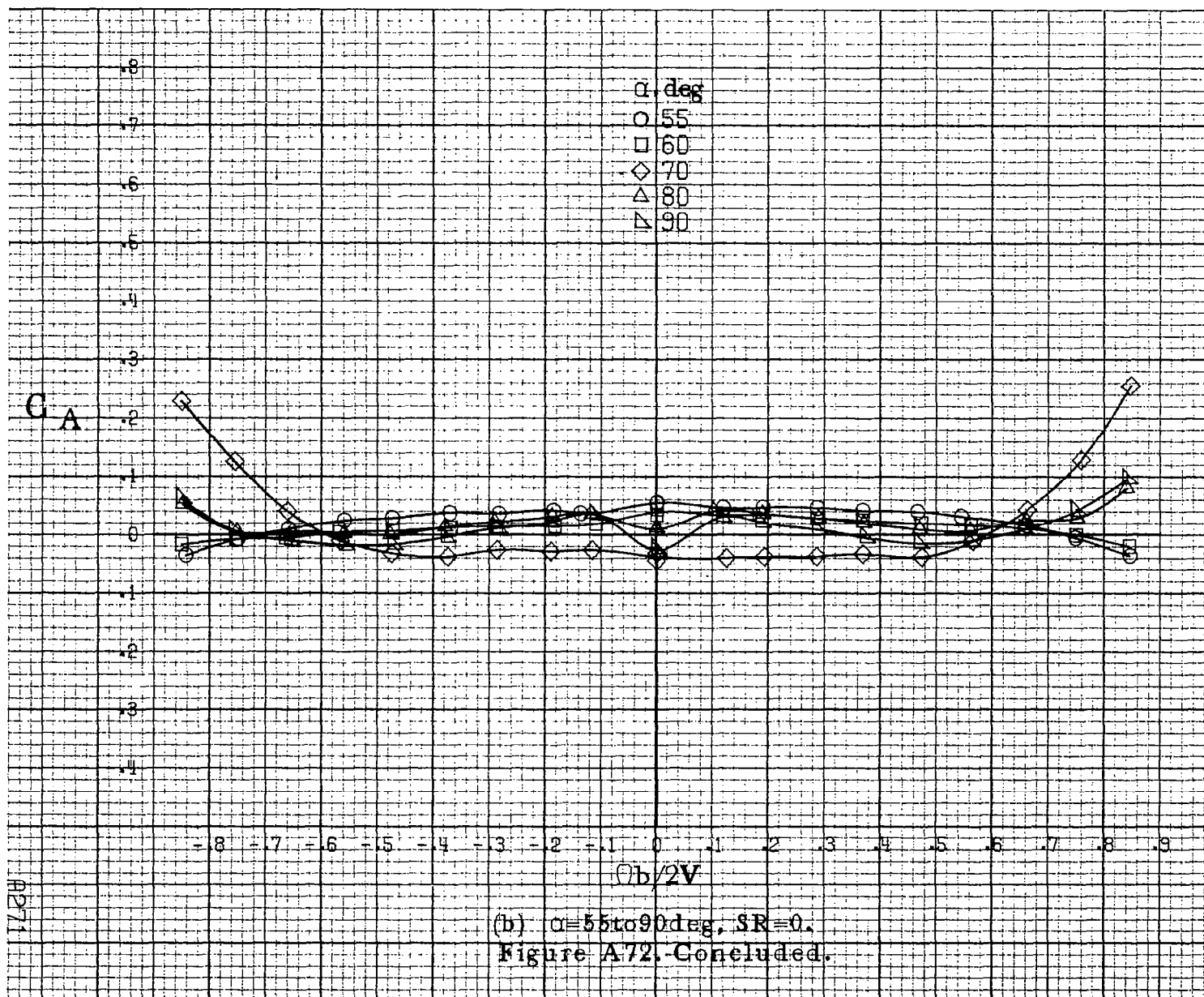
Figure A71. Effect of rotation rate and angle of attack on side-force coefficient for configuration having sharp-edged fuselage bottom with ventrals and strakes off. $\delta_e = 0^\circ$, $\delta_a = 0^\circ$, $\delta_r = 0^\circ$, $\beta = 0^\circ$.

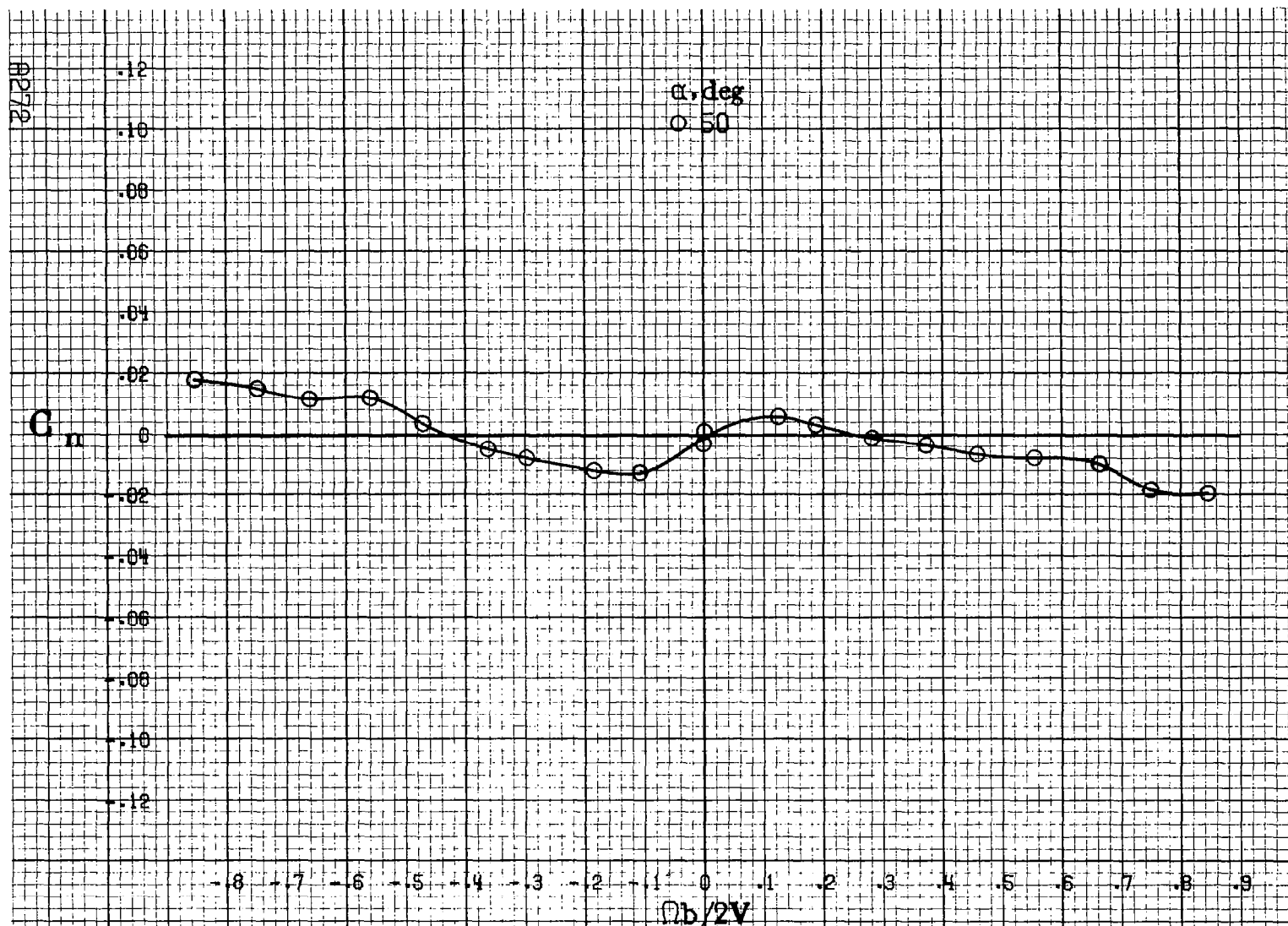




(a) $\alpha = 50^\circ$, $SR=0$.

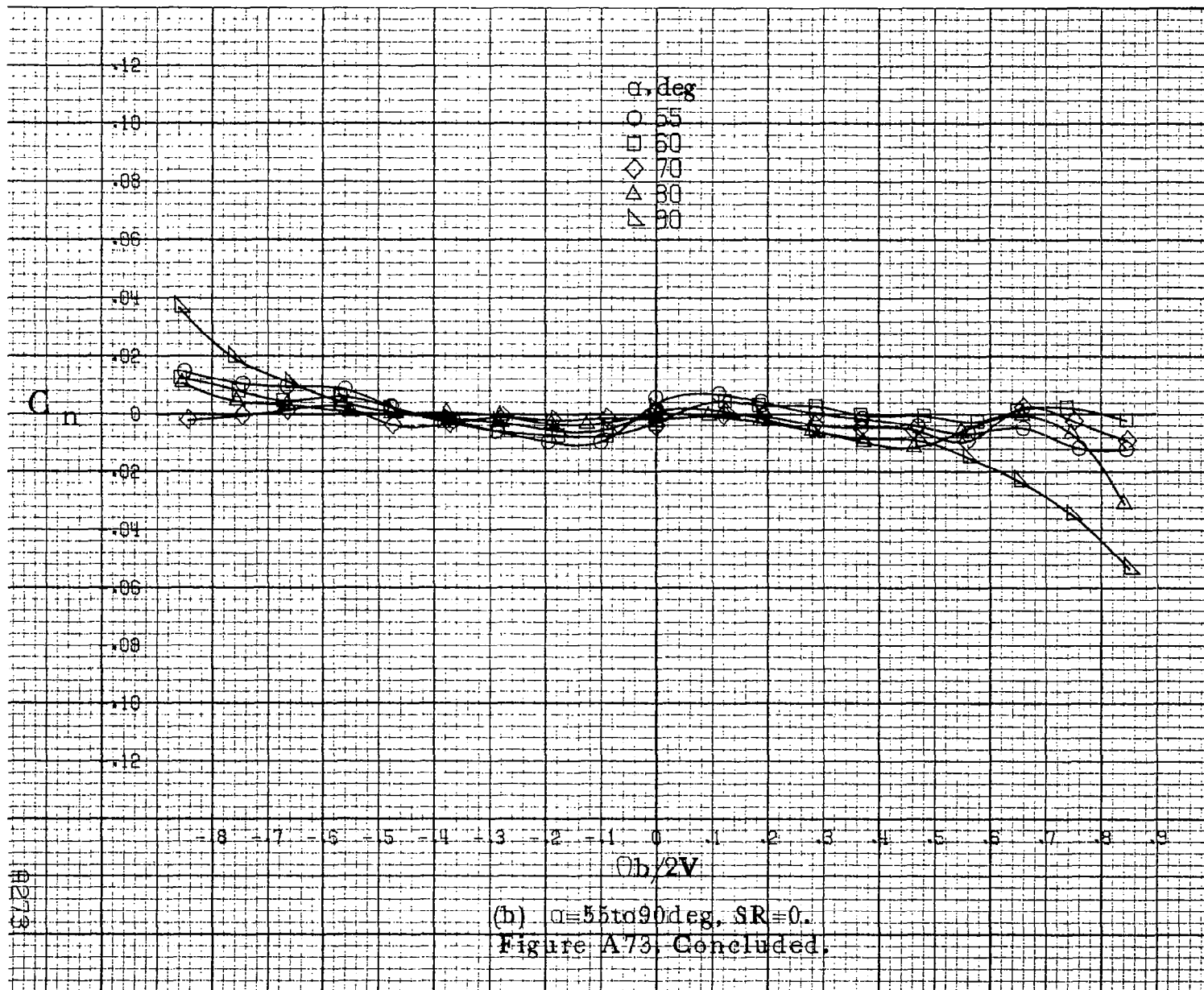
Figure A-72. Effect of rotation rate and angle of attack on axial force coefficient for configuration having sharp-edged fuselage bottom with ventrals and strakes off. $\delta_a = 0^\circ$, $\delta_s = 0^\circ$, $\delta_r = 0^\circ$, $\beta = 0^\circ$.

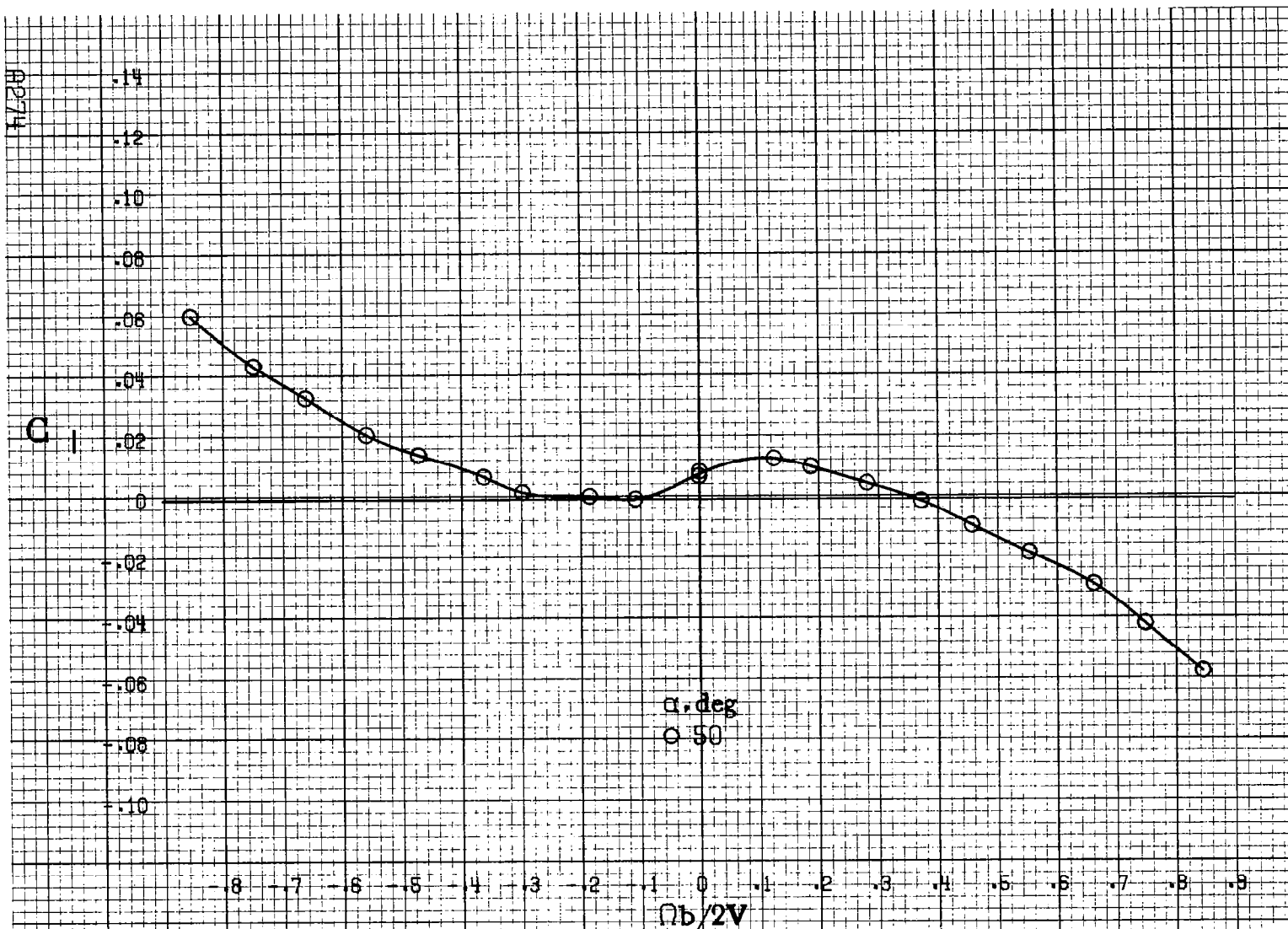




(a) $\alpha = 50 \text{ deg}$, $SR = 0$.

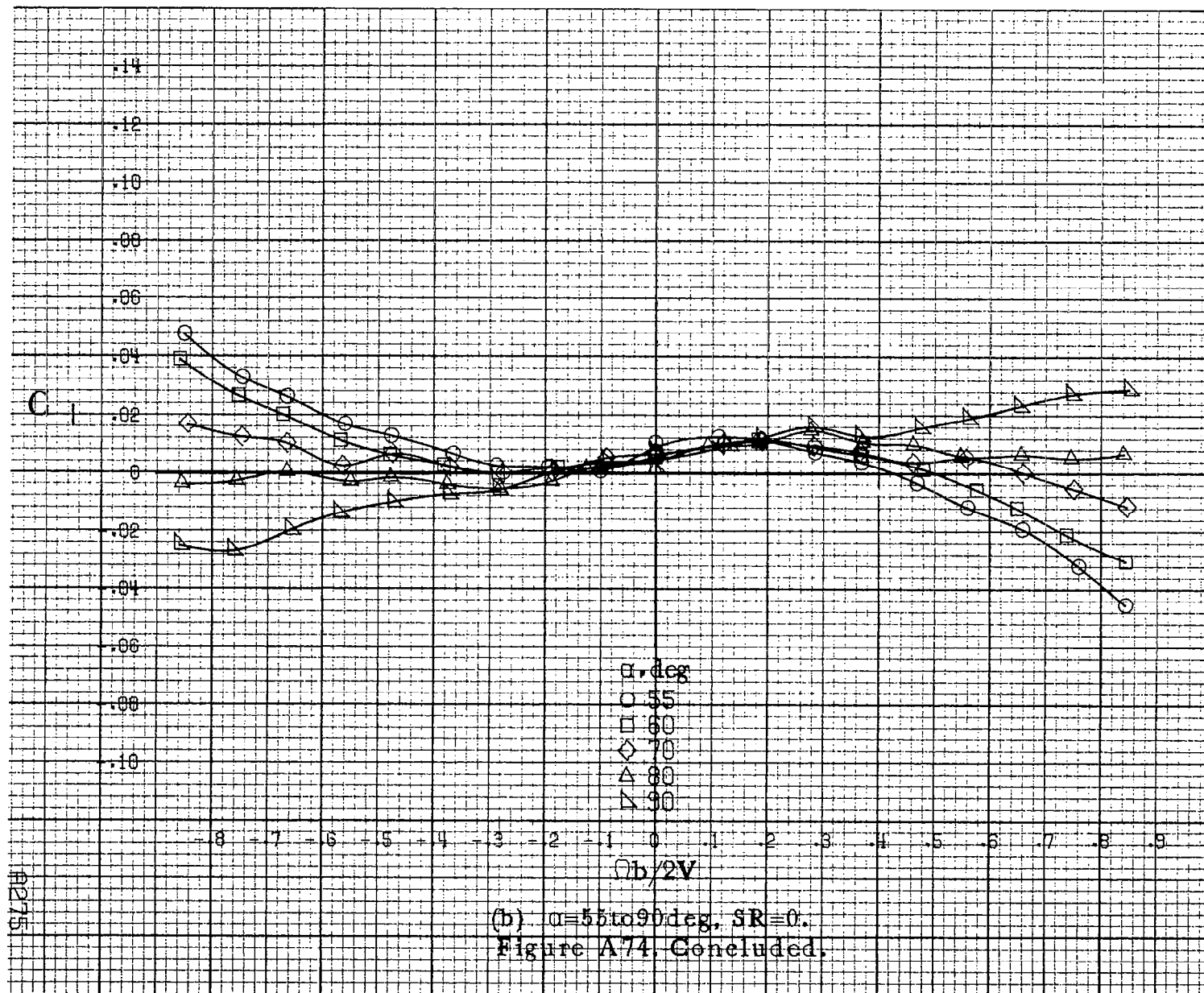
Figure A73.-Effect of rotation rate and angle of attack on yawing-moment coefficient for configuration having sharp-edged fuselage bottom with strakes and engine stacks off. $\delta_e = 0^\circ$, $\delta_a = 0^\circ$, $\delta_r = 0^\circ$, $\beta = 0^\circ$.

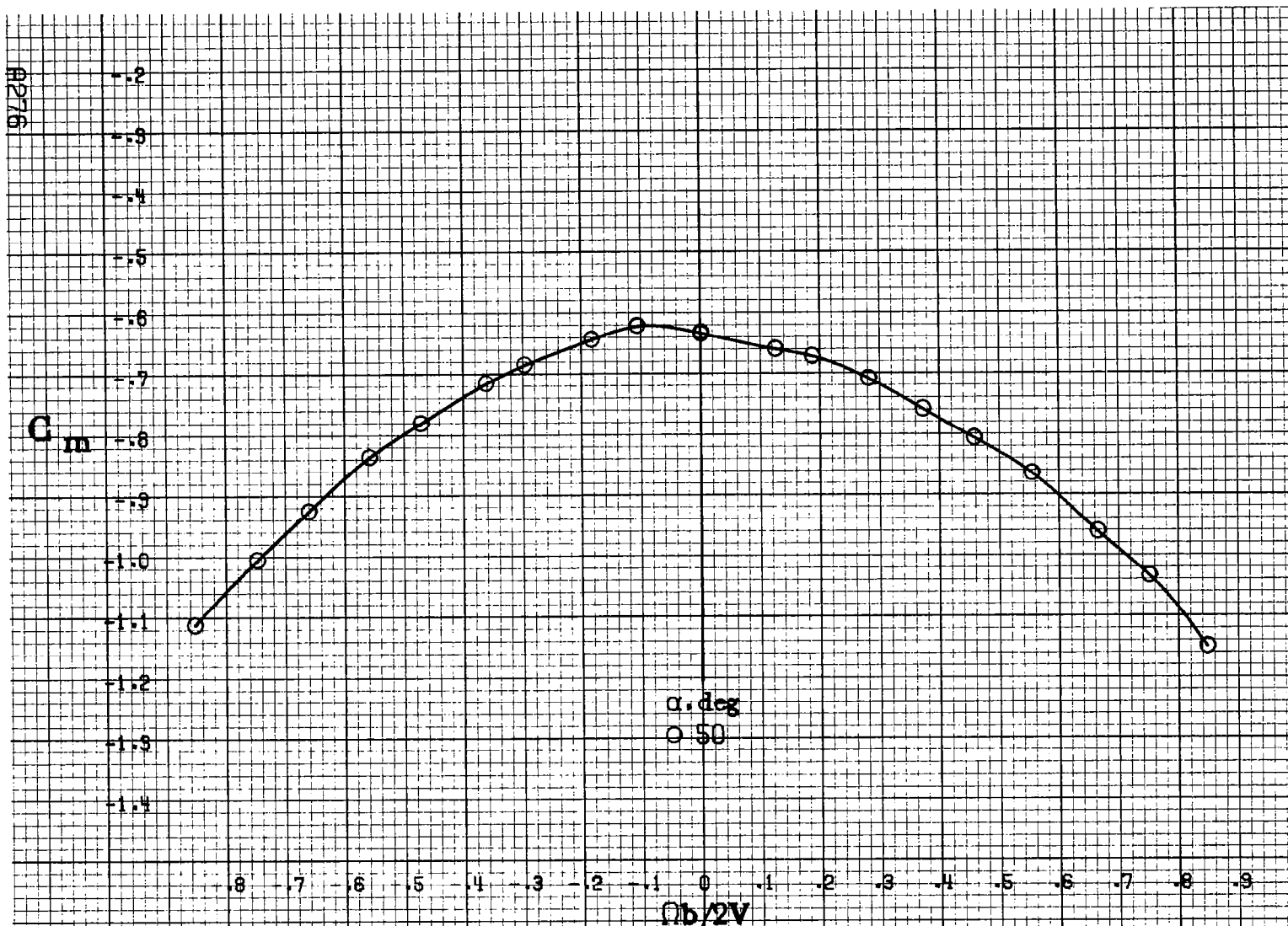




(a) $\alpha = 50^\circ$, $SR = 0$.

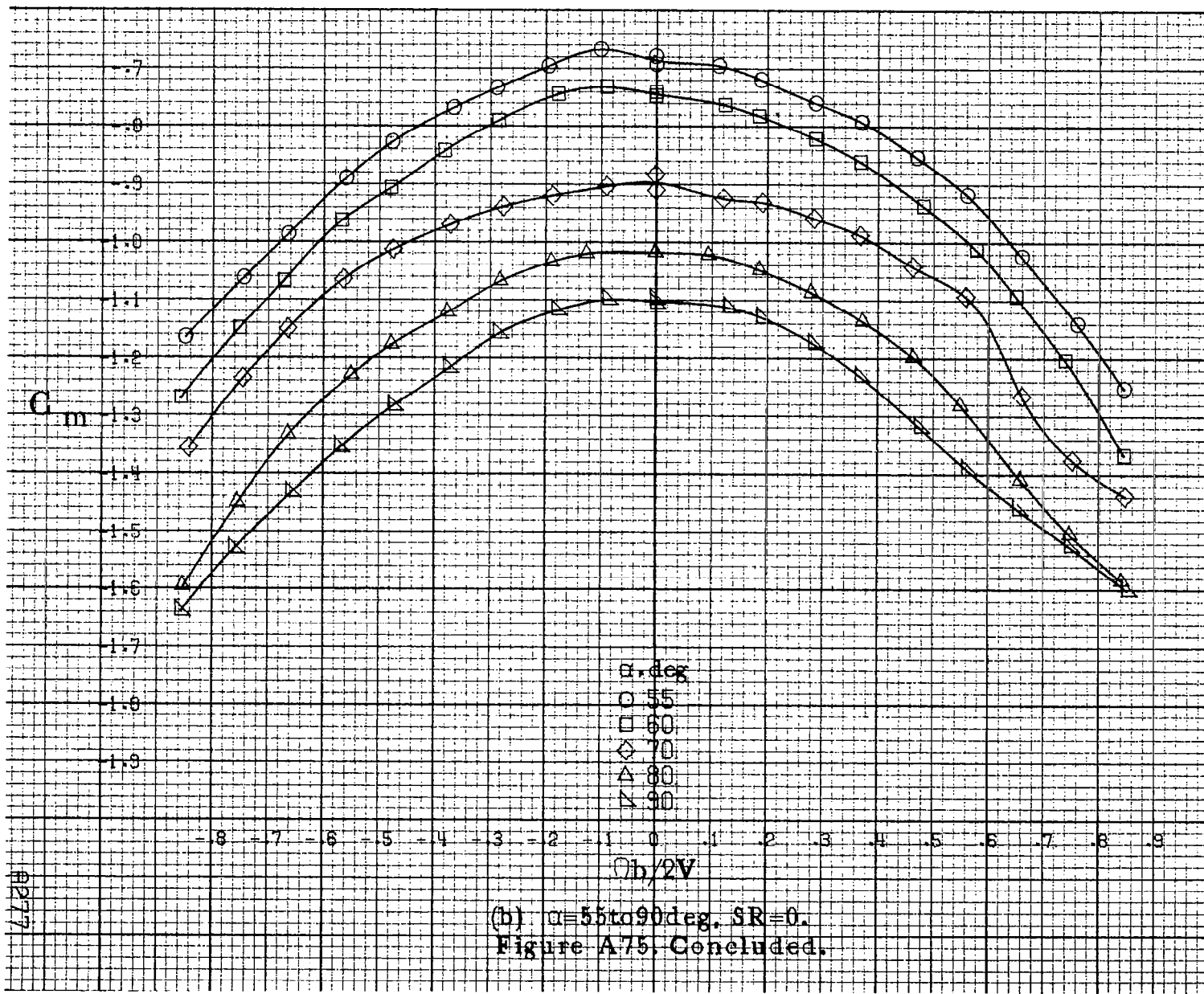
Figure A74. Effect of rotation rate and angle of attack on rolling-moment coefficient for configuration having sharp-edged fuselage bottom with strakes and engine stacks off, $\delta_a = 0^\circ$, $\delta_s = 0^\circ$, $\delta_e = 0^\circ$, $\beta = 0^\circ$.

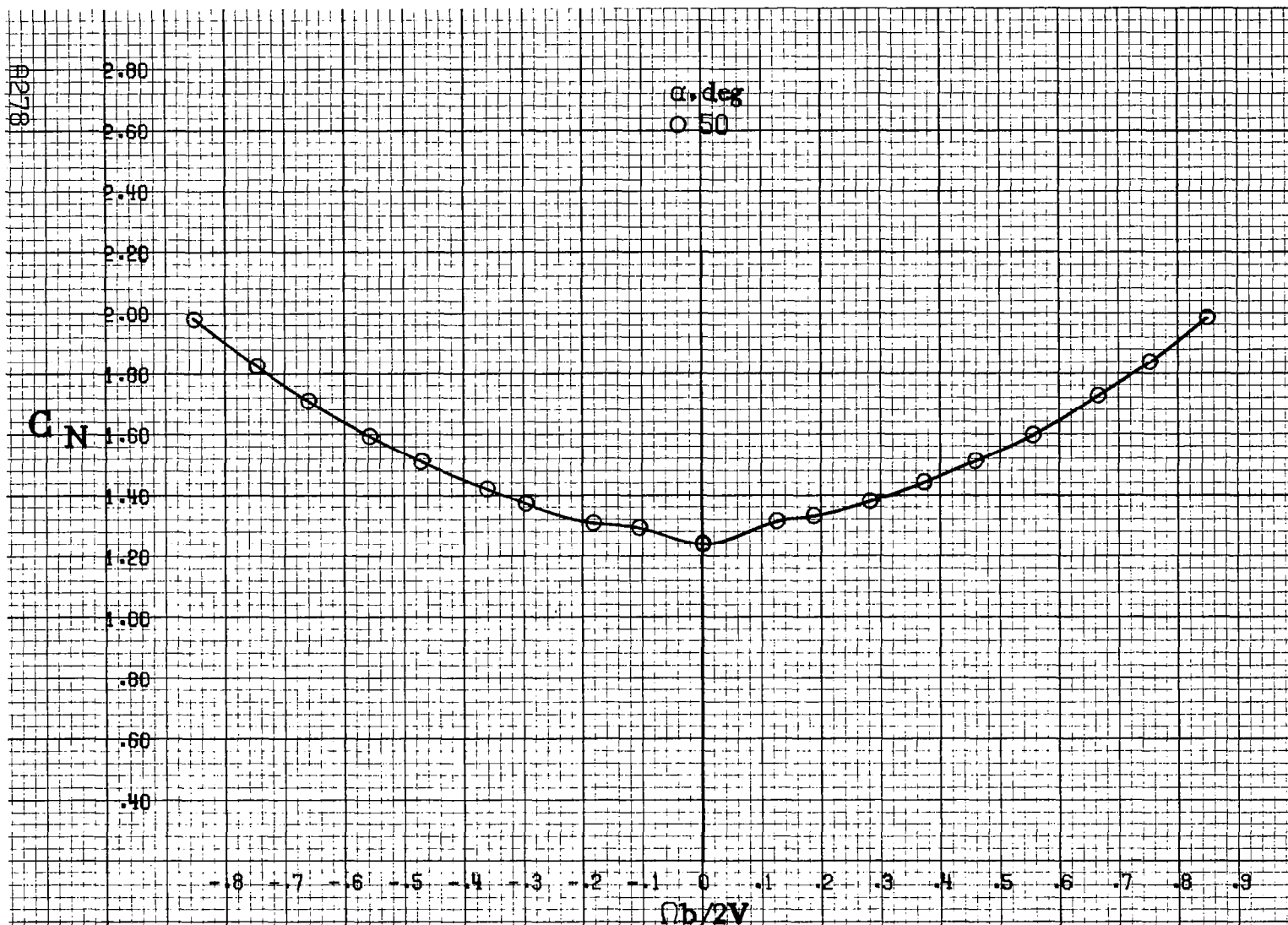




(a) $\alpha = 50^\circ$, $SR = 0$.

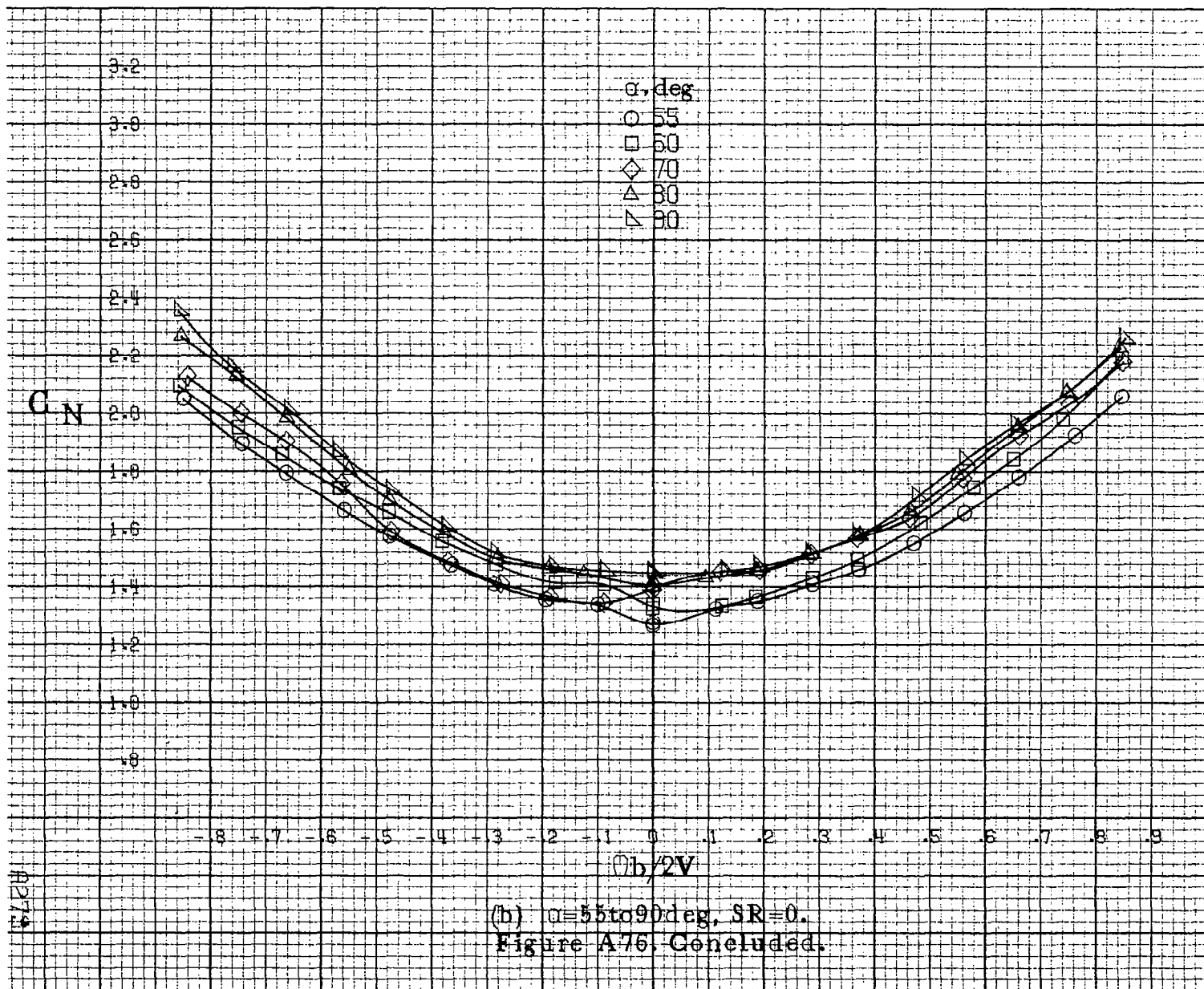
Figure A75. Effect of rotation rate and angle of attack on pitching-moment coefficient for configuration having sharp-edged fuselage bottom with strakes and engine stacks off. $\delta_a = 0^\circ$, $\delta_s = 0^\circ$, $\delta_r = 0^\circ$, $\beta = 0^\circ$.

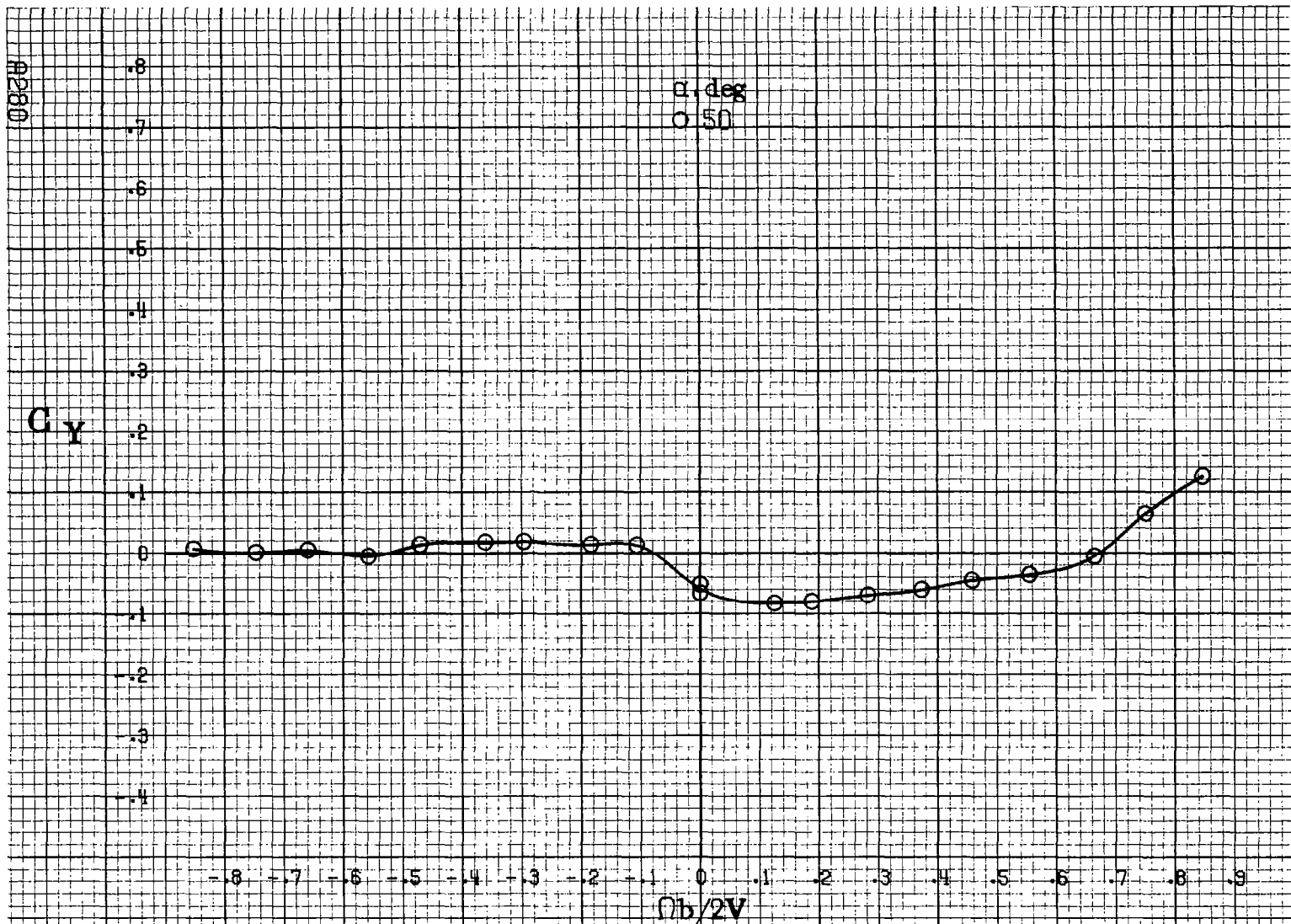




(a) $\alpha = 50 \text{ deg}$, $SR = 0$.

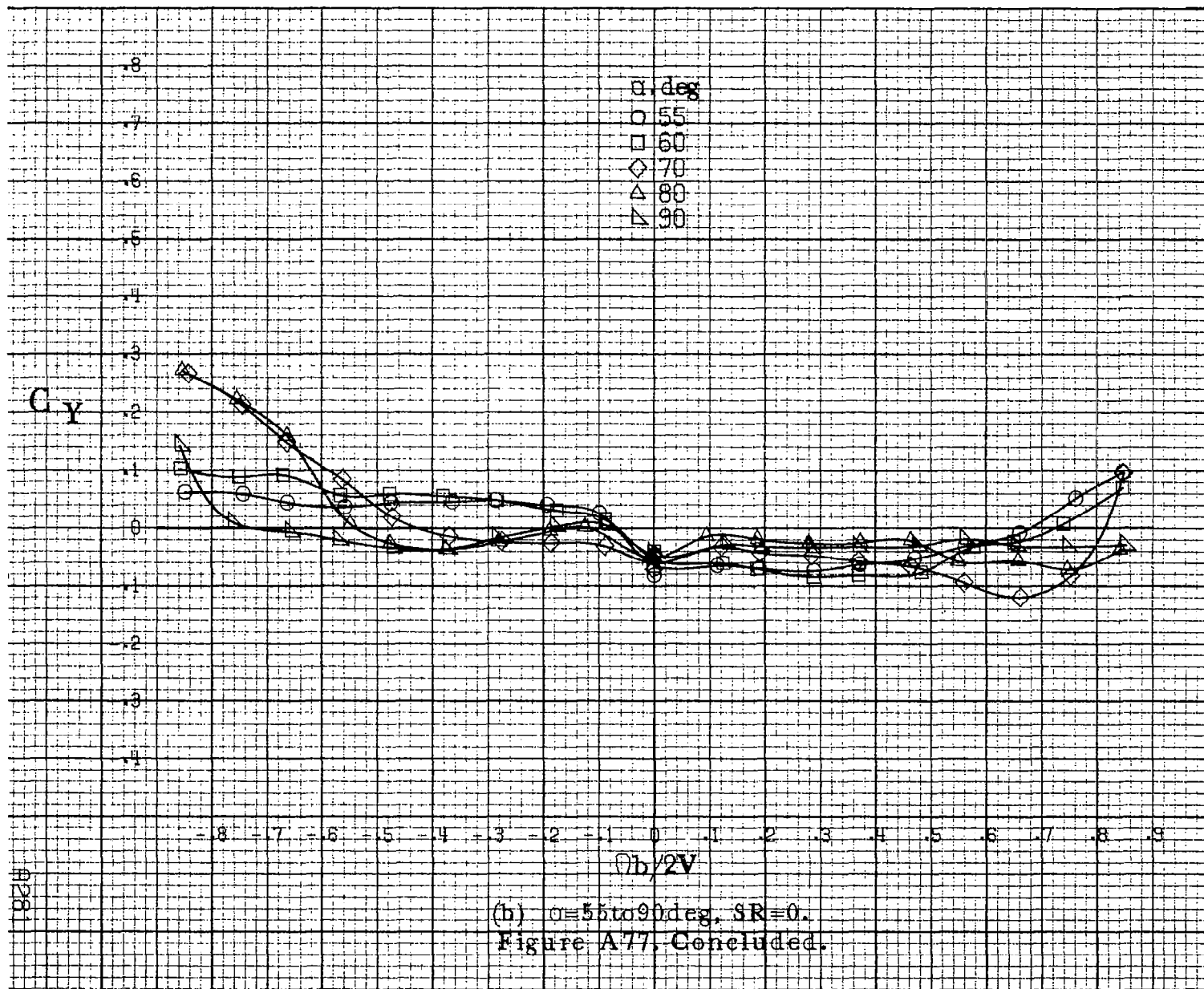
Figure A76. Effect of rotation rate and angle of attack on normal force coefficient for configuration having sharp-edged fuselage bottom with strakes and engine stacks off. $\delta_a = 0^\circ$, $\delta_s = 0^\circ$, $\delta_z = 0^\circ$, $\beta = 0^\circ$.



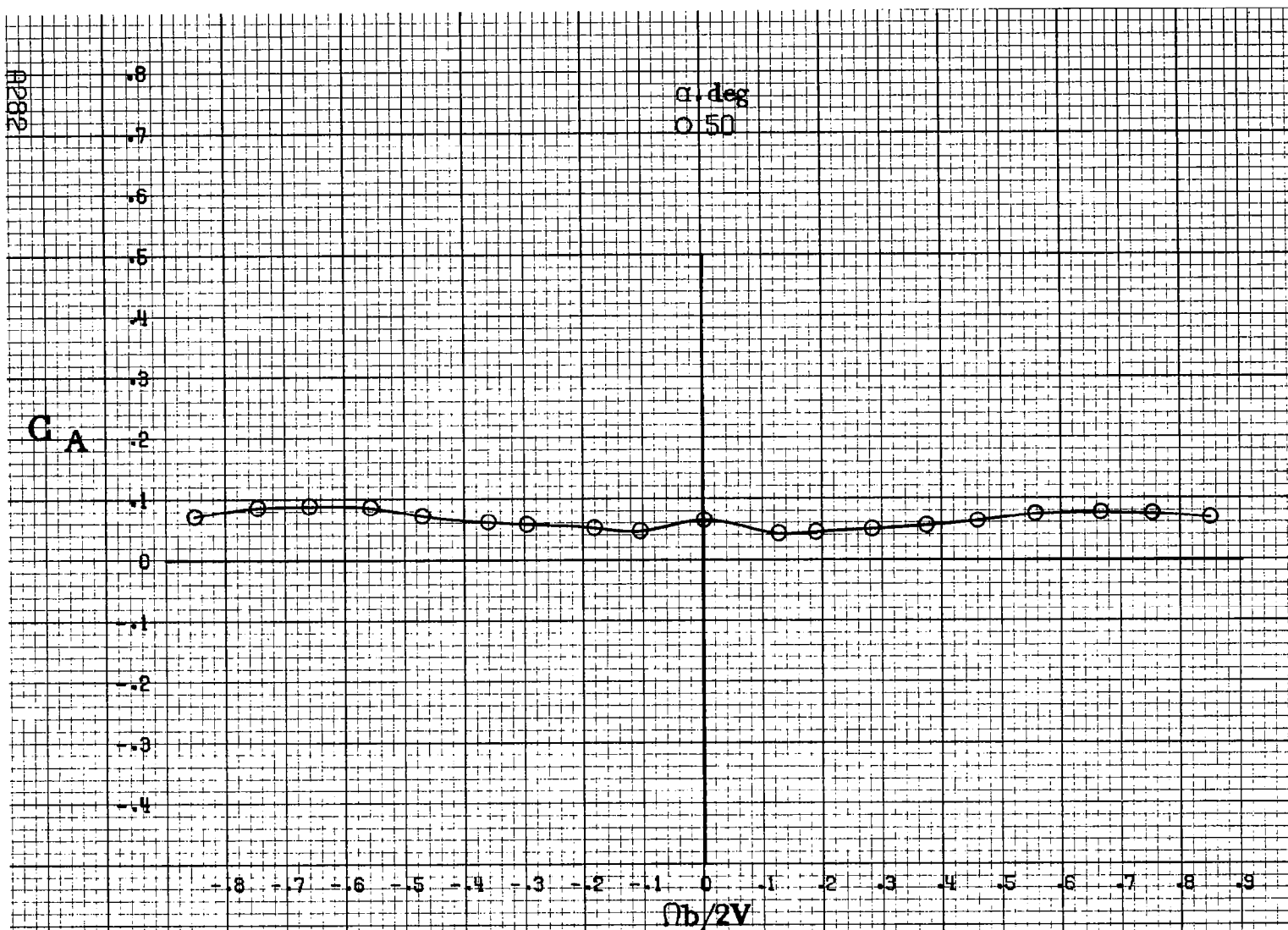


(a) $\alpha = 50^\circ$, $SR = 0$.

Figure A77. Effect of rotation rate and angle of attack on side force coefficient; for configuration having sharp-edged fuselage bottom with strakes and engine stacks off. $\delta_e = 0^\circ$, $\delta_a = 0^\circ$, $\delta_z = 0^\circ$, $\beta = 0^\circ$.

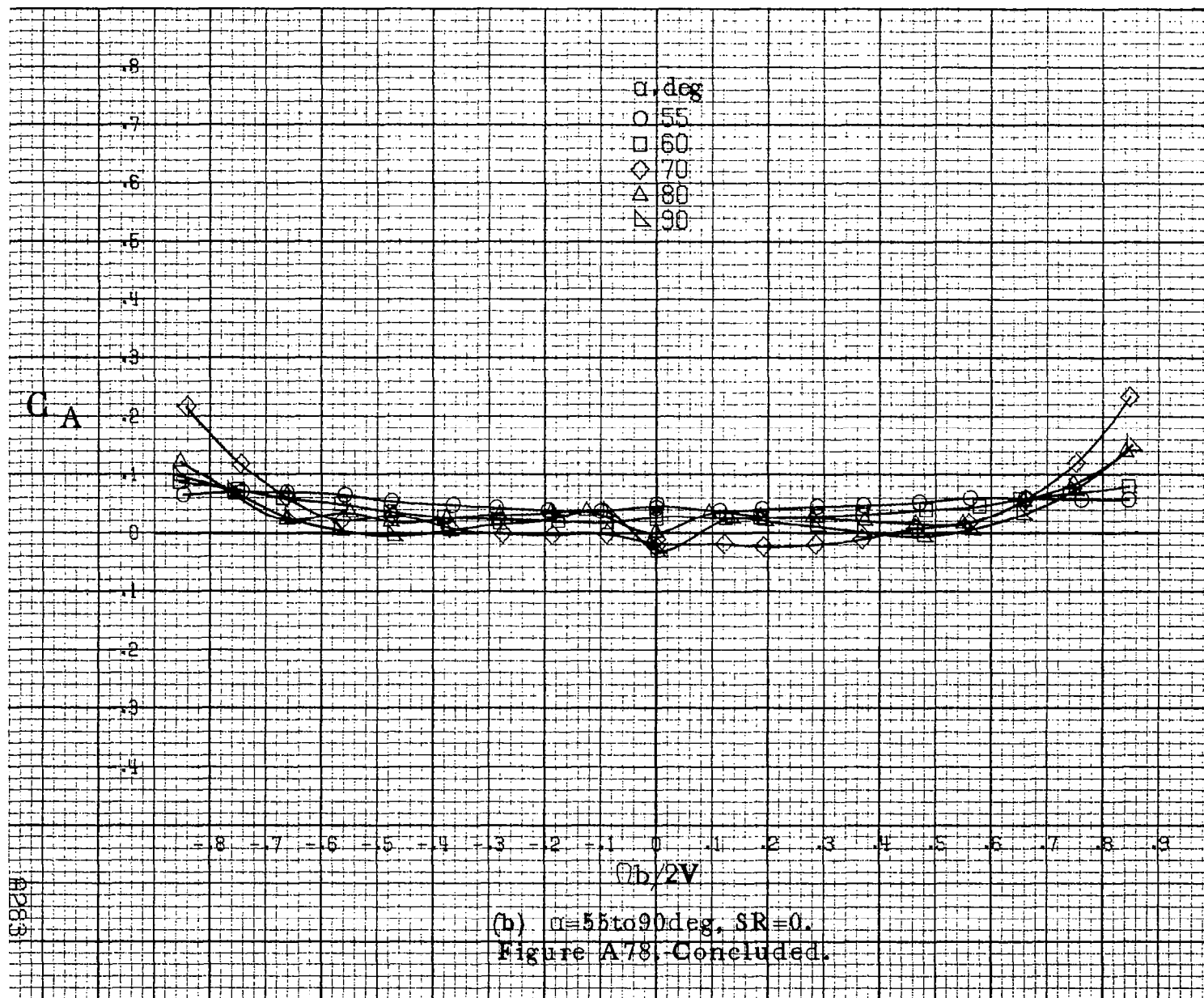


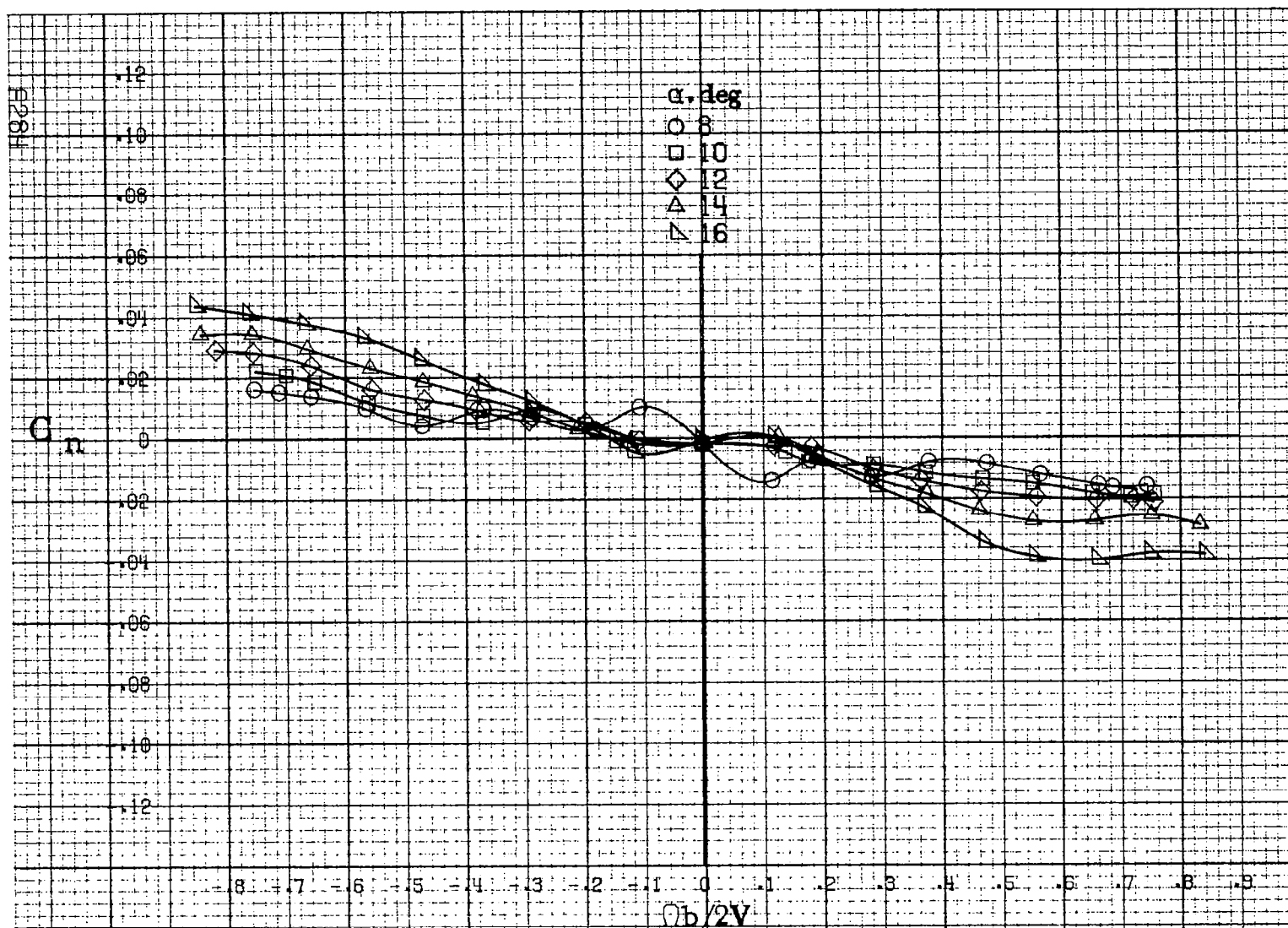
(b) $\alpha = 55$ to 90° , $SR = 0$.
Figure A77. Concluded.



(a) $\alpha = 50$ deg, $SR = 0$.

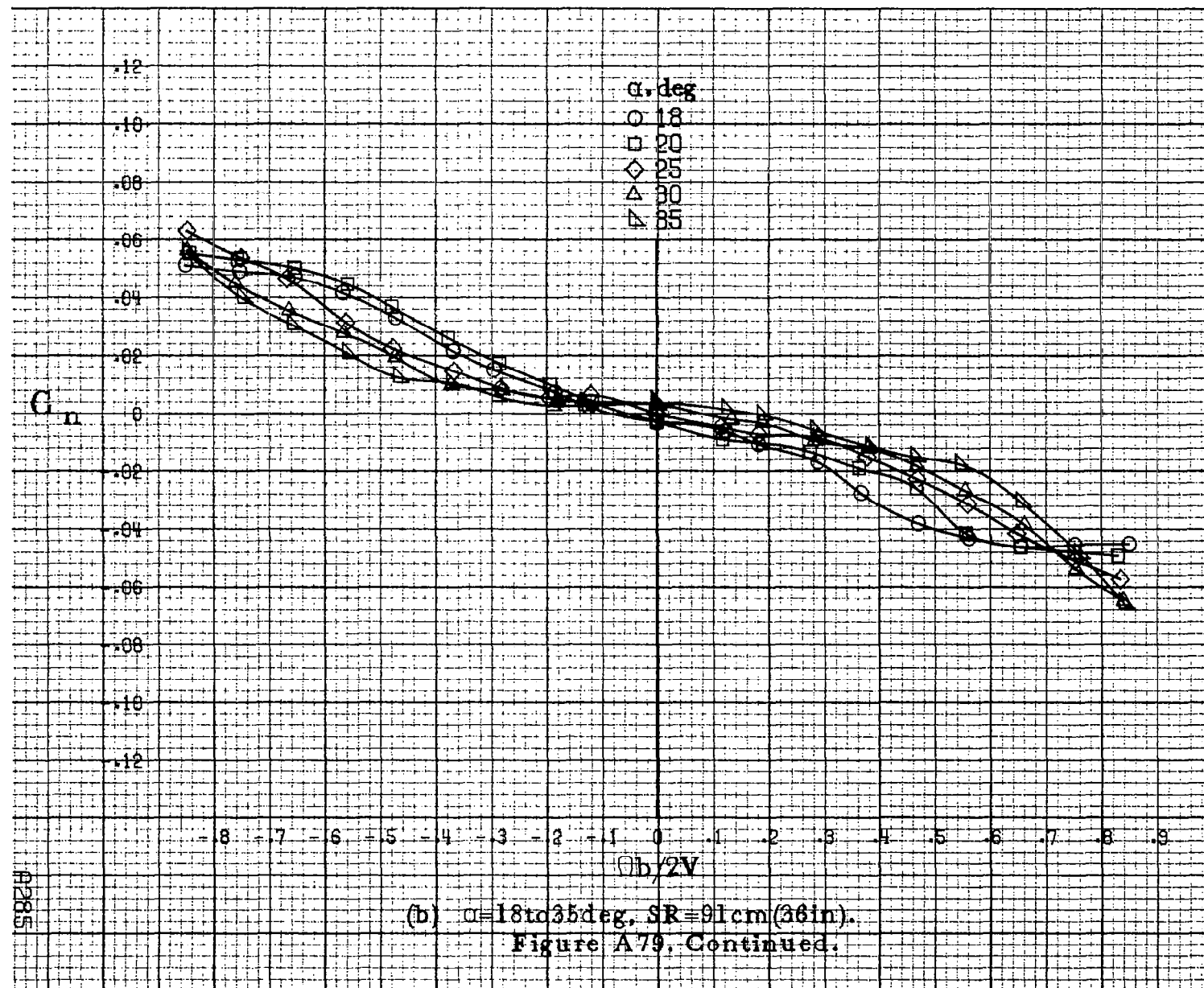
Figure A78. Effect of rotation rate and angle of attack on axial-force coefficient for configuration having sharp-edged fuselage bottom with strakes and engine stacks off. $\delta_s = 0^\circ$, $\delta_e = 0^\circ$, $\delta_r = 0^\circ$, $\beta = 0^\circ$.

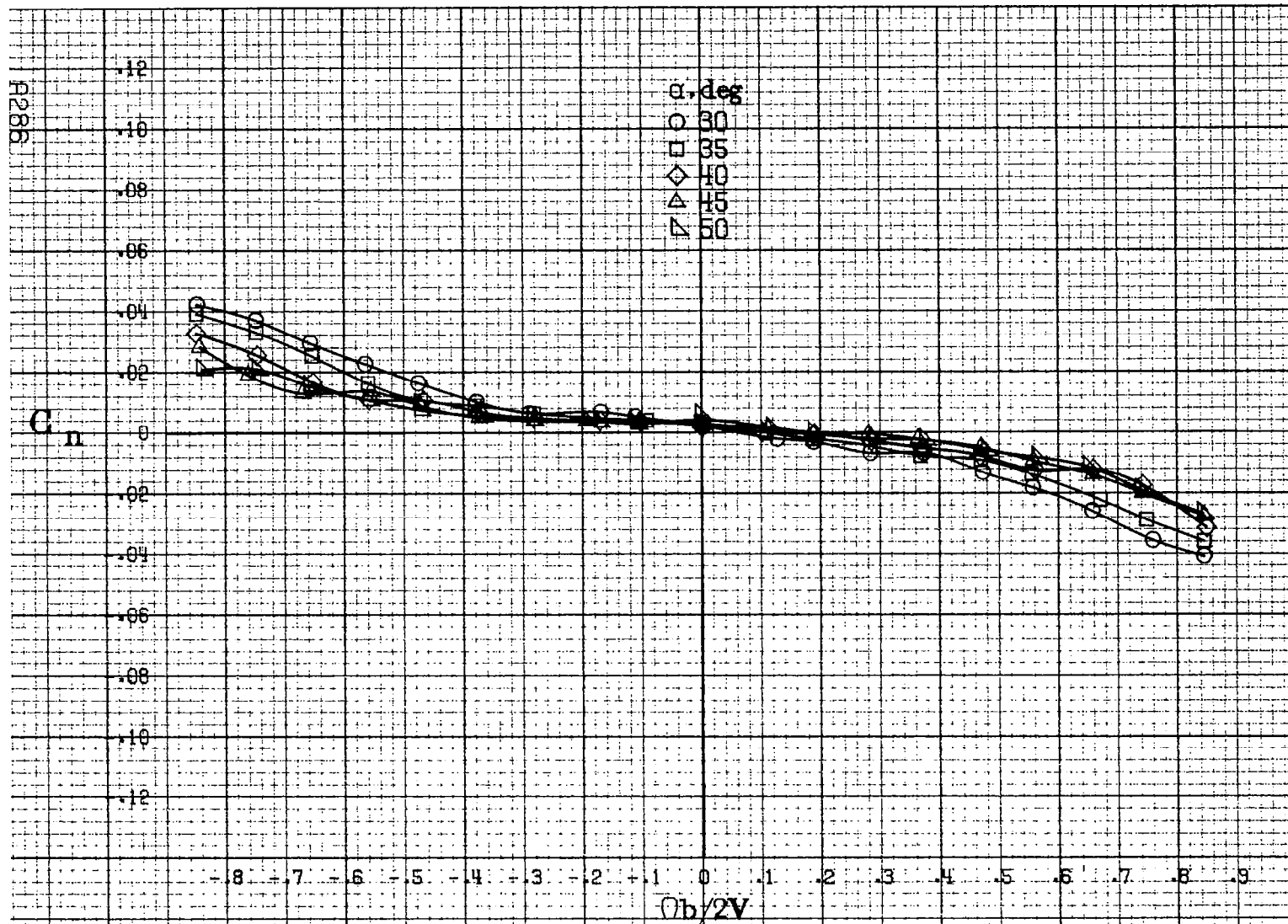




(a) $\alpha=8$ to 16° , $SR=91\text{cm}(36\text{in})$.

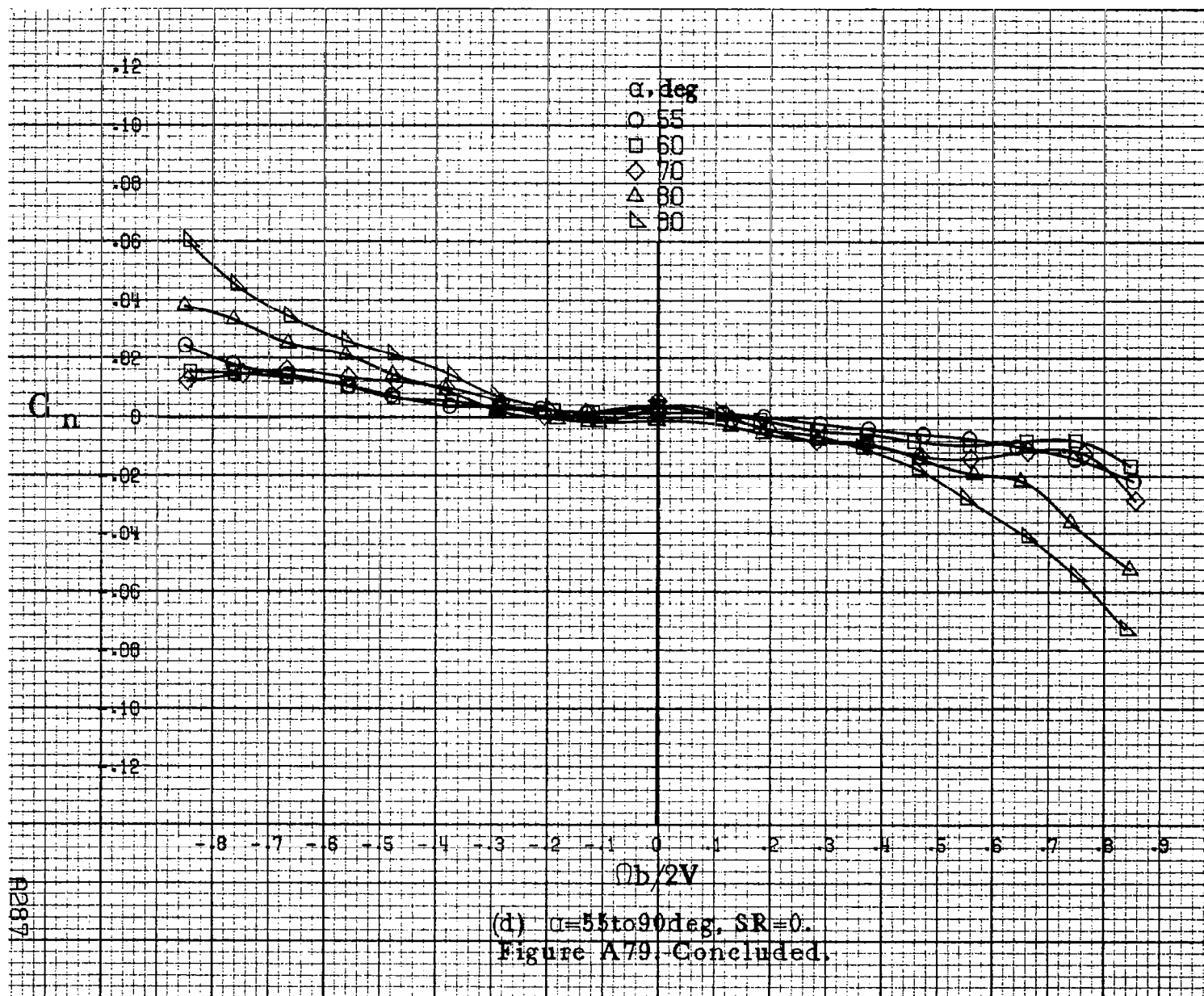
Figure A 79. Effect of rotation rate and angle of attack on yawing-moment coefficient for configuration having sharp-edged fuselage bottom and a 49.8cm (19.6in) span outboard LE wing droop. $\delta_a=0^\circ$, $\delta_s=0^\circ$, $\delta_c=0^\circ$, $\beta=0^\circ$.

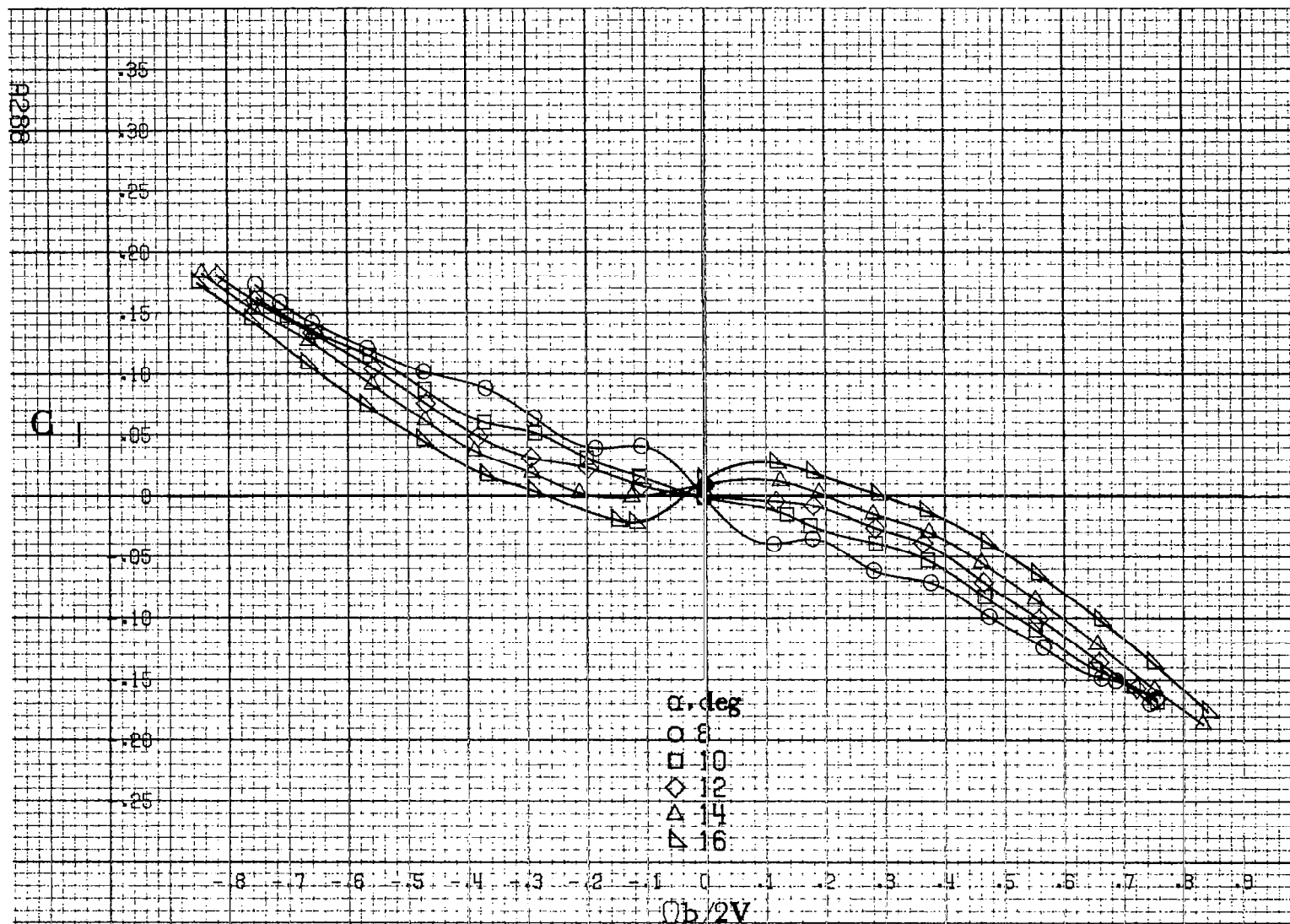




(c) $\alpha=30$ to 50 deg, $SR=0$.

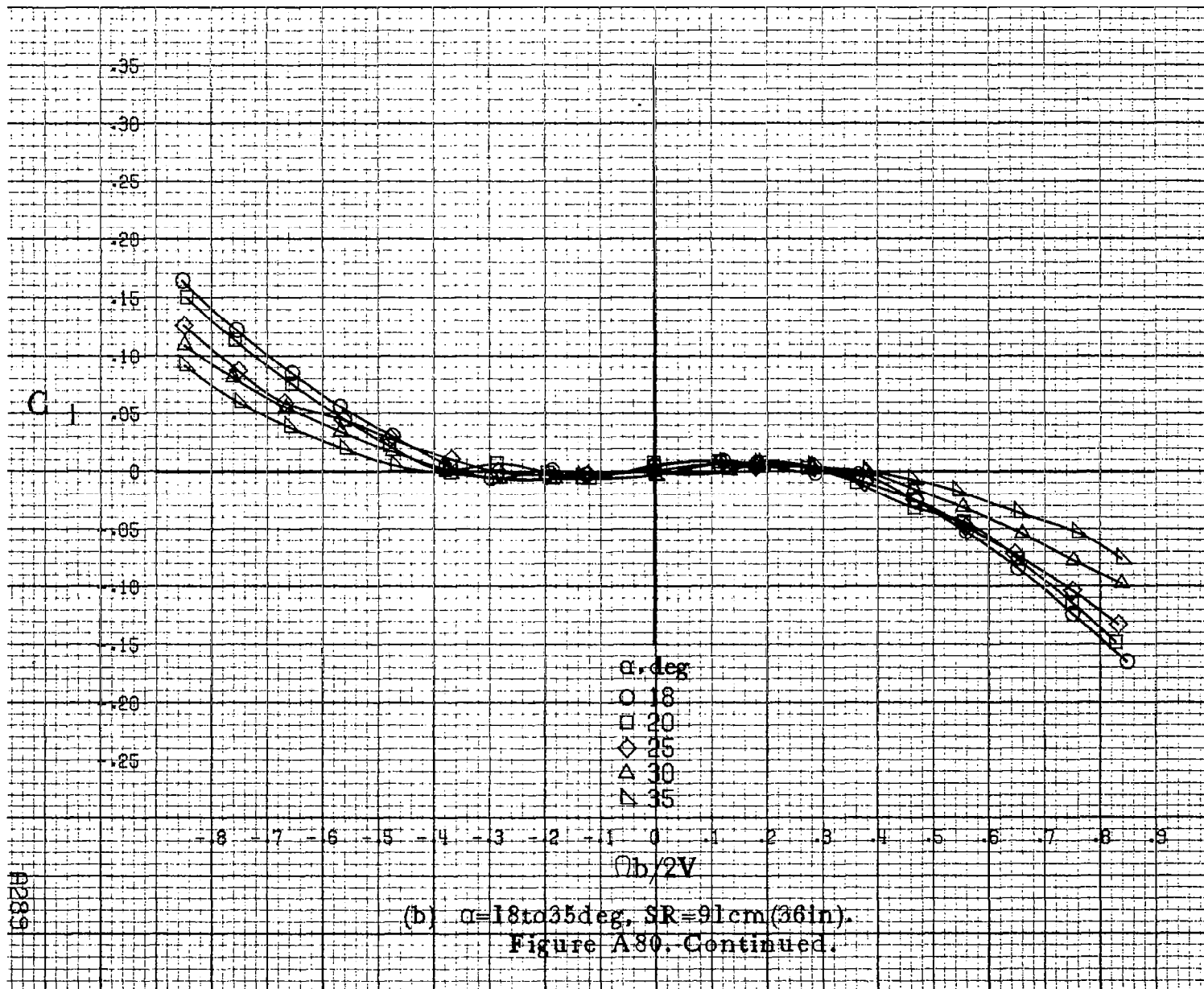
Figure A79. Continued.

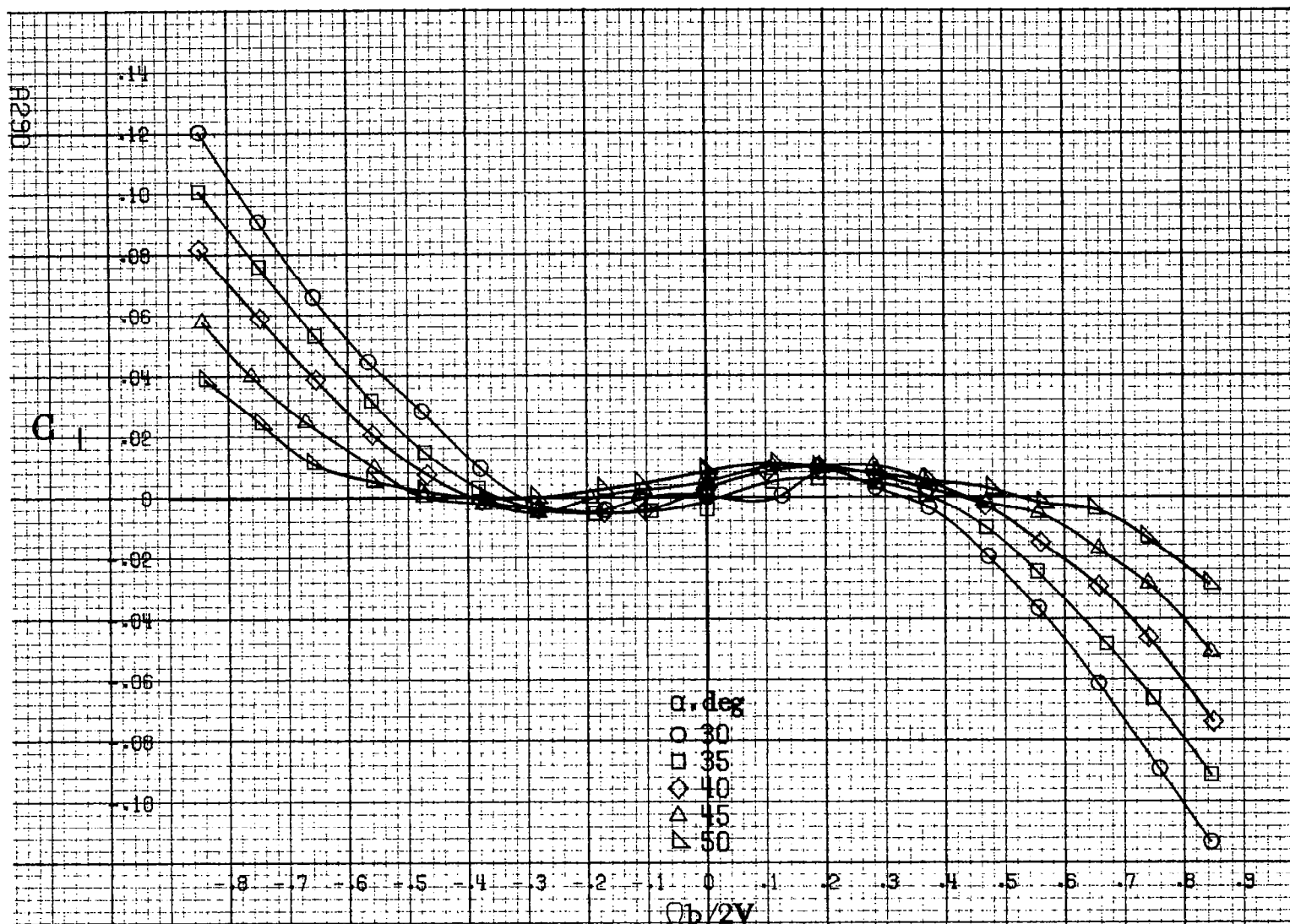




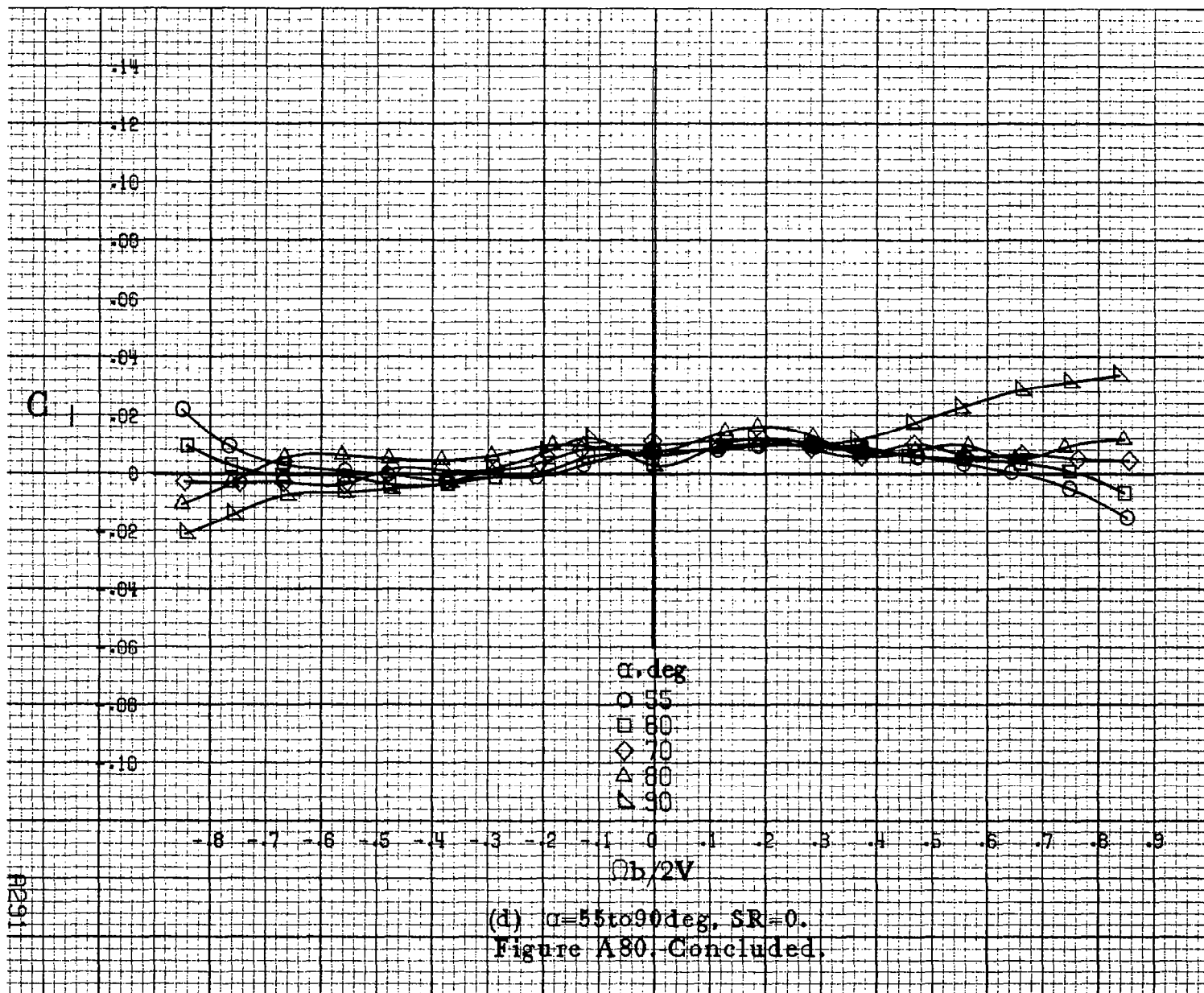
(a) $\alpha=8$ to 16 deg, $SR=91$ cm (36 in).

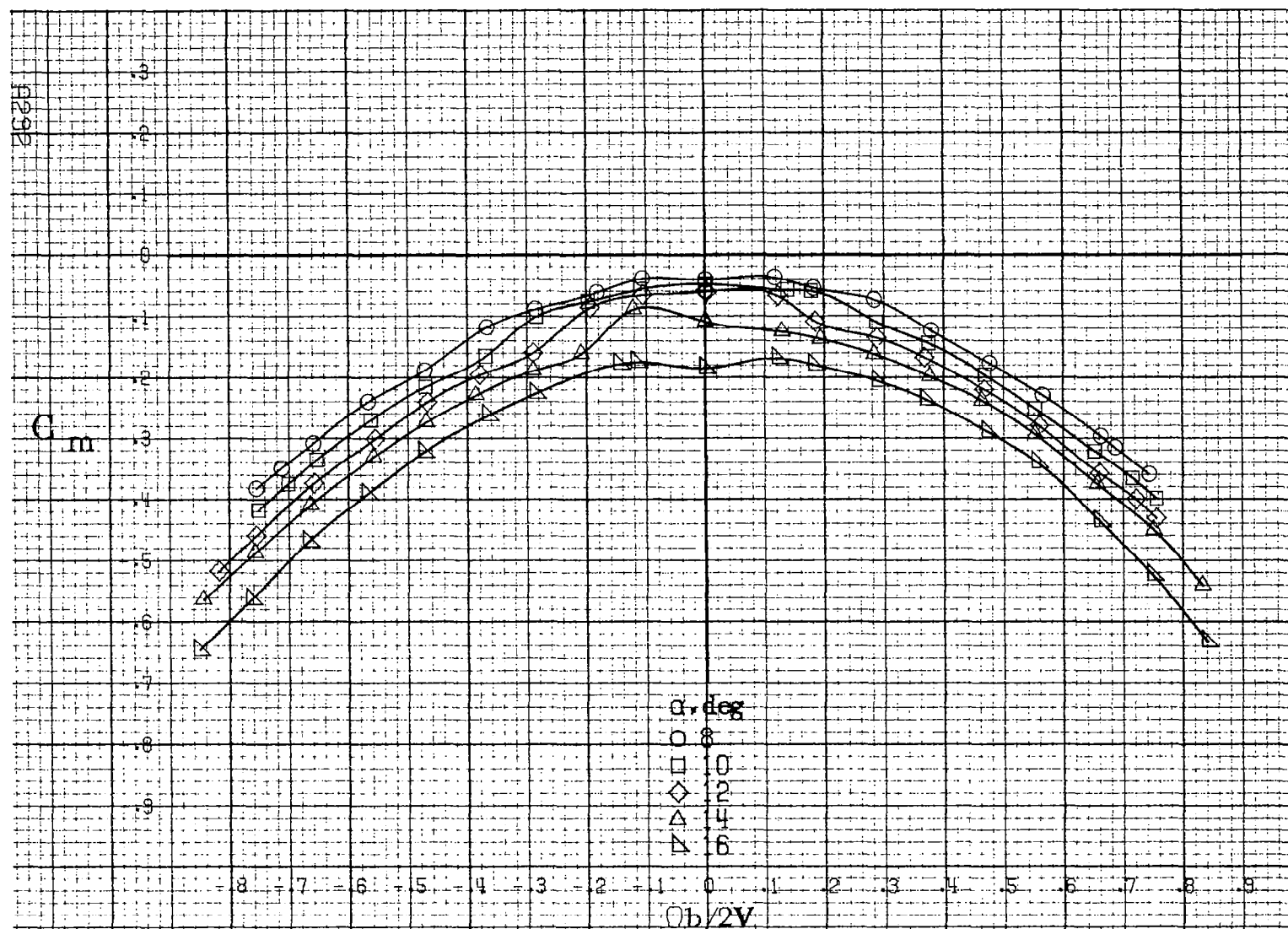
Figure A80. Effect of rotation rate and angle of attack on rolling-moment coefficient for configuration having sharp edged fuselage bottom and a 49.8 cm (19.6 in) span outboard LE wing droop. $\delta_a = 0^\circ$, $\delta_a = 0^\circ$, $\delta_r = 0^\circ$, $\beta = 3^\circ$.





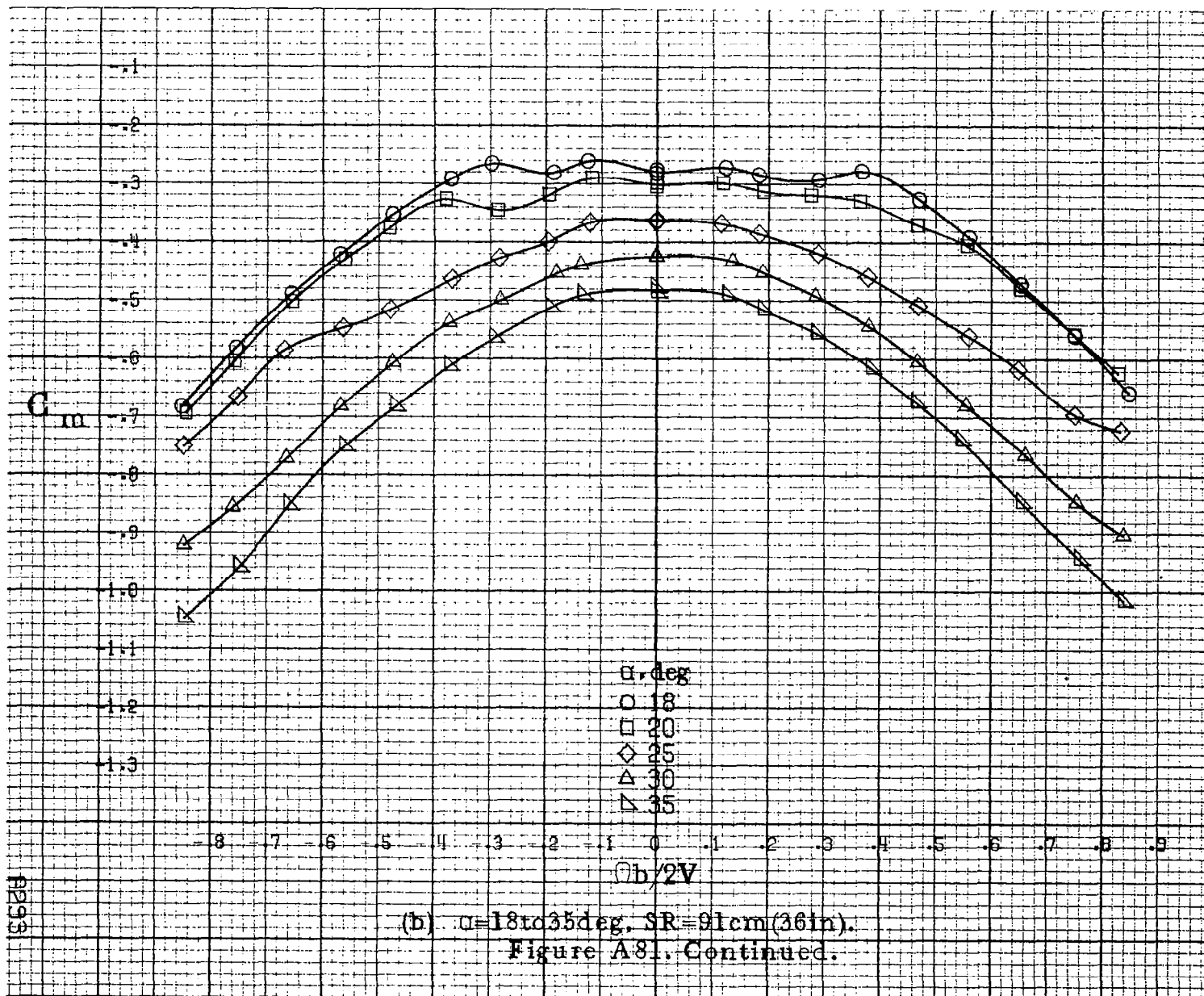
(c) $\alpha = 30$ to 50 deg. $SR = 0$.
Figure A80. Continued.

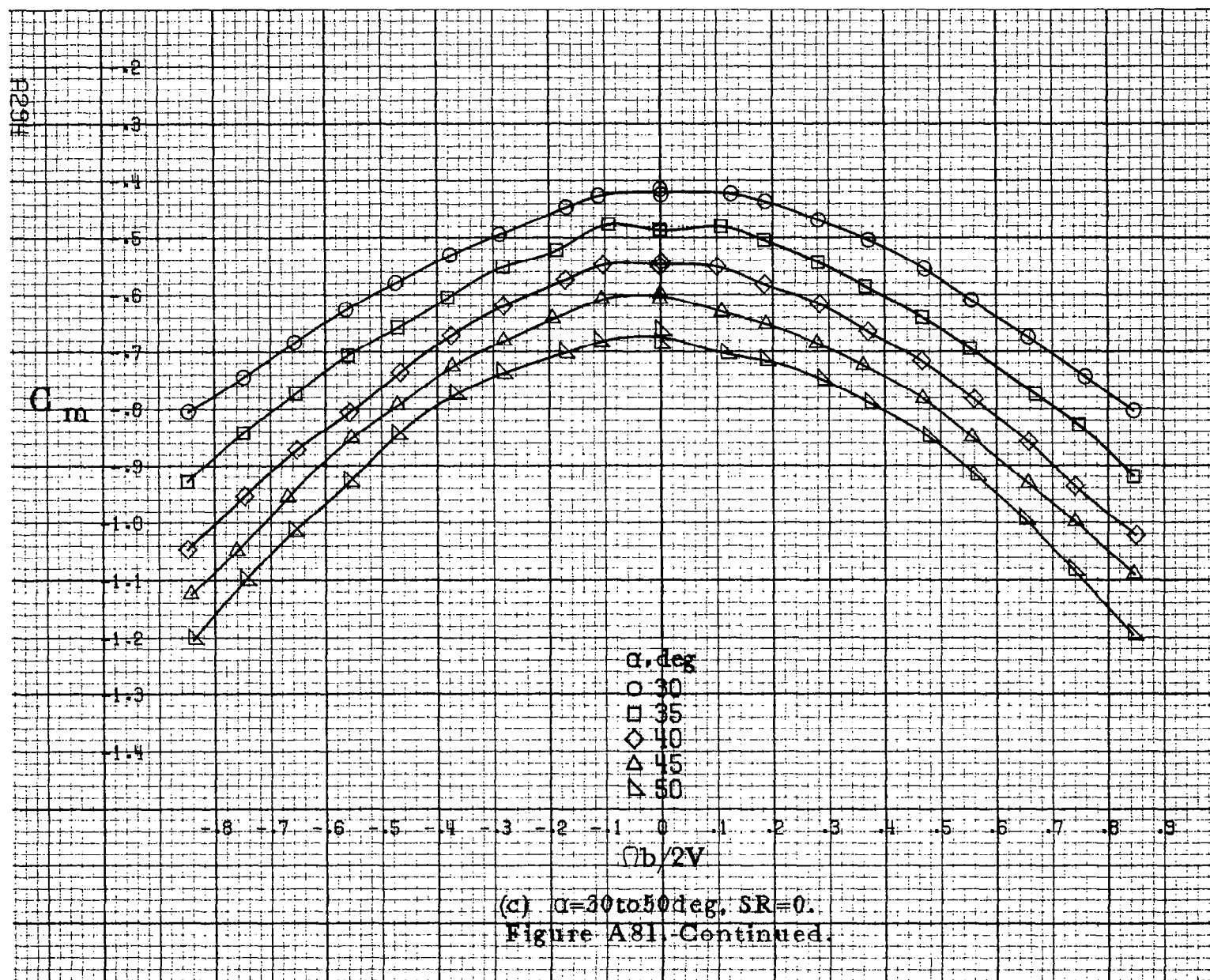


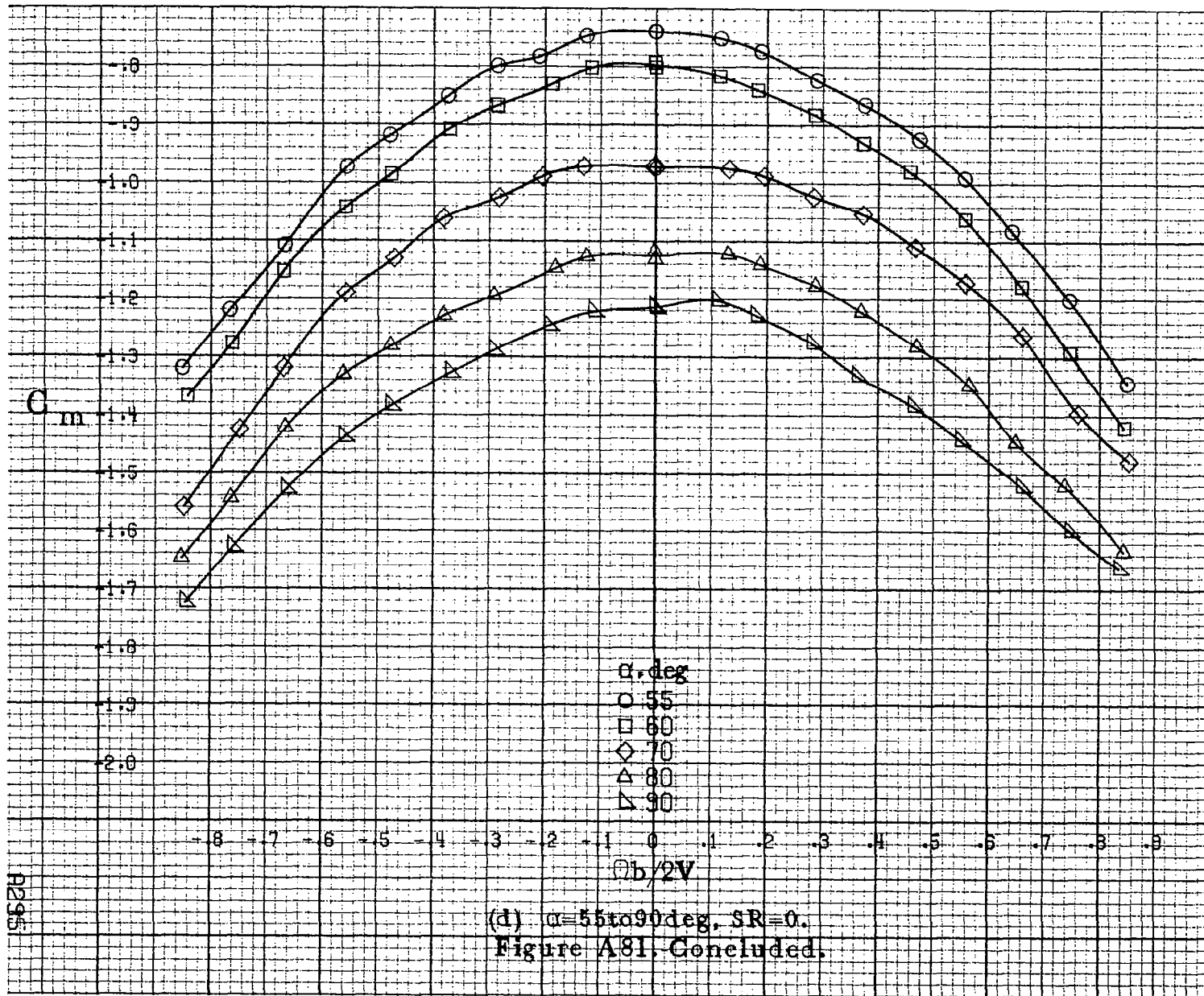


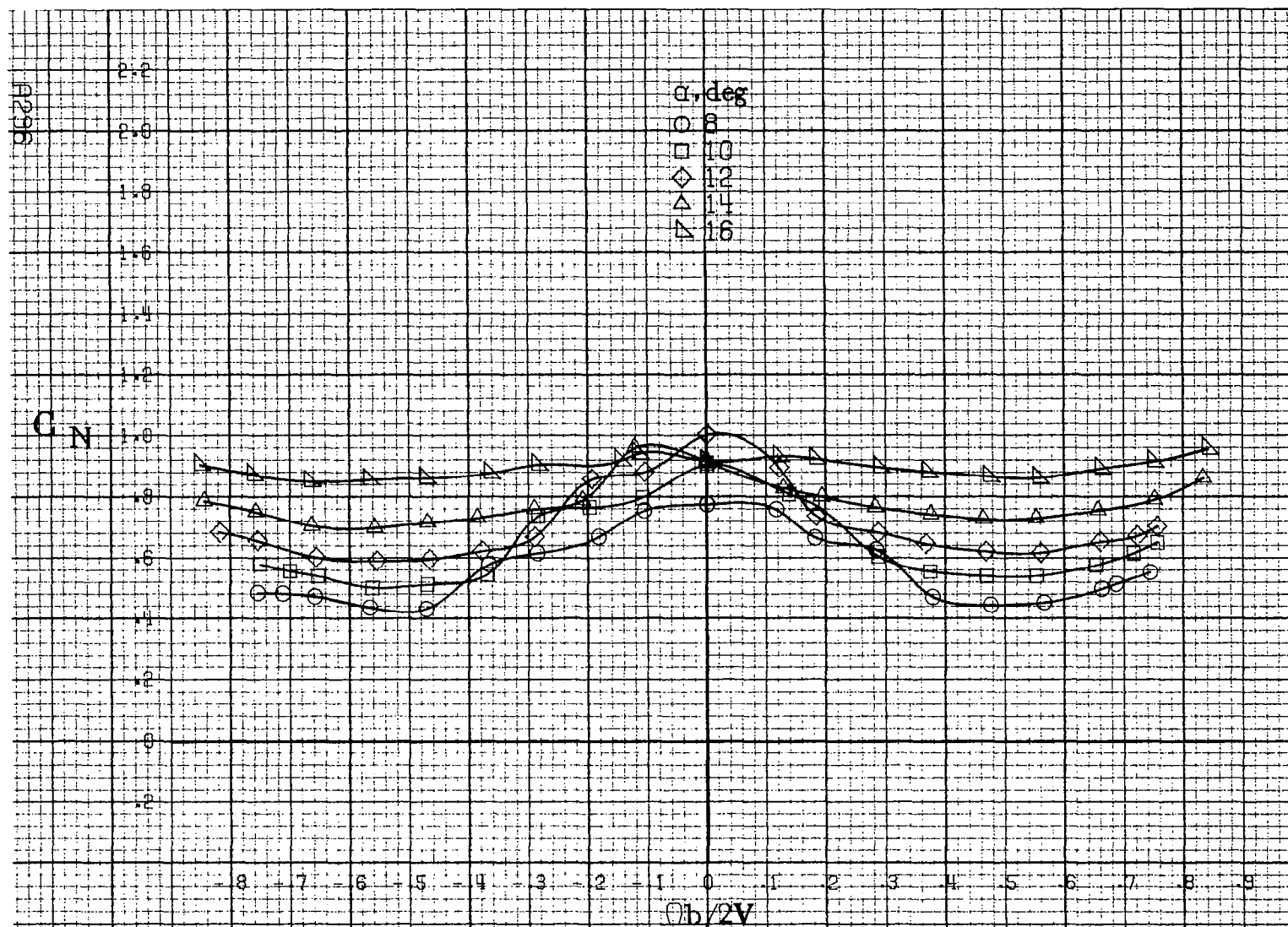
(a) $\alpha = 8$ to 16° , $SR = 91\text{cm}$ (36in.).

Figure A81. Effect of rotation rate and angle of attack on pitching moment coefficient for configuration having sharp edged fuselage bottom and a 49.8cm (19.6in.) span outboard LE wing droop. $\delta_e = 0^\circ$, $\delta_a = 0^\circ$, $\delta_r = 0^\circ$, $\beta = 0^\circ$.



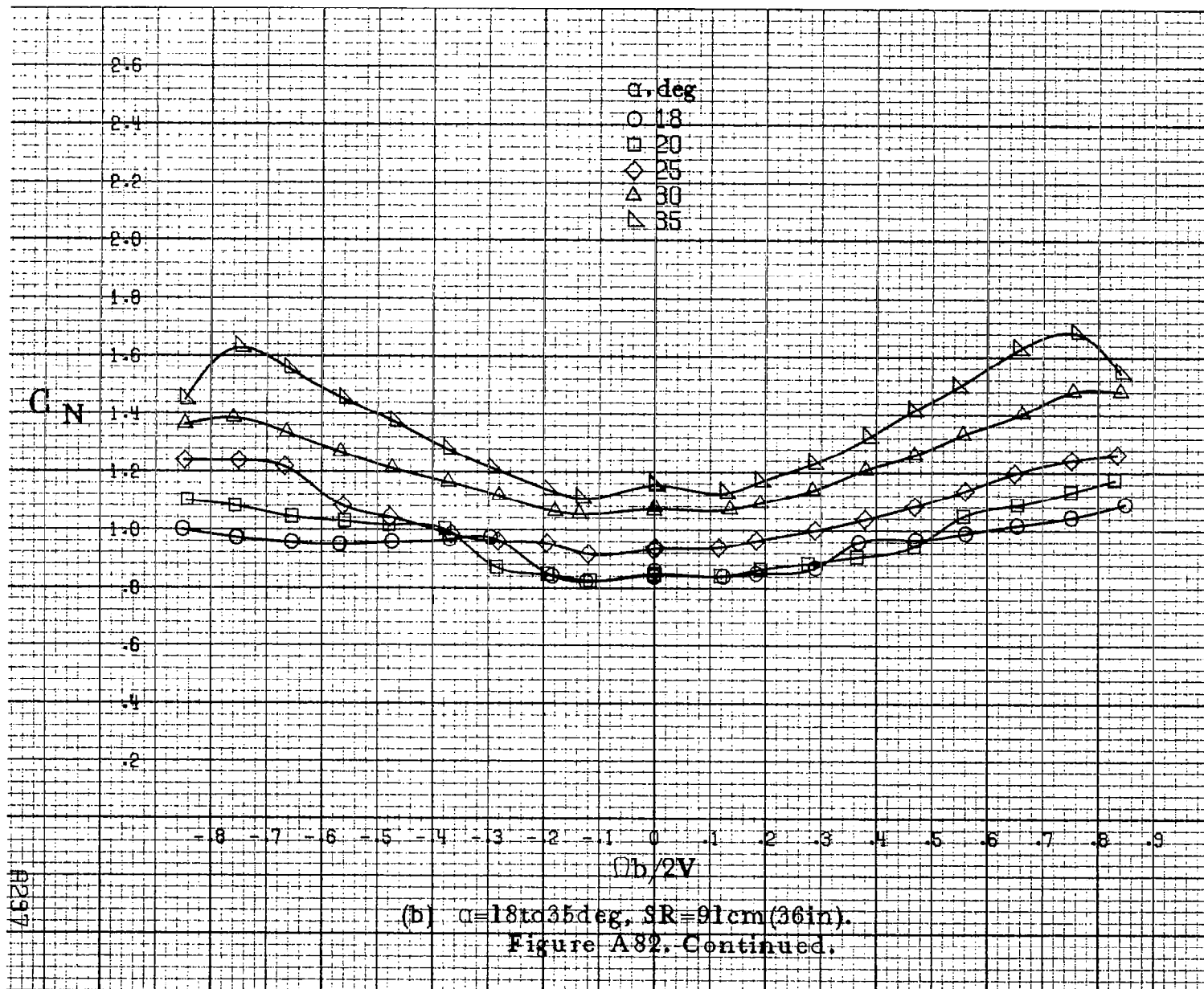


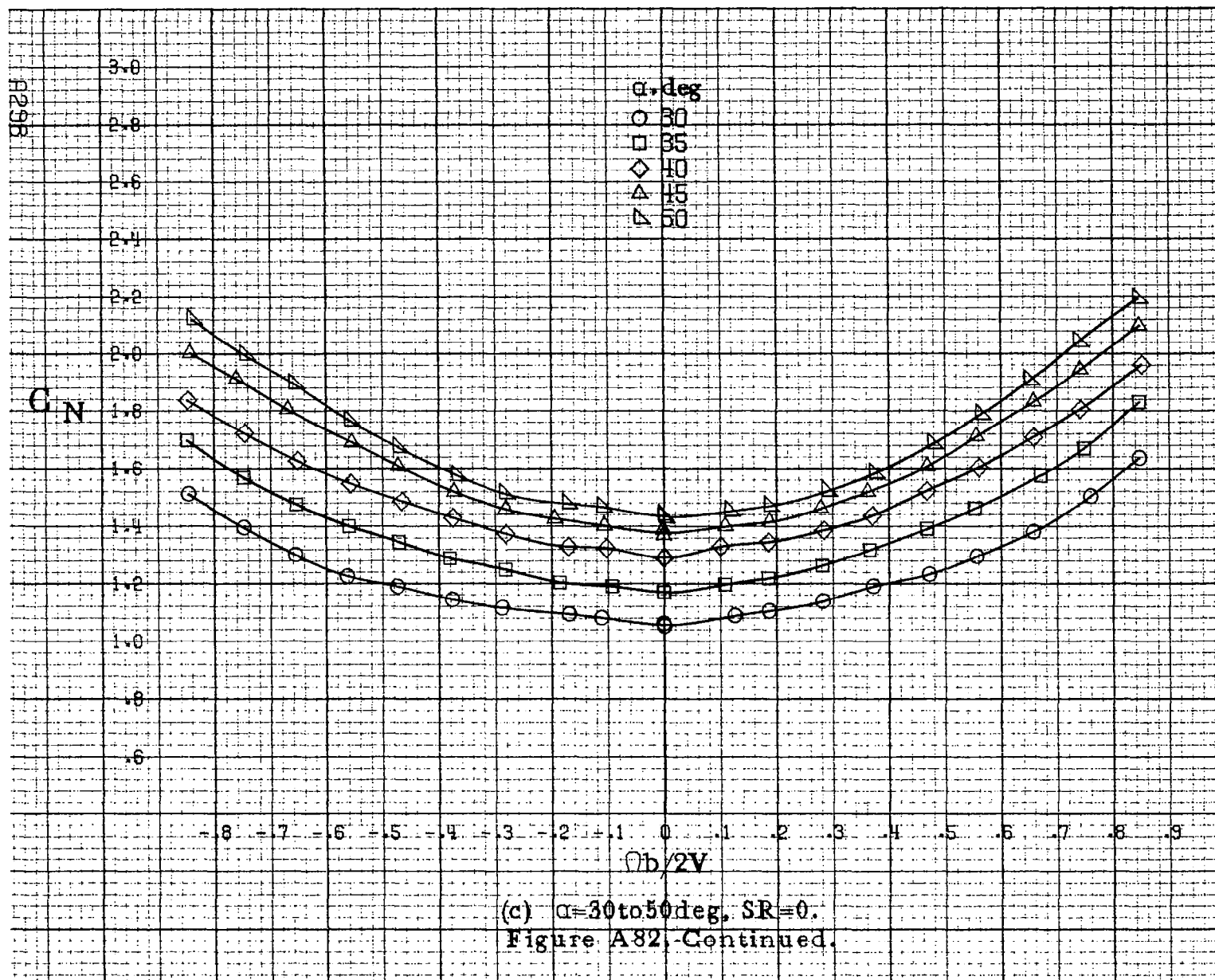


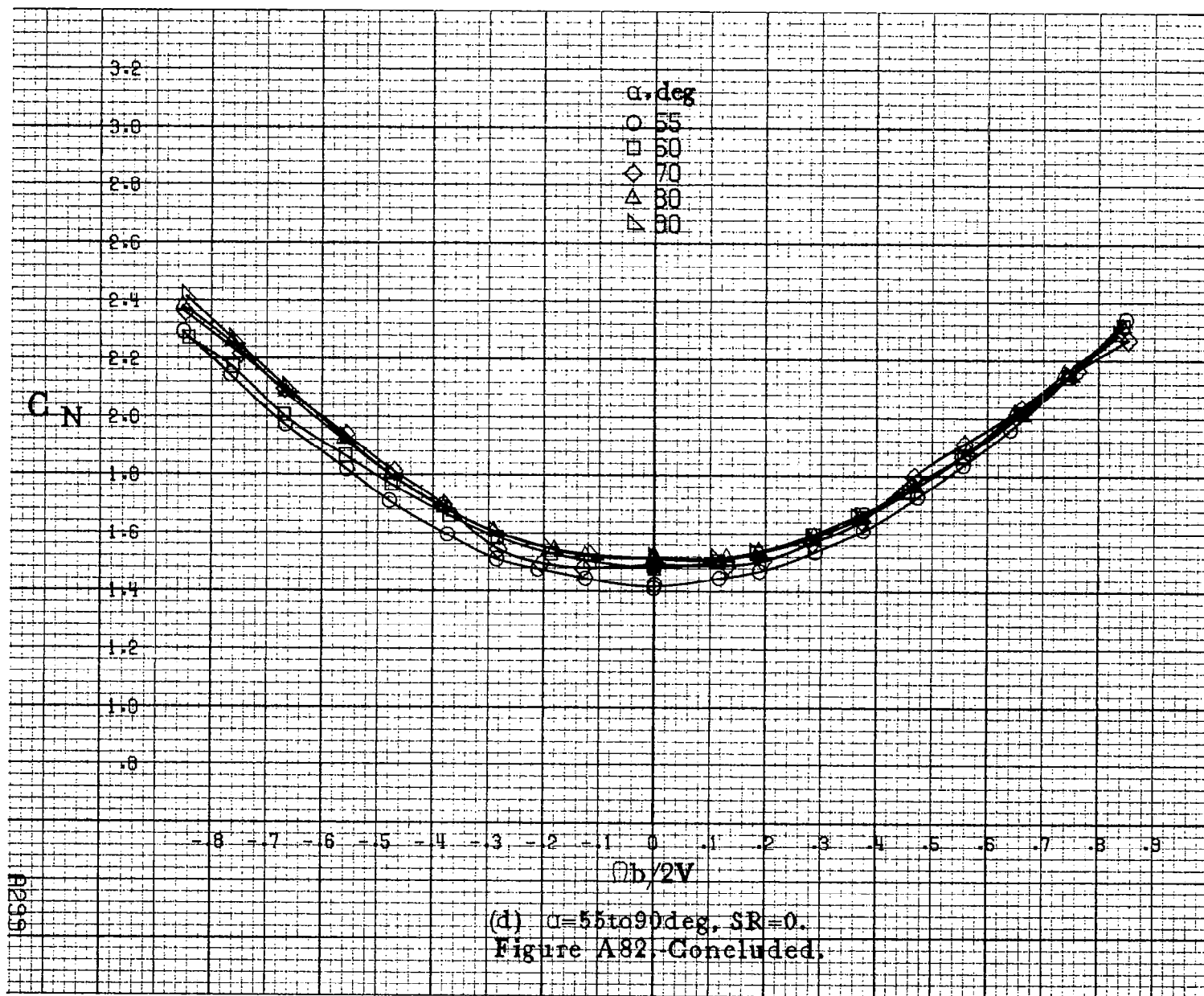


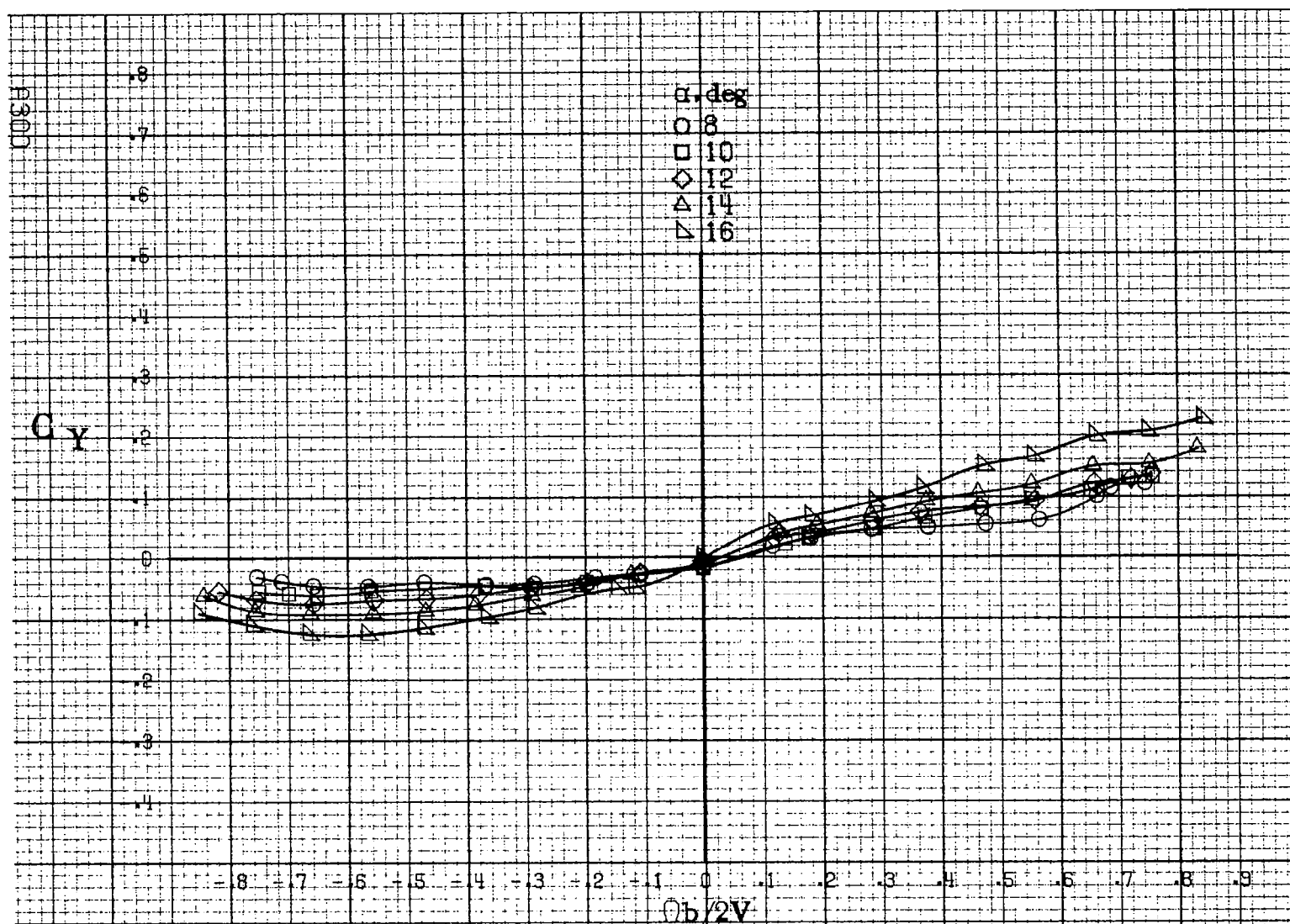
(a) $\alpha=8$ to 16 deg, SR-91cm (36in).

Figure A82. Effect of rotation rate and angle of attack on normal force coefficient for configuration having sharp edged fuselage bottom and a 49.8cm (19.6in.) span outboard LE wing droop. $\delta_e=0^\circ$, $\delta_z=0^\circ$, $\delta_c=0^\circ$, $\beta=0^\circ$.



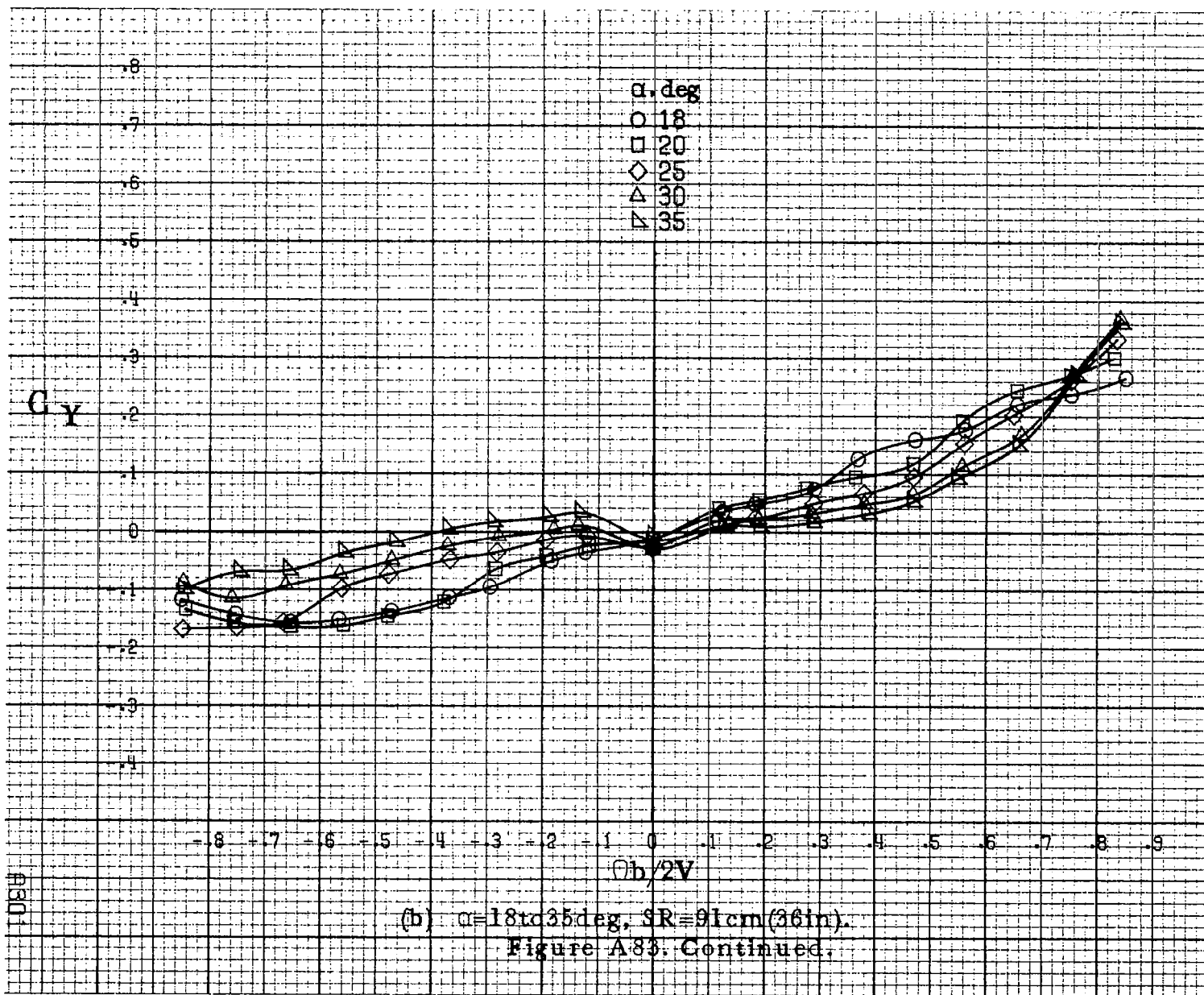


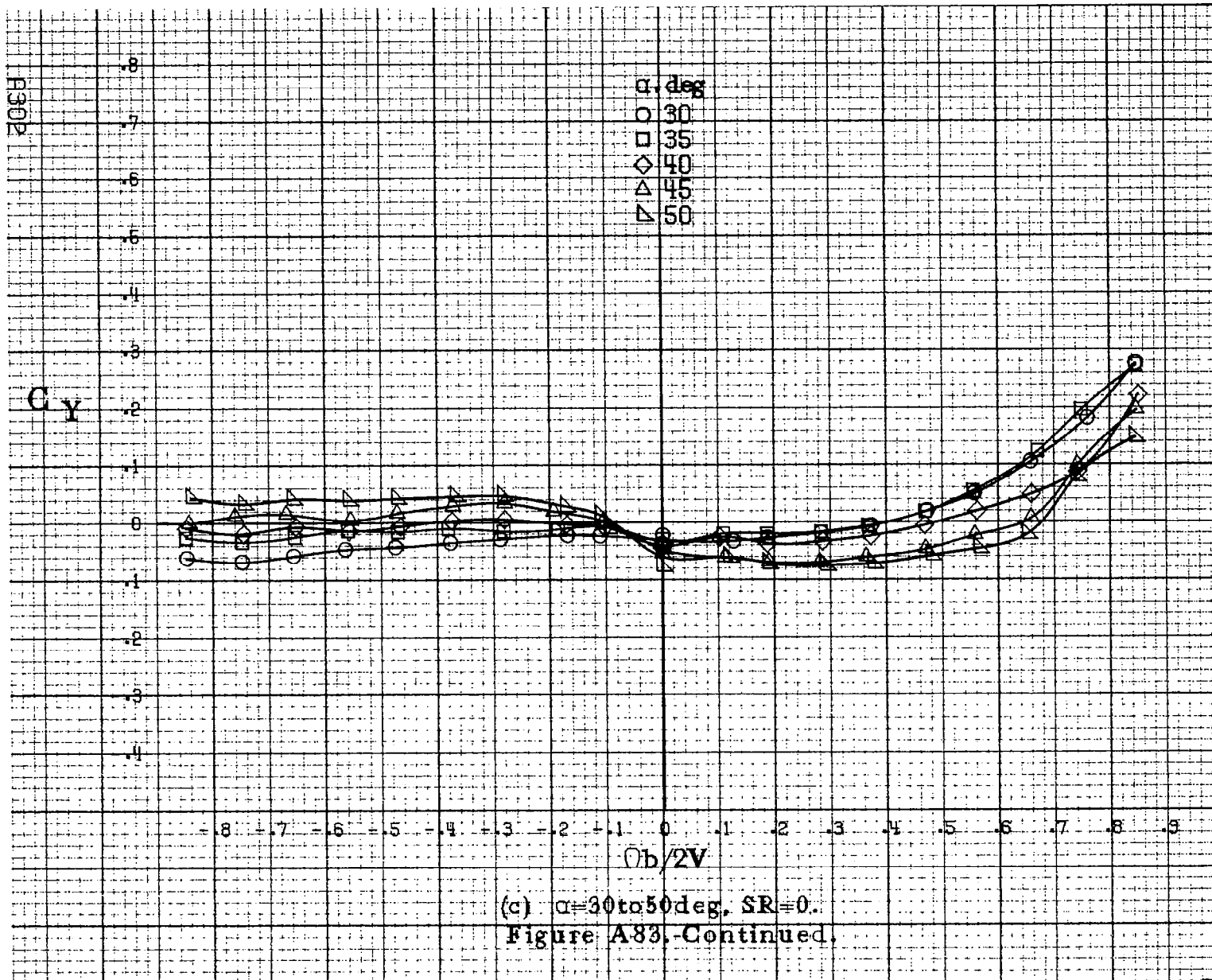


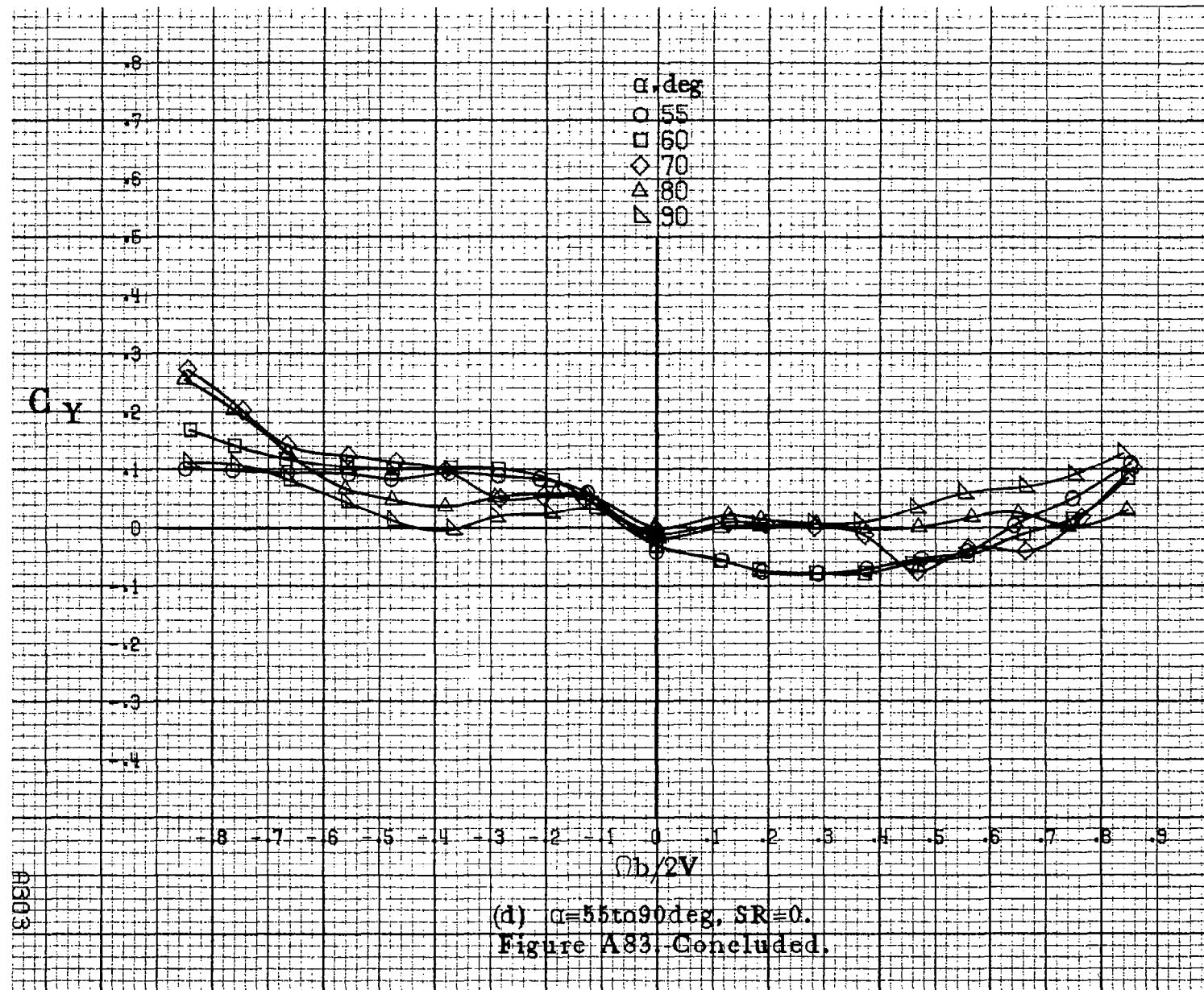


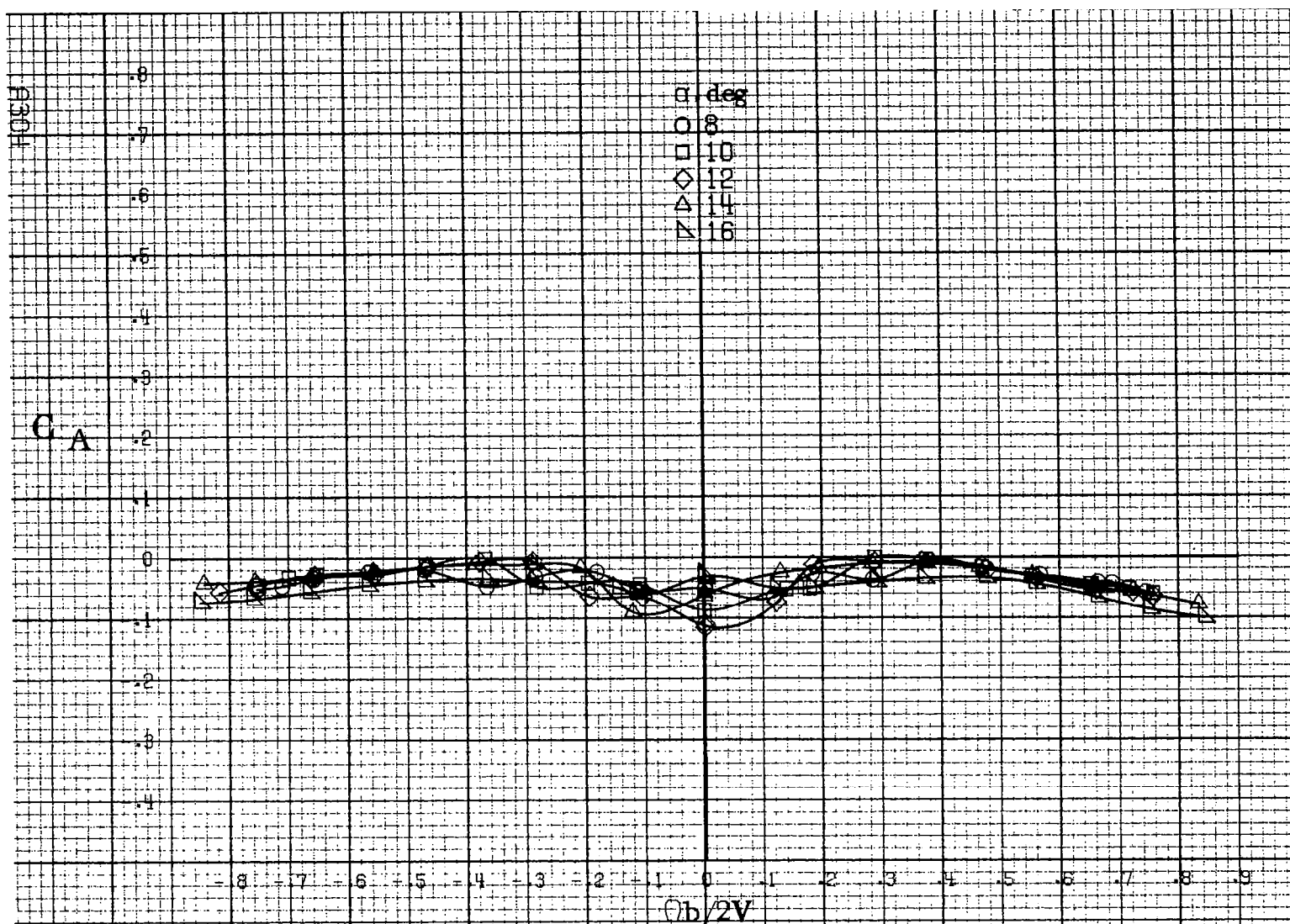
(a) $\alpha=8$ to 16° , $SR=91\text{cm}(36\text{in})$.

Figure A83. Effect of rotation rate and angle of attack on side-force coefficient for configuration having sharp-edged fuselage bottom and a 49.8cm(19.6in) span outboard LE wing droop. $\delta_e=0^\circ$, $\delta_a=0^\circ$, $\delta_r=0^\circ$, $\beta=0^\circ$.



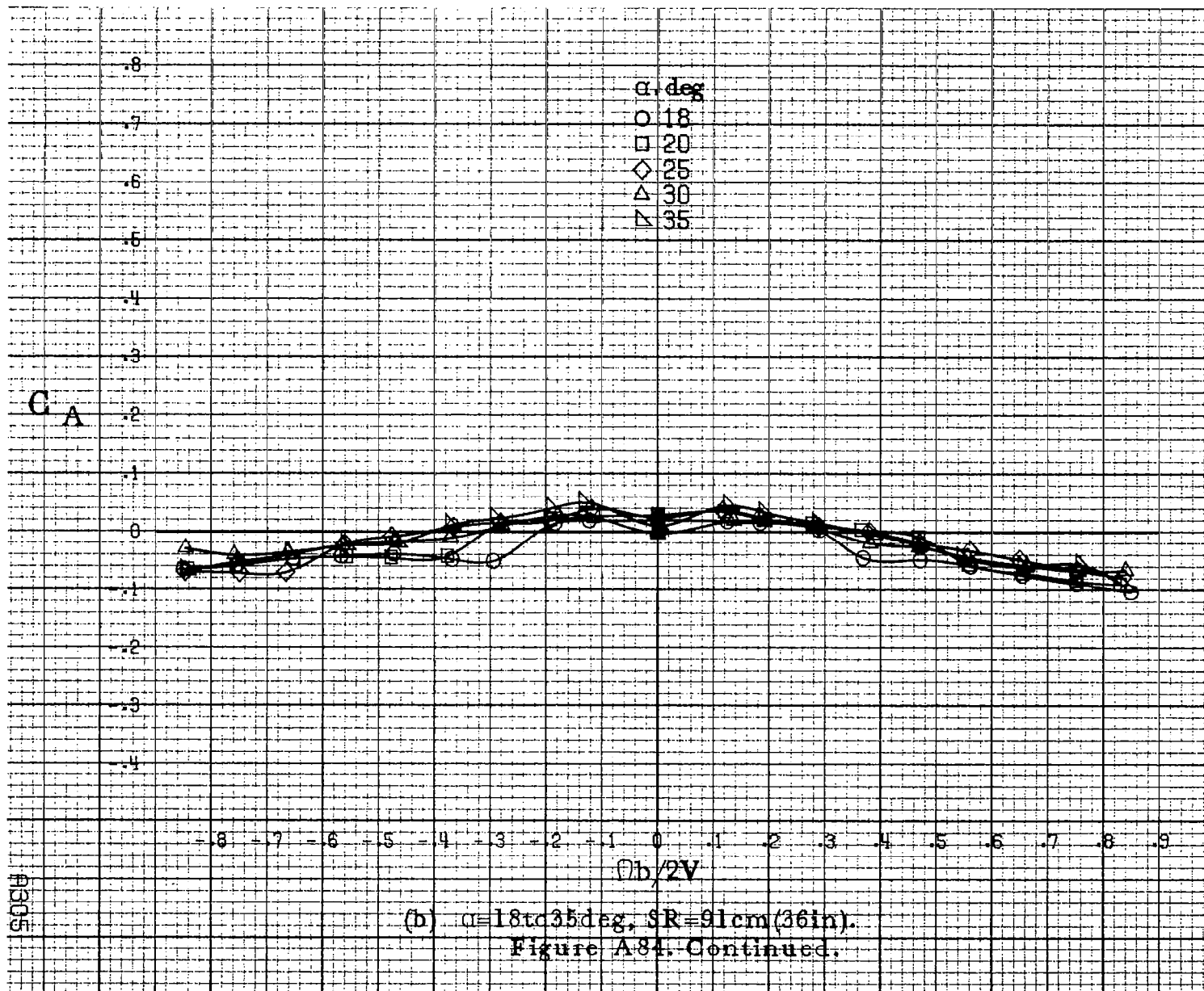


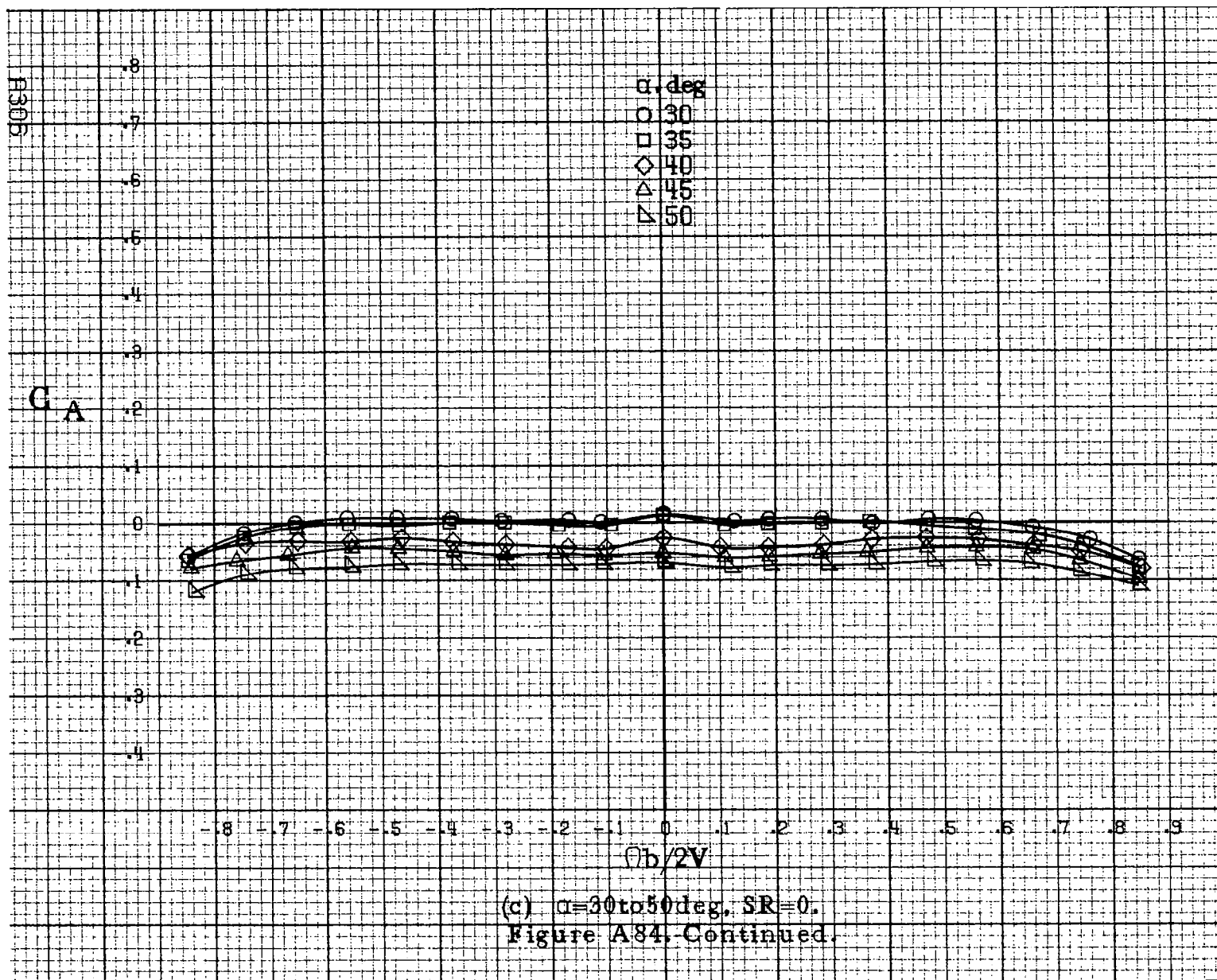


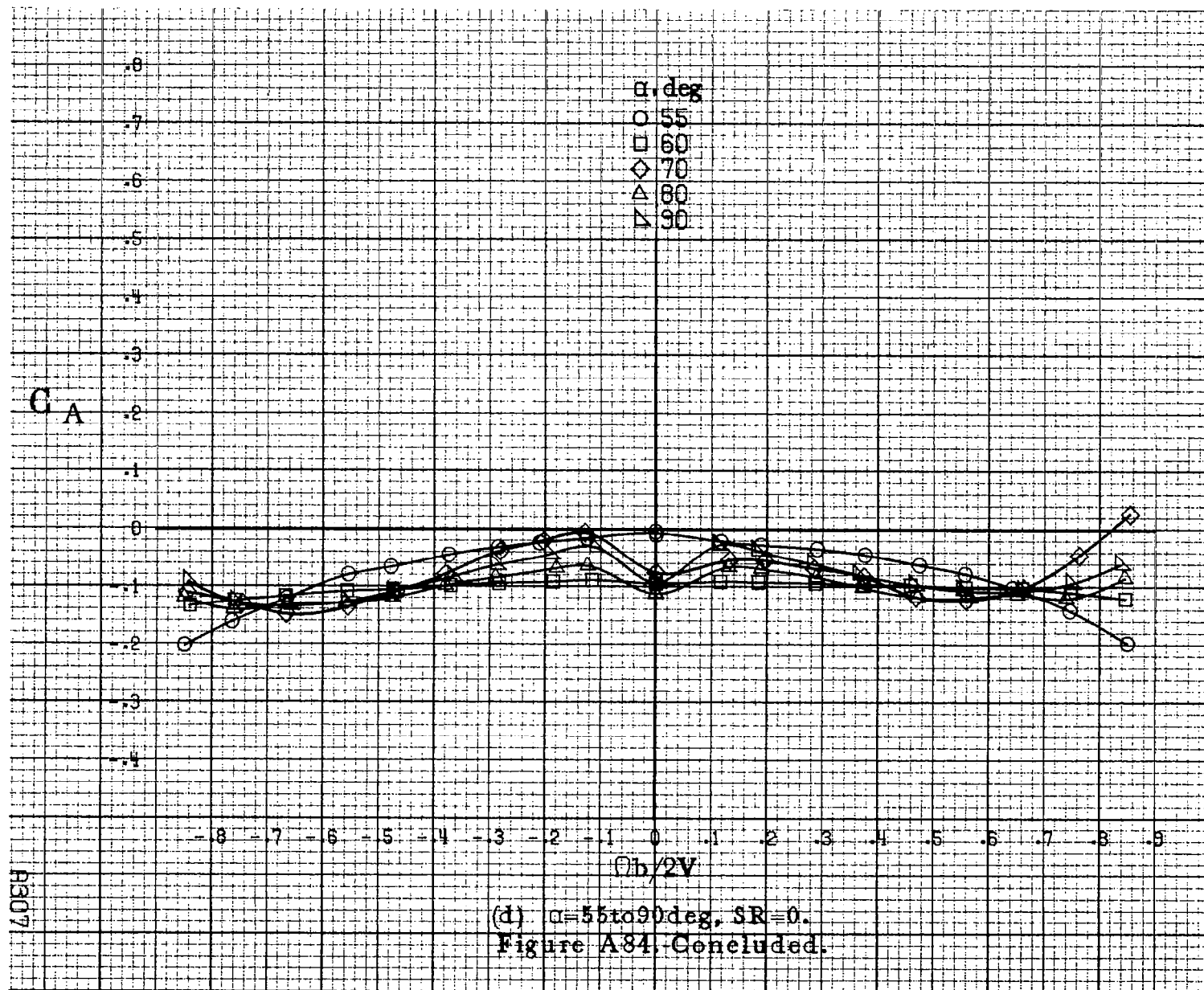


(a) $\alpha = 8$ to 16° , $SR = 91\text{cm}(36\text{in})$.

Figure A84. Effect of rotation rate and angle of attack on axial force coefficient for configuration having sharp-edged fuselage bottom and a 49.8cm(19.6in.) span outboard LE wing droop. $\delta_a = 0^\circ$, $\delta_a = 0^\circ$, $\delta_r = 0^\circ$, $\beta = 0^\circ$.







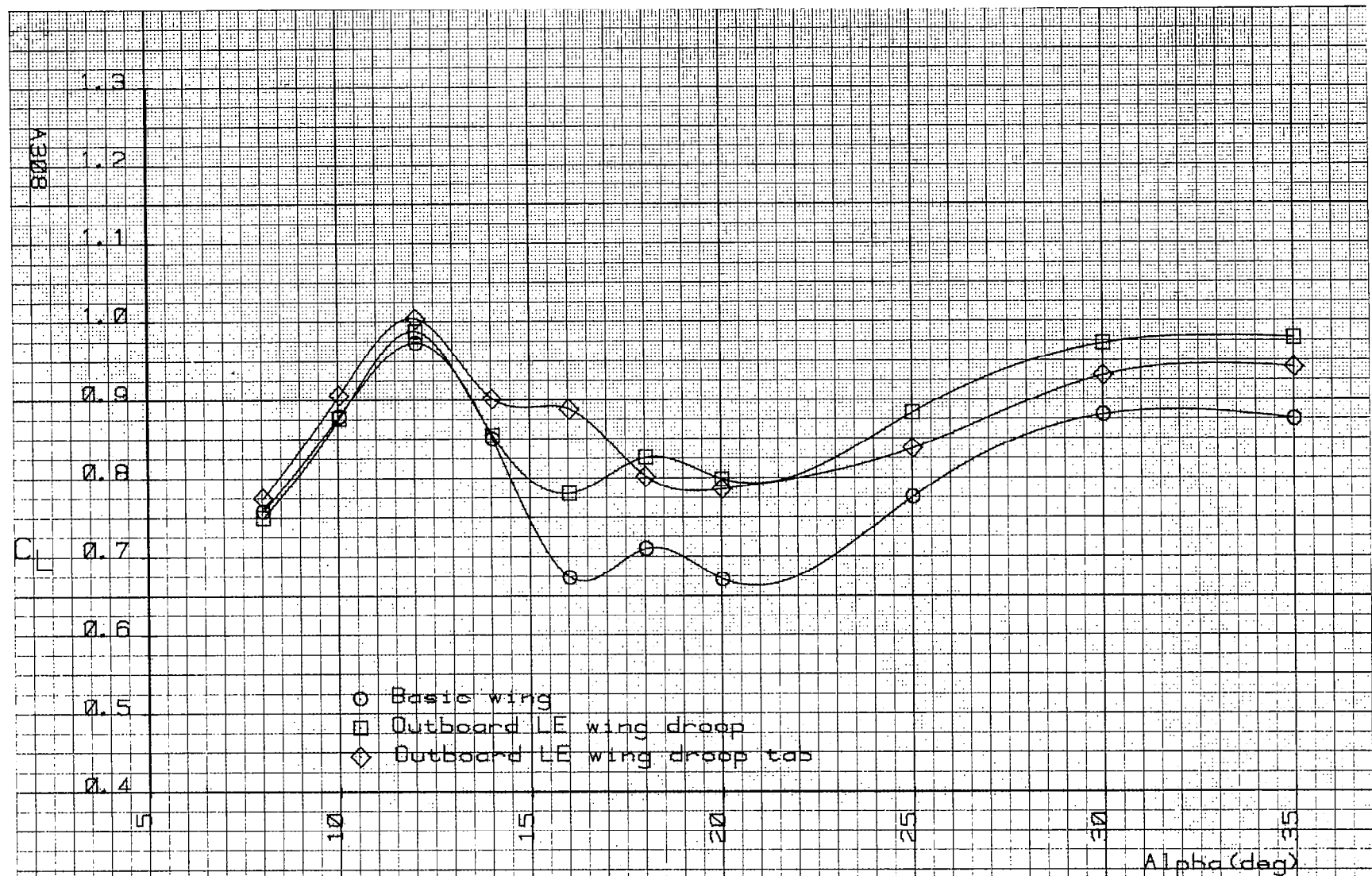


Figure A85. -Lift coefficient as a function of angle of attack for various span LE outboard wing droops.

1. Report No. NASA CR-3099		2. Government Accession No.		3. Recipient's Catalog No.	
4. Title and Subtitle Rotary Balance Data for a Single-Engine Trainer Design for an Angle-of-Attack Range of 8° to 90° .				5. Report Date August 1979	
				6. Performing Organization Code	
7. Author(s) Paul Pantason Waldo Dickens				8. Performing Organization Report No.	
				10. Work Unit No. 505-10-13-07	
9. Performing Organization Name and Address Bihrlle Applied Research, Inc. 400 Jericho Turnpike Jericho, New York 11753				11. Contract or Grant No. NAS1-14849, Task 32	
				13. Type of Report and Period Covered Contractor Report	
12. Sponsoring Agency Name and Address National Aeronautics and Space Administration Washington, DC 20546				14. Sponsoring Agency Code	
15. Supplementary Notes Langley Technical Monitor: James S. Bowman, Jr. Topical report					
16. Abstract Aerodynamic characteristics obtained in a rotational flow environment utilizing a rotary balance located in the Langley spin tunnel are presented in plotted form for a 1/6-scale, single-engine trainer airplane model. The configurations tested included the basic airplane, various wing leading-edge devices, elevator, aileron and rudder control settings as well as airplane components. Data are presented without analysis for an angle-of-attack range of 8° to 90° and clockwise and counter-clockwise rotations covering an $\frac{\Omega b}{2V}$ range from 0 to 0.85.					
17. Key Words (Suggested by Author(s)) General Aviation Spinning Rotary Balance High angle-of-attack wind tunnel data			18. Distribution Statement Unclassified - Unlimited Subject Category 02		
19. Security Classif. (of this report) Unclassified	20. Security Classif. (of this page) Unclassified	21. No. of Pages 324	22. Price* \$11.75		